

UNIVERSAL
LIBRARY

OU_158135

UNIVERSAL
LIBRARY

OSMANIA UNIVERSITY LIBRARY

Call No. 532.1/F 36 R Accession No. G-10639

Author Firth, Frederick R., ed.

Title Rheology ... 1960.

This book should be returned on or before the date last marked below.

RHEOLOGY

Theory and Applications

VOLUME 3

RHEOLOGY

Theory and Applications

Edited by

FREDERICK R. EIRICH

Polytechnic Institute of Brooklyn

Brooklyn, New York

VOLUME 3



1960

ACADEMIC PRESS • New York and London

Copyright ©, 1960, by Academic Press Inc.

ALL RIGHTS RESERVED

NO PART OF THIS BOOK MAY BE REPRODUCED IN ANY FORM,
BY PHOTOSTAT, MICROFILM, OR ANY OTHER MEANS,
WITHOUT WRITTEN PERMISSION FROM THE PUBLISHERS.

ACADEMIC PRESS INC.

111 FIFTH AVENUE
NEW YORK 3, N. Y.

United Kingdom Edition

Published by

ACADEMIC PRESS INC. (LONDON) LTD.
17 OLD QUEEN STREET, LONDON S. W. 1

Library of Congress Catalog Card Number 56-11131

PRINTED IN THE UNITED STATES OF AMERICA

PREFACE

This third volume completes the treatise as planned some time ago. During the time of preparation, however, chapter after chapter became more substantial and for each subject covered at least two more suggested themselves as important enough to be included. Thus, the expansion from the original one-volume work to three volumes appears to have been insufficient and, although plans are as yet indefinite, gaps in the present series as well as further developments in the rapidly growing field may make a fourth volume advisable in the not too distant future.

The present volume, except for two chapters on principles and methodology of measurements, contains chapters devoted to individual topics and to some industrial applications where the rheology of the materials undergoing forming operations is sufficiently well understood. Readers may be reminded that the book has been a long time in the making and that during this period some fields have developed further by making greater strides than others toward a quantitative mathematical or physical formulation. These chapters appear therefore to be of unequal level. Inasmuch as they reflect the present state of the art, however, the purpose of the treatise, that of introducing the reader into unfamiliar fields of rheology, is hoped to be fulfilled.

In view of the venture which "Rheology" represented, it has been most gratifying to find that the first two volumes have been generally well received by critics and public alike. It has encouraged the editor to continue in the same style and with the same organization as that of the first two volumes. The chapters were written by prominent, competent, and articulate authors who were left free to arrange the material to the best of their judgment within the framework and objectives of the book. Inevitably, personal views are often expressed and the chapters were permitted to contain overlapping sections, a policy which the editor explained in the Preface to the second volume.

Despite earlier hopes and intentions, it was again found impractical to unify the nomenclature. The main reason was that the subject matter of Volume 3 is even more diverse than that of the earlier ones and uniformity of treatment lies still in the rather distant future. All the greater efforts have been made to facilitate the use of the book by appending lists of

nomenclature to the chapters and by adding an index which is not only extensively cross-referenced but which might serve as a glossary for the many overlapping or conflicting terms which appear in widely different areas of rheology. The index has been arranged also in conformity with the two earlier volumes so that, taken in conjunction, the three indexes should enable the reader to locate any desired subject matter speedily and conveniently.

Brooklyn, N. Y.
Fall, 1959

FREDERICK R. EIRICH

CONTRIBUTORS TO VOLUME 3

- W. O. BAKER, *Bell Telephone Research Laboratories, Murray Hill, New Jersey*
C. E. BEYER, *Dow Chemical Company, Midland, Michigan*
J. J. BIKERMANN, *Department of Civil and Sanitary Engineering, Massachusetts Institute of Technology, Cambridge, Massachusetts*
A. BONDI, *Shell Development Company, Emeryville, California*
B. E. CONWAY, *Department of Chemistry, University of Ottawa, Ottawa, Canada*
DEAN W. CRIDDLE, *California Research Corporation, Richmond, California*
A. DOBRY-DUCLAUX, *Institut de Biologie Physico-Chimique, Fondation Edmond de Rothschild, Paris, France*
W. L. GORE, *E. I. du Pont de Nemours, Wilmington, Delaware*
I. L. HOPKINS, *Bell Telephone Research Laboratories, Murray Hill, New Jersey*
IRVIN M. KRIEGER, *Case Institute of Technology, Cleveland, Ohio*
JAMES M. MCKELVEY, *Department of Chemical Engineering, Washington University, St. Louis, Missouri*
SAMUEL H. MARON, *Case Institute of Technology, Cleveland, Ohio*
RAYMOND R. MYERS, *William H. Chandler Chemical Laboratory, Lehigh University, Bethlehem, Pennsylvania*
S. OKA, *Department of Physics, Faculty of Science, Tokyo Metropolitan University, Tokyo, Japan*
W. C. ORMSBY, *Department of Mineral Technology, Pennsylvania State College, State College, Pennsylvania*
M. REINER, *Israel Institute of Technology, Haifa, Israel*
BRUNO R. ROBERTS, *The Chemstrand Corporation, Decatur, Alabama*
R. S. SPENCER, *Plastics Basic Research Laboratory, Dow Chemical Company, Midland, Michigan*
RUTH N. WELTMANN, *National Aeronautics and Space Administration, Lewis Research Center, Cleveland, Ohio*
W. A. WEYL, *Department of Mineral Technology, Pennsylvania State University, University Park, Pennsylvania*
A. C. ZETTMAYER, *William H. Chandler Chemistry Laboratory, Lehigh University, Bethlehem, Pennsylvania*
B. H. ZIMM, *General Electric Company, Schenectady, New York*

CONTENTS

Preface.....	v
Contributors to Volume 3.....	vii
Contents of Volumes 1 and 2.....	xv
 1. The Normal-Coordinate Method for Polymer Chains in Dilute Solution	
By B. H. ZIMM	
I. Introduction	1
II. The Elastic Dumbbell	2
III. The Elastic Chain	7
Nomenclature	16
 2. The Principles of Rheometry	
By S. OKA	
I. Introduction	18
II. Capillary Viscometers	21
III. Rotating Coaxial Cylinder Viscometers	29
IV. Oscillating Coaxial Cylinder Viscometers	42
V. Disk Viscometers	51
VI. Concentric Sphere Viscometers	56
VII. Cone and Plate, Double Cone, and Conicylindrical Viscometers	61
VIII. Oscillating Plate Viscometers	65
IX. Falling Sphere Viscometers	70
X. Parallel Plate Plastometers	73
XI. Coaxial Cylinder Viscometers with Axial Motion	77
Nomenclature	80
 3. Viscosity of Suspensions of Electrically Charged Particles and Solutions of Polymeric Electrolytes	
By B. E. CONWAY AND A. DOBRY-DUCLAUX	
I. Introduction	83
II. Simple Strong Electrolytes	85
III. Electroviscous Effects with Impermeable Macromolecular Particles	87
IV. Comparison of Theory with Experiment for the First Electroviscous Effect	92

V. The Second Electroviscous Effect	96
VI. Electroviscous Effects in the Close Approach of Macroscopic Bodies and in Sedimentation	98
VII. The Third Electroviscous Effect	99
VIII. General Expression for the Electroviscous Effects	119
Nomenclature	120

4. The Rheology of Latex

BY SAMUEL H. MARON AND IRVIN M. KRIEGER

I. Introduction	121
II. Literature Resumé	122
III. Experimental Determination of Flow Behavior	125
IV. Dependency of Latex Flow on Shearing Stress	130
V. Dependence of Latex Flow on Concentration	135
VI. Effect of Particle Size and Size Distribution	139
VII. Effect of Temperature	140
VIII. Effect of Electrolytes	140
IX. Some Unsolved Problems in Latex Rheology	141
Nomenclature	143

5. The Rheology of Printing Inks

BY A. C. ZETTMAYER AND RAYMOND R. MYERS

I. The Role of Printing Inks	145
II. Rheological Requirements of Printing Inks	146
III. Ink Production	147
IV. Printing	152
V. Viscometric Study of Printing Inks	157
VI. Tack and Related Phenomena	167
Nomenclature	187

6. Rheology of Pastes and Paints

BY RUTH N. WELTMANN

I. Introduction	189
II. Instruments	190
III. Flow Measurements	193
IV. Physical Considerations	219
V. Product Evaluation	233
Nomenclature	247

7. Atomistic Approach to the Rheology of Sand-Water and of Clay-Water Mixtures

BY W. A. WEYL AND W. C. ORMSBY

I. Analysis of the Problem	249
II. Some Unique Properties of Water	252

III. Surface Properties of Solids Containing Cations of High Charge and Low Polarizability (Quartz, Clay)	258
IV. The Interaction of Minerals with Water	267
V. Summary	295

8. The Rheology of Inorganic Glasses

By W. A. WEYL

I. Introduction: the Importance of the Viscosity of Glass for Its Manufacture	299
II. Methods of Measuring the Viscosity of Glass	301
III. Principles Governing the Polymerization of Ionic Compounds and Formation of Viscous Liquids	303
IV. Factors Determining the Rheological Properties of Glass	309
V. Interpretation of the Viscosity of Some Simple Experimental Glasses of Systematically Varied Compositions	318
VI. Viscosities of Some Commercial Glasses	327
VII. Flow Processes within a Rigid Glass	329
VIII. Summary and Conclusions	337

9. The Rheology of Concrete

By M. REINER

I. Introduction	341
II. Fresh Cement Paste	344
III. Set Cement	346
IV. Mortar	351
V. Concrete	356
VI. Reinforced Concrete	363
Nomenclature	364

10. The Deformation of Crystalline and Cross-Linked Polymers

By I. L. HOPKINS AND W. O. BAKER

I. Introduction	365
II. Polyethylene	388
III. Hard Rubber: A Highly Polar, Cross-Linked Polymer	408
IV. Polyamides: Polar Chain Polymers Examined for Both Long and Short Range Behavior	412
V. Conclusion	425
Nomenclature	426

11. The Viscosity and Elasticity of Interfaces

By DEAN W. CRIDDLE

I. Interfacial Viscosity	429
II. Interfacial Elasticity	439
III. Significance of Interfacial Viscosity and Elasticity	441
Nomenclature	442

12. Rheology of Lubrication and Lubricants

By A. BONDI

I. Fluid Lubricants	444
II. Gelled Lubricants	457
III. Flow Phenomena in Boundary Lubrication	467
Nomenclature	478

13. The Rheology of Adhesion

BY J. J. BIKERMAN

I. Introduction	479
II. Application of Adhesives	480
III. Tackiness	481
IV. Time of Set	485
V. Final Strength	488
VI. Summary	503
Nomenclature	503

14. Rheology in Molding

BY C. E. BEYER AND R. S. SPENCER

I. Introduction	505
II. The Injection Molding Machine	506
III. The Injection Molding Cycle	510
IV. Filling the Mold	514
V. Packing in the Mold	524
VI. Discharge and Sealing	535
VII. Sealed Cooling	537
VIII. Cycle Time	542
Nomenclature	550
General Bibliography	551

15. Rheology of Spinning

BY BRUNO R. ROBERTS

I. Introduction	554
II. Description of the Problem	554
III. Discussion of the Physical Characteristics of Spinnable Materials	556
IV. Flow under Fiber-Forming Conditions	561
V. Evaluation Techniques	568
VI. Interpretation of Phenomena Accompanying the Fiber Formation	571
VII. Summarizing Discussion of Present Knowledge of the Various Rheological Problems Involved in Spinning	575
VIII. Appendix	576
Nomenclature	587

16. Theory of Screw Extruders

By W. L. GORE AND JAMES M. MCKELVEY

I. Introduction	589
II. Flow and Power Formulas	599
III. Operating Equations for Melt Extrusion	602
IV. Extrusion of Non-Newtonian Melts	617
V. Plasticating Extrusion	623
Nomenclature	631
 AUTHOR INDEX	 633
SUBJECT INDEX	645

CONTENTS OF VOLUMES 1 AND 2

VOLUME 1

Introduction to Rheological Concepts

FREDERICK R. EIRICH

Phenomenological Macrorheology

M. REINER

Finite Plastic Deformation

WILLIAM PRAGER

Stress-Strain Relations in the Plastic Range of Metals—Experiments and Basic Concepts

D. C. DRUCKER

Mechanical Properties and Imperfections in Crystals

G. J. DIENES

Dislocations in Crystal Lattices

J. M. BURGERS AND W. G. BURGERS

Mechanical Properties of Metals

J. FLEEMAN AND G. J. DIENES

Some Rheological Properties Under High Pressure

R. B. DOW

Theories of Viscosity

A. BONDI

Large Elastic Deformations

R. S. RIVLIN

Dynamics of Viscoelastic Behavior

TURNER ALFREY, JR., AND E. F. GURNEE

Viscosity Relationships for Polymers in Bulk and in Concentrated Solution

T. G. FOX, SERGE GRATCH, AND S. LOSHAEK

The Statistical Mechanical Theory of Irreversible Processes in Solutions of Macromolecules

J. RISEMAN AND J. G. KIRKWOOD

The Viscosity of Colloidal Suspensions and Macromolecular Solutions

H. L. FRISCH AND ROBERT SIMHA

Streaming and Stress Birefringence

A. PETERLIN

Non-Newtonian Flow of Liquids and Solids

J. G. OLDROYD

Acoustics and the Liquid State

R. B. LINDSAY

AUTHOR INDEX—SUBJECT INDEX

VOLUME 2

Viscoelasticity Phenomena in Amorphous High Polymeric Systems

HERBERT LEADERMAN

Stress Relaxation Studies of the Viscoelastic Properties of Polymers

ARTHUR V. TOBOLSKY

The Relaxation Theory of Transport Phenomena

TAIKYUE REE AND HENRY EYRING

The Rheology of Organic Glasses

ROLF BUCHDAHL

The Rheology of Raw Elastomers

M. MOONEY

The Rheology of Cellulose Derivatives

E. B. ATKINSON

The Rheology of Fibers

R. MEREDITH

The Rheology of Gelatin

A. G. WARD AND P. R. SAUNDERS

Rheological Properties of Asphalts

R. N. J. SAAL AND J. W. A. LABOUT

Rheological Problems of the Earth's Interior

B. GUTENBERG

Experimental Techniques for Rheological Measurements on Viscoelastic Bodies

JOHN D. FERRY

Fundamental Techniques: Fluids

B. A. TOMS

Goniometry of Flow and Rupture

A. JOBLING AND J. E. ROBERTS

AUTHOR INDEX—SUBJECT INDEX

CHAPTER 1

THE NORMAL-COORDINATE METHOD FOR POLYMER CHAINS IN DILUTE SOLUTION*

B. H. Zimm

I. Introduction.....	1
II. The Elastic Dumbbell.....	2
III. The Elastic Chain.....	7
Nomenclature	16

I. Introduction

The method of normal coordinate analysis is the newest, and perhaps the most powerful, of the mathematical tools that have been applied to the theory of high polymers. It was introduced only a few years ago by Bueche¹ and Rouse, Jr.,² working independently. However, normal coordinate analysis has had a long history in other branches of mathematical physics.^{2a}

Perhaps the genesis of the method goes back to Sir Isaac Newton's theory of sound. At that time the theory of differential equations was not yet developed—in fact calculus itself had only just been invented—and Newton was forced to use an artifice to describe the propagation of sound through an elastic medium such as air. His artifice consisted of representing the continuous medium by a chain of weights connected by springs. The sound wave was assumed to propagate down this chain, and in this way the problem of the modes in which such a chain could vibrate came to the fore.

A fairly complete discussion of this problem was accomplished a few years later by two Swiss mathematicians, John and Daniel Bernoulli, in a

* This chapter is the manuscript of a lecture delivered before a joint meeting of the Society of Rheology and the Division of High Polymer Physics of the American Physical Society in New York in February 1956. Although it is not intended to be a comprehensive review of the subject, the Editor has wished to include it because of the special interest of the subject.

¹ F. Bueche, *J. Chem. Phys.* **22**, 603 (1954).

² P. E. Rouse, Jr., *J. Chem. Phys.* **21**, 1272 (1953).

^{2a} L. Brillouin, in his book "Wave Propagation in Periodic Structures" (McGraw-Hill, New York, 1946; Dover, New York, 1953) gives an interesting historical account from which the next few paragraphs are drawn.

correspondence beginning about 1727. They explicitly discussed the normal vibrations, i.e., the ones which would perpetuate themselves down the chain without change of type, and they worked this problem out in quite complete detail. Since that time the analysis of complex systems of masses and springs, and sometimes including damping forces in addition, has usually been reduced by means of a normal-coordinate analysis.

On the other hand, the dynamical theory of the specific heat of solid substances, which was founded by Debye and by Born and von Karman in the early part of this century, is essentially a theory of the normal vibrations of the crystal lattice. Likewise, the normal coordinate theory has been very important—in fact, absolutely necessary—in discussing the design of electrical filter apparatus for communications equipment.

Despite the fact that this problem is well known to almost any student of advanced physics, until very recently it remained unused in the field of high polymers. The mathematical theory of high polymer chains probably dates from the pioneering work of Meyer, Mark, and Guth over twenty years ago. Since that time it has been recognized that the model of a chain of weights connected by springs is a fair representation of the actual high polymer chain. Now such a chain is, of course, very similar to the chain which was discussed by Newton in 1686. There is one difference however, and this difference, which is much more serious in appearance than in actuality, undoubtedly kept people from applying the method of normal coordinates to high polymer chains. The difference lies in the fact that the typical high polymer chain is represented by a freely coiling chain with the universal joints joining the springs, whereas the chains which are discussed in the problems of classical physics are chains arranged in a definite linear framework in space. Now we shall see shortly that if one assumes that the springs of the high polymer chain have zero equilibrium length—and this, in fact, is just the assumption that one wants to make—then it makes no difference whether the chain is coiling or whether it is rigid. The state of each spring is described by the vector distance between its ends. Likewise, since it is a Hooke's law spring, the force between its ends is proportional to this length vector, and both the force and the length vectors project upon the coordinate axes in the same way. Therefore, the projection of each spring upon each coordinate axis acts just as if it were an identical spring laid out along this axis. The chain as a whole can be represented as three identical chains, but in each case stretched out along one of the three coordinate axes. These chains, of course, are each of the classical type.

II. The Elastic Dumbbell

Now let us study the particulars of our model more closely. By way of introduction, let us first take a very simple model, one that consists of only

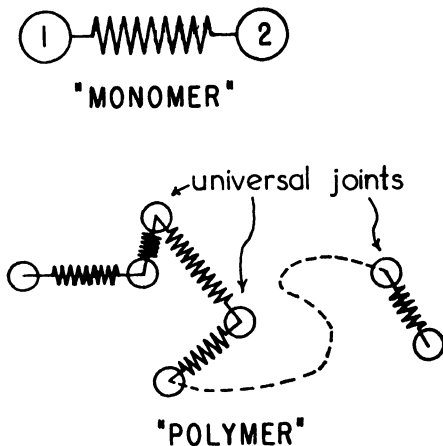


FIG. 1. Two idealized molecular models, whose motions can be given exact mathematical treatment.

one spring and two beads. This is the object depicted at the top of Fig. 1, labeled there "monomer." We assume that the springs have zero equilibrium length. This does not mean, of course, that the molecule which this object represents will have zero length, because thermal motion generally keeps this spring expanded to some extent. At first, however, let us consider the equations of motion neglecting thermal agitation.

We will suppose that this monomer object, which might also be called an elastic dumbbell, is extended in a viscous liquid which impedes its motion. There are then three types of forces and reactions that we have to consider: the force due to the extension of the spring, the force caused by the viscosity of the liquid when one of the beads moves through it, and the inertial reaction caused by the masses of the beads. On the molecular scale the inertial reactions tend to be very much smaller than the other two forces, and for this reason we shall neglect them completely.

We shall assume that the viscous drag on the motion of one of the beads can be represented simply by a force proportional to the velocity of the bead and in the reverse direction. With this very reasonable assumption we get the two following equations of motion for beads one and two:

$$\begin{aligned}\rho \dot{x}_1 &= F_{x1} = -g(x_1 - x_2), \\ \rho \dot{x}_2 &= F_{x2} = -g(x_2 - x_1).\end{aligned}\tag{1}$$

(The dot represents a derivative with respect to time.)

The left-hand side of these equations represents the viscous drag with a resistance coefficient ρ . The velocities of the beads in the x -direction are

\dot{x}_1 and \dot{x}_2 , respectively. These must be equal to the forces on the beads F_{x1} and F_{x2} which are, in turn, equal to the forces exerted by the springs; the latter are given by the right-hand side of the equation, with g the force constant and x_1 and x_2 the x -coordinates of the two beads.

Now this set of simultaneous differential equations can be solved easily by adding and subtracting the two equations to produce two new equations. In this process two quantities naturally make their appearance. These quantities are ξ_0 and ξ_1 as given below.

$$\begin{aligned}\xi_0 &= \frac{x_1 + x_2}{\sqrt{2}} \\ \xi_1 &= \frac{x_1 - x_2}{\sqrt{2}}\end{aligned}\tag{2}$$

The first is, except for a normalization factor, the mean coordinate of the elastic dumbbell. The other is, except for the same factor, the length of the dumbbell. By adding the two equations, we get the following differential equation for ξ_0 , which is easily solved to get a result that ξ_0 is a constant:

$$\dot{\xi}_0 = 0; \quad \xi_0 = \text{constant}.\tag{3}$$

In other words, the center of mass of the dumbbell does not move, as of course it should not, since there is no force acting on the center of mass. By subtracting the two equations we get the following for ξ_1 , and this again has the simple solution given below:

$$\dot{\xi}_1 = -(2g/\rho)\xi_1; \quad \xi_1 = \xi_1' \exp [(-2g/\rho)t]\tag{4}$$

The quantity ξ_1 , therefore, decreases exponentially from its initial value ξ_1' toward 0. The two quantities ξ_0 and ξ_1 , which so markedly simplify the original set of equations, are the normal coordinates of this system.

We are now in a position to be more realistic about our model and introduce thermal agitation or Brownian motion. At the same time, with no increase in complication, we may put our model in a flowing liquid, one that is undergoing shear as a liquid would, for example, in conventional viscometer. Consider the situation in Fig. 2, in which our dumbbell molecule is shown with arrows representing the flow of liquid. The liquid is flowing in the x -direction with a velocity gradient in the z -direction. (For simplicity, we ignore the y -axis.) The equations of motion amplified by the addition of the Brownian motion and the shear-rate terms are the following:

$$\begin{aligned}\rho\dot{x}_1 &= F_{x1} = -kT \frac{\partial \ln \psi}{\partial x_1} - g(x_1 - x_2) + Kz_1, \\ \rho\dot{x}_2 &= F_{x2} = -kT \frac{\partial \ln \psi}{\partial x_2} - g(x_2 - x_1) + Kz_2.\end{aligned}\tag{5}$$

Kz_1 and Kz_2 are the shear-rate terms, K being the rate of shear. The partial derivative terms account for the Brownian motion. These require some explanation. It would seem, at first sight, impossible to introduce Brownian motion, which is a random agitation, into our equations which, up to now, at least, have been completely determined. This is, indeed, only possible if we average over the motions of the large number of identical particles, and it is in this sense that our equation must now be interpreted. The \bar{x}_1 and \bar{x}_2 now become the average motions of particles 1 and 2 in an ensemble of a large number of identical molecules. Under these conditions, we know how to handle the problem of Brownian motion. Brownian motion simply causes diffusion in the ordinary sense, and diffusion obeys Fick's Law; i.e., there is a current which flows from regions of high concentration to regions of low concentration, the strength of the current being proportional to the gradient of the concentration multiplied by kT . This is the origin of the first terms on the right of equations (5). The function ψ is the concentration generalized so that it includes both the concentration of particles 1 and particles 2. This function ψ is commonly called the distribution function of the system.

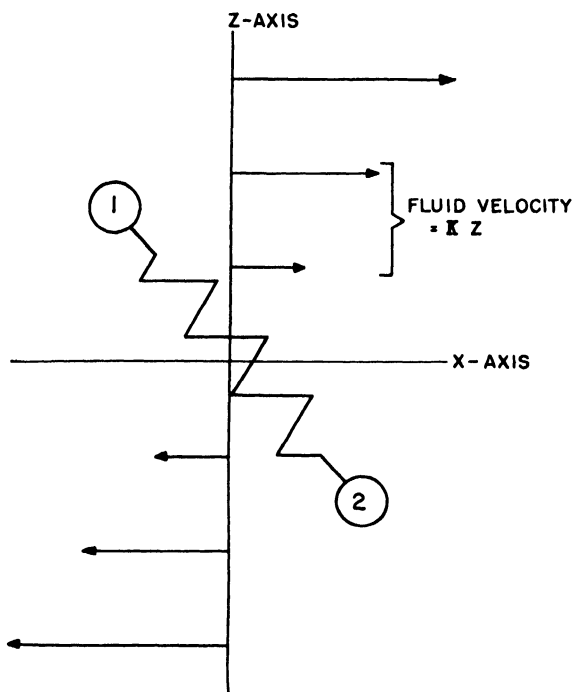


FIG. 2. A model molecule in two-dimensional shearing flow

These new, and more complicated, equations of motion still can be simplified by means of the normal-coordinate transformation. The results of the transformation are the following:

$$\begin{aligned}\rho\dot{\xi}_0 &= -kT \frac{\partial \ln \psi}{\partial \xi_0} \\ \rho\dot{\xi}_1 &= -kT \frac{\partial \ln \psi}{\partial \xi_1} - 2g\xi_1 + K\xi_1 \\ \dot{\zeta}_1 &= \frac{z_1 - z_2}{\sqrt{2}}\end{aligned}\tag{6}$$

Once again ξ_0 occurs in one equation only with itself, and ξ_1 occurs only with itself and with ζ_1 . This mixing of ξ_1 and ζ_1 turns out to be harmless.

The divergence of the rates of flow of the particles is set equal to the rate of accumulation of the particles at a given point to give a second-order differential equation of the familiar type encountered in diffusion theory. From this the unknown function ψ can be determined. It would take us too far afield to give the details of the solution of this equation, since the interested reader may find it in the original literature. It is worth noting, however, that the equation for the problem in hand, the elastic dumbbell molecule in a shearing fluid, can be solved exactly without recourse to approximation. (This was first accomplished, I believe, by J. J. Hermanns.³)

Quantities of particular interest are the mean square extensions of the molecules along the coordinate axes. These are proportional to the mean squares of the normal coordinates ξ_1 and ζ_1 , and expressions for them as calculated from the differential equation are given below.

$$\langle \xi_1^2 \rangle_{av} = (kT/2g)(1 + K\rho/g)\tag{7}$$

$$\langle \zeta_1^2 \rangle_{av} = kT/2g\tag{8}$$

$$\langle \xi_1 \zeta_1 \rangle_{av} = kT K\rho/2g^2 = 2kT K\tau/g\tag{9}$$

$$\tau = \rho/2g\tag{10}$$

We see that, as we predicted originally, the mean square extension of this elastic dumbbell is not zero. It is, in fact, proportional to the temperature and inversely proportional to the strength of the spring. Furthermore, the mean square extension along the x -axis increases with rate of shear. At the same time the average of the cross product term $\xi_1 \zeta_1$, which is zero when the rate of shear is zero, increases proportionately to the rate of shear. The net result is that the molecule extends along a diagonal line inclined somewhat to the x -axis.

³ J. J. Hermanns, *Rec. trav. chim.* **63**, 219 (1944).

A further important quantity is the relaxation time τ . If we return to equation (4), which describes the relaxation of the molecule in the simple case where Brownian motion is neglected, we see that the coefficient of time in the exponential has the dimensions of reciprocal time, and this is, in fact, the reciprocal of the relaxation time of this simple model; i.e., it is the reciprocal of the time needed for the dumbbell to relax to a length which is $1/e$ of the initial value. This same quantity, the relaxation time, which is equal to $\rho/2g$, appears in our equations where Brownian motions have been considered. In fact, the variable that appears in the mean square extension is just the product of the rate of shear and the relaxation time. In other words, the rate of shear is essentially measured in units of the relaxation time.

The relaxation time that we have been talking about is associated with the normal coordinate *one*. There is another relaxation time associated with normal coordinate *zero*; however, this relaxation time happens to be infinite. In general, there will be one relaxation time associated with each normal coordinate, since the original differential equation separates into as many new equations as there are normal coordinates. Later, when we take more complicated models, we will find that there will be many relaxation times of importance.

III. The Elastic Chain

We can polymerize the simple model of the elastic dumbbell into a long chain, as shown in the second half of Fig. 1. This chain is a rather realistic model of a real polymer chain.

To justify this statement, I should point out that the distribution function for the end-to-end length of one of our hypothetical springs is, in fact, of the same mathematical form as the distribution function of the end-to-end length of a chain of rigid bonds joined by freely rotating joints. This form is the Gaussian distribution function, usually taken as a starting point in any investigation of the theory of a polymer chain.

The chain containing many units has, of course, many internal coordinates, and these can be transformed into many normal coordinates. A few of the simplest of these are shown in Fig. 3. As before, there is a normal coordinate which simply represents a translation of the center of mass of the molecule. The next least complicated coordinate is one in which the ends of the molecule move in opposite directions while the center stands still, and this is analogous to the coordinate ξ_1 that we had before.

Then there are more complicated coordinates to which we had no analogy before; these have two, three, or more nodes, and they can be visualized as being related to the normal vibrations of the stretched string studied by students in elementary physics classes. As in the simple case that we have

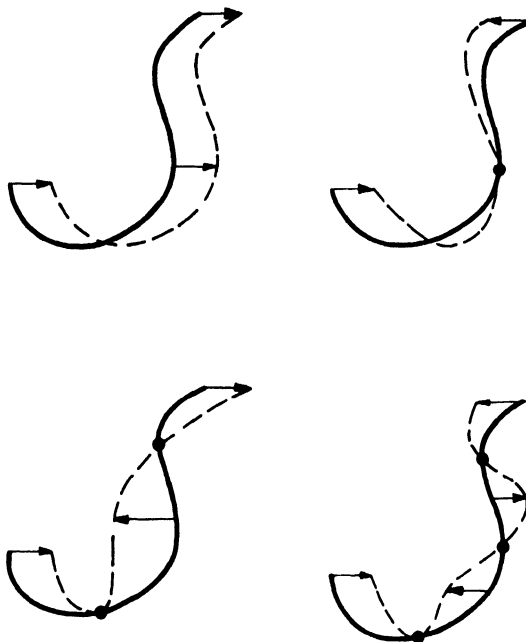


FIG. 3. Schematic representation of the first four normal modes of a chain molecule.

already discussed, however, the use of these coordinates allows the complicated differential equation of the whole chain to be separated into a non-interacting set of equations, each one of which is quite simple and can be easily solved.

There is another complication that should be mentioned at this point. A molecule suspended in a liquid and exerting forces on the liquid causes the liquid to flow, and these currents in the liquid influence the motions of other parts of the same molecule. The situation is shown in Fig. 4, where a particular bead shown at the center of the figure is acted on by a force which drags it toward the right. It, in turn, sets up currents in the liquid around it which are indicated by the curved arrows on the left-hand side of the picture. Unfortunately, an exact description of this situation makes the equations of motion too complicated to be solved. However, if we approximate the curvilinear flow field, which is shown in the left side of the figure, by a rectilinear flow field, shown on the right side of the figure, the equations become simple enough to be solved with hardly any more difficulty than would have been encountered if this flow complication had been neglected completely. The replacement of the curvilinear flow field by an appro-

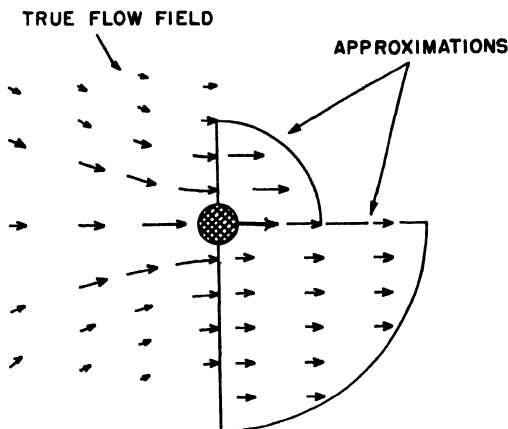


FIG. 4. Replacement of the exact flow field (left) around a moving bead by approximate rectilinear flow fields valid for limited regions (right).

appropriate rectilinear flow field is essentially the approximation that Kirkwood and Riseman made in their theory of intrinsic viscosity. (See below.)

Now let us look at the results of this theory for the high polymer chain. One of the most interesting quantities is the intrinsic viscosity. Since we have a theory that includes relaxation effects, we can calculate intrinsic viscosity for a molecule suspended in oscillating shear as well as in the more usual case of steady-state shear. The results, which show the effect of the various relaxation processes quite clearly, are presented in Fig. 5, where the viscosity is plotted as a function of the frequency of the oscillating shear on a logarithmic scale. The total viscosity falls from a low-frequency plateau to another plateau at very high frequencies; the latter plateau is just the viscosity of the solvent.

To understand what is going on, one need only consider what the molecular processes are in these two extremes. At low frequency (or steady flow) the molecules are being extended by the shear rate, but at the same time they are revolving slowly in the flow gradient. The result is that the energy which is put into them is gradually dissipated by the slippage of the molecule through the fluid. Therefore, energy is lost and a true viscosity appears.

At high frequencies, on the other hand, the molecules, which are essentially springlike, are extended slightly in one phase of the motion. However, before they have a chance to dissipate the energy stored in this extension, the motion reverses itself and the energy stored in the springs is given back to the fluid. There is thus very little energy loss and the viscosity is very small. Instead, a modulus of elasticity appears which corresponds to the springlike action of the molecules. (We do not show the modulus here.)

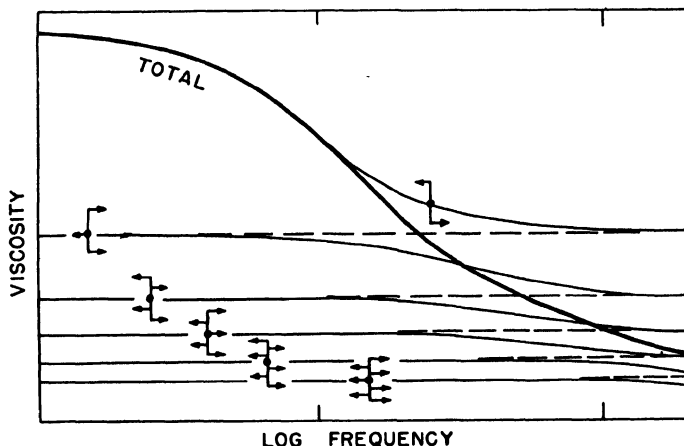


FIG. 5. The real part of the complex viscosity of an isolated chain molecule and its decomposition into contributions from the various normal modes of relaxation.

The curve of viscosity versus frequency is actually a composite curve made up of the contributions of the various relaxation processes corresponding to the various normal coordinates. These are indicated in detail in Fig. 5. About half of the total viscosity is caused by the motions of the simplest of the normal coordinates, the one in which the two ends move in opposite directions. The more complicated types of motion contribute in successively smaller portions to the total viscosity. It is also noteworthy that the relaxation times of these various normal coordinates are different, the simplest normal coordinate having a longer relaxation time than the more complicated ones.

A comparison of this theory with experiments is shown in Fig. 6 and Table I. Figure 6 shows experimental curves of viscosity versus frequency as determined by Rouse and Sittel⁴ on solutions of various samples of polystyrene in toluene. The general agreement in regard to the form of the curve is noteworthy. Furthermore, the relaxation times taken from experimental curves are quite close to those calculated theoretically. This comparison is shown in Table I.

The theory provides a formula which connects the relaxation time with the viscosity of the solution and with known numerical constants. The times calculated from this formula are shown in the next to the last column of this table with the measured experimental times in the last column. It can be seen that while the agreement is not perfect, there is a systematic difference between the theoretical and observed times amounting to about 50 %;

⁴ P. E. Rouse, Jr. and K. Sittel, *J. Appl. Phys.* **24**, 690 (1953).

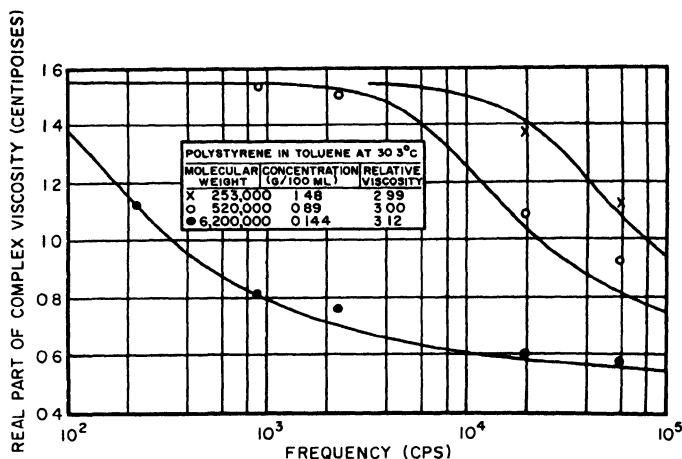


Fig. 6. Experimental viscosity versus frequency for polystyrene solutions. From Rouse and Sittel.⁴

TABLE I
RELAXATION TIMES OF POLYSTYRENE IN TOLUENE^a

$$\tau_{1\text{theor}} = 0.422 M(\eta_{sp}/C)\eta_{\text{sol}}/RT^b$$

<i>M</i>	<i>C</i> , g./ml.	η_{sp}/C	$\tau_{1\text{theor}}$, sec.	$\tau_{1\text{exper}}$, sec.
6,200,000	0.00144	1470	0.81×10^{-3}	1.22×10^{-3}
520,000	0.0089	225	10.3×10^{-6}	16.8×10^{-6}
253,000	0.0148	134	3.00×10^{-6}	4.8×10^{-6}

^a Reference 4.

^b Reference 6.

but this is, in fact, quite small compared with the total range of variation among polymers of different molecular weights.

The difference between the theoretical and experimental times may reflect inadequacies in the theory or may perhaps even be due to experimental complications. It will be necessary for further investigation to settle this point. However, we could point out one source of difficulty which, in fact, has considerable interest of its own.

In Fig. 7 are shown the relaxation curves for the viscosity of solutions of two polymers of the same molecular weight but of which one is a narrow fraction and the other has a broad distribution corresponding to that produced in many common types of polymerizations. It can be seen that the apparent τ_1 's of these two materials would differ considerably even though a certain average relaxation time might be the same.

Although the experiments of Rouse and Sittel were performed on frac-

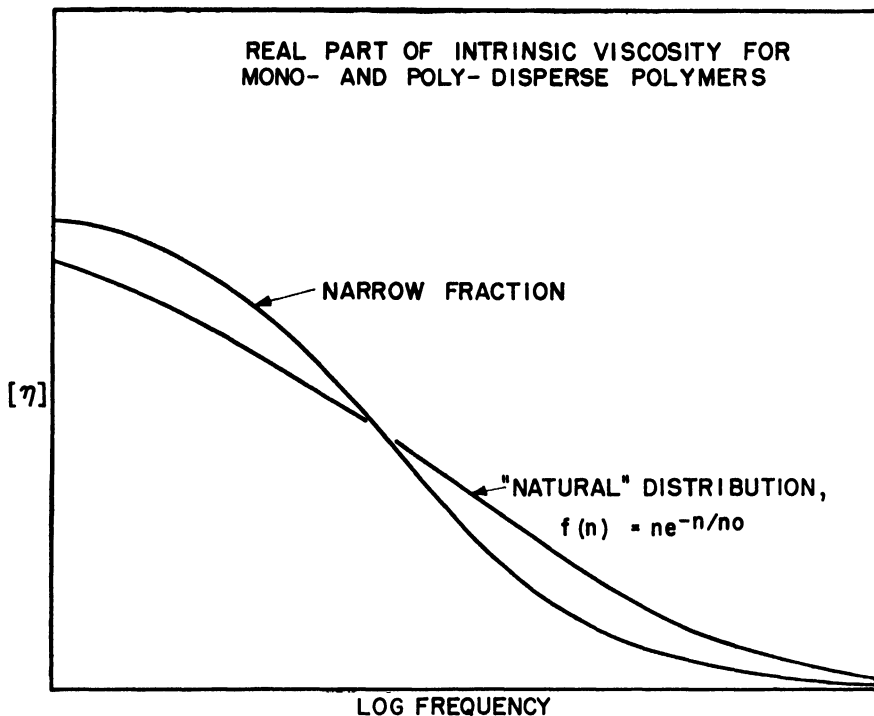


FIG. 7. Real part of the intrinsic viscosity against the logarithm of the frequency for a polymer with a uniform molecular weight and for one with a molecular weight distribution.

tionated materials, the efficiency of fractionation in general, and of the fractionation employed in this case in particular, is unknown. Therefore, we are not at all sure that the curve that they actually obtained corresponds to the narrow fraction curve of Fig. 7 or to something more like the broader curve. And in this fact lies a possible source of the discrepancy in the relaxation times. On the other hand, when we find out more about this subject we may be able to use the difference between curves of materials of different molecular weight distributions to discover something about the molecular weight distributions.

Before we leave the subject of the intrinsic viscosity, another interesting point deserves mention. Some years ago, Kirkwood and Riseman⁵ derived a much quoted relation between the intrinsic viscosity in steady flow $[\eta]_0$ and certain molecular constants, namely, the molecular weight M and

⁵ J. G. Kirkwood and J. Riseman, *J. Chem. Phys.* **16**, 565 (1948).

the root-mean-square distance between the ends of the chain L . We can easily derive a similar formula from our theory⁶ and this is given here.

$$[\eta]_0 = 2.84 \times 10^{23} L^3 / M. \quad (11)$$

The only difference between this formula and Kirkwood and Riseman's original result is in the numerical constant, which is 2.84 in our case and was originally found to be 3.6 by Kirkwood and Riseman. A subsequent revision of some details of the calculations by Kirkwood and associates⁷ reduced this constant to about 3.4, and later Auer and Gardner⁸ showed that another method of carrying out the mathematical details gave the value of 2.90. The latter is very close to our value of 2.84. The small remaining discrepancy can be attributed to some minor differences in the models which could probably be removed if someone were sufficiently interested to do so.

I think this result is interesting in two ways. First, it shows an unexpected dividend of the normal-coordinate method, in that it was possible to obtain a more accurate result than the original Kirkwood and Riseman one with less labor, principally as a result of the simplifications obtained by transforming from the ordinary coordinates into the normal ones.

A further matter of interest is the question of whether this value of 2.84 is in accord with experimental facts. The determination of the experimental value, which has been pursued in particular by Flory and his co-workers, is subject to some uncertainty, and over the past two years the experimental value has shown a tendency to rise. The most recent value of which I am aware⁹ is, in fact, 2.5, with an estimated error of perhaps 10 %. We can say, therefore, that the theoretical and experimental values are now almost in agreement with each other.

I should now like to make a few remarks about branched molecules. The possibility of branching in polymer chains has been a rather mysterious subject until recently, and one which has been blamed for all sorts of discrepancies between accepted ideas and experimental results. In the last few years mathematical analysis of the properties to be expected in branched molecules has made it possible to begin to dispel some of this mystery.

Some time ago a calculation was made of the quantity which might be called the mean square radius of the branched molecule. This is a quantity which, in principle, is measurable by light-scattering. In practice, however,

⁶ B. H. Zimm, *J. Chem. Phys.* **24**, 269 (1956).

⁷ J. G. Kirkwood, R. W. Zwanzig, and R. J. Plock, *J. Chem. Phys.* **23**, 213 (1955).

⁸ P. L. Auer and C. S. Gardner, *J. Chem. Phys.* **23**, 1545 (1955).

⁹ S. Newman, W. R. Krigbaum, C. Laugier and P. J. Flory, *J. Polymer Sci.* **14**, 451 (1954).

TABLE II

THEORETICAL INTRINSIC VISCOSITIES AND RADII OF MOLECULES WITH ONE BRANCH POINT AND f ARMS OF EQUAL LENGTH COMPARED TO THOSE OF A LINEAR MOLECULE OF THE SAME MOLECULAR WEIGHT^a

<i>No. of arms, f</i>	<i>Mean square radius ratio</i>	<i>Viscosity ratio</i>
1 and 2	(1.000)	(1.000)
3	0.778	0.907
4	0.625	0.814
8	0.344	0.632

^a Reference 9a.

the measurement has turned out not to be very useful, probably because the result depends on the degree of polydispersity, which is usually unknown.

It has been observed experimentally that the relation between the intrinsic viscosity and the weight-average molecular weight depends upon the extent of branching. Therefore, if the theoretical relation between these quantities could be obtained, it would offer a means of determining the amount of branching. We have already seen that we were able to find this relation in the case of linear polymers. Calculation of this relation for branched polymers has turned up some rather surprising results.^{9a}

We have already seen that the intrinsic viscosity in the case of linear polymers depends upon the three-halves power of the mean square radius of the molecule. We might expect, therefore, that the same relation would hold true in the case of branched polymers; and, in fact, this hypothesis was proposed by Flory. However reasonable this hypothesis may seem on a dimensional basis, the actual calculations have not borne it out. In fact, the results given in Table II indicate that the intrinsic viscosity varies more nearly with the *square root* of the mean square radius as the number of branch points in the molecule is increased at constant molecular weight.

It is rather difficult to give a convincing explanation of this result in a few words, since the actual flow of liquid through the molecule is a rather complicated process. Nevertheless, the theoretical calculations are strikingly well confirmed by experiment.

Figure 8 shows some experimental results by Schaeffgen and Flory¹⁰ on polyamides. The straight line drawn through the circles representing the experiments on the linear molecule is an empirical relation between the viscosity and the molecular weight. The other two solid straight lines are displaced from it by the square root of the mean square radius, as suggested by our theory. It can be seen that these lines pass through the experimental

^{9a} B. H. Zimm and R. W. Kilb, *J. Polymer Sci.* in press (1958).

¹⁰ J. R. Schaeffgen and P. J. Flory, *J. Am. Chem. Soc.* **70**, 2709 (1948).

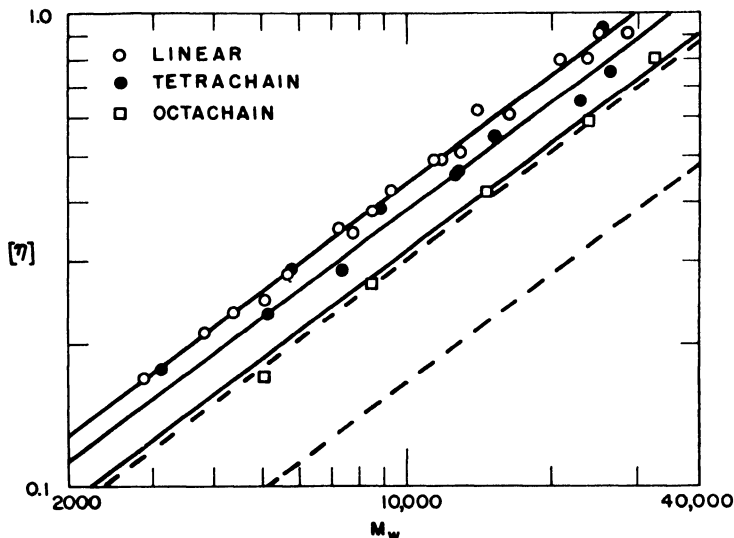


FIG. 8. Experimental results of Schaeffgen and Flory on the viscosity-molecular weight relation for linear and branched polyamides. See text.

points on the branched molecules as well as could reasonably be expected. The dotted lines which represent the hypothesis that the viscosity depends upon the cube of the root-mean-square radius obviously do not fit the experiments at all.

Another subject that can be treated by the normal mode theory is the dependence of viscosity on the rate of shear. The first theory of the intrinsic viscosity gave no dependence of viscosity on the rate of shear at all. However, it has been subsequently found that refinement of the hydrodynamic interaction approximations does introduce a change of viscosity with the rate of shear. We mentioned before that the real curvilinear flow field of a liquid around a moving bead is replaced in our theory by a rectilinear flow field. The strength of this rectilinear field is determined by the average distance between the two pairs of elements whose interaction is being considered.

In the original simple theory an average value of this distance characteristic of the molecule at rest was introduced. An obvious refinement would be to introduce the value of the distance calculated from the simple theory, a value which changes with the rate of shear, as we have seen above in the case of the simple elastic dumbbell model. When this is done, a dependence of viscosity upon the rate of shear appears which is, at least, rather like the experimental dependence; i.e., the viscosity at first decreases rather rapidly with increasing rate of shear and then levels off. Whether the dependence

is quantitatively exact has not yet been determined at the time of writing. The determination must await the results of some rather lengthy numerical computations.

We have described some of the interesting results that have been obtained by the use of normal-mode theory. All of these problems have dealt with single, isolated chains which correspond in practice to dilute solutions of polymers. Some of our most important problems however, concern concentrated solutions or solid polymers where many chains are interacting at once. Normal-mode analysis has proved very useful in this field also, particularly in the hands of Bueche,¹¹ who has applied it boldly and with considerable success to the discussion of the viscoelastic behavior of rubber-like materials. This field is less developed than dilute solution theory, however, in that the exact way in which the polymer chains couple mechanically with each other is still rather mysterious. Mention should also be made of the extensive comparisons between theory and experiment by Ferry and co-workers, which are conveniently summarized in recent reviews.¹²

Finally we ought to mention that the present interest in the relaxation properties of *dilute* polymer solutions stems from the initial work of W. O. Baker, W. P. Mason, J. H. Heiss and H. J. McSkimin of the Bell Telephone Laboratories.¹³

Nomenclature

C	Concentration, weight per unit volume	z	Vertical coordinate
F_{x1}, F_{x2}	z -components of mechanical force	ξ	Vertical normal coordinate
L	Root-mean-square distance between the ends of a polymer chain	η	Viscosity
M	Molecular weight	η_{sp}	Specific viscosity
R	Gas constant per mole	$[\eta]_0$	Intrinsic viscosity for steady flow
T	Absolute temperature	K	Shear rate
g	Spring constant	ξ	Horizontal normal coordinate
k	Boltzmann's constant	$\dot{\xi}$	Rate of change of ξ
t	Time	ρ	Resistance or frictional coefficient
x	Horizontal coordinate	τ	Relaxation time
\dot{x}	Rate of change of x	τ_1	Longest relaxation time for a polymer chain
		ψ	Distribution function

¹¹ F. Bueche, *J. App. Phys.* **26**, 738 (1955).

¹² J. D. Ferry, *Record Chem. Progr. (Kresge-Hooker Sci. Lib.)* **16**, 85 (1955).

¹³ See, for example, W. O. Baker, W. P. Mason, and J. H. Heiss, *J. Polymer Sci.* **8**, 129 (1952); H. J. McSkimin, *J. Acoust. Soc. Am.* **24**, 355 (1952).

CHAPTER 2

THE PRINCIPLES OF RHEOMETRY

S. Oka

I. Introduction..	18
II. Capillary Viscometers	21
1. Non-Newtonian Flow	21
2. Materials with Specified Flow Behavior	23
a. Newtonian Liquids	24
(1) End-Effect	24
(2) Kinetic Energy Correction	24
b. Bingham Solids	25
c. Power Law Flow Curve	28
(1) de Waele-Ostwald's Law	28
d. Development of $f(\tau)$ into Taylor's Series	28
e. Ferry's Flow Law	29
3. Apparent Fluidity	29
III. Rotating Coaxial Cylinder Viscometers	29
1. Inelastic Liquids of Arbitrary Flow Curve	29
2. Liquids with Specified Flow Curve	32
a. Newtonian Liquids	32
b. Bingham Solids	33
c. Power Law Flow Curve (de Waele-Ostwald's Law)	34
d. Development of $f(\tau)$ into Taylor's Series	34
e. Ferry's Flow Law	34
3. Apparent Fluidity	34
4. Hydrodynamic Treatment	36
5. End-Effect	37
a. Theory of the End-Effect for Plane Ends	37
6. Viscoelastic Liquids	40
IV. Oscillating Coaxial Cylinder Viscometers	42
1. Forced Oscillations	42
2. End-Effect	47
3. Free Oscillations	48
4. Outer Cylinder in Oscillation	49
V. Disk Viscometers	51
1. Rotating Disk Viscometers	51
2. Oscillating Disk Viscometers: Free Oscillations	53
a. General Case	54
b. Special Case	55
VI. Concentric Sphere Viscometers	56
1. Rotating Concentric Sphere Viscometers	56

2. Oscillating Concentric Sphere Viscometers	58
a. Forced Oscillations	58
b. Free Oscillations	60
VII. Cone and Plate, Double Cone, and Conicylindrical Viscometers	61
1. Cone and Plate Viscometers	61
2. Double Cone Viscometers.	62
3. Conicylindrical Viscometers.	63
VIII. Oscillating Plate Viscometers	65
1. Newtonian Liquids.	65
2. Edge-Effect	67
3. Wall-Effect	68
IX. Falling Sphere Viscometers.	70
1. Stokes' Law	70
2. Corrections for Stokes' Law	71
a. Effect of Finite Reynolds' Number	71
b. Wall-Effect.	71
c. End-Effect	73
X. Parallel Plate Plastometers	73
1. Newtonian Liquids	73
2. Linear Viscoelastic Bodies.	75
3. Non-Newtonian Liquids	76
XI. Coaxial Cylinder Viscometers with Axial Motion	77
1. Pochettino Viscometer	77
2. Penetrometer	78
3. Oscillating Penetrometer	79
Nomenclature	80

I. Introduction

This chapter is concerned with methods for determining the rheological properties of liquids and gases. We will deal mostly with *inelastic incompressible* fluids manifesting *Newtonian* flow behavior, that is, with materials the rheological properties of which are characterized by a single parameter for isothermal conditions, as discussed in Chapter 16 of Volume I. Many such methods involve measurements of the motion of one surface in contact with the liquid relative to another surface. In the case of liquids of low viscosity, one of these surfaces is in the form of a container to hold the liquid. The surfaces may be effectively at an infinite distance from each other.

The rheological behavior of a Newtonian liquid in an appropriate instrument is obtained in principle by solution of the Navier-Stokes equation for the appropriate boundary conditions. Owing to the existence of a quadratic term in this equation, exact solutions cannot in general be obtained. If the quadratic term is dropped, solutions thus obtained are approximate except in the limiting case of infinitesimally slow motion. The quadratic term corresponds physically to a secondary flow superimposed upon the

flow derived from the simplified Navier-Stokes equation. The solutions discussed in this chapter are obtained from linearized forms of the Navier-Stokes equation and must be considered to a certain extent approximate, except when quadratic terms vanish identically, as in capillary flow. Some discussion of secondary flow has recently appeared in the literature.

Relatively simple results in closed form for the simplified equation can be obtained in general only with certain geometries. In many cases an experimentally convenient form of apparatus is not tractable mathematically. In such circumstances it is customary to obtain solutions for simplified geometries and then to apply empirical or calculated corrections for so-called "end-effects," "edge-effects," and "wall-effects." In this chapter some formal solutions are given for certain rheological instruments with such experimentally convenient geometries. Numerical calculation from the analyses of correction terms may be more or less difficult. Unfortunately, some of these formal solutions are so untractable that they can be regarded as little more than reformulations of the problem. They may, however, indicate convenient approximations for particular cases.

This chapter is also concerned with the measurement of the rheological properties of materials manifesting linear viscoelastic behavior. Formally, such behavior may be characterized by a linearized Navier-Stokes equation, or the generalized Hooke's law equation with a "memory" term. In practice, we will deal mostly with sinusoidally varying stress or strain, under which condition it is customary merely to consider the viscosity or elasticity as complex; this procedure is, however, not strictly justified for resonance methods, since the complex viscosity or elasticity is a function of frequency.

Finally, we consider the steady flow behavior of materials manifesting non-Newtonian behavior. For such behavior the shear stress in steady rectilinear flow is a single-valued monotonically increasing function of the rate of shear, the so-called "flow curve"; thixotropic behavior is thus excluded. Non-Newtonian flow behavior is characterized not only by the shear stress at a given rate of shear under such a flow pattern, but also by the nonzero differences in stresses which act normally on the three mutually perpendicular planes associated with flow. These normal stresses are not considered in this chapter.

The main objective of this chapter is thus to give results for the above types of flow behavior for certain of the more usual geometries, and to show the mathematical procedures involved. For completeness, well-known results for several other arrangements are included. Many variations of the arrangements discussed are possible. Space does not permit the description or listing of these variations; however, from the mathematical procedures given for the typical methods discussed here, the alternative arrangements

TABLE I
CASES DISCUSSED IN THIS CHAPTER

<i>Type of instruments</i>	<i>Type of motion</i>	<i>Rheological properties</i>	<i>Effects considered</i>
Capillary viscometer	Rectilinear flow	Newtonian Non-Newtonian Linear viscoelastic	End-effect No end-effect End-effect
Rotating coaxial cylinder viscometer	Rotation	Newtonian Non-Newtonian Linear viscoelastic	End-effect No end-effect End-effect
Oscillating coaxial cylinder viscometer	Forced oscillation	Linear viscoelastic Newtonian	End-effect
Oscillating coaxial cylinder viscometer	Free oscillation	Linear viscoelastic Newtonian	No end-effect
Rotating disk viscometer	Rotation	Newtonian	{ Edge-effect End-effect Wall-effect
Oscillating disk viscometer	Free oscillation	Newtonian	{ Edge-effect End-effect Wall-effect
Rotating concentric sphere viscometer	Rotation	Newtonian	Wall-effect
Oscillating concentric sphere viscometer	Forced oscillation	{ Linear viscoelastic Newtonian }	Wall-effect
Oscillating concentric sphere viscometer	Free oscillation	{ Linear viscoelastic Newtonian }	Wall-effect
Cone and plate viscometer	Rotation	{ Newtonian Non-Newtonian Linear viscoelastic }	No edge-effect
Double cone viscometer	Rotation	{ Newtonian Linear viscoelastic }	No edge-effect
Conicylindrical viscometer	Rotation	{ Newtonian Non-Newtonian Linear viscoelastic }	No edge-effect No corner-effect
Oscillating plate viscometer	Forced oscillation	{ Newtonian Linear viscoelastic }	Edge-effect Wall-effect

TABLE I—(Continued)

<i>Type of instruments</i>	<i>Type of motion</i>	<i>Rheological properties</i>	<i>Effects considered</i>
Falling sphere viscometer	Rectilinear motion	Newtonian	{ Wall-effect End-effect
Parallel plate plastometer	Compression	{ Newtonian Non-Newtonian Linear viscoelastic }	No edge-effect
Pochezzino viscometer	Rectilinear motion	{ Newtonian Linear viscoelastic }	No end-effect
Penetrometer	Rectilinear motion	Newtonian	No end-effect
Oscillating penetrometer	Axial oscillation	{ Linear viscoelastic Newtonian }	No end-effect

can be treated similarly. Since this chapter is concerned only with mathematical relationships between instrument geometry, observable quantities, and rheological properties, no discussion is given of the scope of each arrangement or of experimental details.

Strictly speaking, the three types of flow behavior considered here, namely, inelastic Newtonian behavior, inelastic non-Newtonian flow, and linear viscoelastic behavior, represent the flow behavior of real liquids only under limiting conditions. In practice, the rheological behavior of a liquid in a given instrument under given conditions may approximate one of these idealized types, and this can be determined by varying the experimental conditions. The cases discussed in this chapter are listed in Table I.

II. Capillary Viscometers

1. NON-NEWTONIAN FLOW

Let us consider the flow of an incompressible liquid through a circular tube, of radius R and length l , as shown in Fig. 1. At each end of the tube are reservoirs, containing pistons exerting pressures $P + p$ and p respectively. In practice P may be a hydrostatic head, and p atmospheric pressure. The tube and reservoirs are the fixed member, and the pistons the movable member. Let Q be the volume of flow in unit time. The rheological behavior of the liquid is specified by the flow curve

$$\dot{\gamma} = f(\tau), \quad (1)$$

where $\dot{\gamma}$ is the rate of shear, which is equal to the velocity gradient for rec-

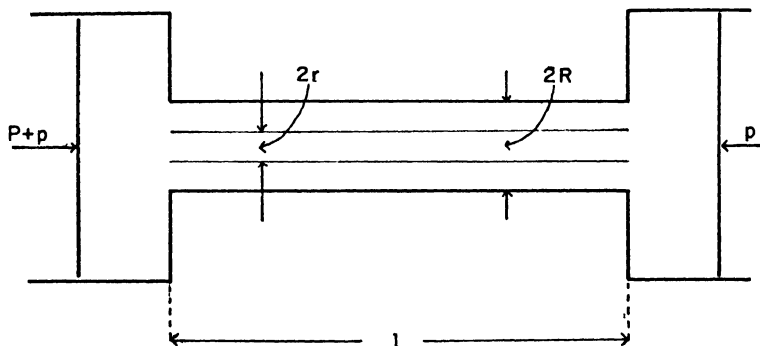


FIG. 1. Flow in a circular tube

tilinear flow, and τ is the shear stress. From the measurement of the relation between P and Q the flow curve may be determined. With regard to the motion of the liquid, the following assumptions are made: (i) the liquid is incompressible; (ii) the motion of the liquid is not turbulent; (iii) the streamlines are parallel to the axis of the tube; that is, the liquid is "telescoping" through the tube; (iv) the motion is stationary; (v) there is no slip at the wall. We will consider first the behavior of the capillary viscometer with liquids of arbitrary flow curve, and subsequently with liquids of specified flow behavior.

Let us consider the cylindrical surface in the liquid of radius r and of length l as in Fig. 1. If we denote the longitudinal shear stress acting on the cylindrical surface by τ , then the resultant force arising from the longitudinal tractions on the cylindrical surface becomes $2\pi r l \tau$. Now for both materials manifesting Newtonian as well as non-Newtonian flow behavior,¹ the difference P in axial normal stress is independent of r (assumption iii). As a consequence of the assumption (iv), the force must be equal to the net driving force $\pi r^2 P$. Hence we have $2\pi r l \tau = \pi r^2 P$, or²

$$\tau = (P/2l)r \quad (2)$$

If we denote the velocity of the liquid at a distance r from the axis of the tube by $v(r)$, the rate of shear is given by $-dv/dr$, and the volume of flow in unit time is given by

$$Q = \int_0^R 2\pi r v(r) dr = \left| \pi r^2 v \right|_0^R - \int_0^R \pi r^2 \frac{dv}{dr} dr$$

The first term on the right-hand side vanishes, because, from assumption

¹ R. S. Rivlin, *Proc. Cambridge Phil. Soc.* **45**, 88 (1948).

² This equation was first derived by G. G. Stokes in 1851.

(v), $v(R)$ must be zero. Substituting $-dv/dr = f(\tau)$ into the above equation and changing the variable of integration from r to τ , we have^{3, 4}

$$D(\tau_R) \equiv \frac{4Q}{\pi R^3} = \frac{4}{\tau_R^3} \int_0^{\tau_R} f(\tau) \tau^2 d\tau \quad (3)$$

where

$$\tau_R = PR/2l \quad (4)$$

denotes the shear stress at the wall. Thus we see that the quantity $4Q/\pi R^3$ is a function of τ_R only.

The relation between P and Q , that is, between τ_R and D , can be directly observed. We need only find the flow curve $f(\tau)$ from the known function $D(\tau_R)$. Cancelling the denominator of equation (3) and differentiating with respect to τ_R , we obtain

$$f(\tau_R) = \frac{3}{4}D(\tau_R) + \frac{1}{4}\tau_R D'(\tau_R)$$

where $D' = dD/d\tau$. Since this relation must hold for any value of τ_R , we shall simply write τ for τ_R . Thus we have the result^{3, 4}:

$$f(\tau) = \frac{3}{4}D(\tau) + \frac{1}{4}\tau D'(\tau) \quad (5)$$

From equations (1) and (2) it can be seen that the relation between the rate of shear and the distance r from the axis of the tube is given by

$$\dot{\gamma} = f\left(\frac{\tau_R}{R} r\right)$$

Thus the rate of shear increases from zero to a maximum $f(\tau_R)$ with increase in r from zero to R . In capillary viscometers the rate of shear cannot be regarded as uniform.

Integration of the equation $-dv/dr = f(\tau)$ leads to the distribution of the velocity

$$v = \frac{R}{\tau_R} \int_{\tau}^{\tau_R} f(\tau) d\tau \quad (6)$$

2. MATERIALS WITH SPECIFIED FLOW BEHAVIOR

If conditions (i) to (v) are complied with, then $\dot{\gamma}$ as a function of τ is obtained from equation (5). The alternative procedure is to *assume* a reasonable flow law, and compare the observed Q - P curve with the curve calculated according to the law. We will now give some examples of Q - P curves for various flow laws.

³ B. Rabinowitsch, *Z. physik. Chem. (Leipzig)* **A145**, 1 (1929).

⁴ M. Reiner, "Deformation and Flow," p. 108. Lewis, London, 1949.

a. Newtonian Liquids

A Newtonian liquid is specified by the flow curve

$$f(\tau) = \tau/\eta, \quad (7)$$

where η is the coefficient of viscosity. Substituting the above relation for equation (3) gives

$$D(\tau_R) = \tau_R/\eta$$

Expressing this relation in terms of Q and P , we get the well-known *Hagen-Poiseuille equation*

$$Q = (\pi R^4/8l\eta)P \quad (8)$$

It can be seen from equation (6) that the distribution of velocity across the tube is parabolic:

$$v = (R^2 - r^2) \frac{P}{4l\eta}$$

Since the assumptions in the previous subsection do not hold in actual capillary viscometers, it becomes necessary to correct the Hagen-Poiseuille equation for certain effects. Here, we will briefly mention only end-effect and kinetic energy corrections.

(1) *End-effect*. Since the ends of the capillary tube are connected with wide vessels, the streamlines are not completely parallel to the axis near the end of the tube. For this reason, the velocity of the liquid in the direction of the axis near the end is less than that in the middle part of the tube. Hence the end-effect may be considered as equivalent to an increase in the effective length of the capillary tube from l to $l + \Delta l$. The correction Δl is sometimes called the *Couette correction*; it is usually written in the form $\Delta l = nR$, but n is variously evaluated. Rayleigh gives 0.824; Scheader, 0.805; and Bond, 0.566.

(2) *Kinetic energy correction*. When the liquid which is moving slowly along the wide tube suddenly finds itself in the capillary tube, it has to move much more quickly, and therefore the pressure falls. The effective pressure difference is smaller than the measured one. Let $\bar{v} = Q/\pi R^2$ denote the average velocity and ρ the density of the liquid. Then this behavior corresponds to substituting $P - m\rho\bar{v}^2$ for P in the Hagen-Poiseuille equation. Consequently we have

$$\eta = \frac{\pi R^4 P}{8lQ} - \frac{m\rho Q}{8\pi l}$$

This correction is sometimes called the *Hagenbach correction*, and the numerical factor m has been variously evaluated as in Table II.

TABLE II^a
VALUES OF m ACCORDING TO SEVERAL AUTHORS

Reynolds	0.50
Hagenbach	0.79
Louette and (independently) Wilberforce	1.00
Boussinesq	1.12
Hiemann	1.124
Swindells	1.12-1.17
Knobbs	1.14
Macobson	1.25-1.55

The Hagen-Poiseuille equation, corrected both for the end-effect and for the kinetic energy, may be written

$$\eta = \frac{\pi R^4 P}{8Q(l + nR)} - \frac{m\rho Q}{8\pi(l + nR)} \quad (9)$$

For experimental determination of the constants m and n the reader should refer to the paper of Swindells.⁶

b. Bingham Solids

Bingham solids are defined by the relation:

$$\left. \begin{aligned} f(\tau) &= 0 & \text{for } \tau \leq \tau_f \\ f(\tau) &= (1/\eta_{pl})(\tau - \tau_f) & \text{for } \tau > \tau_f \end{aligned} \right\} \quad (10)$$

where τ_f is the *yield value* and η_{pl} is the *plastic viscosity*. Thus the Bingham solid is specified by two material constants τ_f and η_{pl} , which are to be determined. Two cases may be distinguished.

(i) $\tau_R \leq \tau_f$, that is, $P \leq 2l\tau_f/R$, since $\tau_R = PR/2l$. From physical considerations it is expected that there will be no flow in this case. This can also be verified from equation (3), since $D(\tau_R)$ becomes zero when $\tau_R \leq \tau_f$.

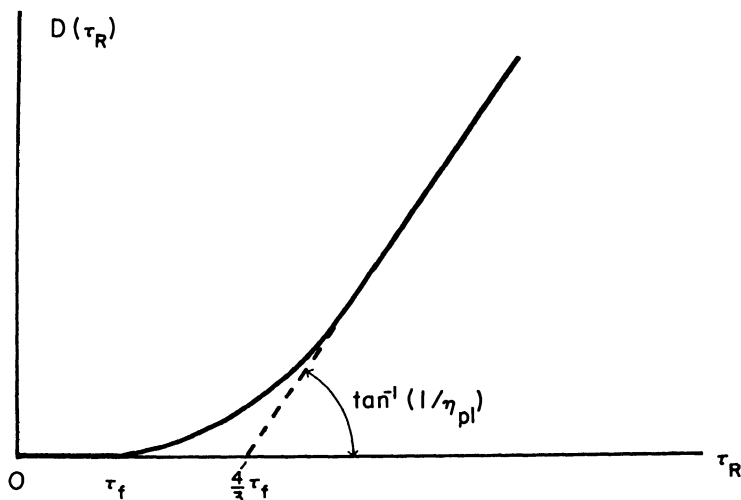
(ii) $\tau_R > \tau_f$, that is, $P > 2l\tau_f/R$. We get from equation (3)

$$D(\tau_R) = \frac{1}{\eta_{pl}} \left[\tau_R - \frac{4}{3} \tau_f + \frac{1}{3} \frac{\tau_f^4}{\tau_R^3} \right] \quad (11)$$

From the above considerations, the relation between $D(\tau_R)$ and τ_R is as in Fig. 2. The curve touches the abscissa at $\tau_R = \tau_f$ and begins to rise at $\tau_R = \tau_f$; the intersection of the asymptote and the abscissa is given by

^a A. C. Merrington, "Viscometry," Arnold, London, 1949.

⁶ J. F. Swindells, J. R. Coe, Jr., and T. B. Godfrey, *J. Research Natl. Bur. Standards* **48**, 1 (1952).

FIG. 2. $D(\tau_R)$ versus τ_R

$\tau_R = (\frac{4}{3})\tau_f$. Then η_{pl} may be calculated from the slope of the asymptote. Equation (11) may be written in terms of P and Q as follows:

$$Q = \frac{\pi R^4}{8l\eta_{pl}} \left[P - \frac{4}{3}p + \frac{1}{3}\frac{p^4}{P^3} \right], \quad (12)$$

where $p = 2l\tau_f/R$. This is the *Buckingham-Reiner equation*,^{7,8} which, when $\tau_f = 0$, reduces of course to the Hagen-Poiseuille equation.

We will now proceed to discuss the distribution of velocity on the basis of equation (6) for the case when $\tau_R > \tau_f$. When $\tau \leq \tau_f$, that is, when r is less than a critical value r_c given by

$$r_c = R(\tau_f/\tau_R),$$

we have from equation (6)

$$v = \frac{1}{4l\eta_{pl}} (R - r_c)^2$$

Thus the velocity is constant and independent of r if r does not exceed the critical radius r_c . When $\tau > \tau_f$, that is, $r > r_c$, we have

$$v = (P/4l\eta_{pl})[R^2 - r^2 - 2r_c(R - r)]^2$$

From the above considerations, the distribution of velocity is as in Fig. 3. Thus the cylindrical portion of radius r moves as if it were rigid. This type of flow is called *plug flow*.

⁷ E. Buckingham, *Am. Soc. Testing Materials, Proc.* **21**, 1154 (1921).

⁸ M. Reiner, *Kolloid-Z.* **39**, 80 (1926).

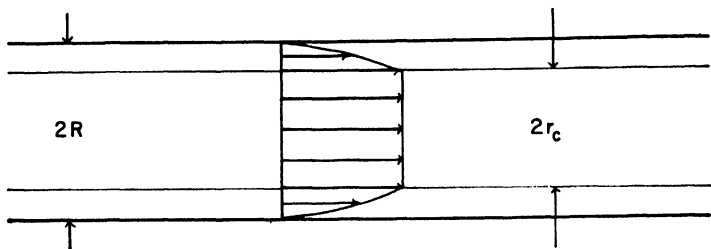
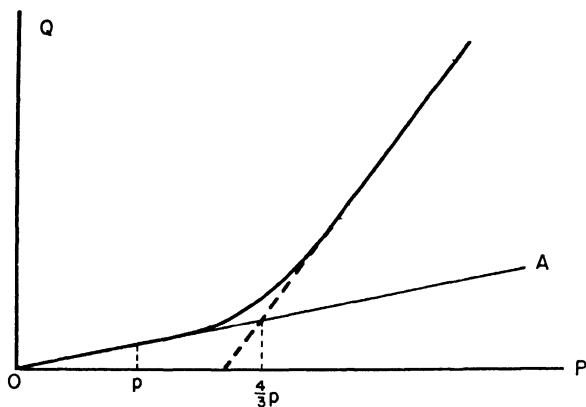


FIG. 3 Plug flow in a circular tube.

FIG. 4. Volume of flow in unit time Q versus the pressure difference P

When there is a slip at the wall, we must add v_R , the velocity of the material at the wall, to the right-hand side of equation (6); that is, a term $\pi R^2 v_R$ must be added to the right-hand side of equation (12). Let us assume that there is a very thin lubricating layer of thickness ϵ next to the capillary wall. The shear stress $\tau_R = PR/2l$ at the wall divided by the viscosity coefficient η_1 of the lubricating layer is equal to the velocity gradient v_R/ϵ ; hence, we have

$$v_R = \epsilon PR/2l\eta_1$$

Adding this term to the right-hand side of equation (12), we get^{9, 10}

$$Q = \frac{\pi R^4}{8l\eta_{p1}} \left[P - \frac{4}{3} p + \frac{1}{3} \frac{p^4}{P^3} \right] + \frac{\pi \epsilon R^3}{2l\eta_1} P$$

The relation between Q and P is shown in Fig. 4. Q first increases linearly

⁹ M. Reiner, "Deformation and Flow." Lewis, London, 1949.

¹⁰ G. Green, "Industrial Rheology and Rheological Structures," p. 26-27. Wiley, New York, 1949.

with increase in P and begins to rise more steeply at $P = p$. The intersection of the asymptote and the straight line OA corresponds to $P = (\frac{4}{3})p$. Thus ϵ/η_1 may be obtained from the slope of the straight line OA, τ_f from the relation $p = 2l\tau_f/R$, and the plastic viscosity η_{p1} from the slope of the asymptote.

c. Power Law Flow Curve

Let us consider the flow curve given by

$$\left. \begin{aligned} f(\tau) &= 0 & \text{for } \tau \leq \tau_f, \\ f(\tau) &= (1/k)(\tau - \tau_f)^n & \text{for } \tau > \tau_f \end{aligned} \right\} \quad (13)$$

This is *Herschel-Bulkley's law*, and the special case $n = 1$ corresponds to the Bingham solid. It is noticed that the dimensions of k differ in general from those of the coefficient of viscosity. In this case also, no flow occurs when $\tau_R \leq \tau_f$, that is, $P \leq 2l\tau_f/R$. This is also clear from equation (3). When $\tau_R > \tau_f$, we obtain

$$D(\tau_R) = \frac{4}{(n+3)k} (\tau_R - \tau_f)^n \left(1 - \frac{\tau_f}{\tau_R}\right) \left[1 + \frac{2}{n+3} \frac{\tau_f}{\tau_R} + \frac{2}{(n+2)(n+3)} \left(\frac{\tau_f}{\tau_R}\right)^2\right]$$

and τ_f is obtained from the point at which the curve of $D(\tau_R)$ touches the abscissa. Thus, if we assume *Herschel-Bulkley's law*, n and k may be obtained from the above relation.

(1) *de Waele-Ostwald's law*. We will examine the special case when $\tau_f = 0$, that is, the case for quasi-viscous flow

$$f(\tau) = (1/k)\tau^n$$

Then we obtain

$$D(\tau_R) = \frac{\tau_R^n}{(n+3)k}, \quad Q = \frac{\pi R^3}{(n+3)k} \left(\frac{PR}{2l}\right)^n,$$

which reduces to the Hagen-Poiseuille equation when $n = 1$. The above formula was first derived by Farrow *et al.*¹¹

d. Development of $f(\tau)$ into Taylor's Series

Let us consider that $f(\tau)$ is developed into power series of $\tau - \tau_f$, where τ_f is the yield value. It may be argued that in the series of $f(\tau)/(\tau - \tau_f)$ all terms with odd powers of $\tau - \tau_f$ should vanish, because $f(\tau)/(\tau - \tau_f)$ corresponds to the fluidity and accordingly it does not change its sign with the change of sign of $\tau - \tau_f$.¹² If we substitute the series for $f(\tau)$ into

¹¹ F. D. Farrow, G. M. Lowe, and S. M. Neale, *J. Textile Inst. Trans.* **19**, 18 (1928).

¹² M. Reiner, "Twelve Lectures on Theoretical Rheology," p. 133. North-Holland, Amsterdam, 1949.

equation (3), we get an expression for $D(\tau_R)$, from which $f(\tau)$ may be determined.

For materials following flow laws of other types the reader should refer to the table of Philippoff's book.¹³

e. Ferry's Flow Law

The flow behavior of polymeric systems at very low rates of shear appears to be in good agreement with the empirical equation proposed by Ferry:¹⁴

$$\dot{\gamma} = f(\tau) = (\tau/\eta)[1 + (\tau/G_i)], \quad (14)$$

where η is the viscosity defined as the limiting value of $\tau/\dot{\gamma}$, and G_i is a constant of the dimensions of stress; following Ferry, this constant is called the *internal shear modulus*. Inserting equation (14) into equation (3) we obtain

$$D(\tau_R) = \frac{\tau_R}{\eta} \left(1 + \frac{4}{5} \frac{\tau_R}{G_i} \right)$$

3. APPARENT FLUIDITY

In Newtonian liquids the fluidity φ , the reciprocal of the coefficient of viscosity, is given by $D(\tau_R)/\tau_R$ as shown in Section II, 2,a. This quantity is not constant in the case of non-Newtonian liquids; however, it has the dimensions of fluidity. Thus, for the capillary viscometer we may define an apparent fluidity given by

$$\varphi_o = D(\tau_R)/\tau_R$$

Then the relation

$$f(\tau_R) = \frac{3}{4}D(\tau_R) + \frac{1}{4}\tau_R D'(\tau_R)$$

may be written in terms of φ_c as follows:¹⁵

$$f(\tau_R) = \varphi_c \tau_R \left[1 + \frac{1}{4} \frac{d \log \varphi_c}{d \log \tau_R} \right] \quad (15)$$

and $f(\tau_R)/\tau_R$ is the apparent fluidity φ_a as usually defined. For Newtonian liquids φ_c is constant and $f(\tau_R) = \varphi_c \tau_R$. The second term in the bracket of equation (15) represents the deviation from Newtonian flow.

III. Rotating Coaxial Cylinder Viscometers

1. INELASTIC LIQUIDS OF ARBITRARY FLOW CURVE

In the rotating cylinder viscometer, a liquid is placed in the annular space between two coaxial cylinders, as in Fig. 5. One of the cylinders is fixed,

¹³ W. Philippoff "Viskosität der Kolloide," p. 46. Steinkopff, Leipzig, 1942.

¹⁴ J. D. Ferry, *J. Am. Chem. Soc.* **64**, 1330 (1942).

¹⁵ I. M. Krieger and S. H. Maron, *J. Appl. Phys.* **23**, 147, 1412 (1952).

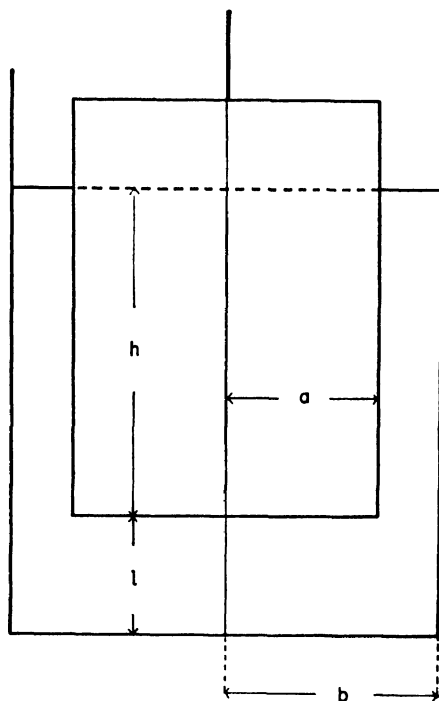


FIG. 5. Coaxial cylinder viscometer

while to the other is applied a torque M . We will consider the performance of such an instrument when M is a constant. Let Ω be the angular velocity $\dot{\phi}$ of the cylinder after reaching a stationary state. From the measurement of the relation between Ω and M , the flow curve of the liquid may be determined. This situation corresponds to the determination of the flow curve from the relation between Q and P in capillary viscometers. We will first consider inelastic liquids of arbitrary flow curve $\dot{\gamma} = f(\tau)$, and subsequently inelastic liquids with specified flow behavior. Finally, the effect of the end with the geometry of Fig. 5 will be considered for a Newtonian liquid, and also for a liquid manifesting linear viscoelastic behavior.

With regard to the motion of the liquid, the following assumptions are made: (i) the liquid is incompressible; (ii) the motion of the liquid is not turbulent; (iii) the streamlines are circles on the horizontal planes perpendicular to the axis of rotation; (iv) the motion is stationary; (v) there is no relative motion between the cylinders and the material in immediate contact with the cylinders; and (vi) the motion of the liquid is the same on each plane perpendicular to the axis of rotation; that is, the motion is two-dimensional. Assumption (iii) corresponds to neglecting the effect of

centrifugal forces, and for small values of Ω this assumption, as well as (ii), may be allowed. Assumption (vi) means neglecting the end-effect.

Let us consider a cylindrical surface in the liquid of radius r and of height h . If we denote the tangential shear stress on the cylindrical surface by τ , then the resultant moment arising from the tangential tractions on the cylindrical surface becomes $2\pi r^2 h \tau$. As a consequence of assumption (iv), this moment must be equal to the torque M applied to the cylinder. Hence we have

$$M = 2\pi r^2 h \tau \quad (16)$$

which corresponds to equation (2) for capillary viscometers. Let the radius of the inner cylinder be a , and that of the outer cylinder be b ; let the value of τ at $r = a$ and $r = b$ be τ_a and τ_b , respectively. Then we have from equation (16)

$$M = 2\pi a^2 h \tau_a = 2\pi b^2 h \tau_b \quad (17)$$

Let us now imagine that the inner cylinder is rotated with a constant angular velocity Ω . If we denote the angular velocity of the liquid particles around the axis by $\omega(r)$, then the rate of shear is given by

$$\dot{\gamma} = -r \, d\omega/dr$$

Then we have from equation (16)

$$2\tau \, d\omega/d\tau = f(\tau),$$

or, integrating under the boundary conditions $\omega(a) = \Omega$ and $\omega(b) = 0$,

$$\omega = \frac{1}{2} \int_{\tau_b}^{\tau} \frac{f(\tau)}{\tau} \, d\tau$$

and

$$\Omega = \frac{1}{2} \int_{\tau_b}^{\tau_a} \frac{f(\tau)}{\tau} \, d\tau \quad (18)$$

Equation (18), which remains unaltered when the outer cylinder rotates and the inner cylinder is fixed, gives the relation between Ω and M corresponds to equation (3) for capillary viscometers.

The relation between the velocity gradient and r is, from equation (16),

$$\dot{\gamma} = f(M/2\pi r^2 h)$$

Therefore, $\dot{\gamma}$ may be assumed to be constant throughout the liquid, *provided that* the clearance is very small, that is, $(b - a)/a \ll 1$.

Now the problem is to find the flow curve $f(\tau)$ from the known relation between Ω and M . Differentiating equation (18) with respect to M and

writing $g(\tau_a)$ for

$$2M \, d\Omega/dM = 2\tau_a \, d\Omega/d\tau_a$$

we have

$$g(\tau_a) = f(\tau_a) - f(s^{-2}\tau_a)$$

where $s = b/a$. From the difference equation the flow curve may be obtained in the form¹⁶

$$f(\tau) = \sum_{n=0}^{\infty} g(s^{-2n}\tau) = 2\tau \sum_{n=0}^{\infty} s^{-2n} \Omega'(s^{-2n}\tau) \quad (19)$$

where $\Omega' = d\Omega/d\tau$. The sum is a slowly convergent one when $s \approx 1$, which may be asymptotically evaluated using the Euler-MacLaurin sum formula.¹⁷

There is another method of obtaining $f(\tau)$ from equation (18). If we set $\tau_a = s^2\tau_b$ and differentiate both sides of the equation with respect to s , keeping τ_b constant, we get¹⁵

$$f(\tau_a) = s(\partial\Omega/\partial s)_{\tau_b} \quad (20)$$

Further discussions for the methods of determination of the flow curve are given in Section III,3.

2. LIQUIDS WITH SPECIFIED FLOW BEHAVIOR

An alternative procedure is to assume as before a reasonable flow curve, and to compare the calculated relation between M and Ω with the observed one.

a. Newtonian Liquids

Substituting τ/η for $f(\tau)$ in equation (18), then from equation (17) we obtain

$$\Omega = \frac{1}{4\pi h} \left(\frac{1}{a^2} - \frac{1}{b^2} \right) \frac{M}{\eta}, \quad (21)$$

which is the well-known *Margules equation*. This equation corresponds to the Hagen-Poiseuille equation for capillary viscometers. The coefficient of viscosity η is determined from the measurable quantity M/Ω .

The rate of shear $\dot{\gamma}$ and its average value $\dot{\gamma}_{av}$ are given by

$$\dot{\gamma} = \frac{2/r^2}{(1/a^2) - (1/b^2)} \Omega, \quad \dot{\gamma}_{av} = \frac{1}{b-a} \frac{2}{(1/a) + (1/b)} \Omega,$$

respectively. $\dot{\gamma}_{av}$ is approximately equal to $a\Omega/(b-a)$, provided that $(b-a)/a \ll 1$.

¹⁶ J. Pawlowski, *Kolloid-Z.* **130**, 129 (1953).

¹⁷ I. M. Krieger and H. Elrod, *J. Appl. Phys.* **24**, 134 (1953).

b. Bingham Solids^{12, 18}

Three cases may be distinguished for the flow behavior of a Bingham solid in a rotating coaxial cylinder viscometer.

(i) $\tau_a < \tau_f$. In this case ω is zero throughout the material and $\Omega = 0$ from equation (18). The material does not flow at all.

(ii) $\tau_b < \tau_f < \tau_a$. Flow occurs when $\tau > \tau_f$. Therefore, flow occurs when r is less than a critical value r_c given by

$$r_c = (M/2\pi h \tau_f)^{1/2}$$

while no flow occurs when r is larger than r_c . This corresponds to plug flow in capillary viscometers. From equation (18) we have

$$\Omega = (1/2\eta_{pl})[\tau_a - \tau_f - \tau_f \ln (\tau_a/\tau_f)],$$

which holds for $\tau_a < s^2 \tau_f$.

(iii) $\tau_f < \tau_b$. In this case ω is greater than zero throughout the material. From equation (18) we have

$$\Omega = \frac{s^2 - 1}{2s^2\eta_{pl}} \tau_a - \frac{\tau_f}{\eta_{pl}} \ln s$$

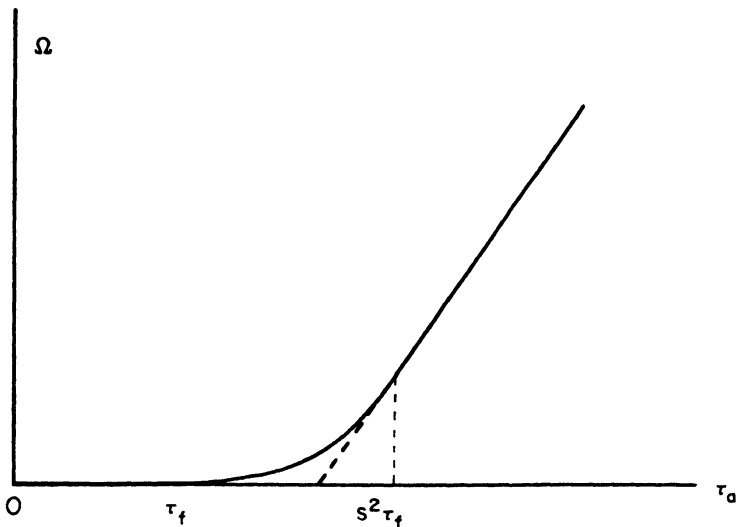


FIG. 6. Angular velocity of the inner cylinder Ω versus τ_a for a Bingham solid

From the above considerations, the relation between Ω and τ_a is as in Fig. 6. The curve is tangential to the abscissa at $\tau = \tau_f$ and is a straight line for $\tau_a \geq s^2 \tau_f$. The intersection of the straight line and the abscissa is

¹⁸ M. Reiner, *Physics* **5**, 321 (1934).

given by

$$\tau_a = \frac{2s^2 \ln s}{s^2 - 1} \tau_f$$

After τ_f is determined, η_{pl} may be obtained from the above equations.

c. Power Law Flow Curve (de Waele-Ostwald's Law)

We obtain from equations (18) and (17)

$$\Omega = \frac{(1/a^{2n}) - (1/b^{2n})}{2n(2\pi h)^n} \frac{M^n}{k}$$

Hence, $\log \Omega$ is in a linear relation with $\log M$, and n is thus obtained from the slope of double logarithmic plot, while k is calculated from the intercept on the ordinate.

d. Development of $f(\tau)$ into Taylor's Series

If we develop $f(\tau)$ into a Taylor's series as in Section II,2, and substitute it into equation (18), then we obtain a relation between Ω and τ_a , from which $f(\tau)$ may be determined.¹⁹

e. Ferry's Flow Law

From equation (3) and (14) the angular velocity of the inner cylinder is found to be

$$\Omega = \frac{\tau_a}{2\eta} \left(1 - \frac{1}{s^2}\right) \left[1 + \frac{\tau_a}{2G_*} \left(1 + \frac{1}{s^2}\right)\right]$$

In terms of the applied torque M and the instrument dimensions, the above equation may be written:²⁰

$$\frac{\Omega}{M} = \frac{1}{4\pi h \eta} \left(\frac{1}{a^2} - \frac{1}{b^2}\right) \left[1 + \frac{M}{4\pi h G_*} \left(\frac{1}{a^2} + \frac{1}{b^2}\right)\right]$$

Thus, Ω/M plotted against M should give a straight line; if this line is extrapolated to zero torque, the viscosity can be obtained. From this line the internal shear modulus G_* can also be found. It is clear that this relationship becomes that of a Newtonian liquid in the limiting case as G_* approaches infinity.

3. APPARENT FLUIDITY

In Newtonian liquids the fluidity is given by

$$\varphi = \frac{4\pi h}{(1/a^2) - (1/b^2)} \frac{\Omega}{M}$$

The quantity is not constant in the case of non-Newtonian liquids. How-

¹⁹ M. Reiner, *Kolloid-Z.* **50**, 199 (1930).

²⁰ H. Leaderman, *J. Polymer Sci.* **13**, 371 (1954).

ever, it has the dimensions of fluidity; it is a function of a and b , or of b and $s = b/a$. Thus for a coaxial cylinder viscometer we may define an apparent fluidity given by

$$\varphi_s = \frac{4\pi b^2 h}{s^2 - 1} \frac{\Omega}{M} = \frac{2\Omega}{(s^2 - 1)\tau_b}$$

Then equation (20) can be written in terms of φ_s as follows:

$$f(\tau_a) = \varphi_s \tau_a \left\{ 1 + \left[\frac{\partial \log \varphi_s}{\partial \log (s^2 - 1)} \right]_{\tau_b} \right\}$$

φ_s is related to the apparent fluidity $\varphi_a = \dot{\gamma}/\tau$ by

$$\varphi_a = \varphi_s \left\{ 1 + \left[\frac{\partial \log \varphi_s}{\partial \log (s^2 - 1)} \right]_{\tau_b} \right\}$$

A convenient and reasonably accurate method for evaluating the quantity

$$\Delta = \left[\frac{\partial \log \varphi_s}{\partial \log (s^2 - 1)} \right]_{\tau_b}$$

would be to employ a single cup and two bobs of the same length but different radii, giving the nearly equal radius ratios s_1 and s_2 . The restriction of constant τ_b is thus equivalent to constant torque. If φ_{s_1} and φ_{s_2} are the apparent fluidities obtained with bobs of radii b/s_1 and b/s_2 , respectively, at the same torque, then

$$\Delta = \frac{\log (\varphi_{s_2}/\varphi_{s_1})}{\log [(s_2^2 - 1)/(s_1^2 - 1)]}$$

This is the *double-bob method* developed by Krieger and Maron.²¹

Using Euler and MacLaurin's method, Krieger and Elrod¹⁷ obtained the following asymptotic solution for $f(\tau)$, which converges rapidly for $s^2 - 1 \ll 1$:

$$f(\tau) = \frac{\Omega}{\ln s} \left[1 + m \ln s + \frac{1}{3} (m \ln s)^2 + \frac{(\ln s)^2}{3} \frac{dm}{d \ln \tau} \right],$$

where

$$m = d \ln \Omega / d \ln \tau$$

Krieger and Maron²² further derived the formula

$$f(\tau_a) = \varphi_s \tau_a \left[1 + k_1 \frac{d \ln \varphi_s}{d \ln \tau_a} + k_2 \left(\frac{d \ln \varphi_s}{d \ln \tau_a} \right)^2 \right]$$

²¹ I. M. Krieger and S. H. Maron, *J. Appl. Phys.* **25**, 72 (1954).

²² S. Oka, *Bull. Kobayashi Inst. Phys. Research* **6**, 108 (1956).

where

$$k_1 = \frac{s^2 - 1}{2s^2} \left(1 + \frac{2}{3} \ln s \right), \quad k_2 = \frac{s^2 - 1}{6s^2} \ln s$$

This applies when s is approximately equal to unity. Thus the flow curve can also be determined by employing a single cup and a single bob. This is the *single-bob method*.²¹ The slope $d \ln \varphi_s / d \ln \tau_a$ is zero for Newtonian fluids and may be constant for many non-Newtonian fluids.

4. HYDRODYNAMIC TREATMENT

The Margules equation can also be derived hydrodynamically, provided that one makes the assumptions (i) to (vi) mentioned in Section III,1. Assumption (vi) does not hold in actual rotating cylinder viscometers due to the effect of the ends. It is, however, possible to take into account end-effects for the case of Newtonian liquids, if we start from the fundamental equations of hydrodynamics.

The Navier-Stokes equation for incompressible Newtonian liquids is

$$\rho \frac{d\mathbf{v}}{dt} = \rho \mathbf{k} - \nabla p + \eta \Delta \mathbf{v}$$

where \mathbf{v} is the velocity, p the pressure, \mathbf{k} the body force per unit mass, ρ the density, and \mathbf{v} and p are determined from the above equation together with the condition of incompressibility $\text{div } \mathbf{v} = 0$. In order to discuss the performance of coaxial cylinder viscometers we write the Navier-Stokes equation in cylindrical coordinates r, ϕ , and z , the axis of the cylinder being taken as the z -axis. From assumption (iii) we have $v_r = v_z = 0$, and v_ϕ and p are independent of the azimuth ϕ . Thus the ϕ -component of the Navier-Stokes equation reduces to

$$\rho \frac{\partial \omega}{\partial t} = \eta \left(\frac{\partial^2 \omega}{\partial r^2} + \frac{3}{r} \frac{\partial \omega}{\partial r} + \frac{\partial^2 \omega}{\partial z^2} \right) \quad (22)$$

where $\omega = v_\phi / r$ denotes the angular velocity of the liquid particles around the axis of rotation. Assumption (iii) means that centrifugal forces are neglected, hence quadratic terms are absent from the above equation. The assumption is justified, provided that the angular velocity is sufficiently small. From the r - and z -components of the Navier-Stokes equation we find that

$$p = \text{constant} - \rho g z$$

Thus the free surface is a horizontal plane. The components of shear stress tensor different from zero are given by

$$\tau_{r\phi} = \eta r \partial \omega / \partial r, \quad \tau_{\phi z} = \eta r \partial \omega / \partial z$$

Let us apply the general equations mentioned above to the rotating co-

axial cylinder viscometer. If we make further assumptions (iv) to (vi), then equation (22) together with the boundary conditions $\omega(a) = \Omega$ and $\omega(b) = 0$ gives

$$\omega = \frac{(1/r^2) - (1/b^2)}{(1/a^2) - (1/b^2)} \Omega$$

The torque M on the inner cylinder is obtained by integrating the moment of the stress $\tau_{r\phi}$ over the cylindrical surface. Hence

$$M = 2\pi a^3 \eta \int_0^h \left(\frac{d\omega}{dr} \right)_{r=a} dz,$$

from which we again obtain equation (21). We notice that equation (21) remains unaltered when the inner cylinder is fixed and the outer cylinder rotates with the angular velocity Ω . In the expression for ω , however, the numerator must be replaced by $(1/a^2) - (1/r^2)$.

5. END-EFFECT

The preceding treatments are valid only for the case of infinitely long inner and outer cylinders. In the case of fluids which cannot support their own weight, an arrangement, for example as shown in Fig. 5, must be adopted. Consequently, there is in general an end-effect. In an actual rotating coaxial cylinder viscometer, there is always a viscous drag due to the stress on the bottom surface of the inner cylinder, and besides, the distribution of the stress on the cylindrical surface differs from that for infinitely long cylinders, because the state of flow is affected by the existence of the ends.

The end-effect may be considered as equivalent to an increase in the effective depth of immersion from h to $h + \Delta h$. Thus for the rotational coaxial cylinder viscometer with the arrangement of Fig. 5,

$$M = \frac{4\pi(h + \Delta h)}{(1/a^2) - (1/b^2)} \eta \Omega, \quad (23)$$

where Δh , the end correction, is in general a function of a , b , h , and the end-gap l .

The end correction Δh is usually obtained experimentally by plotting M/Ω against h , as in Fig. 7. If it is assumed that Δh is independent of h , then a linear relationship between M and h gives Δh . Mooney and Ewart developed a method for making an end correction, which will be discussed in Section VII,2.

a. Theory of the End-effect for Plane Ends

We will consider first the calculation of the end-effect for the arrangement shown in Fig. 5, and subsequently, in a later section, for an arrangement in which the ends of the cylinders consist of coaxial cones with common vertex.

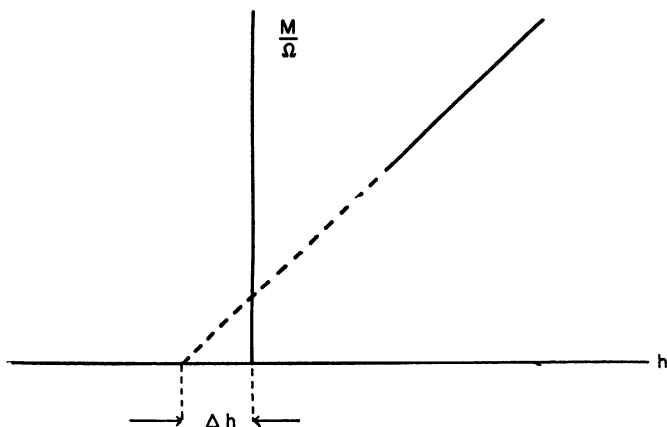


FIG. 7. End correction Δh for a coaxial cylinder viscometer

We will consider here the calculation of the end-effect for the special case of a Newtonian liquid in the arrangement of Fig. 5 as mentioned in the Introduction. It is possible to obtain an expression for Δh as a function of a , b , h , and l . However, it is not possible to obtain an expression for Δh in closed form for the general case.²²

Let us assume without loss of generality that the outer cylinder is fixed. The problem is to find the relation between the angular velocity Ω and the torque M . For this purpose the previous assumptions (i) to (v) are made again. These assumptions will of course hold, provided that the angular velocity Ω is sufficiently small.

In order to obtain a solution of equation (22) satisfying the appropriate boundary conditions, we imagine that the space occupied by the liquid is divided into three regions I, II, and III, as in Fig. 8. Let us denote the angular velocity ω for these regions by $\omega^{(1)}$, $\omega^{(2)}$, and $\omega^{(3)}$, respectively, and take

$$\begin{aligned}
 \omega^{(1)} &= \frac{z+l}{l} \Omega + \alpha \Omega \sum_{n=1}^{\infty} A_n \sin \frac{n\pi z}{l} \cdot \frac{1}{r} I_1 \left(\frac{n\pi r}{l} \right) \\
 \omega^{(2)} &= \frac{(1/r^2) - (1/b^2)}{(1/a^2) - (1/b^2)} \Omega \\
 &\quad + \alpha \Omega \sum_{n=1}^{\infty} B_n \cosh \kappa_n(h-z) \cdot \frac{\rho(\kappa_n r)}{r} \\
 \omega^{(3)} &= \alpha \Omega \sum_{n=1}^{\infty} C_n \sinh \kappa_n(z+l) \cdot \frac{J_1(\kappa_n r)}{r} \\
 &\quad + \alpha \Omega \sum_{n=1}^{\infty} D_n \sinh \kappa_n(z+l) \cdot \frac{\rho(\kappa_n r)}{r},
 \end{aligned} \tag{24}$$

where I_1 is a modified Bessel function of the first kind and first order, and $\rho(\kappa_n r)$ is given by $\rho(\kappa_n r) = J_1(\kappa_n r)Y_1(\kappa_n a) - Y_1(\kappa_n r)J_1(\kappa_n a)$. k_n and κ_n are respectively the n th positive roots of the equations $J_1(kb) = 0$ and $\rho(\kappa b) = 0$. It may be seen that equation (24) satisfies equation (22) as well as the boundary conditions. The nondimensional coefficients A_n , B_n , C_n , and D_n are to be determined from the conditions that the angular velocity ω as well as the components $\tau_{r\phi}$ and $\tau_{\phi z}$ of the stress tensor must be continuous at both boundaries between the regions I and III and the regions II and III. These conditions, in explicit form, are

$$\begin{aligned}
 (-1)^n n \pi I_1 \left(\frac{n \pi a}{l} \right) A_n &= 2 - \sum_{m=1}^{\infty} C_m \frac{J_1(k_m a) \sinh 2k_m l}{(k_m l / n \pi)^2 + 1} \\
 (-1)^n (n \pi)^2 I_2 \left(\frac{n \pi a}{l} \right) A_n \\
 &= \sum_{m=1}^{\infty} C_m \frac{J_2(k_m a) k_m l \sinh 2k_m l}{(k_m l / n \pi)^2 + 1} + \frac{2l}{\pi a} \sum_{m=1}^{\infty} D_m \frac{\sinh 2\kappa_m l}{(\kappa_m l / n \pi)^2 + 1} \\
 (B_n \cosh \kappa_n h - D_n \sinh \kappa_n l) \frac{J_1^2(\kappa_n a) - J_1^2(\kappa_n b)}{\pi \kappa_n^2 J_1^2(\kappa_n b)} \\
 &\quad + \frac{1}{\kappa_n^2} + \sum_{m=1}^{\infty} C_m \frac{J_1(k_m a) \sinh k_m l}{k_m^2 - \kappa_n^2} \\
 (B_n \sinh \kappa_n h + D_n \cosh \kappa_n l) \frac{J_1^2(\kappa_n a) - J_1^2(\kappa_n b)}{\pi \kappa_n J_1^2(\kappa_n b)} \\
 &= - \sum_{m=1}^{\infty} C_m \frac{J_1(k_m a) k_m \cosh k_m l}{k_m^2 - \kappa_n^2}
 \end{aligned} \tag{25}$$

In the derivation of the above equations use was made of theorems on finite Hankel transforms.²³

Now we proceed to calculate the torque M on the inner cylinder. This torque consists of a torque M_1 due to the stress on the bottom surface, and a torque M_2 due to the stress on the cylindrical surface. Then

$$M_1 = 2\pi\eta \int_0^a r^3 \left(\frac{\partial \omega^{(1)}}{\partial z} \right)_{z=0} dr, \quad M_2 = -2\pi a^3 \eta \int_0^h \left(\frac{\partial \omega^{(2)}}{\partial r} \right)_{r=a} dz$$

Substituting equation (24) into these equations we find that

$$M_1 = M_1^0 + M_1', \quad M_2 = M_2^0 + M_2',$$

where

²³ S. Oka and Y. Sato, *Bull. Kobayashi Inst. Phys. Research* **3**, 104 (1953).

$$\begin{aligned}
M_1^0 &= \frac{\pi a^4}{2l} \eta \Omega \\
M_1' &= 2\pi a^3 \eta \Omega \sum_{n=1}^{\infty} A_n I_2 \left(\frac{n\pi a}{l} \right) \\
M_2^0 &= \frac{4\pi h}{(1/a^2) - (1/b^2)} \eta \Omega \\
M_2' &= 4a^2 \eta \Omega \sum_{n=1}^{\infty} B_n \frac{\sinh \kappa_n h}{\kappa_n}
\end{aligned} \tag{26}$$

Hence M may be written²⁴ in the form of equation (23) with

$$\begin{aligned}
\frac{\Delta h}{a} &= \frac{1}{8} \frac{a}{l} \left[1 - \left(\frac{a}{b} \right)^2 \right] \left\{ 1 + 4 \frac{l}{a} \sum_{n=1}^{\infty} A_n I_2 \left(\frac{n\pi a}{l} \right) \right. \\
&\quad \left. + \frac{8}{\pi} \frac{l}{a} \sum_{n=1}^{\infty} B_n \frac{\sinh \kappa_n h}{\kappa_n a} \right\}, \tag{27}
\end{aligned}$$

where the first term in the braces corresponds to the end correction due to the bottom of the inner cylinder without the edge-effect, the second term to the edge-effect, and the third term to the effects of both the end and the free surface. Since the coefficients A_n , and B_n are functions of nondimensional parameters

$$\sigma = a/b, \quad H = h/b, \quad L = l/b,$$

then $\Delta h/a$ is also a function of these three nondimensional parameters σ , H , and L .

A formal solution of the problem of the end-effect has been previously obtained by a different procedure.²² The result is

$$\begin{aligned}
\frac{\Delta h}{a} &= \frac{1}{2} \frac{b}{a} \left[1 - \left(\frac{a}{b} \right)^2 \right] \left\{ \sum_{n=1}^{\infty} E_n \cosh k_n l \cdot J_2(k_n a) \right. \\
&\quad \left. + \frac{2}{\pi} \frac{b}{a} \sum_{n=1}^{\infty} F_n \frac{\sinh \kappa_n h}{\kappa_n b \cosh \kappa_n (l + h)} \right\},
\end{aligned}$$

where E_n and F_n are functions of the three nondimensional parameters σ , H , and L , while k_n and κ_n have the same meaning as before.

6. VISCOELASTIC LIQUIDS²⁰

It has previously been assumed that the liquid is *inelastic*, that is, that the flow is steady. In practice, the average retardation of the liquid may not be vanishingly small, as it is for example in water at room temperature. The angular displacement ϑ of a cylinder as a function of time may be as in Fig. 8, when the torque M applied to the cylinder varies as shown.

²⁴ S. Oka, *Bull. Kobayashi Inst. Phys. Research* **7**, 13 (1957).

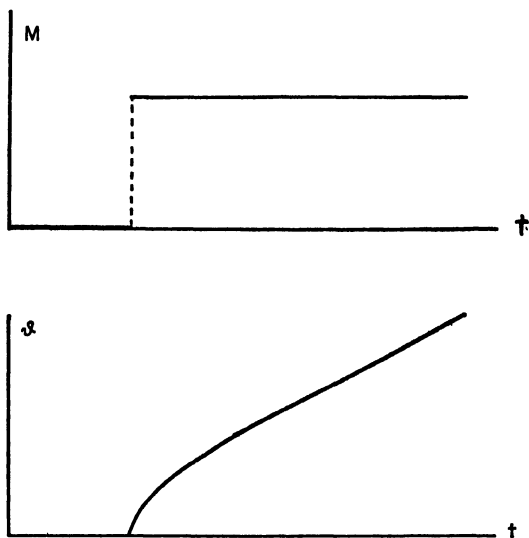


FIG. 8. Time-effect in a coaxial cylinder viscometer

If we consider only times which are *long* compared to the average retardation time, then $\dot{\vartheta}$ is constant and is taken equal to Ω . Thus the non-Newtonian flow behavior of *elastic* liquids may be analyzed in the same way as for the hypothetical inelastic liquid.

A material manifesting *linear viscoelastic behavior* in shear may be specified by either of the equations:

$$\begin{aligned}\gamma(t) &= \int_{-\infty}^t \frac{d\tau(u)}{du} J(t-u) du \\ \tau(t) &= \int_{-\infty}^t \frac{d\gamma(u)}{du} G(t-u) du\end{aligned}\tag{28}$$

where $\gamma(t)$ and $\tau(t)$ are, respectively, shear strain and shear stress at time t , and $J(t)$ and $G(t)$ are, respectively, monotonically increasing or decreasing functions of time (cf. Chapter 1 of Volume II).

Then neglecting inertia, the relation between torque $M(t)$ and angular displacement $\vartheta(t)$ for such a material is given by

$$\vartheta(t) = C \int_{-\infty}^t \frac{dM(u)}{du} J(t-u) du,$$

or

$$M(t) = \frac{1}{C} \int_{-\infty}^t \frac{d\vartheta(u)}{du} G(t-u) du,$$

where

$$C = \frac{1}{4\pi(h + \Delta h)} \left(\frac{1}{a^2} - \frac{1}{b^2} \right)$$

Here Δh is the end-effect as calculated previously for a Newtonian liquid. Thus the elastic part of the creep compliance of a liquid, $J(t) - t/\eta$, may be measured by a suitable torque history.

IV. Oscillating Coaxial Cylinder Viscometers

1. FORCED OSCILLATIONS

Oscillating cylinder viscometers are used to determine the dynamic rheological properties of materials, especially of those which are unable to support their own weight. The angular displacement of either or both cylinders varies sinusoidally with time. If the amplitude is sufficiently small, then we may assume in general that the material in the viscometer manifests *linear viscoelastic behavior*. If the elasticity is negligible, the behavior of the material may be assumed to be Newtonian. The relation between shear stress and shear strain is represented in general by a *complex modulus*

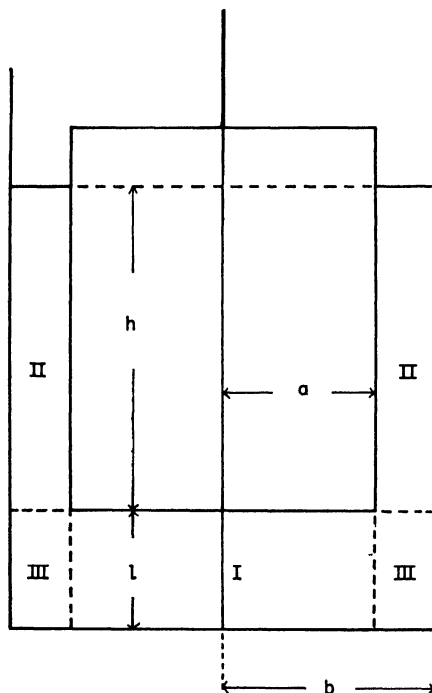


FIG. 9. End-effect in a coaxial cylinder viscometer

$G^*(\omega)$. It is not usually permissible to neglect inertia.²⁵ In the following treatment we will first consider the case where the *outer cylinder is fixed*. The relationships between the amplitudes and phases of the torque and displacement ϑ of the inner cylinder will be considered, taking into account the inertia of the material as well as the effect of the end, as in the previous section.

We will consider the special arrangement in Fig. 9, in which the inner cylinder is suspended by a wire, the upper end of which is twisted sinusoidally through an angle $\psi = \psi_0 \sin \omega t$. The inner cylinder then oscillates with the same frequency, but with different phase, since it is subject to a torque due to the viscous drag of the liquid. Thus we may write for the angular displacement of the inner cylinder

$$\vartheta = \vartheta_0 \sin (\omega t - \delta)$$

We will develop relationships for δ and ϑ_0/ψ_0 as a function of the rheological properties of the material; we will first neglect the end-effect and subsequently extend the analysis to include it.

Let us assume that the material to be investigated is a linear viscoelastic body, the shear stress in which is related to the shear strain $\gamma_{r\phi}$ by the linear relation

$$\tau_{r\phi} = 2G'\gamma_{r\phi} + 2\eta'\dot{\gamma}_{r\phi}$$

where G' and η' are in general functions of ω . Similar relationships apply to $\tau_{\phi z}$ and τ_{zr} . These linear relationships may well apply so long as we treat small oscillations of the material. In terms of the operator

$$\mathbf{G} = G' + \eta' \partial/\partial t$$

the above relations may be written in a simpler form

$$\tau_{r\phi} = 2\mathbf{G}\gamma_{r\phi}$$

and so on. In the case of a Newtonian liquid, G' is zero and η' is a constant equal to η .

Let us assume that the particles perform rotational oscillations around the z -axis. Then the fundamental equation for the angular displacement φ , in cylindrical coordinates, is given by

$$\rho \frac{\partial^2 \varphi}{\partial t^2} = \mathbf{G} \left(\frac{\partial^2 \varphi}{\partial r^2} + \frac{3}{r} \frac{\partial \varphi}{\partial r} + \frac{\partial^2 \varphi}{\partial z^2} \right) \quad (29)$$

This may be obtained from the equation of motion of the volume element $rd\phi dr dz$. Equation (29) reduces to equation (22) when G' is zero. We will

²⁵ H. Markovitz, *J. Appl. Phys.* **23**, 1070 (1952).

now write φ , ψ , and ϑ in complex form:

$$\varphi = \varphi_0 e^{i\omega t}, \quad \psi = \psi_0 e^{i\omega t}, \quad \vartheta = \vartheta_0 e^{i\omega t}$$

The fact that there is a phase difference between ϑ and ψ or φ and ψ means that ϑ_0/ψ_0 and φ_0/ψ_0 are really complex quantities. The operator G becomes the complex modulus

$$G^* = G' + i\omega\eta',$$

and equation (29) becomes

$$L(\varphi_0) \equiv \frac{\partial^2 \varphi_0}{\partial r^2} + \frac{3}{r} \frac{\partial \varphi_0}{\partial r} + \frac{\partial^2 \varphi_0}{\partial z^2} + \beta^2 \varphi_0 = 0 \quad (30)$$

where

$$\beta^2 = \rho\omega^2/G^*$$

We will first *neglect the end-effect* and assume that φ_0 is independent of z . Then we can easily find the solution of equation (30) satisfying the boundary conditions $\varphi_0(a) = \vartheta_0$ and $\varphi_0(b) = 0$. Integrating the moment of the shear stress

$$\tau_{r\phi} = G^* r \, d\varphi/dr$$

over the cylindrical surface we obtain²⁶ for the torque on the inner cylinder

$$M = 2\pi a^2 h G^* \Psi \vartheta, \quad (31)$$

where

$$\Psi = \beta a \frac{J_2(\beta a) Y_1(\beta b) - Y_2(\beta a) J_1(\beta b)}{J_1(\beta a) Y_1(\beta b) - Y_1(\beta a) J_1(\beta b)} \quad (32)$$

The equation of motion of the inner cylinder may be written

$$I\ddot{\vartheta} = K(\psi - \vartheta) - R_0 \dot{\vartheta} - 2\pi a^2 h G^* \Psi \vartheta,$$

where I is the moment of inertia of the inner cylinder, K is the torsion constant of the wire, and $R_0 \dot{\vartheta}$ is a term arising from the internal friction of the wire. K and R_0 are obtained from the natural angular frequency ω_0 and the logarithmic decrement $2\pi\Delta_0/\omega_0$ of free oscillations *in vacuo* by the relation

$$K = I(\omega_0^2 + \Delta_0^2), \quad R_0 = 2I\Delta_0 \quad (33)$$

If we put

$$\vartheta = \vartheta_0 e^{-\Delta_0 t} e^{i\omega t}$$

²⁶ S. Oka and A. Takami, *Bull. Kobayashi Inst. Phys. Research* **3**, 9 (1953).

in the equation of motion of the inner cylinder in free oscillation,

$$I\ddot{\vartheta} + R_0\dot{\vartheta} + K\vartheta = 0,$$

and then separate into real and imaginary parts, we get the above results. Putting

$$\vartheta_0/\psi_0 = qe^{-i\delta}$$

the equation of motion leads to²⁴

$$G^*\Psi = \frac{I}{2\pi a^2 h} \left[\omega^2 + (\omega_0^2 + \Delta_0^2) \left(\frac{e^{i\delta}}{q} - 1 \right) - 2i\omega\Delta_0 \right] \equiv \mu \quad (34)$$

Now μ is a measurable quantity, and G^* is then determined from the above equation. Since, however, G^* is buried in the complex argument of Bessel functions, it is impossible to solve equation (34) for G^* , and so we will confine ourselves to special cases. For a Newtonian liquid of viscosity η , G^* reduces to $i\omega\eta$.

Case (a). $|\beta b| \ll 1$. This is the case where either the inertia term $\rho\omega^2$ is negligible or $|G|^2 = G'^2 + \omega^2\eta'^2$ is sufficiently large. If we expand Bessel functions and neglect higher order terms, we obtain

$$\Psi = 2b/(b^2 - a^2)$$

to a zero approximation and consequently

$$\begin{aligned} G' &= \frac{(1/a^2) - (1/b^2)}{4\pi h} I \left[\omega^2 + (\omega_0^2 + \Delta_0^2) \left(\frac{\cos \delta}{q} - 1 \right) \right] \equiv G_0' \\ \eta' &= \frac{(1/a^2) - (1/b^2)}{4\pi h} I \left[(\omega_0^2 + \Delta_0^2) \frac{\sin \delta}{\omega q} - 2\Delta_0 \right] \equiv \eta_0' \end{aligned} \quad (35)$$

Successive approximations will be most conveniently made by following the method of Markovitz.²⁵ He devised a method of freeing the quantities from the complex arguments of Bessel functions in the combination $J(\xi)Y(\sigma) - Y(\xi)J(\sigma)$ by expanding the functions with argument σ in a Taylor's series about ξ . It can then be shown²⁶ that for the special case when $x = (b - a)/a < 1$,

$$\Psi = 1 + \frac{B_0 + B_2\xi^2 + B_4\xi^4 + \dots}{B_1 + B_3\xi^2 + B_5\xi^4 + \dots}$$

where $\xi = \beta a$, and the coefficients B_n are functions of x . B_n may either be obtained by a method similar to that used by Markovitz or, as was shown by Saito,²⁷ as solutions of certain differential equations. If we neglect terms in ξ^4 and all higher order terms, then G^* can be obtained by solving a quad-

²⁷ N. Saito, *Bull. Kobayashi Inst. Phys. Research* **4**, 266 (1954).

ratic equation with complex coefficients. Neglecting further small quantities we obtain to the first approximation

$$G' = G_0' + \rho\omega^2 a^2 \left\{ \frac{b^2}{2(b^2 - a^2)} \ln \left(\frac{b}{a} \right) - \frac{1}{8} \frac{a}{(a + b)} y \left(3 \frac{b}{a} + 3 - \frac{a}{b} - \frac{a^2}{b^2} \right) \right\} \quad (36)$$

and $\eta' = \eta_0'$, where G_0' and η_0' are given by equation (35).

Case (b). $|\beta a| \gg 1$. This is the case where both G' and $\omega\eta'$ are very small, so that $|G|^2 = G'^2 + \omega^2 \eta'^2$ is negligible. Since the method of Markovitz is not applicable in this case, we will make use of the asymptotic expansions of Bessel functions. Thus we have, to a zero approximation,

$$\Psi = \beta a \cot \beta(b - a),$$

or $\Psi = i\beta a$, provided that $|\beta(b - a)| \gg 1$. Equation (34) then leads to²⁴

$$G' = \frac{1}{\rho\omega^2 a^2} \left(\frac{I}{2\pi a^2 h} \right)^2 \left\{ \left[(\omega_0^2 + \Delta_0^2) \frac{\sin \delta}{q} - 2\omega\Delta_0 \right]^2 - \left[\omega^2 + (\omega_0^2 + \Delta_0^2) \left(\frac{\cos \delta}{q} - 1 \right) \right]^2 \right\} \quad (37)$$

$$\eta' = \frac{2}{\rho\omega^2 a^2} \left(\frac{I}{2\pi a^2 h} \right)^2 \left\{ (\omega_0^2 + \Delta_0^2) \frac{\sin \delta}{q} - 2\omega\Delta_0 \right\} \left\{ \omega^2 + (\omega_0^2 + \Delta_0^2) \left(\frac{\cos \delta}{q} - 1 \right) \right\}$$

If we specify that the system shall always be operated *at resonance*, which means that the imaginary part of $\psi_0/\dot{\vartheta}_0$ is zero, we get, from the equation of motion,

$$[R_0 + 2\pi a^2 \omega^{-1} \operatorname{Im} (G^* \Psi)] \dot{\vartheta}_0 = K \psi_0$$

where $\dot{\vartheta}_0$ is the angular velocity amplitude of oscillation of the inner cylinder and $\operatorname{Im} (G^* \Psi)$ is the imaginary part of the complex quantity $G^* \Psi$. When the inner cylinder oscillates freely in air (vacuo), the second term in the bracket is negligible, and we write $R_0 \dot{\vartheta}_{0A} = K \psi_0$. The subscript *A* indicates the quantity appropriate to motion in air (vacuo). Hence we have

$$\operatorname{Im} (G^* \Psi) = \frac{R_0 \omega}{2\pi a^2 h} \left(\frac{\dot{\vartheta}_{0A}}{\dot{\vartheta}_0} - 1 \right)$$

$$\operatorname{Re} (G^* \Psi) = \frac{I}{2\pi a^2 h} (\omega_0^2 + \Delta_0^2 - \omega^2),$$

the second equation being obtained from the condition of resonance. Thus

G' and η' may be obtained in terms of measurable quantities $\dot{\vartheta}_{0A}/\dot{\vartheta}_0$, ω , ω_0 , and Δ_0 . Simplified results may be obtained for the special cases (a) and (b).

2. END-EFFECT

We will discuss here an exact treatment of the end-effect in the oscillating cylinder viscometer considered above. The method of calculation is quite similar to that used in Section IV,3. The problem is to find a solution of equation (22) satisfying the appropriate boundary conditions. We imagine that the space occupied by the liquid is divided into three regions I, II, and III, as in Fig. 9, and we take the solutions in these regions as follows:

$$\begin{aligned}
 \varphi_0^{(1)} &= \frac{\sin \beta (z + l)}{\sin \beta l} \vartheta_0 + a \vartheta_0 \sum_{n=1}^{\infty} A_n \frac{J_1(\epsilon_n r)}{r} \sin \frac{n \pi z}{l} \\
 \varphi_0^{(2)} &= \frac{a J_1(\beta r) Y_1(\beta b) - Y_1(\beta r) J_1(\beta b)}{r J_1(\beta a) Y_1(\beta b) - Y_1(\beta a) J_1(\beta b)} \vartheta_0 \\
 &\quad + a \vartheta_0 \sum_{n=1}^{\infty} B_n \cos \gamma_n (h - z) \cdot \frac{\rho(\kappa_n r)}{r} \\
 \varphi_0^{(3)} &= \frac{\sin \beta (z + l)}{\sin \beta l} \cdot \frac{(1/r^2) - (1/b^2)}{(1/a^2) - (1/b^2)} \vartheta_0 \\
 &\quad + a \vartheta_0 \sum_{n=1}^{\infty} C_n \frac{J_1(k_n r)}{r} \sin \alpha_n (z + l) \\
 &\quad + a \vartheta_0 \sum_{n=1}^{\infty} D_n \frac{\rho(\kappa_n r)}{r}, \sin \gamma_n (z + l)
 \end{aligned} \tag{38}$$

where

$$\epsilon_n^2 = \beta^2 - (n\pi/l)^2, \quad \gamma_n^2 = \beta^2 - \kappa_n^2, \quad \alpha_n^2 = \beta^2 - k_n^2$$

and k_n and κ_n have the same meaning as in equation (24). The nondimensional coefficients A_n , B_n , C_n , and D_n are to be determined from the conditions at the boundaries between the regions I and III and the regions II and III. Integrating the moment of the stress over the surface of the inner cylinder we find that the torque M is made up of four terms²⁴:

$$\begin{aligned}
 M_1^0 &= \frac{\pi a^4}{2} \beta \cot \beta l \cdot G^* \vartheta \\
 M_1' &= \frac{2\pi^2 a^3}{l} G^* \vartheta \sum_{n=1}^{\infty} n A_n \frac{J_2(\epsilon_n a)}{\epsilon_n} \\
 M_2^0 &= 2\pi a^2 h G^* \Psi \vartheta \\
 M_2' &= 4a^2 G^* \vartheta \sum_{n=1}^{\infty} B_n \frac{\sin \gamma_n h}{\gamma_n},
 \end{aligned} \tag{39}$$

where M_1^0 is the torque due to the stress on the bottom of the inner cylinder without the edge-effect, and M_1' is the torque due to the edge-effect. From the equation of motion of the inner cylinder a complicated equation results; however, it is not possible to determine G^* when the end-effect is taken into account. If we want to treat a Newtonian liquid instead of a linear viscoelastic body, we need only put G' equal to zero in the above treatment.

In an alternative treatment²³, the space occupied by the liquid was divided into two regions instead of three, and consequently the torque M_1^0 did not appear in the expression for the torque M .

3. FREE OSCILLATIONS

Here we will treat free oscillations of the inner cylinder. From the measurement of the frequency ω and the logarithmic decrement $2\pi\Delta/\omega$ the dynamic shear modulus G' and the dynamic viscosity η' may be obtained. For the sake of simplicity, the end-effect will be neglected. If we put

$$\vartheta = \vartheta_0 e^{-\Delta t} e^{i\omega t}, \quad \varphi = \varphi_0 e^{-\Delta t} e^{i\omega t}$$

the operator G becomes

$$G\ddagger = G' + (i\omega - \Delta)\eta'$$

and equation (29) reduces to equation (30) with β^2 replaced by

$$\beta_1^2 = \rho(\omega + i\Delta)^2 / G\ddagger$$

Hence we have

$$M = 2\pi a^2 h G\ddagger \Psi_1 \vartheta,$$

where Ψ_1 is equal to Ψ with β replaced by β_1 . From the equation of motion of the inner cylinder we obtain²⁴

$$G\ddagger \Psi_1 = \frac{I}{2\pi a^2 h} [(\omega + i\Delta)^2 - (\omega_0^2 + \Delta_0^2) - 2i\Delta_0(\omega + i\Delta)] \equiv \mu_1, \quad (40)$$

which determines in principle $G\ddagger$ from measurable quantities ω , Δ , ω_0 , and Δ_0 . Since, as before, it is impossible to obtain $G\ddagger$ from the above equation in the general case, we will consider only special cases.

Case a. $|\beta_1| \ll 1$, that is, either when the inertia term $\rho(\omega + i\Delta)^2$ is negligible or

$$|G\ddagger|^2 = (G' - \Delta\eta')^2 + \omega^2\eta'^2$$

is sufficiently large. Ψ_1 may be approximated as before, and if we neglect terms in $(\beta_1 a)^4$ and higher order terms, we obtain to the first approximation

$$\begin{aligned}
G' &= \frac{(1/a^2) - (1/b^2)}{4\pi h} I(\omega^2 + \Delta^2 - \omega_0^2 - \Delta_0^2) \\
&\quad + \rho(\omega^2 + \Delta^2) \left[\frac{1}{2} \frac{1}{(1/a^2) - (1/b^2)} \ln \left(\frac{b}{a} \right) \right. \\
&\quad \left. - \frac{1}{8} \frac{a^3}{a+b} \left(3 \frac{b}{a} + 3 - \frac{a}{b} - \frac{a^2}{b^2} \right) \right] \\
\eta' &= \frac{(1/a^2) - (1/b^2)}{4\pi h} I \cdot 2(\Delta - \Delta_0) \\
&\quad + 2\rho\Delta \left[\frac{1}{2} \frac{1}{(1/a^2) - (1/b^2)} \ln \left(\frac{b}{a} \right) \right. \\
&\quad \left. - \frac{1}{8} \frac{a^3}{a+b} \left(3 \frac{b}{a} + 3 - \frac{a}{b} - \frac{a^2}{b^2} \right) \right]
\end{aligned} \tag{41}$$

Case *b*. $|\beta_1 a| \gg 1$, that is, when

$$|G_{\dagger}|^2 = (G' - \Delta\eta')^2 + \omega^2\eta'^2$$

is negligible. Using asymptotic expansions of Bessel functions, Ψ_1 becomes $i\beta_1 a$ to a zero approximation, provided that $|\beta_1(b - a)| \gg 1$, and equation (40) reduces to

$$G_{\dagger} = - \frac{\mu_1^2}{\rho a^2(\omega + i\Delta)^2}$$

Hence we obtain

$$\begin{aligned}
G' &= \frac{1}{\rho a^2} \left(\frac{I}{2\pi a^2 h} \right)^2 \left[3\Delta^2 \left(\frac{\omega_0^2 + \Delta_0^2}{\omega^2 + \Delta^2} - \frac{1}{3} \right) \left(\frac{\omega_0^2 + \Delta_0^2}{\omega^2 + \Delta^2} + 1 \right) \right. \\
&\quad \left. - \omega^2 \left(\frac{\omega_0^2 + \Delta_0^2}{\omega^2 + \Delta^2} - 1 \right)^2 - 8\Delta\Delta_0 \frac{\omega_0^2 + \Delta_0^2}{\omega^2 + \Delta^2} + 4\Delta_0^2 \right] \\
\eta' &= \frac{1}{\rho a^2} \left(\frac{I}{2\pi a^2 h} \right)^2 \cdot 2\Delta \left(\frac{\omega_0^2 + \Delta_0^2}{\omega^2 + \Delta^2} - 1 \right) \left(\frac{\omega_0^2 + \Delta_0^2}{\omega^2 + \Delta^2} + 1 - 2 \frac{\Delta_0}{\Delta} \right)
\end{aligned} \tag{42}$$

4. OUTER CYLINDER IN OSCILLATION

A cylindrical bob of radius a is suspended coaxially to a depth h in a viscoelastic liquid contained in a cup of radius b . The cup is caused to oscillate through a very small angular amplitude.²⁸ It is desired to find a relationship between the mechanical properties of the sample and the amplitude and the phase angle of the motion of the bob relative to that of the cup.

For the sake of simplicity, we will neglect here the end-effect. Let us

²⁸ H. Goldberg and O. Sandvik, *Anal. Chem.* **19**, 123 (1947).

write the angular displacement of the cup, bob, and the sample, respectively:

$$\psi = \psi_0 e^{i\omega t}, \quad \vartheta = \vartheta_0 e^{i\omega t}, \quad \varphi = \varphi_0 e^{i\omega t}$$

Then we obtain from equation (30)

$$\varphi_0(r) = (1/r)[AJ_1(\beta r) + BY_1(\beta r)]$$

where the constants A and B are determined from the boundary conditions $\varphi_0(a) = \zeta_0$ and $\varphi_0(b) = \psi_0$. The torque on the bob is given by

$$M = -2\pi a^2 h \beta G^* [AJ_2(\beta a) + BY_2(\beta a)] e^{i\omega t}$$

and from the equation of motion of the bob we get

$$\begin{aligned} \frac{\psi_0}{\vartheta_0} = \frac{I\omega^2 - K}{4abhG^*} [J_1(\beta a)Y_1(\beta b) - Y_1(\beta a)J_1(\beta b)] \\ + \frac{\pi a}{2b} \beta a [J_2(\beta a)Y_1(\beta b) - Y_2(\beta a)J_1(\beta b)], \end{aligned}$$

the damping term $R_0 \dot{\vartheta}$ being neglected. Since G^* is buried in the complex argument of Bessel functions it is impossible to solve the above equation for G^* . For the special case $|\beta a| \ll 1$, Markovitz²⁵ expanded functions with argument βb into a Taylor's series about βa , and obtained the following result, in the present notation:

$$\begin{aligned} \frac{\psi_0}{\vartheta_0} = 1 - \frac{1}{G^*} \left(\frac{I\omega^2 - K}{4\pi h} \frac{b^2 - a^2}{a^2 b^2} + \frac{\rho\omega^2}{8} \frac{(b^2 - a^2)^2}{b^2} \right) \\ + \frac{1}{G^{*2}} \left\{ \frac{(I\omega^2 - K)\rho\omega^2}{32\pi h} \left(4 \ln \frac{a}{b} + \frac{b^2}{a^2} - \frac{a^2}{b^2} \right) \right. \\ \left. + \frac{\rho^2 \omega^4}{192b^2} \left[(b^2 - a^2)(b^4 - 5b^2 a^2 - 2a^4) + 12a^4 b^2 \ln \frac{b}{a} \right] \right\} \\ + \frac{1}{G^{*3}} \left\{ \frac{(I\omega^2 - K)\rho^2 \omega^4}{768\pi h a^2 b^2} \left[12a^2 b^2 (a^2 + b^2) \ln \frac{b}{a} \right. \right. \\ \left. \left. - (b^2 - a^2)(b^4 + 10b^2 a^2 + a^4) \right] \right. \\ \left. - \frac{\rho^3 \omega^6}{9216b^2} \left[24a^4 b^2 (2a^2 + 3b^2) \ln \frac{b}{a} \right. \right. \\ \left. \left. + (b^2 - a^2)(b^6 - 11b^4 a^2 - 47b^2 a^4 - 3a^6) \right] \right\} + \dots \end{aligned} \quad (43)$$

For sufficiently large values of $|G|$, terms in $1/G^*$ and all higher order terms may be neglected.

Oldroyd²⁹ has developed a theory of periodic and steady states of motion of a liquid in an annular gap between coaxial cylinders, assuming that the viscous and elastic properties of the material at small rates of shear can be specified by three constants: a viscosity, a relaxation time and a retardation time. The outer cylinder undergoes forced harmonic angular oscillations about its axis, and the inner cylinder is supported by a torsion wire, as in the case just considered; the amplitude of the oscillation of the inner cylinder is calculated.

Ibrahim³⁰ treated an oscillating coaxial cylinder viscometer of the same type containing a Newtonian liquid. He avoided Bessel functions by replacing $3/r$ by $3/\bar{r}$ in equation (30), where \bar{r} is the average radius $(a + b)/2$. This approximation will be valid, provided that the clearance is very small. In this way he obtained a simple approximate formula for determining the viscosity from ϑ_0/ψ_0 and the angular frequency ω . The result is

$$\eta = \frac{b-a}{2\pi a^3 h} \frac{I\omega^2 - K}{\omega} \left[1 + \left(\frac{2\pi a^3 h \rho \omega^2}{I\omega^2 - K} - \frac{b}{a+b} \right) \right] \frac{\vartheta_0}{\psi_0} \quad (44)$$

V. Disk Viscometers

1. ROTATING DISK VISCOMETERS

A circular disk, under the action of a constant torque M in a *Newtonian fluid* of viscosity η , is assumed to rotate with a constant angular velocity Ω about an axis through its center, perpendicular to the plane of the disk. The problem then is to determine how M and Ω depend upon the viscosity of the fluid, and how this may be calculated from the two observable quantities.

Let us assume, for the sake of simplicity, that the arrangement is such that a circular disk of radius a of infinitesimal thickness rotates between two fixed parallel infinite planes at equal distances from them. If we neglect the edge-effect, that is, if we assume that the distribution of the stress on the disk due to the viscous drag of the fluid is the same as that for an infinite disk, then we have from equation (22)

$$M = (\pi a^4/l)\eta\Omega$$

as was derived by Stokes. Since the correction we have to consider is confined to the space immediately surrounding the edge of the disk, we may treat the edge as if it were the straight edge of an infinite plane. From these considerations Maxwell³¹ deduced that the edge-effect is the same as if a portion whose breadth is $(2l/\pi) \ln 2$ had been added to the surface at its

²⁹ J. G. Oldroyd, *Quart. J. Mech. and Appl. Math.* **4**, 271 (1951).

³⁰ A. A. K. Ibrahim and A. M. Kabi, *J. Appl. Phys.* **23**, 754, 1190 (1952).

³¹ J. C. Maxwell, *Phil. Trans. Roy. Soc. London* **156**, 249 (1866).

edge. Hence the torque M is given by

$$M = (\pi a^4/l)\eta\Omega + 8a^3\eta\Omega \ln 2$$

provided that $l/a \ll 1$. According to Brillouin, the edge correction $(2l/\pi) \ln 2$ is too large and should be multiplied by a factor

$$1 - (6l/\pi a) \ln 2$$

Maxwell also treated the effect of finite thickness of the disk. If the thickness is $2h$, and the distance between the fixed plates is equal to $2l + 2h$, so that the distances between the surfaces is l , it was shown that the breadth of the strip which must be supposed to be added to the surface at the edge will be

$$\frac{2l}{\pi} \left[\ln 2 + \ln \sin \frac{\pi l}{2(l+h)} \right]$$

This of course reduces to $(2l/\pi) \ln 2$ when $h \rightarrow 0$. Although in actual arrangements the influence of the edge is found to be important, no exact treatment has been previously published.

Let us consider that an oblate spheroid with the major axis $2a$ and the minor axis $2c$ rotates with a constant angular velocity Ω in a Newtonian fluid extending to infinity. The torque M due to the viscous drag of the fluid is given by the well-known formula

$$M = \frac{16\pi}{3} \eta\Omega \frac{a^2(a^2 - c^2)^{3/2}}{c(a^2 - c^2)^{1/2} - a^2[(\pi/2) - \sin^{-1}(c/a)]}$$

Taking the limit $c \rightarrow 0$, we obtain for the torque on a circular plate of radius a of infinitely small thickness rotating in an infinite Newtonian fluid

$$M = (2\pi/3)a^3\eta\Omega$$

It is necessary to remark that these formulas are derived on the assumption that each thin confocal ellipsoidal shell rotates as a rigid body. In an actual arrangement, however, the disk is contained in a vessel of finite dimensions, and the assumption is generally no more valid.

We will now give a mathematical treatment of the problem, ignoring secondary flow, for the arrangement of Fig. 10. A circular plate of radius a and thickness $2h$ rotates in a coaxial cylinder of radius b containing a Newtonian fluid of viscosity η . For the sake of simplicity it is assumed that the disk is placed with equal spacing l from the top and bottom surfaces of the cylinder. Concerning the motion of the fluid we make again the assumptions (i) to (v) mentioned in Section III,1.

In order to obtain a stationary solution of equation (29) satisfying the appropriate boundary conditions, we imagine that the space occupied by the fluid is divided into five regions I, II, III, I', and III' as in Fig. 10. We

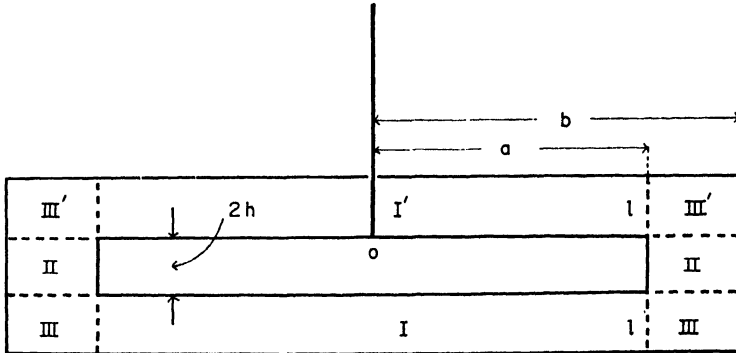


FIG. 10. Disk viscometer

take the origin of the cylindrical coordinates at the center of gravity of the plate, and denote the angular velocity for these five regions by $\omega^{(1)}$, $\omega^{(2)}$, $\omega^{(3)}$, $\omega^{(1')}$, and $\omega^{(3')}$, respectively. From the considerations of symmetry it is clear that $\omega^{(1')} = \omega^{(1)}$ and $\omega^{(3')} = \omega^{(3)}$, so that we need only find $\omega^{(1)}$, $\omega^{(2)}$, and $\omega^{(3)}$. By a mathematical procedure quite similar to that used in Section II,5 we can calculate $\omega^{(1)}$, $\omega^{(2)}$, and $\omega^{(3)}$, and consequently the torque M on the disk. It is then found that M consists of four components M_1^0 , M_1' , M_2^0 , and M_2' , where M_1^0 is the torque on the top or bottom surface of the disk without the edge-effect, M_1' is the torque due to the edge-effect, M_2^0 is the torque on the cylindrical surface of the disk without the end-effect, and M_2' is the torque due to the end-effect. Thus the total torque on the disk may be written in the form²⁴

$$M = \frac{\pi a^4}{l} \eta \Omega \left[1 + \frac{4l}{a} \sum_{n=1}^{\infty} A_n I_2 \left(\frac{n\pi a}{l} \right) + \frac{l}{a^4} \frac{8h}{(1/a^2) - (1/b^2)} + \frac{8l}{\pi a^2} \sum_{n=1}^{\infty} B_n \frac{\sinh \kappa_n h}{\kappa_n} \right], \quad (45)$$

where κ_n , A_n , and B_n have the same meaning as before. The third and the fourth terms correspond to the torque due to the drag on the cylindrical surface, and they vanish for the limiting case of a disk of infinitesimally small thickness. We notice that both the edge correction and the end correction are in general functions of three non-dimensional parameters a/b , a/l , and h/b .

2. OSCILLATING DISK VISCOMETERS: FREE OSCILLATIONS

In spite of the fact that the oscillating disk viscometer method leads to great simplicity of design and lends itself to precise measurements, the evaluation of the results in terms of viscosity still presents difficulties.

Let us consider a plane circular disc of radius a , thickness $2h$, and moment of inertia I , suspended by a long torsion wire of torsion constant K , and let us suppose that it performs torsional free oscillations in a *Newtonian fluid* of viscosity η and density ρ so that at time t the angular displacement of the disk, from its position of rest, is given by

$$\vartheta = \vartheta_0 e^{-\Delta t} e^{i\omega t}$$

It is required to solve the Navier-Stokes equation so as to obtain the velocity distribution within the fluid, to calculate from the velocity gradient at the disk surfaces the damping couple on the disk due to the viscous drag of the fluid, and to deduce equations from which the viscosity may be determined from the observed logarithmic decrement and the period. Approximate theories have been proposed by various investigators both for the case where the fluid is extending to infinity and the case where the fluid is bounded by two infinite parallel plates. However, the effect of finite thickness of the disk is often neglected.

a. General Case

We will present a treatment of the theory of an oscillating disk viscometer for the arrangement of Fig. 10, neglecting secondary flow. It is possible to treat the general case where the cylindrical container is filled with a linear viscoelastic body instead of a Newtonian fluid. The cases previously treated by various investigators are special cases of our general case; however, we will confine ourselves to the case of Newtonian fluids for the sake of comparing our results with those of other investigators.

By a method similar to that used in Section IV,2, we can obtain the damping couple M on the disk due to the drag of the fluid. It is then found,²⁴ corresponding to equation (39), that the damping couple consists of four terms:

$$\begin{aligned} M_1^0 &= \pi a^4 \eta \beta \cot \beta l \cdot \dot{\vartheta} \\ M_1' &= \frac{4\pi^2 a^3}{l} \eta \dot{\vartheta} \sum_{n=1}^{\infty} n A_n \frac{J_2(\epsilon_n a)}{\epsilon_n} \\ M_2^0 &= 4\pi a^2 h \eta \Psi \dot{\vartheta} \\ M_2' &= 8a^2 \eta \dot{\vartheta} \sum_{n=1}^{\infty} B_n \frac{\sinh \gamma_n h}{\gamma_n}, \end{aligned} \quad (46)$$

where the notations have the same meaning as in Section IV,2 except that

$$\beta^2 = \frac{\rho(-i\omega + \Delta)}{\eta}$$

M_1^0 is the damping couple on the top and bottom surfaces of the disk with-

out the edge-effect; M_1' is the couple due to the edge-effect; M_2^0 is the damping couple on the cylindrical surface of the disc without end-effect; and M_2' is the couple due to the end-effect. Since M_1^0 is the principal term in this case, we may write M in the following form:

$$M = \pi a^4 \eta \beta \dot{\vartheta} (1 + \lambda) \cot \beta l, \quad (47)$$

where

$$\lambda = \frac{4\pi}{a l \beta} \sum_{n=1}^{\infty} n A_n \frac{J_2(\epsilon_n a)}{\epsilon_n} + \frac{4h\psi}{a^2 \beta \cot \beta l} + \frac{8}{\pi a^2 \beta \cot \beta l} \sum_{n=1}^{\infty} B_n \frac{\sinh \gamma_n h}{\gamma_n} \quad (48)$$

We can now write down the equation of motion of the disk, taking into account the internal friction in the wire:

$$I \ddot{\vartheta} + R_0 \dot{\vartheta} + K \vartheta = -\pi a^4 \eta \beta \dot{\vartheta} (1 + \lambda) \cot \beta l$$

or expressing, as before, R_0 and K in terms of the natural angular frequency ω_0 and the logarithmic decrement $2\pi\Delta_0/\omega_0$ for free oscillations *in vacuo*:

$$\eta \beta (1 + \lambda) \cot \beta l = \frac{I}{\pi a^4} \left[\frac{\omega_0^2 + \Delta_0^2}{\omega^2 + \Delta^2} \Delta + \Delta - 2\Delta_0 + i\omega \left(\frac{\omega_0^2 + \Delta_0^2}{\omega^2 + \Delta^2} - 1 \right) \right] \quad (49)$$

b. Special Case

For the sake of simplicity we will neglect λ compared to unity, that is, we will neglect both the edge-effect and the effect of finite thickness of the disk, and examine two special cases.

Case 1. $|\beta l| \ll 1$, that is, the case of very small spacing or sufficiently high viscosity. Substituting $1 - (\beta l)^2/3$ for $\beta l \cot \beta l$ and separating both sides of equation (49) into real and imaginary parts, we find

$$\eta = \frac{2Il}{\pi a^4} \left(\frac{\omega_0^2 + \Delta_0^2}{\omega^2 + \Delta^2} \Delta - \Delta_0 \right), \quad (50)$$

which is essentially equivalent to the equations derived by Maxwell³¹ and by MacWood.³² If we neglect the term $\rho l^2/3$ compared to $Il/\pi a^4$, then we have $\omega^2 + \Delta^2 = \omega_0^2 + \Delta_0^2$, and equation (50) reduces to²⁴

$$\eta = \frac{2Il}{\pi a^4} (\Delta - \Delta_0) \quad (51)$$

Equation (50) reduces also to equation (51), provided that $\omega_0/\omega \approx 1$ and $\Delta_0/\omega_0 \ll 1$.

Case 2. $|\beta l| \gg 1$, that is, the case of negligible viscosity or sufficiently

³² G. E. MacWood, *Physica* 5, 374, 763 (1938).

large spacing. Replacing $\cot \beta l$ by the limiting value i and separating both sides of equation (49) (in which λ is set equal to zero) into real and imaginary parts, we find²⁴

$$\eta\rho = \frac{2I^2}{\pi^2 a^8} \frac{1}{\sqrt{\omega^2 + \Delta^2} - \Delta} \left[\frac{\omega_0^2 + \Delta_0^2}{\omega^2 + \Delta^2} \Delta + \Delta - 2\Delta_0 \right]^2, \quad (52)$$

which reduces to

$$\eta\rho = \frac{8I^2}{\pi^2 a^8} \frac{1}{\omega - \Delta} (\Delta - \Delta_0)^2, \quad (53)$$

provided that $\omega_0/\omega \approx 1$ and $\Delta/\omega \ll 1$.

Hollis-Hallett³³ proposed an approximate theory of the problem of a disk of radius a and thickness $2h$ oscillating in an infinite Newtonian fluid. He evaluated the viscous moment acting on the two faces and on the cylindrical surface, on the assumption that the two flat faces form part of an infinite cylinder. Such a scheme of calculation introduces mathematical simplifications into the problem. The result may be written, in terms of our present notation,

$$\eta\rho = \frac{2I^2}{\pi^2 a^8} \frac{1}{\omega - \Delta} \left(\frac{\omega_0^2}{\omega^2} \Delta + \Delta - 2\Delta_0 \right)^2 \left[1 + \frac{2h}{a} + \frac{2}{a} \sqrt{\frac{2\eta}{\rho\omega}} \right]^{-2} \quad (54)$$

neglecting Δ^2/ω^2 compared to unity. Equation (54) should be compared to equation (52). If $\omega_0/\omega \approx 1$ and $\Delta/\omega \ll 1$, equation (54) reduces to

$$\eta\rho = \frac{8I^2}{\pi^2 a^8} \frac{1}{\omega - \Delta} (\Delta - \Delta_0)^2 \left[1 + \frac{2h}{a} + \sqrt{\frac{2\eta}{\rho\omega}} \right]^{-2} \quad (55)$$

If we wish to take into account the edge-effect and the effect of finite thickness of the disk, the exact formula should of course be deduced on the basis of equation (49).

In the foregoing treatment it is assumed that the motion of the fluid is not turbulent. The criterion for nonturbulent motion of a disk has been given by Cochran³⁴ as $\rho\omega a^2/\eta < 10^5$.

VI. Concentric Sphere Viscometers

1. ROTATING CONCENTRIC SPHERE VISCOMETERS

Let us consider a rotating concentric sphere viscometer with the arrangement shown in Fig. 11. The space between two concentric spheres is filled with a *Newtonian liquid* of viscosity η . One of the spheres is fixed, while to the other is applied a constant torque M . Let Ω be the angular velocity of

³³ A. C. Hollis-Hallett, *Proc. Roy. Soc. A* **210**, 404 (1952).

³⁴ W. G. Cochran, *Proc. Cambridge Phil. Soc.* **30**, 365 (1934).

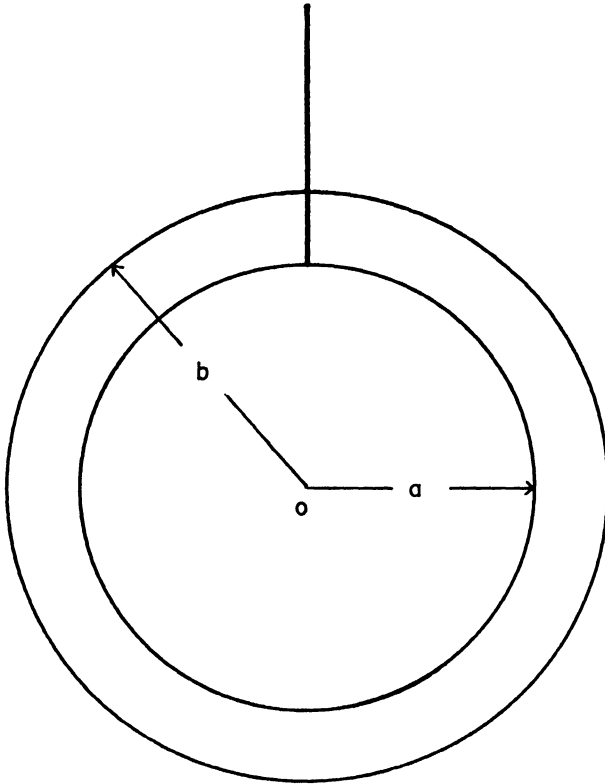


FIG. 11. Concentric sphere viscometer

the sphere in the stationary state. Then η may be determined from the measurement of the relation between M and Ω .

Let us assume that the inner sphere is fixed. In order to find the relation between M and Ω , we also make assumptions (i-v) mentioned in Section III,1, so that secondary flow is again ignored. It can then be shown from the fundamental equations of hydrodynamics that the angular velocity ω of the liquid particles around the axis of rotation is given by

$$\omega = \frac{(1/a^3) - (1/r^3)}{(1/a^3) - (1/b^3)} \Omega,$$

where a and b are the radius of the inner and outer spheres, respectively. The fact that ω is a function of r only means that each thin spherical shell rotates as a rigid body. Integrating over the surface of the inner sphere the moment of the shear stress given by

$$\tau_{r\phi} = \eta r \sin \theta \cdot d\omega/dr$$

(where θ is the angle which the radius vector makes with the axis of rotation), we get

$$M = \frac{8\pi}{(1/a^3) - (1/b^3)} \eta\Omega$$

This equation corresponds to the Margules equation for a coaxial cylinder viscometer and remains unaltered when the outer sphere is fixed and the inner one rotates.

In the case of a hemispherical viscometer³⁵ of the arrangement as in Fig. 12, 8π should be replaced by 4π . Since we have neglected the effect of centrifugal forces, the free surface remains a horizontal plane.

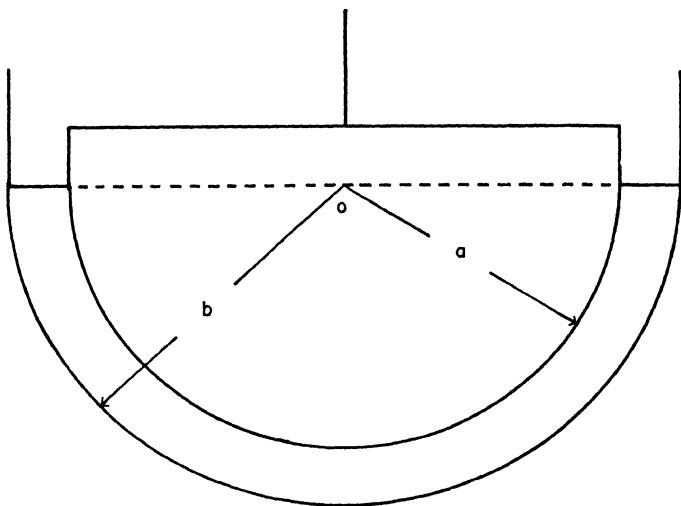


FIG. 12. Hemispherical viscometer

2. OSCILLATING CONCENTRIC SPHERE VISCOMETERS

a. Forced Oscillations

We will discuss the performance of a concentric sphere viscometer both for the cases of forced and free oscillations. Let us assume that the outer sphere is fixed and the inner one is suspended by a wire, the upper end of which is twisted through an angle $\psi = \psi_0 \sin \omega t$. The inner sphere then oscillates with a phase lag δ , owing to the viscous drag of the material between the spheres. Thus at time t the angular displacement of the inner sphere, from its position of rest, may be written $\vartheta = \vartheta_0 \sin (\omega t - \delta)$. We will assume that the material is a *linear viscoelastic body* whose rheological behavior is characterized by the complex shear modulus $G^* = G' + i\omega\eta'$.

³⁵ G. Ungar, *Kolloid-Z.* **69**, 30, 164 (1934).

The problem is to find a relation between the measurable quantities δ and ϑ_0/ψ_0 and the dynamic modulus G' and the dynamic viscosity η' . In the case of a *Newtonian liquid* we need only put $G' = 0$.

The fundamental equation for the angular displacement φ , in spherical polar coordinates r , θ , and ϕ , is given by

$$\rho \frac{\partial^2 \varphi}{\partial t^2} = G^* \left(\frac{\partial^2 \varphi}{\partial r^2} + \frac{4}{r} \frac{\partial \varphi}{\partial r} + \frac{1}{r^2} \frac{\partial^2 \varphi}{\partial \theta^2} + \frac{3 \cot \theta}{r^2} \frac{\partial \varphi}{\partial \theta} \right) \quad (56)$$

Corresponding to the torsional oscillation $\psi = \psi_0 \exp(i\omega t)$ at the upper end of the wire we put for the inner sphere

$$\vartheta = \vartheta_0 e^{i\omega t} = q\psi_0 e^{i(\omega t - \delta)},$$

and similarly

$$\varphi = \varphi_0 e^{i\omega t}$$

From the solution of the above differential equation, which is subject to the boundary conditions $\varphi(a) = \vartheta$ and $\varphi(b) = 0$, we find³⁶ that the torque on the inner sphere is given by

$$M = 4\pi a^3 G^* \Phi \vartheta \quad (57)$$

where

$$\Phi = \frac{2}{3} \beta a \frac{J_{5/2}(\beta a) Y_{3/2}(\beta b) - Y_{5/2}(\beta a) J_{3/2}(\beta b)}{J_{3/2}(\beta a) Y_{3/2}(\beta b) - Y_{3/2}(\beta a) J_{3/2}(\beta b)} \quad (58)$$

and $\beta^2 = \rho\omega^2/G^*$. From the equation of motion of the inner sphere we obtain

$$G^* \Phi = \frac{I}{4\pi a^3} \left[\omega^2 + (\omega_0^2 + \Delta_0^2) \left(\frac{e^{i\delta}}{q} - 1 \right) - 2i\omega\Delta_0 \right] \equiv \mu, \quad (59)$$

where ω_0 and $2\pi\Delta_0/\omega_0$ are, respectively, the angular frequency and the logarithmic decrement for free oscillations of the inner sphere in vacuo. Since G^* is buried in the argument of Bessel functions it is in general impossible to solve equation (59) for G^* . We will examine special cases.

Case a. $|\beta a| \ll 1$, that is, when the inertia is negligible or

$$|G|^2 = G'^2 + \omega^2 \eta'^2$$

is sufficiently large. For the *special case* when $x = (b - a)/a < 1$, Φ can be written

$$\Phi = 1 + \frac{2 B_0 + B_2 \xi^2 + B_4 \xi^4 + \dots}{3 B_1 + B_3 \xi^2 + B_5 \xi^4 + \dots}$$

where $\xi = \beta a$ and B_n 's are known functions of x . Neglecting terms in ξ^4 and all higher order terms we obtain

³⁶ S. Oka and A. Takami, *Bull. Kobayashi Inst. Phys. Research* **4**, 15 (1954).

$$\begin{aligned}
 G' &= \frac{I}{8\pi} \left(\frac{1}{a^3} - \frac{1}{b^3} \right) \left[\omega^2 + (\omega_0^2 + \Delta_0^2) \left(\frac{\cos \delta}{q} - 1 \right) \right] \\
 &\quad + \rho \omega^2 a^2 \left[\frac{1}{3} \left(\frac{b}{a} \right)^3 - \frac{3}{5} \left(\frac{b}{a} \right)^2 + \frac{1}{3} - \frac{1}{15} \left(\frac{a}{b} \right)^3 \right] \left[\left(\frac{b}{a} \right)^3 - 1 \right]^{-1} \quad (60) \\
 \eta' &= \frac{I}{8\pi} \left(\frac{1}{a^3} - \frac{1}{b^3} \right) \left[(\omega_0^2 + \Delta_0^2) \frac{\sin \delta}{\omega q} - 2\Delta_0 \right]
 \end{aligned}$$

In the case of a hemispherical viscometer, 8π should be replaced by 4π .

Case b. $|\beta a| \gg 1$, that is, when $|G|^2 = G'^2 + \omega^2 \eta'^2$ is sufficiently small. Using asymptotic expansions of Bessel functions, equation (59) becomes, to a zero approximation,

$$G^* = -\frac{9}{4} \frac{\mu^2}{\rho \omega^2 a^2}$$

from which G' and η' may be determined from measurable quantities as in Section IV, 1, b.

b. Free Oscillations

Let us denote the frequency and the logarithmic decrement of the free oscillations of the inner sphere by ω and $2\pi\Delta/\omega$. By the same procedure as before we find³⁷ the damping couple M on the inner sphere due to the viscous drag of the linear viscoelastic material as follows:

$$M = 4\pi a^3 G_{\dagger}^* \Phi_1 \vartheta,$$

where

$$G_{\dagger}^* = G' + (i\omega - \Delta)\eta', \quad \beta^2 = \rho(\omega + i\Delta)^2 / G_{\dagger}^*$$

and Φ_1 is defined by Φ with β replaced by β_1 . From the equation of motion of the inner sphere we obtain

$$G_{\dagger}^* \Phi_1 = \frac{I}{4\pi a^3} [(\omega + i\Delta)^2 - (\omega_0^2 + \Delta_0^2) - 2i\Delta_0(\omega + i\Delta)] \equiv \mu_1 \quad (61)$$

In the case of a Newtonian liquid we put G' equal to zero.

Case a. $|\beta a| \ll 1$. In this case we have, to the first approximation,

$$\begin{aligned}
 G' &= \frac{I}{8\pi} \left(\frac{1}{a^3} - \frac{1}{b^3} \right) (\omega^2 + \Delta^2 - \omega_0^2 - \Delta_0^2) \\
 &\quad + \rho a^2 (\omega^2 + \Delta^2) \left[\frac{1}{3} \left(\frac{b}{a} \right)^3 - \frac{3}{5} \left(\frac{b}{a} \right)^2 + \frac{1}{3} - \frac{1}{15} \left(\frac{a}{b} \right)^3 \right] \left[\left(\frac{b}{a} \right)^3 - 1 \right]^{-1} \\
 \eta' &= \frac{I}{8\pi} \left(\frac{1}{a^3} - \frac{1}{b^3} \right) \cdot 2(\Delta - \Delta_0) \\
 &\quad + 2\rho a^2 \Delta \left[\frac{1}{3} \left(\frac{b}{a} \right)^3 - \frac{3}{5} \left(\frac{b}{a} \right)^2 + \frac{1}{3} - \frac{1}{15} \left(\frac{a}{b} \right)^3 \right] \left[\left(\frac{b}{a} \right)^3 - 1 \right]^{-1} \quad (62)
 \end{aligned}$$

In the case of a hemispherical viscometer, 8π should be replaced by 4π .

³⁷ S. Oka, *Bull. Kobayashi Inst. Phys. Research* 6, 37 (1956).

Case b. $|\beta a| \gg 1$. We have, to a zero approximation,

$$G_{\dagger}^{\dagger} = -\frac{9}{4} \frac{\mu_1^2}{\rho(\omega + i\Delta)^2 a^2},$$

from which G' and η' may be determined as in Section IV,3,b.

VII. Cone and Plate, Double Cone, and Conicylindrical Viscometers

1. CONE AND PLATE VISCOMETER

In the cone and plate viscometer a cone with a wide vertical angle is placed on a horizontal flat plate as in Fig. 13. The generator of the cone makes a very small angle α with the plate which is of the order of one degree to two degree. The wedgelike space between the cone and the plate is filled with a liquid to be investigated. One of the surfaces is fixed; the other rotates around the axis of the cone. It is desired to find the relationship between the torque M and angular velocity Ω (or angular displacement ϑ). We will consider Newtonian liquids, materials manifesting linear viscoelastic behavior, and non-Newtonian liquids. We will neglect edge-effects and secondary flow.

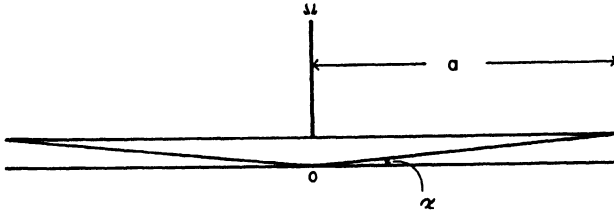


FIG. 13. Cone and plate viscometer

For the case of *Newtonian liquids*, we start with a form of the Navier-Stokes equation in spherical polar coordinates r , θ , and ϕ for the stationary state:

$$\frac{\partial^2 \omega}{\partial r^2} + \frac{4}{r} \frac{\partial \omega}{\partial r} + \frac{1}{r^2} \frac{\partial^2 \omega}{\partial \theta^2} + \frac{3 \cos \theta}{r^2} \frac{\partial \omega}{\partial \theta} = 0 \quad (63)$$

with the boundary conditions:

$$\omega = 0 \quad \text{for} \quad \theta = (\pi/2) - \alpha$$

$$\omega = \Omega \quad \text{for} \quad \theta = \pi/2$$

We find that the solution is a function of θ only, which means that each thin conical shell rotates as a rigid body. Integrating the moment of the shear stress

$$\tau_{\theta\phi} = \eta \sin \theta \cdot d\omega/d\theta$$

over the surface of the disk, we obtain³⁸

$$\begin{aligned} M &= \frac{2\pi a^3}{3} \eta \Omega \left[\int_{(\pi/2)-\alpha}^{\pi/2} \frac{d\theta}{\sin^3 \theta} \right]^{-1} \\ &= \frac{4\pi a^3}{3} \eta \Omega \left[\frac{\sin \alpha}{\cos^2 \alpha} - \ln \tan \left(\frac{\pi}{4} - \frac{\alpha}{2} \right) \right]^{-1} \end{aligned} \quad (64)$$

which is valid for any value of α . For small values of α equation (64) reduces to

$$M = \frac{2\pi a^3}{3\alpha} \eta \Omega \quad (65)$$

As in the case of the rotating cylinder viscometer, this instrument can be used for materials manifesting *linear viscoelastic behavior*, the relations between $M(t)$, $\vartheta(t)$, $J(t)$, and $G(t)$ being as given in Section III,6; the instrument constant K is obtained from the appropriate equation (64) or (65).

An alternative approach leading to equation (65) is to consider a point P on the rotating member at a distance r from O. The velocity at the point P is $r\Omega$, and the thickness of the liquid at P is nearly equal to $r\alpha$; thus the rate of shear $\dot{\gamma}$ is uniform and equal to³⁹ Ω/α . Consequently shear stress τ is uniform and the torque M is then given by

$$M = \int_0^{2\pi} \int_0^a r \cdot \tau r d\phi dr = \frac{2\pi a^3}{3} \tau$$

For a Newtonian liquid we again obtain equation (65).

In the case of a non-Newtonian liquid, it is reasonable to assume that the rate of shear and shear stress are uniform if α is small.³⁹ Thus from the above relations the flow curve $\dot{\gamma} = f(\tau)$ is obtained.

2. DOUBLE CONE VISCOMETER

The arrangement is as shown in Fig. 14, where the liquid fills to a height h the space between two cones with common axis and vertex. The semi-angles of the cones are α and β , and a and b are the radii of the free surface of the liquid. One of the cones is fixed; it is desired to find the relationship between torque M and angular velocity Ω for the other cone.

We will first assume as before that the space between the cones is filled with a *Newtonian liquid*. If we take a spherical coordinate system r , θ , and ϕ whose origin is at the vertex of the cone, then the angular velocity $\omega(r, \theta)$ of a particle satisfies equation (63) with the boundary conditions:

$$\omega(r, \alpha) = 0, \quad \omega(r, \beta) = \Omega$$

³⁸ I. Braun, *Bull. Research Council Israel* **1**, 126 (1951).

³⁹ G. H. Piper and J. R. Scott, *J. Sci. Instr.* **22**, 206 (1945).

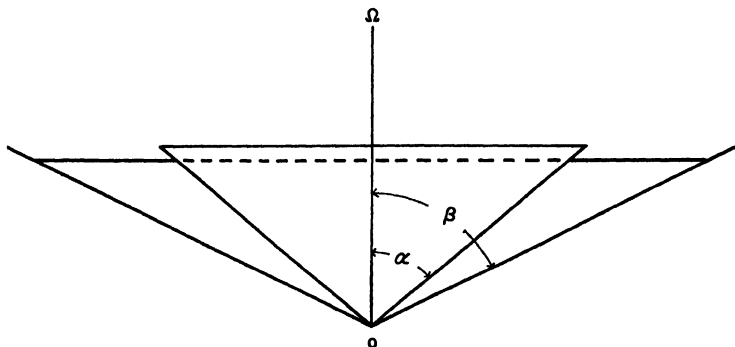


FIG. 14. Double cone viscometer

We find that the solution is a function of θ only:

$$\omega = \Omega \int_{\alpha}^{\theta} \frac{d\theta}{\sin^3 \theta} \left(\int_{\alpha}^{\beta} \frac{d\theta}{\sin^3 \theta} \right)^{-1}$$

where

$$\int_{\alpha}^{\beta} \frac{d\theta}{\sin^3 \theta} = \frac{1}{2} \left(\frac{\cos \alpha}{\sin^2 \alpha} - \frac{\cos \beta}{\sin^2 \beta} \right) + \frac{1}{2} \ln \frac{\tan (\beta/2)}{\tan (\alpha/2)}$$

Hence the only shear stress different from zero is the one acting in the ϕ -direction on a θ -surface, that is,

$$\tau_{\theta\phi} = \frac{\eta\Omega}{\sin^2 \theta} \left(\int_{\alpha}^{\beta} \frac{d\theta}{\sin^3 \theta} \right)^{-1} \quad (66)$$

Thus the torque M is given by

$$M = \frac{2\pi h^3}{3 \cos^3 \beta} \eta\Omega \left(\int_{\alpha}^{\beta} \frac{d\theta}{\sin^3 \theta} \right)^{-1} \quad (67)$$

The viscosity η can be obtained from the measurable quantity M/Ω .

This arrangement can also be used for liquids with *linear viscoelastic behavior*, the relationship between torque $M(t)$ and angular displacement $\vartheta(t)$ being obtained as before. Such an apparatus has actually been used⁴⁰ to measure $G(t)$.

3. CONICYLINDRICAL VISCOMETER

This arrangement consists of a concentric viscometer, with coaxial cones with a common vertex as bases for the cylinder as in Fig. 15. We will first consider the behavior of a *Newtonian liquid* in such a viscometer. If we neg-

⁴⁰ J. M. Watkins, R. D. Spangler, and E. C. McKannan, *J. Appl. Phys.* **27**, 685 (1956).

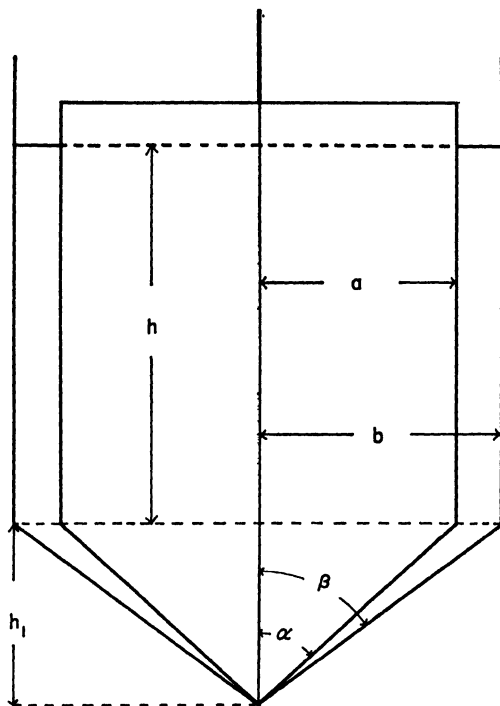


FIG. 15. Conicylindrical viscometer

lect the "corner-effect" at the junction of the conical and cylindrical portions, the viscometer can be considered as a combination of the cylindrical and double-cone arrangements. If h and h_1 are the heights of the cylindrical and conical portions, respectively, then from equations (21) and (67)

$$\frac{M}{\Omega} = \frac{4\pi h\eta}{(1/a^2) - (1/b^2)} \left(1 + \frac{\Delta h}{h}\right),$$

where

$$\Delta h = \frac{h_1}{6 \cos^2 \beta} \left(\frac{1}{\tan^2 \alpha} - \frac{1}{\tan^2 \beta} \right) \left(\int_{\alpha}^{\beta} \frac{d\theta}{\sin^3 \theta} \right)^{-1} \quad (68)$$

Thus with this arrangement the end-effect can be calculated approximately. This arrangement can similarly be used for materials with *linear viscoelastic behavior*. A treatment of the end-effect for slightly non-Newtonian liquids is given by Mooney and Ewart.⁴¹

⁴¹ M. Mooney and R. H. Ewart, *Physics* **5**, 350 (1934).

VIII. Oscillating Plate Viscometers

1. NEWTONIAN LIQUIDS

In an oscillating plate viscometer, a rigid plate is immersed in a liquid to be investigated and performs forced oscillations in a direction in its own

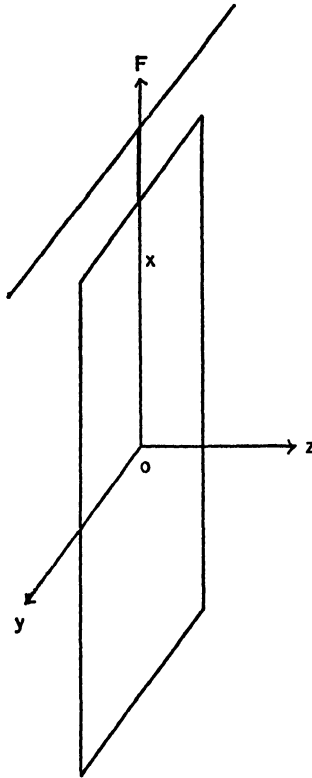


FIG. 16. Oscillating plate viscometer

plane under a driving force $F = F_0 \sin \omega t$ varying sinusoidally with time; the arrangement is as in Fig. 16. The amplitude of oscillation is measured at a resonant frequency. This amplitude is smaller than in air. The reason lies, of course, in the fact that the plate experiences the viscous drag of the liquid. From the measurement of the change in amplitude at resonant frequency the viscosity can be obtained as was shown by Woodward.⁴²

In order to evaluate the force on the plate due to the viscous drag of the fluid the following assumptions are made: (i) the liquid is Newtonian;

⁴² J. G. Woodward, *J. Acoust. Soc. Am.* **25**, 147 (1953).

(ii) the liquid is incompressible; (iii) the amplitude of motion is sufficiently small to avoid turbulence in the liquid; (iv) the initial period is disregarded and the motion of the liquid is independent of the initial conditions; (v) there is no relative motion between the plate and the liquid in immediate contact with the plate; (vi) the thickness of the plate is infinitesimally small; (vii) the edge-effect is negligible; and (viii) the wall-effect is negligible. Under these assumptions the velocity component v_x in the direction of oscillation is obtained from the Navier-Stokes equation

$$\rho(\partial v_x / \partial t) = \eta(\partial^2 v_x / \partial z^2)$$

with the boundary conditions

$$v_x = V_0 \sin \omega t \quad \text{for } z = 0,$$

$$v_x = 0 \quad \text{for } z = \infty$$

as follows:⁴³

$$v_x = V_0 \exp(-kz) \sin(\omega t - kz)$$

where V_0 is the velocity amplitude of the oscillating plate, z is the distance from the plate, k is given by $k = (\rho\omega/2\eta)^{1/2}$, and ρ is the density of the liquid. The viscous drag on the plate of area A is then given by

$$f = 2AV_0(\eta\rho\omega)^{1/2} \sin[\omega t + (\pi/4)]$$

so that the equation of motion of the system under the applied sinusoidal force may be written

$$m\ddot{\xi} + R_0\dot{\xi} + K\xi + 2AV_0(\eta\rho\omega)^{1/2} \exp\{i[\omega t + (\pi/4)]\} = F_0 e^{i\omega t}$$

where m is the mass of the moving system, ξ is the displacement of the plate in the x -direction, $R_0\dot{\xi}$ is the force due to the internal friction, and $K\xi$ is the elastic force. The above equation can be transformed into the form $Z_M V_0 = F_0$, where Z_M is the mechanical impedance defined as the ratio between force and velocity amplitude. We now specify that the system shall always be operated at resonance, which means that the imaginary part of Z_M is zero. Hence we have

$$[R_0 + A(2\eta\rho\omega)^{1/2}]V_0 = F_0$$

When the plate oscillates freely in air, the second term in the bracket is negligible, and we write $R_0 V_{0A} = F_0$, the subscript "A" indicating that the quantities are referred to motion in air (*vacuo*). We next specify that the driving force shall remain constant regardless of the load on the plate,

⁴³ J. W. S. Rayleigh, "Theory of Sound," Vol. II, p. 317. Macmillan, London, 1929.

that is, $F_{0A} = F_0$. Then we obtain from the above equations

$$(2\eta\rho\omega)^{1/2} = (R_0/A)[(V_{0A}/V_0) - 1] \quad (69)$$

The condition that the imaginary part of Z_M is zero at resonant frequency ω is given by

$$m\omega^2 - K + A\omega(2\eta\rho\omega)^{1/2} = 0,$$

so that ω may be regarded as equal to ω_A unless the viscosity is very large. Hence

$$\eta\rho = C[(V_{0A}/V_0) - 1]^2 \quad (70)$$

where

$$C = (R_0^2/2A^2)(m/K)^{1/2}$$

is an instrument constant. The above result is due to Woodward,⁴² and it allows η to be evaluated from the measurable quantity V_{0A}/V_0 .

2. EDGE-EFFECT

As is seen in Section VIII,1, equation (69) and (70) are derived by assuming that both the edge-effect and the wall-effect are negligible, that is, by considering an infinite plate in an infinite liquid. This condition obviously cannot be completely fulfilled in actual cases. Here we will neglect the wall-effect and discuss the theory of edge-effect for a square plate whose sides are of length $2a$. Let us take a rectangular coordinate system x and y parallel to the sides of the square plate, x being the direction of oscillation. Although the terms $\partial^2 v_x / \partial x^2$ and $\partial^2 v_x / \partial y^2$ cannot be regarded as exactly zero, they will surely be negligible compared to $\partial^2 v_x / \partial z^2$. Hence the Navier-Stokes equation becomes

$$\rho(\partial v_x / \partial t) = \eta(\partial^2 v_x / \partial z^2)$$

as before. It can be seen⁴⁴ that the solution subject to the boundary conditions:

$$\begin{aligned} v_x &= V_0 \sin \omega t & \text{for } z = 0, & \quad 0 < |x|, |y| < a, \\ v_x &= 0 & \text{for } z = 0, & \quad |x|, |y| > a, \\ v_x &= 0 & \text{for } z = \infty \end{aligned}$$

is given by

$$\begin{aligned} v_x = \frac{V_0}{2\pi} \int_{-a}^a \int_{-a}^a & \left[\frac{\sqrt{2}k}{R^2} \sin \left(\omega t - kR + \frac{\pi}{4} \right) \right. \\ & \left. + \frac{1}{R^3} \sin(\omega t - kR) \right] z e^{-kR} dx' dy', \end{aligned}$$

⁴⁴ S. Oka and T. Kato, *Bull. Kobayashi Inst. Phys. Research* **7**, 9 (1957).

where

$$R^2 = (x - x')^2 + (y - y')^2 + z^2$$

and k is given by $k = (\rho\omega/2\eta)^{1/2}$. The solution is obtained by making use of the theory of Fourier and Laplace transforms, retaining the previous assumptions except assumption (vii). We then obtain⁴⁴ the force on the oscillating plate due to the viscous drag of the fluid:

$$f = 2AV_0(\eta\rho\omega)^{1/2} \sin\left(\omega t + \frac{\pi}{4}\right) + \frac{32a}{\pi} \eta V_0 \sum_{n=0}^{\infty} \frac{1}{n!} \left(\frac{\rho\omega a^2}{\eta}\right)^{n/2} I_{n-1} \sin\left(\omega t + \frac{5n\pi}{4}\right),$$

where

$$I_n = \int_0^{\pi/4} \frac{1}{\cos^n \phi} d\phi$$

The first term is the same as before and the second term represents the effect of the edge. If $\rho\omega a^2/\eta < 1$, the series is convergent very rapidly, and it may be enough to consider only the first few terms. For example, let $a = 1$ cm., $\rho = 1$ g./cm.³, and $\omega = 2\pi \times 350$ rad./sec. Then the condition $\rho\omega a^2/\eta < 1$ corresponds to $\eta > 47$ poise.

From the equation of motion of the oscillating system and the condition that the system shall always be operated at resonance, we obtain

$$(2\eta\rho\omega)^{1/2} + \frac{8}{\pi a} \eta \sum_{n=0}^{\infty} \frac{1}{n!} \left(\frac{\rho\omega a^2}{\eta}\right)^{n/2} I_{n-1} \cos \frac{5n\pi}{4} = \frac{R_0}{A} \left[\frac{V_{0A}}{V_0} - 1 \right], \quad (71)$$

which is the exact formula for determining the viscosity from measurable quantities. If we neglect the second term on the left-hand side of equation (71), we get equation (69).

3. WALL-EFFECT

We will discuss the performance of an oscillating plate viscometer in a linear viscoelastic body specified by the complex modulus $G^* = G' + i\omega\eta'$, taking into account the wall-effect. For the sake of simplicity, we will neglect here the edge-effect. Let us consider an infinite plate at $z = 0$ in a viscoelastic body bounded by two parallel infinite planes $z = \pm l$, and assume that the plate oscillates by a driving force varying sinusoidally with time in a direction of x in its own plane as in Fig. 17. Thus the problem may be regarded as a two-dimensional one. We make the further assumptions (ii) to (vi) mentioned in Section VIII,1.

From the differential equation

$$\rho \partial^2 u_x / \partial t^2 = G^* \partial^2 u_x / \partial z^2$$

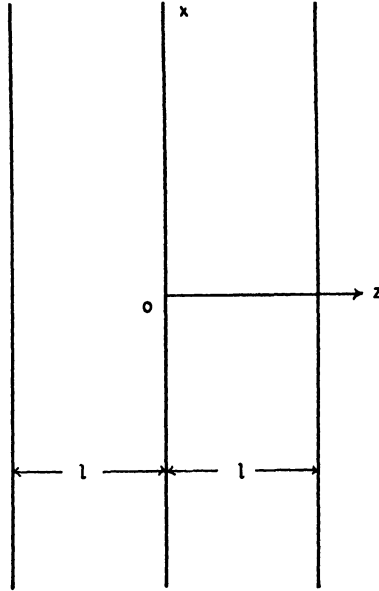


FIG. 17. Wall-effect in an oscillating plate viscometer

and the boundary conditions:

$$\begin{aligned} u_x &= \xi \quad \text{for } z = 0, \\ u_x &= 0 \quad \text{for } z = \pm l, \end{aligned}$$

we obtain the viscous drag due to the viscoelastic body in the form^{45, 46}

$$f = 2AG^*\beta\xi \cot \beta l,$$

where

$$\beta^2 = \rho\omega^2/G^*$$

A is the area of the plate ($2A$ is the total area of both faces), and ξ is the displacement of the plate from the position of rest. The equation of motion of the oscillating system is given by

$$m\ddot{\xi} + R_0\dot{\xi} + K\xi + 2AG^*\beta\xi \cot \beta l = F_0 e^{i\omega t}$$

Hence we have

$$\begin{aligned} \{R_0 + (2A/\omega) \operatorname{Im} (G^*\beta \cot \beta l) \\ + (i/\omega)[m\omega^2 - K - (2A/\omega) \operatorname{Re} (G^*\beta \cot \beta l)]\} V_0 = F_0, \end{aligned}$$

⁴⁵ H. Fuwa and I. Kimura, *Keisoku* **4**, 480 (1954).

⁴⁶ H. Fuwa, *Ôyô Butsuri* **25**, 149 (1956). Due to an oversight, he obtained half our value for the viscous drag.

where $\text{Re } (G^*\beta \cot \beta l)$ and $\text{Im } (G^*\beta \cot \beta l)$ represent the real and imaginary part of the complex quantity $G^*\beta \cot \beta l$. We again specify that the system shall always be operated *at resonance*. We denote as before the velocity amplitude of the plate in the viscoelastic body and in air by V_0 and V_{0A} , respectively. Hence we have

$$\text{Im } (G^*\beta \cot \beta l) = (\omega R_0/2A)[(V_{0A}/V_0) - 1]$$

$$\text{Re } (G^*\beta \cot \beta l) = m\omega^2 - K$$

from which G' and η' may be determined as a function of measurable quantities V_{0A}/V_0 and ω . We will examine two special cases.

Case a. $|\beta l| \ll 1$, that is, negligible inertia or sufficiently small spacing. Putting $\beta l \cot \beta l = 1$ to a zero approximation, the above equations lead to

$$\begin{aligned}\eta' &= (R_0 l/2A)[(V_{0A}/V_0) - 1] \\ G' &= (Kl/2A)[(\omega/\omega_A)^2 - 1],\end{aligned}\tag{72}$$

where ω_A is the frequency of free oscillations of the plate in air.

Case b. $|\beta l| \gg 1$, that is, either when $|G|^2 = G'^2 + \omega^2 \eta'^2$ is negligible or the spacing is large. Putting $\cot \beta l = i$ to a zero approximation, the above equations lead to the following results:

$$\begin{aligned}(G'^2 + \omega^2 \eta'^2)^{1/2} + G' &= (R_0^2/2\rho A^2)[(V_{0A}/V_0) - 1]^2 \\ (G'^2 + \omega^2 \eta'^2)^{1/2} - G' &= (2K^2/\rho\omega^2)[(\omega^2/\omega_A^2) - 1]^2\end{aligned}\tag{73}$$

from which G' and η' may be determined. If G' is equal to zero, that is, for a Newtonian liquid, the first equation reduces to equation (69) as is expected.

IX. Falling Sphere Viscometers

1. STOKES' LAW

If a sphere falls through a fluid of viscosity η , it experiences a resistance from the fluid and will attain a constant or terminal velocity v . Stokes showed that the viscous resistance of the sphere moving with uniform velocity V is

$$F_s = 6\pi a \eta V\tag{74}$$

where a is the radius of the sphere. On the other hand, the force exerted on the sphere is

$$\frac{4\pi}{3} a^3 (\sigma - \rho) g$$

in which σ is the density of the sphere, ρ that of the fluid, and g the accel-

eration due to gravity. Equating this to F_s gives

$$\eta = \frac{2(\sigma - \rho)ga^2}{9V} \equiv \eta_s \quad (75)$$

This is the well-known Stokes law, which relates the viscosity of the fluid to the velocity of the falling sphere.

Stokes' law, and consequently equation (75) are derived on the following assumptions: (i) the motion of the sphere is sufficiently slow; (ii) the fluid is of infinite extent; (iii) there is no slip between the fluid and the sphere; (iv) the sphere is rigid. Assumption (i) may be expressed explicitly in such a way that the Reynolds' number $R = 2a\rho V/\eta$ is negligible compared to unity; otherwise, a correction is necessary. In actual viscometers assumption (ii) is of course not fulfilled, and the wall-effect must be taken into account. There is a considerable weight of evidence to show that assumption (iii) is justified; experiments with spheres of different surface finish confirm this. Assumption (iv) is generally satisfied, because rigid solid spheres are usually used.

2. CORRECTIONS FOR STOKES' LAW

a. Effect of Finite Reynolds' Number

Neglecting R compared to unity, Oseen⁴⁷ obtained the following result:

$$F = F_s(1 + \frac{1}{6}R), \quad (76)$$

whereas Goldstein⁴⁸ obtained for values of R up to and including 2,

$$F = F_s(1 + \frac{1}{6}R - \frac{19}{1280}R^2 + \frac{71}{20480}R^3 - \frac{30179}{34406400}R^4 + \dots) \quad (77)$$

Hence the viscosity is given by η_s divided by the expression in the bracket of equation (76) or (77).

b. Wall-effect

Let us assume that a sphere falls vertically down the axis of an infinitely long cylinder of radius b . Ladenburg⁴⁹ showed that the resistance is approximately given by

$$F_s[1 + (2.1a/b)]$$

⁴⁷ C. W. Oseen, *Arkiv Mat. Astron. Fyz.* **9**, (16) 1 (1913).

⁴⁸ S. Goldstein, *Proc. Roy. Soc.* **A123**, 225 (1927).

⁴⁹ R. Ladenburg, *Ann. Physik* [4] **23**, 447 (1907).

so that

$$\eta = \frac{\eta_s}{1 + (2.1 a/b)}$$

It is found^{50, 51} that this relation is valid for $a/b < 0.06$. The original factor 2.4 was corrected to 2.1 by Faxén.

Faxén⁵² has carried the solution of Oseen's equations to completion, arriving at the result

$$\eta = \eta_s[1 - 2.104(a/b) + 2.09(a/b)^3 - 0.95(a/b)^5] \quad (78)$$

on the assumption that R^2 , $R(a/b)^2$, $(a/b)^6$, and R^2b/a are negligible compared to unity. The formula forms a closer approximation than Ladenburg's. Faxén has also obtained a result valid for finite Reynolds' number. Bacon⁵³ showed that equation (78) is in good agreement with his experimental data up to $a/b < 0.32$. Some of the results are reproduced in Fig. 18. The Faxén relation gives values within 1 per cent of the absolute

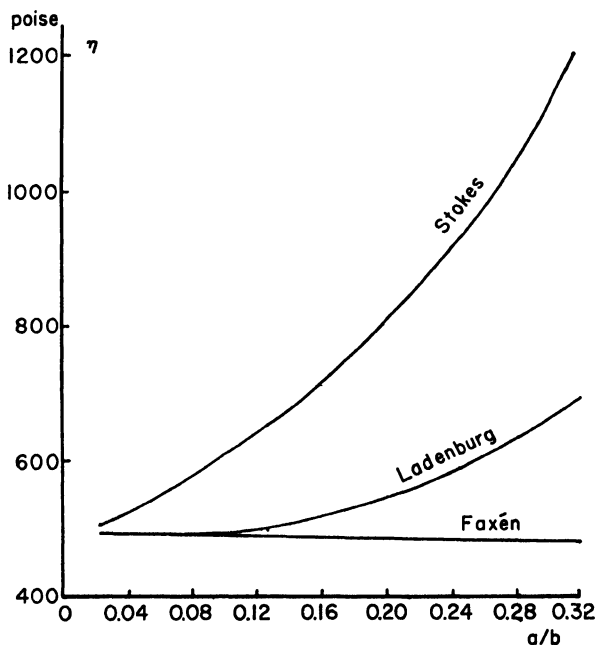


FIG. 18. Apparent viscosities evaluated by several formulas

⁵⁰ C. E. Lemm, *Phil. Mag.* [7] **12**, 589 (1931).

⁵¹ A. D. Arnold, *Phil. Mag.* [6] **22**, 755 (1911).

⁵² H. Faxén, *Arkiv Mat. Astron. Fyz.* **17** (27), 1, (1922-1923).

⁵³ L. R. Bacon, *J. Franklin Inst.* **221**, 251 (1936).

viscosities measured by the capillary tube method over the whole range checked (7.5–3660 poise). Thus the Faxén treatment of the hydrodynamic theory puts the falling sphere method on a basis probably as sound mathematically as that upon which the capillary tube technique rests.

c. End-effect

Since in practice the cylinder is of finite length, the effect of the two ends must be taken into account. Altrichter and Lustig⁵⁴ showed that the effect is a function of a/l , where l is the height of the sphere above the base of the cylinder.

X. Parallel Plate Plastometers

1. NEWTONIAN LIQUIDS

The material under test in the form of a cylinder is placed between parallel circular plates. A constant force F is applied perpendicular to the plates, one of the plates being fixed. From the measurement of the displacement of the other plate, the rheological behavior of the specimen may be determined. Two arrangements are used as shown in Fig. 19.

Case a. The thickness of the specimen h considerably smaller than the diameter. The specimen is larger than the plates; thus the area under compression is constant.

Case b. Thickness as above. The plates are larger than the specimen; thus the volume of the specimen is constant.

We will first investigate the behavior of a material manifesting only Newtonian flow in the plastometer in the two cases. Dienes and Klemm⁵⁵ has developed a theory of a parallel plate plastometer starting from the equation of motion of an incompressible viscous fluid.

First of all, we will make following assumptions: (i) the material is incompressible; (ii) the flow behavior of the material is Newtonian; (iii) no body force acts on the material; (iv) the motion is very slow; (v) there is no relative motion between the plates and the material in immediate contact with the plates; (vi) the plate separation is so small compared to the radius that the velocity component in the perpendicular direction is negligible. Let us take a cylindrical coordinate system r , ϕ , and z whose origin is at the center of the fixed plate. From assumptions (i) to (iv), the Navier-Stokes equation becomes

$$\partial p / \partial r = \eta \Delta v_r, \quad \partial p / \partial z = \eta \Delta v_z$$

From assumption (vi) and the second equation we find that the pressure

⁵⁴ F. Altrichter and A. Lustig, *Physik. Z.* **38**, 786 (1937).

⁵⁵ G. J. Dienes and H. F. Klemm, *J. Appl. Phys.* **17**, 458 (1946).

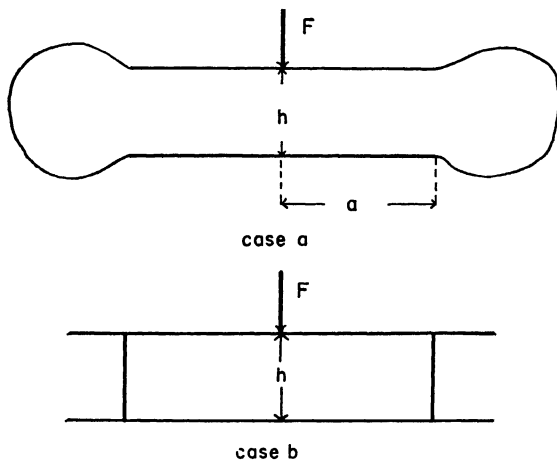


FIG. 19. Parallel plate plastometer

p is a function of r only. Since $v_r = 0$ at the plates from the assumption (v), $\partial v_r / \partial r$ may be negligibly small compared to $\partial v_r / \partial z$, and the first equation gives on double integration

$$v_r = \frac{1}{2\eta} \frac{dp}{dr} z(z - h) \quad (79)$$

Here it is considered that v_r vanishes at $z = 0$ and $z = h$. Integration of the condition of incompressibility

$$\partial(rv_r)/\partial r + \partial(rv_z)/\partial z = 0$$

with respect to z from $z = 0$ to $z = h$ gives

$$-r \frac{dh}{dt} = \int_0^h \frac{\partial}{\partial r} (rv_r) dz,$$

since $v_z = 0$ when $z = 0$, and $v_z = dh/dt$ when $z = h$. The derivation of the above equation differs from that by Dienes and Klemm, and is more general. Inserting equation (79) into the above equation, and integrating and observing boundary conditions regarding p to be finite for $r = 0$ and $p = p_0$ for $r = R$, where p_0 is the atmospheric pressure, we obtain

$$p = -\frac{3\eta}{h^3} \frac{dh}{dt} (R^2 - r^2) + p_0$$

Since the applied force F together with $\pi r^2 p_0$ is in equilibrium with the pressure in the fluid, we get

$$F = -\frac{3\pi}{2} \frac{R^4 \eta}{h^3} \frac{dh}{dt} \quad (80)$$

Case a. We may take $R = a$, and equation (80) becomes

$$-\frac{dh}{dt} = \frac{2F}{3\pi a^4 \eta} h^3,$$

where a is the radius of the circular plates. The above equation can be written as

$$\log (-dh/dt) = 3 \log h + \log (2F/3\pi a^4 \eta) \quad (81)$$

Thus if $\log (-dh/dt)$ is plotted against $\log h$, a straight line of slope 3 is obtained. From the intercept on the ordinate, the value of η , the viscosity is found of the specimen being tested.

Alternatively, equation (81) can be integrated. If h_0 is the thickness at zero time, then the thickness h at a subsequent time t is given by

$$\frac{3\pi a^4}{4} \left(\frac{1}{h^2} - \frac{1}{h_0^2} \right) = F \frac{t}{\eta} \quad (82)$$

We may plot $3\pi a^4/4h^2$ against t , and from the slope of the straight line η is obtained.

Case b. If we express equation (80) in terms of V , the volume of the specimen, we have

$$-\frac{dh}{dt} = \frac{2\pi F}{3V^2 \eta} h^5 \quad (83)$$

Thus if $\log (-dh/dt)$ is plotted against $\log h$, a straight line of slope 5 is obtained. η is obtained from the intercept on the ordinate.

Alternatively, equation (83) may be integrated. Thus we have

$$\frac{3V^2}{8\pi} \left(\frac{1}{h^4} - \frac{1}{h_0^4} \right) = F \frac{t}{\eta} \quad (84)$$

We may plot $3V^2/8\pi h^4$ against t , and η is obtained from the slope of the straight line.

2. LINEAR VISCOELASTIC BODIES⁵⁶

Let us assume that the relationship between shear stress, shear strain, and time is given by the first of equations (28). Then the shear strain in a material subject to constant shear stress τ at zero time is given by

$$\gamma(t) = \tau J(t), \quad (85)$$

where $J(t)$ is the shear creep compliance (cf. Chapter 1 of Volume II). Now t/η is the shear creep compliance for a material manifesting only Newtonian flow. If we assume that the above equations (82) and (84) can be generalized for a material manifesting linear viscoelastic behavior in

⁵⁶ G. J. Dienes, *J. Colloid Sci.* **2**, 131 (1947).

shear, then for a load F applied at zero time we have, respectively, for case a :

$$\frac{3\pi a^4}{4} \left(\frac{1}{h^2} - \frac{1}{h_0^2} \right) = FJ(t) \quad (86)$$

and for case b :

$$\frac{3V^2}{8\pi} \left(\frac{1}{h^4} - \frac{1}{h_0^4} \right) = FJ(t) \quad (87)$$

3. NON-NEWTONIAN LIQUIDS

We shall examine the case of a non-Newtonian liquid whose flow follows de Waele-Ostwald's law:

$$\dot{\gamma} = \tau^n/k$$

According to the theory of Scott,⁵⁷ for case a

$$-\frac{dh}{dt} = \frac{1}{n+2} \left(\frac{3n+1}{2n\pi} \right)^n h^{n+2} \frac{F^n}{ka^{3n+1}} \quad (88)$$

or

$$\frac{n+2}{n+1} \left(\frac{2n\pi}{3n+1} \right)^n \left(\frac{1}{h^{n+1}} - \frac{1}{h_0^{n+1}} \right) a^{3n+1} = F^n \frac{t}{k} \quad (89)$$

If $n = 1$, equations (88) and (89) reduce to equations (81) and (82), respectively. If $\log(-dh/dt)$ is plotted against $\log h$, a straight line is obtained, and n is obtained from the slope, and η from the intercept on the ordinate.

By use of the relation $V = \pi a^2 h$ in equations (88) and (89), we obtain corresponding equations which hold for case b , namely

$$-\frac{dh}{dt} = \frac{\pi^{(n+1)/2}}{n+2} \left(\frac{3n+1}{2n} \right)^n h^{(5n+5)/2} \frac{F^n}{\eta V^{(3n+1)/2}} \quad (90)$$

and

$$\frac{n+2}{\pi^{(n+1)/2}} \left(\frac{2n}{3n+1} \right)^n \frac{2}{5n+3} V^{(3n+1)/2} \left(\frac{1}{h^{(5n+3)/2}} - \frac{1}{h_0^{(5n+3)/2}} \right) = F^n \frac{t}{\eta} \quad (91)$$

These equations reduce to equations (83) and (84). We may again plot $\log h$ against $\log(-dh/dt)$. It should be noted that if the slope is different from 3 or 5, respectively, it may be interpreted as either non-Newtonian flow or viscoelastic behavior. The correct interpretation is obtained from tests under different experimental conditions.

⁵⁷ J. R. Scott, *Trans. Inst. Rubber Ind.* **7**, 169 (1931).

XI. Coaxial Cylinder Viscometers with Axial Motion

An important group of instruments contain coaxial cylinders which move axially with respect to each other, the material being located in the space between the cylinders.

1. POCHETTINO VISCOMETER

We consider first the Pochettino viscometer, as in Fig. 20. The material occupies the space of length h between two coaxial cylinders of radii a and b . We will consider first the behavior of *Newtonian liquids*, and assume that one cylinder is fixed and that the other moves with a constant velocity V . Then from elementary considerations or from the Navier-Stokes equation we obtain for the rate of shear at radius r

$$\dot{\gamma} = \frac{V}{2 \ln (b/a)} \frac{1}{r}$$

The shear stress is thus

$$\tau = \eta \frac{V}{\ln (b/a)} \frac{1}{r},$$

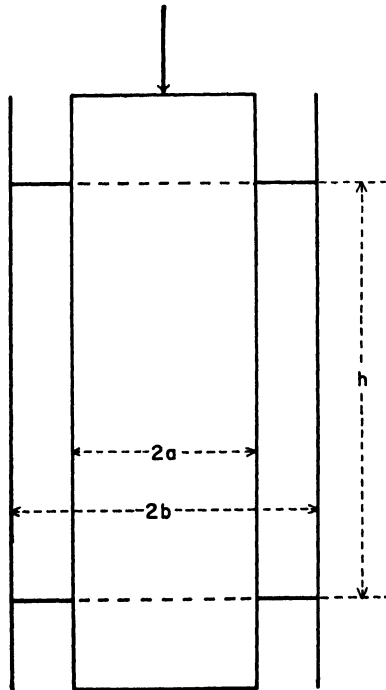


FIG. 20. Pochettino viscometer

from which the viscosity is obtained. This result can be generalized as in previous cases for the measurement of *linear viscoelastic behavior*. This arrangement is restricted to materials of high viscosity which do not flow appreciably under their own weight for the duration of the test.

2. PENETROMETER

The general arrangement of a penetrometer is as shown in Fig. 21. This may be considered as a modification of the Pochettino viscometer for materials of low viscosity. As a consequence of the closed ends of the cylinders, the displacement of the inner cylinder leads to a displacement in the opposite direction of the free surface. We will consider first the behavior of a *Newtonian liquid*, and derive the relationship between constant axial velocity V and axial force F acting on the inner cylinder, assuming that the outer cylinder is stationary and that the motion of the liquid between the cylinders is two-dimensional.

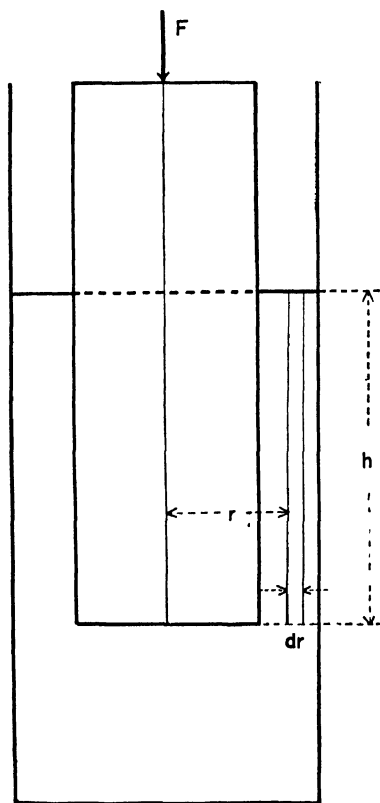


FIG. 21. Penetrometer

The force F is resisted by a tangential stress along the cylindrical surface, together with a pressure p acting axially on the immersed plane end. Let us consider an annulus of liquid of radii r and $r + dr$ and of length h as shown in Fig. 21. Then the rate of shear at radius r is dv/dr , where v is the axial velocity of the liquid. Thus the net shear force on the annulus is

$$\frac{d}{dr} \left(2\pi r h \eta \frac{dv}{dr} \right) dr$$

This is balanced by the hydrostatic pressure p acting on the lower end of the annulus. Thus⁵⁸

$$h\eta \frac{1}{r} \frac{d}{dr} \left(r \frac{dv}{dr} \right) + p = 0, \quad (92)$$

from which we obtain⁵⁹

$$v = -\frac{p}{4h\eta} r^2 + A \ln r + B$$

Now $v = V$ at $r = a$, and $v = 0$ at $r = b$, and also the volume of liquid displaced by the rod must equal the volume forced up around the rod, hence we obtain A , B , and p . The force F acting on the free end of the rod is given by

$$F = -2\pi a h \eta (dv/dr)_{r=a} + \pi a^2 p$$

Hence we obtain finally:

$$F = 2\pi h \eta \left(\ln \frac{b}{a} - \frac{b^2 - a^2}{b^2 + a^2} \right)^{-1} \quad (93)$$

It can be easily seen that the expression in the bracket is positive for any value of $b/a (>1)$. From equation (93), the viscosity η can be experimentally determined. Now since V is proportional to dh/dt , we see that at constant F , h^2 should vary linearly with time. Bikerman considered the case where the force was applied by the weight of the moving rod, and indicated how buoyancy is taken into account. Many technological instruments are similar in design to that in Fig. 21; however, because of complicated geometry, it is not possible to obtain fundamental rheological parameters with them.

3. OSCILLATING PENETROMETER

Let us assume in the above penetrometer that the applied force F varies sinusoidally with time. When it is permissible to neglect inertia of the liquid,

⁵⁸ J. J. Bikerman, *J. Colloid Sci.* **3**, 75 (1948).

⁵⁹ T. L. Smith, J. D. Ferry, and F. W. Schremp, *J. Appl. Phys.* **20**, 144 (1949).

then the force is in phase with the velocity, and the mechanical resistance R_M is given by

$$R_M = 2\pi h\eta \left(\ln \frac{b}{a} - \frac{b^2 - a^2}{b^2 + a^2} \right)^{-1} \quad (94)$$

We will consider finally the behavior of a material manifesting *linear viscoelastic behavior* in an oscillating penetrometer, in which F varies sinusoidally with time, as above. If the complex viscosity η^* defined as

$$\eta^* = \eta' - (iG'/\omega) = G^*/i\omega$$

is substituted for η in the above equation, we get the *mechanical impedance* Z_M (neglecting inertia of the liquid) and this can be measured by a suitable transducer.⁵⁹

If inertia is taken into account, then equation (92) becomes²⁵

$$h\eta^* \frac{1}{r} \frac{d}{dr} \left(r \frac{dv}{dr} \right) - i\omega\rho h v + p = 0,$$

from which we obtain finally for the mechanical impedance Z_M :

$$Z_M = i\omega m + \frac{K}{i\omega} + 2\pi h\eta^* \left(1 + i \frac{\omega\rho A}{\eta^*} \right) \left(\ln \frac{b}{a} - \frac{b^2 - a^2}{b^2 + a^2} \right)^{-1} \quad (95)$$

or

$$Z_M = i\omega m + \frac{K}{i\omega} + 2\pi h \frac{G^*}{i\omega} \left(1 - \frac{\omega^2\rho A}{G^*} \right) \left(\ln \frac{b}{a} - \frac{b^2 - a^2}{b^2 + a^2} \right)^{-1} \quad (96)$$

where m is the mass of the moving system and A is given by

$$A = -\frac{a^4}{2(a^2 + b^2)} - \frac{a^2}{2} \ln \frac{b}{a} + \frac{1}{24} \frac{(b^2 - a^2)^3}{(b^2 + a^2)^2} \left(\ln \frac{b}{a} - \frac{b^2 - a^2}{b^2 + a^2} \right)^{-1}$$

The first two terms on the right-hand side of these equations are due respectively to the inertia of the rod and the elastance of its support, which were neglected in the previous treatment. The third term is the same as in equation (94), except for the factor $(1 + i\omega\rho A/\eta^*)$ or $(1 - \omega^2\rho A/G^*)$. From the above equation the effect of inertia for the case of an inelastic *Newtonian liquid* can be accounted for by writing η for $\eta^* = G^*/i\omega$.

ACKNOWLEDGMENT

The author wishes to express his sincere thanks to Dr. H. Leaderman for valuable advice and criticism.

Nomenclature

A	Area; constant	C	Constant
B	Constant	D	$= 4Q/\pi R^3$

F_s	Stokes' resistance of a sphere	v	Velocity of liquid
$G(t)$	Shear relaxation modulus	α	Apex angle of a cone
G'	Dynamic shear modulus	α_n^2	$= \beta^2 - \kappa_n^2$
G^*	Complex shear modulus, $G^* = G' + i\omega\eta'$	β	Apex angle of an outer cone; $\beta^2 = \rho\omega^2/G^*$
G_{\dagger}^*	Complex shear modulus for damped oscillations, $G_{\dagger}^* = G' + (i\omega - \Delta)\eta'$	β_1^2	$= \rho(\omega + i\Delta)^2/G_{\dagger}^*$
G	$= G' + \eta' \partial/\partial t$	$\dot{\gamma}$	Rate of shear
G_i	Internal shear modulus	γ_n^2	$= \beta^2 - \kappa_n^2$
$ G $	$= (G'^2 + \omega^2\eta'^2)^{1/2}$	δ	Phase lag in forced oscillations
I	Moment of inertia	Δ	Damping factor in free oscillations
$J(t)$	Shear creep compliance	Δ_0	Damping factor in free oscillations in vacuo
K	Torsion constant of a wire; elastic constant	ϵ	Thickness of a thin lubricating layer
M	Torque	ϵ_n^2	$= \beta^2 - (n\pi/l)^2$
P	Pressure difference	η	Viscosity
Q	Volume of flow in unit time	η'	Dynamic viscosity
R	Radius of a capillary tube; Reynolds' number	η^*	Complex viscosity; $\eta^* = G^*/i\omega = \eta' - iG'/\omega$
R_0	Internal friction in a wire	η_l	Viscosity of a lubricating layer
R_M	Mechanical resistance	η_{pl}	Plastic viscosity
V	Volume; velocity of a rigid body	η_s	Viscosity derived from Stokes' law
Z_M	Mechanical impedance	θ	Angle between a radius vector and the z-axis
a	Radius of an inner cylinder (sphere) or a disk	ϑ	Angular displacement of an inner cylinder (sphere)
b	Radius of an outer cylinder (sphere)	ϑ_0	Complex amplitude of the angular displacement
c	Minor axis of an oblate spheroid	κ_n	n th positive root of the equation $J_1(\kappa b)Y_1(\kappa a) - Y_1(\kappa b)J_1(\kappa a) = 0$
$f(\tau)$	Flow curve, that is, rate of shear	ρ	Density of liquid
g	Acceleration of gravity	σ	Density of a sphere; $\sigma = a/b$
h	Depth of immersion of an inner cylinder; half thickness of a disk; distance between two parallel plates	τ	Shear stress
k	Constant in power law flow curve; $k = (\rho\omega/2\eta)^{1/2}$	τ_a	Tangential shear stress on the cylindrical surface of the inner cylinder
k	Body force per unit mass	τ_b	Tangential shear stress on the cylindrical surface of the outer cylinder
k_n	n th positive root of the equation $J_1(\kappa b) = 0$	τ_R	Longitudinal shear stress on the wall of a capillary tube
l	Length of a tube; end-gap	τ_f	Yield value
m	Kinetic energy correction factor; mass	ϕ	Azimuth
n	Couette correction factor	Φ	Dissipation function
p	Pressure; $p = 2l\tau_f/R$	φ	Angular displacement; fluidity
q	$= \partial_0/\psi_0 $	φ_0	Amplitude of the angular displacement
r	Distance; radius vector	φ_a	Apparent fluidity $\dot{\gamma}/\tau$ as usually defined
s	Ratio of radii of an outer and inner cylinder; $s = b/a$		
t	Time		
u	Displacement		

φ_c	Apparent fluidity defined for a capillary viscometer	ω	Angular velocity of a fluid particle around the axis of rotation; angular frequency
φ_s	Apparent fluidity defined for a rotating coaxial cylinder viscometer	ω_0	Angular frequency of free oscillations in vacuo
ψ	Angle of twist	Ω	Angular velocity of a rotating cylinder (sphere)
ψ_0	Amplitude of the angle of twist		

CHAPTER 3

VISCOSITY OF SUSPENSIONS OF ELECTRICALLY CHARGED PARTICLES AND SOLUTIONS OF POLYMERIC ELECTROLYTES

B. E. Conway and A. Dobry-Duclaux

I. Introduction	83
II. Simple Strong Electrolytes	85
III. Electroviscous Effects with Impermeable Macromolecular Particles	87
IV. Comparison of Theory with Experiment for the First Electroviscous Effect	92
V. The Second Electroviscous Effect	96
VI. Electroviscous Effects in the Close Approach of Macroscopic Bodies and in Sedimentation	98
VII. The Third Electroviscous Effect	99
1. Electrical Free Energy and Viscosity of Polyelectrolytes	99
2. Experimental Basis of the Third Electroviscous Effect	102
3. Concentration Effects in the Viscosity of Polyelectrolytes	106
4. Molecular Structure and Degree of Extension of Polyelectrolytes	115
5. Variation of Reduced Specific Viscosity with Rate of Shear	116
VIII. General Expression for the Electroviscous Effects	119
Nomenclature	120

I. Introduction

The presence of electric charges on particles, either in suspension or in solution, imposes certain energetic restrictions on the relative positions of the particles in addition to the usual requirement that one particle cannot occupy the effective volume taken up by another particle. When a fluid containing particles distinct from those comprising the fluid itself, is subjected to shear, there is an extra dissipation of energy in proportion to the rate of shear and to the volume fraction of suspended or dissolved particles, such that the relative viscosity η/η_0 can be written, according to Einstein,¹ as

$$\eta/\eta_0 = 1 + 2.5\phi \quad (1)$$

where ϕ is the ratio of volume of solute particles to the total volume of the solution, η is the viscosity of the solution, and η_0 that of the pure solvent

¹ A. Einstein, *Ann. Physik* **19**, 289 (1906); **34**, 591 (1911).

at the same temperature. It is useful to recall the assumptions on which equation (1) is based, as this equation forms the basis of other equations in which electrical effects are considered.

In equation (1) it is assumed that (a) the suspended particles are large compared with solvent molecules but small compared with the dimensions of the measuring apparatus; (b) the suspended particles are spherical, rigid, and wetted by the solvent; (c) the suspension is sufficiently dilute that no particle causes disturbance to the hydrodynamic flow of solvent past another particle; (d) the effects of gravitation, and inertia and turbulence of solvent are negligible. Experimental tests of equation (1) have been performed by Eirich *et al.*,^{2, 3} using glass spheres and certain spherical spores and fungi and the validity of the concentration dependence coefficient of 2.5 has been demonstrated. The analysis for the case of finite concentrations has been made theoretically by Guth and by Guth and Simha⁴ and later by Vand⁵ who allowed for increments to the viscosity due to hydrodynamic interaction and to doublets formed by shear-induced two-body collisions.

The following type of equation was derived

$$(\eta - \eta_0)/\eta_0\phi = \alpha_0 + \alpha_1\phi$$

α_0 is the Einstein coefficient, and the interaction coefficient α_1 is found to be 7.35. In the derivation of this equation Vand assumed that the spheres participating in two-body collisions, rolled over each other along an arc of a great circle on each sphere and separated when the line joining their centers was perpendicular to the direction of flow. From this mechanism, the collision frequency, the mean life of the doublet, and hence the steady state concentration of doublets were calculated, and allowance was made for their contribution to the viscosity of the suspension. Direct experimental measurements of this effect by Manly and Mason⁶ with pyrex glass microspheres showed, however, that the doublet lifetime and hence the steady state concentration were exactly twice that calculated by Vand. This discrepancy arises since it is found experimentally that the spheres forming doublets do not roll over one another but rotate as a unit. Allowance for this in the theory gives $\alpha_1 = 10.05$. Later experiments by Manly

² F. R. Eirich, *Repts. Progr. Phys.* **7**, 329 (1940).

³ F. Eirich, M. Bunzl, and H. Margaretha, *Kolloid-Z.* **74**, 276 (1936); F. Eirich, and O. Goldschmidt, *ibid.* **81**, 7 (1937).

⁴ E. Guth, *Kolloid-Z.* **74**, 147 (1936); E. Guth and R. Simha, *ibid.* **74**, 266 (1936); see also H. C. Frisch and R. Simha, in "Rheology: Theory and Applications" (F. R. Eirich, ed.), Vol. 1, Chapter 14. Academic Press, New York, 1956.

⁵ V. Vand, *J. Phys. & Colloid Chem.* **52**, 277, 300 (1948); see also T. Duclaux, *Compt. rend.* **223**, 836 (1946).

⁶ R. S. J. Manley and S. G. Mason, *Can. J. Chem.* **32**, 763 (1954).

and Mason⁷ with smaller spheres than those used in their previous work⁶ gave values of $\alpha_1 = 12.7$, the Einstein coefficient being in all cases close to 2.5.

Deviation from the behaviour represented by equation (1) occurs when the particles (a) are nonspherical and assymmetric,^{4, 8} (b) interfere with one another at high concentrations, (c) bear electric charges. Effects due to (c) in relation to both (a) and (b) are the focus of attention in this review.

II. Simple Strong Electrolytes

Poiseuille⁹ was the first to observe in 1847 that the viscosity of electrolytic solutions differed from that of the solvent. Further work was carried out by Arrhenius, Gruneisen, and Schneider and, more recently, accurate data of Jones and Dole¹⁰ were shown to be represented by an equation of the form

$$\eta = \eta_0[1 + A\sqrt{c} + (A^2 - B)c + \dots] \quad (2)$$

where A is zero for nonelectrolytes and positive for all strong electrolytes, and B can be positive or negative but is negative for most salts.

Rearranging equation (2) gives the reduced specific viscosity

$$\frac{(\eta/\eta_0) - 1}{c} = \text{constant} + A/\sqrt{c}, \quad (3)$$

so that, at low concentrations, the *relative* contribution of the ions to the viscosity of the solution *decreases* with increasing concentration, as shown in Fig. 1.

The theory of viscosity of simple electrolytes was first considered by Falkenhagen¹¹ and Falkenhagen and Dole¹² and developed in a general form by Onsager and Fuoss.¹³ It is convenient to summarize the basis of this theory, since the factors giving rise to a concentration-dependent reduced viscosity for simple electrolytes are essentially similar to those which determine the electrical contribution to the viscosity of electrically charged particles of colloidal dimensions.

In any solution of charged particles there are nonuniform zones of distribution of charges, and in an ionic solution each ion is surrounded by an atmosphere of ions having a net charge of opposite sign to that of the

⁷ R. S. J. Manley, and S. G. Mason, *J. Colloid Sci.* **1**, 354 (1952).

⁸ H. B. Bull, *Trans. Faraday Soc.* **36**, 80 (1940).

⁹ J. L. M. Poiseuille, *J. chim. phys.* **21**, [3], 76 (1847).

¹⁰ G. Jones and M. Dole, *J. Am. Chem. Soc.* **51**, 2950 (1929).

¹¹ H. Falkenhagen, *Physik Z.* **30**, 611 (1929).

¹² H. Falkenhagen and M. Dole, *Z. physik. Chem. (Leipzig)* **B6**, 159 (1929).

¹³ L. Onsager and R. M. Fuoss, *J. Phys. Chem.* **36**, 2689 (1932).

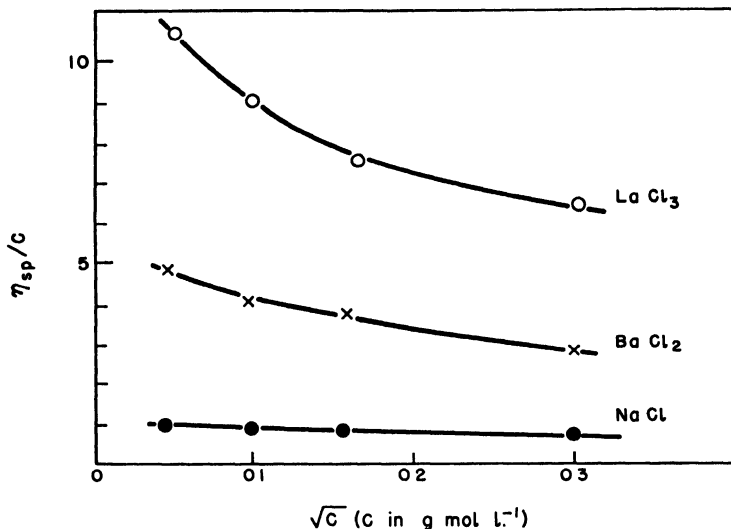


FIG. 1. Reduced viscosity of electrolyte solutions as a function of concentration

central ion. Deformation of these ionic atmospheres by a velocity gradient in the solution gives rise to dissipation of extra energy in the solution. In the unperturbed fluid, the ionic atmosphere has spherical symmetry and an effective radius of $1/\kappa$ where

$$\kappa = \left(\frac{4\pi e^2 N_A}{1000 \epsilon k T} \sum_1^i c_i z_i^2 \right)^{1/2}$$

and e is the electronic charge, N_A Avogadro's number, ϵ the dielectric constant of the solution, and other terms have their usual significance. In a velocity gradient of dv_x/dy , where v_x is a velocity in the direction of the x -coordinate and y is the direction across which the gradient exists, a stationary net deformation of the ionic atmosphere will prevail depending on the rates of deformation and relaxation. If the relaxation time of the ionic atmosphere is τ , a stationary deformation $\tau(dv_x/dy)$ will prevail. Now $\tau = \rho_i/\kappa^2 k T$ where ρ_i is the frictional coefficient of an ion i , so that the average deformation will be

$$\frac{\rho_i (dv_x/dy)}{\kappa^2 k T}.$$

The forces between two ions of charge e at a distance $1/\kappa$ are $e^2 \kappa^2/\epsilon$ and the total transfer of force between the ion and its atmosphere is $1/\kappa$ times this force, that is, $e^2 \kappa/\epsilon$. The order of magnitude of the stress transferred between the ion and its atmosphere is then this transfer of force multiplied

by the displacement of the ionic atmosphere, that is,

$$\text{stress} = \frac{e^2 \rho_i}{\kappa \epsilon k T} \left(\frac{dv_x}{dy} \right)$$

which gives, upon substituting the value of κ^2 , the electrostatic contribution to the stress as

$$\text{stress} \sim \kappa \rho_i \left(\frac{dv_x}{dy} \right) \quad (4)$$

or from the more rigorous general treatment,

$$\text{stress} = \frac{1}{480\pi} \kappa \rho_i \left(\frac{dv_x}{dy} \right) \quad (5)$$

Defining viscosity as stress transferred per unit velocity gradient leads to the electrostatic contribution to viscosity of the solution as

$$\eta_e = \kappa \rho_i / 480\pi \quad (6)$$

which is the behavior found experimentally¹⁰ at low concentrations, since κ is proportional to the square root of the ionic strength. The above is essentially the simplest case of an electroviscous effect.

III. Electroviscous Effects with Impermeable Macromolecular Particles

The hydrodynamic behavior of spherical particles of colloidal dimensions has been discussed with reference to equation (1). When the colloidal particles carry electrical charges, as is usually the case in practice, there is a distribution of gegen-ions about the particle in the same way as with simple electrolytes. The distortion of this ionic atmosphere gives rise to an electrostatic contribution to the viscosity of the suspension having, in principle, the same origin as in the case of simple electrolyte solutions.

The electrostatic contribution to viscosity (the so-called electroviscous effect) of charged colloidal particles was first examined by von Smoluchowsky¹⁴ in 1916, who extended the Einstein equation to allow for electrical effects in a flowing solution of charged spherical particles and gave the following equation, without derivation, for the viscosity η of such a suspension

$$\eta = \eta_0 \left\{ 1 + 2.5\phi \left[1 + \frac{1}{\lambda \eta_0 a^2} \left(\frac{\zeta \epsilon}{2\pi} \right)^2 \right] \right\} \quad (7)$$

where η_0 is the viscosity of the solvent, ϵ its dielectric constant, λ the specific conductivity of the suspension,^{14a} a the radius of the particles (assumed

¹⁴ M. von Smoluchowsky, *Kolloid-Z.* **18**, 190 (1916).

^{14a} The relevant conductivity to be used here is somewhat obscure. Near the col-

spherical), ζ the electrokinetic potential, and ϕ the volume fraction of solute in the suspension. The derivation of the above equation, except for a numerical factor of 1.5 in the numerator of the coefficient of $(\zeta\epsilon/2\pi)^2$, was first given by Krasny-Ergen in 1936.¹⁵ Both equations are derived on the assumption that the particles are sufficiently far away from one another, i.e., in dilute solutions, so that no mutual interaction of double layers occurs.

By comparison with equation (1), it is seen from equation (7) that the increase of viscosity over that of the solvent, on account of electrical forces, is

$$\frac{2.5\phi}{\lambda a^2} \left(\frac{\zeta\epsilon}{2\pi} \right)^2$$

Since the ζ -potential at an interface diminishes with increase of ionic strength, whilst λ increases, the electrical contribution to the viscosity of the suspension must decrease with added salts. The qualitative observation of this behaviour originally gave rise to the term "electroviscous effect" in work on colloidal solutions of natural substances, such as that of Kruyt in 1921 and later in a series of researches by Bungenberg de Jong *et al.*,¹⁶ Loeb,¹⁷ and Hammarsten.¹⁸ However, it is doubtful if the class of substances examined in their work was that to which the classical theory of von Smoluchowsky could be applied.

The electroviscous effect of von Smoluchowsky arises on account of displacement in a velocity gradient, of the effective center of gravity of the gegen-ions in the double layer from a point coincident with the center of gravity of the spherical colloidal particle. During flow, the equilibrium spherical symmetry of the double layer is distorted and gives rise to extra dissipation of energy because of the disturbance of the electrical interaction between the ions in the double layer and charges on the surface of the colloidal particle. The displacement of the ionic atmosphere can be regarded as giving rise to local electric currents of an electrophoretic type, leading

loidal particles the conductivity may not have the same value as the mean over the whole solution, because of the nonuniform ionic concentration in the double layers of the particles; see also p. 95.

¹⁵ W. Krasny-Ergen, *Kolloid-Z.* **74**, 172 (1936).

¹⁶ H. R. Kruyt and H. G. Bungenberg de Jong, *Z. physik Chem. (Leipzig)* **100**, 250 (1921); *Kolloidchem. Beih.* **27**, 1 (1928); for gum arabic see H. R. Kruyt and H. J. C. Tendeloo, *Kolloidchem. Beih.* **29**, 396 (1929); for starch see H. G. Bungenberg de Jong, *Rec. trav. chim.* **43**, 189 (1924); for sodium thymonucleate see *ibid.* **31**, 89 (1930); H. G. Bungenberg de Jong and N. F. De Vries, *ibid.* **49**, 658 (1950).

¹⁷ J. Loeb, "Proteins and the theory of colloidal behaviour," McGraw-Hill, New York, 1922.

¹⁸ E. Hammarsten, *Biochem. Z.* **144**, 383 (1924).

to extra dissipation of energy and hence to an augmentation of viscosity of the solution. Examination of equation (7) shows that a measurable electroviscous effect would not be expected unless the particles were very small, of the order of 5×10^{-6} cm. in radius. This limitation necessarily conflicts with the assumption made in the derivation of the equation, that the effective thickness of the double layer is small compared with the radius of the central colloidal particle. With particles of this size, the assumptions of the theory are only met if the ionic strength is greater than approximately 0.01, which imposes severe experimental limitations. The limitations of particle size were for a long time an obstacle to the verification of the classical equations for the electroviscous effect. Particles of 500 Å could not, at that time, be seen directly, and independent knowledge of their dimensions and symmetry was not available. Use of concentrated solutions, where the electroviscous effects might more easily be examined, is excluded by the requirements in the development of the theory that no overlapping or interaction of double-layers of neighboring particles should occur.

A number of improvements on the von Smoluchowsky-Krasny-Ergen theory have been made in more recent years. The classical theory was limited in that calculations were made for a relatively noncurved double layer, and also no account was taken of the reciprocal action of the cataphoretic potential upon the macroscopic flow of the liquid,¹⁸ which approximation is valid only if the solution is a good conductor. Finkelstein and Cursin¹⁹ developed the theory of the first electroviscous effect by allowing for (i) the diffuse distribution of ions in the ionic atmosphere of the colloidal particle, (ii) the curvature of the double layer, and (iii) the reciprocal effect of the cataphoretic potential on the flow of the liquid. The disturbance of ideal flow behaviour on account of Brownian motion of the particle was not considered. Other assumptions common to the Einstein and von Smoluchowsky treatments were accepted. By integration of the Poisson-Boltzmann equation by a method of successive approximations, the following essential result for the viscosity of the charged suspension was obtained:

$$\eta = \eta_0 \left\{ 1 + 2.5\phi \left[1 + \frac{77}{25} \cdot \frac{z^2 e^2 \bar{p}}{\pi \epsilon k T (\kappa a)^4 a^2 \eta_0} \right] \right\} \quad (8)$$

where \bar{p} is the mean frictional coefficient of the ions, κ the Debye-Hückel reciprocal thickness of the double layer, and ze the charge on the colloidal particle. Substituting the value

$$\zeta = ze / \epsilon \kappa a^2$$

¹⁹ B. N. Finkelstein and M. P. Cursin, *Acta Physicochim. U.R.S.S.* **17**, 1 (1942).

gives

$$\eta = \eta_0 \left\{ 1 + 2.5\phi \left[1 + \frac{77}{25} \cdot \frac{\epsilon \bar{\rho} \zeta^2}{\pi (\kappa a)^2 k T \eta_0} \right] \right\} \quad (9)$$

Numerical comparison between the predictions of equations (9) and (7) under the same conditions of ionic concentration, temperature, and ζ potential, indicates that equation (9) gives an electroviscous contribution about five times that given by equation (7).

The most useful and satisfactory calculations of the first electroviscous effect have been made by Booth²⁰ without the limiting assumption made by von Smoluchowsky that the double layer is thin compared with the radius of the central particle. The Einstein equation is developed as a power series of the charge Q on the particle as

$$\eta = \eta_0 \left[1 + 2.5\phi \left(1 + \sum_1^{\infty} a_n Q^n \right) \right] \quad (10)$$

and a_n is the coefficient of the n th term in Q . Since Q can be expressed in terms of ζ , the following general equation is obtained

$$\eta = \eta_0 \left\{ 1 + 2.5\phi \left[1 + \sum_1^{\infty} b_n \left(\frac{e\zeta}{kT} \right)^n \right] \right\} \quad (11)$$

where b_n is now the coefficient of the n th term in $e\zeta/kT$. Evaluation of the general equation (11) in terms of ionic and solution parameters was made using the method of Fröhlich and Sack²¹ in which is determined the coefficient of viscosity which a volume of uniform fluid would have, if it exhibited the same stress-strain relationships at the surface of a representative spherical volume of solution (much greater in radius than that of the colloidal particle) as would a similar volume of the actual suspension.

The usual hydrodynamic assumptions are made:^{21a} inertia terms are neglected and there is no turbulence; also it is assumed that there is no slip and the liquid is incompressible. The following assumptions are made about conditions at the solid-solution interface. (i) The thickness of the surface phase^{21b} containing the surface charge is very much less than the radius of the particle. (ii) Ions or charges in the surface phase are immobile, i.e., cannot move laterally across the surface. This assumption is probably only valid for proteins where there is definite localization of ionogenic

²⁰ F. Booth, *Proc. Roy. Soc.* **A203**, 533 (1950).

²¹ H. Fröhlich and R. Sack, *Proc. Roy. Soc.* **A185**, 415 (1946).

^{21a} Compare D. C. Henry, *ibid.* **A133**, 106 (1931).

^{21b} The term "surface phase" is defined here as the region near the interface of the particle, which contains the charge. It must presumably be identified with that part of the particle contained in the region corresponding to the outermost 2-3 Å of the radius of the particle.

sites, or for particles where surface heterogeneity leads to localisation of adsorption of ions at certain sites. (iii) The surface charge density at any point remains fixed and unchanged when the electrolyte solution moves. (iv) The potential difference across the surface phase is also unaffected by motion in the liquid. (v) The average distance between the colloidal particles is much greater than the double layer thickness, so that no interaction of double layers (cf. Section V) can occur. No restrictions are placed, however, on the effective radius of the double layer compared with that of the colloidal particle. (vi) The particles are nonconducting spheres. Mathematical development²⁰ of equation (11) leads to

$$\eta = \eta_0 \{ 1 + 2.5\phi [1 + q^* (e\zeta/kT) Z(b) \cdot (1 + b)^2] \} \quad (12)$$

where

$$q^* = \epsilon kT \sum_i n_i z_i^2 u_i^{-1} / \eta_0 e^2 \sum_i n_i z_i^2$$

in which u_i is the ionic mobility of the ions of type i , and $b = \kappa a$, where κ is the reciprocal double layer thickness as defined previously and a is the radius of the colloidal particle. $Z(b)$ is a function of b evaluated numerically and two useful limiting conditions can be formulated: when b is small

$$Z(b) = \frac{1}{200\pi b} + \frac{11b}{3200\pi}$$

and when b is large $Z(b) = \frac{3}{2}\pi b^4$. For a given charge or potential, when b is small, the electrostatic contribution to the viscosity increases approximately as b^{-1} . The more diffuse the double layer (that is, $1/\kappa$ is large) the more is the expected distortion since the double layer then extends into relatively faster flowing regions of the solution; the electroviscous effect is then larger. When b is large (thin double layer), the electrostatic contribution to the overall viscosity tends to zero, since the double layer charge is concentrated near the ion and suffers little distortion because the relative velocity of the flowing fluid near the ions is small. Booth points out that this situation is in contradiction to the classical theories since they apply specifically to thin double layers and predict considerable electroviscous effects for this case. The discrepancy arises from two inadequate assumptions in Krasny-Ergen's theory: (i) The distortion of the initially spherically symmetric double-layer field by the flow of solution causes local electric currents in the electrolyte. In the calculation of the electric energy dissipated in this process the contribution from diffusion due to gradients of chemical potential in addition to those of electrical potential, was neglected. (ii) There is an inconsistency between the equation for the distortion ($\Delta\psi$) of the potential corresponding to the distortion of the initially spherically

symmetric field, and the boundary conditions for the derivative of $\Delta\psi$ with respect to distance from the center of the colloidal particle. The important difference between Booth's theory and earlier theories is that a much lower magnitude of the electroviscous effect is predicted, which is more in accord with experiment (see below).

IV. Comparison of Theory and Experiment for the First Electroviscous Effect

The first attempt at a direct comparison between theoretical predictions of the von Smoluchowsky-Krasny-Ergen theory and experimental data was made by Bull⁸ who attributed the change of viscosity of protein solutions with degree of ionization of the protein, to electroviscous effects. Using ovalbumin, Bull found an electroviscous effect which varied with the apparent ζ -potential at concentrations of less than 1% protein in aqueous solution, but its magnitude was some 90 times less than that predicted by the theory. The protein used by Bull did not completely fulfill the requirements of the classical theory of the electroviscous effect. For example, ovalbumin is not spherical but ellipsoidal with an axial ratio of about 3.5:1; and the Einstein equation does not hold, as is experimentally observed; also, only in the presence of a considerable concentration of neutral salt, will the double layer thickness be less than the "radius" of the protein molecule, as required theoretically. Despite these limitations, the discrepancy between experiment and theory is probably significant. Comparison with the behavior predicted by Booth's theory is more relevant, since here the limitation due to relative double layer thickness is absent. Again, direct comparison is not possible since Bull's data are given in terms of specific conductivity of the whole solution whereas Booth's equation requires knowledge of the individual mobilities of all ions present. However, if all mobilities are assumed equal, as an approximation, a comparison is possible. Booth's equation then becomes

$$\eta = \eta_0 \left\{ 1 + 5.2\phi \left[1 + \frac{1}{\lambda\eta_0 a^2} \left(\frac{\zeta\epsilon}{2\pi} \right)^2 \pi b^2 (1+b)^2 Z(b) \right] \right\} \quad (13)$$

which differs from that given by the classical theories by the factor

$$\frac{5.2}{2.5} \pi b^2 \cdot (1+b)^2 Z(b)$$

in the electroviscosity term. The numerical term (5.2/2.5) arises since Bull found at the isoelectric point that $\eta = \eta_0 (1 + 5.2\phi)$ instead of the Einstein form $\eta = \eta_0 (1 + 2.5\phi)$. The difference in the coefficient of ϕ arises because ovalbumin is anisometric. Table I gives the electrostatic contributions to viscosity of the albumin solution calculated from the equations of Booth

TABLE I
CALCULATED AND OBSERVED VALUES OF THE ELECTROVISCOUS
EFFECT (η_0) WITH OVALBUMIN

pH	Parameter "b"	η_0 Observed	η_0 Krasny-Ergen	η_0 Booth
No NaCl				
5.25	0.0186	0.6	60	0.01
6.62	0.00135	2.9	543	0.02
7.72	0.00594	3.9	934	0.02
9.65	0.0504	4.6	1299	0.2
10.20	0.1661	4.3	1126	0.8
10.85	0.3570	3.2	645	1.4
11.16	0.501	2.5	424	1.55
With 0.01 N NaCl				
5.71	0.7892	0.4	1.44	0.1
7.38	0.7892	0.6	37.3	0.3
8.82	0.7892	0.5	103.5	0.75
10.60	0.8333	0.3	90.8	0.7

and Krasny-Ergen, and compared with experiment. It is seen from Table I that the agreement between experimental results and the figures predicted by Booth's equation is much better than that obtained when comparison is made with the results from the classical theory, particularly at higher pH or in the presence of salt. Some errors in the "b" values used in the equation occur on account of uncertainties in the ionic composition and concentration of Bull's suspensions. If allowance could be made for the uncertain factors better agreement with experiment would be obtained.²⁰ Thus, in the salt-containing solutions, where the ionic composition and concentration are more exactly defined, better agreement is obtained. Allowance must also be made for the fact that the protein is asymmetric. The theory is a striking improvement over the classical theories.

The second attempt at verification of the von Smoluchowsky-Krasny-Ergen theory was made by Briggs²² and Briggs *et al.*^{23, 24} using gum arabic, sodium caseinate, and β -lactoglobulin. If, in equation (7), ζ , η_0 , and λ are made to vary, whereas ϕ and a are kept constant, it should be possible from measured values of ζ , η and λ to test the accuracy of equation (7) by plotting $1/\eta$ against $\zeta^2/\lambda(\eta - \eta_0)$. If equation (7) is correct in form, a straight line will be obtained, whose intercept on the $1/\eta$ axis will give $1/K\phi$ (where K is the constant 2.5 in the Einstein equation) and from whose slope the radius of the particle can be calculated if a value of the effective

²² D. R. Briggs, *J. Phys. Chem.* **45**, 866 (1941).

²³ C. R. Hankinson and D. R. Briggs, *J. Phys. Chem.* **45**, 943 (1941).

²⁴ D. R. Briggs and M. Hanig, *J. Phys. Chem.* **48**, 1 (1941).

dielectric constant^{24a} of the solution is assumed. The treatment here assumes that the volume fraction of solute is constant with varying salt content. Experimentally, with gum arabic, approximately straight lines are obtained for the above plots at zero or low salt content of the solution, but at higher concentrations deviations from linearity occur. Values of $1/K\phi$ vary, however, with concentration of colloid and with salt concentration and the apparent radius decreases as the colloid and/or salt concentration increases.

Similar effects are found with sodium caseinate. With β -lactoglobulin, $K\phi$ is constant with varying pH and salt content indicating, for this substance, a relatively constant effective volume compared with that exhibited by gum arabic or sodium caseinate. The change in viscosity of β -lactoglobulin is thus primarily due to the first electroviscous effect and not due to change in effective volume of the colloid. Qualitatively, therefore, for proteins which approximately meet the conditions for applicability of the classical theories, agreement between the *form* of the experimental and theoretical results is found; but, numerically, predictions from the classical theories are much larger than those found experimentally. Tests of the theories using gum arabic or sodium caseinate (which exhibits non-Newtonian viscosity at relatively low concentrations) are probably without any justification as the morphology of colloids of this kind in solution does not approach that assumed in the theories being examined. Gum arabic and sodium caseinate are more related to the thread-like polyelectrolytes discussed in a subsequent section. It is of interest that the qualitative conclusions of Brigg's work anticipated those given later by Fuoss *et al.*²⁶ using well characterized synthetic polyelectrolytes, although salt effects on the viscosity of sodium polyacrylate had been observed previously by Kern.²⁷

The limitations of the use of hydrophilic colloids illustrate a general difficulty in testing the theories of the electroviscous effect. It is difficult to find an aqueous suspension which satisfies simultaneously all the conditions required by the present theories, viz., that the particles must be (i) spher-

^{24a} Allowance for field effects on the dielectric constant of the solution in the electric double layer at an interface, due to dielectric saturation have been calculated by Conway *et al.*²⁵ for a number of conditions of interfacial potential difference and ionic strength.

²⁵ B. E. Conway, J. O'M. Bokris and I. A. Ammar, *Trans. Faraday Soc.* **47**, 756 (1951).

²⁶ R. M. Fuoss and U. P. Strauss, *Ann. N. Y. Acad. Sci.* **51**, 836, (1949); *J. Polymer Sci.* **3**, 602 (1948).

²⁷ W. Kern, *Z. physik. Chem. (Leipzig)* **A181**, 249 (1938); **A181**, 283 (1938); *Angew. Chem.* **51**, 566 (1938).

ical,^{27a} (ii) insulating, (iii) insoluble, (iv) rigid, (v) unable to swell, (vi) stable over a period of time and in the presence of electrolytes, (vii) with a radius less than 1×10^{-5} cm., and also meet the other conditions listed on pp. 84 and 90.

The first attempt to examine the applicability of the von Smoluchowsky-Krasny-Ergen theory with suspensions designed to meet the above requirements more satisfactorily was made by Dobry,²⁸ using a suspension of spherical nitrocellulose particles of average diameter 3×10^{-6} cm. in water. The particles were charged only because of adsorption of ions. Dobry was unable to verify the von Smoluchowsky effect and suggested possible causes for the discrepancy, e.g., the uncertainty in calculation of the ζ -potential from electrophoretic mobilities using the macroscopic value of the dielectric constant of water (cf. reference 25 and p. 94) and the fact that it is not clear in the classical theory exactly to what part of the solution the specific conductivity term (cf. p. 87) should refer, i.e., to the whole suspension or the liquid immediately surrounding the particles. Dobry²⁸ has also pointed out the limited validity of Stokes' law for charged particles bearing double layers.

Further work has been carried out by Dobry²⁹ using silicon carbide particles and, although a decrease of viscosity of the suspension by added KCl was observed, the classical equation was not found to be applicable. Work on an aged sample 13 years old and of high purity gave a diminished electroviscous effect. However, when carrying an adsorbed monolayer of silicic acid, the suspension exhibited an electroviscous effect which, contrary to the von Smoluchowsky theory and the findings of Briggs *et al.*²²⁻²⁴ with β -lactoglobulin, depended on the *logarithm* of the solution conductivity and not on the conductivity. Such a system is complex and probably does not meet the assumptions of the theory. Further work has been carried out with hydrophobic suspensions of carbon-black by Donnet³⁰ and with AgI by Overbeek *et al.*³¹ The dependence of the "constant" K in the Einstein equation upon dielectric constant of the medium has been examined by Donnet and Marquier³² by addition of ethanol to aqueous suspensions and by raising the temperature. Experiments such as these are not definitive

^{27a} Modern electron-micrographic techniques enable experiments to be made in order to examine if particles in suspensions fulfill this condition, particularly in the case of inorganic hydrophobic sols.

²⁸ A. Dobry, *J. Chim. Phys.* **47**, 402 (1950); **52**, 814 (1955).

²⁹ A. Dobry, *J. chim. phys.* **48**, 28 (1951).

³⁰ J. B. Donnet, *Compt. rend.* **242**, 1169 (1956).

³¹ G. J. Harmsen, J. V. Schooten and J. Th. G. Overbeek, *J. Colloid Sci.* **8**, 64, 72 (1953).

³² J. B. Donnet and P. Marquier, *Compt. rend.* **242**, 771, 1042 (1956).

of a direct relationship to the dielectric constant of the suspension, since simultaneous alterations of the microscopic structure of water^{33, 34} by ethanol addition or increase of temperature, although related to change of the dielectric constant, are unavoidable.

Later work by Dobry³⁵ with five suspensions of spherical ionized particles indicated apparent applicability of the classical theory only when the thickness of the double layer was of the same order as the radius of the particle. Since this is *not* the condition assumed in the derivation¹⁵ of the equation, the results of Dobry again throw doubt on the validity of equation (7). Other work has been done using hydrated thorium oxide.³⁶

V. The Second Electroviscous Effect

In the derivation of equations to represent the first electroviscous effect, it has been assumed that the particles are on the average much further apart than twice the effective radius of the ionic atmospheres of the particles. When this condition is not fulfilled and overlapping of double layers occurs at relatively high concentrations of colloid, an enhancement of viscosity due to electrical repulsion of the double layers occurs and was first examined by Harmsen and co-workers³¹ using AgI sols and also observed by Dobry³⁵ in suspensions of ferric hydroxide, gamboge, and particles of a copolymer of crotonic acid and vinyl acetate. This effect, designated as the *second* electroviscous effect, increases in proportion to the square of the particle concentration, thereby confirming its origin as due to particle interaction, and increases, at constant colloid concentration, with decrease of ionic strength, since under these conditions the effective radius of the double layers increases and interaction by overlapping of double layers is therefore more probable.

The effect arises as follows: in the range of high concentrations of colloid, the particles in the flowing liquid, e.g., *A* and *B* in Fig. 2, have to pass one another. This is only possible if the particles are also displaced in a direction perpendicular to the lines of flow of the liquid. The displacement has been calculated in the case of uncharged particles by Vand and Duclaux³⁷ and causes an extra dissipation of energy. Since the effect depends on the frequency of near encounters between particles, the extra viscosity is proportional to the second and higher powers of the concentration, *i.e.*, the Einstein constant apparently varies with concentration, Fig. 3. When the particles

³³ J. D. Bernal and R. H. Fowler, *J. Chem. Phys.* **1**, 515 (1933).

³⁴ B. E. Conway and J. O'M. Bockris, "Modern Aspects of Electrochemistry" (J. O'M. Bockris, ed.), Chapter 2. Academic Press, New York, 1954.

³⁵ A. Dobry, *J. chim. phys.* **52**, 809 (1955).

³⁶ A. Dobry, *J. chim. phys.* **50**, 507 (1953).

³⁷ V. Vand, *J. Phys. & Colloid Chem.* **52**, 277, 300 (1948); T. Duclaux, *Compt. rend.* **223**, 836 (1946).

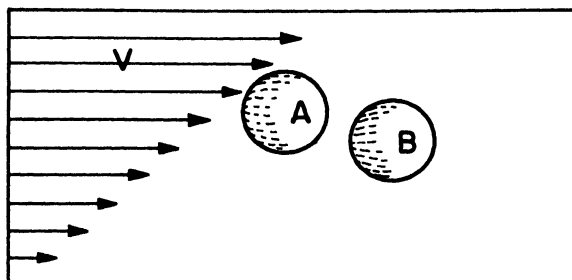


FIG. 2. Approach of two spheres, illustrating origin of the second electroviscous effect

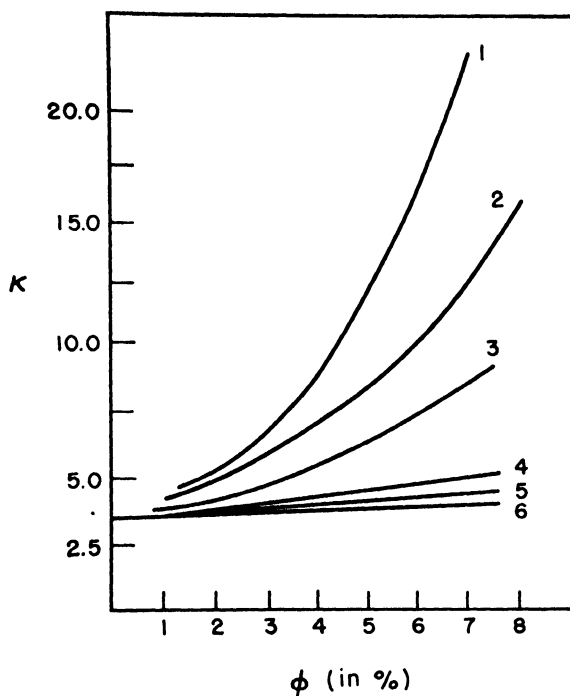


FIG. 3. Apparent dependence of the Einstein coefficient K upon volume fraction ϕ of AgI in dilute nitric acid. Key: 1, 0.035 mg. ion per liter of hydrogen ions; 2, 0.12; 3, 0.49; 4, 2.3; 5, 15.0; 6, 39.0. From Harnsen *et al.*³¹

are charged, the extra displacements will occur over a distance of the order of the radius of the ionic atmosphere of the particles. The electroviscous effect due to the double layer interaction will thus be relatively greater and more easily observed when the double layer thickness is greater than or equal to the particle radius. The effect is thus particularly strong

with small particles,³⁵ and low ionic strengths will therefore favor the presence of the second electroviscous effect.

With AgI sols exhibiting the second electroviscous effect, non-Newtonian behavior is also observed.³¹ This is explained³¹ as follows: the displacement of the particles in passing one another is due to repulsion and the total displacement will be less, the more rapidly the particles pass. Consequently, at high rates of shear the extra dissipation of energy, and hence the enhanced viscosity, will be smaller.

VI. Electroviscous Effects in the Close Approach of Macroscopic Bodies and in Sedimentation

A number of phenomena arise when macroscopic bodies approach each other closely (i.e., to within about 5×10^{-6} cm.), e.g., two parallel plates, or a sphere and a plate. Also in narrow capillaries hydrodynamic properties of liquids, particularly if they are ionic solutions, are anomalous.³⁸

The rate of approach of a sphere under gravity towards a plate or the rate of approach of two parallel plates is very slow at the above distances of separation and is experimentally found to be much slower in electrolyte solutions, an effect which diminishes with increasing ionic strength. These effects are due to the electrical contributions to the viscosity of the medium between the plates. These contributions become greater when bodies approach each other more closely and interaction of their double layers occurs. The origin of the effect is thus, in principle, similar to that giving the second electroviscous effect.

For the close approach of two parallel plates at a separation of $2l$, Elton³⁹ has calculated the apparent viscosity η_a of the medium between the plates, which differs from the normal macroscopic viscosity of the medium on account of electrical interaction between the double layers of the surfaces in close proximity.

Denoting by η the normal viscosity of the medium, by ζ the zeta potential at the phase boundary and by κ the reciprocal radius of the double layer, the apparent viscosity between the plates is

$$\eta_a = \eta + \frac{3\epsilon\zeta^2}{32\pi^2\lambda l^3} (l - \kappa + \kappa e^{-l/\kappa}) \quad (14)$$

or, when $l \gg \kappa$,

$$\eta_a = \eta + \frac{3\epsilon\zeta^2}{32\pi^2\lambda l^2} \quad (15)$$

where ϵ is the dielectric constant and λ the specific conductance of the

³⁸ M. Terzaghi, *J. Rheology* **2**, 253 (1931); J. Macaulay, *Nature* **138**, 587 (1936).

³⁹ G. A. H. Elton, *Proc. Roy. Soc. A* **194**, 239, 275 (1948).

solution. Equation (14) is derived by obtaining the distribution of potential between the plates for a uni-univalent electrolyte and integrating the Poisson-Boltzmann equation for the boundary conditions appropriate to the model.

Similar effects are operative in sedimentation of charged particles. Elton has calculated⁴⁰ the apparent viscosity η_a of a suspension of spherical particles of radius a and finds that

$$\eta_a = \eta + \frac{16c_i \epsilon k T a^3 n}{3\pi\lambda} \sinh^2 \left(\frac{e\zeta}{2kT} \right) \quad (16)$$

which, at small values of ζ , reduces to

$$\eta_a = \eta + \frac{\epsilon \zeta^2 a^3 n}{6\pi\lambda\kappa^2} \quad (17)$$

where c_i is the ionic concentration, ϵ the dielectric constant, n is the number of particles per cc., and other symbols have their previous significance.

Use of equations (16) or (17) to obtain rates of sedimentation of colloidal carborundum at various ionic strengths gives moderate agreement with experiment.⁴⁰

VII. The Third Electroviscous Effect

5

1. ELECTRICAL FREE ENERGY AND VISCOSITY OF POLYELECTROLYTES

The third electroviscous effect arises on account of the change of shape of polymeric colloidal particles in solution when their electrical free energy is changed by ionization and the presence of neutral salts. The problem of the form of nonelectrolytic polymers in solution can be treated in terms of a statistical model in which there is an almost random distribution of segments of a size characteristic of the polymer molecule. Such a treatment⁴¹ leads to the concept of a statistical coil as representing the configuration of the polymer in solution, the average dimensions of the coil being dependent on the polymer-solvent interaction, the size of the statistical links, or segments and their number in the whole molecule and any specific intramolecular interactions (e.g. hydrogen-bonds) in the polymer.

If the polymeric molecule can undergo ionization, e.g., by reaction with a base or by reaction with some other ion-producing substance—as in the quaternization of polyvinylpyridine by butyl bromide—electrostatic repulsion between the like charges introduced on the polymer chain modifies the partial molar free energy of the polymer in solution.

If the average radius of the charged statistical coil (assumed approxi-

⁴⁰ G. A. H. Elton, *Proc. Roy. Soc. A* **197**, 568 (1949).

⁴¹ W. Kuhn, *Kolloid-Z.* **68**, 2 (1934); **76**, 258 (1936).

mately spherical at low degrees of ionization of the polymer) is R , and h is the mean end-to-end distance in the coil,

$$R^2 = 5/36 NA^2[1 + (h^2/NA^2)]$$

which can be written as

$$R^2 = 5/36(h_0^2 + h^2)$$

where h_0^2 is the square of the end-to-end distance in the uncharged polymer coil and is equal to NA^2 , and N is the number of statistical elements of length A . The probability of finding an end-to-end distance between the values h and $h + dh$ in the statistical coil when $h \ll NA$, the maximum extension, is then given in the theory of Hermans and Overbeek⁴² in terms of the electrical free energy G_e of the molecule, as a distribution function

$$h^2 \exp \left(-\frac{3h^2}{2NA^2} - \frac{G_e}{RT} \right) \cdot dh \quad (18)$$

and the mean square end-to-end distance in the charged polymer is then

$$\bar{h}^2 = \frac{\int_0^\infty h^4 \exp \left[-\frac{3h^2}{2NA^2} - \frac{G_e}{RT} \right] \cdot dh}{\int_0^\infty h^2 \exp \left[-\frac{3h^2}{2NA^2} - \frac{G_e}{RT} \right] \cdot dh} \quad (19)$$

This function indicates a higher average of \bar{h}^2 as the electrical free energy change in going from the uncharged to the charged form of the polymer becomes numerically larger. The average extension of the polymer therefore increases as the electrical repulsion energy becomes larger, i.e., as the degree of ionization increases at constant ionic strength. G_e is calculated by Hermans and Overbeek⁴² using the Poisson-Boltzmann equation and has the form

$$G_e = (3z^2e^2/5\epsilon R)(1 + 0.6 \kappa R + 0.4 \kappa^2 R^2)^{-1}, \quad (20)$$

where κ is the Debye-Hückel reciprocal radius of the ionic atmosphere, and ze is the charge on the polyion. The calculation for G_e is based on either a spherically symmetric continuous uniform charge distribution or a Gaussian one in the statistical coil but either assumption leads to essentially the same result. The spatial redistribution of small gegen ions in the polyion coil which necessarily occurs in the charging of the polyion is assumed not to contribute to the free energy term.

Introduction of the average end-to-end length, in terms of G_e , into the expression for R^2 leads to

⁴² J. J. Hermans and J. Th. G. Overbeek, *Rec. trav. chim.* **67**, 761 (1948).

$$y^3 \cdot \frac{(y^2 - 2)}{(y^2 - 1)} = \frac{\beta}{3} \cdot \frac{(1 + 1.2\kappa R + 1.2\kappa^2 R^2)}{(1 + 0.6\kappa R + 0.4\kappa^2 R^2)^2} \quad (21)$$

where y is a dimensionless parameter equal to $6R/h_0\sqrt{5}$ and

$$\beta = \frac{18}{5^{3/2}} \cdot \frac{z^2 e^2}{\epsilon k T h_0}.$$

Two limiting results arise from equation (21): (i) At high ionic strength $y^2 = 2$ and $R^2 = \frac{5}{18} \bar{h}_0^2$, that is, the value for the uncharged coil. (ii) At ionic strength approaching zero

$$y^3 \frac{(y^2 - 2)}{(y^2 - 1)} = \beta/3;$$

when $y^2 > 2$, that is, $h > h_0$, the equation can be written $y^3 = \beta/3$. In other words, it becomes identical with that given by Katchalsky and Gillis.⁴³ By solving equation (21) (e.g., graphically), R can be obtained and related to the viscosity of the polymer solution using the theory of Debye and Bueche⁴⁴ which gives for the intrinsic viscosity $[\eta]$ of the solution

$$[\eta] = 10^{-3} \cdot R^2 f / m \eta_0, \quad (22)$$

where m is the mass of the monomer, f its frictional constant and η_0 , the viscosity of the solvent.

The above treatment by Hermans and Overbeek is limited to small degrees of ionization for which the increase of extension relative to that of the uncharged polymer is small, and also because the Debye-Hückel approximation is used, so that values of electric potential inside or outside the polymer coil must be small.

At high degrees of charging (and hence extension) the assumptions of spherical symmetry and of the Debye-Hückel approximation break down and the above result becomes invalid. The statistics of the stretched flexible chain were considered by Kuhn and co-workers⁴⁵ who derived G_e for less limiting conditions, obtaining

$$G_e = (z^2 e^2 / \epsilon h) [1 + \ln (h^2 / N A^2)] \quad (23)$$

at infinite dilution of the polymeric ions and for the absence of added salts.

For finite ion concentrations,⁴⁶ equation (23) becomes approximately

$$G_e = (z^2 e^2 / \epsilon h) [1 + \ln (6h / \kappa N A^2)] \quad (24)$$

⁴³ A. Katchalsky and J. Gillis, *Proc. Intern. Conf. Macromolecules, Amsterdam*, p. 277 (1949).

⁴⁴ P. Debye and A. M. Bueche, *J. Chem. Phys.* **16**, 573 (1948).

⁴⁵ W. Kuhn, O. Künzle, and A. Katchalsky, *Helv. Chim. Acta* **31**, 1994 (1948).

⁴⁶ O. Künzle, *Rec. trav. chim.* **68**, 699 (1949).

from which \bar{h}^2 follows from equation (19). Thus, the essential result follows that the extension is determined both by the net charge and the ionic strength (through the term in κ). Since the viscosity of a suspension of particles is determined in part by the anisometry of the particles, a new electroviscous effect will appear on account of the dependence of dimensions of the particles on ze (the net charge) and on κ , and hence on degree of ionization of the polymer and on neutral salt concentration. Other more detailed treatments of the above problem have been given⁴⁷⁻⁵¹ (cf. also reference⁵²) and consist in refinements of the general theory.

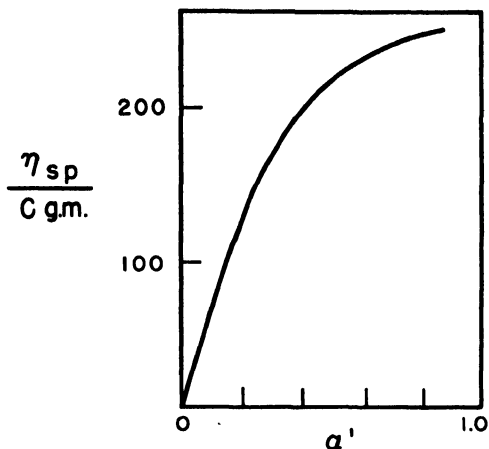


FIG. 4. Reduced specific viscosity of sodium polyacrylate and apparent degree of dissociation α' . From Kern.²⁷

2. EXPERIMENTAL BASIS OF THE THIRD ELECTROVISCOUS EFFECT

Experimental demonstration of an electroviscous effect with substances apparently having the nature of polyelectrolytes was first made in the work of Kruyt and Bungenberg de Jong¹⁶ though the effect was not recognized as a special property of polyelectrolytes, as the materials used by these workers had not been well characterized. The first observation of the third type of electroviscous effect with well defined material was by Staudinger,⁵³ using polyacrylic acid. This type was later studied in more

⁴⁷ S. Lifson and A. Katchalsky, *J. Polymer Sci.* **13**, 43 (1954).

⁴⁸ K. Susuki, *Busseiron Kenkyu* **25**, 77 (1950).

⁴⁹ T. L. Hill, *J. Chem. Phys.* **20**, 1173 (1952).

⁵⁰ G. Kimball, M. Cutler, and H. Samelson, *J. Phys. Chem.* **56**, 57 (1952).

⁵¹ T. Osawa and N. Imai, *J. Polymer Sci.* **13**, 93 (1954).

⁵² P. J. Flory, *J. Phys. Chem.* **58**, 653 (1954).

⁵³ H. Staudinger, *Ber.* **64**, 2095 (1931).

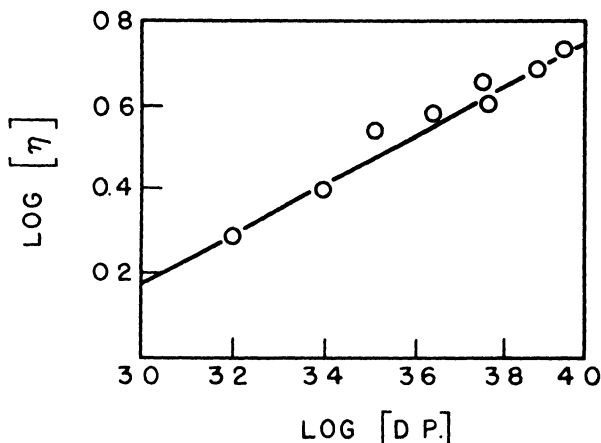


FIG. 5. Intrinsic viscosity $[\eta]$ of polymethacrylic acid in hydrochloric acid solution ($2 \cdot 10^{-3} M$) as a function of degree of polymerization [D.P.]. From Katchalsky.⁵⁵

detail by Kern,^{27, 54} who showed that the viscosity depended both on the degree of polymerization and on the apparent degree of dissociation (α') of the carboxylic groups in the polymer, as shown in Fig. 4. The uncoiling due to ionization predicted by the theories discussed above was indirectly demonstrated in experimental work by Katchalsky.⁵⁵ For unionized polymethacrylic acid the relation between intrinsic viscosity $[\eta]$ and molecular weight is $[\eta] = KM^a$, where K is a constant and a is approximately 0.5, corresponding to unstretched statistical coils. The demonstration of this relation is given in Fig. 5. When the degree of ionization (α) exceeds 0.2, the exponent a increases progressively until at $\text{pH} = 6$ ($\alpha = 0.4$) it reaches a limiting value of 2, and the condition $0.5 < a < 2$ when $2.7 < \text{pH} < 6.0$ is found for polymethacrylic acid (see Fig. 6). Thus, for a sample of given molecular weight, a increases with α , and hence $[\eta]$ and the average molecular extension increase. This conclusion is substantiated by measurements on streaming birefringence, e.g., of poly-4-vinyl-*N*-butylpyridinium bromide,⁵⁶ which is greatly in excess of the very small birefringence of the uncharged poly-4-vinyl pyridine, presumably because the polyion is more extended than the neutral polymer. Addition of neutral salt (for example, 1% KBr to a 0.2% polybromide solution) completely suppresses the birefringence and markedly lowers the reduced specific viscosity to values

⁵⁴ W. Kern, *Z. physik. Chem. (Leipzig)* **A184**, 197, 304 (1939); *Biochem. Z.* **301**, 338 (1939).

⁵⁵ A. Katchalsky, *J. Polymer Sci.* **7**, 393 (1951).

⁵⁶ R. M. Fuoss and R. Signer, *J. Am. Chem. Soc.* **73**, 1901 (1951).

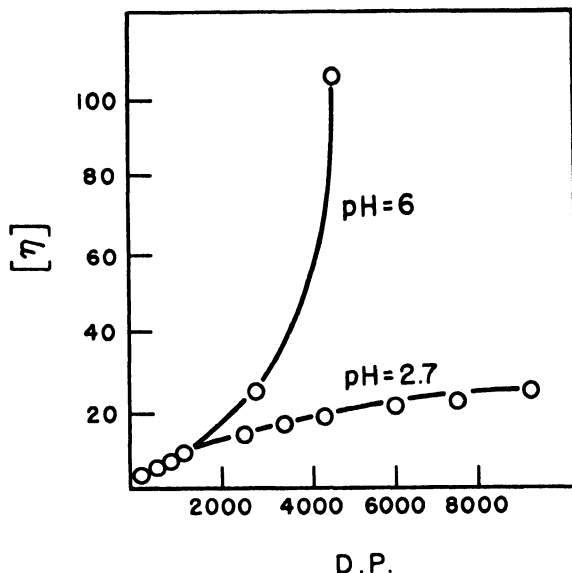


FIG. 6. Dependence of intrinsic viscosity $[\eta]$ on degree of polymerization [D.P.] of polymethacrylic acid at pH 2.7 and pH 6. From Katchalsky.⁵⁵

comparable with those of the uncharged polymer of the same molecular weight. Analogous results were obtained with organic polyacid salts by Arnold and Overbeek,⁵⁷ Markowitz and Kimball,⁵⁸ and Wiederhorn and Brown,⁵⁹ and with polyphosphates by Strauss and Smith⁶⁰ and Saini.⁶¹

Similar birefringence results are found⁵⁵ with polymethacrylic acid; the limiting value of $(d\psi/dq)_{q \rightarrow 0}$, the gradient of orientation angle ψ with respect to rate of shear q as $q \rightarrow 0$, varies in a parallel way (see Fig. 7) with the reduced specific viscosity as the degree of ionization increases. Analogous results are obtained for poly-4-vinyl-*N*-butylpyridinium bromide.⁶² With polyampholytes, e.g., copolymers of vinylpyridine and methacrylic acid, the viscosity increases rapidly upon addition of either acid or base.^{55, 63} Similar effects occur with chainlike proteins, e.g., myosin or sodium caseinate, where the viscosity is a minimum at the iso-electric point. Analogous effects occur with albumins. (See Fig. 8.)

⁵⁷ R. Arnold and J. Th. G. Overbeek, *Rec. trav. chim.* **69**, 192 (1950).

⁵⁸ H. Markowitz and G. Kimball, *J. Colloid Sci.* **5**, 115 (1950).

⁵⁹ N. M. Wiederhorn and A. R. Brown, *J. Polymer Sci.* **8**, 651 (1952).

⁶⁰ U. P. Strauss and E. H. Smith, *J. Am. Chem. Soc.* **75**, 6186 (1953).

⁶¹ G. Saini, *Ann. chim. (Rome)* **41**, 340 (1951).

⁶² P. Kamath, B. Rosen, and F. R. Eirich, *Phys. Rev.* **86**, 657 (1956); B. Rosen, P. Kamath, and F. R. Eirich, *Discussions Faraday Soc.* **11**, 135 (1951).

⁶³ Turner Alfrey, Jr. and H. Morawetz, *J. Am. Chem. Soc.* **74**, 436 (1952).

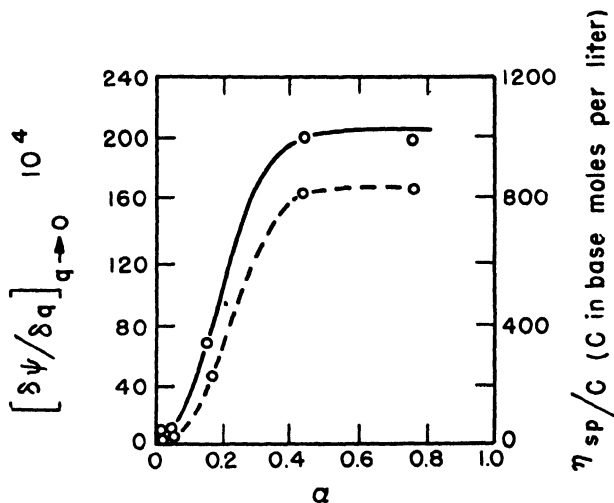


FIG. 7. Limiting rate of change of orientation angle ψ for polymethacrylic acid with shear rate q in streaming birefringence, as a function of degree of ionization α . Dotted curve shows corresponding relation between reduced viscosity and α . From Katchalsky.⁵⁵

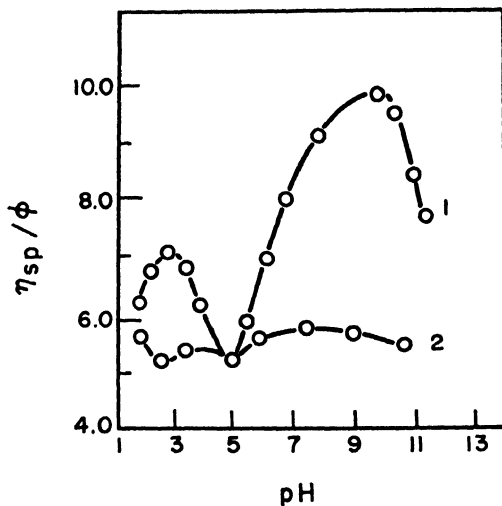


FIG. 8. Dependence of reduced specific viscosity (in terms of volume fraction ϕ) of ovalbumin upon pH. Key: 1, in absence of NaCl; 2, in 0.01 *N* NaCl above pH 7, and in 0.02 *N* NaCl below pH 7.⁸

Pals and Hermans⁶⁴ have made an experimental examination of the theory of Hermans and Overbeek⁴² using carboxymethylcellulose and sodium pectinate; moderate agreement between the observed viscosity behavior and that predicted by the theory is obtained at intermediate values of ionic strength. Experimental test of the theory is impossible at high salt concentrations as the polymer is salted out. An extrapolated value of $y^2 = 1.55$ (see p. 101) instead of 2.0, as required theoretically, is obtained. For low salt concentrations the theory requires $\kappa R < 1$. In the absence of added neutral salts the minimum value of κR is about 0.5 but, in the presence of the least concentration of NaCl used (viz., $0.375 \times 10^{-3} N$), κR is equal to 5. Use of equation (22) requires caution since it gives anomalously low values for the volume occupied by the monomer. Thus, Pals and Hermans have calculated the Stokes radius of the main-chain monomer (glucose) in carboxymethyl cellulose as 0.4×10^{-8} cm., that is, a value some five times smaller than the radius deduced from molecular dimensions in the glucose molecule. Similar disagreement occurs with nonionized polymers.⁶⁵

3. CONCENTRATION EFFECTS IN THE VISCOSITY OF POLYELECTROLYTES

The first systematic work on the concentration dependence of reduced specific viscosity (η_{sp}/c) of polyelectrolytes and the effect of added salts thereon was carried out by Kern²⁷ and later by Fuoss *et al.*^{26, 66-68} The experimental behavior of poly-4-vinyl-*N*-butylpyridinium bromide (PVPBr) with respect to concentration dependence of η_{sp}/c and effect of salts is shown in Fig. 9. The shapes of the η_{sp}/c versus c plots in Fig. 9 are reproduced by many other widely differing polyelectrolytes^{61, 64, 69-79} including those in nonaqueous solution,^{72, 79} so that the behavior observed appears

⁶⁴ D. T. F. Pals and J. J. Hermans, *Rec. trav. chim.* **71**, 433 (1952).

⁶⁵ E. D. Kunst, Thesis, University of Groningen, The Netherlands, p. 43, 1950; J. M. Wilson, *J. Chem. Phys.* **17**, 217 (1949).

⁶⁶ R. M. Fuoss, *J. Polymer Sci.* **3**, 603 (1948); **4**, 96 (1949).

⁶⁷ R. M. Fuoss and G. Cathers, *J. Polymer Sci.* **4**, 97 (1949).

⁶⁸ R. M. Fuoss and W. N. Maclay, *J. Polymer Sci.* **6**, 511 (1951).

⁶⁹ M. Heidelberger and F. E. Kendall, *J. Biol. Chem.* **95**, 127 (1932).

⁷⁰ S. Basu, *Nature* **168**, 341 (1951); *J. Colloid Sci.* **6**, 539 (1950).

⁷¹ E. H. Balazs and T. C. Laurent, *J. Polymer Sci.* **6**, 665 (1951).

⁷² J. Schaefgen, *J. Am. Chem. Soc.* **73**, 4580 (1951); **74**, 2715 (1952).

⁷³ S. Basu, *J. Colloid Sci.* **7**, 53 (1952).

⁷⁴ T. Hekker, *Chem. Weekblad.* **46**, 625 (1950).

⁷⁵ J. Kagawa, *J. Soc. Chem. Ind. Japan* **47**, 544 (1944).

⁷⁶ H. Fujita and T. Homma, *J. Colloid Sci.* **9**, 591 (1954).

⁷⁷ A. Katchalsky and M. Eisenberg, *J. Polymer Sci.* **6**, 145 (1951).

⁷⁸ A. Oth and P. Doty, *J. Phys. Chem.* **56**, 43 (1952).

⁷⁹ J. Schaefgen, Abstracts of American Chemical Society Meeting, Chicago, p. 11J, 1950.

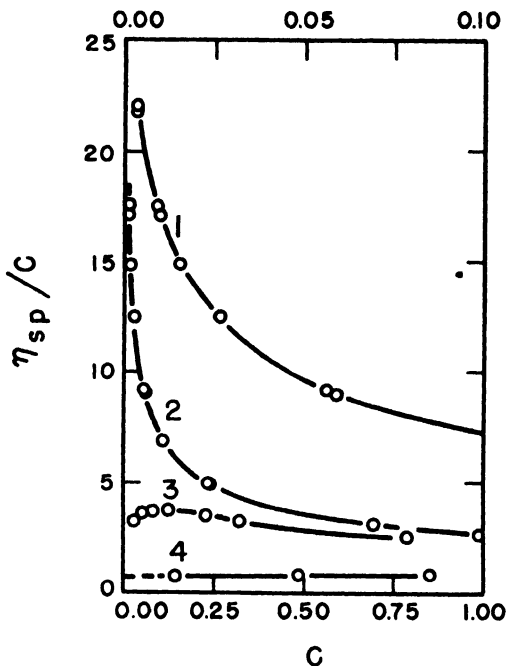


FIG. 9. Dependence of reduced specific viscosity of poly-4-vinyl *N*-butylpyridinium bromide upon polysalt concentration in solutions containing various concentrations of simple electrolyte. Key: 1, in water; 2, in water (upper scale of abscissas); 3, in 0.001 *N* KBr solution; 4, in 0.0335 *N* KBr. From Fuoss and Strauss.²⁶

to be a fundamental property. In the work of Fuoss^{26, 66-68} it appeared that in pure aqueous solution η_{sp}/c increased steadily with dilution and very rapidly at high dilutions.^{79a} In the presence of added salts the viscosity was much lower but at low concentrations of salt η_{sp}/c still increased with dilution until the ionic concentration due to the salt was comparable with that due to the polysalt, when η_{sp}/c went through a maximum and then decreased with further dilution. The effects are similar at lower degrees of ionization of the polymeric electrolyte, but less pronounced, and the viscosities obtained are not so high. In excess of added salt, η_{sp}/c increases with a small uniform slope with increasing concentration of polymer, as in the case of uncharged polymers.

On the assumption that the variation of η_{sp}/c with c was connected with a property of the ionic atmosphere around the particle, Fuoss⁶⁶ proposed

^{79a} F. Eirich [*Discussions Faraday Soc.* **11**, 153 (1951)] was the first to point out that a continuous increase of η_{sp}/c to infinite dilution could not occur but that a maximum should also be observed in the curve for salt-free solution, as later found.

the following empirical relation for the behavior in the absence of salts:

$$\frac{\eta_{sp}}{c} = \gamma + \frac{a}{1 + b\sqrt{c}} \quad (25)$$

or, when $\gamma \ll \eta_{sp}/c$,

$$\frac{\eta_{sp}}{c} = \frac{a}{1 + b\sqrt{c}} \quad (26)$$

and in the presence of salts at an ionic strength μ ,

$$[\eta] = \left(\frac{\eta_{sp}}{c} \right)_{c \rightarrow 0} = A \left(1 + \frac{B}{\sqrt{\mu}} \right)^3 \quad (27)$$

where A , B , a , b , and γ are constants. A is the intrinsic viscosity in the limit of infinite ionic strength and is equal to (or less than^{62, 80}) the intrinsic viscosity of the uncharged polymer; a is a constant depending on the nature and molecular weight of the polymer at infinite dilution; b is related to the influence of the electrostatic repulsion and depends on the net charge of the polyion and increases with decrease of the dielectric constant of the solvent. Equations (25) and (26) apply to a number of polyelectrolytes over certain concentration ranges, as shown in Fig. 10 (see also below); functions of c , and not \sqrt{c} , apply in some other cases.⁷²

The increase of η_{sp}/c with dilution has been explained by Fuoss and Strauss²⁶ as due to the variation of the degree of ionic association between the polyion and its counter ions with concentration of the polysalt. Polymeric electrolytes at moderate or high degrees of ionization behave like simple strong electrolytes in solvents of low dielectric constant on account of the high field of the polyion and its consequent effect in pulling counterions into close proximity to the polyion chain. With increasing dilution the degree of counter-ion association becomes smaller by a mass action effect and the effective net charge on the polymer increases. The extension and hence η_{sp}/c increase with dilution. This effect was first recognized by Kern²⁷ with sodium polyacrylate and by Briggs²²⁻²⁴ with certain natural polyelectrolytes, but a detailed interpretation of the effect was not made. In the presence of a constant salt concentration, the dilution effect operates until the concentration of simple ions from the added salt is greater than that from the polysalt; whereupon the η_{sp}/c decreases with further dilution of polysalt, and the plot of η_{sp}/c shows the familiar maximum which shifts to higher polysalt concentration, the higher the concentration of added simple electrolyte.

⁸⁰ R. M. Fuoss, *Discussions Faraday Soc.* **11**, 125 (1951); cf. P. Doty and G. Ehrlich, *Ann. Rev. Phys. Chem.* **3**, 81 (1952).

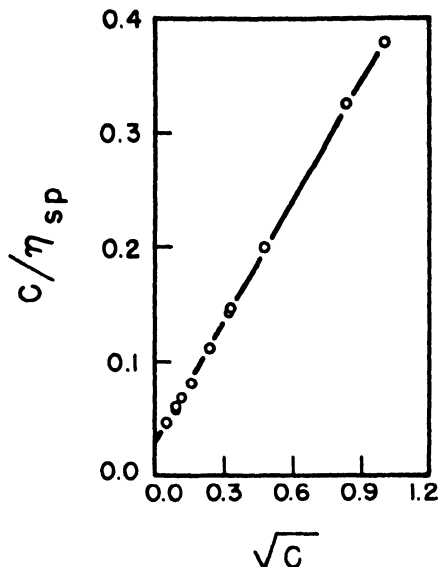


FIG. 10. Test of equation (26) for polyvinyl *N*-butylpyridinium bromide at $q = 2000 \text{ sec}^{-1}$. From Fuoss and Strauss.²⁶

The expansion of the polymer coil with dilution can be eliminated if the ionic strength is kept constant (isoionic dilution) during the dilution, as was demonstrated by Hermans,^{64, 81} whereupon the reduced viscosity-concentration plot becomes linear, as shown in Fig. 11. Direct evidence for strong ionic association, as suggested by Fuoss and Strauss,²⁶ has been given in transport measurements by Wall⁸² using radioactively labeled ions; conductance studies^{78, 83-85} and measurements of the Wien effect⁸⁶ indicate a similar result. The relative birefringence of PVPBr. increases with dilution of the polymer⁵⁶ again indicating an increase of extension of the polyion with dilution. Anomalous heats of dilution of PVPBr.⁸⁷ are also explained by the decrease of ionic association with dilution.

The results of Fuoss *et al.*^{26, 66} indicate a large change of $[\eta]$ from the salt-free solution to one containing excess salt, as well as an increase of the

⁸¹ D. T. F. Pals and J. J. Hermans, *J. Polymer Sci.* **6**, 733 (1950).

⁸² F. T. Wall, J. R. Huizenga, and P. F. Grieger, *J. Am. Chem. Soc.* **72**, 2636, 4228 (1950).

⁸³ R. M. Fuoss and U. P. Strauss, *J. Polymer Sci.* **3**, 246 (1948).

⁸⁴ D. Edelson and R. M. Fuoss, *J. Am. Chem. Soc.* **70**, 2832 (1948).

⁸⁵ A. Veis, *J. Phys. Chem.* **57**, 189 (1953).

⁸⁶ F. G. Bailey, L. A. Patterson, and R. M. Fuoss, *J. Am. Chem. Soc.* **74**, 1845 (1952); *J. Polymer Sci.* **9**, 285 (1952).

⁸⁷ W. Schultz, *Z. Elektrochem.* **58**, 165 (1954).

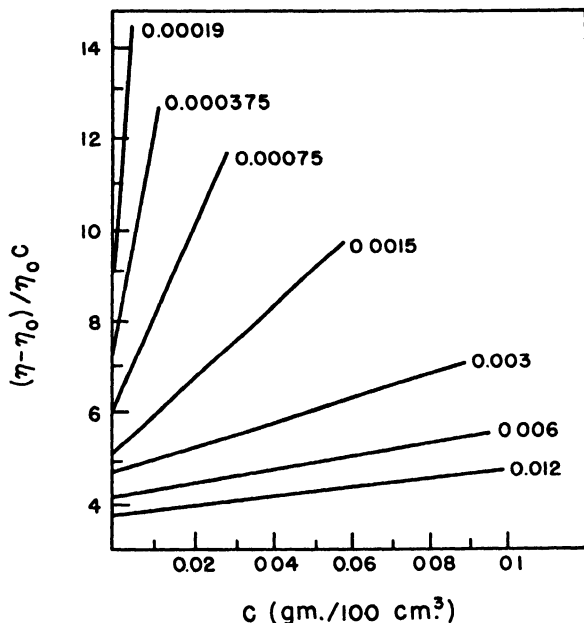


FIG. 11. Dependence of reduced specific viscosity $(\eta - \eta_0)/\eta_0 c$ upon concentration of sodium pectinate in NaCl solution at various isoionic dilutions. Index figures denote the NaCl concentration in millimoles per liter at the limit of zero polysalt concentration. From Pals and Hermans.⁸¹

salt effect $(\Delta\eta_{sp})/c$, with dilution of the polysalt, caused by addition of neutral salts to the salt-free solution. In investigations of the viscosity behavior of thymus sodium deoxyribonucleate (DNA) at low rates of shear and very low concentrations in sensitive Couette viscometers, Pouyet⁸⁸ and Conway and Butler⁸⁹ found that η_{sp}/c decreased at high dilutions (10^{-4} to 2.5×10^{-6} gm./ml.) and that in the limit of zero polymer concentration the effect of added salt on $[\eta]$ was very small or zero, the lines of η_{sp}/c for the salt-free and salt-containing solutions converging to a common intercept at infinite dilution of polymer, as shown in Fig. 12a and 12b. The convergence indicates a small or zero change of extension and shape of this polymer with added salt. This result is consistent with the stiffness inherent in the structure (see reference ¹⁰⁴) of the molecule, as indicated by the electron micrographs of apparently individual DNA molecules, recently obtained by Hall and Litt^{89a}. Confirmation of this effect was obtained by observ-

⁸⁸ J. Pouyet, *Compt. rend.* **234**, 152 (1952).

⁸⁹ B. E. Conway and J. A. V. Butler, *J. Polymer Sci.* **12**, 199 (1954).

^{89a} C. E. Hall and M. Litt, *J. Biochem. Biophys. Cytol.* **4**, 1 (1958).

^{89b} J. A. V. Butler, B. E. Conway and D. W. F. James, *Trans. Faraday Soc.* **50**, 612 (1954).

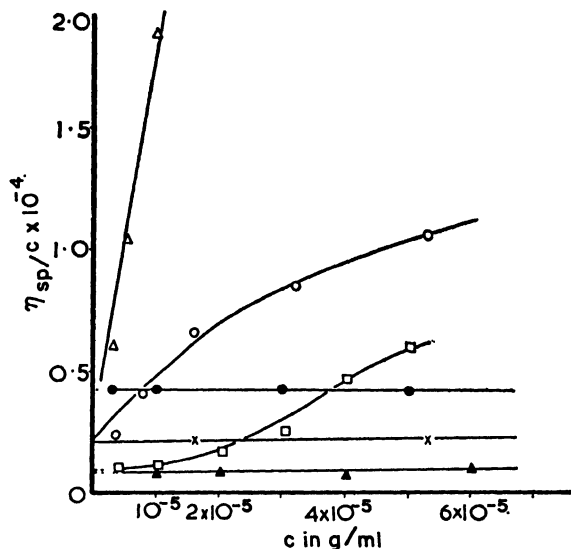


FIG. 12a. Dependence of reduced specific viscosity of three DNA preparations in pure water and in excess 0.1 *M* sodium chloride solution. (From Conway and Butler^{89, 89b}) Key: Δ thymus DNA in water, \bullet in 0.1 *M* NaCl; \circ herring sperm DNA in water, \times in 0.1 *M* NaCl; \square herring sperm DNA (lower molecular weight) in water, \blacktriangle in 0.1 *M* NaCl.

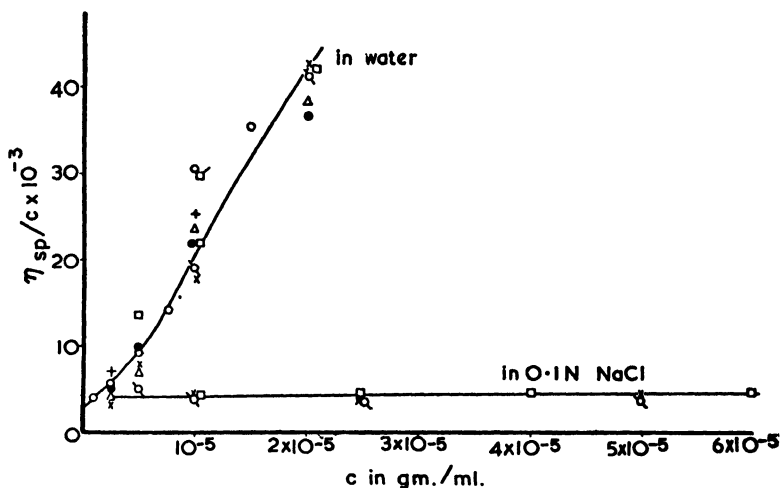


FIG. 12b. Dependence of reduced specific viscosity on concentration of DNA showing reproducibility of points obtained in different experiments with different solutions, and coincidence of $[\eta]$ in water and 0.1 *N* NaCl solutions, within experimental error. From Conway and Butler.^{89, 89b}

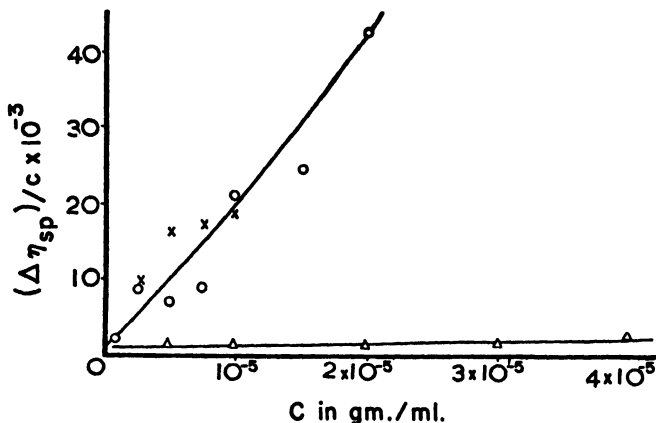


FIG. 13. Change of reduced specific viscosity as a function of DNA concentration observed upon direct addition of a small volume of strong salt solution to constant volumes of DNA solutions initially in pure water. Lower line (Δ points) shows effect with lower molecular weight herring sperm preparation.^{89b}

ing the drop of viscosity of DNA solution at various dilutions, upon addition of 0.1 ml. of a saturated salt solution. The reduced decrease of viscosity caused by the salt addition tended to zero at zero DNA concentration, as shown in Fig. 13. The same conclusion was reached by Signer and Schwander,⁹⁰ who found the birefringence curves for DNA were identical within experimental error in the presence or absence of added salt. The effect of salt on the viscosity of DNA solutions is, however, large at higher concentrations of the polymer and of the same magnitude as that found with other polyelectrolytes. The change of viscosity of DNA with various added salts of different valence types is linear in ionic strength at low salt concentration^{89b} (cf. also reference ⁹¹). The results with DNA indicated the possibility that at high dilutions of other polyelectrolytes η_{sp}/c might *increase* with increasing c and pass through a maximum as occurs in the presence of salts. Using very low concentrations of PVPBr. and sodium polymethacrylate Conway⁹² and Pouyet and Eisenberg⁹³ showed that such an effect occurred in pure water solutions, as shown in Fig. 14. The maximum in η_{sp}/c versus c was demonstrated using a Couette viscometer and eliminating loss of material from the solutions on account of adsorption on the walls of vessels by washing all vessels out

⁹⁰ R. Signer and H. Schwander, *Helv. Chim. Acta*, **34**, 1344 (1951); H. Schwander and H. Cerf, *ibid.* **34**, 436 (1951).

⁹¹ J. Creeth, J. M. Gulland, and D. O. Jordan, *J. Chem. Soc.* p. 1141 (1947).

⁹² B. E. Conway, *J. Polymer Sci.* **18**, 257 (1955).

⁹³ J. Pouyet and M. Eisenberg, *J. Polymer Sci.* **13**, 85 (1954).

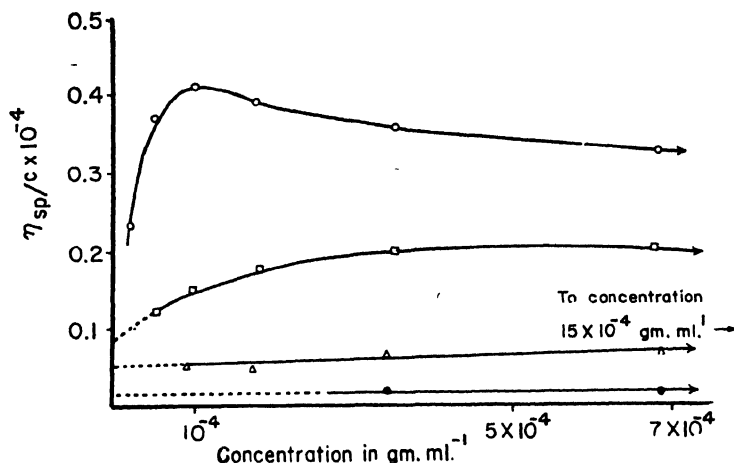


FIG. 14. Curves for reduced viscosity versus concentration of sodium polymethacrylate (60% sodium salt) at low concentrations. Key: ○ in water; □ 0.0001 *M* NaCl; Δ 0.01 *M* NaCl; ● 0.1 *M* NaCl. From Conway.⁹²

several times with the solution of a given concentration and then making up the solution to the required strength again. The maximum arises on account of two competing factors, viz., the second and third electroviscous effects: molecular interaction which increases^{62, 92} in proportion to $[\eta]^2$ and c^2 and molecular contraction as suggested by Fuoss which increases as the polymer concentration increases. The first effect tends to increase η_{sp}/c with increase of c whereas the second effect tends to decrease η_{sp}/c . There is thus a maximum in the curve of η_{sp}/c versus c beyond which one effect overcomes the other.

With samples of sodium polymethacrylate of various molecular weights, Conway⁹² demonstrated the increase of η_{sp}/c with c at zero shear rate in the absence of added salts and showed that the slopes in the low concentration region of the η_{sp}/c versus c lines were proportional to $[\eta]^2$, thus indicating the initial increase of η_{sp}/c with c as due to mechanical or electrical interactions. Similar observations were made by Pals and Hermans⁶⁴ for finite salt concentrations, using sodium pectinate. By using the observed linear dependence of η_{sp}/c upon c at high dilutions and the equilibrium constant⁶⁴ for Na^+ -ion association with 60% neutralized polymethacrylic acid, Conway showed⁹² that the shape of the curve of η_{sp}/c versus c could be predicted in quite good agreement with experiment over a wide range of polymer concentrations, as shown in Fig. 15.

The concentration at which the maximum value of η_{sp}/c occurs, depends

⁹⁴ P. Lawley, Ph.D. Thesis, The University, Nottingham, England, 1953.

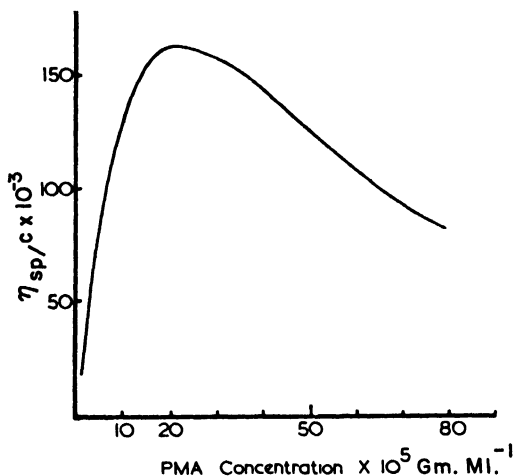


FIG. 15. Curve of reduced specific viscosity versus concentration of sodium (60%) polymethacrylate (PMA) calculated from experimental polymer interaction constant and sodium ion polyion association equilibrium constant. (From Conway⁹²)

on the intrinsic flexibility of the molecule. Deoxyribonucleic acid, which appears to be a rather stiff molecule since $[\eta]$ is almost unchanged by added salt (*cf.* ref. ^{89a}) shows no maximum when η_{sp}/c is plotted against c if values of viscosity extrapolated to zero rate of shear are used. Degraded samples exhibit the maximum, and a finite effect of added salts on $[\eta]_{q=0}$, is found.⁹⁵

The rapid decrease of η_{sp}/c with c at high dilutions raises an important question concerning the determination of intrinsic viscosities. In a Fuoss-type plot, the intrinsic viscosity and salt effect on $[\eta]$ will be much larger than that which is found if the measurements are extended to low concentrations. Under the conditions where the change of sign of the slope of the η_{sp}/c lines occurs it is difficult to obtain viscosity measurements which give accurate differences of the viscosity of the solution compared with that of the solvent, owing to the low concentrations involved. Also traces of electrolytic impurities may have a strong effect on the results. However, in the purest solutions Butler *et al.*⁹⁶ have shown that the maximum is still observed, although it appears at lower concentrations as the solution is more purified. In aqueous solutions at the high dilutions examined, the presence of ions arising from the dissociation of water may effect the results.⁵² Further work in nonaqueous polar solvents, where this difficulty would be absent or reduced, is required. Hydrolysis cannot account for the effect in DNA or sodium polymethacrylate, as may be verified by

⁹⁵ B. E. Conway, *J. Polymer Sci.* **20**, 299 (1956).

⁹⁶ J. A. V. Butler, private communication (1957).

calculation⁹² using the known pK 's; also the effect is observed with PVPBr, a strong polyelectrolyte, where hydrolysis could not occur. If the rapid decrease of η_{sp}/c with c at high dilutions is a real effect, the relative change of intrinsic viscosity of polyelectrolytes with excess added salt is much less than has hitherto been supposed, and much of the high viscosity of polyelectrolytes at higher concentrations must be attributed to electrostatic and mechanical interaction.

This view has been suggested and examined by Butler, Conway and James,^{99b} who showed that an attractive electrostatic interaction could arise by various polyions sharing counter ions (cf. references^{97, 99}) in their ionic atmospheres. Excess salt would destroy the attractive effect and the viscosity will decrease. Such an attractive effect appears to account for the gels formed, for example, with Ca polymethacrylate,⁹⁷ where the ionic interaction forces are stronger than with the monovalent Na salt. Deuel⁹⁸ has argued against such a view in the case of pectinates but Conway has supported it by experiments with magnetic models⁹⁹ of polyelectrolytes. However, qualitatively similar predictions follow if the high viscosity at higher concentrations were due to overlapping and repulsion of the double layers of the extended polyions, i.e., to the second electroviscous effect. The latter effect is proportional to the square of the concentration and could account for the interaction effect observed; it is also known³¹ to give rise to non-Newtonian viscosity even with particles of low asymmetry, so that the strong non-Newtonian viscosity of polyelectrolytes, which is much diminished by the presence of salts,⁹⁰ may arise from the second electroviscous effect. Contributions from the first electroviscous effect are considered⁴² to be small in polyelectrolyte solutions, but no direct evidence for this has been offered.

4. MOLECULAR STRUCTURE AND DEGREE OF EXTENSION OF POLYELECTROLYTES

The equilibrium average extension depends on the intramolecular cohesion and on steric hindrance to rotation. These factors determine the dimensions of the statistical chain element and hence the average radius of the statistical coil. It is doubtful if fully ionized polymeric ions reach the configuration of straight rods.^{78, 100-103} Special effects due to intramolecular

⁹⁷ F. T. Wall and J. W. Drennan, *J. Polymer Sci.* **7**, 83 (1951).

⁹⁸ H. Deuel, G. Huber, and L. Asyas-Weiss, *Helv. Chim. Acta* **33**, 563 (1950).

⁹⁹ B. E. Conway, *J. Chem. Educ.* **31**, 477 (1954).

¹⁰⁰ J. D. Ferry, D. C. Udy, F. C. Wu, G. E. Heckler, and D. B. Fordyze, *J. Colloid Sci.* **6**, 429 (1951).

¹⁰¹ A. Dobry, *J. chim. phys.*, to be published.

¹⁰² H. Deuel and H. Neukom, *J. Polymer Sci.* **4**, 759 (1949).

¹⁰³ J. V. Kubal and N. Gralen, *J. Colloid Sci.* **3**, 457 (1948).

H-bonding, e.g., in polymethacrylic acid, restrict the degree of uncoiling of the molecule with ionization. In DNA the probable existence of a double helical chain structure¹⁰⁴ makes this molecule particularly rigid and the degree of coiling appears to be much smaller than with some synthetic polymers. Urea denaturation of DNA apparently causes the molecule to change to a more flexible form, where the effect of added salt on $[\eta]$ becomes measurable.⁹⁵ When the degree of coiling is large, the viscosity can become almost independent of molecular weight.¹⁰⁵ The effect of urea on the viscosity of DNA has been attributed to a process similar to the denaturation of proteins. Evidence for a scission of the molecule by urea denaturation has been given by Alexander and Stacey¹⁰⁶ but has not been confirmed.¹⁰⁷ The differences of behaviour of DNA observed by various authors, appear to be attributable, in part, to the different biological sources of the polymers used, viz., from thymus gland or herring sperm.

5. VARIATION OF REDUCED SPECIFIC VISCOSITY WITH RATE OF SHEAR

Influence of shear rate on the viscosity has not been observed in cases where the first electroviscous effect exists alone, e.g., in dilute suspensions of spherical particles. A viscosity dependent on shear rate has, however, been found³¹ at higher concentrations of colloid where the second electroviscous effect is operative. With polymeric electrolytes, the non-Newtonian viscosity is considerable, particularly at low salt concentrations or high polyion concentrations; the effect increases with degree of ionization. At high polyion concentrations in the presence of excess added salt, non-Newtonian behavior is still observed. However, at concentrations of polyion less than 0.01% there is little non-Newtonian behavior up to gradients of 1000 sec.⁻¹ In the absence of salts, the dependence of η_{sp}/c on rate of shear is observable down to 10^{-5} gm./ml. with fully neutralized polymethacrylic acid, and $[\eta]$ values must be obtained by extrapolation of η_{sp}/c with respect both to c and q to $c = 0$, $q = 0$. For extrapolation, measurements are best made in a Couette apparatus.^{90, 108, 109}

From the theory of Kuhn and Kuhn,¹¹⁰ Katchalsky and Sternberg¹¹¹

¹⁰⁴ J. D. Watson and F. H. C. Crick, *Nature* **171**, 737 (1953).

¹⁰⁵ C. Sadron and R. Kocher, *Makromol. Chem.* **10**, 172 (1953).

¹⁰⁶ P. Alexander and K. Stacey, *Trans. Faraday Soc.* **50**, 303 (1954); *Biochem. J.* **60**, 194 (1955); *Nature* **176**, 162 (1955).

¹⁰⁷ P. Doty and S. A. Rice, *Biachim. et Biophys. Acta* **16**, 446 (1955); *J. Am. Chem. Soc.* **79**, 3937 (1957).

¹⁰⁸ A. G. Ogston and J. Stanier, *Biochem. J.* **54**, 4 (1953).

¹⁰⁹ A precision Couette viscometer with an electrostatic restoring device so that it can be used as a null instrument, has recently been described by E. H. Frei, D. Treves, and H. Eisenberg, *J. Polymer Sci.* **25**, 273 (1957).

¹¹⁰ W. Kuhn and H. Kuhn, *Helv. Chim. Acta* **28**, 1533 (1945).

¹¹¹ A. Katchalsky and N. Sternberg, *J. Polymer Sci.* **10**, 253 (1953).

calculated the viscosity at zero shear. They assumed that the particles approximate to rigid rods, for which they obtained

$$(\eta_{sp})_q = (\eta_{sp})_{q=0}(1 - aq^2 + bq^4 - cq^6 + \dots) \quad (29)$$

where $(\eta_{sp})_q$ is the specific viscosity at a gradient q and $(\eta_{sp})_{q=0}$ is the corresponding value at zero rate of shear. For small gradients

$$(\eta_{sp})_q = (\eta_{sp})_{q=0}(1 - aq^2) \quad (30)$$

which gives for the efflux time (from an Ostwald viscometer) of the solution (t_s) and of the solvent (t_0)

$$\frac{t_s}{t_0} = \frac{\eta_s}{\eta_0} \left(1 + \frac{ap^2r^2}{3\eta_0^2l^2} \right) \quad (31)$$

where η_s is the viscosity of the solution at a gradient $q = 0$, η_0 the viscosity of the solvent, p the hydrostatic pressure, r the radius of the capillary, and l its length.

In a series of measurements with the same solution but in viscometers with different capillary radii, the ratio t_s/t_0 is a linear function of r^2 at constant pressure, as shown in Fig. 16. The intercept of this line on the ordinate axis (Fig. 16) gives the viscosity at zero gradient. This procedure was theoretically developed and applied experimentally by Weissenberg and

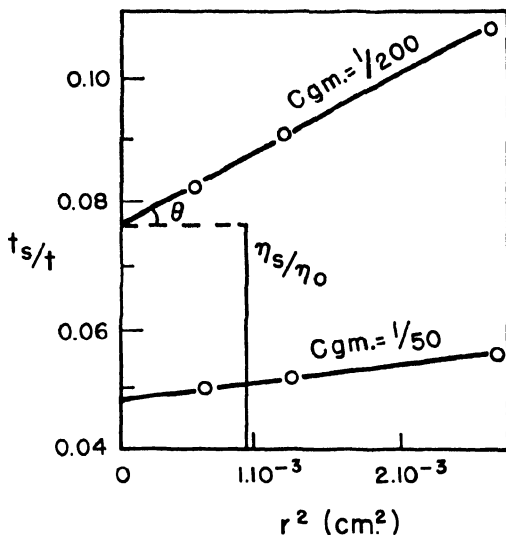


FIG. 16. Plot of t_s/t versus r^2 in cm.^2 , from viscosity measurements on sodium polymethacrylate ($\alpha = 0.5$) in three viscometers of different radii and at two base mole concentrations. η_s/η_0 is the reciprocal of the relative viscosity at $q = 0$ and $\tan \theta = \alpha(P^2R^2/3\eta_0^2l^2)$. From Katchalsky and Sternberg.¹¹⁰

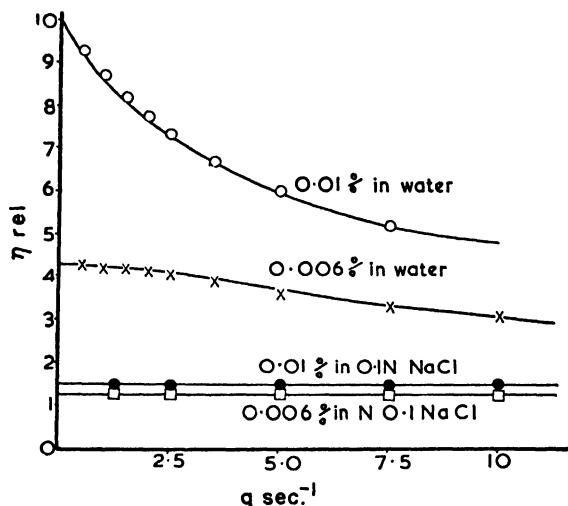


FIG. 17. Effect of rate of shear on the relative viscosity of DNA solutions in water and NaCl solution. From Signer and Schwander.⁹⁰

associates¹¹² in 1929. A more general and complex relation between viscosity and rate of shear than that derived by Kuhn was obtained.

Ackermann and co-workers¹¹³ studied the effect of velocity gradient on the viscosity of solutions of carboxymethyl cellulose and showed that the decrease of viscosity over the shear rate range 0–800 sec.⁻¹ was 12%. The magnitude of the effect depends on polymer concentration, degree of ionization, and salt concentration. For DNA, for example, at 0.1% in pure aqueous solution η_{sp} decreases by 90% over the range $q = 0.5$ to 116 sec.⁻¹ The Kuhn theory predicts a much smaller effect of shear than that observed; also the effect should be quadratic in q . The behavior only approximates to this at low concentrations and in salt-containing solutions, as shown in Fig. 17 for DNA under various conditions. In dilute solutions, the conditions are more close to those assumed in the theory^{111, 114} (viz., orientation of noninteracting rods) and better agreement between theory and experiment is found. The line of η against q should have a zero slope as $q \rightarrow 0$ and, consequently, linear extrapolations of η_q to $q = 0$ are probably invalid and are due to lack of data at very low gradients. Confirmation of a zero slope of η_q versus q at very low shear rates has been obtained

¹¹² K. Weissenberg, B. Rabinowitz, and R. Eisenschitz, *Mitt. deut. Materialprüfungsanstalt. Sonderhefte* **9**, 21 (1929).

¹¹³ F. Ackerman, D. T. F. Pals, and J. J. Hermans, *Rec. trav. chim.* **71**, 56 (1952).

¹¹⁴ See also F. R. Eirich, ed., "Rheology: Theory and Applications," Vol. 1, Chapter 14. Academic Press, New York, 1956.

recently¹¹⁵ using a precision viscometer.¹⁰⁹ At higher concentrations the shear effect must be due to strong ionic interaction⁹⁰ since, for example, for DNA, $[\eta]$ is almost independent of ionic strength (so that changes of polymer dimensions can be neglected), yet the non-Newtonian viscosity is much diminished by addition of excess of simple electrolytes. Similar effects occur with other polyelectrolytes.^{91, 92} Part of the effect of shear rate may be on the first electroviscous effect, but little information is available.

Strauss and Fuoss¹¹⁶ have made a careful study of the shear dependence of reduced viscosity of PVPIBr and represented their results by an empirical function

$$(\eta_{sp}/c)_q = (\eta_{sp}/c)_{q=0} \{1 - [\alpha(\eta_{sp}/c)_{q=0} \cdot q]\} \quad (32)$$

where q is the velocity gradient, and α is a constant depending on the polymer and its degree of ionization. The relative effect of shear rate increases upon dilution since η_{sp}/c increases upon dilution (except at the lowest concentrations).

Equation (32) is not satisfactory for all polymers over a wide range of q values since η_{sp}/c is not usually linear in q . At high concentrations the function is concave, approximating to an hyperbola between the axes of η_{sp}/c and q . At low concentrations a bend over of η_{sp}/c with decreasing q occurs,^{90, 115} and at very low shear rates (5–0.5 sec.⁻¹) the behavior approximates to that predicted by Kuhn and Kuhn.¹¹⁰ In the presence of considerable salt concentrations ($>0.01 N$) the relation (32) holds over a wider range of shear rates.

VIII. General Expression for the Electroviscous Effects

The general expression for viscosity of a suspension is (cf. equation 1)

$$\eta = \eta_0(1 + K\phi + K'\phi^2 + \dots), \quad (33)$$

where only the first term in ϕ is usually taken and K depends on the form of the particle and on electrical effects. K can be subdivided into three terms K_1 , K_2 , K_3 , corresponding to each of the electroviscous effects:

$$\eta = \eta_0(1 + [K_1 + K_2 + K_3]\phi). \quad (34)$$

As each factor is a function of ϕ , a power series

$$\eta = \eta_0(1 + a_1\phi^{1/2} + a_2\phi + a_3\phi^2 + \dots) \quad (35)$$

may be written. Separation of the constituent effects is difficult but has been

¹¹⁵ H. Eisenberg, *J. Polymer Sci.* **25**, 257 (1957).

¹¹⁶ U. P. Strauss and R. M. Fuoss, *J. Polymer Sci.* **8**, 593 (1952).

attempted by Dobry³⁶ for suspensions of thorium hydroxide obtained from ThCl_4 by hydrolysis. This colloid is positively charged with Cl^- gegen ions. The hydrolysis forms free aqueous HCl which is in equilibrium with the colloidal hydroxide. The hydrochloric acid can be removed by dialysis but this also affects the net charge of the colloidal particles. During dialysis of the hydrated oxide, the constant K increases from 16 to 193 on account of change of electrolyte concentration from 16×10^{-4} to 1×10^{-4} mol./liter. Dobry showed that the reduced viscosity was independent of concentration, of the shape of the particles, and of the velocity gradient, thus apparently indicating the occurrence of only the first electroviscous effect. However, light-scattering and electron microscopy showed that the particles are in fact chainlike, and the degree of coiling varies with the colloid and with the HCl concentration. Quantitative differentiation of the three electroviscous effects was therefore not possible.

Nomenclature

a	Exponent in $[\eta]$ versus molecular weight relationship; radius of a (spherical) particle	z	Valence of an ion, i.e., formal charge on the ion
A	Length of a statistical segment in a polymer coil	α	Degree of ionization of a polymer
c	Concentration of a solute in moles per liter or base moles per liter	α'	Apparent degree of ionization of a polymer
e	Electronic charge	ϵ	Static dielectric constant of a solution or solvent
G_e	Electrical free energy contribution	ζ	Zeta potential
\bar{h}	Mean end-to-end distance in a statistical coil	$[\eta]$	Intrinsic viscosity
k	Boltzmann's constant	η	Viscosity of a solution
N	Number of statistical segments in a coil	η_0	Viscosity of the solvent
N_A	Avogadro's number	η_{sp}	Specific viscosity of a solution
q	Shear rate	κ	Reciprocal radius of the ionic atmosphere
\bar{R}	Average radius of a statistical coil	λ	Specific conductivity
t	Time (of flow in a viscometer)	μ	Ionic strength
T	Absolute temperature	ρ_s	Frictional coefficient of an ion
		ϕ	Volume fraction of a solute in a solution
		ψ	Orientation angle (in birefringence)

CHAPTER 4

THE RHEOLOGY OF LATEX

Samuel H. Maron and Irvin M. Krieger

I. Introduction.....	121
II. Literature Resumé.	122
III. Experimental Determination of Flow Behavior.....	125
1. Instruments.	125
2. Treatment of Data	127
a. Capillary Viscometer.	127
b. Concentric Cylinder Viscometer.	129
IV. Dependence of Latex Flow on Shearing Stress.....	130
V. Dependence of Latex Flow on Concentration.....	135
VI. Effect of Particle Size and Size Distribution.....	139
VII. Effect of Temperature	140
VIII. Effect of Electrolytes	140
IX. Some Unsolved Problems in Latex Rheology.....	141
Nomenclature	143

I. Introduction

The term *latex* was originally used to designate the milky liquid which is obtained from certain trees, particularly *Hevea brasiliensis*, and which yields natural rubber on coagulation. More recently the term latex has been used to designate not only the above natural products, but also aqueous colloidal dispersions of high polymeric materials prepared synthetically by emulsion polymerization. Although it is also possible to prepare latices by dispersion of high polymers in aqueous or other media, such dispersions are outside the scope of the present chapter. The discussion here will be confined to the rheology of natural latex, and to synthetic latices prepared from the monomers by emulsion polymerization.

From a physicochemical standpoint, both natural and synthetic latices are colloidal dispersions of high polymeric materials in water which are stabilized by the presence of protective agents adsorbed by the disperse phase. In the case of natural rubber latex the system contains polyisoprene dispersed in water, as well as resins, sugars, proteins, electrolytes, and some ingredients still undefined. Besides, the commercially available latex contains also added ammonia or other stabilizers. In natural latex the dispersed particles are more or less spherical, they carry a negative charge,

and their size may range from several hundred angstroms up to 10 or more microns in diameter. Synthetic latices, on the other hand, may vary widely in composition of the dispersed polymer, and the stabilizers employed may be soaps of various kinds, synthetic emulsifiers, or both. The latices generally contain also some electrolyte. The particles in synthetic latices are spherical, they are as a rule negatively charged, and their size distribution, which may be wide, is usually narrower than that of natural latex. Further, the average particle size of synthetic latices can be controlled by the mode of preparation so as to yield products ranging all the way from about 300 A. up to 10 or more microns in diameter.

At concentrations below about 25 % solids, both natural and synthetic latices exhibit Newtonian flow behavior, and hence the measurement of their viscosities introduces no particular problems. However, at higher concentrations latices exhibit "pseudoplastic" flow, with the deviation from Newtonian behavior being generally more pronounced in the synthetic latices than in the natural ones. This behavior immediately introduces the problems of flow measurement, reduction of data to results independent of the instruments and their dimensions, and the question of how the results are to be expressed and presented. Besides this dependence of flow behavior on the rate of shear or shearing stress in the laminar region, we also have the problems associated with turbulent flow in non-Newtonian systems, and the effects on the flow of such variables as polymer composition and concentration, nature and concentration of protective agents and other ingredients, particle size and its distribution, temperature, and electrical environment. Very few complete answers are as yet available to many of the questions which can be raised.

The plan of this chapter is (a) to review the information available on the flow behavior of natural and synthetic latices; (b) to discuss briefly measurement of latex flow behavior and reduction of data to rate of shear-shearing stress curves; (c) to present available information on the effect of various variables on the flow behavior; and (d) to mention some problems connected with latex rheology which are still unsolved, and upon which more information is highly to be desired. The latter problems are to a large degree those facing the entire field of rheology.

II. Literature Resumé

Latex dispersions have relatively low viscosities compared to other fluid forms of polymer. Thus, a latex containing 60 % by weight of polymer is often more fluid than a 2 % solution of the polymer in an organic solvent. Since the technical uses of latex are greatly dependent upon its viscosity, it is not surprising to find a number of rheological studies in the literature on the flow properties of latex, and particularly on the effect of concentration on the viscosity.

Most of the published work on latex rheology pertains to natural rubber latex, and was performed in "practical" nonabsolute instruments under conditions where little or no attention was given to the non-Newtonian flow characteristics. In studies of this type, for example, De Vries,¹ Stevens,² and others³ have shown that many factors beside concentration affect the viscosity of natural latex. Among these are the age and condition of the tree yielding the latex, the time and method of tapping, as well as the stabilizers introduced to preserve the latex. De Vries also demonstrated that dilution of a latex with ammonia is more effective than dilution with water in decreasing latex viscosity.

The viscosity of natural latex is particularly dependent on concentration, with the increase in viscosity being very pronounced above 60% solids.⁴ De Vries¹ showed that the increase was steeper than exponential. Again, Bary⁴ found that the Arrhenius equation

$$\log \eta_r = \frac{Kw}{1 + (n-1)w} \quad (1)$$

where η_r is the apparent relative viscosity, w the weight fraction of rubber and K and n empirical constants, did not climb rapidly enough to fit the data. Bachle,⁵ who used for his measurements a Höppler falling ball viscometer, attempted to represent his data by the Guth formula

$$\eta_{sp} = 2.5v + 7.8v^2 \quad (2)$$

where η_{sp} is the specific viscosity and v the volume fraction of disperse phase. He found the equation to be inapplicable above $v = 0.45$.

Rhodes and Smith⁶ and Sekar and Wahab,⁷ using the Höppler instrument among others, proposed several new viscosity-concentration functions. For preserved natural latex they gave the equation

$$\log \eta = 0.034 + 0.952 \tan w \quad (3)$$

while for a centrifuged concentrate

$$\log (\eta + 0.0309) = 0.143 + \frac{1.014r}{1 - w} \quad (4)$$

¹ O. De Vries, *Arch. Rubbercult. Ned.-Indië* **7**, 409 (1923).

² H. P. Stevens, *Bull. Rubber Growers' Assoc.* **2**, 214 (1920).

³ E. A. Hauser and W. Kelly, "Latex." Reinhold, New York, 1930.

⁴ P. Bary, *Rev. gén. caoutchouc* **11**, 3 (1934).

⁵ O. Bachle, *Kautschuk* **12**, 210 (1936); *Rubber Chem. and Technol.* **10**, 675 (1937).

⁶ E. Rhodes and H. F. Smith, *Rubber Chem. and Technol.* **13**, 474 (1938).

⁷ E. Rhodes, H. F. Smith, K. Sekar, and C. Wahab, *India Rubber J.* **97**, 21 (1939); *J. Rubber Research Inst. Malaya, Commun.* **9**, 171 (1939).

where r is the weight ratio of dry rubber to serum. Smith⁸ also proposed the formula

$$\log \eta_r = a + br \quad (5)$$

where a and b are constants, while Houwink and Klaassens⁹ attempted to fit the data of Rhodes and Smith to the modified exponential function of Papkov

$$\log \eta_r = Kv^\alpha \quad (6)$$

where K and α are constants. To cover the concentration range from 0 to 69% solids, they used $\alpha_1 = 1.00$ for the range 0–15%, $\alpha_2 = 1.18$ from 15 to 30%, and $\alpha_3 = 1.70$ above 30% solids.

Despite the dependence of the viscosity of natural latex on shear stress, the above-mentioned studies neglected this important variable. They must be considered, therefore, as measurements of apparent viscosity at an approximately fixed shearing stress which may be different in each study. One of the earliest attempts to investigate the non-Newtonian behavior of latex was that of Madge,¹⁰ who used a Redwood viscometer to measure the effects of concentration, temperature, and alkalinity, and a Couette viscometer to determine the effect of rate of shear. Madge found the *hevea* latex to be non-Newtonian, and clearly showed that the latex possessed no yield point. Nevertheless, in an effort to set up a viscosity specification test for *hevea* latex, Jordan and co-workers¹¹ assumed the latex to possess a yield point and a limiting viscosity in the Bingham¹² sense, and proceeded to develop a simple capillary instrument for determination of the two Bingham constants from efflux rate measurements at two different pressure heads. The Crude Rubber Committee¹³ of the Division of Rubber Chemistry of The American Chemical Society accepted Jordan, Brass, and Roe's apparatus for a tentative specification method, and also recommended the rotational viscometer of Mooney and Ewart¹⁴ for the same purpose. The work of Jordan and associates was criticized sharply by van Gils,¹⁵ who pointed out the desirability of obtaining the complete rate of

⁸ H. F. Smith, *J. Rubber Research Inst. Malaya, Commun.* **11**, 44 (1941); *Rubber Chem. and Technol.* **15**, 301 (1942).

⁹ R. Houwink and K. H. Klaassens, *Kolloid-Z.* **99**, 160 (1942).

¹⁰ E. W. Madge, *Trans. Inst. Rubber Ind.* **10**, 393 (1935); *Rubber Chem. and Technol.* **8**, 501 (1935).

¹¹ H. Jordan, P. Brass, and C. Roe, *Ind. Eng. Chem.* **9**, 182 (1937); **11**, 377 (1939).

¹² E. C. Bingham, *Natl. Bur. Standards (U. S.), Sci. Paper* **278** (1916).

¹³ Crude Rubber Committee, Division of Rubber Chemistry, American Chemical Society, *Ind. Eng. Chem., Anal. Ed.* **11**, 593 (1939).

¹⁴ M. Mooney and R. H. Ewart, *J. Appl. Phys.* **5**, 350 (1934).

¹⁵ G. E. van Gils, *Arch. Rubbercult. Ned.-Indië*, **24**, 403 (1940); *Rubber Chem. and Technol.* **14**, 137 (1941).

shear-shearing stress curve without prejudicial assumptions. Thus far no such results have been published for natural latex.

Prior to the recent publications of the authors and their co-workers, to be discussed more fully below, very little significant information has been published on the flow behavior of synthetic latices. The only studies to which reference need be made here are those of Livingston¹⁶ on Neoprene latex, and of Winding *et al.*¹⁷ on 70:30 butadiene-styrene GR-S latex. Livingston, investigating the creaming behavior of Neoprene latex mixtures, measured the flow behavior of Neoprene latex in a concentric cylinder viscometer, and found the latex to be pseudoplastic in character. Nevertheless he assumed the existence of a yield point, and proceeded to correlate the values of the latter with creaming ability. Winding, Bauman, and Kranich, in turn, studied the flow properties of stripped, vented, and unvented GR-S latex in pipes and capillaries. They found the latex to be non-Newtonian and to show a continual decrease of viscosity with increase in the shearing stress. By using the Newtonian approximation to convert their data to rate of shear and shearing stress, and then plotting the log of the shear stress versus the log of the rate of shear, they found linear relationships in many cases. However, they made no attempts to obtain analytic relationships for the flow equation followed by the latices.

III. Experimental Determination of Flow Behavior

From the results of previous investigations, as reviewed above, it is evident that latex is a non-Newtonian fluid. Further, our own and other observations have shown that uncompounded latices are not thixotropic; i.e., their flow behavior is instantaneously reversible. The first object of latex rheology is therefore the determination of the relationship between the rate of shear $\dot{\gamma}$ and the shearing stress τ . To be suitable for this purpose, a viscometer must be an absolute instrument which permits variation of the shearing stress over the desired range. This requirement rules out most of the "practical" viscometers, as these are capable only of measuring relative viscosities.

1. INSTRUMENTS

The most widely used absolute viscometers are of the concentric cylinder and capillary types. Properly designed instruments of either type may be employed for latex measurements. A concentric cylinder viscometer should have a narrow clearance; that is, $s = R_2/R_1$, where R_2 and R_1 are the radii of the outer and inner cylinders, should be as small as possible, and prefer-

¹⁶ H. K. Livingston, *Ind. Eng. Chem.* **39**, 550 (1947).

¹⁷ C. C. Winding, G. P. Bauman, and W. L. Kranich, *Chem. Eng. Progr.* **43**, 527, 613 (1947).

ably below 1.10. While this design feature makes mechanical alignment of the cylinders critical, it does offer some important advantages. First, with a narrow clearance most of the viscous drag will be exerted on the cylinder walls, so that the "end-effects" produced by top and bottom surfaces can be approximated by an empirically determined correction of the length of the inner cylinder. Second, with smaller s values, higher rates of shear are obtainable with reasonable angular velocities. And, third, calculations of the true rates of shear are more accurately and easily made when s is near unity. Another desirable feature in a concentric cylinder viscometer for latex use is complete immersion of the inner cylinder in the sample. Such immersion minimizes any errors caused by centrifuging, the Weissenberg effect, or variation in sample level. Finally, it is advisable to provide the viscometer with a cover or vapor space to prevent or reduce evaporation and skin formation on the latex surface. An instrument which meets these specifications quite well is the Mooney-Ewart conicylindrical viscometer.¹⁴ However, difficulty is encountered occasionally in using this instrument with latices which are mechanically unstable. When an unstable latex is subjected to the frictional pressure exerted by the shaft riding in the lower bearing of the viscometer, coagulation of the latex takes place, and the torque required for rotation of the inner cylinder is increased above its correct value.

In order to obtain a wide range of shearing stresses in a capillary viscometer, provision must be made for varying the applied pressure and for changing the capillary bore. Pressures up to about 1,000,000 dynes/cm.² are desirable, and several capillaries of radii between 0.2 and 0.7 mm. should be available. The capillary lengths should be at least fifty times their radii in order to minimize the importance of the end-effects. With such capillaries it will usually be possible to operate at flow rates where the kinetic energy correction is negligible. The capillary tubes should be made of a resistant glass if they are to withstand the hot oxidizing solutions required for removal of latex films.

Capillary viscometers offer several distinct advantages over concentric cylinder instruments. First, capillary viscometers are usually simpler and less expensive to construct. Second, end-effects, Weissenberg effect, heat buildup, misalignment, and centrifuging errors are either absent, or they can be rendered negligible by proper design. Third, high rates of shear are more readily attained in capillary than in rotational instruments. And, finally, calculation of the true rate of shear is simpler for capillary viscometers than for concentric cylinder systems.¹⁸⁻²⁰

¹⁸ I. M. Krieger and S. H. Maron, *J. Appl. Phys.*, **23**, 147 (1952).

¹⁹ I. M. Krieger and H. Elrod, *J. Appl. Phys.*, **24**, 134 (1953).

²⁰ I. M. Krieger and S. H. Maron, *J. Appl. Phys.*, **25**, 72 (1954).

Maron and co-workers²¹ have developed a capillary viscometer which is very satisfactory for latex studies. This instrument, of all glass construction, is convenient, accurate, and absolute, and permits measurements over a shear stress range from about 5 to 3000 dynes/cm.². A modified form of this instrument, applicable to shear stresses between about 0.06 and 20 dynes/cm.², has been described by Maron and Belner.²² For shear stresses higher than ca. 3000 dynes/cm.² the authors use a positive displacement capillary instrument in which known rates of flow are obtained by means of a motor-driven syringe. The pressure drops across the capillary are determined with strain-gage transducers.

Recently, cone and plate viscometers have been developed in which the rate of shear is uniform throughout the fluid being sheared. The commercial versions of this instrument, such as the Ferranti-Shirley viscometer, may be suitable for latex studies provided the latices are mechanically stable. With mechanically unstable latices the close clearances employed in these instruments will operate essentially as mechanical stability test devices²³ and cause partial, or even total, coagulation of the latex sample under test.

2. TREATMENT OF DATA

a. Capillary Viscometer

In a capillary viscometer the shearing stress at a distance r from the axis of a capillary tube of radius R and length L is

$$\tau = rP/2L \quad (7)$$

where P is the pressure drop caused by viscous resistance. The rate of shear, in turn, is the gradient of fluid velocity u , or

$$\dot{\gamma} = -du/dr \quad (8)$$

The experimentally measured variable is the volume rate of flow Q or

$$Q = \int_0^R \pi r^2 \dot{\gamma} dr = \frac{8\pi L^3}{P^3} \int_0^{\tau_w} \phi \tau^3 d\tau \quad (9)$$

where $\tau_w = RP/2L$ is the shearing stress at the capillary wall and $\phi = \dot{\gamma}/\tau$ is the fluidity.

Equation (9) can be integrated if we know or assume the relation between $\dot{\gamma}$ and τ , that is, the flow equation. In the Newtonian case, where ϕ is a

²¹ S. H. Maron, I. M. Krieger, and A. W. Sisko, *J. Appl. Phys.* **25**, 971 (1954).

²² S. H. Maron and R. J. Belner, *J. Appl. Phys.* **26**, 1457 (1955).

²³ S. H. Maron and I. N. Ulevitch, *Anal. Chem.* **25**, 1087 (1953).

constant, equation (9) yields on integration the Poiseuille equation, namely,

$$\phi = \frac{8LQ}{\pi R^4 P} \quad (10)$$

If the fluid is non-Newtonian, it is frequently possible to assume over limited ranges²⁴⁻²⁹ the exponential flow equation

$$\tau^N = \eta' \dot{\gamma} \quad (11)$$

or

$$\phi = \dot{\gamma} / \tau = \tau^{(N-1)} / \eta' \quad (12)$$

where N and η' are constants. N is an index of non-Newtonian behavior ($N = 1$ in the Newtonian limit) and η' is the viscosity at unit shearing stress. For this flow equation integration of equation (9) yields

$$Q = \frac{\pi R^3}{\eta'(N+3)} \left(\frac{RP}{2L} \right)^N \quad (13)$$

If equation (11) applies, then a plot of $\log Q$ versus $\log P$ should be linear, with slope equal to N . With N determined, η' may be evaluated from the intercept. $\dot{\gamma}$ and ϕ then follow from equations (11) and (12). The expression $\tau_w = RP/2L$ remains valid even in the non-Newtonian case.

However, it is possible to deduce the nature of the flow curve from equation (9) without knowing or assuming the flow equation. For a non-Newtonian fluid in a capillary viscometer an apparent fluidity ϕ_c may be defined by means of the Poiseuille relation

$$\phi_c = \frac{8LQ}{\pi R^4 P} \quad (14)$$

On substitution of equation (14) into equation (9), we obtain

$$\phi_c = \frac{4}{\tau_w^4} \int_0^{\tau_w} \phi \tau^3 d\tau \quad (15)$$

This integral equation of the capillary viscometer is a relation between ϕ_c and τ_w , and does not contain any instrumental dimensions. Consequently, ϕ_c - τ_w data from different capillary viscometers may be compared directly.

²⁴ I. M. Krieger and S. H. Maron, *J. Colloid Sci.* **6**, 528 (1951).

²⁵ S. H. Maron, B. P. Madow, and I. M. Krieger, *J. Colloid Sci.* **6**, 584 (1951).

²⁶ S. H. Maron and B. P. Madow, *J. Colloid Sci.* **8**, 130 (1953).

²⁷ S. H. Maron and B. P. Madow, *J. Colloid Sci.* **8**, 300 (1953).

²⁸ S. H. Maron and S. M. Fok, *J. Colloid Sci.* **10**, 482 (1955).

²⁹ S. H. Maron and A. E. Levy-Pascal, *J. Colloid Sci.* **10**, 494 (1955).

Solution of this equation, first obtained by Weissenberg, may be expressed in the form²⁰

$$\phi = \phi_c [1 + \Delta_c(\tau_w)] \quad (16)$$

where $\Delta_c(\tau_w)$ is given by

$$\Delta_c(\tau_w) = \frac{1}{4} \frac{d \log \phi_c}{d \log \tau_w} \quad (17)$$

Consequently, all that need be done to obtain the true fluidity ϕ is to evaluate ϕ_c , plot $\log \phi_c$ versus $\log \tau_w$, and differentiate graphically the resulting plot. $\Delta_c(\tau_w)$ is then $\frac{1}{4}$ of this slope, and ϕ follows from equation (16). Once ϕ values are available at various τ_w 's, they may be plotted against each other to give the flow curve.

b. Concentric Cylinder Viscometer

In a typical concentric cylinder viscometer the sample is confined between a cup of radius R_2 and a bob of radius R_1 and length L . The measured torque M is that required to produce a steady relative angular velocity Ω between the cylinders, and the shearing stresses τ_1 and τ_2 produced in a fluid at the inner and outer cylinders are, respectively,

$$\tau_1 = \frac{M}{2\pi R_1^2 L} \quad (18)$$

$$\tau_2 = \frac{M}{2\pi R_2^2 L} \quad (19)$$

Finally, it can be shown that Ω and the τ 's are related by the expression

$$\Omega = -\frac{1}{2} \int_{\tau_1}^{\tau_2} \frac{\dot{\gamma}}{\tau} d\tau = -\frac{1}{2} \int_{\tau_1}^{\tau_2} \phi d\tau \quad (20)$$

where $\phi = \dot{\gamma}/\tau$.

For a Newtonian fluid ϕ is a constant and equation (20) yields on integration

$$\phi = \frac{2\Omega}{\tau_1(1 - s^2)} \quad (21)$$

where $s = R_2/R_1$. Again, for a fluid obeying the exponential flow equation (11), integration of equation (21) gives

$$\Omega = \frac{1}{2N\eta'} \left(\frac{R_2^{2N} - R_1^{2N}}{R_2^{2N}} \right) \left(\frac{M}{2\pi R_1^2 L} \right)^N \quad (22)$$

When equation (22) is applicable, a plot of $\log \Omega$ versus $\log M$ yields a

straight line of slope equal to N . With N known, η' can be found from the intercept, and $\dot{\gamma}$ and ϕ may be found from equations (11) and (12).

An asymptotic solution of equation (20) without assuming a flow equation was obtained by Krieger and Elrod.¹⁹ Their result can be expressed in the generalized form²⁰

$$\phi = \phi_s[1 + \Delta_s(\tau_1)] \quad (23)$$

Here ϕ is the true fluidity and ϕ_s the fluidity as calculated from equation (21). Again $\Delta_s(\tau_1)$ is given by

$$\Delta_s(\tau_1) = k_1 \left(\frac{d \log \phi_s}{d \log \tau_1} \right) + k_2 \left(\frac{d \log \phi_s}{d \log \tau_1} \right)^2 \quad (24)$$

where

$$k_1 = \frac{s^2 - 1}{2s^2} (1 + \frac{2}{3} \ln s) \quad (25)$$

and

$$k_2 = \left(\frac{s^2 - 1}{6s^2} \right) \ln s \quad (26)$$

To handle these equations, ϕ_s is calculated first from the experimental data, then $\log \phi_s$ is plotted versus $\log \tau_1$, and the plot differentiated graphically to obtain $d \log \phi_s / d \log \tau_1$. These slopes, along with the instrumental constants k_1 and k_2 , give then $\Delta_s(\tau_1)$, and the latter, introduced into equation (23), yield finally the true fluidities at the various values of τ_1 .

Examples of the application of these various equations to latex, and of the superposition of the results from capillary and rotational viscometers, may be found in publications from this laboratory.²⁴⁻³⁰ The only point which need be illustrated here is the superposition of the results obtained with both capillary and rotational viscometers when the data were handled by means of equations (16) and (23), i.e., without assumption of a flow equation. Figure 1 gives a plot of ϕ versus τ for a 62.2% solids synthetic latex measured in a capillary viscometer and in a rotational viscometer with two different clearance ratios. The three sets of points may be seen to fall very well on the same curve.

IV. Dependence of Latex Flow on Shearing Stress

As was pointed out above, no published data are available for natural rubber latex which give unambiguously the relation between shear stress and rate of shear. Whatever data are available merely show that natural rubber latex is non-Newtonian at the higher concentrations, with the flow

³⁰ S. H. Maron and R. J. Belner, *J. Colloid Sci.* **10**, 523 (1955).

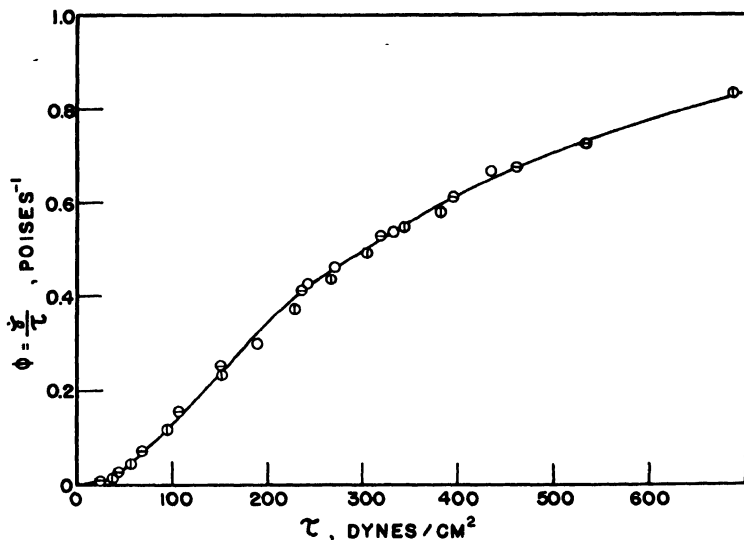


Fig. 1. Fluidity-shear stress plot for a 62.2% solids latex at 30°C. in capillary and concentric cylinder viscometers. Key: Φ , concentric cylinder a; Θ , concentric cylinder b; \circ , capillary.

being of the type generally referred to as pseudoplastic. Consequently, all of the following will be confined to the discussion of the relation between rate of shear and shearing stress observed with synthetic latices.

Krieger, Maron, and Madow^{24, 26} have shown that 50:50 butadiene-styrene copolymer latex emulsified with rosin soap is Newtonian in flow behavior up to a concentration of about 25% solids and is non-Newtonian at higher concentrations. This dividing line of ca. 25% solids between Newtonian and non-Newtonian flow has also been observed in latices of high butadiene content emulsified with both rosin and fatty acid soaps,^{25, 28, 30} in Neoprene latex,²⁹ and in latex mixtures.²⁷

Figure 2 shows the typical shape of flow curves for synthetic latex above ca. 25% solids. These curves are very near to linear at concentrations just above 25% solids and then deviate more and more from linearity as the concentration is raised. In all cases the curves are found to be concave upwards, indicating pseudoplastic flow, and in no instance do they show a yield point. At sufficiently high shear stresses the slope of each curve becomes constant, and consequently the latex approaches under these conditions Newtonian flow behavior with a limiting viscosity determined by the nature of the latex and its concentration. The higher the concentration for a given latex, the larger is this high shear stress limiting viscosity. Again, Maron and Belner³⁰ have found that latex above a volume fraction

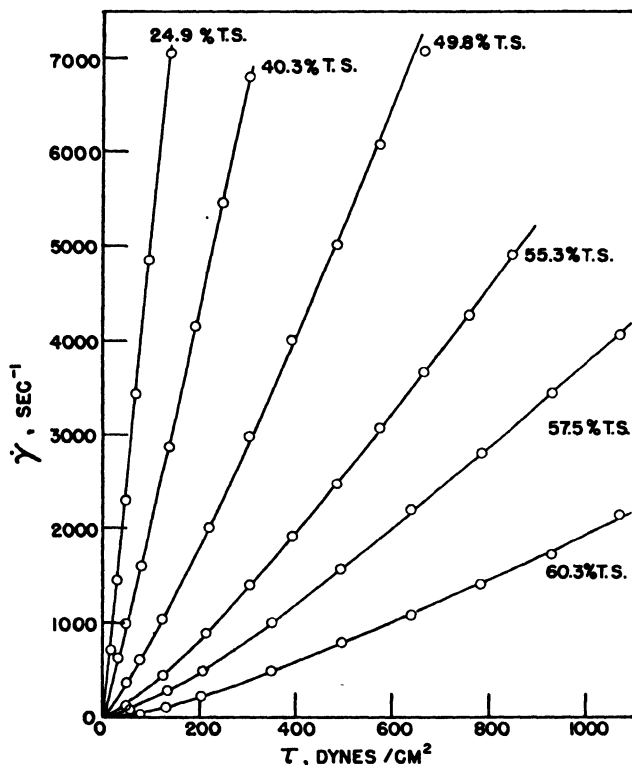


FIG. 2. Rate of shear-shear stress plot for a GR-S latex at various total solids contents and 30°C.

$v = 0.28$ and below $v = 0.54$ exhibits also Newtonian flow at very low shear stresses. The shear stress below which Newtonian flow set in ranged from $\tau = 4$ dynes/cm.² at $v = 0.28$ down to $\tau \simeq 0$ at $v = 0.54$ for the particular latex studied. No such approach to Newtonian flow was observed above $v = 0.54$. For any given concentration of latex the low shear Newtonian viscosity is in all cases higher than the high shear limit. These results indicate that the complete variation of the viscosity of a latex with shear stress or rate of shear in the non-Newtonian range can be represented schematically by a curve such as shown in Figure 3. One such curve corresponds to each fixed concentration, with the curves for higher concentrations lying above those for the lower ones.

A problem of considerable importance is the mathematical representation of these flow curves, i.e., the nature of the flow equation. Maron and associates²⁴⁻²⁷ have shown that in some instances equation (11) may be used to represent the relation between τ and $\dot{\gamma}$ over at least reasonable ranges of τ .

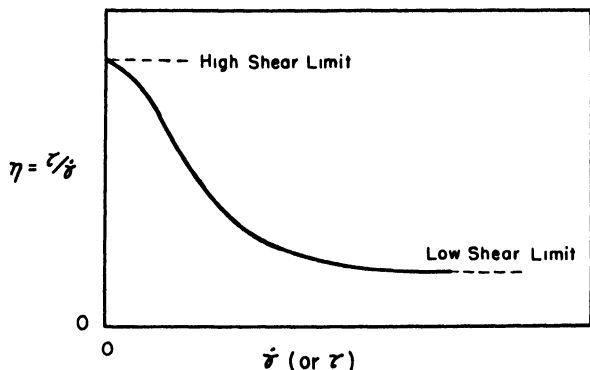


FIG. 3. Schematic diagram of complete flow curve for a latex of fixed concentration in non-Newtonian range.

They further found that up to ca. 40 % solids a single set of N and η' values was sufficient to represent the flow curve over the entire region studied. However, above ca. 40 % solids two sets of N and η' values were required, one for the lower shearing stresses and another for the higher ones. The N values, which measure deviation from Newtonian behavior, were found to range from $N = 1$ (Newtonian) up to $N = 2.6$ for ca. 62 % solids latex, while the η' values varied from the viscosity of water up to values as high as a million times that of water.

However, experience has shown that for many latex systems, as well as different samples of the same system, equation (11) is not valid even for limited ranges of τ .²⁸⁻³⁰ In the latter instances it was found possible to represent the flow behavior up to ca. 60 % solids by the relation

$$\eta_r^{1/2} = \frac{A + B\tau}{1 + C\tau} \quad (27)$$

for shear stresses above 50 dynes/cm²,^{28, 29} and by

$$\eta_r^{1/2} = \frac{A + B\tau^{1/2}}{1 + C\tau^{1/2}} \quad (28)$$

for shear stresses between 0.08 and 20 dynes/cm².³⁰ In these equations η_r , the relative viscosity, is defined as $\eta_r = \tau/\dot{\gamma}\eta_0$, while A , B , and C are parameters dependent on concentrations and temperature. These equations are purely empirical in character, and it is doubtful whether they have any general validity.

Ree and Eyring³¹ proposed in 1955 a generalized theory of flow which

³¹ T. Ree and H. Eyring, *J. Appl. Phys.* **26**, 793, 800 (1955).

considers a system to be composed of a number of flow units of different relaxation times and gives for the viscosity $\eta = \tau/\dot{\gamma}$ the relation

$$\eta = \sum b_i \frac{\sinh^{-1}(\beta_i \dot{\gamma})}{\beta_i \dot{\gamma}} = \sum b_i \theta_i \quad (29)$$

In this equation b_i and β_i are parameters characteristic of a particular flow unit and dependent on concentration and temperature, while the indicated summation has to be carried over the number of flow units required to represent η as a function of $\dot{\gamma}$. Maron and Pierce³² applied equation (29) to the latex flow data of Maron and Fok²⁸ on the supposition that the latex consists of two flow units, a Newtonian solvent unit and a polymer particle unit which may be non-Newtonian. On this basis equation (29) takes the form

$$\eta = a + b_1 \theta_1 = a + b_1 \frac{\sinh^{-1}(\beta_1 \dot{\gamma})}{\beta_1 \dot{\gamma}} \quad (30)$$

where a is the contribution made to the viscosity by the solvent, and $b_1 \theta_1$ that made by the latex particles. A plot of η versus $\dot{\gamma}$ predicted by equation (30) has the general shape shown by Fig. 3. At high values of $\beta_1 \dot{\gamma}$, $\theta_1 = 0$ and $\eta = a$. Again, when $\beta_1 \dot{\gamma} \rightarrow 0$, $\theta_1 = 1$ and $\eta = a + b$. The latter is also the expression for the viscosity of the system at lower concentrations when the flow becomes Newtonian. Consequently, this equation predicts for the non-Newtonian region Newtonian high and low shear limits of $\eta = a$ and $\eta = a + b$, respectively, and an intermediate viscosity variation with $\dot{\gamma}$ similar to that observed.

Maron and Pierce also found that equation (30) reproduced quantitatively the dependence of η on $\dot{\gamma}$ over the entire range of the latter variable studied and at all concentrations and temperatures. A typical example of the agreement obtained is shown in Fig. 4. However, application of the Ree-Eyring theory by Maron and Sisko³³ to the low shear data of Maron and Belner³⁰ showed that in this region three flow units are required to represent the data, that is, η is given now by

$$\eta = a + b_2 \theta_2 + b_3 \theta_3 \quad (31)$$

One of these flow units is the Newtonian solvent, while the other two are latex particle units of different relaxation times.

The equations given by the Ree-Eyring theory for the flow of a system in the non-Newtonian range are too complicated for substitution into and integration of equations (9) or (20). Further, to use these theoretical equa-

³² S. H. Maron and P. E. Pierce, *J. Colloid Sci.* **11**, 80 (1956).

³³ S. H. Maron and A. W. Sisko, *J. Colloid Sci.* **12**, 99 (1957).

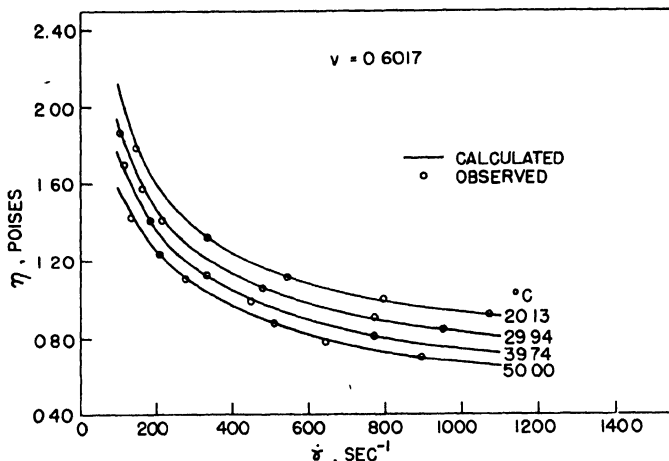


FIG. 4. Comparison of observed viscosities with those calculated by equation (30) for 62.0% total solids latex. ($\nu = 0.6017$). Key: —, calculated; O, observed.

tions τ and $\dot{\gamma}$ data are required. Hence these equations can be applied only to experimental results which have already been processed without assumption of a flow equation to convert the observables to τ - $\dot{\gamma}$ plots, or to equivalent ϕ - τ or η - $\dot{\gamma}$ plots.

The practice employed at present by the authors is to process experimental data without assumption of a flow equation, and then to plot the results as either $\phi = \dot{\gamma}/\tau$ versus τ or $\eta = \tau/\dot{\gamma}$ versus $\dot{\gamma}$. A set of curves thus obtained is shown in Fig. 5. These results can be left and used in graphical form, or, if desired or possible, mathematical functions can be fitted to the data.

V. Dependence of Latex Flow on Concentration

The viscosity of latex is very dependent on concentration. The increase of viscosity with concentration is relatively slow below 40% solids, more rapid between 40% and 50–55% solids, and extremely sharp above the latter concentrations. In general, the increase of viscosity with concentration is not as pronounced with natural latex as it is with the synthetic ones. With synthetic latices it is not unusual to find the viscosity of a 60% solids latex to be a million or more times that of water.

Some of the relations which have been employed to represent the variation of the viscosity of natural latex with concentration have been mentioned in Section II. In all these relations the viscosity, relative viscosity, or specific viscosity employed have been calculated on the basis of Newtonian behavior, with no attempt being made to take into consideration shear stress or rate of shear as a variable. The only latex systems in which

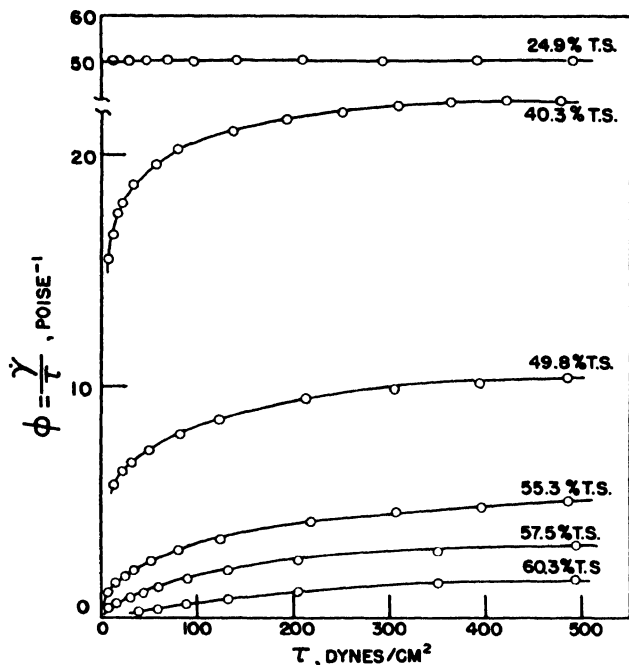


FIG. 5. Fluidity-shear stress plot for a GR-S latex at various total solids (T.S.) contents and 30°C.

cognizance was taken of the latter effect are the synthetic latices investigated by the authors.

Maron and co-workers²⁵⁻²⁷ have found that it is possible in some synthetic latex systems to represent the dependence of flow behavior on concentration by means of the relation

$$\log \frac{\eta'}{\eta_0} = \frac{\alpha b v}{1 - \alpha v} \quad (32)$$

where η' is the viscosity at unit shear stress as it appears in equation (11), η_0 is the viscosity of water, and v the volume fraction of polymer in the latex, whereas α and b are constants. When applicable, equation (32) is capable of representing the flow behavior of a latex all the way from $v = 0$ up to at least $v = 0.60$, that is, a polymer content higher than 60% solids. However, when equation (11) is unsatisfactory, then equation (32) is not applicable. For such instances the Eilers³⁴ equation, modified to the form

$$\eta_r = \left(1 + \frac{\alpha v}{1 - \beta v} \right)^2 \quad (33)$$

³⁴ H. Eilers, *Kolloid-Z.* **97**, 313 (1941).

has been found to be satisfactory.²⁸⁻³⁰ In this equation $\eta_r = 1/\phi\eta_0 = \tau/\dot{\gamma}\eta_0$ while α and β are fitted constants.

Both of these equations can be tested readily by graphical means. A rearrangement of equation (32) gives

$$\frac{v}{\log \eta'/\eta_0} = \frac{1}{\alpha b} - \frac{v}{b} \quad (34)$$

and hence a plot of the quantity on the left versus v should yield a straight line from which the constants can be obtained. Again, rearrangement of equation (33) yields

$$(\eta_r^{1/2} - 1)/v = \alpha + \beta(\eta_r^{1/2} - 1) \quad (35)$$

and hence a plot of $(\eta_r^{1/2} - 1)/v$ versus $(\eta_r^{1/2} - 1)$ should be linear if the equation is applicable.

In the case of the Ree-Eyring theory, the variation of the parameters a and b in equation (30) with concentration at any given temperature can be represented by the relations (32)

$$a = \frac{\eta_0}{(1 - \epsilon v)^2} \quad (36)$$

and

$$b_1 = \frac{K_b(\epsilon v)^2}{(1 - \epsilon v)^3} \quad (37)$$

In these equations η_0 is the viscosity of water, K_b is a constant dependent on temperature, and ϵ is a temperature independent constant. The same equations have been found applicable³³ to a and b_2 in equation (31). However, the dependence of β_1 and β_2 on concentration is different, as is also that of b_3 and β_3 .^{32, 33} A discussion of the variation of these parameters with temperature has been given by Maron and Pierce.³²

According to Einstein's theory³⁵ for suspensions of rigid spherical particles,

$$\lim_{v \rightarrow 0} \eta_{sp}/v = 2.50 \quad (38)$$

The extent to which this expectation is realized with synthetic latices can be deduced from the above equations. For small values of v equation (32) reduces to the form

$$(\eta'/\eta_0) - 1 = 2.303\alpha bv$$

or

$$\eta'_{sp}/v = 2.303\alpha b \quad (39)$$

³⁵ A. Einstein, *Ann. Physik* [4] **19**, 289 (1906).

Again as $v \rightarrow 0$, equation (33) reduces to

$$\eta_{sp}/v = (\eta_r - 1)/v = 2\alpha \quad (40)$$

and equation (36) to

$$\eta_{sp}/v = 2\epsilon \quad (41)$$

These equations are not quite correct because, in calculating the volume fraction v , no account was taken of the volume occupied by the adsorbed layer of emulsifier on the latex particles. Now, Maron *et al.*²⁵ have shown that the true volume fraction v_t is related to v by the relation

$$v_t/v = \gamma = 1 + (6\Delta/D_s) \quad (42)$$

where Δ is the thickness of the adsorbed monolayer of emulsifier, and D_s is the volume-to-surface average diameter of the dispersed particles as determined by soap titration.³⁸⁻³⁸ On eliminating v between equation (42) and equations (39-41), we obtain

$$\eta'_{sp}/v_t = 2.303ab/\gamma \quad (43)$$

$$\eta_{sp}/v_t = 2\alpha/\gamma \quad (44)$$

and

$$\eta_{sp}/v_t = 2\epsilon/\gamma \quad (45)$$

The values for η'_{sp}/v_t obtained from equation (43), and based on data obtained through use of equation (11), ranged from 2.03 to 2.25^{25, 26}. On the other hand, data processed without assumption of a flow equation, and based on the use of η_{sp} instead of η'_{sp} , gave limiting values of η_{sp}/v_t through equation (44) which ranged from 2.42 to 2.82²⁸⁻³⁰, and through equation (45) values of 2.60 and 2.67^{32, 33}. The results given by equations (44) and (45) are near the expected 2.50 value, and they indicate that the flow behavior of dilute latices is in good accord with the Einstein theory of dilute suspensions of spherical particles.

Equations (32), (33) and (36) predict, respectively, that the viscosity will become infinite at a volume fraction given by $v_\infty = 1/\alpha$, $v_\infty = 1/\beta$, and $v_\infty = 1/\epsilon$. When corrected by means of equation (42) for the volume occupied by the monolayer of emulsifier adsorbed upon the latex particles, these expressions become $v_\infty = \gamma/\alpha$, $v_\infty = \gamma/\beta$, and $v_\infty = \gamma/\epsilon$. The values of v_∞ obtained by means of the latter equations for various types of butadiene-styrene latices ranged from 0.68 to 0.77.^{25, 26, 28, 30, 32, 33} These results

²⁶ S. H. Maron, M. E. Elder, and I. N. Ulevitch, *J. Colloid Sci.* **9**, 89 (1954).

²⁷ S. H. Maron, M. E. Elder, and C. Moore, *J. Colloid Sci.* **9**, 104 (1954).

³⁸ S. H. Maron and M. E. Elder, *J. Colloid Sci.* **9**, 263 (1954).

are in good accord with $v_{\infty} = 0.74$ expected for rhombohedral close packing of uniform spheres, and values somewhat larger than 0.74 for spheres not uniform in size. However, in the case of Neoprene latex v_{∞} was found to range from 0.55 to 0.61.²⁹ These lower values suggest that in Neoprene the viscosity becomes infinite when the particles are closely packed in cubical rather than in rhombohedral array, i.e., with six rather than twelve closest neighbors.

VI. Effect of Particle Size and Size Distribution

Hevea latex, being a natural product, is not subject to much variation in either particle size or its distribution. Further, in order to preserve a certain uniformity in properties, latices from various trees and sources are frequently blended, and thereby differences which may be present are to a large degree wiped out. Consequently particle size and size distribution effects are questions which have not been investigated in connection with the flow behavior of natural latex.

However, this is not the case with synthetic latices. These may be prepared in average particle sizes ranging from several hundred angstroms up to several microns, and the size distribution can also vary within extremely wide limits.³⁹ Some latices may show a very narrow distribution, such as the much studied Dow 580G polystyrene latex, while others may have broad distribution curves with one or more peaks in them.³⁹ Under such circumstances the question of the effect of particle size and its distribution on flow becomes important.

Experience with latex polymerization has shown that, for the same solids content, large particle size latices are more fluid than corresponding latices of small particle size. However, it has not been established that the increase in fluidity is due entirely to increase in particle size. In order to make large particle size latices, polymerization recipes must be employed in which the amount of emulsifier used is considerably lower than in recipes for small particle size latices. Under such conditions the emulsifier-polymer ratio in the large and small particle size latices is quite different, as is also the fraction of the surface covered with emulsifier. What effects these latter factors have on fluidity of latex is still unknown; and, until they are evaluated, it will be impossible to establish unambiguously the effect of particle size on latex flow.

The only study which has been reported on the influence of particle size distribution on latex flow is that by Maron and Madow.²⁷ They studied the flow behavior of mixtures of two latices, both of which were heterogeneous in particle size, but whose average particle diameters differed by a factor of two. They found that, for mixtures of all proportions of the two

³⁹ S. H. Maron, C. Moore, and A. S. Powell, *J. Appl. Phys.* **23**, 900 (1952).

latices up to a total volume fraction of ca. 0.45, the $\log(\eta'/\eta_0)$ values were intermediate between those of the two constituents and were essentially linear with the composition, expressed as the fraction by volume of one constituent. Above a total volume fraction of 0.45, the plots showed minima which shifted toward greater proportions of the larger particle size latex as the total concentration increased. Further, the Einstein relation³⁸ was found to be obeyed reasonably well by the mixtures, while v_∞ was found to go through a maximum when the composition was about 75% of the larger particle size latex. Whereas v_∞ was 0.74 for the smaller particle size latex and 0.77 for the larger one, the maximum gave $v_\infty = 0.81$, indicating that mixtures of the two latices were capable of giving denser packing than the individual latices. These observations suggest that polydisperse latices should be capable of exhibiting flow to concentrations higher than corresponding monodisperse systems.

VII. Effect of Temperature

There are no published data on the effect of temperature upon the flow behavior of natural rubber latex. The only reference we have been able to find is the statement by Madge¹⁰ that the viscosity of natural rubber latex decreases sharply, and probably exponentially, with temperature.

For synthetic latices, in turn, there is available only one detailed study, that of Maron and Fok²⁸ on the flow behavior of a butadiene-styrene latex between 20° and 50° C. This study shows that the decrease of the viscosity of the latex with temperature results primarily from the decrease of the viscosity of the water medium. As a consequence the relative viscosity of a latex of given concentration changes very little with temperature, and the flow involves an activation energy which differs only slightly from that of pure water. Further, the deviation of the latex from Newtonian behavior has been found to be essentially independent of temperature and to be a function only of concentration and shear stress. An analysis of these data in terms of the Ree-Eyring theory has been given by Maron and Pierce.³²

VIII. Effect of Electrolytes

Ordinary electrolytes which are compatible with latex have generally a tendency to lower its viscosity. The effect is the more pronounced the higher the concentration of the added electrolyte. However, too much added electrolyte may produce agglomeration of the particles and eventual coagulation of the latex.

The effect of anions on the viscosity of latices is relatively smaller than the effect of the cations, since in general most latices are negatively charged. Latices containing soaps usually cannot tolerate multivalent cations, since

the soaps of such ions are insoluble, and hence the latices are destabilized. Among the monovalent cations the action of the potassium ion is unique, since potassium salts and potassium soaps give much more fluid latices at a given concentration than any of the other monovalent cations. Although the above observations are common knowledge among latex chemists, no study has as yet been published on the quantitative effect of electrolytes on either the viscosity of latex or its non-Newtonian behavior.

While most ordinary electrolytes lower the viscosity of latex, certain other electrolytes, such as sodium silicofluoride, and polyelectrolytes, such as sodium or ammonium alginate and sodium acrylate, raise it. These substances, as well as others, are known as thickeners. They are usually agents which promote the creaming and sometimes also the gelation of latices.

IX. Some Unsolved Problems in Latex Rheology

From the above discussion it is apparent that information is very meager on the flow behavior of natural latex. While the situation for synthetic latices is better, we still do not have a complete understanding of the behavior of these systems. Some of the deficiencies in the picture are peculiar to latices, while others are common to the entire field of non-Newtonian rheology.

The key problem in the entire field is the cause of non-Newtonian flow. Many rheologists ascribe all non-Newtonian behavior to orientation under shear. Although such effects may be operative when the suspended particles are unsymmetrical, it is difficult to extend this explanation to systems such as latices where the suspended particles are essentially spherical and, in many cases, rigid. To us a vital clue to the cause of non-Newtonian flow in latices is the observation that this phenomenon only appears when the volume fraction exceeds about 25 %. This suggests that, at least in these systems, the origin of non-Newtonian behavior is a crowding effect, and that contributions resulting from orientation and from particle-particle and particle-medium interactions are secondary.

A second deficiency which impedes the logical study of non-Newtonian flow is the lack of a simple and theoretically interpretable flow law, i.e., an analytic function relating the rate of shear $\dot{\gamma}$ and the shearing stress τ . While such a flow law is no longer necessary to obtain $\dot{\gamma}$ and τ from viscometric data, this task might be considerably eased if equations (9) and (20) could be integrated. A more important advantage would be the possibility of expressing the flow behavior of a fluid by means of the parameters of its flow equation, rather than by means of graphs or tables. While many empirical and semitheoretical flow laws have been proposed, none has been shown to be applicable to a wide class of fluids. And, although the Ree-

Eyring theory looks very promising as a general flow law, the equations yielded by this theory are difficult and tedious to handle, and the parameters of the equation are not always easily interpretable.

This brings us to the question of how the flow results are to be expressed. Most latex chemists, accustomed to thinking in Newtonian terms, insist on the expression of latex flow results in terms of a single parameter, the "viscosity." From the very definition of non-Newtonian flow it is evident that such an economy of expression of flow results is impossible. Nevertheless, the problems still remain of how many parameters are required to characterize the flow behavior and how these parameters are to be used in practical and theoretical problems. In our present state the most satisfactory way of expressing the results appears to be the $\phi = \dot{\gamma}/\tau$ versus τ or the $\eta = \tau/\dot{\gamma}$ versus $\dot{\gamma}$ plot. Although such a plot presents the desired information, it does not permit the ready use of the results, and it is not convenient for mathematical application. Again, while analytic functions can often be fitted to the curves, the functions are not always the same, and neither are the parameters. Consequently, intercomparison of flow results becomes difficult and confusing.

Beside these questions affecting the entire field of non-Newtonian flow, there are also some which apply specifically to latex, both natural and synthetic, and which require further elucidation. First, more information is required on the flow behavior of latices at very low shearing stresses in order to define more fully the shape of the flow curve. Second, we know as yet very little about the rheological effects of polymer composition, kind and amount of emulsifier, temperature, particle size, and particle size distribution. Third, systematic studies are required to define the action of electrolytes in latex, not only with a view to the type of electrolyte and its concentration but also from the standpoint of the theory of the electroviscous effect. Fourth, it is known that latices exhibit flow at concentrations beyond v_{∞} and that the flow behavior in those regions is not the same as below v_{∞} . Investigation of this concentration range should be of great interest. Fifth, no data are available on the flow behavior of latex in the turbulent region. Yet this region is of great importance practically, for the shear rates employed during polymerization and in subsequent handling place the latex in turbulent flow. Finally, most applications of latex require its compounding with various ingredients. This compounding modifies tremendously the flow characteristics and frequently imparts thixotropy to the system. As the processing conditions and the properties of the products formed are greatly dependent on the flow properties of the compounded latices, rheological information on such latices is needed, and would be of great help to the latex technologist.

Nomenclature

A, B, C	coefficients	Δ_c	correction term for capillary viscometer
D_s	particle diameter, volume to surface average	Δ_s	correction term for concentric cylinder viscometer
K, K_b	coefficients	Ω	angular velocity
L	length of capillary or cylinder	$\alpha, \alpha_1, \alpha_2, \beta$	coefficients
M	torque	γ	volume correction factor ($\gamma = v_i/v$)
N	exponent in flow equation	$\dot{\gamma}$	rate of shear
P	pressure drop	ϵ	coefficient
Q	volume rate of flow	η	viscosity
R	radius of capillary	η_0	viscosity of medium
R_1	radius of inner cylinder	η'	viscosity at unit shear stress
R_2	radius of outer cylinder	η_r	relative viscosity ($\eta_r = \eta/\eta_0$)
a, b, b_1, b_1, b_2, b_3	coefficients	η_{sp}	specific viscosity ($\eta_{sp} = \eta_r - 1$)
k_1, k_2	instrumental constants of concentric cylinder viscometer	η'_{sp}	specific viscosity at unit shear stress ($\eta'_{sp} = \eta'/\eta_0 - 1$)
r	radial coordinate; rubber-to-serum weight ratio	$\theta, \theta_1, \theta_2, \theta_3$	Eyring function [$\theta(x) = x^{-1} \sinh^{-1}x$]
s	radius ratio of concentric cylinder viscometer ($s = R_2/R_1$)	τ	shear stress
u	velocity	τ_u	shear stress at capillary wall
v	volume fraction of suspended phase	τ_1	shear stress at inner cylinder
v_t	total volume fraction, polymer plus soap	τ_2	shear stress at outer cylinder
v_∞	volume fraction at which flow ceases	ϕ	fluidity ($\phi = 1/\eta$)
w	weight fraction of suspended phase	ϕ_c	apparent fluidity in capillary viscometer
Δ	thickness of soap monolayer	ϕ_s	apparent fluidity in concentric cylinder viscometer

CHAPTER 5

THE RHEOLOGY OF PRINTING INKS

A. C. Zettlemoyer and Raymond R. Myers

I. The Role of Printing Inks.....	145
II. Rheological Requirements of Printing Inks	146
III. Ink Production	147
1. Premixing	147
2. Roll Milling.....	149
IV. Printing	152
1. Fountain Phase	152
2. Distribution Phase	153
3. Transfer Phase.....	154
4. Penetration Phase	156
V. Viscometric Study of Printing Inks	157
1. Theoretical Background.....	157
a. Printing Ink Flow Behavior	157
2. Instruments and Measurement	159
3. Status of the Viscometric Approach in Ink Rheology	162
4. The Mechanisms of Anomalous Viscosity in Inks	163
VI. Tack and Related Phenomena	167
1. The Nature of the Splitting Ink Film	167
2. Force Analysis of Tack	168
3. Instrumentation	169
4. Cohesive Strength of Liquids and Dispersions	172
5. The Rheology of Film Application by Rolls	176
Nomenclature	187

I. The Role of Printing Inks

In the production of the printed page, an ink meets a remarkable number of rheological requirements. Poured or scraped from the can into the press fountain, it must feed properly onto the fountain roller; distribute, transfer, and suffer structural breakdown over some twenty rollers in the distributing system; cover the printing form adequately without filling in fine half tones in pictures; transfer the message to the paper without serious squash out yet with no unprinted areas in solids; and then it must set on the porous paper sufficiently fast to prevent offset on rollers or paper. All this must be accomplished to supply the web of paper, moving through the press at speeds up to 25 miles per hour, with about 20 pounds of ink per ten inch page width to print 90,000 copies. In a few seconds, the ink is

compressed, stretched, sheared, fractured and kissed, and finally when it meets the paper, it is transferred and set-dried in a fraction of a second.

The complexity of this problem is multiplied by the variety of types of printing and of printed matter. From postage stamps to packages and from breadwraps to books, each ink is adapted to one or more of the different types of printing: gravure with indented printing plates, lithographic with work and nonwork areas at roughly the same level, letterpress with raised type, and flexographic with raised rubber plates. A host of variations in these processes and in types of presses cause further differences in rheological requirements of the various inks employed.

Printing inks constitute 2% of the dollar volume of the nation's fourth ranking industry. They are both the keystone and the common denominator of the graphic arts. Outside of the esthetic appeal that one ink may have over another, the chief means of judging the quality of an ink is by its flow properties; as a consequence, printing ink rheology is closely identified with its technology.

II. Rheological Requirements of Printing Inks

Practically all printing inks are suspensions of solid pigment particles in complex vehicles. In recent years, the traditional oleoresinous oil-based vehicles have been displaced percentagewise by the invasion of heatset inks based on resins dissolved in petroleum solvents, flexographic inks based on resins in alcohol, and steamset inks based on resins in glycols. Latexes appear to be headed toward limited use in the field; plastisols have also been considered.

Printing inks are usually pseudoplastic and possess a stress-versus-shear rate curve which is essentially linear only in the range of shear rates from 50 to 500 sec^{-1} ; below this range a decided curvature toward the origin is encountered. As a consequence they seldom can be characterized by a single parameter such as viscosity, except under conditions of high shear or when bracketing a viscosity range. Broad ranges of viscosity and of pigment concentrations are presented in Table I.

TABLE I
VISCOSITIES OF PRINTING INKS

<i>Types</i>	<i>Per cent pigment</i>	<i>Viscosity, poises</i>
Gravure	10-30	0.5-10
Flexographic	10-40	1-100
Letterpress	20-80	10-500
Newsink	8-12	2-10
Lithographic	20-80	100-800

Printing inks are probably the most precisely controlled commercial solid-in-liquid dispersions. To achieve adequate reduction of pigment agglomerates to below $2\ \mu$ for essentially all particles present, inks are usually manufactured, or at least finished, on a three-roll mill. But whether dispersed in a colloid mill, ball mill, or roll mill, rheological demands must be met if the process is to be most efficient. In fact, the rheology of printing inks begins in the premixer, where the pigment is first wetted by vehicle.

The rheological requirements of a printing ink will be followed through the manufacturing stages starting with the most commonly used change-can premixer, followed by the three-roll mill, and progressing through the fountain, distribution, transfer, and penetration phases of letterpress printing.

III. Ink Production

1. PREMIXING

The change-can or pony mixer is used to effect initial blending of the pigments and the vehicle. A typical mixer is illustrated in Fig. 1 where the can has been cut away to show the shape and direction of motion of the mixing blade. The usual procedure is to introduce the vehicle and part of the pigments and to add additional pigment as the wetting progresses in order to minimize dusting.

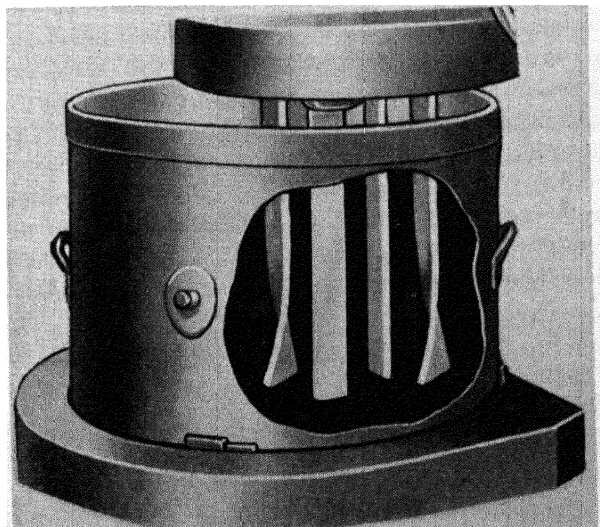


FIG. 1. Typical change-can mixer used for blending pigments with vehicles

An "intensive mixing" procedure has been developed by Hoback¹ and described by the New York Paint Production Club.² Accordingly, a limited amount of vehicle is used with all the pigment so that wetting down occurs in about 2 min. and at a high level of viscosity. After subsidence or "break" of the paste, the additional vehicle is added to give the mixture a proper consistency in preparation for the roller mill. At the higher viscosity in "intensive mixing," air is largely eliminated, the pigment is more finely dispersed, and lumps are eliminated.³

Rheological properties are changing constantly during the premix operation; generally, viscosity increases at the start. The most suitable conditions for each type of pigment-vehicle combination must be determined empirically; and as a consequence, there is need for a more careful elucidation and control of the process. No satisfactory method has been developed for deciding that the premixing is completed, such as the method of sediment volumes which is employed in dispersions made from low viscosity vehicles.

The "consistency" or rheological nature of the ink usually determines which is the most suitable mixer to employ. For relatively low viscosity the high speed turbine type of mixer is frequently used. In this mixer, high local shear rates accomplish dispersion; and the pumping action of the impeller circulates the fluid, bringing all portions of the batch into the high energy zone. For high viscosity and extremely short inks, mixers must employ a positive displacement shearing action where all portions of the batch are brought into the agitation zone through rotation of the mixer tub, through eccentric motion of the impeller shaft, or both. A recently developed angular mixer, Fig. 2, has combined features of both high speed impeller shear and positive displacement mixing action.⁴

Rheological properties influence the effectiveness of the mixing operation and determine the mixer power consumption. Metzner⁵ has shown that it is possible to employ a generalized Reynolds number for pseudoplastic materials obeying the relationship that stress = constant \times (shear rate)ⁿ, to correlate power consumption with turbine type mixer size and speed. Pseudoplastic flow properties tend to stabilize the flow pattern, and

¹ W. H. Hoback, *Practical Aspects of Pigment Dispersion*, *Offic. Dig. Federation Paint & Varnish Production Clubs* **316**, 255-297 (1951).

² New York Paint Production Club, *Offic. Dig. Federation Paint & Varnish Production Clubs* **311**, 977-1000, December (1950).

³ This subject is covered in National Printing Ink Research Institute Project Report No. 2, August 1946 on the Beken Mixer. American representatives are Bramley Machinery Corp., Edgewater, New Jersey.

⁴ Troy Engine and Machine Company, Troy, Pennsylvania, describes this mixer in Catalog GP-50.

⁵ A. B. Metzner and R. E. Otto, *AIChE Journal*, **3** (1), 3 (March, 1957).

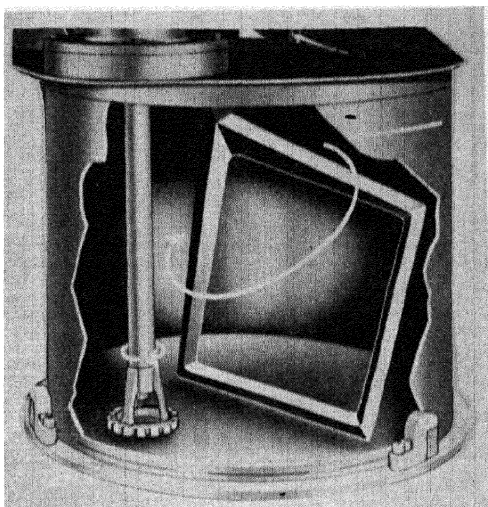


FIG. 2. The Troy angular mixer which combines high speed shear with thorough material turnover.

pseudoplastic fluids require higher levels of the Reynolds number to achieve complete turbulence than do Newtonian fluids.

2. ROLL MILLING

Most inks are finished on a roll mill where the fluid is subjected to increasingly higher rates of fluid shear between successive rolls operating at higher speeds and closer clearances. The three-roll mill having a feed nip and an apron nip is most commonly used. The clearance between the rolls depends on a number of variables, especially on ink viscosity and force on the rolls. A clearance of $10\ \mu$ would correspond to a tight setting in the final or apron nip. In recent years a "floating roll" mill has come into wide usage.⁶ The design of this type of mill is such that only two points of mill adjustment are required instead of the customary four points. The center roll is self-positioning and self-aligning. Figures 3A and 3B are schematic diagrams of conventional and floating roll mill designs.

Little or no crushing of primary pigment particles occurs in the roll mill. Its chief function is to disperse pigment agglomerates through fluid shear and particle-particle attrition. The largest agglomerates are crushed between the rolls, whereas the smaller agglomerates are dispersed mostly by hydraulic shear, which has been estimated to be of the order of magnitude of $50,000\ \text{sec}^{-1}$. It is the largest agglomerates which show up on the commonly used grind gage for estimating the fineness of grind of the

⁶ L. Maus, W. C. Walker, and A. C. Zettlemoyer, *Ind. Eng. Chem.* **47**, 701 (1955).

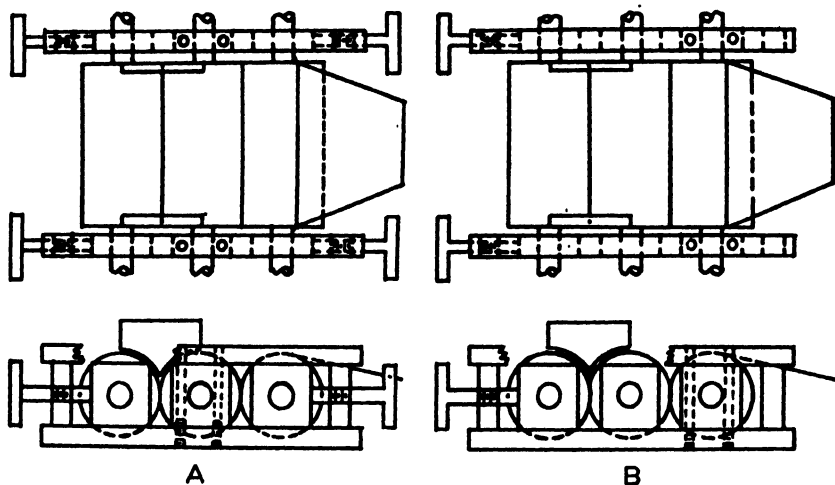


FIG. 3. Schematic diagrams of three-roll mills, top and side views. A. Conventional type—the center roll is fixed and the two outer rolls are positioned (four point adjustment). B. Floating roll type—the center roll is free to align itself between one fixed and one movable outer roll, thus requiring only two points of adjustment.

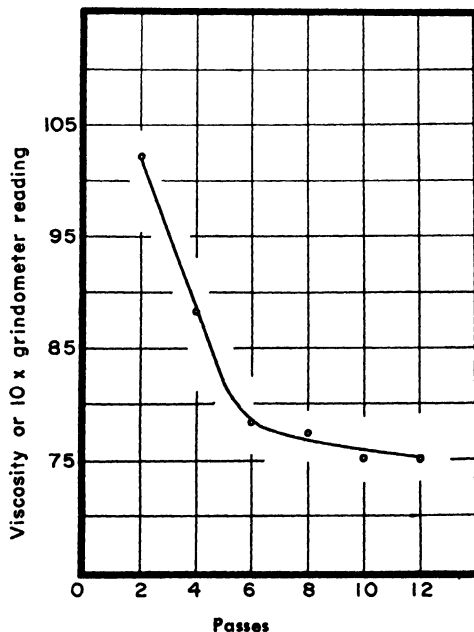


FIG. 4. Reduction of ink viscosity and fineness of grind with number of passes through a roll mill. Fineness of grind is a measure of maximum particle size.

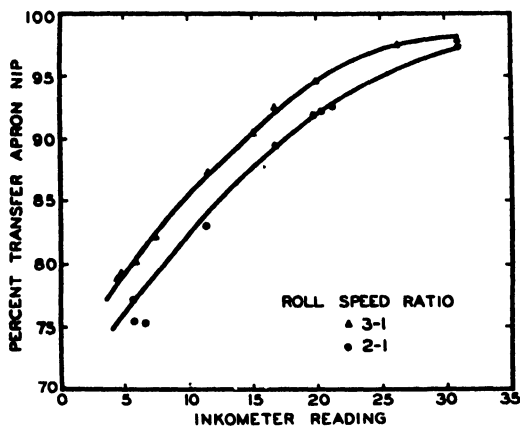


FIG. 5. Apron nip transfer in the roll mill as a function of Inkometer reading of commercial inks.

dispersion.⁷ Both production rate and fineness of grind appear to be proportional to the apron nip clearance in many instances. It has been found that the reduction in viscosity per pass and the decrease in fineness of grind follow a first order rate equation,⁸ as shown in Fig. 4. There is evidence, however, that this is partly due to the fact that reduction in viscosity effected by dispersion and by heating on one pass allows the mill to operate at a closer setting on the next pass.

Production rate R , in volume per unit time, of a three-roll mill depends on four factors: the quantity of ink Q entering the feed nip, the fractional transfers f and a from slow to fast roll at the feed nip and apron nip, respectively, and the fraction of ink t removed from the apron roll by the take-off knife. The relationship is given by the equation

$$R = \frac{taf}{1 - a + at} Q. \quad (1)$$

Q for a given mill is a function of roll speed, force between the rolls, and ink viscosity. The transfer factors a and f appear to depend primarily on roll speed ratio and on ink rheological properties as yet to be elucidated,⁹ but generally grouped under the term viscoelasticity.

The film leaving the mill nip splits somewhere between the surface of the slow roll and the center of the nip; that is, the split occurs closer to the fast roll than desirable for highest efficiency. Figure 5 shows that the percentage transfer for a variety of commercial inks increases with the

⁷ W. C. Walker and A. C. Zettlemoyer, *Am. Ink Maker* **28**, 7, 31 (1950).

⁸ Roughly speaking, $-d\eta/dn = K\eta$ rather than $-d\eta/dt = K$.

⁹ A. Voet, *J. Phys. & Colloid Chem.* **51**, 1037 (1947).

TABLE II
RELATIONSHIP OF PERCENT TRANSFER TO INK PROPERTIES^a

<i>Ink. No.</i>	<i>Inkometer reading^b</i>	<i>Viscosity, poises</i>	<i>Per cent transfer</i>
3:1 Roll speed ratio			
1	4.3	77	78.9
2	4.4	65	79.2
3	5.6	62	80.3
4	7.2	59	82.2
5	11.2	64	87.3
6	14.8	87	90.6
7	16.5	125	92.5
8	19.7	487	94.7
9	26.2	135	97.7
10	30.9	103	98.0
2:1 Roll speed ratio			
11	5.6		75.6
3	5.6	62	77.3
12	7.1		75.3
4	7.2	59	78.1
5	11.2	64	83.2
7	16.5	125	
8	19.7	487	92.3
13	19.9	412	92.3
14	21.0	124	92.8
15	30.9	125	97.7

^a From T. A. Sparta, M.S. Thesis, Lehigh University, Bethlehem, Pennsylvania, October, 1954.

^b Model B-45, Roller composition 1C-6513, low speed, 30°C.

reading on an Inkometer which is a two-roll instrument simulating a press, described on page 170.

Roll mill productivity can sometimes be increased by additives which increase Inkometer reading and lead to more complete transfer from slow to fast roll. Inkometer reading and the transfer factor generally increase with ink viscosity; the data of Table II show that these empirical values correlate better than does viscosity. In addition to purely mechanical factors such as state of blade wear, blade angle, and blade pressure, take-off knife efficiency depends on ink film thickness and ink viscosity.

IV. Printing

1. FOUNTAIN PHASE

The first shear of appreciable magnitude encountered by an ink during printing occurs when it leaves the press fountain via the fountain roller.

The chief requirement in this initial phase of printing is that the ink follow the fountain roll and not deplete itself adjacent to the roll which starts it on its way through the press. Correlation between measured rheological properties and behavior does not seem to be completely revealing, but it is known that inks with excess structure perform poorly in the fountain. Inks with good length, that is, those which readily form threads, will generally behave well in the fountain, whereas short inks often will not properly follow the roll. Length usually correlates with plastic viscosity divided by dynamic yield value.¹⁰ A short ink has a high dynamic yield value-plastic viscosity quotient (see page 165); a long ink generally has no recognizable yield value and is characterized by a quotient which approaches zero.

On the other hand, once it has started through the press, an ink with both a high yield value and a high viscosity will function properly. Presumably, the cohesive forces are sufficiently great in such cases to allow the ink to follow the fountain roll.

2. DISTRIBUTION PHASE

The function of the distributing system of a press is to break down any structure present in the ink and to distribute a uniform film on the form rollers. In this phase the ink is subjected to a discontinuous shear. Voet¹¹ has calculated that the ink is sheared about $\frac{1}{20}$ of the time and that the stresses developed are high (of the order of 10^8 dynes/cm.²). Although the ink is at rest most of the time, the period of rest is probably less than a second; this time is believed to be too short to allow much structure to develop.

The length of the ink is apparently the rheological property of most importance in the distribution phase. If the ink is too short—e.g., if the formulation is “dry” due to high pigment loading—the ink will not follow the rolls properly, and poor or uneven distribution will result. On the other hand, if the ink is too long, flying or misting may occur. Misting occurs when in the course of splitting, an ink filament necks down at two or more places leaving fragments suspended in the air. High shear rheological properties during the rupture of thin filaments need to be explored to shed light on this problem.

In gravure printing, Bowles¹² suggests that inks should be dilatant. If this concept is correct, the ink would stiffen under mechanical action, and

¹⁰ A. C. Zettlemoyer, W. C. Walker, J. M. Fetsko, and R. R. Myers, *Intern. Bull. Printing and Allied Trades* **73**, 60 (1956).

¹¹ A. Voet, “Ink and Paper in the Printing Process,” p. 51. Interscience, New York, 1952.

¹² R. F. Bowles, *J. Oil & Colour Chemists' Assoc.* **33**, 72 (1950).

clean wiping prior to printing could take place on the surface of the intaglio plate. Yet the ink could still be transferred during printing from the recessed areas to the paper, perhaps aided by the absence of high shear at the instant of impression.

It should be recognized that distribution on a roller system and other aspects of ink transfer are little understood and deserve serious analysis. If organic solvents in combination with resins are chosen haphazardly, fewer than 5% of the combinations will distribute and transfer well on the roller system of a given press. The required combination of wetting and rheological properties has not been delineated sufficiently to permit formulations to be made on a scientific basis.

3. TRANSFER PHASE

From the time the ink leaves the can until the finished print emerges, the treatment of a printing ink can be characterized by the single word, transfer. In the sense used here, the process by which the ink leaves the press is referred to as transfer; the ink is transferred from the plate or rubber blanket to the paper concurrently with a partial drainage of vehicle into the paper, and finally the printed sheet is withdrawn from the plate or blanket. In the transfer to paper, the ink is under high compression followed by high tension. Thus, an ink with a high degree of resistance to deformation or high viscosity is needed. If the viscosity is too low, the ink on halftone dots will be forced out from the center to the sides of the dots and will produce distortion and poor reproduction. When the ink is short, mottling of solid areas will usually tend to be minimized; long filaments will not form. Then less uneven coverage is likely to develop as the shorter filaments subside.

When the printing form is separated from the paper, the ink film is split for the last time. The resistance of the ink film to rapid splitting is called tack, and in this particular transfer the problem of tack becomes most prominent. If the tack of an ink is too great, the paper may be ruptured before the ink film splits, giving rise to a phenomenon called picking. In the transfer phase as a whole, the ink should have as high a viscosity as can be obtained, consistent with the requirement that no picking of the paper takes place. Splitting force increases with press speed, therefore more viscous inks can be used at low press speeds than at high speeds. In wet multicolor printing, the tack of an ink is also of importance for proper trapping where the tack of each successive ink must be less than that of the previous one so that the split will always take place in the last-down film.

In the transfer phase of printing on paper, drainage of ink into the pores begins as the impression is made. Since the pores are small and the printing pressures are high (from 100 to 500 lb. per inch of roll width), the ink is

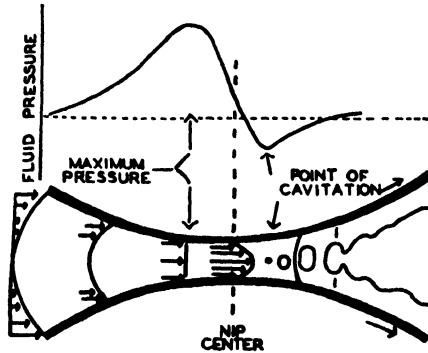


FIG. 6. Pressure and velocity profiles for a Newtonian fluid splitting between two rolls turning at the same speed.

subjected to a high stress. The length of time that this high stress acts is very short so that only partial drainage occurs during this interval, despite the high pressures. In this step, the viscosity of the ink at high shear stresses is more important than its low shear viscosity. It may be noted that the ink might become more concentrated in pigment because of drainage, and thereby develop increased tack. On nonporous stocks such as cellophane or metals, of course, such drainage cannot occur. When the ink film is sufficiently thick to cover all the depressions, the amount transferred y has been found¹³ to depend on the ink film thickness x according to the equation

$$y = b + f_r (x - b) \quad (2)$$

where b is the amount of ink immobilized during the impression and f_r is the fraction of the residual ink film split to the stock. Recently, f_r has been found¹⁴ to correlate with the ratio of yield value to plastic viscosity. This ratio, considered to be a measure of "shortness," has been thought to be related to f_r because little or no shear takes place near the region in the nip between separating rolls where the splitting action takes place.

The flow pattern and pressure distribution¹⁵ of an ideal fluid in a roll nip (without slippage) are pictured in Fig. 6. A quite similar situation exists in the nip between plate and paper during printing and between the rolls in a roll mill. No shear takes place at the maximum and minimum in the pressure distribution curve. Cavitation begins near or at the minimum, as is explained later. Maximum rate of shear, up to thousands of reciprocal seconds occur near the center of the nip. The high pressure on the entrance side of the nip creates a pumping action so that more fluid passes

¹³ W. C. Walker and J. M. Fetsko, *Am. Ink Maker* **33**, 12, 38 (1955).

¹⁴ A. C. Zettlemoyer, R. F. Scarr, W. D. Schaeffer, *TAGA 9th Ann. Proc.* 75 (1957).

¹⁵ R. E. Gaskell, *Trans. Am. Soc. Mech. Engrs.* **72**, 334 (1950).

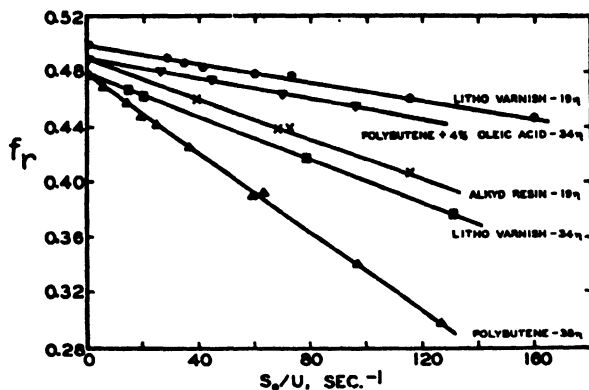


FIG. 7. Split of the residual ink film to paper during printing as a function of ink shortness. The inks were made from two carbon blacks in five vehicles.

through the nip than indicated by the clearance. That the minimum occurs at about zero absolute pressure when a film is split (as opposed to the situation when the rolls are completely immersed) is becoming increasingly clear.¹⁶ If the non-Newtonian nature of the ink and penetration into the paper are taken into account, it can be recognized that the flow pattern may be more complicated than that suggested in Fig. 6. According to the picture presented, splitting is initiated where the shear rate is low. For this reason, the low shear data of plastic viscosity and yield point from precision rotational viscometry up to a few hundred reciprocal seconds might be expected to correlate with the f_r values from transfer data. In Fig. 7, quite good correlation is indicated for a variety of dispersions between f_r and S_0/U .

Transfer to the paper poses a host of problems, not all of which arise from irregularities in paper surface and quality. One problem in which some headway has been made in recent years is that of wet multicolor trapping and the related phenomenon of picking, where the uses of certain test instruments have been demonstrated.¹⁷

4. PENETRATION PHASE

The penetration phase follows the transfer phase and involves the drainage of the vehicle into the pores of the paper. As already mentioned, part of this drainage occurs in the transfer phase under high stresses. Most

¹⁶ Printing, Packaging and Allied Trades Research Association, Annual Report 1953-1954, p. 26.

¹⁷ A. C. Zettlemoyer, C. T. Dickert, W. C. Walker, and R. R. Myers, Preprint booklet, Meeting of Paint, Plastics and Printing Ink Division of the American Chemical Society, Kansas City, Missouri, p. 95, 1954.

of the penetration phase usually occurs in the first minutes.¹⁸ This process proceeds entirely under the stresses induced by capillary action, since those due to the printing pressure are no longer operative. The most fruitful studies of penetration of liquids into paper have been performed by Tollenaar.¹⁹

Rapid drainage of a vehicle of moderately low viscosity is needed to set the ink sufficiently to permit the print to be handled prior to drying. If the drainage is not rapid enough, sticking or offsetting to the sheet above will occur; however, if the drainage is excessive, insufficient binder will be left in the film to bond the pigment properly, and a "chalky" condition will result. Thus, intermediate rheological properties are required to prevent occurrence of either of these extreme conditions.

In recent years, an interesting combination of rheological properties has enabled the development of a variety of gloss inks, in which the resin has been selected so as to be somewhat insoluble in the remainder of the vehicle and yet to be readily dispersible. During the penetration phase, the discrete particles of resin are left on the surface while some of the vehicle drains into the stock, leaving a smooth and glossy film due to the holdout.

V. Viscometric Study of Printing Inks

1. THEORETICAL BACKGROUND

a. Printing Ink Flow Behavior

The fundamentals of the rheology of dispersions and the principles of its measurement have been described in detail in Chapter 14, Volume 1, by Frisch and Simha. Rheological concepts for dispersions such as printing inks have developed in a somewhat unusual fashion, however, and require brief mention here.

It is not possible to describe printing ink dispersions by means of a single material constant such as can be done with the continuous phase from which it is made. Nonetheless, the printing ink rheologist must find ways to characterize dispersions by physical constants, and the most significant of these is viscosity. The introduction of solid particles, as for example pigments or extenders, into a vehicle to produce a product of commercial value invariably results in non-Newtonian or anomalous flow behavior. As a result, the flow of an ink is far more difficult to characterize and is less clearly understood than the flow of pure liquids.

¹⁸ R. R. Coupe and A. H. Smith, *J. Oil & Colour Chemists' Assoc.* **39**, 8, 579 (1956).

¹⁹ D. Tollenaar and G. Blokhuis, *Appl. Sci. Research* **A2** (2), 125 (1950); D. Tollenaar, *Appl. Sci. Research* **A3** (6), 451 (1953); D. Tollenaar, *Intern. Bull. Printing and Allied Trades* **67**, 16 (1954); D. Tollenaar and P. Ernst, *Technical Association of the Graphic Arts, 8th Proc.*, 37 (1956).

Einstein²⁰ derived the first equation for calculating the viscosity of a Newtonian suspension from the concentration of pigment. Printing ink systems, however, do not obey the relation between volume concentration and viscosity defined by his equation, nor do they obey strictly any of the known relations in which a single viscosity parameter is employed. Many investigators have worked on extensions of the Einstein equation to take into consideration important factors in ink systems such as particle shape and particle-vehicle interaction,²¹⁻²⁴ particle sediment volume,^{25, 26} and particle area.²⁷

Although the basic factors in anomalous flow have long been recognized,^{28, 29} only recently has substantial progress been made in elucidating the mechanism involved.³⁰ In the case of dispersions, viscous anomalies stem from two primary causes: particle disturbances such as rotation of clusters, and immobilization of vehicle in interstices of aggregates or on pigment surfaces.

Several workers have attempted the application of rheology to dispersion technology. Among these are Bingham³¹ who recognized that different dispersions exhibit different anomalies, Green³² who established a basis for industrial utilization of rheological data, Reiner³³ who developed a theoretical treatment of sources of anomalies in general which has recently been used³⁴ to advantage in the printing ink field, and Voet and Suriani³⁵ who established a simple relation between relative plastic viscosity and the ratio of pigment to vehicle volume:

$$\log U_R = K\phi \quad (3)$$

U_R is the ratio of plastic viscosity of the dispersion to the viscosity of the

²⁰ A. Einstein, *Ann. Physik* **19**, 289 (1906); **34**, 591 (1911).

²¹ V. Vand, *Nature* **155**, 364 (1945); *J. Phys. & Colloid Chem.* **52**, 277 (1948).

²² R. H. Brailey, Preprint booklet, Meeting of Paint, Plastics and Printing Ink Division of the American Chemical Society, New York, 1951.

²³ E. Guth and R. Simha, *Kolloid-Z.* **74**, 266-75 (1936).

²⁴ A. Voet and L. R. Suriani, *Am. Ink Maker* **30**, 37 (1952).

²⁵ J. S. Gourlay, *J. Oil & Colour Chemists' Assoc.* **34**, 385 (1951).

²⁶ J. V. Robinson, *Trans. Soc. Rheol.* **1**, 15 (1957).

²⁷ A. C. Zettlemoyer and G. W. Lower, *J. Colloid Sci.* **10**, 29 (1955).

²⁸ F. R. Eirich, M. Bunzl, and H. Margaretha, *Kolloid-Z.* **75**, 20 (1936); F. R. Eirich and R. Simha, *Monatsch. Chem.* **71**, 67 (1937).

²⁹ E. Guth, *Kolloid-Z.* **74**, 147 (1936).

³⁰ M. Reiner, "Deformation and Flow." Lewis, London, 1949.

³¹ E. C. Bingham, "Fluidity and Plasticity." McGraw-Hill, New York, 1922.

³² H. Green, "Industrial Rheology and Rheological Structures." Wiley, New York, 1949.

³³ M. Reiner, see reference 30.

³⁴ J. C. Miller, unpublished work.

³⁵ A. Voet and L. R. Suriani, *J. Colloid Sci.* **7**, 1 (1952).

vehicle, and ϕ is the ratio of pigment volume to vehicle volume. The constant K varies from system to system but appears to characterize the rheological behavior of any one dispersion.

2. INSTRUMENTS AND MEASUREMENT

Theoretically, the ideal viscometer is a parallel plate assembly of infinite area. However, certain compromises must be made in the interests of practicality of design. Hence, the most satisfactory instrument for gathering fundamental data on inks is the precision rotational viscometer.

One of the earliest rotational viscometers was that of Couette,³⁶ modifications of whose design have found their way into the printing ink field in the form of the rotating spindle types. Examples are: (1) the Stormer viscometer³⁷ which enables one to time the descent of a weight attached to a revolving spindle; (2) the Brookfield viscometer whose chief virtue is its portability and whose distinguishing feature is its ability to measure torque directly from the moving spindle; and (3) a more recent design based on the Brookfield principle and called the Drage viscometer.³⁸

Of far more fundamental import in the study of printing inks have been the rotating cup versions of Couette's viscometer. Green³⁹ designed a rotational viscometer specifically for printing inks which currently is of more than historical value despite the advent of at least two other rotational viscometers which have been used in printing ink rheology. One of these, similar to Green's and designed by Buchdahl *et al.*,⁴⁰ is referred to as the Sun precision rotational viscometer; the other, by Myers and Zettlemoyer⁴¹ is called the Squibb viscometer, and is shown schematically in Fig. 8. By means of a completely frictionless torque-measuring suspension, this viscometer has enabled a new region of low shear viscometry to be investigated (for example, see page 166).

Although the temperature rise in a rotational viscometer cannot be measured directly in the fluid under study without disturbing the laminar shear, the rise has been demonstrated to be highly significant.^{42, 43} This Laboratory was the first to point out that the temperature rise can be 50°C. at 550 sec.⁻¹ shear rate in a modern precision rotational viscometer; tem-

³⁶ M. Couette, *Ann. chim. et phys.* **21**, 433 (1890).

³⁷ A. J. Stormer, *Trans. Am. Ceram. Soc.* **11**, 597 (1909).

³⁸ A. G. Epprecht, *F.A.T.I.P.E.C., Compt. rend. 2^e Congr., Noordwijk, Holland* **1953**, p. 125.

³⁹ H. Green, *Ind. Eng. Chem., Anal. Ed.* **14**, 576 (1942).

⁴⁰ R. Buchdahl, J. G. Curado, and R. Braddicks, Jr., *Rev. Sci. Instr.* **18**, 168 (1947).

⁴¹ R. R. Myers and A. C. Zettlemoyer, *SPE Journal* **11**, 43 (1955), U. S. Patent 2,796,758 (1957).

⁴² G. W. Lower, W. C. Walker, and A. C. Zettlemoyer, *J. Colloid Sci.* **8**, 116 (1953).

⁴³ R. N. Weltmann and P. W. Kuhns, *J. Colloid Sci.* **7**, 218 (1952).

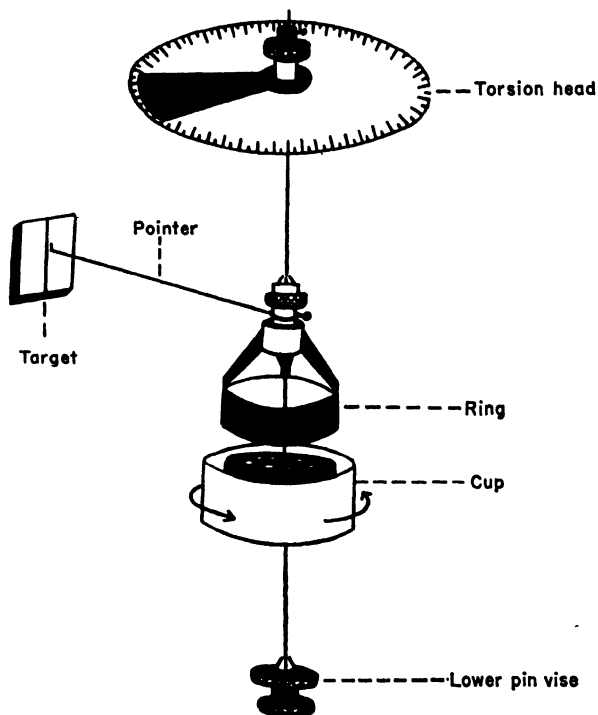


FIG. 8. Schematic diagram of the Squibb viscometer. Features include no friction torque assembly, annular space for sample to give double shear area, and adjustable head to give null point operation.

perature measurements were made at the sides of the annular space on the cup and on the bob. The best way to define the steps needed to control the temperature is in terms of energy input per unit area per unit time.⁴² If steps are not taken to control the temperature, the flow curve may be curved in the direction of lower viscosity as the shear rate is increased. Ordinary mineral oils, vegetable oils and litho varnishes show no evidence of non-Newtonian behavior when the temperature is properly controlled.

Cone-and-plate attachments can be made for practically any of the existing rotational viscometers. This design is due to Mooney⁴⁴ and is commercially available. The plate is driven and the cone makes an angle of about 3° with the plate so that the rate of shear is the same at all radii. The need for only small samples of material, the ease (but not precision) of temperature control, and high shear rates achieved are advantages which have led to current investigations in printing ink rheology.

⁴⁴ M. Mooney and R. H. Ewart, *Physics* 5, 350 (1934).

Printing inks exhibit the usual viscosity anomalies associated with pseudoplastics, and in addition they often fail to produce a reproducible stress-shear rate relation. At some critical speed, which depends somewhat on the geometry as well as on the nature of the ink, flow curves often fail completely. The type of hysteresis described by Green is present; but in addition, the untenable situation occurs in which stress actually decreases with increased shear. On reduction of shear, the descending slope appears somewhat uniform, but undoubtedly suffers from slippage or the formation of voids.

An interesting adjunct to rotational viscometry has been used on printing inks by Voet⁴⁶ who adapted the dielectric constant method of Bruggeman⁴⁶ to flowing systems. The dielectric constant of a dispersion depends more on the particle shape and the amount of aggregation than on particle size. For irregular particles the dielectric constant ϵ for the dispersion is related to that of the medium ϵ_{med} by the equation

$$\epsilon = \epsilon_{\text{med}} (1 + 3fV) \quad (4)$$

The magnitude of the form factor f depends on the orientation of the particle with respect to the electric field, with the result that ϵ decreases with shear in dispersions of low dielectric solids such as metal powders and carbon blacks, and in general depends on the relative dielectric constants of the medium and the pigment.

The dielectric constant technique, along with the similar methods of dielectric loss and conductivity, have augmented the value of rotational viscometry as a fundamental instrument in studying dispersions. The importance of agglomeration or flocculation as the pigment concentration is increased has been amply demonstrated by this approach. Of particular interest is the possibility of detecting incipient gel formation or aggregate growth at much lower shear rates than have been studied heretofore.

The empirical flow test of Bowles⁴⁷ also utilizes a rotational viscometer. After shearing at a definite rate, the rotation is stopped and the decrease in torque with time is measured. The two arms of the curve obtained have been related to various required properties in the printing operation.

Another interesting use of the rotational viscometer in ink technology has been in the study of rates of thixotropic breakdown of inks at constant rates of shear.⁴⁸ An attempt to divorce the kinetic aspects of shear breakdown as measured by rate studies from the thermodynamic aspects as exemplified by the flow curve has been made by Miller.⁴⁹ He concluded

⁴⁶ A. Voet, *J. Phys. & Colloid Chem.* **51**, 5 (1947).

⁴⁶ D. Bruggeman, *Ann. Physik* **24**, 636 (1935).

⁴⁷ R. F. Bowles, *J. Oil & Colour Chemists' Assoc.* **31**, 87 (1948); **34**, 339 (1952).

⁴⁸ R. N. Weltmann, *Rev. Sci. Instr.* **16**, 184 (1945).

⁴⁹ J. C. Miller, unpublished work.

that this approach warrants much more attention than it has received up to the present time. More recent work by Knauss⁵⁰ indicates that energy input is the proper parameter on which to base breakdown studies, rather than shear rate as usually employed.

Two viscometers of the vibrating reed type have been used in the evaluation of printing inks: the Ultra-Viscoson⁵¹ and the RCA viscometer.⁵² Interesting results concerning the thixotropic behavior of inks have been obtained using both of these instruments, but most of the findings have been of a qualitative nature. For example, position-sensitivity of the probe has been used as evidence of pseudoplasticity.

3. STATUS OF THE VISCOMETRIC APPROACH IN INK RHEOLOGY

The basis of the Bingham, Green, and Reiner approaches is the flow curve, which is a representation of stress versus the rate of shear. Valuable correlations of flow curve data with structure parameters have been found. The correlations have been interpreted in terms of particle shape, particle aggregation, interactions involving the liquid, and the other tenets.⁵³⁻⁵⁵ Such interpretations are the first step toward gaining sufficient insight into the behavior of suspended particles to permit changes of preparation or composition of industrial dispersions to be made in the most logical direction; however, they do not show promise of unfolding the whole story because the viscometric method involves changes in structure as the data are taken. The reason for determining viscosity at various shear rates is not the gathering of data at the shear rates used in printing (which are much higher), but the elucidation of this structure.

The complexities of printing ink flow arise from the fact that inks are concentrated dispersions and also involve problems in the surface chemistry of pigments. The forces emanating from the surface of the discontinuous phase of a dispersion, as well as the complex hydrodynamic behavior of concentrated dispersions, give rise to deviations from the behavior predicted by Einstein and require the use of a flow curve as a means of expressing rheological information. The effects listed below not only give rise to correction factors in the original Einstein equation but also result in a variable deviation, for reasons which will become apparent in the mechanistic picture about to be presented. This variable generally is manifested as pseudoplasticity (decreased viscosity with increased shear) rather than

⁵⁰ C. J. Knauss, unpublished work.

⁵¹ W. Roth and S. R. Rich, *J. Appl. Phys.* **24**, 940 (1953).

⁵² J. G. Woodward, *J. Colloid Sci.* **6**, 481-91 (1951).

⁵³ C. F. Goodeve and G. W. Whitfield, *Trans. Faraday Soc.* **34**, 511 (1938).

⁵⁴ T. H. Hazlehurst and H. A. Neville, *J. Phys. Chem.* **44**, 592 (1940).

⁵⁵ G. B. Moses and I. E. Puddington, *Can. J. Chem.* **29**, 996 (1951).

as dilatancy or rheopexy (increased viscosity with increased shear). Only the pseudoplastic case is considered here.

A broad classification of the complex effects which might be encountered in the rheology of dispersions has been made by Reiner:⁵⁶

(a) *Particle-liquid interaction*. Included here are bond formation, polarization, induction, and dispersion forces; the last mentioned are often the most potent of the van der Waal's attractive forces.⁵⁷

(b) *Particle-particle interaction*. The role of the solvent in transmitting residual surface forces from one particle to another is important. The possibility of altering the attraction of one particle for its neighbors has been realized in the established practice of lowering the surface energy of pigments and extenders via coating with polar organic compounds and resins.

(c) *Disturbances leading to pseudoplastic behavior*. Concavity toward the rate of shear axis will result if the particle is not a sphere or not rigid, for then it can distort or align itself with shear. Four mechanisms have been recognized which account for disturbances of this nature and are discussed in the next section.

The state of subdivision has an enormous effect upon the area of the solid. Since interactions depend upon the extent of the surface as well as on its nature, the effect of fine subdivision on the rheology of suspensions is enormous. One significant effect of particle size is that dilatant systems are formed in highly deflocculated suspensions comprising small solid particles. Because solvent is released on increasing the shear rate, flocculation gives rise to pseudoplasticity and indicates incomplete wetting of the solid by the liquid. More important to the printing process, thixotropy (time dependent viscosity change) often appears in easily flocculated dispersions.

Anomalies in rheological behavior usually can be *detected*, but not analyzed quantitatively by means of flow curves. Because of the great technical importance of the non-Newtonian behavior of inks and other dispersions, a brief description follows of the recognized sources of anomalies and of the methods used to ascertain them.

4. THE MECHANISMS OF ANOMALOUS VISCOSITY IN INKS

Of all the complex effects which can be imparted by pigments, three were just shown to result in pseudoplastic behavior. Each can contribute to the magnitude of the anomaly obtained. If any one appears to be inoperative in rotational viscometry, the cause may be the inability of the

⁵⁶ M. Reiner, see reference 30, p. 56.

⁵⁷ S. Brunauer, "Physical Adsorption," Vol. 1 of Adsorption of Gases and Vapors, p. 190. Princeton Univ. Press, Princeton, New Jersey, 1943.

rheologist to detect it with the instruments at his disposal, rather than the absence of such an effect.

Particle-liquid interactions give rise to immobilization via adsorption which, being a reversible process, may lead to anomalies. Pseudoplasticity occurs whenever the range of applied stress produces shear energies which span the energy equivalent of the adsorption link. Since these bonds are progressively weaker as the adsorbed layers extend further from the surface, particle-liquid interactions are most likely to be observed at low shearing stress. *Particle-particle interactions* result in a more or less steric immobilization in which vehicle is trapped in the interstices of clusters of particles. If these clusters are broken down reversibly on shearing, the apparent viscosity is decreased in a manner which produces pseudoplasticity.

The opinion has been reached that the interest of the ink chemist and perhaps of virtually all manufacturers of dispersions should lie in a delineation of the type of particle-vehicle and particle-particle interactions encountered. Viscometry provides at least an insight into the nature and range of the adsorption forces emanating from pigment surfaces. Rheological methods can be used to measure the shearing stresses required to overcome separately the forces resulting from random orientation, aggregation, or particle enlargement via adsorption.

Reiner lists four criteria by which the type of interaction can be ascertained by means of flow curves. The first is based on the *response of relative viscosity to temperature* but is difficult to apply because a complete specification of experimental conditions must be made,⁵⁸ such as whether viscosities are to be determined at constant stress, at constant shear rate, or at constant energy input. The second criterion is the *reversibility of the flow curve*, indicates whether or not an aggregate is built up as an ordered array. The third is the *existence of a lower limit of nonlinearity*, which may or may not depend upon the sensitivity of the measuring instrument, and which would clarify the problem of whether or not a particular dispersion possessed a solid-type structure. The fourth, believed to give the most promising results in applying theory to practice, is the *relation of inherent viscosity at zero rate of shear to that at infinite shear as the concentration of pigment is increased*; a change in the ratio would imply that secondary structures are present in which solvent is immobilized by a network involving the particles. For additional details the reader is referred to Reiner's excellent description of "structural viscosity," already cited.

The viscometric approach can be summarized by listing the types of flow curves which can be used in characterizing printing inks. For convenience, the Newtonian flow curve has been called Type I and is represented by a straight line of slope η through the origin (Fig. 9).

⁵⁸ A. B. Bestul and H. V. Belcher, *J. Appl. Phys.* **24**, 696 (1953).

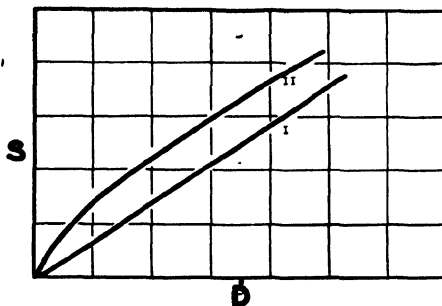


FIG. 9. Typical flow curves obtained by plotting stress (S) versus rate of shear (\dot{D}). Key: I, Newtonian—vehicles and thin inks; II, Pseudoplastic—typical of most inks. Recommended nomenclature for Type II flow is *Shear Thinning*.^{58a}

In the flow curves of most printing inks an apparent linear portion is attained at shear rates as low as 50–100 sec.⁻¹ In the absence of additional information, this curve can be characterized as Type II (Fig. 9) and can be used in determining so-called *plastic viscosities* and *yield values*, which are not dealt with extensively in this chapter because they have only empirical value. Artfully, however, the slope U and the intercept S_0 of the flow curve can be used to characterize inks as we have seen. The ratio S_0/U has been called “shortness.”

If the slope of this linear portion is less than the viscosity calculated from the Einstein equation, the flow curve cannot possibly maintain linearity; if it were to do so, the viscosity at high shear rates would be less than the ideal value based on the volumetric and shape factors alone. Consequently, one can predict with assurance that a flow curve cannot be continuously linear if the slope is less than the calculated ideal viscosity. That the apparent linearity is accidental in some cases and results from the fact that the flow curve approaches an inflection point was demonstrated by Ostwald.⁵⁹ He was the first to investigate the high shear phenomena of anomalous systems and found that the concavity was reversed, just as predicted above, giving rise to a third type of flow curve (Type III, Fig. 10). This reversal was not due to the onset of dilatancy but resulted from the gradual disappearance of the structure responsible for the viscous anomaly. Thus, the Ostwald curve is pseudoplastic at low shear but eventually settles down to an extensive range of Newtonian behavior. Theoretically, dilatancy or rheopexy can set in at the upper end of the curve, which means that a *system* can exhibit both pseudoplastic and dilatant behavior. Printing inks *may* actually behave as Newtonian systems under the conditions found in the distribution phase, but must assume

^{58a} R. R. Myers, D. R. Brookfield, F. R. Eirich, J. D. Ferry, and R. N. Traxler, *Trans. Soc. Rheol.* **3**, in press (1959).

some pseudoplastic character in the post-printing phase either as a result of drainage into the substrate or from physical changes in the film after deposition. Structure buildup may be physical or it may be induced by chemical change as in the oxidation-polymerization of oils.

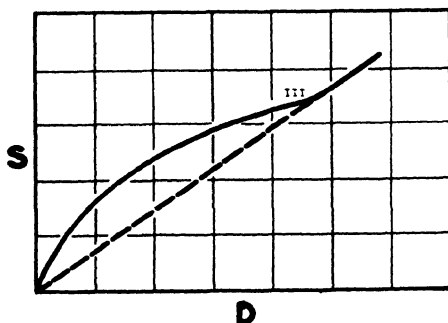


FIG. 10. Ostwald flow curve produced by anomalous systems, obtained by plotting stress (S) versus rate of shear (\dot{D}).

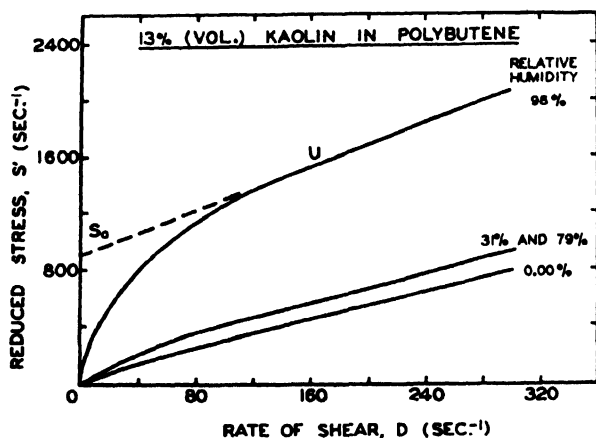


FIG. 11. Flow curves of dispersions made from clays stored at various relative humidities.

Generally, structures of the strength needed to resist excessive penetration of a porous substrate can be observed only at exceedingly low shear stresses. Even then, their contribution to the properties of a film at rest can only be inferred from flow data. For example, dispersions made from clays conditioned at various relative humidities⁶⁰ produced flow curves in the low shear range that followed the trend shown in Fig. 11. Observe the slight upward displacement of the flow curve when a monolayer of

⁶⁰ R. R. Myers, J. C. Miller, and A. C. Zettlemoyer, *J. Appl. Phys.* **27**, 468 (1956).

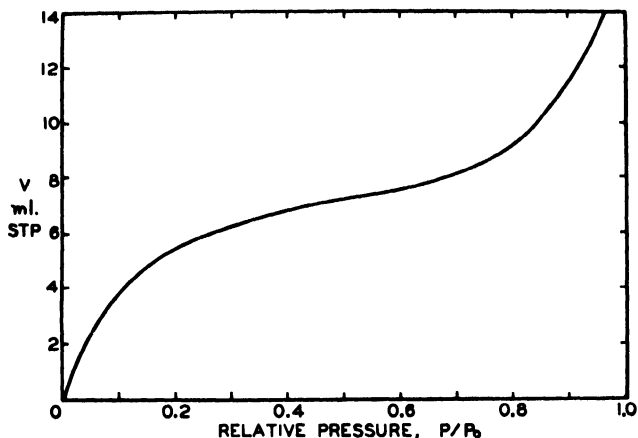


FIG. 12. Water isotherm of a kaolinite clay showing the small water uptake between 0.3 and 0.8 relative humidity.

water was adsorbed on the clay surface before compounding the dispersion. This displacement is a reflection of a noticeable "shortening" of the system (yield value divided by plastic viscosity increases); but it is nowhere near as drastic a change as when water is allowed to accumulate to multilayer depths on the clay surface.

Comparison of Fig. 11 with the isotherm representing the adsorption of water on clay at 25° C. (Fig. 12) clarifies the points made in the preceding paragraph. Figure 12 gives unmistakable evidence that the uptake of water in the humidity range from 0.30 to 0.80 does not increase significantly; on the other hand, the 0.30 to 0.80 "plateau" differs from the 0.00 and 0.90 relative humidity points. Drastic changes in water content of the extender are reflected in drastic changes in the low shear flow curves of the resulting dispersion. Kruyt and Van Selms⁶¹ have explained this change in consistency by postulating that water bridges connect the individual particles, thereby creating particle-particle contacts through the aqueous film. These contacts become more potent as the depth of the film is increased sufficiently to allow it to provide an excess of water in the capillaries between adjacent particles.

VI. Tack and Related Phenomena

1. THE NATURE OF THE SPLITTING INK FILM

In spite of the advances described in the preceding section, the conclusion has been reached in many quarters that the viscometric approach to the

⁶¹ H. R. Kruyt and F. G. van Selms, *Rec. trav. chim.* **62**, 407, 415 (1943).



FIG. 13. Filamentation in a roll nip. The side view was taken using a microflash technique by Lars Sjodahl, Interchemical Corporation, Chicago, Illinois.

study of printing inks is destined to be incomplete. The chief reason for this stand is the fact that the shear pattern in a rotational viscometer does not resemble that encountered by the ink at most stages of the printing process. In addition, the behavior of the system undergoing continuous shear is quite different from its behavior during the intermittent shear which occurs in its repeated passage through roller nips.

Whether the split is between rolls, or between roll and plate, or plate and paper, Sjodahl⁶² has shown that the ink splits in filaments, as evidenced by the side view of a roller system shown in Fig. 13. This finding, coupled with the fact that split takes place exceedingly rapidly in practice, has given rise to the concept that viscoelasticity is involved. Thus, it would be expected that viscosity alone would sometimes fail to account for ink behavior on a press, although not all printing ink rheologists agree that elasticity is involved. Some believe that tack is related solely to viscosity, in a manner not yet elucidated.

2. FORCE ANALYSIS OF TACK

Under the conditions in which the tack of printing inks is manifest, the material undergoes a type of flow reminiscent of the elongation of a filament (see Chapter 15). The chief point of departure from this model occurs when

⁶² L. Sjodahl, Paper presented at the First Annual Meeting of the Technical Association of the Lithographic Industry, Chicago, Illinois, April, 1949; *Am. Ink Maker* **29**, 31 (1951).

the forces involved in the *formation* of the filament are considered. It is conceivable that the dynamic requirements for filament formation are larger than those required for its subsequent elongation. Stefan⁶³ has calculated the force F required to separate two plates of radius a from distance h_1 to final distance h_2 :

$$F = \frac{3\eta a^4}{4t} \left(\frac{1}{h_2^2} - \frac{1}{h_1^2} \right) \quad (5)$$

where t is the time required to effect the separation, h_2 is the initial clearance h_1 the final clearance, and a the plate radius. This equation was developed for the elongation of a single filament and appears to be valid for times in excess of one second. However, separation times of this order of magnitude are unrealistic in the case of the split of printing inks in a roller system. Furthermore, the separation of parallel plates in a direction normal to their surfaces does not exactly duplicate the situation existing on a roller system. Consequently, a new equation must be sought.

3. INSTRUMENTATION

The oldest technique for measuring "tack" depends upon the craftsman's middle finger by which he pats out a dab of ink on the paper to printing thickness and then discerns the resistance to the snap of the finger away from the film. In spite of its primitive and subjective nature, the method is still widely and successfully used.

The mechanical tack finger of Green⁶⁴ was an attempt to attach a number to the craftsman's test. It has been supplemented by the design of Curado,⁶⁵ in which the alternate compressive and tensile forces impressed on an ink are measured by a piezoelectric crystal. Both of these devices differ from practice in that the split involves motion of the surfaces normal to each other and in that the milling of air into the ink by the rollers is not duplicated in the test.

The closest approach which has been made to the measurement of the tack of an ink as found on the press was made by Reed⁶⁶ who designed an instrument called the Inkometer. This instrument measures the torque exerted upon one roll of a simple distributing system as the ink is being worked. The torque is transmitted through a linkage to a balance arm above the torque roller on which readings are taken as depicted in Fig. 14.

The Inkometer has been used successfully in routine control tests in

⁶³ M. J. Stefan, *Sitzber. Akad. Wiss. Wien. Math-Naturw. Kl. Abt. II* **69**, 713 (1874).

⁶⁴ H. Green, *Ind. Eng. Chem., Anal. Ed.* **13**, 632 (1941).

⁶⁵ Although Curado's data have not been published, they indicate that tensile strengths above 15 p.s.i. are not found in printing inks.

⁶⁶ R. F. Reed, *Am. Ink Maker* **17**, 27 (1939).

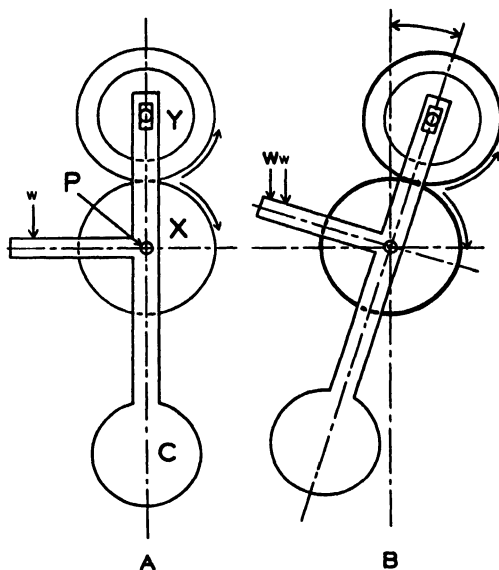


FIG. 14. Diagrammatic illustration of the Inkometer principle. A. The instrument rotating without ink at the outset is zeroed by adjusting weight w . B. When the inked rollers X and Y rotate, the additional weight W required to realign the assembly about shaft P is a measure of the torque exerted by the splitting ink film. C is a counterweight.

the manufacture of inks, in correlations with trapping in wet multicolor printing,⁶⁷ in correlations with the transfer of inks on three-roll mills,⁶⁸ and in an empirical test for ink stability, particularly in heatset and steamset inks. These inks dry by burning off and water sorption (thus precipitating the resin), respectively.

Limitations of the Inkometer are that it does not exactly duplicate a printing press, partly because the optimum ink film thickness for measurement is several times greater than that found on presses ($7\ \mu$) and partly because equilibrium readings are exceedingly difficult to obtain. Superimposed upon these drawbacks is the fact that the torque roller is made of a rubber composition, and no composition has been developed which will insure the permanency of the characteristics of such rollers. On one occasion the solvent may be absorbed by the rollers, producing a gradual increase in torque; on another, solvent or plasticizer may exude from the rollers and produce a diminution of the Inkometer reading. Distortion of

⁶⁷ A. C. Zettlemoyer, C. T. Dickert, W. C. Walker, and R. R. Myers, see reference 17.

⁶⁸ This finding is covered by National Printing Ink Research Institute Project Report No. 32 on Ink Transfer through the Three-Roll Mill.

the composition roller is always present. Some attempts have recently been made to attach the Inkometer directly to the distribution system of presses.⁶⁹

Other measurements of the forces involved in the splitting of ink films have been provided by Duffie⁷⁰ and Voet and Geffken⁷¹ who measured the decrease in kinetic energy suffered by a rolling cylinder as it passes over an inked surface set on an inclined plane. This work culminated in the concept of tack as an energy density, with energy requirements dependent upon the volume of ink transferred from plate to roller. One of the problems in experimenting with the inclined plane tackmeter arises from the difficulty in obtaining good, reproducible contact between the ink film and surface to be wetted. Sometimes the cylinder is covered with paper to simulate printing, but the pressures achieved are not nearly as great as on printing presses.

Banks and Mill⁷² sought an answer to the question of how great a tensile force can be supported by an ink film by a method based on impact loading. Their conclusion, that the pressure in the interior of an ink film cannot fall below zero absolute, has in effect declared that a fundamental difference exists between a printing ink and a solid or pure liquid, for these materials can maintain tensions much higher than the equivalent of one atmosphere.

The importance of tack in industrial processes has led to the adoption of many empirical testing instruments such as the Gardner Touch Controller, Gardner Magnetic Tack Test, and Blom Tack Tester.⁷³ One of the simplest and most used empirical techniques for measuring tack is the rolling ball⁷⁴⁻⁷⁶ test, which consists of timing the descent of a ball over a tacky film on an inclined plane. Its limitations are best described by pointing out that the descent is influenced by the amount of material pushed ahead of the ball as well as the retardation due to splitting behind the ball. The rolling cylinder^{77, 78} is a variation of this technique.

⁶⁹ *Patra Ann. Rept.* 1953.

⁷⁰ E. Duffie, private communication.

⁷¹ A. Voet and C. F. Geffken, *Ind. Eng. Chem.* **43**, 1614 (1951).

⁷² W. H. Banks and C. C. Mill, *J. Colloid Sci.* **8**, 139 (1953).

⁷³ H. A. Gardner and G. G. Sward, "Physical and Chemical Examination of Paints, Varnishes, Lacquers and Colors," 11th ed., pp. 155, 156. Gardner Laboratory, Inc., Bethesda, Maryland, 1950.

⁷⁴ R. H. Gilbert, V. F. Downing, and T. E. Kalber, Paper presented at the Third Annual Meeting of the North Jersey Section Science Groups of the American Chemical Society, Newark, New Jersey. January, 1951.

⁷⁵ J. L. Overholt and A. C. Elm, *Ind. Eng. Chem.* **32**, 378 (1940).

⁷⁶ H. Wolff and G. Zeidler, *Paint Technol.* **1**, 387 (1936).

⁷⁷ B. V. Deryagin, S. M. Sovokin, and A. P. Poretskayeo, "Physico-Chemical Fundamentals of the Printing Process." Graphic Institute, Moscow, 1937.

⁷⁸ A. Voet and C. F. Geffken, see reference 71.

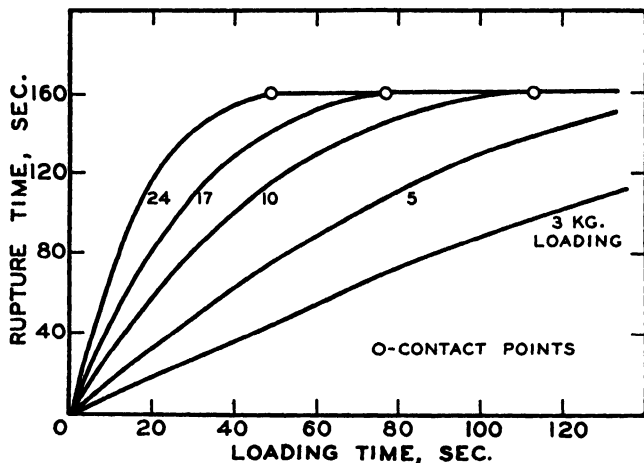


FIG. 15. Determination of contact points of a mineral oil from times of rupture and loading. From H. Heidebroek and E. Pietsch, *Forschung* **12**, 74-87 (1941).

One significant experimental condition must be met in the measurement of tack. Scott⁷⁹ showed that it was mandatory that intimate contact be made between the liquid and solid surfaces. Heidebroek and Pietsch⁸⁰ arrived at the same conclusion in a study of the forces required to pull one block from another connected with a simple liquid, and found that a limiting impulse (Ft) for separation was reached only after a given weight had been applied for a definite time. Figure 15 shows that the rupture time reached a maximum only after complete contact was achieved.

Bikerman⁸¹ has concluded that only viscous forces are involved in the peeling of a flexible substrate from a plane surface in contact with a Newtonian liquid. Apparently viscometry, if conducted properly, would provide the material constants needed to characterize the low shear flow behavior of a system under tension, but additional knowledge of the flow pattern (i.e., the kinematics) is needed before a complete description can be given of tack on roll systems.

4. COHESIVE STRENGTH OF LIQUIDS AND DISPERSIONS

Various methods of estimating the theoretical strength of liquids under tension have been used,^{82, 83} many of which give very high values (20,000

⁷⁹ J. R. Scott, *Paint Technol.* **10**, 218 (1944).

⁸⁰ E. Heidebroek and E. Pietsch, *Forsch. Gebiete Ingenieurw.* **12**, 74 (1941).

⁸¹ J. J. Bikerman, *Trans. Soc. Rheol.*, **2**, (1958).

⁸² S. W. Benson and E. J. Gerjoux, *J. Chem. Phys.* **17**, 914 (Oct. 1949).

⁸³ S. Glasstone, "Textbook of Physical Chemistry," 2nd ed., p. 479. Van Nostrand, New York, 1946.

atmos. for water). Recent theoretical developments^{84, 85} give tensile strengths an order of magnitude lower.

Experimental measurements of the stress that a liquid will withstand before cavitation have been made with a number of different techniques.⁸⁶⁻⁹² None of the measurements have given values over 300 atmos. tension, and those stresses were obtained under stringently sterile conditions. Experimental verification of the theoretical tensions has not yet been achieved because of foreign particles, small gas bubbles, the surface of the container, etc. An impure liquid should cavitate at the interface of foreign nuclei at much lower tensions than the values obtained under carefully controlled conditions. Theoretically, the tensile strength of a liquid is expressed as⁹³

$$P = T(\alpha/\beta) - P_A. \quad (6)$$

For most liquids β , the coefficient of compressibility, is of the order of magnitude of 10^{-4} /atmos. and α , the coefficient of thermal expansion, is about 10^{-3} /deg. Consequently, the value of P derived theoretically is thousands of atmospheres. And yet, these values are not obtained experimentally. The reason is attributed to the presence of nuclei which serve to form cavities long before the theoretical tension has been reached.

The splitting of an ink film is therefore believed to represent a combination of viscous flow in the time allotted and of fracture resulting from the stress exceeding the elastic limit of the ink. The number of nuclei and their interfacial attraction apparently determine the forces involved in the process.

In the case of rapid separation of two parallel plates, the liquid yields by laminar shear only insofar as its cohesive strength will permit. If the separation rate is sufficiently high to develop internal stresses that exceed the cohesive strength, the liquid will fracture as a brittle solid. This type of behavior has long been construed as elastic, but in the final analysis it does not even depend on the molecular properties of the material. Viscosity is involved because the product of viscosity and separation rate determines the internal stress, as will be shown later.

⁸⁴ L. Bernath, *Ind. Eng. Chem.* **44**, 1310 (1952).

⁸⁵ H. N. V. Temperley, *Proc. Phys. Soc. (London)* **A58**, 436 (1946).

⁸⁶ L. J. Briggs, *J. Appl. Phys.* **19**, 1062 (1948).

⁸⁷ R. Budgett, *Proc. Roy. Soc.* **A86**, 25 (1912).

⁸⁸ R. B. Dean, *J. Appl. Phys.* **18**, 446 (1944).

⁸⁹ H. H. Dixon, *Proc. Roy. Dublin Soc. [N.S.]* **14**, 229 (1914).

⁹⁰ W. B. Kenrick, C. S. Gilbert, and K. L. Wismer, *J. Phys. Chem.* **28**, 1297 (1924).

⁹¹ H. N. V. Temperley and R. Chambers, *Proc. Phys. Soc. (London)* **A58**, 420 (1946).

⁹² R. S. Vincent, *Proc. Phys. Soc. (London)* **A55**, 41 (1943).

⁹³ S. Glasstone, see reference 83, p. 480.

The kinematics of roll application are even more complicated than with parallel plates. The work of Sjodahl⁹⁴ using microflash techniques has been described. From shadowgraphs of splitting films on the downstream side of a roller system, filaments of liquid were observed to be attached to both rollers. It is evident from Fig. 13 that rupture of the filaments constitutes the final splitting of the film rather than the incipient split. High speed motion pictures of the external or final aspects of the split were obtained by the Interchemical Corporation Laboratories.⁹⁵ Banks and Mill⁹⁶ obtained photographs of filaments at the separating side of the nip of a totally immersed pair of rolls. None of these workers studied the nip region in which the filaments are created.

From previous work, Blokhuis⁹⁷ described the probable sequence of action of the film splitting as cavitation, bubble expansion, and finally elongation and rupture of the filaments. Coincident with these findings was the experimental fact that rapid separation of a thin film produced forces or energies lower than predicted by Stefan's equation, from which one must conclude that a rupture occurred akin to fracture of a solid. The patterns left in a viscous liquid by the rapid separation of parallel plates⁹⁸ are not smooth but have jagged valleys and peaks, with the peaks all connected like a range of mountains with small ridges branching off the main range.

It is clear that the basic concept of the kinematics of film splitting involves filamentation of the material being split. Rheology enters into this picture in at least two ways: the duration and magnitude of the stresses involved is of interest in the design of mills and presses; and the flow pattern of the filament during elongation is of concern in the study of misting often encountered in the press room. The effect of the pigment on the initial phase of film splitting, i.e., in the formation of the filaments via cavitation, may well turn out to be a means for lowering the stress requirements by serving as nuclei for the formation of cavities.⁹⁹ Furthermore, the presence of dissolved air in the vehicle or of air milled into the ink at the nip may likewise assist in the cavitation, perhaps by the formation of small cells of undissolved air. A test of this hypothesis has been made by operation of the Inkometer with a polybutene-CaCO₃ dispersion under progressively lower ambient pressures. Figure 16 is a plot of the Inkometer

⁹⁴ L. Sjodahl, see p. 31 of reference 62.

⁹⁵ Interchemical Corporation Laboratories, *Am. Ink Maker* **33**, (1), 51 (1951).

⁹⁶ W. H. Banks and C. C. Mill, *Proc. Roy Soc.* **A223**, 414 (1954).

⁹⁷ G. Blokhuis, *Intern. Bull. Printing and Allied Trades* **73**, 64 (1956).

⁹⁸ Anonymous, *Allgem. Papier-Rundschau* **1952** (4), 154 (1952).

⁹⁹ J. C. Miller, Ph. D. Dissertation, Lehigh University, Bethlehem, Pennsylvania, (October, 1956).

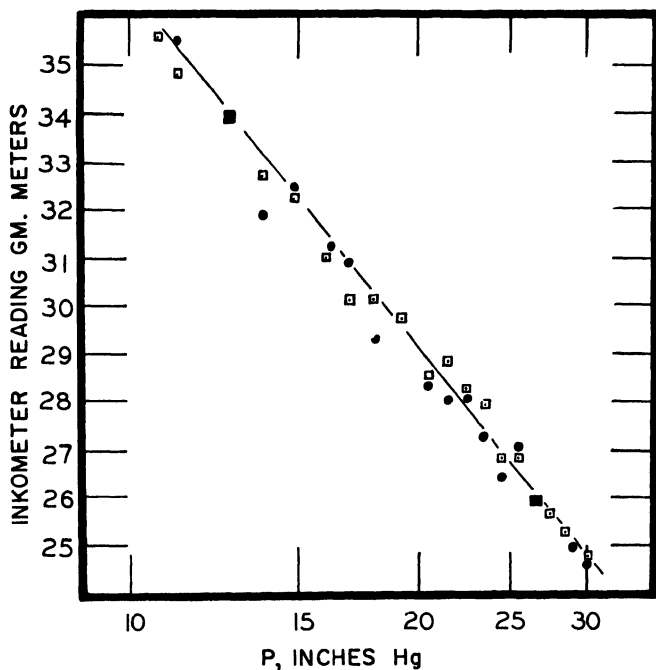


FIG. 16. Effect of ambient pressure on Inkometer reading

reading versus the logarithm of the absolute pressure which shows two significant findings:

(1) The stress requirements of both the polybutene vehicle and the dispersion of calcium carbonate increased linearly with a logarithmic decrease in pressure. In other words, if T represents tack in dyne-cm. of torque, then

$$P_A/P_0 = \exp (b - T/m). \quad (7)$$

(2) The slope is of greater magnitude for unpigmented systems than for inks made from the same vehicle.

An interpretation of the constants b and m has not been made; however, with tack readings in dyne-cm. of torque, b is expressed in identical units and can be called the tack reading at a relative pressure of unity (i.e., at atmospheric pressure). The inverse slope m also is expressed in dyne-cm. which can be viewed as a work term (ergs) rather than as a torque. Since a low m is characteristic of a nonpigmented system, it relates to the ease of cavitation. In view of other complexities of the behavior of dispersions, this statement appears to be an oversimplification of the true situation.

Because of the ability of liquids to cavitate, and because of the tendency

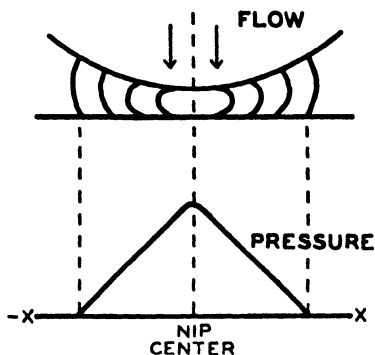


Fig. 17. Velocity and pressure profiles for a roll moving toward a plate

of pigments and extraneous nuclei to assist cavitation, the role of viscosity in tack remains an unknown factor. If some material constant other than viscosity contributes to the lessening of the forces required to split an ink film, then it must be singled out so that its contribution can be measured. On the other hand, if the chief variable in tack is the ease of formation of cavities, the problem may have a simple solution in ordinary mechanical terms.

5. THE RHEOLOGY OF FILM APPLICATION BY ROLLS

Attempts to elucidate the flow of liquids in a roll nip date to a paper by Reynolds¹⁰⁰ on the hydrodynamics of lubrication. Flow streamlines were presented for different situations involving a flat plate and a roll. Some of the situations discussed by Reynolds are applicable to the moving roller system that comprises a printing press. Figure 17 shows the velocity profiles of the liquid under the influence of a roll moving perpendicularly toward the plate.

When a couple is applied to the roll, and the plate moves at the same linear velocity, the flow pattern inside the nip is skewed, as shown in Fig. 18. Descriptions of the flow and pressure profiles have been attempted using special forms of the Navier-Stokes equations but are not taken up here. Most of the solutions consider the material (steel or plastic) to leave the roll at the position of minimum clearance.¹⁰¹⁻¹⁰⁴ While not evident in the velocity profile of Fig. 18, the liquid must adhere to the surfaces to give the tacky type of film splitting discussed here.

¹⁰⁰ O. Reynolds, *Phil. Trans. Roy. Soc. London* **177**, 157 (1886).

¹⁰¹ G. Archivelli, *Kautschuk* **14**, 23 (1938).

¹⁰² D. D. Eley, *J. Polymer Sci.* **1**, 539 (1946).

¹⁰³ E. Marboe, *Chem. Eng. News* **27**, 2198 (1949).

¹⁰⁴ J. Orowan, *Proc. Inst. Mech. Engrs. (London)* **150**, 140 (1943).

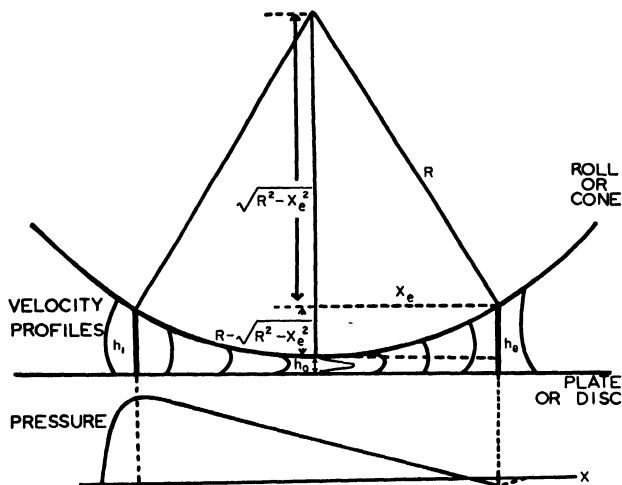


FIG. 18. Velocity and pressure profiles for a roll rotating on a plate.
Geometry of a roll nip.

Gaskell¹⁰⁵ in a paper on the calendering of plastic materials first considered the problem of the flow and pressure distribution of an incompressible liquid of limited extent on an infinitely long roll system. From a material balance on the flow in the nip, he concluded that the velocity profiles must be as shown in Fig. 18 and that the liquid follows the rolls until the distance of separation is equal to the clearance at the entrance. Gaskell's boundary conditions limit the application of Fig. 18 to the region between h_1 and h_2 (which are equal), and is based on the concept that adhesion to at least one of the rolls is zero.

The complex flow pattern that exists in a roll nip has only recently been elucidated. The area of research described below was designed to shed light on tack,¹⁰⁶ which in the parlance of the ink maker is a measure of the resistance of a film to rapid splitting.

Roll application of liquid films¹⁰⁷ involves a response to a tangential stress (Schubspannung) and a stress applied normal to the confining surfaces (Zugspannung). As a consequence, experimental procedures designed to measure tack by impressing on a film only one of these components are destined to provide only partial solutions.

We have already seen that attempts to rate inks by rotational viscometry (schub) have failed. The inability of tack fingers (zug) to provide a better

¹⁰⁵ R. E. Gaskell, *Trans. Am. Soc. Mech. Engrs.* 72, 334 (1950).

¹⁰⁶ Tack is a dynamic manifestation of the cohesive strength of liquids; in contrast, another concept of tack exists that depends on adhesive properties.

¹⁰⁷ This discussion will be confined to Newtonian liquids.

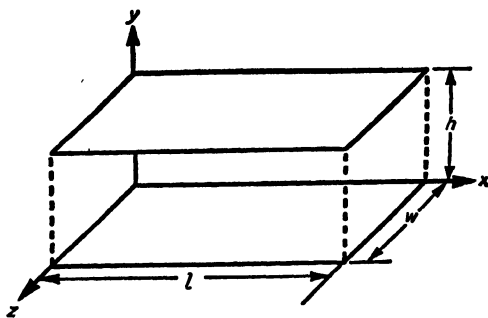


FIG. 19. Element of Area of Contact between Rolls

correlation is not quite so evident because they are not in as much use as viscometers. They fail, nevertheless, to provide the proper geometry and motion.

The only way to simulate press conditions is to adopt a roll design for the measurement of tack. Even after this decision has been reached, a choice must be made between two totally different ways of measuring the "tack force": by continuous reading of a torque¹⁰⁸ or by the capture of a transient pressure pulse as a selected segment of the roll surface passes through the nip.¹⁰⁹

Recently conducted studies on the kinematic aspects of film splitting¹¹⁰ have led the authors to conclude that it may not be necessary to measure the dynamic (force) components of tack. Traditionally, rheological studies are conducted with the objective of relating kinematic terms to dynamic terms using proportionality constants descriptive of the mechanical properties of the system. The proper sequence of events is to describe the kinematic aspects before attempting to measure the forces involved. Roll application of films has recently passed the first of these goals.

The fundamental dynamic quantity in roll application is the pressure P developed by the wedge of liquid as it is alternately compressed and distended on its passage through the roll nip. The basic kinematic quantity is the shear rate, commonly expressed as the shear profile of Fig. 18. Unfortunately, nip kinematics are not confined to the relatively simple family of shear profiles shown in the figure. Hydrodynamic shear through the nip is only the starting point of the history of a sheared film.

Let us start with a slowly rotating pair of rolls (or Discone, since the information in this section was obtained on that instrument). A torque is applied to one or both of the rotating members in order to overcome two

¹⁰⁸ The Inkometer provides the best example of this type of measurement, cf. Fig. 14.

¹⁰⁹ J. T. Bergen and G. W. Scott, *J. Appl. Mech.* **18**, 101 (1951).

¹¹⁰ J. C. Miller and R. R. Myers, *Trans. Soc. Rheol.*, **2**, in press, (1959).

types of viscous retarding forces: the laminar shear in the liquid wedge and the flow of the free boundary, which we have already seen is highly irregular. Up to this point the only mechanical property of the material which must be considered is its viscosity.

If an element of the area of contact between disk and cone is represented by the parallel plane model of Fig. 19, the force driving the fluid from left to right in the figure is represented by

$$f_1 = phw \quad (8)$$

while the viscous retarding force on the roll surfaces is¹¹¹

$$f_2 = Slw \quad (9)$$

Since the forces balance,

$$phw = Slw \quad (10)$$

or

$$S = Ph/l = Pdy/dx \quad (11)$$

Differentiation with respect to the y -coordinate produces

$$dS/dy = dP/dy \cdot dy/dx = dp/dx \quad (12)$$

From the rheological equation of state for a Newtonian liquid,

$$S = \eta D = \eta du/dy \quad (13)$$

differentiation provides¹¹²

$$dS/dy = \eta d^2u/dy^2 \quad (14)$$

Therefore,

$$d^2u/dy^2 = (1/\eta)dp/dx \quad (15)$$

It is apparent from the last equation that one of the prime determinants of u (the velocity of a given layer of liquid) is the pressure differential in the direction of flow. In order to show the exact relation between u and dp/dx it is necessary to integrate twice, using the model of Fig. 18. The first integration produces,

$$\eta \frac{du}{dy} = \frac{dp}{dx} y + B,$$

and the second,

$$u\eta = \frac{dp}{dx} \frac{y^2}{2} + By + C \quad (17)$$

¹¹¹ This analysis was provided by R. D. Hoffman of our laboratory.

¹¹² Gaskell's paper (1950) covers the development from here on.

Substitution of the boundary conditions that $u = U$ when $y = h$ gives

$$U\eta = \frac{dp}{dx} \frac{h^2}{2} + Bh + C, \quad (18a)$$

and when $y = 0$ gives

$$U\eta = C \quad (18b)$$

where U is the rim velocity of the cone and disk. Therefore,

$$B = -\frac{1}{2}h\frac{dp}{dx} \quad (19)$$

Equation (17) can now be written

$$u\eta = \frac{dp}{dx} \left(\frac{h^2}{2} - \frac{yh}{2} \right) + U\eta \quad (20)$$

or

$$u = U + \frac{1}{2\eta} \frac{dp}{dx} (h^2 - yh) \quad (21)$$

This equation is not in terms of measurable quantities. However, from the volume rate of flow Q we can develop the further knowledge that:

$$Q = \int_0^h u \, dy \quad (22a)$$

$$= Uh + \frac{1}{2\eta} \frac{dp}{dx} \int_0^h (y^2 - yh) \, dy \quad (22b)$$

$$= Uh - \frac{h^3}{12\eta} \frac{dp}{dx} \quad (22c)$$

Therefore,

$$\frac{dp}{dx} = \frac{12\eta}{h^3} (Uh - Q) \quad (23)$$

Furthermore,

$$Q = Uh_1 \quad (24)$$

and therefore,

$$\frac{dp}{dx} = \frac{12U\eta}{h^2} \left(1 - \frac{h_1}{h} \right) \quad (25)$$

The development from this point is purely geometrical. In the case of

the Discone, Equation (25) can be integrated using the geometry of Fig. 18, in which

$$\begin{aligned} h &= h_0 + R - \sqrt{R^2 - x^2} \\ &= h_0 + R - R \left(1 - \frac{x^2}{R^2} \right)^{1/2}. \end{aligned} \quad (26)$$

Binomial expansion of the term in parenthesis gives

$$\left(1 - \frac{x^2}{R^2} \right)^{1/2} = 1 - \frac{x^2}{2R^2} - \frac{1}{8} \frac{x^4}{R^4} + \dots \quad (27)$$

Now, using this relation, we obtain

$$h = h_0 + R - R + \frac{x^2}{2R} = h_0 \left(1 + \frac{x^2}{2Rh_0} \right). \quad (28)$$

From Fig. 18, the variable can be changed from x to θ ,

$$\tan \theta = \left(\frac{h}{h_0} - 1 \right)^{1/2} = \frac{x}{(2Rh_0)^{1/2}} \quad (29)$$

so that

$$dx/d\theta = (2Rh_0)^{1/2} \sec^2 \theta. \quad (30)$$

Therefore

$$\frac{dp}{d\theta} = \frac{dp}{dx} \frac{dx}{d\theta} = \frac{12U\eta(2Rh_0)^{1/2}}{h_0^2} \left(\cos^2 \theta - \frac{h_1}{h_0} \cos^4 \theta \right) \quad (31)$$

The reason for the conversion of the argument from x to θ is now clear. Integration of equation (31) produces the soluble but complicated relation for pressure:

$$\begin{aligned} P = 12 (2Rh_0)^{1/2} U\eta h_0^{-2} [& \frac{1}{4} \sin 2\theta + \frac{\theta}{2} - h_1/h_0 (\frac{3}{8}\theta \\ & + \frac{1}{4} \sin 2\theta + \frac{1}{32} \sin 4\theta)] + C \end{aligned} \quad (32)$$

The solution of this general relation for p depends on the limiting conditions imposed at the start. The constants which must be evaluated (experimentally or arbitrarily) are the ratio of initial to minimum clearance h_1/h_0 , and the constant of integration C .

Hoffman¹¹³ recognized that both the symmetry and location of the pressure profile depend strongly on conditions which still must be selected arbitrarily, and organized the solutions of equation (31) for the following cases.

¹¹³ R. D. Hoffman, the authors' laboratory.

Case 1. Complete immersion of the rolls. This condition was assumed by Banks.¹¹⁴ The additional assumption that $p \theta = 0$ at $\theta = \pm 90^\circ$ does not necessarily evolve as a proper limiting condition for p . The solution becomes

$$p = 4U\eta(2Rh_0)^{1/2}/h_0^2 \sin \theta \cos^3 \theta \quad (33)$$

and is symmetrical with respect to the origin.

Case 2. dp/dx is zero at the plane of no shear. This situation, which is the basis of the foregoing paragraphs, imposes an apparently different complexion on the equation. The material balance of fluid in the nip requires at the entrance (x_1) and the exit (x_e) that:

$$dS/dy = dp/dx = 0, \quad (34)$$

and furthermore, that $h = h_1 = h_e$ at this point. The symmetry between entrance and exit values about the line of minimum clearance should be noted in contrast with the asymmetrical velocity and pressure profiles.

If $dp/dx = 0$, p is constant when $x = x_1$ or x_e . Gaskell put p equal to one atmosphere at x_e for the calendering of plastic materials that wetted only one roll, and solved equation (32). The result, adapted for the Disc-cone and for the change in argument from x to θ , was

$$P = 12U\eta(2Rh_0)^{1/2} h_0^{-2} \{ \frac{1}{4} (\sin 2\theta - \sin 2\theta_1) (1 - h_1/h_0) + \frac{1}{2} (\theta - \theta_1) (1 - 3h_1/4h_0) - (h_1/32h_0) (\sin 4\theta - \sin 4\theta_1) \} \quad (35)$$

where θ_1 is *not* to be identified with the angle of rotation of the cone.

$$\tan \theta_1 = [(h_1/h_0) - 1]^{1/2} \quad (36)$$

Equation (24) is used in the determination of h_1 ; h_0 is measured or calculated in either case with poor precision.

Case 3. p is negative at the exit plane of no shear. As a special case of Gaskell's analysis¹¹² the situation is taken in which the liquid wets both rolls and therefore does not separate from the surface at ambient pressure. This picture is more realistic for milling, printing, roll coating, and adhesives application. The chief difference between this limiting condition and case 2 is that the liquid undergoes tension as soon as x exceeds x_e . No liquid or paste is capable of withstanding much tension (practical systems fracture at tensions far less than those calculated from equation 6). It is unlikely that P will become large enough to cause p to drop below zero p.s.i. absolute; negative pressures are nevertheless possible in theory.

¹¹⁴ W. H. Banks and C. C. Mill, *Proc. Roy. Soc.* **A223**, 414 (1954).

Both Banks and Curado, and more recently Strasburger¹¹⁵ have obtained evidence that the minimum lies in the vicinity of zero p.s.i. absolute. Tensions of this order of magnitude in conjunction with pressures capable of reaching hundreds of atmospheres prevent the pressure profile from obeying the symmetrical relation of equation (21).

The inconstancy of viscosity in printing inks further complicates the roll application of films. Gaskell¹⁰⁵ considered "viscoplastic" materials; Gatecombe¹¹⁶ modified equation (32) to include the pressure dependence of viscosity; Pasley¹¹⁷ considered the effect of viscoelastic systems upon nip flow.

Equations of this nature are of interest in understanding the forces involved in roll coating. When pressure drops below a certain critical value (as determined by the $U\eta$ product) the liquid cavitates, as shown in the schematic drawing in Fig. 6 for a similar situation. Although Banks and Mill describe the fully grown cavities in the immersed roll system, no direct observation was possible of the cavities at their instant of formation until Miller⁹⁹ photographed them with a specially built roll system consisting of a cone rotating on a disk with its apex coincident with the center of rotation of the disk. This device is shown in Fig. 20, and has been named the Discone.

The nip was viewed directly through the glass disk (from the rear as positioned) and the fluid was split between the disk and a polished metal cone which were independently driven to avoid slippage. Pictures were taken under $10\times$ to $60\times$ magnification at two millionths of a second exposure time as the film thickness, pressure and speed were varied. Motion pictures were also taken at 2000 frames per second.

At slow speeds the contribution to the tack force was found to be confined to two purely viscous flow components: laminar shear through the nip, and flow of the free boundary of material on either side of the nip, particularly on the downstream side in the region of ultimate splitting. At some critical velocity, depending on viscosity, the flow pattern passed abruptly to a second regime characterized by the appearance of cavities.

Three typical patterns are shown in Fig. 21. In each of these exposures three regions are identifiable: the bank (top), the nip or contact area, and the cavitation and filamentation region. The low shear velocity was 0.2 cm./sec.; moderate, 15 cm./sec.; and high, 31 cm./sec. What appear to

¹¹⁵ H. Strasburger, *J. Colloid Sci.* **13**, 218 (1958).

¹¹⁶ E. K. Gatecombe, *Trans. Am. Soc. Mech. Engrs.* **67**, 177 (1945); see also M. Finston, Paper No. 50-SA-13, Presented at meeting of American Society of Mechanical Engineers, St. Louis, Missouri, June, 1950.

¹¹⁷ P. R. Pasley, *J. Appl. Mech.* **24**, 602 (1957).

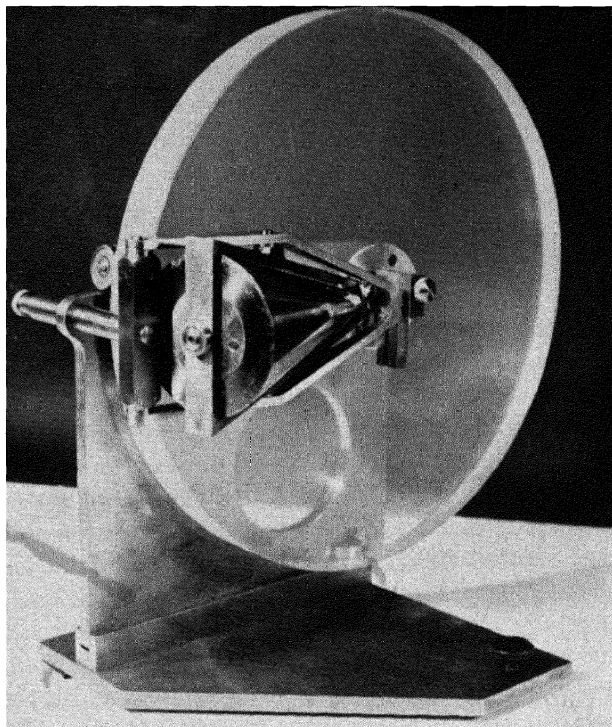


FIG. 20. Filamentation apparatus used in the photographic study of fluids splitting at different speeds, pressures, and nip geometry. Disk and cone are rim-driven

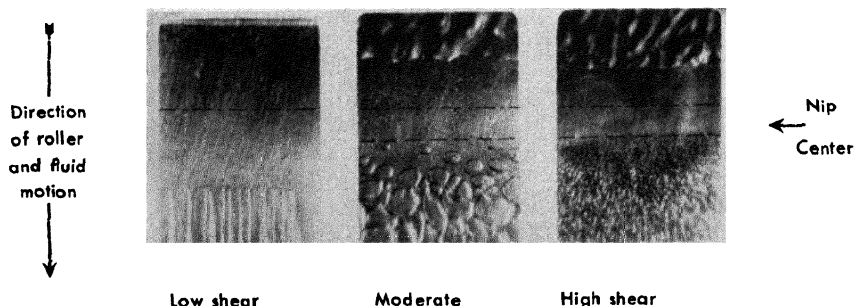


FIG. 21. Typical flow patterns inside a roll nip taken at exposure times of two millionths of a second

be streamers at the edges of the arches at the bottom of the low shear picture are webs of liquid perpendicular to the roller surface.

At the two higher velocities, the second regime is evident in the form of roughly circular discontinuities in the contact region which had been clear at lower tangential velocities. At moderate shear the discontinuities are elliptical cavities which contact one or both of the roller surfaces. At high shear a large increase in their number can be seen, and further, they appear as almost perfect circles or bubbles.^{118, 119}

The most interesting new concept introduced by this work is that cavitation occurs when the shear rate is practically zero. Initial contact of the wetted surfaces occurs when the clearance between the rollers becomes equal to h_1 , where $\frac{1}{2}h_1$ is the depth of ink on each roller. This contact is represented by a plane, transverse to the flow direction; and at this plane the pressure is built up to its highest value by the presence of a bank of liquid at clearances greater than h_1 . As the liquid moves through the nip, the clearance decreases and forces the planar area of the model to bow forward at the center and assume a parabolic configuration. The velocity gradient produced by the parabolic configuration is a maximum at the minimum clearance and decreases as the surfaces begin to separate.

At distance $x_0 (= -x_1)$ the velocity vector envelope again becomes linear; once again the area becomes planar, thereby indicating no shear. After passing the plane of no shear the area loses its identity, for either the material cavitates or it flows into the webs previously described. Ultimately the bubbles coalesce, then implode. This sequence of events leaves, attached to both rollers, filaments which are elongated by the increasing separation until the stresses become high enough to cause rupture. The film separation is then complete.

The high speed motion pictures obtained at 2000 frames per second¹²⁰ verified and amplified the sequence of action described above. The additional observation at velocities low enough to have well-defined arches coexisting with bubbles was that the arches penetrated explosively into the bubble as the bubble approached the interface; the motion was opposite the direction of roll movement. Since the pressure of the air on the external side of the interface is atmospheric, the push of the arch back into the bubbles indicates that the bubble pressure is significantly lower than atmospheric.

The second regime appears when the tension in the liquid exceeds the cohesive strength of the material and causes it to cavitate prior to the ultimate split. This regime is characterized by one viscous contribution and two elastic responses: peripheral flow of the liquid at the interface of the ex-

¹¹⁸ J. C. Miller and R. R. Myers, *Trans. Soc. Rheol.* **2**, 237 (1958), in press.

¹¹⁹ R. R. Myers, J. C. Miller, and A. C. Zettlemoyer, *J. Colloid Sci.*, in press.

¹²⁰ High speed cinematography was performed in the Bell Laboratories, New York.

panding cavity or bubble, and contributions from surface tension and the PV product of any gases in the cavity.

Quantitative measurements of the cavitation rate (i.e., the number of bubbles per unit volume of liquid) as a function of film thickness, roller velocity, and applied force established a linear increase in the number of cavities with roller velocity above the critical velocity. A slight decrease in the number of cavities occurred with increasing force on the cone.

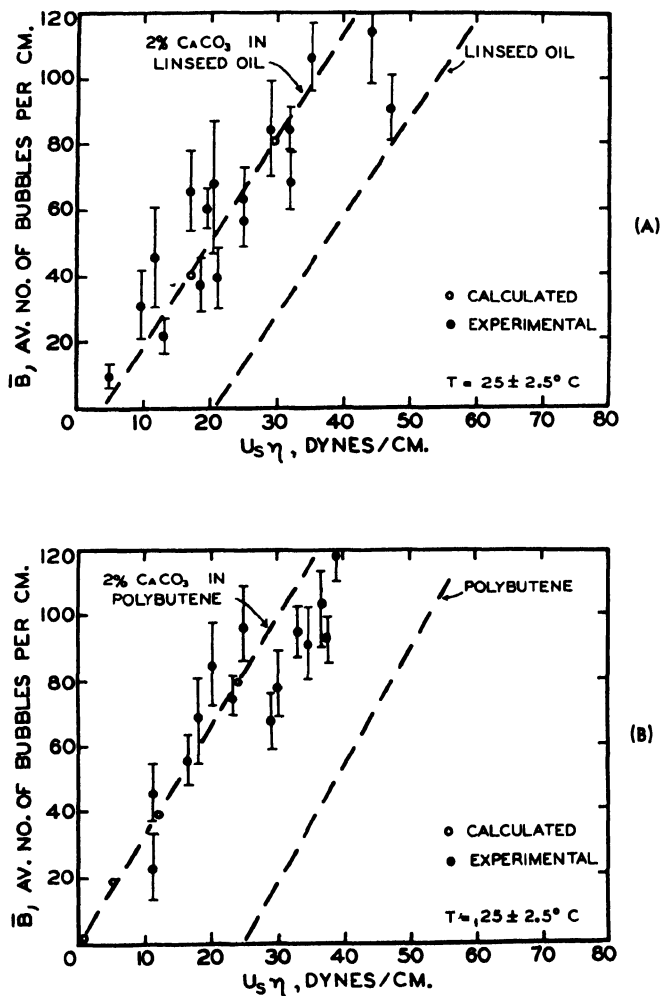


FIG. 22. Cavitation of fluids as a function of the velocity-viscosity product. (A) calcium carbonate in linseed oil. B, calcium carbonate in polybutene.)

Plots of the number of bubbles versus the velocity-viscosity product for two liquids, a 220-poise polybutene and a 165-poise linseed oil at 25°C., appear in Fig. 22A and B. They indicated no differences due to the chemical composition of the liquid. Introduction of dispersed particles of calcium carbonate catalyzed the bubble formation significantly.

Examination of the magnitude of the forces during the sequence of the splitting suggested that surface tension is the most important force resisting separation. Consequently, the highest tension on the film occurs during the formation of bubbles rather than during the elongation of the resulting filaments.

The conclusions reached from the "Discone" work must be considered preliminary. While it seems certain to the authors that bubble formation rather than film elongation is responsible for most of the force or energy required to split ink films, this decision is still open to question. The next stages in the development of our understanding of ink splitting and transfer should prove highly interesting.

Fundamental and applied studies of film splitting by rolls are still in their infancy. The next decade should provide advances in this field rivaled in practical importance by no other branch of rheology.

Nomenclature

<i>a</i>	Plate radius; fraction of ink transferred from slow to fast roll in apron nip of a three-roll mill	<i>p</i>	Pressure on fluid element in roll nip
<i>b</i>	Thickness of ink immobilized during impression in printing, in microns; tack at relative pressure of unity	<i>P</i>	Pressure or tension on film
<i>f</i>	Form factor (shape of pigment aggregates); fraction of ink transferred from slow to fast roll in feed nip of a three-roll mill	<i>P_A</i>	Ambient pressure
<i>f_r</i>	Fraction of residual ink film split to stock after amount <i>b</i> is immobilized	<i>P₀</i>	Atmospheric pressure
<i>F</i>	Force	<i>Q</i>	Quantity of ink entering roll mill in volume per unit time per unit roll length; volume rate of flow
<i>h</i>	Distance between plates or rolls	<i>R</i>	Roll radius; production rate of roll mill in volume per unit time per unit roll length
<i>h₀</i>	Initial film thickness on rolls	<i>S</i>	Stress in dynes/cm. ²
<i>h_e</i>	Film thickness at roll exit	<i>S₀</i>	Yield value as determined by extrapolation of flow curve
<i>K</i>	Constant in relation between viscosity and volume fraction	<i>t</i>	Time; fraction of ink transferred from apron roll by takeoff blade
<i>m</i>	Reciprocal of slope of tack relation	<i>T</i>	Temperature, absolute; torque in dyne-cm.
		<i>u</i>	Velocity of elementary layer through roll nip
		<i>U</i>	Rim velocity; plastic viscosity; slope of "linear" portion of flow curve

U_R	Relative plastic viscosity	β	Coefficient of compressibility
V	Volume	δ	Dimensionless counterpart of roll radius
x	Distance from nip center (horizontal coordinate); ink film thickness on plate before printing, in microns	ϵ	Dielectric constant of dispersion
y	Distance from plate (vertical coordinate); thickness of ink transferred to stock during printing, in microns	ϵ_{med}	Dielectric constant of medium
z	Dimensionless counterpart of distance from center of roll nip	θ	Angle between radii drawn to roller where film thicknesses are h and h_0
α	Coefficient of thermal expansion	ϕ	Ratio of pigment to vehicle volume
		η	Viscosity of Newtonian material; apparent or average viscosity of an ink in dyne sec./cm. ²

CHAPTER 6

RHEOLOGY OF PASTES AND PAINTS

Ruth N. Weltmann

I. Introduction	189
II. Instruments	190
1. Orifice-Capillary	190
2. Relative Motion	191
3. Rotation	191
4. Vibration	193
5. Extension-Compression	193
III. Flow measurements	193
1. Newtonian Flow	194
2. Plastic Flow	198
3. Pseudoplastic and Dilatant Flow	201
4. Thixotropic Flow	205
5. Rheoplectic Flow	216
6. Turbulent Flow	217
IV. Physical Considerations	219
1. Aging	219
2. Pretreatment and Operational Application	220
3. Temperature	221
4. Dispersion and Ingredients	222
5. Surface Active Agents	226
6. Grinding and Mixing	230
V. Product Evaluation	233
1. Control	233
2. Flow in Pipes	236
3. Pastes	240
4. Paints and Lacquers	242
Nomenclature	247

I. Introduction

Pastes and paints are suspensions which consist of either solid-liquid or liquid-liquid mixtures. The latter are often referred to as emulsions. Both paints and pastes are most frequently dispersions of microscopic or colloidal particles. Their flow behavior is of primary importance in all stages of their existence. The rheological properties of the ingredients are among the determining factors for the final product. The flow during grinding

determines the degree of mixing, the color, and other physical characteristics. Most important of all, it is the purpose of such materials to serve in applications involving flow, as in coating, spraying, dipping, brushing, printing, and other spreading operations.

The nature of such suspensions is rather complex, so that their flow behavior cannot be described by a single parameter, as would be desired by the practical investigator. Consequently, complete stress-strain curves are required to give a clue to the pattern of behavior of these materials when used for their intended purposes.

This chapter considers practical methods of measuring the flow properties of such suspensions and interpreting the obtained stress-strain curves. This must be done in such a manner as to provide information on the behavior of these materials, when they are applied to surfaces that have various physical characteristics and when they are subjected to different stresses and strains or are made to flow through channels under changing temperature conditions. In addition, suggestions are presented to indicate the type of rheological properties preferred for given conditions of application and the means of improving them. It is with this last purpose in mind that an attempt is made to show how some of the primary ingredients and their physical characteristics, together with the physical conditions of mixing, storing, and aging, can influence the flow behavior of the final product.

II. Instruments

To measure the flow of a material, instruments registering shear rates and forces are needed. The simplest qualitative indication is obtained by observing the material as it flows from an object such as a glass rod, putty knife, or paint brush. Crude as this way of judging the quality and suitability of a material is, many craftsmen still prefer this subjective method of testing to more complex objective instrumentation.

1. ORIFICE-CAPILLARY

The simplest flow instruments are related to the subjective methods and allow a measured volume of material to flow through an orifice. The time of flow of a given volume is then an indication of the consistency of the material. Examples of orifice instruments are: the Ford cup, the Zahn cup, and the Saybolt viscometer. The last is a more elaborate instrument and is usually equipped with a constant temperature bath. It is used most frequently to measure the consistency of oils. For heavier materials which do not flow under gravity alone, pressures are applied and the orifice is lengthened. Such instruments are called extrusion viscometers, of which

the Severs extrusion meter¹ is one example. By extending the length of the orifice and by making its diameter small, one of the oldest viscometers, the capillary viscometer^{2, 3} is obtained which permits flow either by gravity alone or by application of pressures.

2. RELATIVE MOTION

Another type of viscometer is based on the principle of measuring the speed of an object moving through the paste or liquid. The Gardner bubble tube⁴ presents this type in its simplest form, where the object is an air bubble which rises in a sealed tube filled with liquid. The bubble tube can be employed for all kinds of oils, including materials of water viscosity. In the Hoeppler-type viscometer,⁵ a solid ball of varying density serves as the object. The fall of the ball can be electrically timed between two contacts and the time is a measure of the consistency of the material. In the band viscometer,^{6, 7} a band moves through the material. In other cases, a plunger might be forced through a tubing or into the material, as in the case of the penetrometer; or a ball might be made to slide down an inclined plane or to move horizontally through the material.^{8, 9} The Gardner Mobilometer¹⁰ measures the time required for a disk with holes to fall through the material which is contained in a cylindrical vessel of given length. Many variations of similar instruments have been investigated and are being employed. A survey of instruments can be found in the literature.¹¹

3. ROTATION

To increase the relative speed of motion in a finite sample, the moving object can be shaped in the form of a spindle or paddle which is made to rotate in a fixed volume of material. The time of rotational motion under

¹ K. Parker and L. Tritsch, *Modern Plastics* **30**, (6), 129-34, 218 (1953).

² E. C. Bingham, "Fluidity and Plasticity." McGraw-Hill, New York, 1922.

³ W. Ostwald, *Kolloid-Z.* **36**, 99-117, 157-167, 248-259 (1925).

⁴ H. A. Gardner and H. C. Parks, *Paint Mfrs.' Assoc. U. S. Tech. Circ.* **265**, pp. 414-428 (1926).

⁵ F. Höppler, *Chemiker-Ztg.* **57**, 62-63 (1933).

⁶ F. Wachholz and W. K. Asbeck, *Kolloid-Z.* **93**, 280-297 (1940).

⁷ H. H. Hull, *J. Colloid Sci.* **7**, 3 (1952).

⁸ H. L. Röder, "Rheology of Suspensions." Paris, Amsterdam, 1939.

⁹ H. Freundlich and H. L. Röder, *Trans. Faraday Soc.* **34**, 308-316 (1938).

¹⁰ H. A. Gardner and G. G. Sward, "Physical and Chemical Examination of Paints, Varnishes, Lacquers, and Colors," 11th ed. Gardner Laboratory, Bethesda, Maryland, 1950.

¹¹ G. W. Scott Blair, "Survey of General and Applied Rheology." Pitman, New York, 1944.

a given force for a predetermined number of revolutions or the force required for a constant time interval of rotational motion is measured, as an indication of the consistency of the material. This type of instrument is extensively employed in industry. The Brookfield viscometer, a spindle-type instrument, is widely used in production applications¹² since it is easy to employ and can be dipped in almost any size container. The Stormer viscometer, having a paddle as the rotational member, is the most widely used instrument in the paint industry; the Brabender viscometer¹³ is one of its more common modifications. Rotational viscometers of the concentric cylindrical form have most desirable features and are widely used in research,¹⁴⁻³⁵ since they subject the material to a type of flow which can be most readily analyzed mathematically, especially if the rotating members are designed so that the shearing stress is practically constant throughout the sheared sample. Some of these viscometers are built to record the stress-strain curves directly and automatically in accordance with a preset stress-strain sequence.³¹⁻³³ In the modified Stormer-type viscometer²¹ the

¹² R. L. Bowles, R. P. Davie, and W. D. Todd, *Modern Plastics* **33**(3), 140, 142, 144, 146, 148 (1955).

¹³ C. R. Wicker and J. A. Geddes *ASTM Bull.* **120**, 11-18 (1943).

¹⁴ J. Pryce-Jones, *Kolloid-Z.* **129**(213), 96 (1952).

¹⁵ M. Mooney and R. H. Ewart, *Physics* **5**, 350 (1934).

¹⁶ R. F. MacMichael, *J. Ind. Eng. Chem.* **7**, 961 (1915).

¹⁷ H. Green, *Ind. Eng. Chem., Anal. Ed.* **14**, 576 (1942).

¹⁸ H. Green, "Industrial Rheology and Rheological Structures." Wiley, New York, 1949.

¹⁹ R. N. Traxler, J. W. Romberg, and H. E. Schwyer, *Ind. Eng. Chem., Anal. Ed.* **14**, 340 (1942).

²⁰ R. N. Traxler, H. E. Schwyer, and J. W. Romberg, *Ind. Eng. Chem.* **36**, 823 (1944).

²¹ E. K. Fischer, "Colloidal Dispersions." Wiley, New York, 1950.

²² R. Buchdahl, J. G. Curado, and R. Braddicks, Jr., *Rev. Sci. Instr.* **18**, 168 (1947).

²³ J. W. Smith and P. D. Applegate, *Paper Trade J.* **126**, (23), 60-66 (1948).

²⁴ E. Hatschek, *Kolloid-Z.* **13**, 88 (1913).

²⁵ P. S. Williams, *Discussions Faraday Soc.*, No. **11** (1951).

²⁶ E. Helmes, *Chem.-Ing.-Tech.* **7**, 390-394 (1953).

²⁷ C. A. R. Pearce, *J. Sci. Instr.* **30**, 232-236 (1953).

²⁸ M. Couette, *Ann. chim. et phys.* [6] **21**, 433-510 (1890); *J. phys.* **9**, 566 (1890).

²⁹ C. F. Goodeve and G. W. Whitfield, *Trans. Faraday Soc.* **34**, 511-20 (1938).

³⁰ E. W. Merrill, *J. Colloid Sci.* **9**(1), 7-19 (1954).

³¹ E. W. Merrill, *ISA Journal* **3**(4), 124-128 (1956).

³² R. N. Weltmann and P. W. Kuhns, *Natl. Advisory Comm. Aeronaut. Tech. Note No. 3510* (1955).

³³ R. N. Weltmann and P. W. Kuhns, *Lubrication Eng.* **13**(1), 43-50, (1957).

³⁴ A. F. H. Ward, S. M. Neale, and N. F. Bilton, *Phys. of Lubrication. Brit. J. Appl. Phys.* **1**, 12-18. (1951). Supplement No. 1, 12-18 (1951).

³⁵ E. M. Barber, J. R. Muenger, and F. J. Villforth, Jr., *Anal. Chem.* **27**, 425-429 (1955).

inner cylinder or bob is the rotor while in the Couette-type viscometer²⁸ the outer cylinder or cup is driven. Other types of rotational viscometers have been built which shear the material between a rotating cone and a flat plate.³⁶⁻³⁹ In this type of rotational viscometer, constant shearing stress is obtained throughout the sample if the clearance between cone and plate is properly designed.

4. VIBRATION

Instead of rotating, the measuring member can be made to vibrate or oscillate. The amount of damping is then used to calculate the consistency of the material. Lately, upper audio or lower supersonic vibrations of a reed⁴⁰ or a disk⁴¹ have been used to measure the consistency in this manner. This type of viscometer seems specially suited for solving automatic control problems and also measuring the dynamic properties of the sample.

5. EXTENSION-COMPRESSION

In another type of viscometer, the material flows by extension or compression between two members such as plane parallel plates. An instrument in which pull is exerted to extend the material under test is the Tackmeter,⁴² which is well suited for measuring the consistency of oils and paints, whereas the Dienes and Klemm⁴³ and Williams⁴⁴ parallel-plate viscometers provide compression and are designed to measure the consistency of very viscous materials such as stiff latices and synthetic plastics.

III. Flow Measurements

From the foregoing it appears that numerous instruments are available for the flow measurement of paints and pastes. However, some of those instruments are not capable of giving sufficient information to evaluate the complex flow characteristics that most pastes and paints exhibit. A complex flow behavior cannot be catalogued by a single viscosity value at any one temperature, since it will also be a function of applied shear and duration of shear application. Although a flow measurement at one rate of shear might suffice for a given problem such as might be encountered

³⁶ R. McKennel, *Proc. 2nd Intern. Rheol. Congr., Oxford*, 1953 pp. 350-359 (1954).

³⁷ H. Markovitz, L. J. Elyash, F. J. Padden, and T. W. DeWitt, *J. Colloid Sci.* 10(2), 165-173 (1955).

³⁸ J. E. Roberts, British Ministry of Supply Rept. ADE 13/52, London, 1952.

³⁹ R. S. Higginbotham, *J. Sci. Instr.* 27, 139, (1950).

⁴⁰ W. Roth and S. R. Rich, *J. Appl. Phys.* 24, (1953).

⁴¹ J. G. Woodward, *J. Acoust. Soc. Am.* 25, (1953).

⁴² H. Green, *Ind. Eng. Chem., Anal. Ed.* 13, 632 (1941).

⁴³ G. J. Dienes and H. F. Klemm, *J. Appl. Phys.* 17, 458 (1946).

⁴⁴ I. Williams, *Ind. Eng. Chem.* 16, 362 (1924).

in production control, only the knowledge of the flow pattern of the material over an extended range of shearing stress and rate of shear makes it possible to choose the proper one-point viscosity control instrument. Thus, most flow investigations require instruments which are capable of applying different, constant rates of shear to the material and of measuring the resulting stresses. For the purpose of determining rates of shear and shearing stresses in rational units, the geometry of the instrument should permit the application of calculations based on a corresponding model of flow. Only a few types of instruments lend themselves to simple flow calculations. They are the capillary viscometer, the parallel plate viscometer, the band viscometer, and the rotational viscometers. Of these only the rotational viscometers are suited to a complete analysis of the flow of all types of materials. For an analysis of the models of flow in the parallel-plate viscometer and band viscometer, the reader is referred to the literature,^{6, 7, 42-45} since these instruments are little used for the measurement of paints and pastes. The models of flow in the capillary viscometer, the extrusion viscometer, the concentric cylinder viscometer and the cone and plate viscometer, however, will be treated here briefly. Since a mathematical treatment of the models of flow in these instruments is given in another chapter of this volume⁴⁶ only the results of the mathematical derivations will be presented here and it will be shown how these equations can be applied to the actual flow measurements and can be used in the interpretation of the rheological flow properties.

1. NEWTONIAN FLOW

The basic law of viscosity, defined as the internal friction of a nonelastic liquid, was deduced by Newton⁴⁷ and can be visualized by a simple model. Suppose a liquid is contained between two parallel plane plates of area A separated by the distance x . While one plate is stationary, the other plate is made to move at a constant velocity v by applying a force F so that the flow in the liquid is laminar. Then the relation between the force per unit area, F/A , or shearing stress, and the change in velocity v over the distance x , or rate of shear, defines the coefficient of viscosity μ . In short,

$$F/A = S = \mu(dv/dx) \quad (1)$$

The unit of viscosity is the poise, when the shearing stress is given in dynes/cm.² and the rate of shear in seconds⁻¹. The plot of shearing stress

⁴⁵ M. J. Stefan, *Sitzber. Akad. Wiss. Wien Math.-naturw. Kl., Abl. II* **69**, 713 (1874).

⁴⁶ See S. Oka, Chapter 2 in this volume.

⁴⁷ I. Newton, "Principia," F. Cajori, ed., "Sir Isaac Newton's Mathematical Principles of Natural Philosophy and His System of the World." University of California Press, Berkeley, California, 1947.

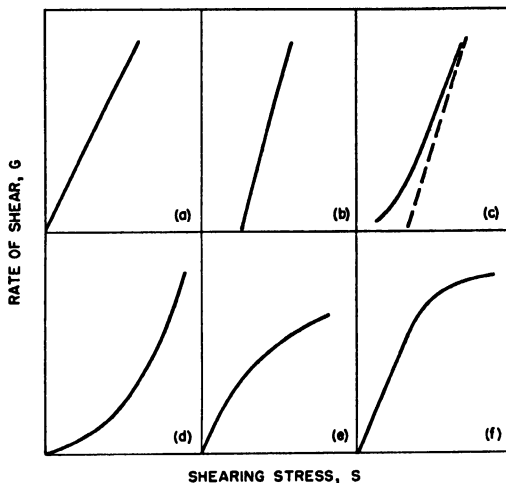


FIG. 1 Schematic flow curves. (a) Newtonian. (b) Plastic. (c) Plastic in capillary. (d) Pseudoplastic. (e) Dilatant. (f) Turbulent.

versus rate of shear is termed the flow curve. A linear flow curve passing through the origin (Fig. 1a) as given by equation (1) defines a material as Newtonian. In this case $\mu = f(S) = \text{constant}$ and any one point will determine the complete flow pattern, i.e., the viscosity is single-valued. Hence any type of instrument can be used to measure the viscosity of a Newtonian material. Although many ingredients which are used in the manufacture of paints and pastes, such as solvents, water, certain oils, some resins, and some varnishes, show Newtonian behavior, the majority of materials that are composed of more than one ingredient, including most pastes and paints, exhibit non-Newtonian flow behavior.

Poiseuille^{48, 49} worked out the equation for laminar Newtonian flow in capillary tube viscometers. If a volume of material V flows through a capillary in a given time t under a pressure P , equation (1) becomes, after integration, when the shearing stress is expressed as a function of the rate of shear,

$$\frac{PR}{2L} = \frac{\mu 4VR}{\pi R_w^4 t} \quad (2a)$$

and

$$\mu = \frac{\pi P t R_w^4}{8 L V} \quad (2b)$$

⁴⁸ J. L. M. Poiseuille, *Compt. rend.* **15**, 1167 (1842).

⁴⁹ W. H. Herschel, "Experimental Investigations Upon the Flow of Liquids in Tubes of Very Small Diameter by J. L. M. Poiseuille," *Rheol. Mem. (Soc. Rheol.)* (1940).

where μ is in poises, if P is the applied pressure in dynes/cm.², R_w is the inside radius of the capillary in centimeters and R is any radius from zero to R_w , L is the length of the capillary in centimeters, V is in cubic centimeters, and t is in seconds. From equation (2a) it can be seen that the shearing stress, $S = PR/2L$, is zero at the center of the capillary (at $R = 0$) and varies from zero to a maximum, which is obtained at the wall of the capillary at $R = R_w$. In practical applications the rate of shear, or velocity gradient, $G_w = 4V/\pi R_w^3 t$, and the shearing stress, $S_w = PR_w/2L$, at the wall of the capillary are often used to plot shearing stress-rate of shear curves. This same equation is also used for calculating the laminar flow in extrusion viscometers and for plotting flow curves from extrusion data.

In the concentric cylinder rotational viscometer, the test sample is sheared between two cylinders rotating with a relative angular velocity ω . The resulting torque T on one cylinder is measured and is a function of the viscosity. For Newtonian materials, when the shearing stress is again expressed as a function of rate of shear, equation (1) becomes after integration,

$$\frac{T}{2\pi R^2 h} = \mu \frac{2\omega}{R^2(1/R_b^2 - 1/R_c^2)} \quad (3)$$

and

$$\mu = \frac{T}{\omega} K$$

where μ is in poises, if K is an instrument constant in cm.⁻³,

$$K = (1/R_b^2 - 1/R_c^2)/4\pi h,$$

R_b is the bob radius in centimeters, h is the bob height in centimeters, R_c is the cup radius in centimeters, R is any radius between the cup and the bob radius; T is measured in dyne-centimeters and ω is in seconds⁻¹. From equation (3) it can be seen that the shearing stress, $S = T/2\pi R^2 h$, varies inversely with the square of the radius; for small clearances, when $R_c \approx R_b$, the variation in shearing stress over the annulus is small.

The instrumental constant K was derived under the assumption that the concentric cylinders have no ends, or rather that the contribution to the torque because of their ends was negligible compared to the torque arising between the cylindrical surfaces. In a well-designed instrument that may well be the case. However, a test is always indicated to determine more definitely whether to neglect or to correct for end-effects. The

TABLE I
PRACTICAL DIMENSIONS FOR A CONCENTRIC CYLINDER ROTATIONAL VISCOMETER
AND END-EFFECT CORRECTIONS

Cup radius R_c (cm.)	Bob radius R_b (cm.)	Bob height h (cm.)	Instrumental constant K (per cm. ³)	End effect ^a Correction (%)	End effect corrected K (per cm. ³)
2.40	2.20	3.60	0.75×10^{-3}	13.4	0.65×10^{-3}
1.75	1.56	3.53	1.76×10^{-3}	14.2	1.51×10^{-3}
1.50	1.30	5.10	2.33×10^{-3}	2.1	2.28×10^{-3}
1.45	1.30	5.10	1.82×10^{-3}	1.7	1.79×10^{-3}
1.40	1.30	5.10	1.25×10^{-3}	1.6	1.23×10^{-3}
1.35	1.30	5.10	0.66×10^{-3}	1.5	0.65×10^{-3}
0.60	0.55	5.10	0.84×10^{-3}	1.2	0.83×10^{-3}

^a All end effects were obtained for a distance of about 1 cm. between the bottom of the cup and that of the bob.

literature offers many suggestions to minimize the end-effects^{32, 50} and to correct for them experimentally.^{18, 21, 51, 52}

A few practical values of cup and bob dimensions and the corresponding corrections necessitated by the end-effects are given in Table I. A constant end-effect correction can be applied only if the clearance between cup and bob is small in relation to the radii and very small in relation to the distance between the bottom of the cup and that of the bob. Otherwise, the end-effect correction might vary with viscosity.⁵¹ End-effects above approximately 5% are high and can introduce appreciable errors. For materials which do not adhere to the surface of the cup and bob it has been suggested¹⁷ that grooved rotating members be provided to minimize slip-page.

In another type of rotational viscometer a cone and plate rotate with respect to each other. This instrument is so designed that the shape of the cone compensates for the increase in radius so that the rate of shear is practically constant over the clearance between cone and plate. In such a viscometer the Newtonian viscosity is given³⁶ as

$$\mu = \frac{3T\beta}{2\pi R^3\omega} \quad (4)$$

where μ is in poises, if R is the radius of the cone in centimeters, β is the

⁵⁰ M. Mooney and R. G. Ewart, *Physics* **5**, 350 (1934).

⁵¹ C. H. Lindsley and E. K. Fischer, *J. Appl. Phys.* **18**, 11 (1947).

⁵² E. Hatschek, "Viscosity of Liquids." Van Nostrand, Princeton, New Jersey, 1928.

angle between cone and plate in radians, T is the torque in dyne-centimeters, and ω is the angular velocity in radians per second.

2. PLASTIC FLOW

Materials exhibiting plastic flow do not flow until the applied shearing stress exceeds a minimum value. This minimum shearing stress f , designated by Bingham² as yield value, is indicated on the flow curve by an intercept on the shearing stress axis (Fig. 1b). Thus, the equation for a plastic material, also called a Bingham body, is

$$S - f = U(dv/dx) \quad (5)$$

where U is the coefficient of plastic viscosity. After the yield value is exceeded, the flow curve of the material is linear. The yield value is believed to be a measure of the force of flocculation per unit area which exists between the suspended particles. Materials consisting of a suspension of highly flocculated particles show a pronounced yield value effect.

Examples of truly plastic materials in accordance with Bingham's straight line concept are very rare, although some carbon black, quartz, and glass-bead suspensions were found⁵³ to exhibit truly plastic flow at least up to the highest rates of shear at which they had been measured.

The term apparent viscosity η is frequently used in the investigation of non-Newtonian materials. Apparent viscosity is defined as the ratio of shearing stress to rate of shear, so that

$$S = \eta(dv/dx) \quad (6)$$

Comparing this equation with equation (5) shows that

$$\eta = U + \frac{f}{dv/dx} \quad (7)$$

and thus η decreases with increasing rates of shear even for constant U and f . The apparent viscosity η is frequently used since it is readily obtainable with many viscometers, although it has very little physical meaning when the flow behavior of non-Newtonian materials is studied, unless it is specified for a definite condition of shearing stress and rate of shear.

It is not surprising that only very few truly plastic materials are encountered, since they might be considered a limiting case for materials exhibiting viscous and elastic flow components. The most simple type of a viscous and elastic material is the Maxwell body. Its equation of flow can be expressed for $dv/dx = G$ being constant at any given S , that is, if only stress relaxation is considered, as

$$G = \frac{S - S_0(e^{-t/\tau})}{\mu(1 - e^{-t/\tau})} \quad (8)$$

⁵³ H. Green and R. N. Weltmann, *Ind. Eng. Chem., Anal. Ed.* **15**, 3 (1943).

where G is the mean rate of shear, S_e is the total elastic shearing stress, also called yield stress, t is the duration of strain, and τ is the relaxation time. Equation (8) is adequately representative of many flow curves which are obtained from shear experiments, since the rate of shear, being the applied parameter in many viscometers, is frequently held constant during the stress relaxation of the sheared sample. Equation (8) reverts to equation (5) if the relaxation time τ is constant, since then $e^{-t/\tau}$ is constant so that $S_e(e^{-t/\tau})$ corresponds to f and $\mu(1 - e^{-t/\tau})$ corresponds to U in equation (5). Even though the relaxation time of many viscous and elastic materials is not constant, but increases with increasing rates of shear, it frequently approaches one prominent value and thus is almost a constant above a certain rate of shear. Consequently, many of these materials show a flow behavior similar to that described in equation (5) at all but the very low rates of shear. Under those circumstances the flow behavior of the material might be interpreted by using the straight portion of the flow curve in accordance with equation (5) as if the material had true plastic flow behavior. This method of interpretation is used throughout this chapter for materials whose major part of the measured flow curve approaches linearity. In many of those cases the stress intercept might not agree with a constant Bingham yield value concept but might result from elastic flow behavior and thus might vary with rate of shear. Nevertheless the above analysis of the flow curve is useful, since it makes possible a practical and rather simple description of the flow properties of numerous materials, including many pastes and paints, and since it permits in many cases a valid interpretation of the flow behavior during and after the application procedures. Equation (8) reverts to equation (1) if the relaxation time τ is small compared to t , which is the case for Newtonian materials.

The shearing stress, $S = PR/2L$, in the center of a capillary or extrusion viscometer is always zero. Since a plastic material does not flow until a finite shearing stress at least equal to the yield value stress f is applied, a plastic can never be made to flow in the center of a capillary, and plug flow exists. Therefore, a straight line similar to the flow curve shown in Fig. 1b for a plastic can never be obtained with capillary and extrusion viscometers, but can only be approached asymptotically at high shearing stresses (Fig. 1c). Buckingham⁶⁴ derived the following equation for evaluating the plastic viscosity of a Bingham body from the flow curve in a capillary viscometer, if slippage flow, end-effects, and kinetic energy effects are assumed absent.

$$U = \frac{\pi P t R_w^4}{8 L V} \left[1 - \frac{8 L f}{3 R_w P} + \frac{1}{3} \left(\frac{2 L f}{R_w P} \right)^4 \right] \quad (9)$$

⁶⁴ E. Buckingham, *Proc. Am. Soc. Testing Materials* **21**, 1154 (1921).

Although Green¹⁸ showed that the Buckingham equation is not valid in the region of very low rates of shear, it nevertheless is a good description of the model of flow for true plastic materials in a capillary viscometer. However, it is difficult to use the Buckingham equation for rigid calculations of the two plastic parameters U and f , since plug flow persists even at high flow rates, and frequently the third term in the bracket on the right side of equation (9) cannot be neglected.

Some investigators,⁵⁵ when measuring pastes with an extrusion viscometer, plot the reciprocal of the rate of shear against the apparent viscosity and obtain at the higher rates of shear an apparently straight line with an intercept on the apparent viscosity axis. This suggests that these materials acquire the flow characteristics of Bingham plastics (equations 5 and 7) at the rates of shear at which this plot becomes linear.

In the concentric cylinder rotational viscometer, equation (5) becomes, after integration,⁵⁶ if shearing stress is expressed as a function of rate of shear,

$$S - S_0 = \frac{T - T_0}{2\pi R^2 h} = U \frac{2\omega}{R^2(1/R_b^2 - 1/R_c^2)} \quad (10)$$

and

$$U = \frac{T - T_0}{\omega} K$$

and

$$f = \frac{T_0 K}{\ln (R_c/R_b)}$$

where T_0 and S_0 are the torque and stress intercepts at $\omega = 0$. Since the shearing stress at the bob (equation 10) is larger than that at the cup, flow of a plastic material with yield value will start in layers close to the bob, while layers close to the cup will remain unsheared, yielding plug flow. The amount of plug flow for the same material will increase with increasing clearance between cup and bob. It is obviously difficult to give a meaningful interpretation to a flow curve if plug flow persists over the complete range or even over a large portion of the applied shearing stresses. Indeed, it is for this reason that the capillary viscometer is thought to be unsuited for the measurements of plastics. In a rotational viscometer the amount of plug flow can be calculated by considering that flow starts at the bob surface when the shearing stress at the bob S_b is equal to the yield value so that $S_b = R_b^2 f / R^2$ or $T = 2\pi R_b^2 h f$ and that flow over the

⁵⁵ G. B. Moses and I. E. Puddington, *Can. J. Research* **B27**, 616-628 (1949).

⁵⁶ M. Reiner and R. Rivlin, *Kolloid-Z.* **43**, 1 (1927).

clearance is complete; i.e., the straight line relation commences when the shearing stress at the cup S_c equals the yield value so that $S_c = R_c^2 f / R^2$ or $T = 2\pi R_c^2 h f$. Thus, when S_c is substituted for S and

$$\frac{f}{K} \frac{\ln (R_c/R_b)}{2\pi R^2 h}$$

for S_0 in equation (10) which is then rearranged for ω explicitly, plug flow ends at

$$\omega_P = \frac{f}{U} \left[\frac{R_c^2}{2R_b^2} - \frac{1}{2} - \ln (R_c/R_b) \right] \quad (11)$$

Equation (10) can be used for meaningful flow interpretations only if $\omega_P \ll \omega_{\max}$.

True plastic flow curves obtained with a concentric-cylinder rotational viscometer are shown in Fig. 2⁶³ for glass beads and quartz suspended in Nujol and for carbon black pigment in glycerin. The experimental data are in agreement with equations (10) and (11), indicating true plastic flow behavior. Also, the curves taken at increasing and decreasing rates of shear coincide, as they should, in the case of true plastic flow.

3. PSEUDOPLASTIC FLOW AND DILATANT FLOW

The flow curves of pseudoplastic materials are convex to the shearing-stress axis as shown in Fig. 1d indicating a decreasing apparent viscosity with increasing rate of shear. This is in accordance with equation (8) for

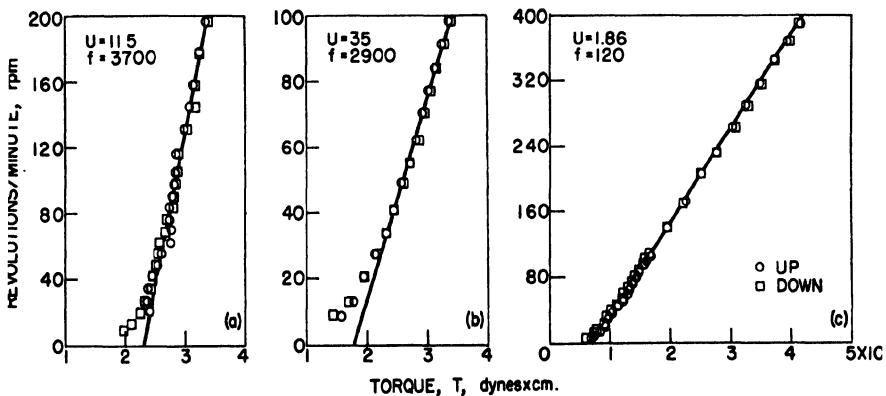


FIG. 2. Concentric-cylinder rotational viscometer flow curves of true plastic materials. Temperature = 30° C. (U , in poises; f , in dynes/cm.²; $G \sim 0.73 \times$ r.p.m. in sec.⁻¹; $S \sim 1.6 \times 10^{-2} \times T$ in dynes/cm.² for $R = R_m$). (a) Carbon black in glycerin. (b) Quartz in Nujol. (c) Glass spheres in Nujol. After Green and Weltmann.⁶³

viscous and elastic materials, when no one prominent relaxation time exists, but τ is a function of the applied shearing rate and is of the same order of magnitude or larger than the time t . The viscosity most frequently used to describe pseudoplastic materials is the apparent viscosity (equation 6), determined at a given rate of shear. Some investigators⁵⁷ prefer to use a tangent viscosity similar to the plastic viscosity U (equation 5) at a given rate of shear. Frequently flow starts at an infinitely small shearing stress, so that at extremely low rates of shear an initial Newtonian viscosity is sometimes postulated. Other investigators⁵⁸ fit an empirical power function to the pseudoplastic flow curve so that

$$dv/dx = S^N/\mu^* \quad (12)$$

After integration of equation (12) and assuming N to be constant the mean rate of shear G in a concentric cylinder rotational viscometer and in a capillary viscometer becomes

$$G = CS^N/\mu^* \quad (13)$$

In this equation N and μ^* are constants of the material. The quantity N is a measure of the degree of pseudoplasticity and for this reason has been called structure number.⁵⁹ The rate of shear correlation factor C depends on the viscometer that is employed and is always a function of N . For pseudoplastic materials the structure number N is always larger than 1.

The decrease in apparent viscosity, $\eta = \mu^*S^{(1-N)}/C$, with increasing shearing stress S is attributed to shear alignment, deinking, and uncoiling of molecules or to changes in shape of suspended elastic particles due to the directional shearing action.

Examples of pseudoplastic materials are numerous. Most high polymers, latices, starch pastes, and many emulsions exhibit this type of flow.

Dilatant^{60, 61} materials on the other hand show increased resistance to flow when agitated since their viscosity increases with increasing rate of shear. The dilatant flow curve is concave to the shearing stress axis (Fig. 1e). Vinyl resin pastes, beach sand, and some carbon black suspensions, for example, exhibit dilatant behavior. Dilatancy is said to be caused by close packing of the suspended particles. At higher rates of shear more of the liquid is trapped in the voids and the particles rub against each other because of lack of lubrication, thus increasing the resistance with increasing rates of shear. This theory is somewhat substantiated by the observa-

⁵⁷ R. V. Williamson, *Ind. Eng. Chem.* **21**, 1108-1111 (1929).

⁵⁸ F. D. Farrow, G. M. Lowe, and S. M. Neale, *J. Textile Inst. Trans.* **19**, 18-31 (1928).

⁵⁹ R. N. Weltmann, *Natl. Advisory Comm. Aeronaut. Tech. Note No. 3397* (1955).

⁶⁰ O. Reynolds, *Phil. Mag.* [5] **20**, 469-480 (1885).

⁶¹ H. Freundlich and F. Juliusberger, *Trans. Faraday Soc.* **30**, 333-338 (1934).

tion that the dilatant flow behavior of a material is readily transformed into other flow types by a change of solid-liquid ratio or by additions of other ingredients. Some investigators designate the dilatant material by a viscosity obtained from a tangent on the flow curve at a point of given rate of shear while others use the power equation (13), where N is said to be a measure of the degree of dilatancy and is always less than 1 for a dilatant material.

For capillary and extrusion viscometers the value of C in equation (13) is equal to $4/(N + 3)$ assuming N to be constant over the cross section of the sheared sample. Therefore, it has been suggested that the expression for the viscosity in equation (2b) be multiplied by the factor $4/(N + 3)$ in the evaluation of pseudoplastic and dilatant flow curves obtained with these viscometers. However, experiments indicate that for many materials N varies as a function of rate of shear, when measurements are made over a wide range of rates of shear. Since in capillary and extrusion viscometers the change in rate of shear over the sheared sample is large, because the shearing stress in such viscometers varies from zero to a maximum at the tube wall, the apparent viscosity of such materials, and sometimes also N , will vary accordingly along the tube radius and the flow rate in the cylindrical layers will differ with the radial distance. Under these conditions, the total flow rate will be a measure of an effective viscosity of the material at the applied pressure, which most likely is weighted in favor of the lowest viscosity⁶² existing within the cross sectional area. For dilatant materials the lowest viscosity occurs at the lowest rate of shear and thus most likely near the center of the tube, while for pseudoplastic materials the highest rate of shear will give the lowest viscosity, that is, near the tube wall. Thus a flow curve obtained in capillary and extrusion viscometers for pseudoplastic and dilatant materials, when plotted in accordance with equation (2) for $R = R_w$ or any mean value of R , is not a rate of shear versus shearing stress curve. The interpretation of such a flow curve is possible only if the materials do not deviate appreciably from Newtonian flow. In many other cases such measurements can lead to a false analysis of the flow behavior of the tested sample. When a more rigorous mathematical treatment is applied^{58, 63, 64} misinterpretations are minimized.

To obtain true rate of shear versus shearing stress curves for pseudoplastic and dilatant materials requires that the shearing stress be constant throughout the sheared sample. This is the case only in Newton's model of flow where the material is sheared between two parallel plates and thus in concentric cylinder viscometers of infinite radii. The shearing stress in a

⁶² R. N. Weltmann and P. W. Kuhns, *J. Colloid Sci.* **7**, (3), 218-226 (1952).

⁶³ B. Rabinowitch, *Z. physik. Chem. (Leipzig)* **2**, 145 (1929).

⁶⁴ M. Reiner, "Deformation and Flow." Lewis, London, 1949.

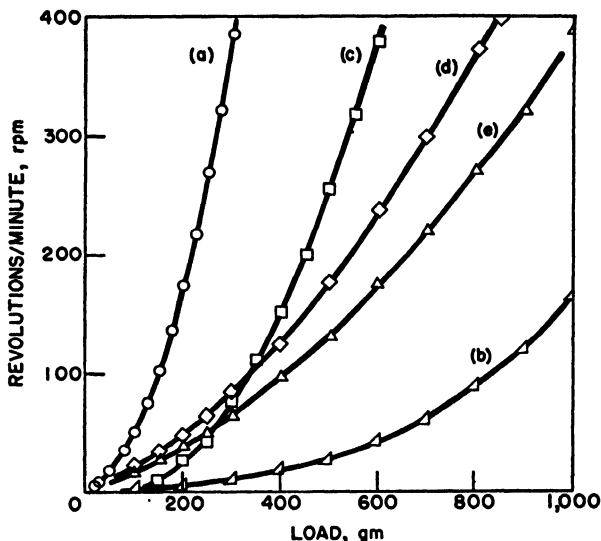


FIG. 3. Concentric-cylinder rotational viscometer flow curves of pseudoplastic materials. Temperature = 30° C., * = 90° C. ($G \sim 0.95 \times \text{r.p.m. in sec.}^{-1}$; $S \sim 1.74 \times \text{load in dynes/cm.}^2$ for $R = R_m$). (a) 1% sodium alginate in water. (b) 2% sodium alginate in water. (c) 10% acid-modified corn starch paste in water.* (d) 1.95%, 4000-c.p.s. grade methyl cellulose solution in water. (e) 2.29%, 1500-c.p.s. grade methyl cellulose solution in water. After Fischer.²¹

practical concentric cylinder rotational viscometer varies from cup to bob. Its change depends on the cylinder dimensions and can be small if the viscometer is properly designed. Therefore, a properly designed rotational viscometer is well suited for measuring pseudoplastic and dilatant materials. The flow curves are almost true rate of shear versus shearing stress curves and lend themselves to valid flow interpretations.

The flow curves of pseudoplastic and dilatant materials obtained on a rotational viscometer are evaluated either by determining an apparent viscosity by using equation (6) or by using equation (10), where U is the tangent viscosity at a specified shear and S_0 is an intercept. Many investigators have made use of the fact that some pseudoplastic and dilatant materials give a logarithmic straight-line relationship of rate of shear and shearing stress (equation 12) and have used the power term N and the constant μ^* of equation (13) to designate the flow behavior of the materials. The equation for C for concentric cylinder rotational viscometers, assuming again N to be constant over the cross section of the sheared sample, is

$$C = \left\{ \frac{1 - (R_b/R_c)^{2N}}{N[1 - (R_b/R_c)^2]} \right\} \left(\frac{R}{R_b} \right)^{2(N-1)}$$

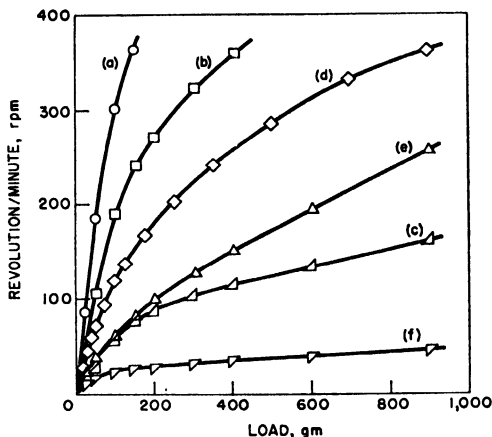


FIG. 4. Concentric-cylinder rotational viscometer flow curves of dilatant materials. Temperature = 30° C. ($G \sim 0.25 \times \text{r.p.m. in sec.}^{-1}$; $S \sim 1.13 \times \text{load in dynes/cm.}^2$ for $R = R_m$). (a) 11.3 vol. % iron oxide in aqueous solution of sodium lignin sulfonate. (b) 1.7 vol. % iron oxide in aqueous solution of sodium lignin sulfonate. (c) 12.4 vol. % iron oxide in aqueous solution of sodium lignin sulfonate. (d) 39.2 vol. % barium sulfate in same solution. (e) 46.9 vol. % starch in ethylene glycol. (f) 50.8 vol. % starch in ethylene glycol. After Fischer.²¹

The quantity C approaches 1 for $R_b/R_c \rightarrow 1$, and R is the radius that was used in the determinations of the flow curve rates of shear and shearing stresses (equations 3 and 10). In a properly designed rotational viscometer, N can be considered to be constant over the sheared annulus, since the change in shearing stress from cup to bob is small, and C does not differ much from 1 even for large values of N . For example, in a concentric cylinder rotational viscometer of $R_b/R_c = 0.95$, $C \approx 1.05$ for $N = 10$, if $R = R_m = \frac{1}{2}(R_b + R_c)$ is used in the calculations.

In Fig. 3 flow curves are shown of pseudoplastic materials such as sodium alginate, starch, and methyl cellulose solutions as obtained with a concentric cylinder rotational viscometer.²¹ Figure 4 gives examples of dilatant materials.²¹ As is shown, iron oxide, barium sulfate suspensions and certain starch mixtures can exhibit dilatant behavior.

4. THIXOTROPIC FLOW

Many materials and certainly most paints and pastes show thixotropic behavior in addition to being plastic, pseudoplastic, or dilatant. Thixotropy was first defined by Peterfi⁶⁵ as an isothermal, reversible sol-gel-sol transformation. Translated, the word thixotropy means change by touch, indi-

⁶⁵ T. Peterfi, *Wilhelm Roux' Arch. Entwicklungsmech. Organ.* **112**, 660 (1927).

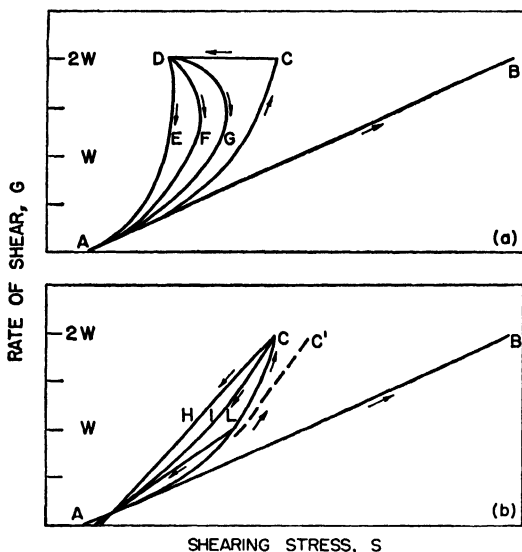


Fig. 5. Schematic flow behavior of thixotropic materials. Reversible change of thixotropic structure with: (a) time of application of a constant rate of shear; (b) increasing rates of shear.

cating that the material decreases in viscosity on shear, but builds up again when at rest. More recently, the definition of thixotropy has been broadened^{66, 67} to include materials which exhibit an isothermal reversible transformation from a higher to a lower viscosity gel. It has also been found that this transformation can be brought about either by an increase in rate of shear followed by a rest period or by the application of a constant rate of shear over a period of time followed again by a rest period. What happens when a thixotropic plastic material is agitated is shown schematically in Fig. 5. Such a material would produce a flow curve similar to line AB if its flow could be measured without stirring. When increasing rates of shear from zero to $2W$ are applied, breakdown will occur and result in curve AC.

Thixotropic breakdown with time is described in Fig. 5a. While a constant rate of shear of $2W$ is applied over a period of time, the consistency of the material decreases continuously from C to D, where it reaches an equilibrium value, the lowest it can experience at the given rate of shear of $2W$. Only a higher rate of shear will be able to decrease the consistency further. If the shear is discontinued at point D, the buildup in consistency necessary for the material to regain its original structure will follow along

⁶⁶ H. Freundlich, "Thixotropy." Hermann, Paris, 1935.

⁶⁷ H. Green and R. N. Weltmann, in "Colloid Chemistry, Theoretical and Applied." (J. Alexander, ed.), Vol. 6, pp. 328-347. Reinhold, New York, 1946.

curve E , F , or G , depending on the time which the particular material requires for the rebuilding process. A similar pattern is found if the shear is discontinued at any point between C and D .

Thixotropic breakdown with increasing rate of shear is illustrated schematically in Fig. 5b. When the shear is discontinued at C , the material can return to its original state along curves such as H , I , or AC , depending on the time required for rebuilding its structure. If it returns instantaneously to its original structure, the material might be considered to be pseudoplastic rather than thixotropic since a hysteresis loop, similar to ACH or ACI , is considered to be a necessary characteristic for thixotropic behavior. If the increase in rate of shear from zero to W at point L required time t , then the successive increase in rate of shear from W to $2W$ along line LC will again take time t , if the rate of increase in rate of shear is to remain constant. Thus, the decrease in consistency between point L and C is caused not only by an increase in rate of shear but also by the elapsed time t which was required to increase the rate of shear from W to $2W$, provided that the increased agitation is successively applied to the same sample. This might not be the case if the rate of shear W is applied to one sample and the rate of shear $2W$ to another sample, since then the time element might be the same for each sample, requiring time t to bring sample 1 to rate of shear W and also time t to bring sample 2 to rate of shear $2W$. In that case, the up curve for sample 2 will not go to C but only to C' , which means the decrease in consistency is less. When the shear at C' is discontinued, the material will follow a similar pattern to that described when the shear was assumed discontinued at point C .

Similar curves are obtained for thixotropic pseudoplastic and thixotropic dilatant materials. Particles of various shapes produce thixotropy, but particles of uniform shapes such as spheres do so to a lesser degree than particles of anisotropic configurations such as long needles or thin disks. In paints thixotropy is quite common and in some applications even an asset. A minute addition of water to a paste of titanium dioxide in linseed oil will increase greatly the degree of thixotropy exhibited by this suspension. As can be seen from the two photomicrographs of Fig. 6,⁶⁸ the appearance of the flow structure is completely changed after a minute amount of water has been added. Flow curves which were obtained for these two suspensions indicate a substantial increase in yield value and in degree of thixotropic structure with almost no change in plastic viscosity on the addition of the few drops of water. Speculation on the structural requirements responsible for thixotropic behavior are given in the literature.¹⁸

In most capillary and extrusion viscometers the material is sheared through a given length of capillary under an applied pressure and is then

⁶⁸ R. N. Weltmann, *J. Soc. Cosmetic Chem.* **7**, 599-618, 1956.

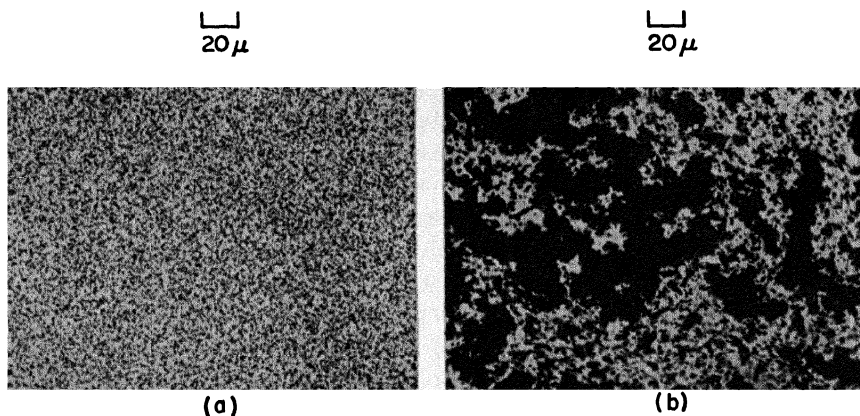


FIG. 6. Photomicrographs of two suspensions of titanium dioxide pigment in linseed oil. (a) No water. (b) With a few drops of water. After Weltmann.⁶⁸

discarded. To obtain a second point on the flow curve, a fresh sample of the material is subjected to a different applied pressure and is again discarded. Thus, each sample of material is subjected to one pressure only for approximately the same period of time. This makes these viscometers incapable of producing the characteristic hysteresis loops for thixotropic materials. A thixotropic material subjected to the above treatment will follow a flow pattern similar to that shown schematically in Fig. 5b for flow curve AC' whether the shear rate is increased or decreased. In addition, the viscosity of a thixotropic material changes with change in shearing stress, so that all the considerations discussed for the measurements of pseudoplastic and dilatant materials in capillary and extrusion viscometers are valid. Hence the flow properties of thixotropic materials are difficult to obtain from flow curves that are measured with these viscometers, on account of the complexity of the flow pattern within the cross section of the tubes. In fact, for most thixotropic materials measured with capillary and extrusion viscometers, the flow curves are slightly concave toward the rate-of-shear axis, simulating pseudoplastic flow behavior (Fig. 1d). It is thus even difficult to recognize the non-Newtonian type of flow behavior of a material from a study of its capillary tube flow curve.

Rotational viscometers, however, have many advantages for the measurement of thixotropic materials. Since, if properly designed, they measure almost true rate of shear versus shearing stress curves, the flow behavior of most non-Newtonian materials including thixotropic behavior can be interpreted from these flow curves. Thus, the investigator is able to analyze the flow type of the test sample and to correlate its flow properties to the operational rate of shear of application. For the measurement of thixotropic

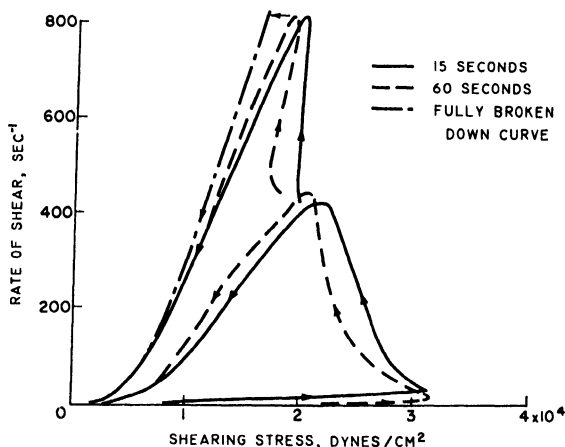


Fig. 7. Flow curves for a grease showing breakdown in structure. Temperature = 0°C . The time refers to the time taken to measure a complete up or down curve. After Weltmann and Kuhns.³³

materials, it is important to determine at least two flow curves where one (the up curve) can be obtained at increasing and the other one (the down curve) subsequently at decreasing rates of shear under controlled timing conditions. It is suggested to obtain such flow curves for at least two different maximum or top rates of shear. These flow curves can be most readily produced with automatic recording rotational viscometers,^{23, 25-27, 31-33, 36, 69, 70} which have become increasingly popular in rheological research. In the investigation of thixotropic materials it is frequently important to measure also the decrease in consistency after increasing periods of time during which constant different rates of shear are applied to the same sample. In any case, an additional flow curve measurement is required after the sample is left undisturbed for a longer period of time to determine if the structure recovers with time, as is expected from thixotropic behavior, or if it is permanently broken down. The up and down flow-curves which were obtained for some lubricant greases³³ showed hysteresis loops typical of thixotropic behavior. To illustrate this, flow curves of one such grease, which were recorded with an automatic concentric cylinder viscometer^{32, 33} for three different timing conditions, are shown in Fig. 7. Repeated flow measurements showed that these hysteresis loops were not caused by thixotropic behavior, but that the structure of this grease was permanently broken down unless the temperature was raised. This change in structure is demonstrated in Fig. 8.³³ The first flow curve at the left was repeatedly

⁶⁹ R. N. Weltmann, *Rev. Sci. Instr.* **16**, 184-191 (1945).

⁷⁰ J. Pryce-Jones, *J. Oil & Colour Chemists' Assoc.* **19**, 295-337 (1936).

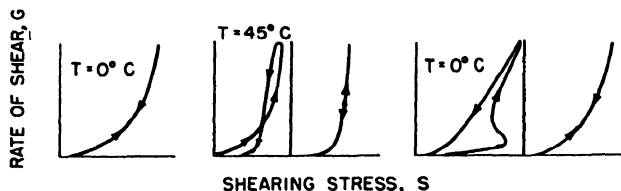


FIG. 8. Increase in flow structure of a grease, that seemed permanently broken down, by raising the temperature. $T = T_e$. After Weltmann and Kuhns.³³

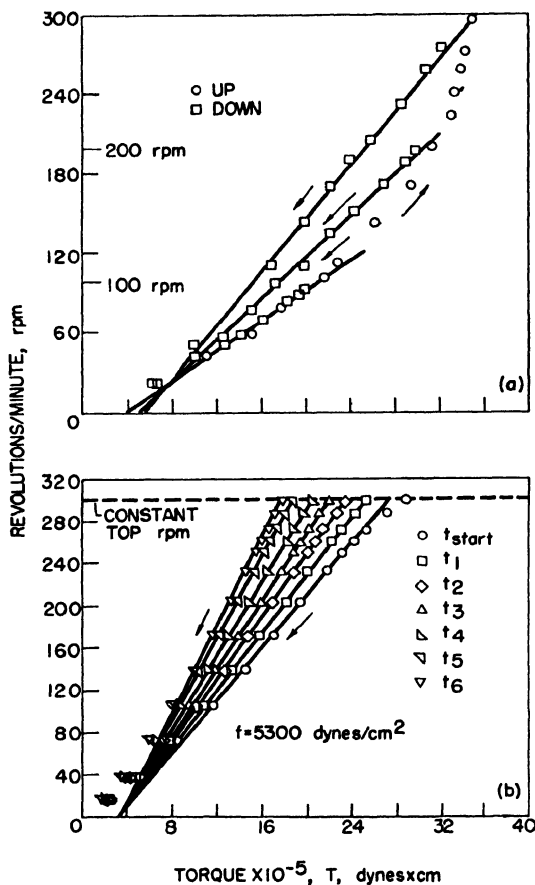


FIG. 9. Concentric-cylinder rotational viscometer flow curves of thixotropic plastic materials. Temperature = 30°C . ($G \sim 0.73 \times \text{r.p.m. in sec.}^{-1}$; $S \sim 1.6 \cdot 10^{-2} \times T$ in dynes/cm.² for $R = R_m$). (a) Flow curves for a silicone fluid at three top rates of shear. (b) Thixotropic breakdown of a pigment suspension with time of application of a constant rate of shear at 300 r.p.m., $t_{\text{start}} = 7$, $t_1 = 16$, $t_2 = 29$, $t_3 = 66$, $t_4 = 121$, $t_5 = 315$, $t_6 = 880$ sec. and $t_5 < t_E < t_6$. After Weltmann.^{71, 72}

obtained for four months. However, when the temperature was raised from 0° C. to 45° C. some structure was recovered as is indicated by the following three flow curves. This structure was completely broken down again when the material was sheared at 0° C., as is indicated by the identity of the two flow curves at the extreme right and left in Fig. 8.

The flow curves shown in Fig. 9 were obtained with a concentric cylinder rotational viscometer for materials which exhibit the flow behavior of thixotropic plastics. Repeated measurements indicated thixotropic behavior and the partial linearity of the down flow curves indicates plastic behavior. Figure 9a⁷¹ shows the up and down flow-curves for a silicone fluid, indicating the decrease in thixotropic structure by the hysteresis loops. Figure 9b⁷² shows how a pigment suspension changes in consistency with the duration of a constant shear rate on account of thixotropic breakdown. Additional flow curves of thixotropic plastic suspensions which were also obtained on a concentric cylinder rotational viscometer are illustrated in Fig. 10^{17, 53, 73} to demonstrate the difference in the degree of thixotropic structure by the variations in curvature of the up curves and in the area of the hysteresis loops.

From the straight part of the down curves, Figs. 9 and 10, the plastic viscosity and the yield value intercept can be calculated by using equation (10). These plastic viscosities and yield values are indicative of the flow behavior of a sample when subjected to the maximum rate of shear of the flow curve during the time that was required to make the up-curve measurement. For each maximum rate of shear, there is a maximum breakdown in structure, which is obtained after a certain time of application, namely the equilibrium time t_E (Figs. 9b and 10b). The curve that connects all points of shearing stress that are obtained after the respective shear rate is applied for a time equal or larger than the equilibrium time has been called the "equilibrium flow curve".

From Figs. 9 and 10, it is indicated that the plastic viscosity decreases with increasing rate of shear and with increasing duration of a constant rate of shear. The torque intercept, however, increases only with increasing rate of shear, but remains constant when a constant rate of shear is applied over increasing periods of time. It has been suggested⁴⁷ that the torque intercept is proportional to a yield value intercept, which is composed of two parts: (1) one part that remains constant with increasing rate of shear and thus might be proportional to the Bingham yield value, and (2) another part that varies with the applied rate of shear and thus might be proportional to a power input which is required to keep the material at that structural state which it attained by the application of the maximum rate of

⁷¹ R. N. Weltmann, *Ind. Eng. Chem.* **40**, 2 (1948).

⁷² R. N. Weltmann, *J. Appl. Phys.* **14**, 7 (1943).

⁷³ E. K. Fischer, *J. Colloid Sci.* **5**, 271-281 (1950).

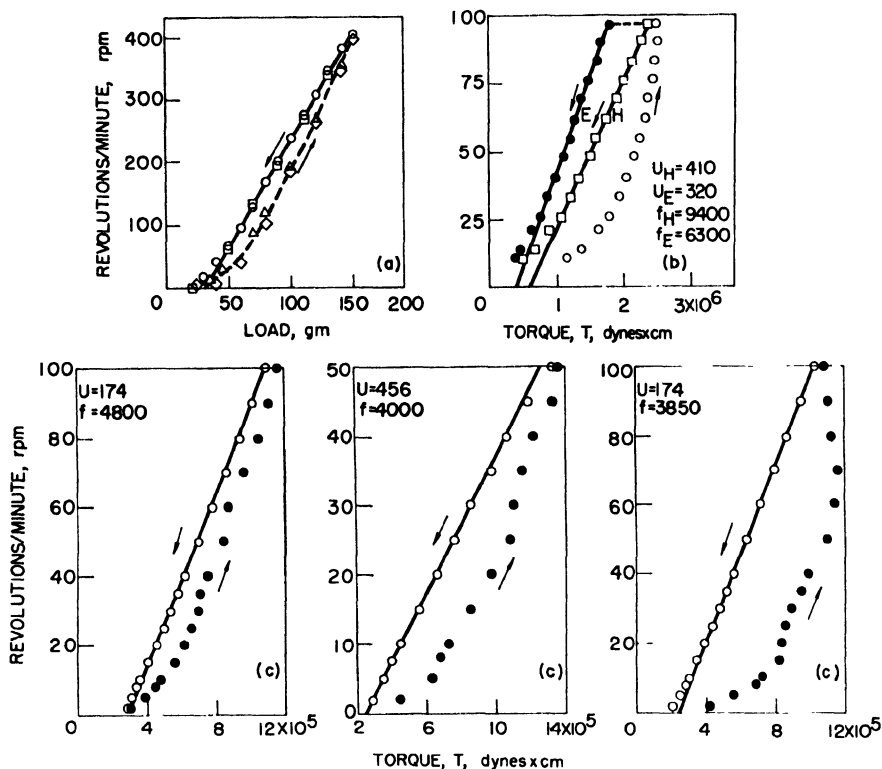


Fig. 10. Concentric-cylinder rotational viscometer flow curves of thixotropic plastic materials. Temperature = 30° C. (U , in poises, f in dynes/cm.²). (a) Flat black paint ($G \sim 0.95 \times \text{r.p.m. in sec.}^{-1}$, $S \sim 1.74 \times \text{load in dynes/cm.}^2$ for $R = R_m$). After Fischer.⁷² (b) Pigment suspension ($G \sim 0.73 \times \text{r.p.m. in sec.}^{-1}$; $S \sim 1.6 \times 10^{-2} \times T$ in dynes/cm.² for $R = R_m$). After Green and Weltmann.⁵² Key: (H) rapidly measured; (E) measured at $t \geq t_E$. (c) Three different pigment suspensions measured at the same time rate exhibiting different hysteresis loop areas, indicating different degrees of thixotropy ($G \sim 0.73 \times \text{r.p.m. in sec.}^{-1}$; $S \sim 1.6 \times 10^{-2} \times T$ in dynes/cm.² for $R = R_m$). After Green.¹⁷

shear of measurement. It is also possible that the part of the yield value intercept corresponding to the Bingham yield value will change with a change in thixotropic structure.

A few suggestions have been made as to the evaluation of the degree of thixotropic breakdown in thixotropic plastic materials. For a qualitative evaluation the area of the loop between the up curve and the down curve can be used as a measure of the degree of thixotropic structure (Fig. 10). The larger area indicates the higher degree of thixotropic behavior provided the rate of shear is increased at the same constant time rate. For a quanti-

tative measure of thixotropic behavior coefficients of thixotropic breakdown can be used, where M_v ^{53, 67, 74} and V_v ^{67, 74} indicate the structural change with increasing rate of shear and B_v ^{67, 72, 74} indicates the structural change with increasing duration of a constant rate of shear. The equations are

$$\begin{aligned} M_v &= \frac{U_1 - U_2}{\ln(\omega_2/\omega_1)} \\ V_v &= \frac{(f_2 - f_1)}{(U_1 - U_2)} \\ B_v &= -\frac{dU}{dt} t \end{aligned} \quad (14)$$

The coefficient M_v can be defined as the loss in shearing stress per unit increase in rate of shear, V_v is the change in yield value intercept with change in plastic viscosity at increasing rates of shear, and B_v is the change in plastic viscosity with time multiplied by the time period of constant shear application. This empirical method is useful for the practical evaluation of the flow of thixotropic plastic materials. An analytical treatment of thixotropic breakdown of such materials has been made,⁷⁵ based on the same experimental data.

Another coefficient of thixotropic breakdown has been suggested.²⁹ It is given as

$$\theta = G(\eta - \eta_0) \quad (15)$$

Other investigators^{26, 76, 77} have suggested the use of equilibrium flow curves to describe a thixotropic material. This introduces the difficulty that equilibrium flow curves are frequently of the same shape as pseudoplastic flow curves and thus are straight lines only in rare cases. In addition, the measurement of an equilibrium flow curve is very time consuming since its measurement takes in the order of 30 min. and more. Another objection to the use of equilibrium curves is that the most valuable information about a thixotropic material, namely, its successive change in structure, is discarded if only the end conditions represented by the equilibrium flow curve are considered.

It is difficult to evaluate mathematically the flow of pseudoplastic and dilatant materials; it seems even more difficult to do so if these materials have the additional complication of being thixotropic. In all these cases the

⁷⁴ H. Green and R. N. Weltmann, *Ind. Eng. Chem., Anal. Ed.* **18**, 167 (1946).

⁷⁵ S. E. Dahlgren, *Trans. Chalmers Univ. Technol., Gothenburg* No. **159** 18 pp. (1955).

⁷⁶ R. Buchdahl and J. E. Thimm, *J. Appl. Phys.* **16**, (1945).

⁷⁷ G. W. Lower, W. C. Walker, and A. C. Zettlemoyer, *J. Colloid Sci.* **8**, 116-129 (1953).

flow parameters N and η , or μ^* and N , or U and f , provided that they are obtained under specified conditions of stress, strain, and duration of flow, can be used if the material is to be tagged. Otherwise, more information is obtained by considering more than one complete flow curve. For instance, the amount of change in curvature of the up curve indicates the amount of change in consistency with increasing rates of shear, and a very large loop area for a given timing cycle indicates more change in thixotropic structure than a smaller one. Thixotropic pseudoplastic flow curves of an emulsion are shown in Fig. 11¹⁸ and thixotropic dilatant flow curves of a vinyl plastisol are demonstrated in Fig. 12.⁷⁸ Both sets of curves were obtained on a concentric cylinder rotational viscometer.

Thixotropy is defined as an isothermal process. However, it is almost impossible to increase the rate of shear or to apply a constant rate of shear over an extended time period without causing temperature increases in the sample even if an instrument with an accurately controlled temperature bath is used. Thus, questions have arisen whether the hysteresis loop is due to thixotropic or temperature changes, especially when the viscosity of the sample decreases appreciably with temperature increases. Many investigators have treated this problem.^{62, 71, 78-85} From all indications it would seem that the hysteresis loop is influenced by temperature and thus its area, if the flow curve could be obtained without any temperature increases, would in most cases be somewhat smaller than measured. For this reason it is suggested that the temperature be measured at the cup and bob surface and that those temperatures be used for evaluating the approximate temperature change over the clearance between cup and bob. An equation which permits such a temperature evaluation by successive approximation is given in the literature.⁶² In the same reference it is shown that the temperature effects become less serious at any given rate of shear with a smaller cup-bob distance, provided good temperature control is available. When high viscosity materials are measured, a separation of the two effects is important, since the temperature effect for such materials is large because of high heat capacity and high viscosity. A decrease in cup-bob clearance alone at high rates of shear is then not always sufficient, and temperature corrections of the flow measurements might be essential to

⁷⁸ W. D. Todd, *Offic. Dig. Federation Paint & Varnish Production Clubs* **325**, 98 (1952).

⁷⁹ H. Blok, *Ingenieur (Utrecht)* **60**, 58 (1948).

⁸⁰ R. N. Weltmann, *Ind. Eng. Chem., Anal., Ed.* **15**, 424 (1943).

⁸¹ A. Bondi, *J. Appl. Phys.* **16**, 539-544 (1945).

⁸² S. Kyropoulos, *Forsch. Gebiete Ingenieurw.* **3**, 287 (1932).

⁸³ M. Muskat and F. Morgan, *J. Appl. Mechanics* **10**, A131 (1943).

⁸⁴ S. M. Neale, *Phil. Mag.* [7] **34**, 577 (1943).

⁸⁵ S. P. Jones Jr. and J. K. Tyson, *J. Colloid Sci.* **7**, 3 (1952).

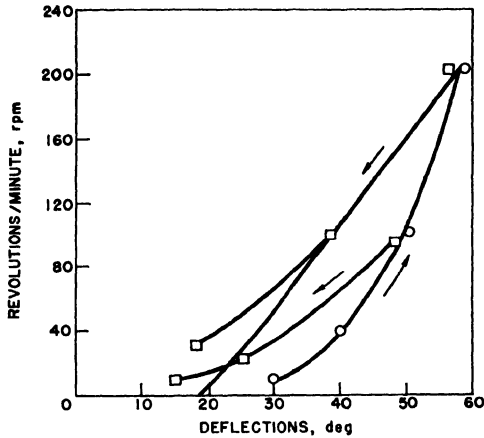


FIG. 11. Concentric-cylinder rotational viscometer flow curves of a thixotropic pseudoplastic emulsion. Temperature = 30° C. ($G \sim 0.73 \times \text{r.p.m. in sec.}^{-1}$; $S \sim 12.5 \times \text{deflections in dynes/cm.}^2$ for $R = R_m$). After Green.¹⁸

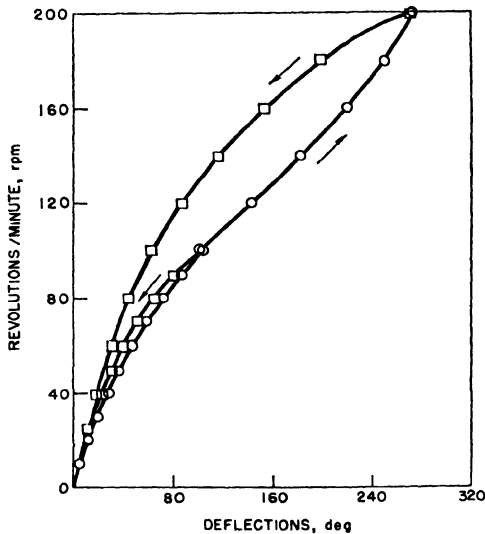


FIG. 12. Concentric-cylinder rotational viscometer flow curves of a thixotropic dilatant vinyl plastisol. Temperature = 30° C. ($G \sim 0.73 \times \text{r.p.m. in sec.}^{-1}$; $S \sim 17.8 \times \text{deflections in dynes/cm.}^2$ for $R = R_m$). After Todd.⁷⁸

obtain the true flow curves. The cone and plate rotational viscometer will minimize temperature effects, as has been shown in the literature,³⁶ because of its small shear area and very small clearance of less than 0.010 in. at the outside rim.

5. RHEOPECTIC FLOW

The behavior and the mechanism of a rheopectic material are not well understood. According to the literature, the word "pectous," which means solidified or curdled, was first used by Graham⁸⁶ for sols which changed to a jelly. Freundlich and Juliusberger⁸⁷ found that some thixotropic substances, such as vanadium oxide suspensions, can be solidified by orienting the particles when a gentle shear action is applied and that in contrast to dilatancy no immediate liquefaction is observed when the shear is removed. This phenomenon, they called "rheopexy." No flow measurements could be found for these sols and thus the paper seems to refer to a qualitative study only. Since it is frequently difficult to differentiate between thixotropic structure and the existence of yield value, a rheopectic material might be redefined as either a thixotropic or a plastic material that will solidify when subjected to a certain shear and will not regain its more fluid structure immediately after shear removal. According to the literature, rheopexy will most likely occur in suspensions which contain anisometric particles. While solidification in dilatancy is connected with the mechanism of close packing of highly dispersed particles, it is said to be caused in rheopectic materials by an almost perfect orientation of anisometric particles. Since the latter represents a state of higher equilibrium than the former, it is not surprising that the dilatant material liquefies instantly on removal of the shear, while a rheopectic material remains solidified at least for a period of time.

Figure 13 shows a flow curve of a material, which was obtained with a rotational viscometer, that could be defined as "rheopectic" although it does not adhere strictly to the definition given. The material is essentially a suspension of chrome yellow in linseed oil. The flow curve shows that the paste behaves at first like a Newtonian liquid, that means it has a constant Newtonian viscosity with increasing rates of shear. However, at a certain "critical" rate of shear, the Newtonian liquid changes almost instantaneously to a slightly thixotropic plastic with a plastic viscosity somewhat higher than its liquid viscosity and with a substantial yield value. The material remains plastic with further increase in rate of shear. At decreasing rates of shear, the plastic viscosity and yield value decrease slightly, but the material remains a plastic even at the lowest applied rate of shear. Apparently a finite time of rest is required to bring the material back to its state of liquid fluidity. After a couple of hours, a measurement of the flow curve would again be like that shown in Fig. 13. Materials exhibiting this type of flow behavior are infrequent but were occasionally encountered in

⁸⁶ T. H. Graham, *Phil. Trans. Roy. Soc. London* **A151**, 184 (1861).

⁸⁷ H. Freundlich and F. Juliusberger, *Trans. Faraday Soc.* **31**, 920 (1935).

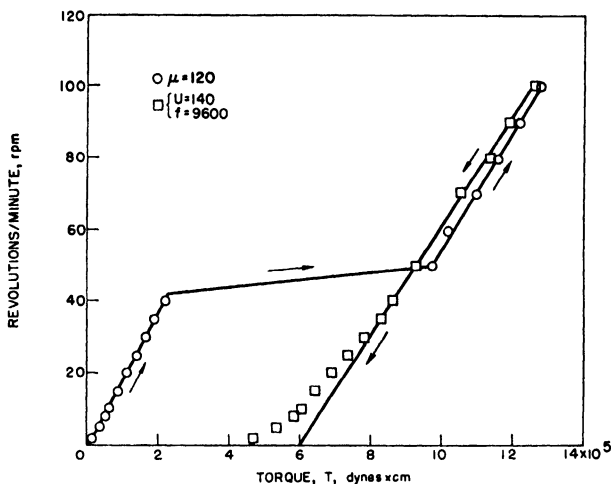


FIG. 13. Concentric-cylinder rotational viscometer flow curve of a rheopectic pigment suspension. Temperature = 30° C. (U , in poises; f , in dynes/cm.²; $G \sim 0.73 \times$ r.p.m. in sec.⁻¹; $S \sim 1.6 \times 10^{-2} \times T$ in dynes/cm.² for $R = R_m$).

studies of the behavior of pastes such as are used in the lithographic printing process.

6. TURBULENT FLOW

The foregoing types of flow assumed laminar behavior and streamline flow, so that distinct layers of material would pass each other. In turbulent flow, no distinct layers are observed. All layers mix with one another by forming eddy currents, swirls, and vortices. Turbulent flow occurs when the rate of shear exceeds a certain critical value. The criterion for the onset of turbulence is frequently expressed as critical or transition Reynolds number. The Reynolds number, Re , is a dimensionless quantity.⁸⁸ For Newtonian materials

$$Re = \frac{vx}{\mu/\rho} \quad (16)$$

where v is the mean velocity, x is an instrument length parameter, ρ is the density, and μ/ρ is the Newtonian kinematic viscosity. At a certain critical value of the Reynolds number, laminar flow will turn into turbulent flow; then all the previously discussed flow types become indistinguishable and a flow curve is obtained as shown schematically in Fig. 1f. It is similar to the flow curve of a dilatant material, but in the case of turbulence, it does not mean that the viscosity of the material increases with increasing rate of

⁸⁸ O. Reynolds, *Phil. Trans. Roy. Soc. London* **A174**, 935-982 (1883).

shear; it rather indicates that with increasing shearing stress the degree of turbulence increases, so that a part of the increased stress is used to increase the number of eddy currents rather than to increase the flow of the bulk of material.

Most studies of turbulent flow have been made on liquids flowing in pipes. In studying turbulent flow in a pipe, it has been found that the flow rate increases approximately with the square root of the applied pressure.

The transition value of the Reynolds number indicating the start of turbulent flow is independent of the Newtonian material being investigated but depends to some extent on the instrumental conditions. Turbulent flow can occur in pipes when the value of the Reynolds number exceeds 2000,⁸⁸ if the pipe diameter D is the instrument length parameter in equation (16). Below this critical value, the flow is always laminar. With care, critical Reynolds numbers as high as 20,000 have been realized. For capillary tubes and extrusion viscometers, these same critical values should be approximately correct.

Empirical equations have been established for turbulent flow of Newtonian materials in pipes and capillaries. They are for $Re = Dv\rho/\mu$ for smooth pipes

$$1/\sqrt{\varphi} = 2 \log (Re\sqrt{\varphi}) - 0.8 \quad (17)$$

and for rough pipes

$$1/\sqrt{\varphi} = 2 \log (D/2k) + 1.7 \quad (18)$$

where the friction factor φ is

$$\varphi = \frac{2DP}{\rho L v^2} = \frac{64}{Re}$$

and the grain diameter k indicates the surface roughness.

Thus, for turbulent flow in smooth pipes the flow velocity depends on the Reynolds number Re and hence is a function of the viscosity, while in rough pipes the flow velocity is independent of viscosity. For more detailed information on turbulent flow of Newtonian fluids in pipes and for graphs of $1/\sqrt{\varphi}$ against $Re\sqrt{\varphi}$ for smooth pipes and pipes of various surface roughness, the reader is referred to the literature^{89, 90} and Chapter 12, Vol. II.

In a well-dimensioned concentric cylinder rotational viscometer, turbulent flow is infrequent; however, it can occur and the flow curve must then be rejected. Turbulent flow sets in at a higher rate of shear in viscometers where the outside cylinder rotates than in those where the inner cylinder

⁸⁹ H. Rouse and J. W. Howe, "Basic Mechanics of Fluids." Wiley, New York, 1953.

⁹⁰ E. N. da C. Andrade, "Viscosity and Plasticity." Chemical Publishing, New York, 1952.

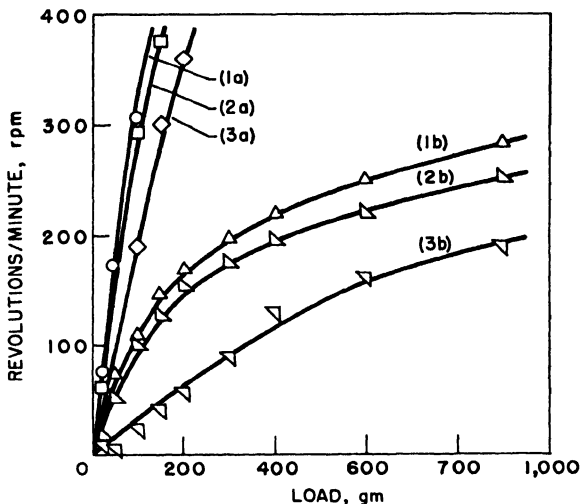


FIG. 14. Aging studies on dilatant iron oxide suspensions in a 10% solution of sodium lignin sulfonate. Temperature = 30°C . ($G \sim 0.25 \times \text{r.p.m. in sec.}^{-1}$; $S \sim 1.13 \times \text{load in dynes/cm.}^2$ for $R = R_m$). Key: (a) 11.3 vol. %. (b) 12.1 vol. %. (1) one week; (2) one day; (3) one hour. After Fischer.²¹

is the rotor.⁹¹ Redimensioning of the cup and bob arrangement can often prevent turbulence in the same material. A definite value for a transition Reynolds number in rotational viscometers has been suggested,²⁸ and calculations for certain conditions necessary for the occurrence of turbulence in such viscometers have been made.^{28, 32, 91}

IV. Physical Considerations

Pastes and paints can change their flow characteristics with aging, pre-treatment, application of shear, type of application, temperature, type of dispersion, physical and chemical characteristics of the solid and liquid ingredients, the addition of special surface-active agents, and the extent of grinding and mixing. This discussion will permit only a brief survey of the various factors.

1. AGING

The aging of dispersions can cause an increase as well as a decrease in consistency. This change in consistency is usually associated with a chemical change which could be a reaction between solid and liquid phase, or with changes in the rate of flocculation arising from surface sorption changes. Most changes caused by aging are irreversible and usually more rapid in the beginning than later. Figure 14 demonstrates the change of

⁹¹ G. I. Taylor, *Proc. Roy. Soc. A***157**, 546-578 (1936).

two dilatant red iron oxide suspensions because of aging during one week.²¹ Thixotropic and plastic pigment suspensions were found to change in plastic viscosity, yield value, and degree of thixotropic structure while standing for a couple of months. All three factors can either increase or decrease during aging and each can do so independently of the other. Thus, it is well to provide for the change in consistency of the final product during storing over a reasonable period of time.

2. PRETREATMENT AND OPERATIONAL APPLICATION

Newtonian materials will always show the same resistance to flow, no matter how they are treated before application or what the rate and type of application are. Almost the same applies in the case of true plastic materials as long as the rate of shear on application is great enough to overcome the yield value stress and its associated plug flow in all types of application, even if the application requires the plastic material to flow through extremely small openings. This, however, is no longer true in the case of pseudoplastic, dilatant, thixotropic, and rheopectic materials. While the treatment of the material just before application will not affect the flow behavior of pseudoplastic and dilatant materials, the rate and type of application will greatly determine their flow behavior, since the former's resistance to flow will decrease whereas the latter's will increase with increasing shear rates. Thus, at high rates of shear of application, as is the case when paper is coated by machine, the pseudoplastic material will have a lower operational consistency than that measured on the viscometer. This factor might account for smudging, an overly thin coating, or too much penetration into the paper. The operational consistency of the dilatant material, on the other hand, might be so high that it might tear the paper. A thixotropic material will decrease in viscosity but at the same time increase in yield value intercept with an increase in rate of shear. Thus, at a high rate of shear application the yield value intercept might become too high to permit flow through small openings, which might be one requirement of a specific application.

The treatment that is given to a thixotropic material before its application can also affect its performance during application. A coating application such as dipping is performed at a low rate of shear. More intense agitation at higher rates of shear than used for dipping will change the consistency of a thixotropic material more than the dipping operation would. Thus, if the rest period between agitation and dipping application is not enough to permit the recovery of the thixotropic breakdown experienced during agitation, the consistency of the dipping material will, at the time of operation, be different from that which had undergone no agitation

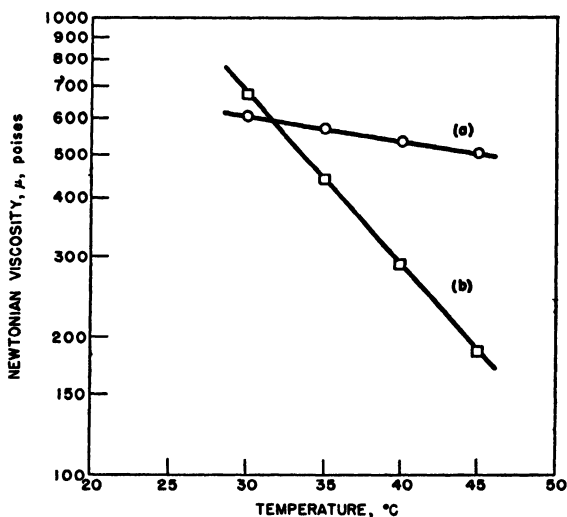


FIG. 15. Temperature-viscosity function for Newtonian behavior at low rates of shear. (a) Silicone fluid. (b) Polybutene oil. After Weltmann.⁷¹

prior to dipping. Any pretreatment at a rate of shear lower than that of application will not affect the performance characteristics of the material.

3. TEMPERATURE

The consistency, that is, the viscosity or the plastic viscosity, of most materials decreases with an increase in temperature. In exceptional cases an increase in viscosity with increasing temperature is measured, which is usually connected with a chemical and surface reaction. However, when no chemical reaction occurs the change in viscosity with temperature follows approximately Andrade's law^{90, 92} which for Newtonian materials is $\mu = ae^{b/T_0}$. This law can be approximated over limited temperature ranges by the following equation

$$\mu = Ae^{-BT_0} \quad (19)$$

where A and B are constants of the tested material and T_0 is the temperature. The slope B of this line is frequently constant for a family of materials such as linseed oils bodied to different viscosity or different viscosity silicone fluids. However, it differs appreciably for the different types of materials, as is shown in Fig. 15 for a silicone fluid and a polybutene oil. Relationships similar to equation (19) are obtained for non-Newtonian materials so that the apparent and plastic viscosity can be substituted for

⁹² E. N. da C. Andrade, *Nature* **125**, 309, 582, (1930).

the Newtonian viscosity in equation (19). The yield value, however, has a tendency to increase with temperature, although no absolute rule could be established. Thus, when the application of the material causes an increase in temperature during operation, which is almost always unavoidable at high rates of shear, the consistency at the operational temperature has to be considered in order to interpret the performance characteristics.

Another effect of temperature might be evaporation, which can cause manifold viscosity increases during operation. This problem is, for instance, encountered in high-speed printing with a vapor-set ink and in paint-spraying applications.

4. DISPERSION AND INGREDIENTS

A paint and paste dispersion can be either a liquid dispersed in another liquid (emulsion) or a solid ground in a liquid (suspension). A mixture or multiple of each type of dispersion is also frequently encountered, for example, in pastes for textile coating and printing. In this chapter only simple dispersions will be discussed.

The flow properties of dispersions change appreciably with the percentage of each constituent.⁹³⁻⁹⁵ In suspensions the liquid is frequently a mixture of two or more oils. If the viscosity of each of them is known, a mixture of desired viscosity μ can be obtained by using a logarithmic relationship, similar to Arrhenius' law⁹⁶ for mixtures of sols, so that

$$\mu = \mu_1 e^{[p \ln (\mu_2/\mu_1)]/100} \quad (20)$$

This equation gives good practical results. In this equation, μ_1 and μ_2 are the viscosities of the two oils forming the mixture and p is the volume percentage of the heavier liquid. Figure 16 gives experimental verifications of equation (20) for seven oil mixtures.⁹⁷

Arrhenius' law⁹⁶ $\mu = \mu_0 e^{\alpha c}$, where α is a constant, relates the suspension viscosity μ to the solid concentration c and to the solute viscosity μ_0 . Similar equations have been established experimentally for solid particles of different shapes^{98, 99} suspended in liquids. Einstein's classical equation¹⁰⁰ gives the first term of the semilogarithmic power law of Arrhenius' equation and calculates α to be equal to 2.5. This equation was derived under

⁹³ H. L. Bredée and J. de Booy, *Kolloid-Z.* **79**, 31-49 (1937).

⁹⁴ K. Hess and W. Philippoff, *Ber.* **70**, 639 (1937).

⁹⁵ W. Philippoff, "Viskosität der Kolloide." Steinkopf, Dresden and Leipzig, 1942. (Reprinted in English by Edwards, Ann Arbor, Michigan, 1944.)

⁹⁶ S. Arrhenius, *Z. physik. Chem. (Leipzig)* **1**, 285-98 (1887).

⁹⁷ R. N. Weltmann and H. Green, *J. Appl. Phys.* **14**, 11 (1943).

⁹⁸ F. Eirich, M. Bunzl, and H. Margaretha, *Kolloid-Z.* **74**, 376 (1936).

⁹⁹ F. Eirich, H. Margaretha, and M. Bunzl, *Kolloid-Z.* **75**, 20 (1936).

¹⁰⁰ A. Einstein, *Ann. Physik* [4] **19**, 289 (1906); [4] **34**, 592 (1911).

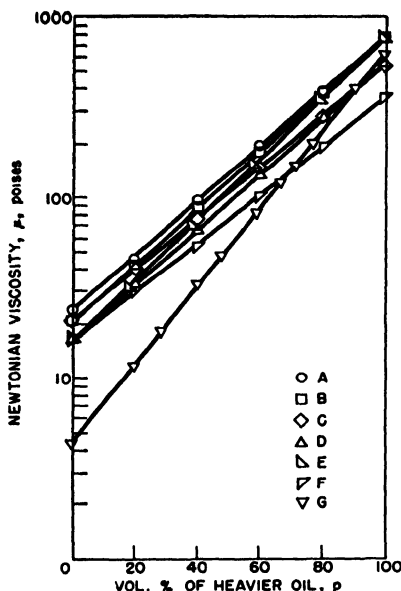


FIG. 16. Newtonian viscosity at low rates of shear of a mixture of two oils as function of the volume content of the heavier oil. Temperature = 30° C. Key: (A) Two isobutylene oils; (B) isobutylene and mineral oils; (C) linseed and mineral oils; (D) two linseed oils; (E) isobutylene and linseed oils; (F) two linseed oils; (G) N.B.S. standard viscosity and mineral oils. After Weltmann and Green.⁹⁷

the assumption that the suspension is so dilute that the spherical and nondeformable particles do not interfere with each other, hence, Newtonian flow was assumed. The value c is then the specific volume concentration. Other theoretical equations have been suggested. Reference to them can be found in the literature.⁹⁵ For plastic flow a more complicated logarithmic law has been empirically established.⁹⁷ For the plastic viscosity U and for the yield value f the equations are

$$U = (\mu_0 + A)e^{Bc} \quad (21a)$$

and

$$f = Me^{nc} \quad (21b)$$

where c is the percent volume concentration of the dispersed solid, μ_0 is again the viscosity of the liquid phase, the constants B , M , and n are related to the particle size, shape, and surface, whereas A was found to be independent of particle size but might depend on particle shape and surface. Since A is zero in Arrhenius' equation for Newtonian materials, A in equation (21a) might be a function of the interference of the particles with

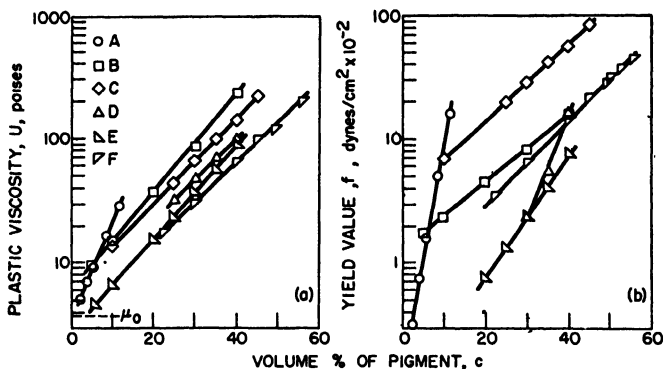


Fig. 17. Consistency of pigment suspensions as function of pigment volume content. Temperature = 30° C. (a) Plastic viscosity. (b) Yield value. Key: (A) carbon black; (B) leaded zinc oxide; (C) green seal zinc oxide; (D) basic carbonate white lead, sample one; (E) antimony oxide; (F) basic carbonate white lead, sample two. After Weltmann and Green.⁹⁷

each other in a non-Newtonian suspension. Figures 17a and 17b show logarithmic plots of plastic viscosity and yield value against volume percent of solid⁹⁷ for solid-liquid pastes of various pigments suspended in the same liquid. In Figs. 18a and 18b the same type of plot is shown for one pigment, a leaded zinc oxide which was heated¹⁰¹ in order to obtain it in particles of different average particle size, d_3 , with respect to specific surface.^{94, 102} The different sized particles were suspended in the same liquid. Figure 18c demonstrates that B and n decrease with increasing average particle size d_3 . Other investigators¹⁰³ have found similar relationships for mineral powders suspended in high viscosity asphalts. These empirical laws are of practical value for systems like paints and pastes since these materials are restricted in the variety of their components.

At a certain solid-liquid content some suspensions show dilatant behavior. Table II²¹ lists the liquid content at which dilatancy occurs in a few selected suspensions.

Very little information is available in regard to the investigation of liquid-liquid dispersions. An emulsion might, for example, consist of water in oil or oil dispersed in water. To stabilize the emulsion, an emulsifying agent is frequently added. In Fig. 19 are plotted the plastic viscosities and yield values of four different oil-water emulsions, with emulsifying agents added, against the percentage water content. At the point of maximum viscosity,

¹⁰¹ H. Green and G. S. Haslam, *Ind. Eng. Chem.* **19**, 1, 53, (1927).

¹⁰² H. Green, *J. Franklin Inst.* **204**, 713 (1927).

¹⁰³ R. N. Traxler, H. E. Schwyer, and L. R. Moffatt, *Ind. Eng. Chem.* **29**, 489-492 (1937).

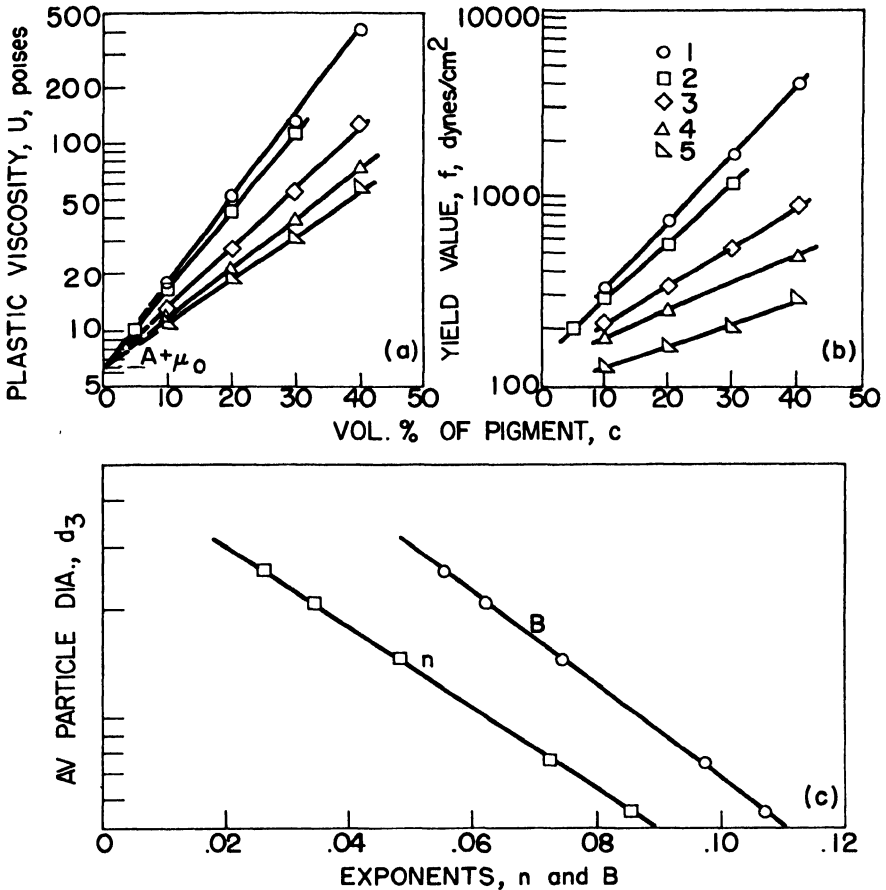


FIG. 18. Consistency of leaded zinc oxide suspensions with particles heated to different average diameters d_3 (in microns), as function of pigment volume content. Temperature = 30° C. (a) Plastic viscosity. (b) Yield value. Key: (1) $d_3 = 0.55$; (2) $d_3 = 0.75$; (3) $d_3 = 1.44$; (4) $d_3 = 2.08$; (5) $d_3 = 2.50$. (c) Particle size d_3 as function of constants B and n in equation (21). After Weltmann and Green.⁹⁷

inversion of the emulsion phases starts and becomes very pronounced after the yield value maximum is passed. It should be noticed that both the plastic viscosity and yield value increase and decrease rapidly with a change in water content. This indicates that only a slight change in the liquid-liquid ratio can change the flow characteristics of emulsions substantially. The emulsions of Fig. 19 were mixed in a colloid mill. Although different mixture procedures would alter the results in a quantitative way, the trend of the curves would be similar.

TABLE II
LIQUID CONTENT AT WHICH DILATANCY WAS OBSERVED FOR
DIFFERENT PIGMENT SUSPENSIONS
(Fischer²¹)

<i>Solid</i>	<i>Water (vol. %)^a</i>	<i>Formamide (vol. %)^a</i>	<i>Carbon tetrachloride (vol. %)^b</i>
Starch (slight acid modification)	38	—	59
Starch (gum type)	35	—	62
Calcium carbonate	55	43	50
Lithol toner	53	43	—
Barium sulfate	39	32	—
Carbon black	33	33	—
Chrome yellow	31	29	31
Zinc oxide	30	—	33
Zinc oxide, acicular	18	—	—
Iron oxide, red	12	14	18

^a Contained 10% of sulfonated lignin.

^b Contained 10% of Aerosol OT.

5. SURFACE ACTIVE AGENTS

Viscosity, plastic viscosity, and yield value can change on addition of surface active agents. They can either increase or decrease together, or one of the flow properties can increase while another one is decreasing. Also, a material exhibiting one type of flow behavior can acquire a different type of flow behavior after the addition of surface active agents. This is especially pronounced when dealing with dilatant materials, since only a slight addition will counteract the close-packing effect. The effects of additions of surface active agents to pigment suspensions and emulsions are manifold and often difficult to explain. Surface active agents are supposed to change the interfacial tension; however, one finds that some of these agents hardly change the surface tension of water. Their supposed purpose is better dispersion, more rapid and intimate liquid contact with the solid particle, better wetting and a stabilizing action with respect to liquid-liquid dispersions. The expression "better dispersion" as used here combines two different mechanisms which are deaggregation and deflocculation. Deaggregation is a mechanical or chemical separation of single particles contained in an aggregate. The aggregate consisting of these unit particles is glued together in such a fashion as to prevent the liquid from penetrating into the aggregated mass and thus surrounding each unit particle. Deflocculation, on the other hand, can only be effected by chemical means. Mechanical force does not change the state of flocculation. A flocculate is a loose but connected structure of particles, where the particles are far enough

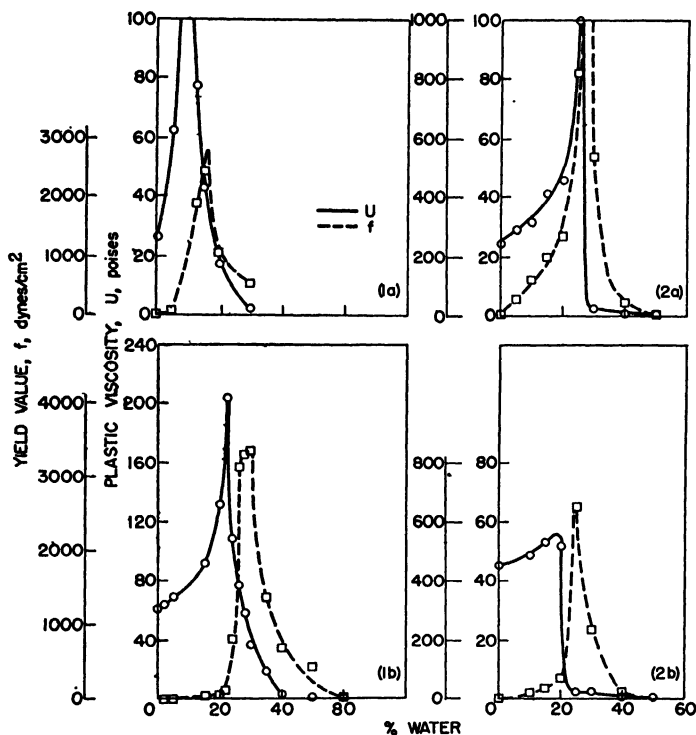


FIG. 19. Consistency of oil-water emulsions as functions of per cent water content. Temperature = 30° C. (a) Water-mineral oil. (b) Water-linseed oil. (1) Emulsifying agent 4% oleic acid and 2% triethanolamine; (2) emulsifying agent 10% mannide monooleate and 2% triethanolamine.

apart to permit the liquid to surround them, but apparently close enough for strong forces to exist between the particles so that the material will not start to flow until enough shearing stress is applied to overcome these forces. This shearing stress is proportional to the yield value. A chemical surface reaction between solid and liquid or a coating of the solid particles can change these forces, in that the yield value will either increase or decrease depending on whether the affinity of the particles to each other or to the surrounding medium becomes greater or less.

In Tables III and IV,^{21, 104} are listed the flow properties of suspensions before and after the addition of a number of surface active agents. Table IV²¹ shows how the addition of water changes the flow properties and how additions of some of the surface active agents can counteract at least to a certain degree the effects of water on the flow properties of the suspensions.

¹⁰⁴ E. K. Fischer and C. W. Jerome, *Ind. Eng. Chem.* **35**, 336-343 (1943).

TABLE III
CHANGE IN FLOW PROPERTIES OF IRON-BLUE DISPERSIONS ON
ADDITIONS OF SURFACE ACTIVE AGENTS
(Fischer²¹)

Reagent	Iron blue					
	29.8% by volume in glycerol		20% by volume in mineral oil		28% by volume in linseed varnish	
	<i>U</i> (poises)	<i>f</i> (dynes/ cm. ²)	<i>U</i> (poises)	<i>f</i> (dynes/ cm. ²)	<i>U</i> (poises)	<i>f</i> (dynes/ cm. ²)
None (control)	8.3	37	106	6,900	90	2,600
Octyl ester sulfosuccinic acid (Na salt)	8.3	260	32	5,500	78	2,200
Dibutyl phenyl phenol sulfonate (Na salt)	8.6	830	81	6,350	98	2,200
Alkyl aryl sulfonic acid (Na salt)	14 ^a	0	61	9,000	92	2,400
Lauryl alcohol sulfate (Na salt)	8.8	130	38	2,700	83	2,300
Lecithin	57	1,400	23	410	85	2,400
Alkyl aryl sulfonate (Na salt) A	8.8	130	74	6,600	84	1,800
Alkyl aryl sulfonate (Na salt) B	9.9	350	69	5,200	81	1,700
Diethyl amino ethyl stearyl acid amide	70	8,000	77	4,400	81	2,300
Secondary fatty alcohol sulfate (Na salt)	7.3	300	89	9,300	114	1,700
Zinc naphthenate	^b	^b	47	4,400	78	2,200
Water	—	—	^b	^b	^b	^b

^a Calculated at low rate of shear, dilatant at higher rates of shear.

^b Too high to measure on available viscometer.

Frequently, additions of small quantities of water, when immiscible with the continuous phase, act as a flocculation agent for pigment powders, as was shown in Fig. 6. One explanation for this is that polar compounds like water form connecting bridges between the particles and thus induce a flocculated structure. The effect of water is an important consideration, since hydrophilic pigments, when in the powder state, take up the water from the surrounding atmosphere, so that when they are mixed into a liquid medium, the water often produces flocculated suspensions. In line with this reasoning, a process has been patented¹⁰⁵ which claims to prevent

¹⁰⁵ A. M. Taylor and A. R. Chapman, U. S. Patent 1,824,177, September, 1931.

TABLE IV
CHANGE IN FLOW PROPERTIES OF PIGMENT DISPERSIONS ON ADDITION OF WATER
(Fischer¹¹)

Reagent	Before water addition		After water addition	
	U (poises)	f (dynes/cm. ²)	U (poises)	f (dynes/cm. ²)
<i>26% Titanium Dioxide by Volume in Mineral Oil</i>				
None (control)	a	a	a	a
Zinc naphthenate	35	2,900	53	4,400
Lecithin	22	1,300	18	1,500
Octyl ester sulfosuccinic acid (Na salt)	40	3,600	31	3,200
<i>31% Titanium Dioxide by Volume in Bodied Linseed Oil</i>				
None (control)	58	740	a	a
Zinc naphthenate	44	780	60	1,440
Lecithin	68	8,200	50	10,000
Octyl ester sulfosuccinic acid (Na salt)	61	3,400	55	6,400
<i>27% Ultramarine Blue by Volume in Bodied Linseed Oil</i>				
None (control)	33	1,000	a	a
Lecithin	24	0	25	90
Octyl ester sulfosuccinic acid (Zn salt)	19	220	170	4,100

a Too high to measure on the available viscometer.

flocculation in lacquers by additions of hygroscopic organic liquids to pigments.

Sometimes hydrophillic coatings like gum arabic, agar, gum tragacanth, alginates, and dextrin are used to treat pigments, as is purposely done in another patent¹⁰⁶ to implant controllable thixotropic properties to a paint. Water is also frequently added to promote and control flocculation and thixotropic behavior in a pigment suspension. Flocculation can be desirable to prevent hard settling of the pigments and to control the surface finish of a coating. In the case of basic lead sulphate, the use of steam has been suggested¹⁰⁷ to promote flocculation. Small quantities of polar compounds other than water and immiscible with the continuous phase—such as alcohol, glycerin, glycol and butanol—are also used as flocculation agents for

¹⁰⁶ D. L. Gamble and L. D. Grady, U. S. Patent 2,135,936, November, 1938.

¹⁰⁷ W. J. Clapson, U. S. Patent 2,315,188, March, 1943.

pigment powders. In the case of hydrophilic pigments suspended in water or in an aqueous solution, oils and oil-soluble agents, such as lecithin or xylene, will frequently induce flocculation.

6. GRINDING AND MIXING

This is not intended to be a paragraph on the technique and efficiency of grinding and mixing. It is included only to highlight the importance of rheological factors in grinding and to point out the changes in flow properties with the degree and type of mixing.

The output of a three-roller mill increases with an increase in viscosity of the material as shown in Fig. 20.²¹ In these tests a variety of materials of known viscosity, measured on a rotational viscometer, were passed over a 5 × 11-in. three-roll laboratory mill, and the time was measured for a given volume of material to traverse the system of rollers for identical roller settings. The results indicate that an increase of the viscosity for the grinding operation tends to increase the grinding efficiency. The curve in Fig. 20 can be considered only as an indication of a trend, since the plastic viscosities measured at the rate of shear of the rotational viscometer are not necessarily the same as the operational viscosities on the three-roller mill. Apparently, the yield value does not greatly affect the grinding efficiency; as long as it is low enough so that the material flows readily from the feed rollers.

In ball-mill grinding, the viscosity is also an important factor. In practice the degree and efficiency of grinding can be controlled by adjusting the flow properties of the material. According to the literature,²¹ a practical

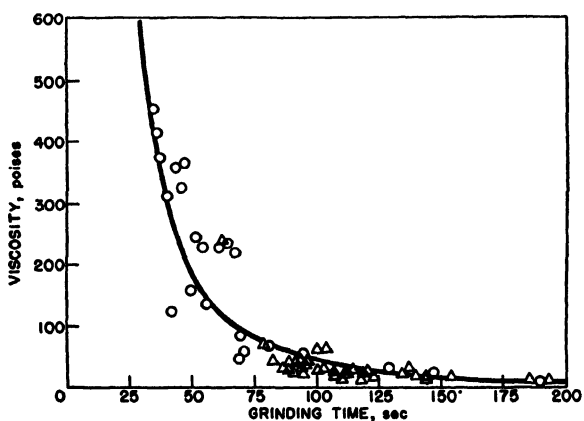


FIG. 20. Required time for samples of same volume, but of different viscosity to pass through a 5-by 7-in. three-roller laboratory mill. Key: ○, Newtonian viscosity of varnishes; △, plastic viscosity of pigment suspensions. After Fischer.²¹

viscosity for good operation in laboratory steel ball mills of 1 gal. or less capacity has been estimated to be about 10 poises, while in steel ball mills 5 ft. in diameter an operational viscosity as high as 200 poises is said²¹ to be still practical. Pebble and porcelain ball mills, however, should be operated at a somewhat lower viscosity on account of the smaller weight of the grinding media. Those approximate viscosity limits are estimations of the actual viscosities existing during the mixing operation. The viscosities that the materials have before mixing will differ substantially from those existing during the mixing operation. The flow properties change during processing because of increase in temperature, increased degree of deaggregation, increase in wetting, and generally improved interaction between solid and liquid phases.

In fact, Fischer¹⁰⁸ has shown by photomicrographs that increasing deaggregation occurs when grinding an iron blue pigment in a linseed oil. From microscopic observations he concluded that the increase in color strength parallels the reduction in aggregate size as the milling continues. Most pigment suspensions show an increase in color strength with continued grinding, accompanied by a change in flow properties. The effect of ball milling on the color strength and on the flow properties of a carbon black pigment suspended in a mineral oil is demonstrated in Fig. 21. The trend shown in Fig. 21 was found to be representative for many materials. Because the rate of shear is higher during milling than in a viscometer, a pseudoplastic material will have a lower viscosity, while a dilatant one will have a higher viscosity during mixing than was measured on the viscometer. The viscosity of a thixotropic material will decrease substantially, while its yield value might increase during milling. Thus, to evaluate grinding performance the consistency of the material at the operational grinding conditions and at the different steps of processing has to be determined.

Another illustration of the effect of the degree of mixing on the flow properties of a material is given in Fig. 22.¹⁰⁹ In this figure, flow curves are shown which were obtained by cooking two samples of the same starch at the same constant temperature but at two different mixing rates of shear. The rate of shear during mixing in the double boiler was about twice that of the Corn Industries viscometer, which is a rotational viscometer with a propeller-type rotor. By chance, it happened that the flow curve taken with the rotational viscometer of the one starch sample that was cooked and mixed for half an hour in the double boiler, coincided with the flow curve of the other starch sample, which was cooked and mixed about 1.25 hr. in the Corn Industries (C.I.) viscometer. Thus, it is shown that the mixing at the higher rate of shear in the double boiler accomplished in 30 min. the

¹⁰⁸ E. K. Fischer, *Ind. Eng. Chem.* **33**, 1465 (1941).

¹⁰⁹ W. G. Bechtel and E. K. Fischer, *J. Colloid Sci.* **4**, 3 (1949).

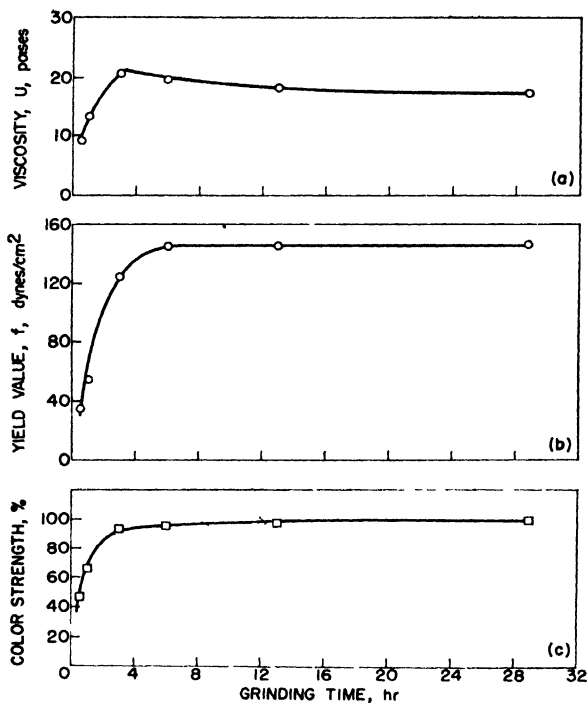


FIG. 21. Change in flow properties and color strength of a suspension of carbon black in mineral oil as function of time of ball milling. (Ball size = 0.8 in., ball charge = 500 gr.) (a) Plastic viscosity. (b) Yield value. (c) Color strength.

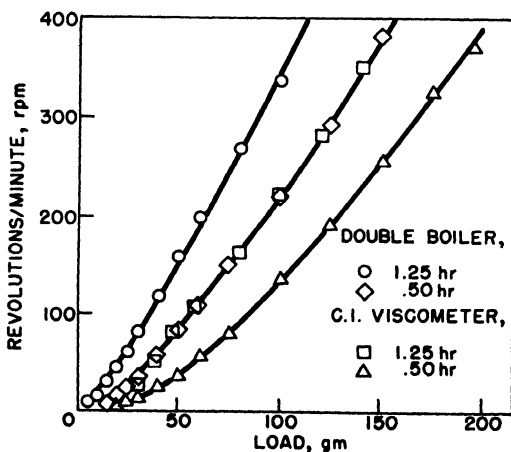


FIG. 22. Rotational viscometer flow curves of starch for different cooking periods and agitation rates. Temperature = 30° C. ($G \sim 0.90 \times \text{r.p.m. in sec.}^{-1}$; $S \sim 1.74 \times \text{load in dynes/cm.}^2 \text{ for } R = R_m$). After Bechtel and Fischer.¹⁰⁹

same degree of mixing that could be obtained with the C.I. viscometer at the lower rate of shear only after 75 min.

V. Product Evaluation

Product evaluation includes some preoperational as well as operational aspects. Before a product is manufactured, its application is known, and thus certain deductions are possible as to the flow behavior that might be most desirable for best operation. In order to control the flow behavior of any material, an instrument must be selected to make flow measurements, which permits a sufficiently good interpretation of the flow properties of the product, so that the manufacturer will be able to tell whether two batches of one material or of different materials will have equal flow behavior under all conditions of operational application. The manufacturer would also want to predict from the flow measurements the physical difference in application behavior. In the preoperational stage, physical effects which occur in manufacture and storing, such as temperature effects, evaporation, mixing procedures, and shelf life, must be studied. In the operational stage, the flow properties of the product must be correlated to actual operational performance characteristics. To do that, special techniques are frequently required that differ for each application. In addition, the knowledge of the flow properties is frequently used to achieve a more efficient and better controlled operation in manufacture and application.

1. CONTROL

In correlating the performance characteristics of a material with the flow properties, the control of the product is of primary importance since operational shear, temperature, and other physical effects during application can only be evaluated if those factors have been studied separately on materials of exactly the same composition and flow properties.

Control is, of course, a must when reproducing a once satisfactory product and also when describing its flow specifications.

In many industries which deal with the manufacture of pastes like paints, varnishes, various food products, paper pulps, medical items, coatings of various kinds, ceramic slurries, printing inks, latices, asphalts, and cements, one of the main factors of control of the manufacturing process is the measurement of consistency. In most cases, one-point measurements are employed, which frequently lead to erroneous results even if obtained with a properly designed viscometer in which the shearing stress is almost constant throughout the test sample.

For demonstration purposes, three materials, a thixotropic plastic, a true plastic, and a Newtonian, are considered in Fig. 23. The one-point value of the apparent viscosity obtained at a rate of shear equal to A is the

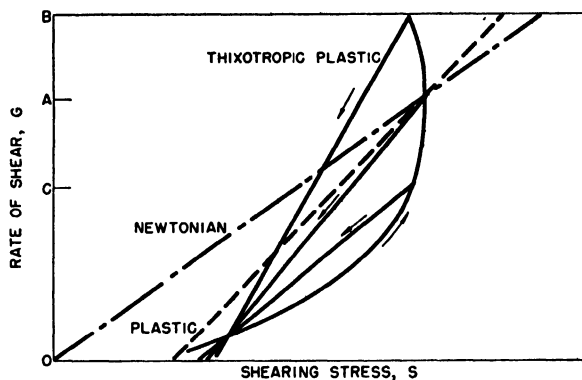


FIG. 23. Schematic flow curves of a Newtonian, true plastic, and thixotropic plastic material to demonstrate the difference in flow behavior at different rates of shear.

same for all three materials. However, these materials look different and behave entirely differently even when applied at this same rate of shear of $G = A$, where all three have the same apparent viscosity. In coating paper or textiles, for instance, at $G = A$, the Newtonian might penetrate into the substratum, while the other two because of their yield value might remain on top, which could result in differences in color, surface appearance, surface strength, and strike-through to the other side. A study of the flow curves indicates that the Newtonian will flow readily from a spatula at extremely low rates of shear, while the plastic as well as the thixotropic materials will show reluctance to do so because of their yield values. After flow has been initiated, and certainly at rates of shear $G > A$, both the plastic and thixotropic materials will flow more rapidly than the Newtonian because of their lower plastic viscosities.

At operational rates of shear $G = B$ and $G = C$, all three materials have different apparent viscosities. The apparent viscosity of the Newtonian material is the same as it was at $G = A$; so is its flow behavior. While the apparent viscosity of the true plastic material changes substantially from $G = A$ to $G = C$ or B , its flow behavior remains unaltered since its plastic viscosity and yield value, which are the factors determining the flow behavior, are constant for all rates of shear. The flow characteristics of a true plastic material change only if the applied rate of shear is so low as to induce plug flow.

For the thixotropic material, the apparent viscosities are very different at $G = C$ and B from that at $G = A$. For this material a change in apparent viscosity indicates a change in plastic viscosity and yield-value intercept, as can be seen from studying the complete flow curves, and thus

its flow behavior is entirely different at the different operational speeds. At $G = B$ the thixotropic material has a lower apparent viscosity than it had at $G = A$, which in reality means a lower plastic viscosity but a higher yield-value intercept. Thus at $G = B$, the material flows more readily if considered in bulk, but less readily when made to flow into small crevices than it does at $G = A$. For silk screen printing, for instance, a high yield value at the instant of operation would spell failure because, for sharp and detailed image printing, the material has to be able to flow into all corners of the fine screen. On the other hand, a paste that is too fluid at the operational speed will run under the wire, and thus the image will blur. The thixotropic plastic material has a very high viscosity at $G = C$; thus, when used for coating purposes at those low rates of shear, it might not be able to follow the coating rollers, or its viscosity might be so high as to tear the base material instead of coating it.

This demonstration should induce the careful investigator to measure at first entire flow curves of all materials in order to learn about the type of flow of the products with which he is concerned. Only then will it be possible to select a suitable control instrument. One-point instruments have desirable features since they are simple and fast in operation and since they can frequently be used to control the production batches by an automatic feedback system which is used either to add ingredients when necessary or to shut off the mixing operation at a desired consistency. The latter is done with success in the starch industry. The starch is agitated and mixed at a given temperature, and its one-point viscosity is measured with a paddle-type rotational viscometer.¹¹⁰ The pasting process, as this mixing procedure is called, is ended at the instant the one-point viscosity indicates the desired value, which is predetermined and varies for different commercial starch pastes. As long as the flow properties of materials are known, one-point instruments are, in many cases, well suited for controlling even highly non-Newtonian materials. However, in the case of non-Newtonian materials, precautions should be taken against changes in test conditions.

For materials that are used in high rate of shear application, it is desirable to obtain the flow curves at the same high shearing rates. Rotational viscometers are frequently incapable of supplying those rates of shear because of mechanical difficulties, unless special design features are employed.¹¹¹ Nevertheless, the rotational-viscometer flow curves have the advantage of not only indicating the flow type of the material but also permitting extrapolation so that sometimes certain conclusions can be drawn in regard to the flow behavior that the material will have at the higher rates of shear of application. For additional flow information, vis-

¹¹⁰ C. C. Kesler and W. G. Bechtel, *Anal. Chem.* **19**, 16-21 (1927).

¹¹¹ W. K. Asbeck, D. D. Laiderman, and M. Van Loo, *J. Colloid Sci.* **7**, 3 (1952).

cometers capable of subjecting the materials to higher rates of shear, such as extrusion instruments, can be used, but the correct interpretation of such flow measurements is often difficult, especially in the case of highly non-Newtonian materials.

2. FLOW IN PIPES

Since many slurries, pastes, and paints are pumped through pipes during their manufacture and in application, a discussion of their flow behavior in pipes seems important. In addition, this discussion will illustrate that rotational-viscometer flow curves frequently permit an interpretation of the flow behavior of materials at higher rate-of-shear applications than the viscometer is capable of producing.

The pressure that is necessary to pump a material through a pipe line system at a given flow rate depends on the pressure loss in the total pipeline system. Pressure losses are incurred by the viscous resistance of the material in the straight pipe line and in the pipeline transitions such as bends, valves, elbows, and pipe expansions and contractions. The viscous losses in straight pipelines are frequently large compared to the pipe transition losses, so that the latter can sometimes be neglected.

The pressure loss for an entire pipeline system is

$$\Delta P = \rho \frac{v^2}{2} \left[\frac{L}{D} \varphi + C_L \right] \quad (22)$$

where ρ is the density of the material, v is the mean velocity which is determined from the flow rate, L and D are the entire length and mean diameter of the pipe line system, respectively, φ is the friction factor, which represents the flow resistance of the material and is given in equation (18) for Newtonian liquids, and C_L is the sum of all pressure loss coefficients^{59, 112} obtained from all pipeline transitions in the pipeline system. It is obtained from the total-pressure losses. Thus, if static-pressure losses are measured, recalculations have to be made to obtain the total-pressure transition losses in contractions and expansions.^{112, 113}

The friction factor φ can be obtained from a generalized friction diagram such as is shown in Fig. 24.^{59, 114} This diagram has been used to obtain the friction factor for Newtonian, Bingham plastic, pseudoplastic, and dilatant materials in laminar and turbulent flow as a function of the Reynolds number and the pertinent non-Newtonian parameters. Experimental flow

¹¹² R. N. Weltmann and T. A. Keller, *Natl. Advisory Comm. Aeronaut. Tech. Note No. 3889*, (1957).

¹¹³ W. H. McAdams, "Heat Transmission," 3rd ed. McGraw-Hill, New York, 1954.

¹¹⁴ R. N. Weltmann, *Ind. Eng. Chem.* **48**, 386-387, 1956.

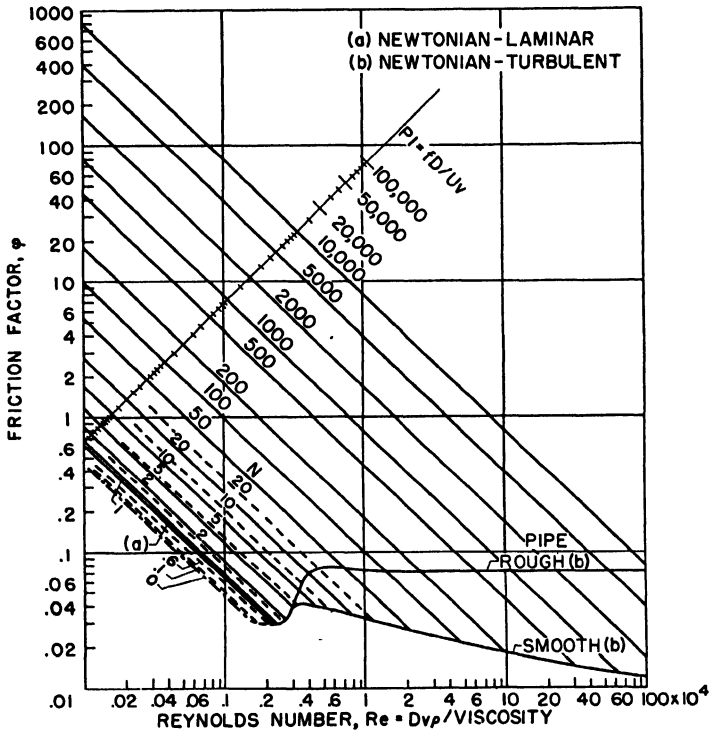


FIG. 24. Generalized friction diagram for Newtonian and non-Newtonian flow in pipelines. After Weltmann.^{59, 114}

data^{112, 115-118} have been used^{59, 112} to illustrate the validity of this friction diagram. Other composite friction diagrams have been suggested^{119, 120} which use different non-Newtonian flow parameters.

The flow of Newtonian materials in pipelines is well understood and is given by Poiseuille's equation (equation 2) in the laminar range of flow behavior and by equations (17) and (18) in the turbulent range. The fric-

¹¹⁵ R. H. Wilhelm, D. M. Wroughton, and W. F. Loeffel, *Ind. Eng. Chem.* **31**, 662 (1939).

¹¹⁶ G. E. Alves, D. F. Boucher, and R. L. Pigford, *Chem. Eng. Progr.* **48**, 385-393 (1952).

¹¹⁷ M. D. Wining, M. Sc. Thesis in Chemical Engineering, University of Alberta, Edmonton, Canada, 1948.

¹¹⁸ C. C. Winding, G. P. Bauman, and W. L. Kranich, *Chem. Eng. Progr.* **43**, 527 (1947).

¹¹⁹ A. B. Metzner and J. C. Reed, *A.I.Ch.E. Journal* **1**(4), 434-440, (1955).

¹²⁰ E. B. Christiansen, N. W. Ryan, and W. E. Stevens, *A. I. Ch. E. Journal* **1**(4), 544-548 (1955).

tion diagram for Newtonian fluids is presented by curve *a* for laminar flow and by curves *b* for turbulent flow in Fig. 24. One curve *b* is for smooth pipes and the other curve *b* is for a pipe with a very rough inside surface. The lines for pipes of medium roughness lie between the two curves *b*.¹¹³ The viscosity which is used to calculate the Reynolds number is the Newtonian viscosity. Thus, the pressure loss of a Newtonian material in a pipeline is a unique function of the Reynolds number.

The flow of non-Newtonian materials in pipelines is not quite as well understood. However, the Buckingham equation (equation 9) was used to determine the laminar flow of Bingham plastics in pipe lines^{59, 114, 121, 122} and the power equation (equation 13) was used to determine the laminar flow of pseudoplastic and dilatant materials in pipe lines.^{59, 114, 119}

For a Bingham plastic in laminar flow the friction factor is¹²²

$$\varphi = \frac{64}{\text{Re}} \frac{\text{Pl}}{8s} \quad (23)$$

where $\text{Pl} = f D/Uv$ and is called the plasticity number⁵⁹ and *s* is the ratio of yield value to shearing stress at the pipe wall. Since *s* is a unique function of *Pl*, the friction factor for Bingham plastics in laminar flow is fully determined from *Re* and *Pl*. It is found from Fig. 24 at the intersection of the Reynolds number and the plasticity number. The Reynolds number in this case is calculated by using the plastic viscosity, and the plasticity number is calculated by using the plastic viscosity and the yield value of the plastic material. Since both flow parameters are independent of the rate of shear, the rate of shear in the pipeline does not have to be known.

For pseudoplastic and dilatant materials in laminar flow the friction factor is^{59, 114}

$$\varphi = \frac{64}{\text{Re}} \left(\frac{N + 3}{4} \right) \quad (24)$$

Thus the friction factor for pseudoplastic and dilatant materials is fully determined from *Re* and *N*. It is found from Fig. 24 at the intersection of the Reynolds number and the structure number. The Reynolds number in this case is calculated by using the apparent viscosity of the material at the flow condition that prevails in the pipeline. This flow condition is given by the rate of shear and temperature in the pipeline. The rate of shear in the pipeline for the flow of pseudoplastic and dilatant materials in laminar flow is

$$G_p = 2v(N + 3)/D \quad (25)$$

¹²¹ E. L. McMillen, *Chem. Eng. Progr.* **44**, 537-546 (1948).

¹²² B. O. A. Hedström, *Ind. Eng. Chem.* **44**, 651-656 (1952).

Thus, the apparent viscosity that is to be used in the Reynolds number has to be measured in the viscometer at the pipeline rate of shear or to be calculated for this rate of shear by extrapolation from equations 12 and 13. Sometimes the structure number N also varies with rate of shear and has then to be obtained for the pipeline rate of shear in a similar manner.^{59, 112}

Experimental data seem to indicate that turbulent flow in pipelines sets in for non-Newtonian materials at a Reynolds number at which the lines of constant plasticity number and structure number intercept the curve b for turbulent Newtonian flow that corresponds to the respective pipeline roughness. Thus, in turbulent non-Newtonian flow the friction factor is a unique function of the Reynolds number. For Bingham plastics the Reynolds number is calculated by using the plastic viscosity since it remains constant with increasing rates of shear. For pseudoplastic and dilatant materials the Reynolds number is calculated by using an estimated apparent viscosity which is obtained by extrapolation to infinite rate of shear.^{29, 59, 112} Since in turbulent flow the rate of shear is high but difficult to evaluate, it is assumed that the apparent viscosity thus determined is a close estimate of the actual apparent viscosity of the material in turbulent flow.

Figure 25 illustrates the validity of the friction diagram for determining

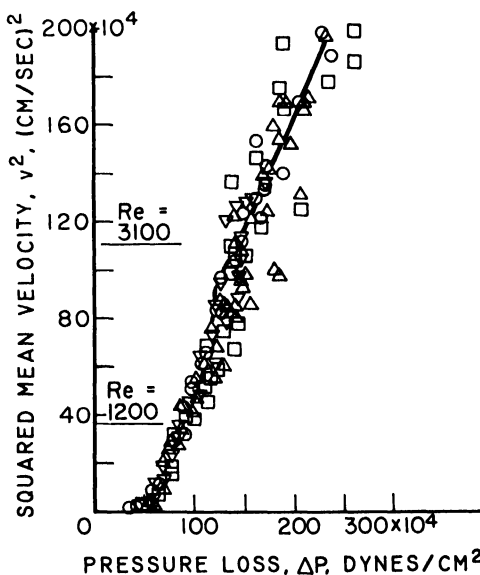


FIG. 25. Comparison of calculated (solid line) and measured pressure losses (points) of a pseudoplastic material in a $\frac{3}{8}$ -in. pipeline in laminar and turbulent flow. The different point symbols represent four different experiments. After Weltmann and Keller.¹¹²

the pressure losses of a pseudoplastic material in laminar and turbulent flow, in a straight pipeline. The solid line was calculated by using the appropriate apparent viscosities and structure number to determine the friction factor from the friction diagram (Fig. 24). The flow properties η and N were obtained from a concentric cylinder rotational viscometer flow curve at the rates of shear corresponding to the flow rates in the pipeline. The pressure loss was calculated from equation (22). The points are measurements from four different experiments. Some deviations between the calculated and experimental data are apparent in the transition region. These same deviations occurred with a Newtonian liquid¹¹² indicating a nonideal transition region in the pipeline, probably on account of nonuniformity in diameter and surface roughness.

To determine the pressure loss in an entire pipeline system, the transition loss coefficients C_L have to be evaluated. For many transitions they have been experimentally determined for Newtonian liquids and can be found in a handbook.¹²³ Frequently they are referred to as "numbers of velocity head." The transition loss coefficients for a few non-Newtonian materials have also been experimentally determined.¹¹² This same reference¹¹² uses the results from these experiments for an analysis, which permits the determination of the pressure losses that occur when such or similar non-Newtonian materials are passed through pipeline transitions, provided that the transition loss coefficients for Newtonian liquids are available for the same transitions. This analysis is quite useful since transition loss coefficients for Newtonian liquids are frequently given in the manufacturer's specifications, even for the very complicated transitions.

3. PASTES

Pastes can be solid-liquid dispersions, liquid-liquid dispersions, colloidal suspensions, and solutions. Thus, all of the many types of flow behavior that have been described and analyzed in the previous paragraphs can be encountered when studying the rheological properties of pastes. Some correlation between flow properties and application behavior was given throughout this chapter for purposes of demonstration. Also, flow curves of various pastes were shown to illustrate the variety of flow types encountered when dealing with pastes. In the following, an attempt will be made to treat some miscellaneous pastes which are not treated elsewhere in the book and to correlate their flow behavior with their performance characteristics in production and application.

Some miscellaneous pastes of everyday household use and their flow

¹²³ J. H. Perry, ed., "Chemical Engineers' Handbook," 3rd ed. McGraw-Hill, New York, 1950.

TABLE V
CONSISTENCY OF A FEW POPULAR HOUSEHOLD PASTES^a

<i>Paste</i>	<i>U</i> (<i>poises</i>)	<i>f</i> (<i>dynes/cm.²</i>)	<i>Flow type</i>	<i>Degree of thixotropy</i>
Water	0.01	0	Newtonian	None
Honey	115	580	Thixotropic plastic	Slight
Mustard	2.94	390	Thixotropic plastic	Slight
Mayonnaise	6.33	850	Thixotropic plastic	Slight
Margarine	7.77	480	Thixotropic plastic	Very marked
Ketchup	0.83	150	Thixotropic plastic	Slight
Burma shave	3.46	210	Thixotropic plastic	Very marked
Other shaving cream	2.55	220	Thixotropic plastic	Very marked
Clay-water suspension	—	—	Thixotropic dilatant	Slight

^a Data taken from Green.¹⁸

behavior are presented in Table V to give the reader a perception of consistency and flow types.

The rheological problem of the ketchup manufacturer is to make the ketchup to such a consistency that it can easily be poured from a serving bottle and yet will flow slowly enough to prevent spilling. That requires a rather critical adjustment and control of yield value at the rate of shear to which it will be subjected by the user.

Shaving creams, like toothpastes and artist colors, are manufactured in a continuous process. Therefore, their consistency during the production process has to be adjusted for easy piping and later for ready flow-out from the consumers' tubes.

The manufacturers of medical and food products such as various salves, penicillin, and canned baby foods have used rheological measurements to adjust the consistency of their products and for control purposes. In the dairy, flour, and starch industries, rheology is mainly used for automatic control purposes by shutting off the mixing and cooking process at a previously determined "consistency end point." Similar use of rheology is made in the preparation of varnishes and resins.

The manufacturers of glues and adhesives measure the change in consistency with temperature to obtain an indication of the stickiness and

performance characteristics of their product upon application and drying. They then use the consistency obtained at one or more temperatures for product control.

For high speed processes, such as printing and paper coating, the paste has to be of sufficiently low consistency to follow the rollers and not to tear the substratum at the high stresses that are developed. Thus, for high speed processes dilatancy is disastrous. However, dilatant materials can be used in low speed coating processes, and in fact some of the materials used for furniture decorations—for instance, artificial leather cloth and also some oilcloth coatings—have shown dilatant flow behavior. But even in the case of slow-coating processes, the manufacturer would prefer non-dilatant pastes, since they are much easier to handle and to control. When coating with plastic and pseudoplastic materials, for instance, flocculation can be induced if a matte finish is desired and reduced if a highly glossy surface finish is to be obtained. This is difficult to do with dilatant materials.

Many slurry pastes such as bentonites, asphalts, and cements, are mixed automatically in a continuous manufacturing process to a predetermined consistency by employing viscosity-indicating instruments. These instruments are used to actuate electromechanical means which in turn will affect additions of preselected ingredients, if required, until the material has the desired consistency.

4. PAINTS AND LACQUERS

Many commercial paints have flow characteristics similar to thixotropic plastic materials. The range of flow properties encountered by the consumer of commercial paint products is summarized in Table VI.²¹ The rheological properties were measured with a Stormer-type concentric cylinder viscometer at a rate of shear that probably was not entirely the same as the operational rates of shear in paint applications. Nevertheless,

TABLE VI
FLOW PROPERTIES OF COMMERCIAL PAINTS
(*Fischer*²¹)

<i>Product</i>	<i>U</i> (<i>poises</i>)	<i>f</i> (<i>dynes/cm.</i> ²)	<i>Degree of</i> <i>Thixotropy</i>
Enamels, gloss	1.4-3.9	0-30	Nil to slight
Enamels, semigloss	1.0-3.5	50-120	Slight
Flat or matte paints	0.6-1.0	20-100	Slight to marked
Wall, water-dispersible ^a	0.2-1.4	10-100	Slight to marked
Primers, metal	0.3-1.2	0-100	Nil to marked
Varnishes	0.9-2.9	0	Nil

^a Diluted as recommended by manufacturer.

TABLE VII
APPROXIMATE TIME OF LEVELING OF OIL FILMS ON A NONPOROUS SURFACE AS
FUNCTION OF VISCOSITY AND FILM THICKNESS
(Data taken from Fischer.²¹)

<i>Viscosity (poises)</i>	<i>Leveling time (min.)</i>	<i>Film thickness (mils.)</i>
<0.5	<1.0	0.5 to 5.0
2.0	5.0	0.5
2.0	<0.5	≥0.5
10.0	>120	0.5
10.0	10	≥0.5

the data should present an interesting comparison, since they all were taken at the same rate of shear. The table indicates the similarity in flow properties of all types of commercial paints with plastic viscosities of less than 4 poises and yield values not exceeding 120 dynes/cm.².

The rheological behavior of a paint and a lacquer during and after application determines the smoothness and perfection of the resulting film surface. Paints and lacquers can be applied to a substratum by brushing, dipping, flow coating, and spraying. In all cases the flow out of the material between the time of application and drying will determine to some extent the characteristics of the finished surface.

The time that is required for flow-out of oils of different viscosity on a nonporous surface depends on the layer thickness, as shown in Table VII.²¹ These data lead to the expected conclusions that leveling to a smoother film takes less time with lower viscosity materials and for films of larger film thickness. These conclusions should also be applicable to the leveling of paint films, however, only if the operational viscosity is considered which, at the moment of deposition on the substratum, is very different from that of the bulk material contained in the spray gun and which continues to increase while drying and leveling proceeds. It is said²¹ that the flow-out will be complete in about 1 min. after deposition of the material for very thin films if the viscosity does not exceed 1 poise. However, most materials require a longer flow-out time, since the viscosity is frequently higher than 1 poise at 1 min. after deposition, either on account of a fast rate of viscosity increase during the spraying process or on account of a higher original viscosity of the bulk material.

The rates of shear that are produced by brushing paints on a surface were estimated by Williamson *et al.*¹²⁴ to range from 130 to 260 sec.⁻¹. He arrived at these values by determining the rate of shear at which the order

¹²⁴ R. V. Williamson, G. D. Patterson, and J. K. Hunt, *Ind. Eng. Chem.* **21**, 1111-1115 (1929).

TABLE VIII
CHANGE IN FLOW PROPERTIES OF A BRUSHED BLACK ENAMEL
ON SOLVENT EVAPORATION
(Fischer⁷³)

<i>Time</i> (min.)	<i>U</i> (poises)	<i>f</i> (dynes/cm. ²)	<i>Type of flow</i>
0	1.9	0	Newtonian
2.5	14.0	24	Plastic
5.0	30.0	520	Thixotropic plastic
7.5	167.0	6200	Thixotropic plastic

of apparent viscosities of thixotropic paints exhibiting entirely different flow behavior coincided with the order of ease of flow indicated by practical brushing tests. This value could also be obtained by assuming that the brushing velocity is about 20 cm./sec. for a distance between substratum and brush of about 0.1 cm. Asbeck¹¹¹ estimates brushing rates of shear of about 100 times those given by Williamson. Various other investigators tried to correlate the flow properties of paints with their brushing behavior¹²⁵⁻¹²⁸ and found that paints have good brushing properties if the plastic viscosities range from 2 to 5 poises and the yield values from 400 to 1400 dynes/cm.². For nitrocellulose lacquers a viscosity ranging from 0.16 to 1.18 poises was found to be preferable.¹²⁹ The reason for the lower viscosity in the latter case might very well be that the nitrocellulose lacquers increase very rapidly in viscosity during and after application. To demonstrate this point, Table VIII⁷³ shows the rate of increase in plastic viscosity and yield value on solvent evaporation for a brushed black enamel paint, which is certainly rapid but less so than it would be for a nitrocellulose lacquer.

A paint is considered to have good brushing properties when all brush marks disappear during the drying process. This might be achieved by rapid flow-out caused by low viscosity and yield value or by taking advantage of the thixotropic properties of the material. The former has the disadvantage that it frequently leads to sag marks and "curtains," since the low consistency causes the material to continue to flow after application until drying is sufficiently advanced. In fact, the danger of sagging is always present if the film is applied in a layer that is too thick. The thixo-

¹²⁵ W. H. Droste, *Farben-Ztg.* **37**, 619-620, 655-657, 694-695 (1932).

¹²⁶ W. H. Droste, *Chem. Fabrik* **7**, 249-250 (1934).

¹²⁷ R. Houwink, "Elasticity, Plasticity and Structure of Matter." Cambridge Univ. Press, London and New York, 1937.

¹²⁸ J. E. Arnold, *Paint Technol.* **9**, 163-166 (1944).

¹²⁹ J. H. Coughlin and R. F. Wint, *Offic. Dig. Federation Paint & Varnish Production Clubs* **263**, 694-696 (1946).

tropic properties have the advantage of giving the material the low operational consistency needed for initial flow-out in order to prevent brush marks and to obtain good leveling.¹³⁰ At the same time, they provide the material with a mechanism for increase in consistency by means of the thixotropic buildup of structure that can be effective immediately after application. However, a too rapid thixotropic increase in structural consistency can also be detrimental, because leveling and flow-out are not instantaneous. It has indeed been shown^{131, 132} that thixotropic materials which decrease in consistency rapidly with rate of shear but rebuild their structure slowly exhibit the best leveling characteristics and that a too rapid increase in thixotropic structure can produce poor leveling.

Gel-lacquers that are used for dipping operations and produce coatings with a film thickness up to 0.015 in. can range in viscosity from 20 to 40 poises.¹³³ For the usual dip-lacquer finishes, however, the viscosity has to be substantially less, since the applied coatings are only about $\frac{1}{10}$ the thickness of those obtained with the gel-lacquers. The viscosity requirements for flow coating operations should be similar to those for dip-lacquer operations, since the process of drying and film forming is similar.

The viscosity of paints and lacquers, that are applied by spray-gun operations range from 0.4 to 1.2 poises.²¹ For hot spray lacquers applied at around 170° F., the viscosity should be adjusted to about 2 poises at room temperature, so that it will be less than 1 poise at the spraying temperature. The viscosity of hot plastic paints that are sprayed at temperatures around 300° F. should be less than 1.5 poises.¹³⁴ The viscosity is usually adjusted to the required value by additions of solvent. The viscosity of the bulk material has to be so low for spray-gun operations because the viscosity of the material will increase substantially during the spraying process; namely, from the time the material leaves the spray gun to the time when it hits the substratum on which it is to be coated. The increase in viscosity will, of course, depend on the volatility of the solvent and on the temperature of operation. The change in flow properties of a typical material can account for an increase in viscosity to six times its original viscosity at a normal spraying distance of 8 to 12 in. A study of many of these factors was made by Bogin.¹³⁵

When applying a paint by spraying, the droplet size of the spray will greatly influence the appearance of the finished surface. A fine spray will produce a glossy surface, whereas a coarse spray will give a matte finish,

¹³⁰ E. L. McMillen, *Ind. Eng. Chem.* **23**, 676-679 (1931).

¹³¹ B. Saunders, *J. Oil & Colour Chemists' Assoc.* **31**, 95-106 (1948).

¹³² M. E. D. Jarret, *J. Oil & Colour Chemists' Assoc.* **31**, 337-378 (1948).

¹³³ C. J. Malm and H. L. Smith, *Ind. Eng. Chem.* **38**, 937-941 (1946).

¹³⁴ H. L. Aldrich, *Paint, Oil, Chem. Rev.* **110**(2), 8, 30, 31, 34 (1947).

¹³⁵ C. Bogin, *Paint, Oil, Chem. Rev.* **103**(15), 7; (16), 16 (1941).

unless leveling-out occurs before drying is completed. The drop size of the spray is determined by the physical properties of the paint and the type of atomizer employed. Paint spray guns are most frequently gas-atomizing nozzles, where the paint is atomized by the impingement of a high-velocity gas stream, which is usually air. The literature¹⁸⁶ gives an empirical equation for the mean droplet size produced by a gas-atomizing nozzle, when the liquid is a Newtonian fluid. In this equation the mean droplet diameter D_0 is defined as a drop with the same ratio of volume to surface as the total sum of all drops formed. The equation is

$$D_0 = \frac{585\sqrt{\sigma_L}}{(v_A - v_L)\sqrt{\rho_L}} + 597 \left(\frac{\mu_L}{\sqrt{\sigma_L\rho_L}} \right)^{0.45} \left(1000 \frac{Q_L}{Q_A} \right)^{1.5} \quad (26)$$

where D_0 is in microns, if the surface tension of the liquid σ_L is in dynes per centimeter, the density of the liquid ρ_L in grams per cubic centimeter, the viscosity of the liquid μ_L in poises, the relative velocities of the liquid v_L and air v_A in meters per second, and where Q_L is the liquid volume flow rate and Q_A is the air volume flow rate. Although this equation is not dimensionally correct, it fits well the experiments and is said to be generally applicable to Newtonian liquids of $19 < \sigma < 73$, $0.7 < \rho < 1.2$, and $0.003 < \mu < 0.5$, provided that the gas or air velocity is subsonic. Since in paint spraying those conditions are almost met, although paints have frequently slightly higher viscosities and often deviate at least somewhat from true Newtonian behavior, it is felt that the above equation is adequate to evaluate the effects of the physical properties of wet paints on the droplet size of the spray. It is seen from equation (26) that, if the ratio of air volume flow rate to liquid volume flow rate is large compared to 10^3 , the term containing this ratio becomes insignificantly small and D_0 depends primarily on the surface tension; on the other hand, if this same ratio is equal to 10^3 and smaller, D_0 depends substantially on the viscosity. For production paint spray guns having a ratio of Q_A/Q_L in the order of 10^3 (the usual gas volume flow rate is about 4 to 8 ft.³/min. at 40 p.s.i. pressure, and the liquid volume flow rate, being rather small, is in the order of 10^{-2} ft.³/min.), the viscosity term in equation (26) is not negligible and D_0 will increase with an increase in paint viscosity.

One of the most common defects of spray-gun-applied films is "orange peel," which is recognized by surface ripples that are similar in appearance to those on the skin of an orange. The following mechanism has been suggested as a reason for the formation of "orange peel." The ripples could be instigated by the irregular pattern that is formed by the coalescence of liquid particles when the subsequent air blast impinges on the deposited

¹⁸⁶ S. Nukiyama and Y. Tanasawa, *Trans. Soc. Mech. Engrs. (Japan)* **5**, 18, 63 (1939); J. H. Perry, (See ref. 123 J. H. Perry).

material while it is still wet. Because of evaporation, the plastic viscosity and yield value increase. At the same time cooling takes place, also increasing the viscosity of the material, so that the material hitting the object might have increased in viscosity and yield value to such an extent that the leveling time becomes substantially greater than the drying time, preventing the film from flowing out before drying is completed; thus the ripples remain in the finished film. The presence of water in the composition is said to be conducive to orange peel and its removal has been suggested.¹³⁷ However, other investigators⁷³ found that water causes orange peel only when it induces yield value, since the flocculated pigment will then prevent good atomization and reduce flow-out and gloss. In a few applications, a slight degree of orange peel is desirable to give the surface a regular small pattern so as to assist in hiding more objectionable surface blemishes.

Nomenclature

A	Area	R	Any radius of capillary and pipe ($0 \leq R \leq R_w$) and of rotational viscometer ($R_b \leq R \leq R_c$)
a, A	Constants		
b, B	Constants		
B_U	Coefficient of thixotropic break-down	R_b	Radius of inner cylinder (bob)
		R_c	Radius of outer cylinder (cup)
C	Rate of shear correlation constant	Re	Reynolds number $Re = Dv\rho/\text{viscosity}$
C_L	Transition loss coefficient	R_m	Midpoint radius $R_m = \frac{1}{2}(R_b + R_c)$
c	Solid concentration in suspension	S	Shearing stress
dv/dx	Rate of shear or velocity gradient	S_e	Total elastic shearing stress
D	Pipe diameter	s	$s = f/S_w$
D_0	Mean droplet diameter	T	Torque
F	Force	Te	Temperature
f	Yield value	t	Time
G	Rate of shear or velocity gradient, assuming constant viscosity	U	Plastic viscosity
h	Height of inner cylinder (bob)	V	Volume
K	Instrument constant	V_U	Coefficient of thixotropic break-down
k	Grain diameter indicating surface roughness	v	Velocity, also mean velocity
L	Length of pipe and capillary	x	Coordinate perpendicular to the shear, also length parameter
M	Constant	α	Constant
M_U	Coefficient of thixotropic break-down	η	Apparent viscosity
n	Constant	η_0	Residual apparent viscosity
N	Exponent for viscosity power function, or structure number	θ	Coefficient of thixotropic break-down
P	Pressure	μ	Newtonian viscosity
ΔP	Pressure loss	μ_0	Solute viscosity in suspension
p	Percentage by volume	μ^*	Material constant
Pl	Plasticity number $Pl = fD/Uv$	ρ	Density
Q	Volume flow rate	σ	Surface tension

¹³⁷ C. A. Hochwalt and P. E. Marling, *Ind. Eng. Chem.* **27**, 190-192 (1935).

τ	Relaxation time	L	Refers to liquid
β	Cone angle	0	Refers to intercept when not otherwise specified
φ	Friction factor $\varphi = 2DP/\rho Lv^2$	p	Refers to plug flow
ω	Angular velocity	w	Refers to wall of capillary and pipe
SUBSCRIPTS			
A	Refers to air	1, 2	Refers to different conditions
E	Refers to equilibrium condition		

CHAPTER 7

ATOMISTIC APPROACH TO THE RHEOLOGY OF SAND-WATER AND OF CLAY-WATER MIXTURES

W. A. Weyl and W. C. Ormsby

I. Analysis of the Problem	249
II. Some Unique Properties of Water.	252
III. Surface Properties of Solids Containing Cations of High Charge and Low Polarizability (Quartz, Clay).	258
1. Ways of Lowering the Surface Energy of Solids.	260
a. Polarization of Surface Ions	260
b. Adsorption of Anions Leading to Charged Particles	261
c. Distortion of the Surface Structure Leading to an Electrical Double Layer.	261
d. Adsorption of Dipoles	262
e. Interaction of Solids with Water and Formation of a Gouy-Freundlich Diffuse Double Layer	262
2. The Unique Features of the Clay Minerals	263
3. Plasticizing of Nonplastic Minerals	264
IV. The Interaction of Minerals with Water.	267
1. Basic Phenomena	267
a. Rigidity of Water Films	267
b. Sedimentation.	269
c. Acidity and Electric Conductivity of Suspensions	271
d. Electrokinetic Phenomena	272
e. Thixotropy of Suspensions.	276
f. Flow of Water through Porous Media.	278
g. Flocculation and Deflocculation.	280
h. Adhesion Properties	284
i. "Green Strength" of Clay	286
j. Volume Changes on Drying	286
2. Rheology of Sand-Water Mixtures.	288
3. Rheology of Clay-Water Mixtures.	290
V. Summary.	295

I. Analysis of the Problem

The rheological properties of mixtures of fine grained minerals with water are of ever increasing practical interest. Concrete is a mixture of natural and synthetic minerals with water, and its rheological properties

are important for the construction of buildings and highways. The secondary recovery of oil calls for a better knowledge of flow phenomena involving water, oil, and rocks. Flotation processes become more important each day as the sources of concentrated minerals are being exhausted. In all these processes the nature of the liquid and the nature of the solid are just as important as their distribution, particle sizes, and shapes. As it is not possible to consider all interesting materials, two types have been chosen which may be considered extremes: sand and clay. Other non-metallic minerals have properties between these two extremes; most of them resemble sand more closely than they do clay.

The mixing of sand with water and the making of mud pies has been a favorite pastime of children for ages. Mankind, in its early childhood, learned to mix clay with water and take advantage of the plasticity of the mixture and of the strength of the product after it had been shaped by hand and dried; a process which marks the beginning of the oldest technology, ceramics.

The atomic structures of these materials, sand (quartz), clay, and water are well known. It has been found that there are several clay minerals which differ in their structures and in their properties. The application of X-rays and of the electron microscope has helped greatly to identify and to classify the different clay minerals.¹

In spite of the knowledge concerning the positions of the atoms, their distances, and their bond angles in clay and quartz, no satisfactory explanation has yet been given for the difference between the rheological properties of a clay-water and a sand-water mixture.

Sand-water mixtures are not plastic. On drying they lose their strength, but they show no shrinkage. This behavior is characteristic for most minerals and indicates that in the wet state the quartz grains must have touched one another.

Clay-water mixtures are typically plastic and can be molded into intricate shapes. Drying a clay-water mixture produces a solid which has considerable strength (green strength of ceramic bodies). The substantial decrease of volume during drying indicates that the particles do not touch one another when wet but that the water is the continuous phase in which the solid particles are suspended. Different clay minerals show this behavior to different degrees so that for practical purposes it is often useful to work with mixtures of different clays and nonplastics in order to obtain sufficient green strength but avoid excessive shrinkage.

In order to give an atomistic explanation for the rheology of mineral-

¹ G. W. Brindley, "X-ray Identification and Crystal Structures of Clay Minerals." Mineralogical Society, London, 1951.

water systems the complexity of the interaction has to be broken down into well-defined partial problems.

From a crystal chemical point of view, the clay minerals can be described as arrays of Si^{4+} , Al^{3+} , O^{2-} , and OH^- ions with or without Mg^{2+} or Fe^{3+} ions. These ions are arranged in a fashion similar to that of the mica crystals, i.e., in parallel sheets of fairly high symmetry. Most important for the crystal chemistry of the clay minerals is the fact that the building units are the normal SiO_4 , AlO_6 , or MgO_6 groups which also are the constituents of numerous minerals.

The rheological properties and the base exchange capacities of various clay minerals differ but the building units are the same. Other minerals, such as the zeolites, show base exchange properties; however, these minerals do not form plastic bodies with water but behave like sand. Which structural factors determine the unique rheological properties of clays?

When clay minerals are dispersed in water, their migration in an electrical field indicates that they are not electrically neutral but that they seem to carry an excess negative charge. Attempts have been made to attribute this lack of electroneutrality to defects, e.g., to Fe^{2+} or Mg^{2+} ions occupying positions which normally should be held by Al^{3+} ions. Defects of this sort develop at high temperature but are not characteristic for crystals which, like the clay minerals, have formed at low temperature. Furthermore, even a perfect quartz crystal when sufficiently subdivided and immersed in water forms negatively charged particles. What is the origin of the excess charge which these minerals assume when suspended in water?

Once we have a clear picture of the origin of the negative charge we can understand why cations are attracted to negative surfaces and why these chemisorbed cations can be replaced easily by others (base exchange). We can understand that the degree of hydration of the clay minerals will depend on the nature and the hydration tendency of these chemisorbed cations. It is more difficult, however, to account for the apparent rigidity of a system which consists of solid particles separated by water films which can be several hundred molecules thick. The plasticity of a wet clay is the result of a relatively thick water film which has been rendered immobile.

In order to explain the rheological properties of sand-water mixtures mixtures and clay-water mixtures, it is necessary to first give an atomistic picture of water in contact with solids. Such a picture could be derived on the basis of the better known behavior of water toward salts containing cations of high field strength.

The high activity of the surface of clay and its influence on water is well appreciated. An atomistic approach to the problem has to account for

its unusually strong surface forces. For this purpose the origin of surface forces of ionic solids is reviewed and four mechanisms are discussed which can lower the surface energy of a solid.

Once the forces acting between water and clay are understood, it becomes possible to appreciate the contribution of particle size and shape. No matter what the forces are between the solid and liquid phase, spherical particles cannot give a plastic medium when dispersed in water. The kinematics of plastic flow and its physicochemical aspects are equally important.

It is the object of this paper to sketch a new atomistic approach to a group of rheological phenomena which are as interesting from a scientific viewpoint as they are important for technology. It is realized that relatively few data on viscosities and experimental conditions have been incorporated into this account. From a quantitative viewpoint, the (literature) data on viscosities of clay-water systems are rather confusing. This is true because of the use of a wide variety of experimental methods and materials. Frequently, experiments are made which are strictly empirical. Time effects and shear-rate variations are often overlooked (single point determinations are sometimes used in attempts to characterize the viscous behavior of clays). Furthermore, an extremely wide variety of results are obtained when particle shape, particle size, and mineral composition are varied. These variables have not been adequately investigated. Restricted studies of specific systems have been made. However, these investigations have not led to a satisfactory explanation of viscous and plastic behavior in clay-water systems. For these reasons we believe that the somewhat qualitative (chemical) approach is most appropriate at this time.

The more pertinent references on clays and the deformation behavior of clay-water systems have been covered (see specifically references 23, 30, 31-35, 41a, b, 45-51, 59, 61 and 62). Naturally the literature on the many and varied aspects of clay-water properties was critically reviewed. However, no attempt was made to compile a comprehensive survey of this literature. This would have entailed an undue amount of detail and would have detracted from the over-all theme of the paper.

II. Some Unique Properties of Water

Physical chemists are well aware of the fact that liquid water has anomalous properties. Whether one refers to "hydrogen bonding" or to molecular "association," no concept of its structure has yet been proposed which explains all of the facts. Many liquids, e.g., alcohols, acetic acid, are of the "associated" type, i.e., they are polymerized both in the liquid and in the vapor state. Water vapor consists of single molecules which do not have the slightest tendency to form dimers like acetic acid.

Water is also unique in its ionizing solvent power. It can dissolve and

ionize more salts than any other solvent. Conventional concepts such as the importance of the dielectric constant or the dipole moment for ionization and ion-dipole interaction fail completely to account for these facts. Hydrocyanic acid should be much superior to water as a solvent because its dielectric constant is 50 % higher than that of water. Liquid ammonia is also a good solvent, but neither HCN nor liquid NH_3 can dissolve salts which contain highly charged cations such as $\text{Al}_2(\text{SO}_4)_3$ or $\text{Th}(\text{NO}_3)_4$.

In our approach to the chemistry of the solid state² we come to the conclusion that reactions are governed primarily by two basic principles: (1) establishment of electroneutrality in the smallest possible volume element and (2) maximum screening of the cations. These two principles also apply to solubility.

According to Bernal and Fowler,³ liquid water represents a three-dimensional, infinitely extending network of anions and cations. Each cation is screened by two anions (the coordination number of the proton is 2) and each anion is tetrahedrally surrounded by four equidistant cations. If one adds to this description of the geometry that the field strength of the cation must be high because of the small size so that the binding forces are strong, one would expect this description to apply to the structure of a crystal.

In order to understand the fluidity of water, one has to realize that the above picture of its structure is a description of the location of the proton over a time average. The protons can change their positions without losing screening, which means that they do not have to overcome a major energy barrier. They can temporarily submerge in the electron cloud of one of their two O^{2-} ions so that only over a time average do the protons assume positions which are equidistant from both O^{2-} ions.

An excess of protons in water does not produce defined H^+ or H_3O^+ ions, that is, units which have characteristic absorption bands or Raman spectra. The properties of water which contain an excess of OH^- ions or of protons can be better understood if it is treated as a defective structure rather than as a solvent containing individual OH^- or H^+ ions in solution.

With respect to the atomic structure of aqueous solutions, Frank and Evans⁴ introduced a very important pictorial concept: the "iceberg," a microscopic region of water which surrounds the solute molecule, atom, or ion with some kind of quasi-solid structure. The name "iceberg" is not supposed to imply that the structure of this volume element of water resembles the atomic structure of one of the forms of ice.

When a rare gas atom or a nonpolar molecule dissolves in water at

² W. A. Weyl, *J. Soc. Glass Technol.* **35**, 421 (1951). See also, this series, Vol. 3, Chapter 8.

³ J. D. Bernal and R. H. Fowler, *J. Chem. Phys.* **1**, 515 (1933).

⁴ H. S. Frank and M. W. Evans, *J. Chem. Phys.* **13**, 507 (1945).

room temperature it seems to modify the structure of the solvent in the direction of greater "crystallinity." The water builds a microscopic "iceberg" around the solute, the extent of which increases with the size of the atom or molecule. For charged particles, the field strength will be an important factor determining the size of the iceberg.

According to Frank and Evans, one must expect that the intrusion of a large atom such as argon or radon into the structure of water will produce two antagonistic effects: (1) The ordinary solvent action: loosening of the water structure, gain in entropy. (2) Iceberg effect: change of water towards greater crystallinity, loss of entropy. At low temperature this effect overshadows the first one so that the solubility of most gases in water shows a minimum when plotted against temperature.

The presence of ions in water lowers its entropy because of the new ordering principle which is introduced by their fields. We can assume that around an ion, especially around one of high charge, the protons have lost their mobility and that the water in this region has changed into an "iceberg." The hydration entropy of all ions is negative.

The immobilization of the protons also affects the viscosity of water. Water has an anomalous viscosity from every point of view. As compared with NH_3 , H_2S , and CH_3OH , the fluidity of water is abnormally low. The structural picture, on the other hand, which describes water as a three-dimensional network of ions and explains its tensile strength, suggests that H_2O should be rigid. The abnormally high fluidity of water is the result of the mobility of the protons. Conditions which increase the tendency of the protons to remain within the electron clouds of O^{2-} ions and change water from a three-dimensional network of ions towards an aggregate of molecules lower its viscosity. This can be accomplished by the application of pressure. Compression of water decreases its volume and increases the electron density of the O^{2-} ions. We may now assume that the increase of the electron density of an O^{2-} ion makes it more S^{2-} -like and favors interpenetration of the proton into its electron cloud, whereas decreasing its electron density makes it more F^- -like and favors the formation of a three-dimensional network. Water, unlike other liquids, becomes more fluid under pressure.

The addition of ions to water can produce both effects. Singly charged, large ions increase the fluidity of water in the same fashion as increased pressure. For small ions or ions with a charge greater than one, the "iceberg" effect predominates so that the viscosity of water is increased.

The two antagonistic effects can be seen easily from the data of the ionic elevations of the fluidity of water as determined by Bingham⁵ (Table I).

⁵ E. C. Bingham, *J. Phys. Chem.* **45**, 885 (1941).

TABLE I
IONIC ELEVATIONS OF FLUIDITY
(After Bingham⁵)

<i>Anion</i>	<i>Fluidity, rhes</i>	<i>Cation</i>	<i>Fluidity, rhes</i>
F^-	-13.6	Li^+	-14.0
Cl^-	+0.28	Na^+	-9.6
Br^-	+3.09	K^+	+0.28
I^-	+7.58	Rb^+	+1.86
NO_3^-	+3.06	Cs^+	+2.59
		NH_4^+	+0.44
		Mg^{2+}	-36.5
		Ca^{2+}	-31.3
		Sr^{2+}	-28.4
		Ba^{2+}	-25.3
		Al^{3+}	-70.5
		Fe^{3+}	-52.2
		Cu^{2+}	-34.7
		Zn^{2+}	-35.6
		H^+	-6.41

Again, the close similarity between the effects of Mg^{2+} and Cu^{2+} ions or Ca^{2+} and Zn^{2+} ions indicates that this phenomenon is due strictly to the electrical field of the particle and is not related to chemical binding forces between the ions and adjacent water dipoles. If the effect of ions on the viscosity of water would involve the binding forces between ions and water molecules, the electronic structure of the ion should have a major influence.

This concept of the interaction of water and ions of high charge can explain the unique solvent power of water with respect to compounds containing cations with a threefold or fourfold charge. Water can accommodate ions of high charge within its structure because the shift of the protons away from the cations produces a volume element of water which has a proton deficiency and an excess negative charge. Such a volume element can neutralize the positive charge of a cation within a relatively short distance. This neutralization of an excess charge is a feature which no other solvent has to offer. From the viewpoint of screening, liquid ammonia should be superior to water. From the viewpoint of ion dipole interaction, liquid HCN should be a better solvent. However, the only salts which ionize completely and which can produce electrical conductivity in anhydrous HCN are alkali salts. The salts of the alkaline earths are practically insoluble in HCN, and compounds with trivalent or tetravalent cations ($SbCl_3$, $AsCl_3$, $SnCl_4$, SnI_4) go into solution as molecules but do not form solvated Sb^{3+} , As^{3+} , or Sn^{4+} ions, in spite of the high dielectric constant of liquid HCN.

It is only logical to assume that the concepts of Frank and Evans concerning the effect of the electrical fields of dissolved ions on the structure of water also apply to the electrical fields which originate in the surface of solids. We may assume that the surfaces of quartz, glass, or clay can project the fields of their ions into water and cause the protons to become less mobile. In the bulk of the water a proton can assume several positions which are approximately equivalent energetically and which are separated by low energy barriers. In the field of a strong cation at least one of these positions becomes less probable than the others, namely, that position within the electron cloud of the O^{2-} ion which is adjacent to the Si^{4+} ion. It is immaterial to our problem whether the surface of the solid tightens or loosens the electron clouds of adjacent O^{2-} ions; it is important only that the protons do not occupy the three possible positions with equal probability. By increasing the probability of protons assuming positions either farther away or closer to the surface, a solid can surround itself with a rigid film of water which has a lower or a higher than average proton density. The unique role of the proton with respect to its screening makes possible a liquid structure in which the proton density can gradually change from one value to another.

This concept will be used as the basis for an atomistic picture of the interaction between water and clays.

Thermodynamic data reveal that the presence of Al^{3+} ions in water causes a structural change which has been described by Frank as the formation of an "iceberg." The volume elements of water which surround atoms (argon) or ions have lost their mobility. We postulated that water is a liquid only because of the unique ability of the proton to enter the electron clouds of either one of its two neighboring oxygen ions. A strong cation in aqueous solution surrounds itself with a volume of water which has a lower than average proton density, because it repels protons into the more distant of all possible positions. The same applies to water which is in contact with a solid of high surface energy (clay). The adhering film loses its mobility.

The rigidity of an "adhering film" of water tapers off with the distance from the wall. For this reason the thickness of the rigid film cannot be uniquely defined, but it depends upon the method which is used to determine the depth action. In order to find out how far the force field of a surface can affect the structure of water, one has to use a method which keeps thermal and mechanical motion at a minimum.

Hosler and Hosler⁶ determined the spontaneous freezing point of small quantities of water. Ice formation, i.e., nucleation, reveals that the depth

⁶ C. L. Hosler and C. R. Hosler, Sci. Rept. No. 1, Contract A. F. 19 (604)-140 Pennsylvania State University, University Park, Pennsylvania, 1952.

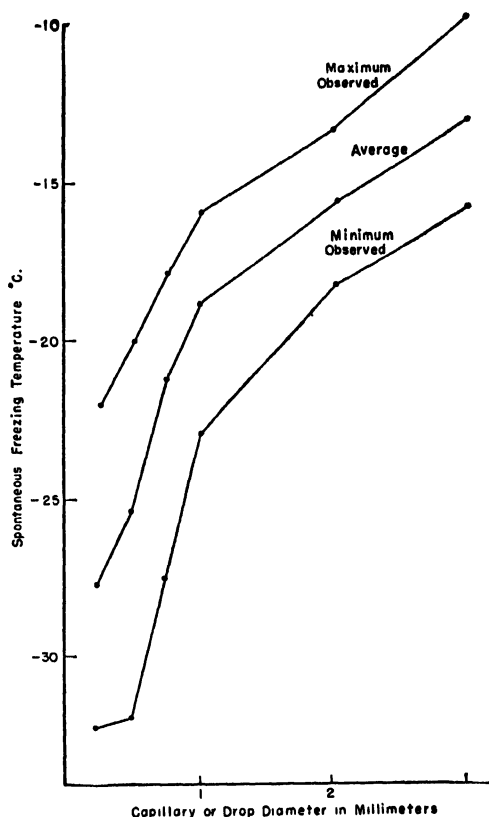


FIG. 1. Variation of spontaneous freezing temperature with capillary diameter. (After C. L. Hosler and C. R. Hosler.⁶)

action of a glass wall extends for several millimeters into the supercooled water (Fig. 1). Many investigators have established that the degree of supercooling of water increases with decreasing size of the droplet or with decreasing diameter of the capillary. This relation has been attributed to the greater probability of nucleus formation in large volumes than in small volumes.

The effect of the surface upon the structure of water leads to an energy barrier which has to be overcome in order to form an ice crystal. Hosler and Hosler found that thermal currents of the water which may result from rapid cooling or which may be mechanically induced enhance the formation of ice. Convection currents or stirring interferes with the depth action of the wall on the structure of the supercooled liquid.

Another phenomenon which reveals the depth action of a pure silica surface on water is the variation of the contact angle of a liquid on quartz

with the humidity of the atmosphere. Bartell and Bristol⁷ found that in the absence of water, acetylene tetrabromide had an advancing contact angle of 10° on quartz. If the ambient atmosphere contained water this contact angle increased gradually and reached 38° for 100 % humidity. These measurements reveal that the contact angle of acetylene tetrabromide on quartz depends on the thickness of the water film and that the surface forces of this film must change as the water film becomes thicker.

III. Surface Properties of Solids Containing Cations of High Charge and Low Polarizability (Quartz, Clay)

All investigators of clay agree on one point, namely, that clay minerals have a particularly "active" surface. The meaning of this activity is not sharply defined, but their absorbing power for foreign molecules as it is utilized in the bleaching of oils or their power to retain water at elevated temperature or low vapor pressure are expressions for their surface forces. There is also no doubt that the intensity of the surface forces of clay is intimately connected with the rheological properties of clay-water mixtures. This is substantiated by the behavior of clays of different plasticity with respect to their water vapor pressure⁸ or their heats of wetting.

Gruner found that a mixture of water and a plastic clay (Wildsteiner Ton) in the molar ratio 4:1 had a vapor pressure of only 3 mm., that is, one-fourth of that of the free water at the same temperature (15°C). A nonplastic kaolin (Zettlitz) had a vapor pressure of 11 mm when mixed with water in the same ratio, thus indicating that its effect on the vapor pressure of water is very weak.

The work of Rosenow⁹ on the adsorption of water by different clays which were stored over 10 % sulfuric acid brings out the same relation between attraction forces of these minerals for water and their plasticity. The heats of wetting of these clays goes parallel with their adsorption power. Table II shows the wide variations of these properties for clays from different localities and for a finely ground quartz.

This focuses our attention on the question concerning the origin of the unusually strong surface forces which seem to be characteristic for clay minerals. The surface area alone cannot explain the magnitude of their surface energy, because finely ground quartz or feldspar does not become plastic in spite of having a large surface area. In order to understand the high surface energy of clay, the origin of the surface energy will be discussed

⁷ F. E. Bartell and K. E. Bristol, *J. Phys. Colloid Chem.* **44**, 86 (1940).

⁸ E. Gruner, *Z. anorg. u. allgem. Chem.* **215**, 1 (1933).

⁹ M. Rosenow, Dissertation, Hanover, Germany, 1911, quoted from H. Salmang, "Die physikalischen und chemischen Grundlagen der Keramik," p. 40. Springer, Berlin, 1951.

TABLE II
WATER ADSORPTION AND HEAT OF WETTING FOR VARIOUS
CLAYS AND FINE QUARTZ

<i>Clay</i>	<i>H₂O adsorbed</i>	<i>Heat of wetting cal./gm.</i>
Ebernhahn	11.5%	3.059
Loethain	9.0	1.919
Loethain, fine	9.5	2.764
Wildstein	8.0	1.830
Lautersheim	7.5	1.747
Zettlitz	5.9	.791
Hirschan	3.0	.796
Quartz, fine	0.7	.147

briefly and the methods will be described which can lower the surface energy of a solid.

The origin of the surface energy of solids is closely related to the origin of the solid state. In a previous publication,¹⁰ an hypothesis has been advanced according to which matter was formed under energy conditions (temperature and radiation) which were so different from those prevailing today that most of the particles which had formed are no longer stable. In order better to screen their positive cores, the atoms have to undergo a reshuffling of their electrons. The fact that most elements are solid at room temperature is the result of the polymerization of atoms, a process which improves the screening of their cores.

The surface energy of a NaCl crystal is thus attributed to the fact that the surface ions are not properly screened or that they do not have their normal coordination numbers of six. This condition has been realized since the early calculations of the lattice energies of crystals by Born, Madelung, and many others.

Many scientists attempted to calculate the surface energy of a NaCl crystal and the deviation of its surface structure from that of the bulk. Their calculations apply to NaCl, a solid which contains only singly charged ions.

All these attempts to calculate the surface energy of simple solids ignore one of the most important features, namely, that a distortion of the surface of a solid must have a "depth action" in order to produce a gradual transition from the normal bulk structure to the distorted surface structure.

Verwey¹¹ writes: "All previous authors agree that the deformation of

¹⁰ W. A. Weyl, "Structure and Properties of Solid Surfaces" (R. Gomer and C. S. Smith, eds.), Chapter 4, pp. 147-184. Univ. of Chicago Press, Chicago, Illinois, 1953.

¹¹ E. J. W. Verwey, *Rec. trav. chim.* **65**, 521 (1946).

the lattice is mainly restricted to the outermost atomic layer. In order to avoid too complicated calculations we have assumed that the atomic positions in the second layer are normal and that no dipoles exist in the ions of this layer."

This assumption is not valid, at least not for solids which contain cations of high field strength and negligible polarizability.

1. WAYS OF LOWERING THE SURFACE ENERGY OF SOLIDS

Unfortunately, there is no method which allows us to measure the surface energy of a solid. A freshly formed surface undergoes a number of changes; for example, it adsorbs gases and vapors. In order to derive a picture of the surface properties of quartz, clay, or similar minerals, we have to examine the mechanisms which can lower the surface energy of a solid.

a. Polarization of Surface Ions

The first change which a freshly formed surface can undergo is the polarization of the surface ions. This process is instantaneous; it involves only a deformation of the electron clouds. This change of the electron density distribution around the core produces a dipole.

The cube faces of ideal surfaces of NaCl or of MgO should be described as an array of cations and anions with incomplete coordination. Ions which are located in a surface undergo polarization because they are exposed to electrical fields. Surface ions are part of the asymmetrical units:

crystal ... anion-cation-space

crystal ... cation-anion-space

These two asymmetrical units extend forces into space which differ both in sign and in magnitude, because of the state of polarization of the surface ions. In the surface of NaCl or MgO, we may neglect the polarization of the cations but not of the anions.

The forces emanating from the anions are decreased by a relatively strong polarization which originates in the asymmetrical field of the cation-anion-space unit where the Cl^- or the O^{2-} ions are exposed to the fields of the Na^+ or Mg^{2+} ions and have no partner at the opposite side. The electron clouds of the anions are pulled towards the cation. This deformation induces a dipole in the anion which decreases its negative field.

We may describe the effect of the different polarizabilities of the ions as one which changes a surface emanating a checkered positive and negative field of equal intensity into one emanating stronger positive and weaker negative forces.

The magnitude of the contribution of this change to the lowering of the surface energy depends on the polarizability of all ions involved. It

can be high for solids which contain cations of high polarizability like Pb^{2+} and Hg^{2+} ions, but it is a minimum for silica or alumina because the small cations, Si^{4+} and Al^{3+} , have negligible polarizabilities.

b. Adsorption of Anions Leading to Charged Particles

The formation of silver iodide from aqueous solutions containing equal quantities of potassium iodide and silver nitrate does not lead to electrically neutral crystals of AgI . The precipitate consists of crystals which have negative excess charges. The solubility product of AgI is very low, of the order of 10^{-7} , so that for analytical purposes one may neglect the concentration of Ag^+ ions which remain in solution if equal numbers of molecules of a silver salt and potassium iodide are allowed to react. The system gains energy by screening the Ag^+ ions in the surface of the crystals with the highly deformable I^- ions rather than with water. The formation of AgI crystals which contain only the polarizable I^- ions in their surfaces requires the participation of fewer Ag^+ ions or of more I^- ions in the precipitate than would correspond to the stoichiometric ratio. Conversely, the supernatant liquid does not contain equal concentrations of Ag^+ and I^- ions but an excess of Ag^+ ions.

Verwey and Kruyt¹² demonstrated that minute crystals of AgI , containing only 10^6 molecules, each have a deficiency of 10^3 Ag^+ ions when formed from a solution containing equimolecular amounts of AgNO_3 and KI .

Whenever a solid contains ions of widely different polarizabilities and its anion to cation ratio is low, so that it does not permit satisfactory screening of the cation, the formation of negatively charged particles provides a means to lower the free energy of the system by decreasing the surface energy of the solid phase. This mechanism is responsible for the stability of many colloids.

c. Distortion of the Surface Structure Leading to an Electrical Double Layer

The polarization of the surface ions changes the checkered positive-negative field of a NaCl or of a MgO cube face into one which emanates weak negative and strong positive fields.

Such a surface can lower its free energy by undergoing a geometrical rearrangement which will better screen the cations, so that the positive forces emanating into space are weakened just as the negative ones. As the screening of the cations is much more important than that of the anions, a surface structure may result which does not contain cations in the extreme outer layer. This is particularly true for those solids where the cation has a small size, low polarizability, and a fairly high charge.

Instead of emanating a checkered plus-minus field of equal intensities,

¹² E. J. W. Verwey and H. R. Kruyt, *Z. physik. Chem. (Leipzig)* **A167**, 137, 149, 312 (1933).

the surface of MgO consists of deformed oxygen ions as the extreme outer layer and slightly recessed Mg^{2+} ions. Formally, one can describe such a surface as consisting of an array of dipole molecules, MgO, the negative parts of which extend into space. This electrical double layer is responsible for the failure of these crystals to adhere. The repulsion between the double layers of crystals in close proximity leads to a phenomenon which has been called "fluidization." The dry powder flows like a liquid because there is no friction between the particles.

d. Adsorption of Dipoles

Usually the conditions under which the surface forms make it possible that foreign substances participate. Instead of forming a surface film with an excess of anions over cations, the crystal can adsorb foreign anions or dipole molecules. The role which this contamination plays in determining the surface energy of solids is so great that some workers in the field of surface chemistry are inclined to attribute most phenomena to contaminations.

e. Interaction of Solids with Water and Formation of a Gouy-Freundlich Diffuse Double Layer

We have seen that the demand of a solid for better screening its surface can immobilize a water film to a considerable depth by repelling protons (Section II). The unique structure of water and the absence of OH^- ions and protons as discrete entities produces a singular effect which is unknown for solutions of electrolytes containing a sufficient number of discrete hydrated anions and cations: the establishment of a diffuse double layer within a liquid.

When quartz grains are brought into pure water, the latter becomes acid and electrically conducting. The acidity of this system is out of proportion to the low solubility of quartz in water and to the very low dissociation constant of silicic acid. Ruff and Hirsch¹³ found that fine quartz powder can produce a pH of 4.85 in conductivity water.

The system quartz-water lowers its free energy by a process in which H_2O dissociates and the OH^- ions are made available for the screening of the Si^{4+} ions in the quartz surface. The OH^- ions impart a negative charge to the quartz and the corresponding H_3O^+ ions in the water produce acidity and are responsible for the increased electrical conductivity of the supernatant liquid.

Using 0.005 *N* HCl instead of pure water makes it more difficult for the silica to be screened by OH^- ions. Therefore, the particles remain electrically neutral.

¹³ O. Ruff and B. Hirsch, *Z. anorg. u. allgem. Chem.* **173**, 14 (1928).

A more accurate description of this interaction would have to consider the particular structure of water and avoid reference to OH^- and H_3O^+ ions as discrete units. The surface of silica produces a film of water which has a lower than average proton density. This description accounts for the fact that the proton density and the electrical potential in the adhering film gradually changes with the distance from the surface (diffuse double layer).

The electrical charge of small particles suspended in water was discovered by Quincke¹⁴ when he observed that these particles migrate toward one pole of a battery (cataphoresis or electrophoresis). Twenty years later von Helmholtz¹⁵ developed his theory of the electrical double layer.

In order to account for the various electrokinetic phenomena, Gouy¹⁶ and Freundlich and Rona¹⁷ proposed a modification of the Helmholtz concept. They suggested that the potential changes gradually with the distance from the surface because the outer part of the electrical double layer consists of adsorbed ions which are under two antagonistic influences: attraction by the electrically charged solid and dissipation in the liquid by thermal motion. These two effects cause the potential to taper off gradually from the surface of the solid toward the dispersing medium (Gouy-Freundlich diffuse electrical double layer).

According to our approach to the subject, the diffuse character of the double layer is the result of the nonexistence of H^+ and OH^- ions as discrete units. We prefer to speak of water as a medium which can assume defective structures. In order to match the structure of water having a lower than average proton density with that having a higher than average proton density a finite transition zone is needed. The electrical potential has a gradient, tapering off gradually just as the rigidity of the adhering water film tapers off with the distance from the solid. The potential gradient diminishes if electrolytes are added because all cations and anions except the H^+ and the OH^- ions are discrete units and in their hydrated state they can form a double layer of the Helmholtz type.

2. THE UNIQUE FEATURES OF THE CLAY MINERALS

In the preceding section the structural changes have been discussed which lower the surface energy of a solid and which make it impossible to derive its surface energy from its lattice energy or from the chemical binding forces. It must be possible, however, to account for the unusual surface activity of some clay minerals at least in a qualitative fashion.

¹⁴ G. Quincke, *Ann. Physik* [2] **113**, 531 (1861).

¹⁵ H. von Helmholtz, *Ann. Physik* [3] **7**, 337 (1879).

¹⁶ G. Gouy, *J. phys.* **9**, 457 (1910).

¹⁷ H. Freundlich and P. Rona, *Sitzber. preuss. Akad. Wiss., Physik.-Math. Kl.* **20**, 397 (1920).

The structure of all clay minerals consists essentially of mica-like layer lattices in which the ultimate building units are SiO_4 , AlO_6 , and MgO_6 groups.¹ A part of the O^{2-} ions contain protons, that is, they participate in the structure as OH^- ions. These groups are linked together in the direction of the a and b axis forming silica, gibbsite, and brucite layers. In the direction of the c axis the structure terminates, so that layers form which are limited to 7 to 30 Å. All clay minerals have in common that they are "infinitely extending" networks only in two dimensions. Thus, these minerals consist of stacks of sheets. On account of this structural characteristic, clay minerals occur as anisodimensional particles, either thin plates mostly less than $2\ \mu$ in diameter or as elongated tubes and laths.

The chemical composition of the clay minerals excludes major polarization effects as a means of lowering the surface energy, because the small noble gaslike cations, Si^{4+} , Al^{3+} and Mg^{2+} , are not sufficiently polarizable.

The compositions alone, however, cannot possibly account for the high surface activity of clays because their ultimate building units occur in many other minerals which do not show plasticity, e.g., zeolites.

This leads to the conclusion that the unique feature of clay minerals lies in their dimensions. Their dimensions are too small for permitting a distortion of the surface structure which has to be accompanied by a depth action. The formation of an electrical double layer of the Helmholtz type is extremely effective in lowering the surface energy of those solids which contain cations of low polarizability and high field strength. This distortion of the surface structure, however, requires a gradual transition into the normal lattice. Most clay minerals do not possess sufficient depth to utilize this means of lowering the surface energy.

The surface properties of montmorillonite and pyrophyllite may serve as an illustration for this factor. Both minerals have basically the same composition $\text{Al}_2(\text{Si}_4\text{O}_{10})(\text{OH})_2$ and the structures of their elementary cells are the same. According to Hofmann *et al.*,¹⁸ the montmorillonite differs from pyrophyllite primarily in the manner in which the layers are stacked up. According to Maegdefrau and Hofmann,¹⁹ the layers in the montmorillonite are stacked up without an orienting principle which, according to our concept, is unfavorable for a depth action. As a result, the montmorillonite is an extremely surface active mineral and the pyrophyllite may be called hydrophobic; it is not easily wet and a pyrophyllite-water mixture is not plastic.

3. PLASTICIZING OF NONPLASTIC MINERALS

Among the naturally occurring minerals some of the clay minerals have unique rheological properties because of their high surface energies com-

¹⁸ U. Hofmann, K. Endell, and K. Wilm, *Z. Krist.* **A86**, 340 (1933).

¹⁹ E. Maegdefrau and U. Hofmann, *Z. Krist.* **A98**, 229 (1937).

bined with platelike or lathlike habitus. It is of basic interest to examine the possibility of plasticizing other minerals, natural or synthetic, in order to evaluate the extent to which these factors contribute to the rheology of the mineral-water system.

Fluorspar, CaF_2 , is a typically nonplastic mineral. The Ca^{2+} and the F^- ions have low polarizability. The anion to cation ratio is only two, so that a CaF_2 crystal should have a fairly high surface energy. Indeed, Dundon²⁰ found that CaF_2 had the highest surface energy of those inorganic compounds which he investigated. The complete lack of plasticity of artificial CaF_2 must, therefore, be due to the unsuitable shape of the particles. The little octahedra which form when an aqueous solution of NaF is allowed to react with a soluble calcium salt tend to produce a rather dense packing. However, if one starts out with an anisodimensional crystal of an insoluble calcium salt, e.g., the platelike $\text{Ca}(\text{OH})_2$ or the more needlelike CaCO_3 , one can obtain anisodimensional CaF_2 crystals by a topochemical reaction. Cohn²¹ obtained a fairly plastic $\text{CaF}_2\text{-H}_2\text{O}$ mixture by allowing a dispersion of slaked lime, that is, a suspension of $\text{Ca}(\text{OH})_2$ crystals, to react with a very dilute solution of HF . His experiments demonstrate the importance of the particle shape and they prove that high surface energy alone is not sufficient for producing plasticity.

Atterberg²² discovered that BaSO_4 is fairly plastic. He determined the degree of plasticity by the amount of water which has to be added to change a workable mixture (one which can be rolled out into a cylinder) into one which can flow. The "flow limit" was determined by bringing the mixture into a porcelain dish, dividing it into two parts by means of a spatula and shaking the dish. The "flow limit" referred to the minimum water content which permitted the two parts to join together on gentle shaking. Atterberg found that the difference between "roll-out limit" and "flow limit" was greatest for the typically plastic clays. Barium sulfate was given the plasticity number 8. A mixture of 100 parts BaSO_4 with 14 parts H_2O could be rolled out and one which contained 22 parts of water, that is, 8 parts more, would flow.

Wilson²³ examined the plasticity of mineral-water mixtures by means of an instrument which recorded a stress-strain curve for a bar twisted at a rate of 3 to 4 r.p.m. He arrived at some interesting generalizations, based on a large number of measurements. Plasticity, according to Wilson, is the result of the presence of a stable viscous film held on the surface of some finely subdivided minerals. Both shape and specific surface activity are considered important for retaining the water film. Cleavage which favors

²⁰ M. L. Dundon, *J. Am. Chem. Soc.* **45**, 2658 (1923).

²¹ R. Cohn, *Z. angew. Chem.* **24**, 1209 (1911).

²² A. Atterberg, *Z. angew. Chem.* **24**, 928 (1911).

²³ E. O. Wilson, *J. Am. Ceram. Soc.* **19**, 115 (1936).

platelike crystals is favorable for producing plasticity. No minerals give plastic mixtures which approach those of clays.

The usefulness of clay minerals in ceramics is based on the fact that a clay-water mixture can hold in suspension nonplastic minerals, e.g., quartz or feldspar. This property permits the shaping of articles by slip casting, by extrusion, or by working on the potter's wheel. There is an ever increasing demand for methods which make it possible to plasticize materials which are more refractory than clay, e.g., pure silica, alumina, zirconium oxide, beryllia, etc.

Podszus,²⁴ as well as Ruff and his associates,²⁵⁻²⁷ were the first ones to carry out systematic work in this direction and their efforts met with partial success. They ground SiO_2 , Al_2O_3 and ZrO_2 very fine and made slip casting possible by chemical treatments. Small particle size combined with the proper surface treatment (acids or hydrolyzing salts) can produce some plasticity in otherwise nonplastic materials. This work supported the view that any theory of plasticity should be based on surface chemistry.

Ruff and Mozala²⁷ describe in detail their method of plasticizing ZrO_2 and similar refractory oxides. The treatment consists in calcining the oxide at 1450°C and milling it wet to a particle size of the order to $0.5\ \mu$. This finely subdivided oxide reacts with acids, for example, HNO_3 or HCl . The degree of reaction is proportional to the time of milling. The material was considered plastic when it was possible to obtain shapes by casting the slip into a plaster mold.

This procedure is typical for all other refractory oxides except MgO , which cannot be treated with aqueous solutions of acids but requires a nonaqueous dispersing medium. Thompson and Mallet²⁸ were able to plasticize calcined MgO by milling it in absolute alcohol for 17 hours.

This brief excursion into the field of plastic mineral-water mixtures, other than clay, brings out that some plasticity can be developed in a large number of minerals provided that they are milled to a fine particle size. Plasticity does not require the presence of a "colloidal phase" which had been considered essential by early workers. As a matter of fact, Hauth,²⁹ who determined the optimum pH conditions which produce a castable slip of fused, finely ground alumina, emphasized that the chemical treatment with acids or bases should not be carried on so far that a large amount of colloidal material is formed. He found that even with respect to pH changes

²⁴ E. Podszus, *Kolloid Z.* **20**, 65 (1917).

²⁵ O. Ruff, *Z. anorg. u. allgem. Chem.* **133**, 187 (1924).

²⁶ O. Ruff and W. Goebel, *Z. anorg. u. allgem. Chem.* **133**, 220 (1924).

²⁷ O. Ruff and J. Mozala, *Z. anorg. u. allgem. Chem.* **133**, 193-219, 416 (1924).

²⁸ J. G. Thompson and M. W. Mallet, *J. Research Natl. Bur. Standards* **23** (2), 319 (1939).

²⁹ W. E. Hauth, *J. Am. Ceram. Soc.* **32**, 394 (1949).

Al_2O_3 is not basically different from clays, provided that the particles are sufficiently fine. He worked with slips which contained particles the size of which was less than 100μ ; 50 % were smaller than 10μ and 10 % smaller than 1μ .

IV. The Interaction of Minerals with Water

Rheology provides the basis for subdividing all matter into three states of aggregation: gases, liquids, and solids. It is not surprising, therefore, that whenever a material has rheological properties which make it difficult to bracket it with one of these three groups, the temptation arises to call it a "fourth state of aggregation."

van Iterson,³⁰ who studied the flow properties of clay bodies under pressure, emphasized that their rheological properties differ from the plasticity of solids, in particular of metals, and of liquids. He suggested that a plastic clay body be called a fourth state of aggregation, a suggestion which reminds one of the times when physical chemists began to be interested in the rheology of glasses. They also suggested that glasses represent the fourth state of aggregation.

In order to develop a theory of the plasticity of clay-water mixtures one has to examine all phenomena which are associated with the high plasticity of clays. In the past, workers in this field developed theories which accounted for only one or two phenomena but which were not applicable to the others. In order to avoid this shortcoming, the most characteristic phenomena involving clay minerals and their interactions with water will be listed and explained on the basis of our atomistic concepts.

1. BASIC PHENOMENA

a. The Rigidity of Water Films

A mixture of clay and water which may contain up to 50 % water does not flow under its own weight. In such a body, water is the continuous phase and the clay particles are surrounded by water films which must be rigid. The thickness of these films depends upon the nature and the size of the clay particles and can reach several hundred molecular layers. Depending upon the method which is used for examining the rigidity of the water film, different values are obtained because its rigidity tapers off gradually. Observing the motion of gas bubbles in bentonite suspensions, Hauser and Reed³¹ found that as little as 0.05 % bentonite is sufficient to stop their rise to the surface. This means that 1 gm. of this highly active clay mineral can immobilize, so to speak, 2 liters of water.

³⁰ F. K. Th. van Iterson, "Plasticiteitsleer," p. 183. Deventeer, Liège, Belgium, 1945.

³¹ E. A. Hauser and C. E. Reed, *J. Phys. Chem.* **40**, 1169 (1936); **41**, 911 (1937).

Norton and Johnson³² studied the properties of monodispersed clay-water systems and calculated the thickness of the water film. For a mixture of kaolinite (0.32μ diameter and 0.04μ thick) they found a film thickness of 0.005μ corresponding to approximately 60 molecules of water. The film thickness decreases with increasing pressure. Grim and Cuthbert³³ emphasized the fact that strong changes in the flow properties take place when the film thickness exceeds that which can be immobilized. They call attention to the fact that some clay minerals require considerable time to bring about the full interaction with water.

The concept that the clay particles are separated by a layer of rigid water is substantiated by the volume changes which accompany the drying of a clay body (see Section IV, 1, j). The only solid form of water which is known is ice.

For this reason Macey³⁴ suggested that the geometry of the structures of ice and the basal plane of montmorillonite favors epitaxis. He attributes the plasticity of clay and the low permeability of clay beds for water to an oriented overgrowth of "ice" on the clay surface. However, Macey's own findings,³⁵ namely, that even the smallest stresses are sufficient to deform clay, speak against an identification of the "rigid water film" with ice. In addition to this discrepancy, the density of the water film excludes it from being identical with ordinary ice.

Recently Williamson³⁶ reviewed the physical relationship between clay and water and came to the conclusion that the "ice" theory is not a satisfactory explanation. Other minerals of the same geometry do not give oriented overgrowth with ice and do not reveal plasticity.

The epitaxis theory, "ice on clay," was extremely convenient because it was the only way to account for the rigidity of the water film.

Our approach to the atomic structure of water, in particular our interpretation of the iceberg theory (see Section II), solves one of the basic difficulties confronting those who want to explain the plasticity of clay bodies. Water can be immobilized by electrical fields by a mechanism which bears no relation to its crystallization. The rigidity of the water film which surrounds the clay particles tapers off gradually. This is important with respect to the observation that clay bodies yield under the smallest stresses. Our atomistic explanation of the nature of the rigid phase does not conflict with the volume relation between ice and water, a difficulty encountered by Frank and Evans.⁴

³² F. H. Norton and A. L. Johnson, *J. Am. Ceram. Soc.* **27**, 77 (1944).

³³ R. E. Grim and F. L. Cuthbert, *J. Am. Ceram. Soc.* **28**, 90 (1945).

³⁴ H. H. Macey, *Trans. Brit. Ceram. Soc.* **41**, 73 (1942).

³⁵ H. H. Macey, *Trans. Brit. Ceram. Soc.* **43**, 5 (1944).

³⁶ W. O. Williamson, *Trans. Brit. Ceram. Soc.* **50**, 10 (1951).

b. Sedimentation

Measurements of the sedimentation volume of a finely subdivided solid in different liquids provide useful information about its surface energy. The relation between the two entities, however, is not simple and at first glance may seem paradoxical. For particles which have the same size and shape, the sedimentation volume increases with increasing surface energy of the solid. It may seem paradoxical that the stronger the surface forces of the particles, the looser should be the aggregate which they form on sedimentation.

A closer analysis of the mechanism of sedimentation, however, reveals the reason for this relationship. The particles move in the dispersing medium because they are subjected to gravity or to centrifugal force. Two particles which come into contact either slide over one another or adhere. Adhesion takes place when the external forces are less than or equal to the binding forces between the two particles.

Liquids which are good screeners for the electrical fields of the surface ions are conducive to small sedimentation volumes. This relation is of practical interest because the sedimentation volume controls the amount of solids in ceramic casting slips.

Harkins and Gans³⁷ performed a series of experiments which elucidate this interaction. Titanium dioxide suspended in benzene (free of water) had a relatively high sedimentation volume and was very sensitive to additions of oleic acid or other long chain acids. A monomolecular layer of oleic acid decreased the sedimentation volume to one-third of the original, because the hydrocarbon chains act as a lubricant which permits gliding. The adhesion forces between TiO_2 crystals are weakened when their surfaces are coated and screened by the long chain fatty acids.

de Waele and Mardles³⁸ found that the centrifuged volume of TiO_2 is larger in xylene than in the more polar and, therefore, better screening *n*-butyl alcohol. However, the centrifuged volume of TiO_2 in *n*-butyl alcohol does not expand when the sediment is permeated with xylene. This experiment proves that the sedimentation volume is determined only by the forces acting between the solid particles and not by the forces between the solid and the liquids. The forces between the solid particles are modified by the chemisorbed molecules. The removal of a lubricant, after it has served its purpose, does not lead to the state of higher potential energy which a system would have assumed if no lubricant had been present.

The extent to which a liquid can screen the surface of a solid can be

³⁷ W. D. Harkins and D. M. Gans, *J. Phys. Chem.* **36**, 86 (1932).

³⁸ A. de Waele and E. W. J. Mardles, *Proc. Intern. Rheol. Congr. 1st Congr. Scheveningen*, Part II, p. 166 (1949).

TABLE III
SEDIMENTATION VOLUME AND SPECIFIC VISCOSITY OF ZnO SUSPENSIONS
(After Davis⁴⁰)

Liquid	Sedimentation volume cc./gm.	Specific viscosity
Benzyl alcohol	2.2	0.25
Linseed oil	2.3	0.26
Nitrobenzene	2.5	0.26
Ethyl alcohol	2.9	0.28
Mineral oil	2.9	0.3
Toluene	2.6	0.4
Water	4.5	0.5
Chloroform	3.8	0.6

estimated from the heat of wetting. Bartell and Almy³⁹ determined the heat of wetting of different liquids on silica gel and found that water had the highest heat of wetting, and the nonpolar liquids the lowest: water, 19.0 cal./gm.; nitrobenzene, 15.2; benzene, 12.5; carbon tetrachloride, 8.5; and hexane, 7.0.

Table III shows the relation between the specific viscosity of a suspension and the sedimentation volume, according to Davis.⁴⁰ Zinc oxide is suspended in different liquids. There is a certain parallelism between specific viscosity and sedimentation volume, because both properties are controlled by the surface forces of the ZnO particles. Liquids which are poor screeners for ZnO (chloroform) cannot lower its surface forces. Strong surface forces, in turn, lead to high viscosity and to a large sedimentation volume.

Recent experiments^{41a,b} on the sedimentation of clay in aqueous solutions of wetting agents illustrates the importance of the screening qualities of solutions in determining sedimentation behavior. Electrodialyzed kaolinite suspensions (25 % solids) containing 0.5 % by weight of anionic, nonionic, and cationic wetting agents were allowed to settle for six days and the resulting sedimentation volumes compared with that obtained with water. The sedimentation volumes produced with anionic solutions were generally smaller and those obtained with cationic solutions were larger than that volume produced with water alone (Fig. 2). Solutions with nonionic wetting agents produced sedimentation volumes either larger or smaller than that

³⁹ F. E. Bartell and E. G. Almy, *J. Phys. Chem.* **36**, 985 (1932).

⁴⁰ N. Davis, *Ind. Eng. Chem.* **24**, 1137 (1932).

^{41a} Office Naval Research Tech. Rept. No. 61 (4th Sect.) Contract N6ONR269 T.O. 8, NR 032-264. Pennsylvania State University, University Park, Pennsylvania, March, 1955.

^{41b} W. C. Ormsby, R. M. Witucki, and W. A. Weyl, *Natl. Acad. Sci.-Natl. Research Council, Publ.* **456**, 251-272 (1956).

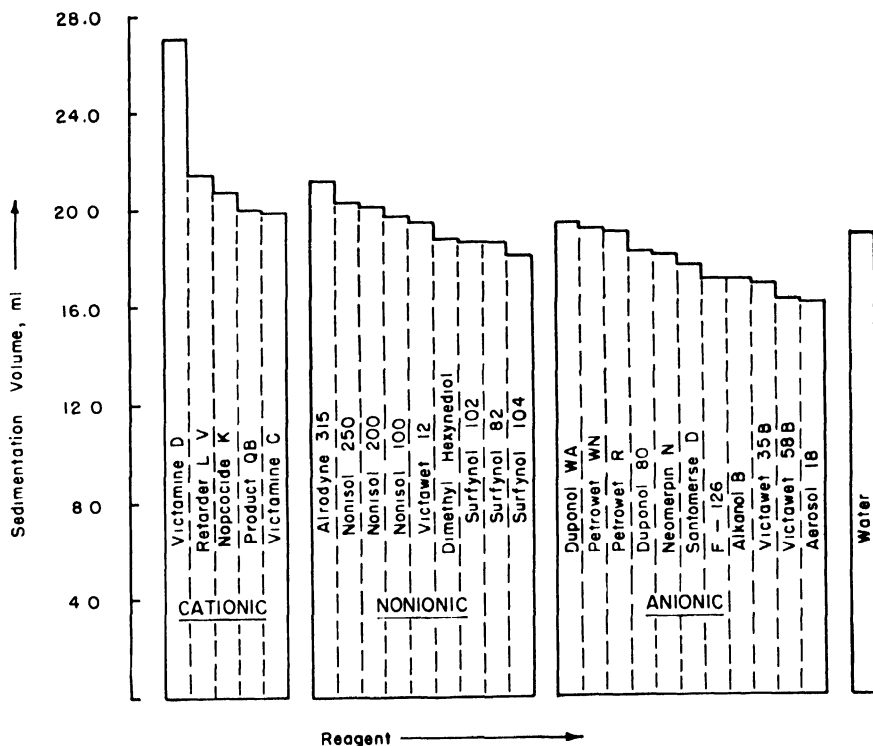


FIG. 2. Sedimentation volumes of kaolinite suspensions (25% solids) as a function of wetting agent additions (0.5%).

of water; no consistent trend was noted. There seems to be no simple relation between sedimentation volume and solution pH or surface tension. The improved screening qualities of water containing anionic reagents is attributed to the presence of large anions which enables the surface forces of the clay particles to be satisfied in a smaller volume. On the other hand, cationic reagents furnish relatively small anions and a relatively large volume is required to satisfy the surface forces of the solid. Nonionic reagents may fall in either group.

c. Acidity and Electrical Conductivity of Suspensions

Water becomes electrically conducting when finely powdered quartz is added. Depending upon the amount of quartz and its particle size, the water also becomes an acid and its pH can fall as low as 4.8.

This phenomenon has been observed and described several times.^{13,42}

⁴² G. van Praagh, *Nature* **143**, 1068 (1939).

No satisfactory explanation could be given because conventional concepts cannot account for the occurrence of such a high acidity as the result of a practically insoluble substance. Quartz is slightly soluble in water but this solubility cannot account for the acidity because of the low value of the dissociation constant of silicic acid.

In the same way, the addition of bentonite to pure water increases its electrical conductivity and its hydrogen ion concentration. The electrical conductivity of a dilute aqueous solution of HCl is a function of its concentration and its hydrogen ion activity, but no such relation exists for water which has been "acidified" by bentonite. Hauser and Reed³¹ studied the influence of the particle size of bentonite suspensions on its base exchange capacity, its pH, and its electrical conductivity. They examined several fractions between 14 and 87 m μ average equivalent spherical diameter. The acidity of the suspensions increased with increasing concentration of the bentonite. The electrical conductivity was found to be a function of the concentration and the particle size of the bentonite, but there was no relation between the electrical conductivity of the suspensions and their hydrogen ion activities. The finer the particle size of the bentonite, the greater the obstacles which the carriers of the electrical current have to overcome in their path. As we learn from the work of the same authors,³¹ the smaller the particles of bentonite, the larger is the volume of water which they can immobilize. With decreasing particle size the discrepancy increases between the hydrogen ion activity as determined by a static method (pH) and that derived from a dynamic method (electrical conductivity).

d. Electrokinetic Phenomena

Quincke¹⁴ in 1850 discovered that small particles immersed in water assume an electrical charge. Some twenty years later von Helmholtz¹⁵ developed his theory of the electrokinetic phenomena. Gouy¹⁶ and Freundlich and Rona¹⁷ suggested a modification to the Helmholtz theory (Gouy-Freundlich diffuse electrical double layer). They suggested that the potential changes gradually with the distance from the surface. If the outer part of the double layer consists of adsorbed ions they must be subjected to two antagonistic influences; attraction by the electrically charged solid and dissipation by thermal motion. These two effects cause the potential to decrease gradually from the interface toward the dispersing medium.

According to our approach (Section III, 1,e), the diffuse character of the double layer is due to the fact that H⁺ and OH⁻ ions do not occur in solution as discrete units. We treat water as a continuous network of O²⁻

and H^+ ions which can deviate from stoichiometric composition. The change of water with a lower than average proton density into that with a higher than average proton density requires a transition zone. Thus, the electrical potential tapers off gradually in the same fashion as the rigidity of a water film tapers off with the distance from the solid. The potential gradient in such a zone is very sensitive to electrolytes because cations and anions other than H^+ and OH^- ions do not need to form a diffuse double layer.

Electrokinetic phenomena occur when external forces disturb the static equilibrium of a liquid system which contains dispersed, charged particles. For example, a particle surrounded by a diffuse double layer does not take along the total layer when it falls under the influence of gravity (Dorn effect) or when it migrates in an external electrical field (electrophoresis). Somewhere the electrical double layer "breaks off" and the exact place where that happens depends upon the disturbing force.

This concept explains satisfactorily the four major electrokinetic phenomena: sedimentation potential (Dorn effect), streaming potential, electroosmosis, and electrophoresis.

Our approach is based upon the assumption that the surface of quartz interacts with water in the same fashion as a highly charged cation. Both surround themselves with a film of water which has a lower than average proton density. A film of nonstoichiometric, immobilized water lowers the positive charge of a hydrated cation, for example, of an Al^{3+} or Th^{4+} ion. This unique mechanism makes it possible for water to dissolve and to dissociate substances such as $Al_2(SO_4)_3$ or $Th(NO_3)_4$, that is, salts which are insoluble in all other solvents, even in liquid ammonia and hydrocyanic acid.

Suspensions and solutions, however, differ in their response to mechanical forces. The quartz particle can be subjected to mechanical forces and it moves under the influence of gravity; a single Al^{3+} or Th^{4+} ion does not. A quartz particle during its fall comes in contact with water of stoichiometric composition. The particle increases its negative excess charge, because more protons can be expelled from the adhering film into water which has a stoichiometric composition than into water which already has an excess of protons. Using the conventional terminology, quartz falling through a column of water picks up, so to speak, more and more OH^- ions and leaves behind a trail of protons. This process, which causes the "iceberg" around the quartz to grow, leads to a potential difference between the top of the water column (positive) and the bottom where the quartz particles settle (Dorn effect or sedimentation potential).

If a fine powder of quartz is allowed to settle from its aqueous suspension upon a quartz plate, the rigidity of the water film and the Coulomb re-

pulsive forces prevent the two solids from coming into close contact. Within a certain distance, thousands of water molecules apart, the quartz particle ceases to fall but continues its Brownian motion.⁴³

The streaming potential is essentially the same as the sedimentation potential, only that here the solid, with its diffuse electrical double layer, remains stationary whereas the liquid moves under an external force. The faster the liquid is pressed through a capillary or through a plug of quartz powder, the greater is the quantity of the electrical double layer which is sheared off from the walls of the tube or from the quartz grains and the higher becomes the potential.

The potential at the surface of shear between the streaming liquid and the glass has been called the "zeta potential" by H. Freundlich. This "zeta" or "electrokinetic" potential depends upon the forces which are applied, because the latter determine the place where shear occurs.

In the same fashion, as motion of the particles through the liquid medium can develop a potential difference, the application of an external field can produce motion. If the solid remains stationary, this phenomenon is called "electroosmosis." If the liquid is stationary and the solid moves in an electrical field, it is called "electrophoresis."

It is characteristic for the nature of the Gouy-Freundlich double layer that these phenomena are subdued when electrolytes are present. The electrokinetic phenomena disappear nearly completely when the concentration of electrolytes exceeds the order of 10^{-3} moles/liter. The classical work of Freundlich and his associates⁴⁴ illustrates the complexity of the interaction of different electrolytes with a glass surface as expressed by the change of the zeta potential. Our approach provides an atomistic explanation.

In contact with solutions of four electrolytes, KCl, BaCl_2 , $\text{La}(\text{NO}_3)_3$, and $\text{Th}(\text{NO}_3)_4$, in concentrations of 10^{-6} moles/liter (Fig. 3), the zeta potential is nearly doubled in the case of KCl but only slightly increased by BaCl_2 ; $\text{La}(\text{NO}_3)_3$ has little influence and $\text{Th}(\text{NO}_3)_4$ reverses the sign.

The addition of KCl can improve the screening of the glass surface because screening anions are now available and K^+ ions can replace some protons of the chemisorbed OH^- ions, improving the screening power of the O^{2-} ions. As a result, the first addition (10^{-7} and 10^{-8} moles/liter) of KCl increases the negative charge of the surface. As the concentration of K^+ ions increases (K^+ ions, unlike the H^+ ions, do not need to remain a large distance away from the surface) they participate in the structure of the adhering film and decrease the diffuse character of the double layer. With increasing concentration of KCl, the Gouy-Freundlich diffuse double layer

⁴³ A. von Buzagh, *Kolloid Z.* **47**, 370 (1929); **51**, 105, 230 (1930).

⁴⁴ H. Freundlich, E. Ettisch, and P. Rona, *Z. physik. Chem. (Leipzig)* **116**, 401 (1925).

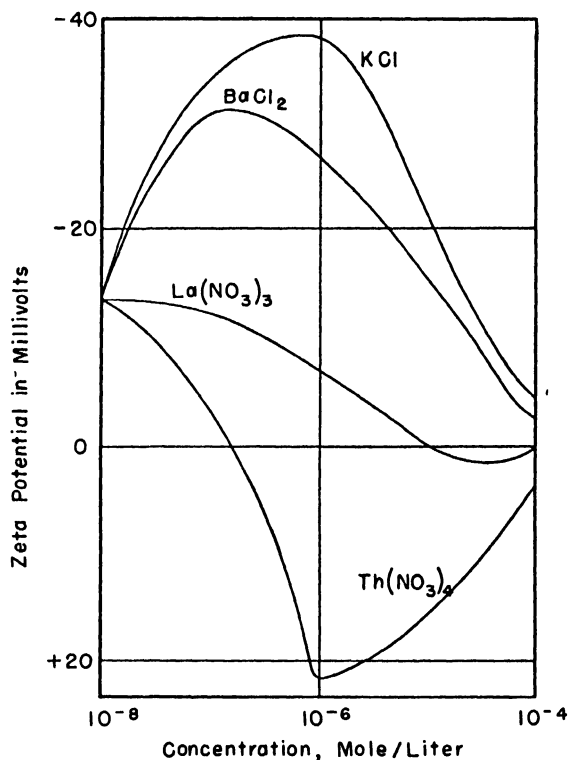


FIG. 3. Electrokinetic potentials at glass-solution interfaces. (After H. Freundlich, E. Ettisch, and P. Rona.⁴⁰)

changes into a Helmholtz double layer. From Fig. 3 one can see that this process has eliminated the diffusivity of the double layer when the concentration of KCl reaches the order of 10^{-3} moles/liter: the zeta potential has become zero.

The addition of thorium nitrate produces a different effect. The negative zeta potential is lowered by Th^{4+} ions so that it becomes zero at a concentration of 10^{-7} moles/liter, but further additions produce a new positive zeta potential. This reversal of the sign indicates that a solution of $\text{Th}(\text{NO}_3)_4$ does not contain only hydrated Th^{4+} ions. A thorium nitrate solution contains complexes in which several hydrated Th^{4+} ions share OH^- ions. The thorium ion has the highest charge of any stable monatomic cation. Its large size and its high coordination number makes it possible for it to surround itself with a large number of anions. At a concentration of 10^{-6} moles of $\text{Th}(\text{NO}_3)_4$ per liter, the glass surface with its chemisorbed Th^{4+} ions is screened by water with a lower than average proton density. However, the

number of protons which have to be repelled from this volume of water is smaller than the number of excess charges which are introduced into the glass surface by the adsorbed Th^{4+} ions. As a result, the glass surface assumes a positive excess charge. The positive charge of some colloids (ThO_2 , ZrO_2 , TiO_2) is due to the same relation. The response of the zeta potential of the surface toward solutions of BaCl_2 and of $\text{La}(\text{NO}_3)_3$ is intermediate between that of KCl and $\text{Th}(\text{NO}_3)_4$.

e. Thixotropy of Suspensions

Some plastic systems have yield values which decrease if the system is subjected to mild vibrations. This phenomenon, called "thixotropy," is characteristic for certain clay suspensions. When a fluid suspension of montmorillonite in water is poured into a test tube and allowed to stand for some time, it changes into a rigid gel and does not flow out if the test tube is turned over. However, tapping of the test tube is sufficient to liquefy the gel. This process is not accompanied by a heat effect and can be repeated indefinitely. It indicates that the structural features which are responsible for the rigidity of the gel can be disturbed by slight vibrations.

As far as an explanation of the mechanism of thixotropy is concerned, there are essentially three schools of thought. One group of scientists, in particular Freundlich,⁴⁵ von Engelhardt,⁴⁶ and Hauser,⁴⁷ assume long range electrical forces which permit the individual particles to interact over distances of the order of 1000 Å.

Another group, Usher,⁴⁸ Kuhn,⁴⁹ and Hofmann,⁵⁰ prefer a mechanical picture according to which the particles touch one another, adhere on contact, and build up a spacious network resembling a house of cards.

A third group explains the rheology of clay-water mixtures by assuming that the water which surrounds the clay particles becomes rigid. This view is shared by Macey,³⁴ McBain,⁵¹ Grim and Cuthbert.³³

Thixotropy has been observed in many systems involving a great variety of solids, e.g., clay, carbon, iron oxide, and organic substances (indanthrene dyes). The phenomenon is not restricted to water as the dispersing medium but may also occur in benzene. Maybe even more spectacular than the variety of compositions are the wide concentration limits in which the phenomenon has been observed. The solid to liquid ratio which permits thixotropy varies from 1:1 to 1:2000. It is reasonable to expect that the

⁴⁵ H. Freundlich, *Actualités sci. et ind.* No. 267 (1935).

⁴⁶ W. von Engelhardt, *Kolloid Z.* **102**, 217 (1943).

⁴⁷ E. A. Hauser, *Chem. Revs.* **37**, 287 (1945).

⁴⁸ F. L. Usher, *Proc. Roy. Soc.* **A125**, 143 (1929).

⁴⁹ W. Kuhn, *Z. physik. Chem. (Leipzig)* **A161**, 564 (1931).

⁵⁰ U. Hofmann, *Kolloid Z.* **125**, 86 (1952).

⁵¹ J. W. McBain, *J. Phys. Chem.* **30**, 239 (1926).

TABLE IV
THIXOTROPY, SEDIMENTATION VOLUME, AND DIMENSIONS OF CLAY PARTICLES
(After Hofmann⁵⁰)

	<i>Shape and dimensions (mμ) of crystals</i>	<i>Water content cc./3 gm. clay</i>	<i>Sedimentation volume cc./gm. clay</i>
Kaolin	Plates, 500 \times 500 \times 15	5.5	4.5
Halloysite	Laths, 2000 \times 100 \times 50	10.0	10.0
Ca-Bentonite	Plates, 700 \times 700 \times 15	8.0	5.0
Na-Bentonite	Plates, 700 \times 700 \times 2	30.0	40.0

solidification of a suspension of graphite as observed by McDowell and Usher⁵² in organic media (ratio 1:1) is caused by direct contact of the particles or their forming a house of cards. The strongly anisodimensional character of clay minerals makes it possible for a few per cent of solid matter to form a house of cards which has a very large volume. This explanation, however, does not explain why this phenomenon can also appear in a 0.05 % montmorillonite suspension in water.⁵¹ Thixotropy is a phenomenon which requires anisodimensional particles and relatively loose packing.

It seems to be an established fact that the sol-gel transformation does not lead to a definite geometrical alignment of the particles. The strength of thixotropic gels increases with decreasing particle size. Hauser and his associates have greatly contributed to the elucidation of the mechanism of the sol-gel transformation by observing the process in the ultramicroscope. The Brownian molecular motion comes to a standstill and in truly thixotropic systems of highly dispersed bentonite fractions, the particles which have ceased to move seem to be clearly separated from each other by the water.

The findings of Hauser are in no way contradictory to the findings of Hofmann,⁵⁰ who studied suspensions which contained higher concentrations of the clay, a condition which is conducive to the formation of a "house of cards" (Table IV).

The thixotropy was measured by determining the water content of a sol containing 3 gm. of the clay which sets after 6 sec. when poured in a glass tube 2.0 cm. wide.

In order to give an atomistic explanation for this reversible process one may conveniently divide it into two steps: the endothermic dissociation of water or the formation of volume elements with lower and higher than average proton density, and the exothermic interaction between the clay surface and the water which has the lower proton density. The net result of the two steps is a sol-gel transformation with no apparent heat effect.

⁵² C. M. McDowell and F. L. Usher, *Proc. Roy. Soc. A***131**, 564 (1931).

In some cases the sol-gel transformation takes several hours but can be accelerated by very mild vibrations. This phenomenon has been called "rheopexy" by Freundlich and Juliusburger.⁵³

f. Flow of Water through Porous Media

We assumed that in contact with a solid, water changes into a phase which has a higher or a lower proton density depending upon the nature of the solid. In both cases the water film loses its fluidity. This concept, namely, that water in close proximity to solids ceases to be a Newtonian liquid and assumes structural viscosity, explains the flow behavior of water through narrow capillaries, for example, porous ceramic materials.

Volkova⁵⁴ measured the effect of the particle size upon the rates of capillary flow of water and of toluene through beds of powdered quartz. These beds can be treated as bunches of capillary tubes. The ratio of the rates of flow for the two liquids should be constant and be independent of the size of the pores. Volkova found that this ratio is constant only for quartz grains which are larger than 0.01 mm. With decreasing size of the grains, however, the rate of flow of water decreased more than that of toluene. These experiments indicate that the immobilizing effect of the quartz upon water is greater than that upon toluene.

Similar phenomena were observed by other workers. Recently, Henniker⁵⁵ reviewed the literature on this subject and made an important contribution. He found that the flow rate of distilled water through a porcelain filter candle having a pore radius of 0.05μ was 20 % lower than that of an aqueous solution of KCl. He measured the streaming potential and found it too small to account for this effect. He wrote: "A tentative explanation links the intense electric field existing in the electrical double layer with the augmentation of the viscosity of liquids in the presence of strong fields."

According to our approach, the porcelain surface produces a film of water which has a lower than average proton density. The repulsion of protons into more remote positions immobilizes the water. The addition of an electrolyte such as KCl produces two effects. First, the K^+ and Cl^- ions improve the screening of the porcelain surface and thus weaken its influence upon the water. Second, these ions disturb the immobilized film by their electrical fields. Recent experiments of Hosler and Hosler⁶ showed that the degree to which a given volume of water can be supercooled decreases sharply when small amounts of salts were added. Additions to the system which lower the freezing point increase the rate of formation of ice nuclei.

⁵³ H. Freundlich and F. Juliusburger, *Trans. Faraday Soc.* **31**, 920 (1935).

⁵⁴ Z. V. Volkova, *Acta Physicochim. U. R. S. S.* **4**, 635 (1936).

⁵⁵ J. C. Henniker, *Revs. Modern Phys.* **21**, 322 (1949); *J. Colloid Sci.* **7**, 443 (1952).

Macey,³⁴ in connection with studies of the drying mechanism, investigated the flow of water and other liquids through clay. He found that liquids such as benzene, nitrobenzene, and pyridine passed through clay 100,000 to 1,000,000 times as fast as water through the same clay. In comparing the behavior of clay-water with other clay-liquid systems, Macey writes: "Differences in particle size, arrangement and possibly interlamellar swelling all play their part, but they cannot alone account for the large order of difference in the rates of flow found." This relation between flow rate, presence of electrolytes, and nature of the wall is of paramount interest for ceramics, for soil science, and for biophysics. Our approach introduces a new parameter into the treatment of flow through capillaries, namely, the thickness of the wall. The forces which a solid exerts upon a liquid, e.g., when flowing through a capillary, depend upon the dimensions of the capillary including the thickness of its wall.

The flow of aqueous solutions of wetting agents through clay has been investigated^{41a, b} with apparatus commonly employed in the evaluation of drilling muds.⁵⁶ In these tests a kaolinite suspension (25 % solids) was placed in a filter cup and subjected to an air pressure of 15 p.s.i. The rate of filtration was measured as a function of time and was found to depend on the type of filter cake produced by the clay. Results with various wetting agents (Fig. 4) indicate that an anionic reagent produces a dense structure of the filter cake whereas nonionic and cationic reagents produce a loose structure. Apparently the better screening afforded by the anionic wetting agent permits a closer approach of the clay particles which leads to a denser structure. On the other hand, nonionic and cationic wetting agents produce a more open structure.

Flow of liquids through porous media provides evidence for the depth action which a solid produces in a liquid. Recently, Martin and Mohiuddin⁵⁷ reported a phenomenon which strikingly illustrates the depth action of a surface and the failure of the conventional approach to provide an explanation.

"In an investigation of the fascial spaces of the face and neck, rubber latex was used as an injection material. Unfortunately, when efforts were made to inject various spaces with latex by means of a large syringe and metal needle, the latex always solidified in the needle and would not flow, no matter how high a pressure was used. After consultation, ammonia and other alkalies were first mixed with the latex, but to no avail; it always solidified almost immediately in the needle. The idea then occurred to us to try glass needles made by drawing out a glass tube over a Bunsen burner. Very surprisingly the rubber flows perfectly through them. The latex solidi-

⁵⁶ W. F. Rogers, "Composition and Properties of Oil Well Drilling Fluids," pp. 112, 268. Gulf Publishing Co., Houston, Texas, 1953.

⁵⁷ C. P. Martin and S. O. Mohiuddin, *Science* **118**, 364 (1953).

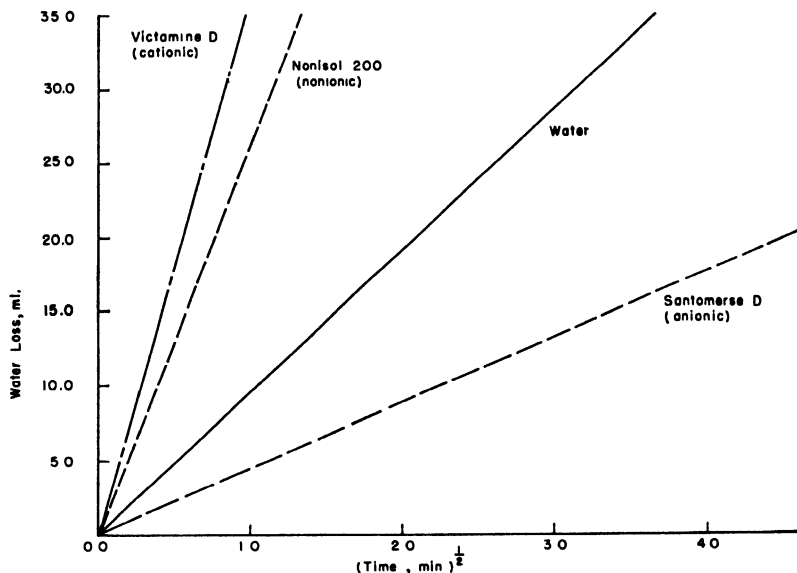


FIG. 4. Relative filterabilities of kaolinite suspensions (25% solids) as a function of wetting agent additions (0.95% by weight).

fies in any metal needle but flows freely through a glass needle of the same bore. We venture no explanation of this phenomenon, but since the fact is not apparently well known, this note may save others from considerable trouble and disappointment."

The interaction between two media affects their mechanical properties, a phenomenon which is utilized in improving the strength of high polymers and elastomers. Carbon black as a "filler" for rubber has unique properties. Present trends in developing new engineering materials take advantage of the effect of the depth action which results at the contact between metals and oxides, carbides, or nitrides.

g. Flocculation and Deflocculation

In the second half of the eighteenth century, French ceramists discovered that clay-water suspensions became more fluid when alkali was added. Through the addition of potash, clay could be made castable with about half the amount of water which was necessary without alkali. This discovery was kept secret for more than a hundred years.

The interaction of clay minerals with salts, acids, and bases is of paramount importance for agriculture, ceramics, and several other technologies. Chemically speaking, clay minerals are alumino-silicic acids. A heteropoly acid can react with bases and forms salts and its anion can copolymerize

with other anions which have a tendency to polymerize, i.e., to form iso- or heteropoly acids (phosphates).

The principle features of the interaction of clay with soluble salts can best be seen from a new field of analytical chemistry: paper chromatography. Chromatography is based on the screening of a solid, either alumina, silica, or paper. If paper is wetted with an aqueous solution of $\text{KCl} + \text{NaCl} + \text{LiCl}$ some of the protons of the cellulose or its oxidation products are replaced by K^+ , Na^+ , and Li^+ ions. The large K^+ ion has a weak electrical field, its "contrapolarizing effect" is smallest and, as a result, the replacement of a H^+ ion of an OH or COOH group by a K^+ ion improves the screening of the cellulose. Na^+ has a similar but weaker effect. Li^+ ions, having the strongest contrapolarizing effect among the alkalies, cannot contribute much to the screening of the surface. As a result, if a stream of a suitable liquid is allowed to flow through the paper, it replaces and carries away the three salts but at different rates. Because of its better screening effect, KCl is retained more strongly than NaCl . LiCl is the poorest screener among the three halides and, consequently, it is the first to be replaced by the solvent molecules. Thus, under controlled conditions the three salts can be separated in a stream of a solvent. Paper impregnated with the chlorides of the alkaline earths behaves similarly to one containing the three alkalies. The Ba^{2+} ions have the weakest field and are retained most strongly, whereas the Mg^{2+} ions are the ones which can be washed out most easily. As far as their mobilities are concerned the alkaline earth ions follow the series Ba^{2+} , Sr^{2+} , Ca^{2+} and Mg^{2+} . These experiments are the key to the interaction of clays with electrolytes.

The same process which we perform in the laboratory with a strip of paper or a few grams of activated alumina has been going on in nature on a gigantic scale for millions of years. The weathering of rocks produces soluble alkali salts, the K^+ ions are retained by the soil minerals, and the Na^+ ions are washed into the oceans where they have accumulated over geological periods.

The base exchange capacity is expressed in milliequivalents of cations per 100 gm. of clay. Its magnitude depends upon the nature of the minerals, as can be seen from the following data⁵⁸: montmorillonite, 60–100 meq./100 gm.; attapulgite, 25–30; illite, 20–40; kaolinite, 3–15.

Only a few of the numerous investigations on the deflocculation of clay slips by salts lend themselves to theoretical interpretation. Most plastic clay minerals are contaminated by organic matter (humic acid), which has a profound influence on the rheological properties.

In addition, clays contain soluble salts and some clays contain considerable quantities of ferric hydroxide. All these substances have to be re-

⁵⁸ R. E. Grim, *J. Geol.* **50**, 225 (1942).

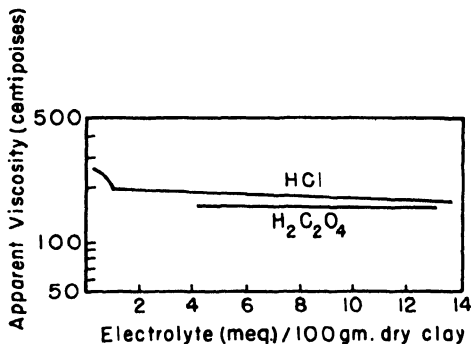


FIG. 5a. Viscosity relations on addition of acids to a suspension (16% by weight) of electrodyalized kaolinite. (After Johnson and Norton.⁶⁹)

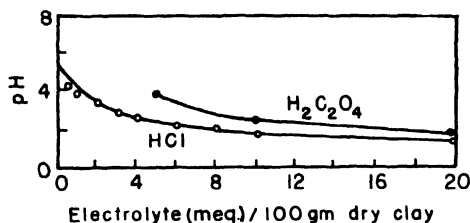


FIG. 5b. Titration relations on addition of acids to a suspension (16% by weight) of electrodyalized kaolinite. (After Johnson and Norton.⁶⁹)

moved in order to obtain a clear picture of the effect which the alkalis have on the viscosity of clay. Johnson and Norton⁶⁹ give a detailed description of the methods which are available for the purification of a kaolinite. They describe the effects which the different impurities have on the response of clays to alkalis. Lignite or humic acid, for example, causes clay to form a strongly thixotropic suspension when alkali is added. Digesting the clay for several days with hydrogen peroxide destroys the organic matter. Alkali and soluble calcium salts can be removed by electrodyalisis.

Figures 5 and 6 show how the viscosity and the pH of a purified kaolinite suspension respond to the addition of an acid and of a base. No drastic change occurs upon the addition of HCl. The viscosity at first is lowered slightly but further additions have no effect. The titration curve is substantially the pH of water with increasing additions of HCl.

The titration curve with NaOH, however, is most revealing. Until approximately 4 meq. of NaOH are added little change takes place. The clay surface exerts a buffering action comparable to that of a weak acid (aluminosilicic acid). Beyond this point further addition of NaOH causes

⁶⁹ A. L. Johnson and F. H. Norton, *J. Am. Ceram. Soc.* **24**, 64, 189 (1941).

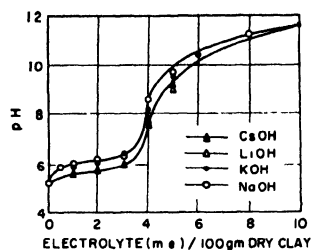
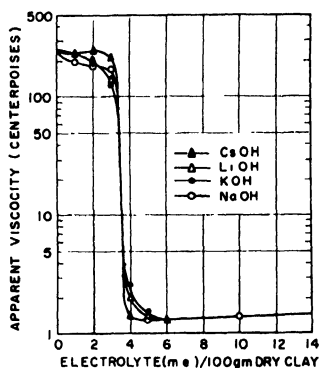


FIG. 6a. Viscosity relations on addition of hydroxides of alkali metals to a suspension (16% by weight) of electrodyalized kaolinite. (After Johnson and Norton.⁵⁹)

FIG. 6b. Titration relations on addition of hydroxides of alkali metals to a suspension (16% by weight) of electrodyalized kaolinite. (After Johnson and Norton.⁵⁹)

TABLE V
MINIMUM VISCOSITY OF A 16% KAOLIN SUSPENSION IN CENTIPOISES
(After Johnson and Norton⁵⁹)

Cation	Hydroxide	Carbonate	Silicate	Oxalate	Sulfate	Chloride
Cs	1.3					
Li	1.3					
K	1.3					
Na	1.3	1.7	1.7		80	140
NH ₄				2.0		
Ba	70					
Sr	90					
H	250			150		170

the pH to increase rapidly and the viscosity to drop. The same effect can be obtained with the other alkalis, LiOH, CsOH, and KOH; the curves are essentially identical but show differences in details.

Table V summarizes some of the results obtained by Johnson and Norton. For several reagents this table lists the maximum degree of deflocculation (expressed by the minimum viscosities which could be obtained). Complete deflocculation requires the presence of OH⁻ ions in the suspending medium. This can be achieved only by alkali hydroxides or by those alkali salts (carbonate, silicate) which hydrolyze.

The addition of a deflocculant caused the viscosity to decrease gradually until approximately 4 meq. were added. The exact point lies between 3.5 and 4.5 and depends on the purity of the kaolin. At this point the viscosity drops with great suddenness to less than $\frac{1}{100}$ of its original value.

The pH value of the clay slip (16% clay) is approximately 5.3. This value gradually increases upon the addition of hydroxides to 6.0, but after 4 meq. alkali hydroxide, $\text{Sr}(\text{OH})_2$ or $\text{Ba}(\text{OH})_2$, have been added it increases much more rapidly.

h. Adhesion Properties

The gradual addition of water to clay leads to a stage in which the mixture is "sticky," i.e., where it adheres to a wettable surface such as glass. This phenomenon is characteristic for clay-water mixtures in a certain composition range which depends upon the nature of the clay mineral, its particle size, the presence of electrolytes, and on the external pressure.

According to Mellor,⁶⁰ the minimum amount of water which produces stickiness decreases with increasing pressure. According to Grim,⁶¹ a Na^+ clay is less sticky than the corresponding H^+ clay.

The observations of von Buzagh⁴⁸ concerning the adhesion of quartz particles to glass can be used to derive an atomistic explanation of the adhesion of clay (see also Section IV, 1,d).

A dilute suspension of quartz particles was allowed to settle upon a horizontal glass plate. When the submerged glass plate was carefully turned over some of the particles fell off, others adhered. Particles of approximately 3μ were best suited for the experiment, larger ones fell off, and those which were much smaller remained at too great a distance from the plate. The addition of electrolytes affects the adhesion. A modified method for studying the phenomenon was based on tilting the glass plate and measuring the angle where the particles began to slide off.

For a certain particle size von Buzagh found that in pure water 50% of the particles did adhere and 50% fell off. This condition could be easily changed into 95% adherence by adding to the water the following concentrations of electrolytes: LiCl , 1.4 mM./liter; NaCl , 1.0; KCl , 0.4; CaCl_2 , 0.04; SrCl_2 , 0.03; BaCl_2 , 0.02; $\text{Th}(\text{NO}_3)_4$, <0.002 . The effectiveness of the electrolytes in increasing the adhesion follows the Schulze-Hardy Rule. This suggests the following atomistic explanation:

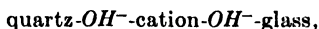
Very small quartz particles surround themselves with water of a lower than average proton density because they lack the necessary volume for developing a distorted surface structure which sufficiently screens the surface cations (see Section III, 1,c). On settling they take along a halo of rigid water which prevents direct contact with the glass plate. At a certain point the repulsive forces between the negative charges of the glass surface and the particles come into play. The rigidity of the Gouy-Freundlich diffuse double layer causes the particles to come to rest in a position which

⁶⁰ J. W. Mellor, *Trans. Brit. Ceram. Soc.* **5**, 72 (1906).

⁶¹ R. E. Grim, *Illinois State Geol. Survey, Bull.* **68**, 268 (1944).

is determined by their size and by the electrolyte concentration of the water. The smaller the particles, the less chance they have to screen their surface by the formation of an electrical double layer and the stronger are their forces upon the water so that these are the ones which produce the largest halo of rigid water. They stop falling at a considerable distance from the glass, where they still continue their Brownian motion. Because of the large distance between the glass surface and the quartz grain and because of the tapering off of the rigidity of the Gouy-Freundlich double layer, these particles can glide or fall off under the smallest shear forces.

Particles which are much larger than 3μ fall off because of their greater weight. In between these two extreme particle sizes there is one range which causes strong adhesion because the following Coulomb attraction forces come into play: negative quartz (with its adhering film which has a lower than average proton density)—water (which is positive because it has a higher than average proton density)—negative glass (surface coated by water which has a lower than average proton density). A positive layer of water with a higher than average proton density is, so to speak, sandwiched between two negative layers of water. This system has a certain rigidity but can flow when the shear forces are sufficiently strong or when the distance is very large. Such a system can change into one where the solids are brought into close contact, for example,



or where their surface cations may even share OH^- ions. These conditions materialize when window panes touch during shipping so that water is condensed at the spots of contact. The panes are glued together and the adhesion forces are of the same magnitude as the binding forces within the glass so that they can no longer be separated without damaging the glass.

In principle the same mechanism operates in many commercial glues, e.g., sodium silicate which is used as an adhesive for cardboard. The surface chemistry of cellulose resembles that of clay or alumina gel to such an extent that the two media, filter paper and activated alumina, can be used interchangeably in chromatography.

The mechanism of the interaction between colloids and electrolytes, as it is treated here, explains the Schulze-Hardy Rule. The stability of some colloids and the zeta potential of surfaces are affected by salts; a phenomenon which has been explained as the result of a lowering of the excess charge of the particles by adsorption of ions of the opposite sign. When comparing the effects of different cations on colloids, for example, of additions of KCl , BaCl_2 , and AlCl_3 , one finds that their effectiveness with respect to flocculation is not proportional to their charge. The ratio of the numbers of K^+ ions, Ba^{2+} ions, or Al^{3+} ions which are necessary to produce

the same effect is approximately 1000:100:1. Why should 1000 K^+ ions or 100 Ba^{2+} ions be required for accomplishing the neutralization which can be achieved by a single Al^{3+} ion?

The Schulze-Hardy Rule involves the two basic principles which govern chemistry, namely, the establishment of electroneutrality within the smallest volume and that of maximum screening of cations. The surface of an electrically neutral particle whose cations are not sufficiently screened can improve its screening by the chemisorption of anions (OH^- , Cl^- , etc.), a process which violates the principle of electroneutrality. However, if screeners such as a Cl^- ion or water of lower than average proton density is available which is neutralized by a cation of high charge, for example, an Al^{3+} or Th^{4+} ion, then the surface can improve its screening by sharing these negative screeners with the positive ions—a process which does not violate the principle of electroneutrality.

i. "Green Strength" of Clay

Ceramic bodies have to be plastic and workable but, in addition, they have to retain their shape on drying and the shapes must have considerable mechanical strength. Shapes made from sand-water mixtures have no strength after the water has evaporated. According to Holdridge,⁶² the strength of a clay body increases rapidly with the removal of the water but no effort is made to obtain the maximum strength because it is rather difficult to remove the last 2–3% water by drying at low temperature.

During the drying process ceramic bodies become sufficiently strong so that they can be trimmed, handles can be attached, or they can be turned on the lathe and even immersed in an aqueous suspension of a glaze slip. In the preceding chapter the adherence of quartz particles to a glass plate was explained (see Section IV, 1,h). The same explanation applies to the forces acting in a sand-water and in a clay-water mixture. The major difference between these two systems develops when the water evaporates. The sand grains are large and can lower their surface energies by forming a Helmholtz double layer (see Section III, 1,c). The clay particles cannot, but they have to retain water in order to be screened. As the water films become thinner the Coulomb forces increase, the water becomes less mobile and its vapor pressure drops sharply. During the transition from the "leather hard" to the "white hard" condition the particles come closer together and the ultimate state of drying brings about a sharing of OH^- ions by adjacent clay particles.

j. Volume Changes on Drying

The wet clay after having been molded into the proper form is allowed to dry. This process is accompanied by characteristic volume changes which

⁶² D. A. Holdridge, *Trans. Brit. Ceram. Soc.* **51**, 401 (1952).

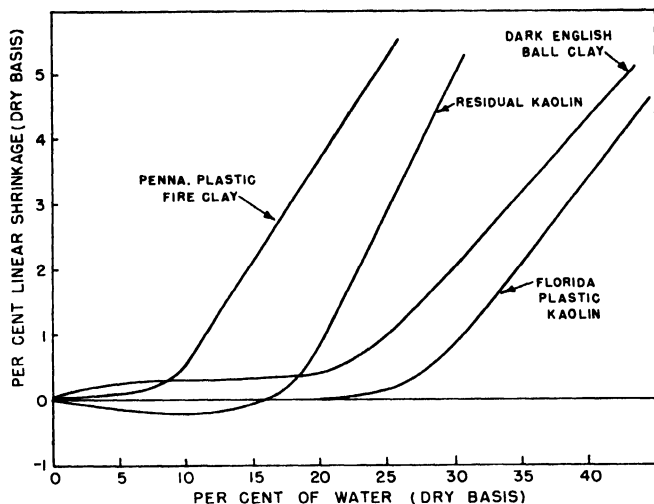


FIG. 7. Linear drying shrinkage curves for several clays. (After Norton.⁶⁴)

are of practical interest and theoretical significance. The fact that a clay body shrinks on drying and that its shrinkage stops rather abruptly when a characteristic water content has been reached agrees with the concept that each clay particle is surrounded by water. The volume changes which accompany the drying of clay speak against the existence of a honeycomb structure of contiguous particles. The abrupt cessation of shrinkage at a certain low water content makes it improbable that plasticity is the result of the binding action of a colloidal gel.

The presence of soluble silicic acid leads to the formation of a gel between the individual particles and produces a small "secondary shrinkage." Haines⁶³ produced such a "secondary shrinkage" in a kaolin suspension, which, by itself, did not show it, by adding some gelatine which simulates the drying shrinkage of colloidal silicic acid.

Norton⁶⁴ made a systematic study of the volume effects which result from the drying of mineral-water mixtures. Figure 7 shows schematically how the volume changes when the water is removed at a temperature of 50–100°C.⁶⁵

The "primary shrinkage" corresponds to the decrease of the thickness of the water film between the particles. The particles come closer together and the interstitial volume decreases proportionally to the amount of water lost. At some characteristic water content the shrinkage stops and

⁶³ W. B. Haines, *J. Agr. Sci.* **13**, 296 (1923).

⁶⁴ F. H. Norton, *J. Am. Ceram. Soc.* **16**, 86 (1933).

⁶⁵ F. H. Norton, "Elements of Ceramics," p. 110. Addison-Wesley, Cambridge, Massachusetts, 1952.

the samples retain their volume during further drying. At this stage the water film has reached the minimum thickness which still permits screening. Any water which is removed after this stage comes from the pores, and air begins to enter the pores of the clay body.

From then on the process does not correspond to an equilibrium with the atmosphere. The remaining water is immobilized, its vapor pressure has decreased to such an extent that it has lost its ability to redistribute within practical times. The tendency of the water to escape is no longer uniform over the whole clay body but it depends strongly on the relative position of the clay crystals, i.e., on the previous mechanical treatment. Williamson⁶⁶ has pioneered in elucidating this phenomenon. During the shaping processes, such as extrusion, slip casting, or kneading, the anisodimensional particles have become more or less oriented (see Section IV, 3). The forces which the particles exert upon the water are a function of their mutual orientation and density of packing. This, in turn, causes the water of different parts of the ware to assume different vapor pressures so that in this stage drying produces warpage. The different volume changes in different parts of the piece may lead to cracks. The drying shrinkage of a slip-cast clay disk reveals different values for its thickness and for its diameter. During casting of the clay slip the platelike particles orient themselves parallel to the walls of the plaster mold.

Removal of the last few per cent of water leads to the sharing of OH⁻ ions at points of contact and the surface of the individual crystals becomes less screened. The suppression of one mode of screening usually accentuates another. Thus, the removal of the screening water film accentuates the rearrangement of surface ions and this distortion increases the volume. This phenomenon is particularly noticeable for coarser clay fractions or for non-plastic materials. Depending on the nature of the material and its particle size, the removal of the last few per cent of water either produces a secondary shrinkage or an expansion. Those materials which can lower their surface energy by the formation of an electrical double layer show expansion because of the depth action which has to accompany any change of geometry within the surface.

2. RHEOLOGY OF SAND-WATER MIXTURES

Wet sand can be formed into simple shapes which are sufficiently strong to carry their own weight. These shapes lose their strength on drying unless the sand contains some clay. A sand-water mixture can lose its water without showing a perceptible shrinkage. This indicates that the single grains nearly touch one another when wet.

What is the nature of the forces which hold the wet quartz grains to-

⁶⁶ W. O. Williamson, *Am. J. Sci.* **245**, 645 (1947); **252**, 129 (1954).

gether? Lindenthal,⁶⁷ in the author's laboratory, performed a number of qualitative experiments in order to elucidate the nature of the interaction between quartz and a liquid.

Potter's flint (finely ground quartz, minus 200 mesh) was used for these experiments. The addition of quartz powder lowers the pH of distilled water and increases its electrical conductivity (see Section IV, 1,c), because each grain surrounds itself with a film of water which has a lower than average proton density. If the water contained molecules which can screen the surface, e.g., glycerol, the electrical conductivity increases less than that of pure water. The demand of the quartz surface for OH^- ions decreases when glycerol is available so that fewer protons are produced which can carry a current. The electrical conductivity of a 40 % glycerol solution in water did not change when quartz powder was added.

The rheological properties of a sand-water mixture are the result of the forces acting between the quartz particles and those acting between the particles and the water. The quartz grains repel one another because they have assumed a negative excess charge. The negative quartz surface and the interstitial water which is positive because it has a higher than average proton density attract one another. These Coulomb attractive forces are responsible for the mechanical strength of the sand-water shape.

The addition of glycerol interferes with this mechanism. In the presence of a screener, such as glycerol, there is no need for the water to dissociate and, as a result, neither the quartz surface nor the interstitial water assumes an electrical charge. For this reason the addition of glycerol to a sand-water mixture leads to an unexpected result: The viscous glycerol solution produces a less viscous slurry with the same amount of quartz powder than the more fluid pure water.

In order to test the strength of the binding forces, the quartz-water mixture was filtered, the filter turned over, and the cone was placed on a lucite plate. The strength of the cone could be tested by tapping the edge of the plate. The higher the glycerol concentration of the liquid phase (5-30 %), the earlier the cone began to slump.

A diluted solution of sodium hydroxide produces an even stronger effect than glycerol. It is not possible to make a cone with a 1 *N* NaOH solution. The cone slumps under its own weight and does not require a vibration of the lucite plate in order to flow.

A 1 *N* HCl solution makes it much more difficult for the quartz surface to acquire a screening water film. The charge difference between surface film and interstitial liquid decreases and the slurry filtered very easily. The surface of the cone did not retain HCl in the way it retained NaOH;

⁶⁷ J. W. Lindenthal, M. Sc. Thesis, Ceramics Dept., Pennsylvania State University, University Park, Pennsylvania, 1952.

it looked dry and the cone did not slump under its own weight. On vibrating the support, however, the cone collapsed. A shape made of a sand-HCl mixture is mechanically much weaker than one made with pure water.

In spite of the completely different rheological behavior of these mixtures, the volume of liquid which was retained by the quartz was nearly the same for all solutions. These results support the view that the volume of the liquid in the cone is determined primarily by the pore volume of the quartz grains which are in close contact with one another. This is one of the basic differences between a quartz-water mixture and a clay-water mixture.

A wet shape of sand is held together by the Coulomb attractive forces between the negatively charged quartz surface and the positive charge of the interstitial water which has a higher than average proton density. The addition of molecules (glycerol) or ions (OH^-) which can screen the surface lowers its charge. The diffuse potential changes into a Helmholtz double layer and the strength of the cone drops. The contact points between the single grains can share some OH^- ions, a process which provides some strength when the pore water evaporates. Most silicate minerals (kyanite, feldspar) behave more or less like quartz.

Sand-water mixtures exhibit a phenomenon which is called dilatancy. They behave like a rigid solid when a sudden pressure is applied but flow under slow sustained pressure. Particles of approximately spherical shape have a good chance to approach close packing. Under an external force such a system can rearrange only when sufficient space is provided for regrouping. Due to the temporary volume expansion during regrouping, the water at the surface of wet sand disappears. This phenomenon can be observed when one steps on wet sand while walking along a beach. Around each footstep, a dry zone appears because the close-packed grains have to loosen their packing in order to regroup. Dilatancy is a phenomenon which depends upon the geometry of the particles and which is not affected by the forces between solid and liquid. Dilatancy is characteristic for close-packed systems and not for those which show plasticity. Plasticity has as a prerequisite a looser packing of the particles.

3. RHEOLOGY OF CLAY-WATER MIXTURES

Quartz and alumina have been plasticized by milling to a particle size of approximately 1μ (see Section III, 3). The small size of the particles is conducive to strong surface forces. The main reason why clay-water mixtures are so much more workable than other finely subdivided minerals lies in their morphology; the individual particles are either thin plates or rods. Le Chatelier⁶⁸ considered the anisodimensional shape of the clay

⁶⁸ H. Le Chatelier, "La Silice et les Silicates," p. 462. Hermann, Paris, 1914.

particles the main factor which determines the plasticity and he proved his point by converting mica into a plastic clay-like substance.

The rheology of clay-water mixtures involves, therefore, two basically different but equally important aspects: the surface chemistry of these minerals and their morphology. The former accounts for the intensity of the interaction between clay and water; the latter governs the kinematics of the deformation process.

Hauser⁴⁷ called the clay particle a "colloidal micelle," emphasizing that colloids are not a separate group of substances but rather matter of an unusually high surface to volume ratio. "This condition," Hauser wrote, "causes matter to exhibit reactivity which is not predictable on the basis of chemical composition alone." Hauser was fully aware of the weakness of classical chemistry, particularly its failure to account for the chemical properties of finely subdivided matter, i.e., of particles with dimensions between 1 and 500 μ . "The fact that a substance having one, two, or all three possible dimensions lying within this range will exhibit properties which cannot be predicted or explained by simple analysis or by reasoning of classical chemistry calls for an explanation." The explanation which Hauser wanted can now be given. It cannot be based on the surface-to-volume ratio alone, but must also include the effect of the absolute dimensions. It is impossible for very small particles to lower their surface energy by that structural change which can occur in the surface of larger particles of the same substances. It is the lack of "depth" of a surface layer which raises its chemical potential when the particles reach the dimensions of colloids. The surface forces are the result of the incomplete coordination of ions which are located in the surface, particularly along edges and at corners. These ions, being incompletely screened, attract charged particles. The whole unit consisting of the solid particle with its diffuse electrical double layer was called the "micelle" by Hauser.

The clay minerals may be classified as colloids because colloidal properties can be expected even if only one of the three dimensions of a particle falls into the colloidal range.

In order to overcome the limitations of classical chemistry, new concepts had to be developed which could explain the intensity of the surface forces of small particles, their negative excess charge and, finally, the rigidity of thin films of water.

In an attempt to elucidate the second, i.e., the kinematic aspect of the rheology of clays, one faces another serious difficulty, namely, the lack of reproducible data. Macey³⁵ was the first to recognize that a workable clay-water mixture is deformed even by the smallest forces and that this deformation stiffens the mixture (shear hardening).

Workable clay-water mixtures are neither Bingham liquids nor can they

be described according to the idealized stress-strain function which is used for truly plastic media. The behavior of these mixtures cannot be measured with one of those devices which produce data, the evaluation of which is based on the assumption of a certain type of stress-strain relation. As the exact nature of this relation is unknown, only those measurements are valid which produce homogeneous strain distribution in the sample. This excludes, among others, the frequently used torsion test.

Buessem and Nagy⁶⁹ recently made a careful analysis of this situation which led to a new experimental approach to the rheology of workable clay-water mixtures. They performed some simple compression tests of cylinders which had been prepared in a special way and followed the changes in the texture of the bodies by means of an X-ray method described by Brindley.⁷⁰

In order to obtain data which are valid, it is absolutely essential to start out with a test piece which contains the kaolinite crystals in random positions. This was achieved by rolling balls of approximately 15-cm. diameter, discarding the oriented outer parts and using cylinders cut out from the interior. Compression tests of cylinders of different heights between lubricated glass plates gave practically identical stress-strain curves, which indicates that this simple device produced uniform strain distribution. The results confirmed the X-ray evidence of randomness of the kaolinite crystals in the samples before they were subjected to the tests.

All stress-strain curves started at the zero point of the coordinate, which means that even a very small stress produced a finite deformation. Samples which had been compressed to a certain stress and then relieved from it gave a new stress-strain curve on repeating the test. The sample had become more rigid.

The work of Buessem and Nagy agrees with the observations of Macey and explains why other workers found yield values. Previous workers did not start out with a randomly oriented clay mixture but with one which was predeformed (through extrusion, tamping, casting, etc.) and which, therefore, was "shear-hardened."

The difficulties encountered in earlier efforts to measure the rheological properties of clay bodies are due to the fact that any deformation of a clay-water mixture produces two irreversible changes: (1) orientation of the clay particles relative to the direction of the compressive stresses, and (2) increase of the strength due to this orientation.

The stress-strain history of a workable clay-water mixture, i.e., the way the test piece has been prepared, determines the extent to which these two

⁶⁹ W. R. Buessem and B. Nagy, *Natl. Acad. Sci.—Natl. Research Council, Publ.* **327**, 480-491 (1954).

⁷⁰ G. W. Brindley, *Mineral. Mag.* **30** (220), 71 (1953).

changes have occurred and also its rheological properties. This point has been frequently neglected and samples were tested which had a complicated and sometimes undefined texture.

As far as the texture is concerned, Williamson⁶⁶ has made some valuable contributions in connection with his work on the effect of the microstructure of clay bodies on the distribution of moisture. Although his work is not concerned with the rheology of clay, his optical methods for following the change of the texture are of direct interest to workers in the field of rheology. The work of Williamson⁶⁶ and that of Buessem and Nagy⁶⁹ make it possible for the first time to present an acceptable picture of the rheology of the clay-water system and to explain the basic difference between clay and finely ground quartz.

A system which contains spherical or nearly spherical particles, such as quartz-water, can be deformed only if some of the particles are forced into other layers of particles. This means that some "bonds" have to be broken and new "bonds" have to be formed, a process which requires a temporary expansion of the volume (dilatancy).

The deformation of a system which contains platelike or rodlike particles proceeds in a basically different fashion. For anisodimensional particles, a rotational movement of the particles contributes to the change of shape. This movement of flaky particles does not require the rupture of "bonds." Flakes and rods can glide along each other without losing their contact. According to Buessem and Nagy, this gliding process connected with the rotational movement of the particles represents the characteristic feature of the rheology of workable clay-water mixtures. Obviously, for isodimensional particles a rotational movement could not contribute to a change of shape.

The intensity of the interaction (clay-water) has been recently studied^{41a, b} using the experimental approach of Buessem and Nagy.⁶⁹ Recognizing the importance of the kinematics of the deformation process, a procedure was adopted wherein tests were made on randomly oriented samples. A simple compression test was used and the effects of aqueous solutions of various types of chemicals upon the deformation behavior of purified kaolinite were investigated. Among the types of reagents tested were inorganic acids and bases, polyhydric alcohols, and wetting agents. Some of the most notable effects were obtained with the various types of wetting agents, namely, nonionic, anionic, and cationic reagents. Results obtained with two different sets of these three types of wetting agents are shown in Figs. 8 and 9. Cationic, nonionic and anionic reagents gave radically different effects. The chemical nature of the liquid medium seems to be of paramount importance since the surface tensions of the solutions were about the same (greatest variation, 0.8 dynes/cm.), pH's were all in the acid range,

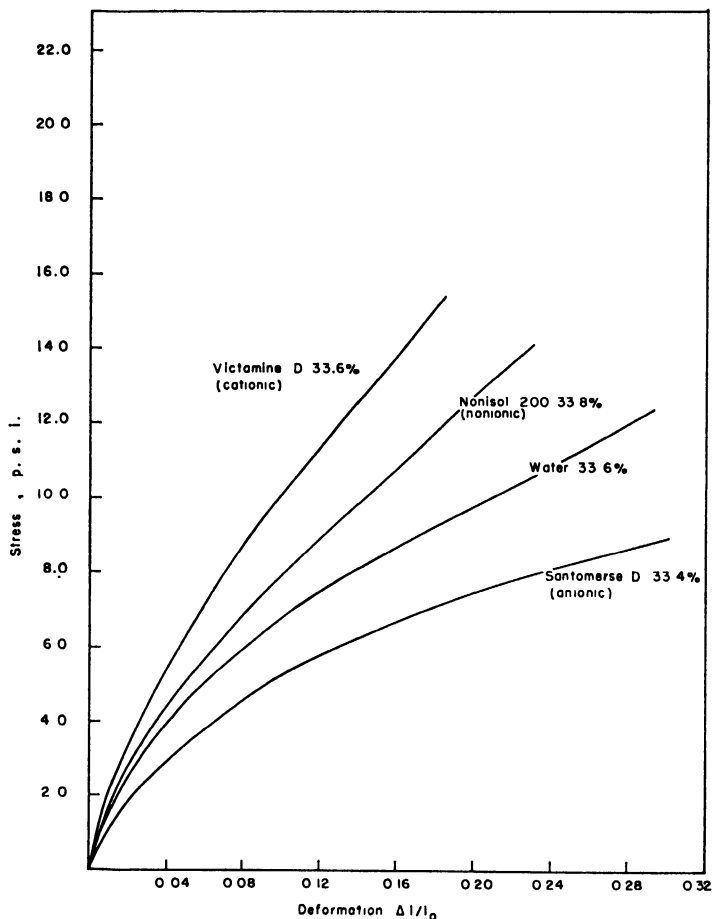


FIG. 8. Plastic stress-deformation curves for Georgia kaolinite as a function of wetting agent solutions (0.95 weight %); moisture contents as indicated.

and moisture content variations were too small to account for the large differences in behavior. It is apparent that the screening ability of the solution in contact with the clay was enhanced by the presence of anionic wetting agents and was subdued by the presence of cationic and nonionic reagents.

The results show that a greater immobilizing effect on the water is produced by the poorer screening solutions since, in all cases, essentially the same volume of liquid is available for satisfying the surface forces of the clay. The anionic reagents provided adequate screening in a smaller volume of water, thus resulting in a greater degree of lubrication and greater ease of deformation.

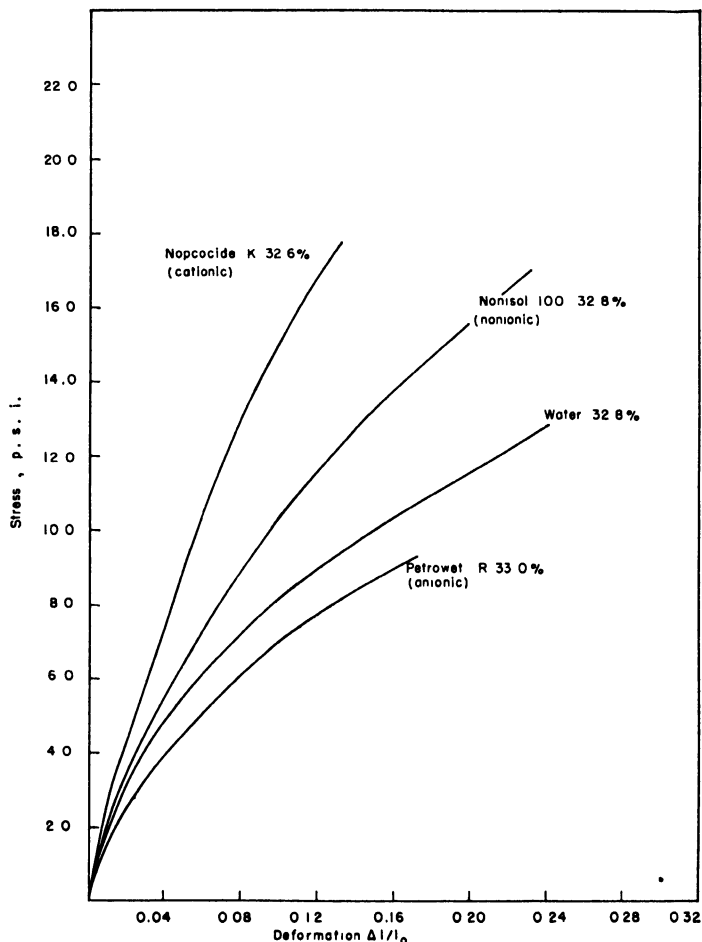


FIG. 9. Plastic stress-deformation curves for Georgia kaolinite as a function of wetting agent solutions (0.85 weight %); moisture contents as indicated.

V. Summary

An atomistic approach to the origin of the surface energy of solids reveals that its value can be lowered by four processes. The electronic polarization of the surface ions is an instantaneous process which is particularly effective if the surface contains cations of high polarizability (PbI_2 or HgS). The cations of quartz or clay have negligible polarizabilities so that the deformation of the electron clouds of the surface ions cannot contribute much to the lowering of their surface energies.

The rearrangement of surface ions and chemisorption are the only

processes which these minerals can use for lowering their surface energy. A profound change of the surface structure which leads to the formation of a "double layer" requires a finite transition zone from the distorted to the normal lattice. The dimensions of many clay minerals do not provide the space necessary for the establishment of such a low energy layer—a condition which governs the surface chemistry of dust, thin films, membranes, and capillaries. Our approach forces us to conclude that the capillary force of a tube not only increases with decreasing diameter but, for thin walled tubes (less than 1μ), it also increases with decreasing thickness of the wall.

The chemical composition of clay minerals keeps the effect of polarization at a minimum. Rather the dimensions of the crystals make it impossible to form a low energy surface layer. As a result, the specific surface energy of clay is much higher than that of other minerals which have similar compositions. This expresses itself in an unusually strong absorptive power and in the chemisorption of anions: thus clay particles suspended in water assume a negative excess charge.

The atomic structure of water, its unique properties as an ionizing solvent for salts containing ions of high charge, and the entropy changes occurring in water when atoms, ions, or molecules are brought into solution, were used as a basis for developing a plausible explanation for the rigidity of water in contact with solids. The concept explains the viscosity of clay slips and the flow of water through porous media. Water is treated as a substance which can form a defective structure. Its H^+ to O^{2-} ratio can deviate from the normal composition, H_2O , in both directions without the formation of individual OH or H^+ ions. Water in contact with solids can assume a higher or a lower than average proton density, but deviation in either one of the two directions impairs mobility. Both the composition and the rigidity of the water taper off with the distance from the interface, so that no definite value can be assigned to the thickness of the rigid water film.

This approach provides an atomistic interpretation for the concept of a diffuse electrical double layer (Gouy-Freundlich double layer), a concept which is essential for the understanding of all electrokinetic phenomena.

The rheology of sand-water and clay-water mixtures involves two equally important aspects: (1) the forces acting between the solid particle and the water, and (2) a kinematic aspect which involves the geometry of the particles. Spherical particles tend toward "close packing" (small sedimentation volume). They can show dilatancy but not thixotropy and plasticity. Plasticity requires separation of the particles by water and "loose packing" (large sedimentation volume).

It is a characteristic feature of a randomly oriented clay-water mixture

that it undergoes deformation under the smallest stresses, but, during this deformation, the individual crystals become oriented and the mixture develops strength. This feature makes it impossible to interpret the rheological properties of a clay body without referring to its previous mechanical history.

CHAPTER 8

THE RHEOLOGY OF INORGANIC GLASSES

W. A. Weyl

I. Introduction: The Importance of the Viscosity of Glass for Its Manufacture	299
II. Methods of Measuring the Viscosity of Glass	301
III. Principles Governing the Polymerization of Ionic Compounds and Formation of Viscous Liquids	303
1. Definition of Glass	303
2. Kinetics of Glass Formation	305
3. Atomic Structure of Inorganic Glasses	307
IV. Factors Determining the Rheological Properties of Glass	309
1. Temperature	309
2. Time	311
3. Composition of the Glass	313
a. The Anion to Cation Ratio	314
b. Binding Forces within the Polyhedra	316
c. Polarizability of the Cation	316
d. Size of the Cation	317
V. Interpretation of the Viscosity of Some Simple Experimental Glasses of Systematically Varied Compositions	318
VI. Viscosities of Some Commercial Glasses	327
VII. Flow Processes within a Rigid Glass	329
1. Low Temperature Bending of Glasses	329
2. Aging and Compacting of Glasses	330
3. Internal Friction	332
4. Cutting of Glass with a Diamond	336
VIII. Summary and Conclusions	337

I. Introduction: The Importance of the Viscosity of Glass for its Manufacture

The viscosity is the property of a glass which dominates its manufacture. The change of the viscosity of a molten salt (silicate, borate, phosphate) as a function of temperature decides whether or not the melt forms a glass on cooling. The economy of glass making is largely determined by its viscosity inasmuch as the rate of forming a homogeneous glass free of undissolved sand and of gas bubbles determines the speed of this operation. In the temperature region of 1400°C. to 1500°C. the viscosity of most commercial glasses is of the order of 10 to 100 poises. After the melt has become

sufficiently homogeneous and the gas bubbles have had a chance to rise to the surface and to escape, the temperature is lowered in order to raise the viscosity to approximately 10^4 poises. The temperature region in which a glass assumes this viscosity is called its working range. When its viscosity exceeds 10^7 poises a glass can hold its shape. The temperature at which a glass reaches the viscosity of $10^{7.6}$ poises has been defined as the "softening point" of the glass.

If the glassware after receiving its final shape were cooled without taking the proper precautions it would develop an unequally strained condition which can be recognized from the birefringence and it might even fracture on account of the thermal shock. Most glassware has to be heat-treated (annealed) in order to relieve a major part of its stresses. Some glasses are heat-treated in order to introduce a desirable stress distribution (compressional stresses in the outer layer) which makes them less sensitive to mechanical shock.

The maximum viscosity of a glass which still can be measured is of the order of 10^{15} poises (strain point). Below the strain point ($\eta = 4 \times 10^{14}$ poises) a glass may be called a rigid solid. The importance of the viscosity of glass for its technology extends, therefore, over the wide range from 10 to 10^{15} poises. In addition to the absolute viscosity the manufacturer of glassware is also interested in the temperature coefficient of its viscosity. In the old days of glass making, when all glass forming operations were carried out by hand, the skilled workmen could adjust the operation according to the viscosity of the glass. Today most glasses are fed into machines and the speed of these machines is determined by the "rate of setting." Glasses with a low temperature coefficient of viscosity are called "long" or "sweet," those with a high coefficient are called "short." The temperature coefficient of the viscosity is one of the factors which determine the rate of setting of a glass. The length of the working range is a function of the temperature coefficient of the viscosity, the specific heat, the emission spectrum (especially in the infrared), and the absolute temperature at which the glass has to be worked.

The brittleness of glass, i.e., its inability to flow under stress at room temperature, dominates its mechanical properties. It is this lack of flow or creep which makes glass suitable for large astronomical mirrors, which must have the greatest possible degree of rigidity.

The fact that a homogeneous system undergoes a viscosity change from 10 to 10^{15} poises represents a challenge to a physicist who is interested in rheological phenomena. Unfortunately, viscosity measurements over this whole range are very difficult because they require a variety of methods which are not applicable to overlapping temperature regions. It is important

for a scientist to be aware of the experimental difficulties in order to judge properly the limitations of the data on viscosity and their interpretation.

II. Methods of Measuring the Viscosity of Glass

The low temperature viscosity of a glass can be measured by the time which is necessary to stretch a glass fiber under a known load. This method which is widely used for viscosities exceeding 10^8 poises has been developed by H. R. Lillie.¹ For this purpose the glass is drawn into a uniform fiber and suspended in a vertical furnace. The details of the method can be taken from the original work of Lillie¹ and from later workers²⁻⁸ who used and modified this method.

Robinson and Peterson⁷ modified an existing formula for the viscosity (η in poises) as follows:

$$\eta = 19600 \frac{m(l_0 \cdot l_1)}{v(l_1 - l_0)} (t_2 - t_1)$$

where l_0 is the original length of the glass fiber in centimeters; l_1 , its length after the run; v , the volume of the fiber (cm.^3) in cubic centimeters; m , the load in grams; and $t_2 - t_1$, the time of viscous flow in minutes.

In the temperature region where the viscosity is so high that it can be measured by the fiber elongation method, the glass still has a measurable elasticity. For this reason the elongation cannot be measured beginning with t_0 , that is, the time where the load m is applied, but some time (several hours in the range of 10^{15} poises) has to elapse until a steady rate of flow is observed. The "softening point" of a glass is determined by heating the upper part (10 cm.) of a uniform fiber 0.6 mm. in diameter of a standardized length (22.9 cm.) at a rate of 5°C. per minute. The temperature at which this fiber elongates under its own weight at a rate of 1 mm. per minute is the "softening temperature" and represents the low temperature limit of the working range (see Littleton⁹). For an average soda-lime silicate glass of the density 2.5 this temperature indicates a viscosity of approximately $10^{7.6}$ poises.¹⁰

¹ H. R. Lillie, *J. Am. Ceram. Soc.* **16**, 619 (1933).

² F. H. Norton, *Glass Ind.* **16**, 143 (1935).

³ G. J. Bair, *J. Am. Ceram. Soc.* **19**, 347 (1936).

⁴ N. W. Taylor, E. P. McNamara, and J. Sherman, *J. Soc. Glass Technol.* **21**, 61 (1937).

⁵ N. W. Taylor and P. S. Dear, *J. Am. Ceram. Soc.* **20**, 296 (1937).

⁶ N. W. Taylor and R. F. Doran, *J. Am. Ceram. Soc.* **24**, 103 (1941).

⁷ H. A. Robinson and C. A. Peterson, *J. Am. Ceram. Soc.* **27**, 129 (1944).

⁸ J. P. Poole, *J. Am. Ceram. Soc.* **32**, 215 (1949).

⁹ J. T. Littleton, *J. Am. Ceram. Soc.* **10**, 259 (1927).

¹⁰ H. R. Lillie, *J. Am. Ceram. Soc.* **14**, 502 (1931).

Viscosities which are smaller than 10^7 poises can be measured by a method which was devised originally by Margules.¹¹ The molten glass is brought between two concentric refractory cylinders, one the crucible, the other a spindle. One of the cylinders is rotated under a given torque and the other, usually the outer one, remains stationary. The rate of rotation or the angular velocity depends upon the viscosity of the liquid and on the dimensions of the apparatus. This method has been used in the high temperature viscosity measurements of soda-lime-silicate glasses by Washburn and co-workers.¹²

Many modifications of the Margules method have been used for measuring the viscosity of glasses. A considerable improvement of this method was introduced by English¹³ who used a platinum crucible and a porcelain rod with a platinum-iridium shoe as the spindle, thus avoiding corrosion of the refractory and the contamination of the glass by alumina. In most instances the viscosity was obtained by calibration with standards of known viscosities at room temperature rather than by calculations based on the dimensions of the cylinders. Lillie¹⁴ modified this method so that absolute values could be obtained and the range of usefulness was extended to 10^8 poises. Lillie¹⁵ gives the cylindrical container a uniform angular motion and measures the torque on an inner cylinder which is suspended in the glass by means of a torsion member. By varying the effective length of the cylinder it was possible to eliminate the apparatus constant, extrapolate to cylinders of infinite length and, thus, calculate the absolute viscosity without the need of referring to standards. In the high viscosity range (10^8 poises) the outer cylinder is turned through a small angle and the time is measured which elapses until the inner cylinder returns to its original position.

Thus the most widely used methods for measuring the viscosity of glass are based on two principles, elongation of a fiber under a constant load and application of shear forces to glass between two concentric cylinders (Margules). Other methods which have been proposed are based on the motion of a platinum sphere through the molten glass. It is very cumbersome to find the precise location of a free falling sphere. X-rays and electrical signals have been suggested for this purpose. Several workers obtained good results by using a suspended platinum sphere, but in all these cases the danger exists that gas bubbles form at the platinum sphere which

¹¹ M. Margules, *Sitzber. Akad. Wiss. Wien, Math.-naturw. Kl., Abt. II* **83**, 588 (1881).

¹² E. W. Washburn, G. R. Shelton, and E. E. Libman, *Univ. Illinois Eng. Expt. Sta. Bull.* No. **140** (1924).

¹³ S. English, *J. Soc. Glass Technol.* **7**, 25 (1923); **8**, 205 (1924); **9**, 83 (1925).

¹⁴ H. R. Lillie, *J. Am. Ceram. Soc.* **12**, 505 (1929).

¹⁵ H. R. Lillie, *Phys. Rev.* **36**, 347 (1930).

falsify the results. For details, Eitel's¹⁶ book should be consulted which offers a complete survey over the different experimental methods which have been used for measuring the viscosities of glasses and slags.

III. Principles Governing the Polymerization of Ionic Compounds and Formation of Viscous Liquids

1. DEFINITION OF GLASS

The word "glass" is used with two different meanings, one referring to the material which is used for making bottles, windows, etc., and the other referring to an amorphous solid which has characteristic rheological properties. In physical chemistry all substances which solidify gradually on cooling by increasing their viscosity to such an extent that crystallization becomes impossible are called "glassy" or "vitreous," provided that this solidification on cooling and the softening on heating are reversible processes.¹⁷ In the physicochemical sense "glass" includes a great variety of chemically unrelated substances, elements (glassy selenium), salts (sodium metaphosphate), oxides (SiO_2 , B_2O_3), sulfides (As_2O_3), and a large number of organic substances (sugar and some polymers). All these materials have in common that their melt hardens gradually on cooling and that the resulting brittle solid lacks the long range order which is characteristic for crystals. The thermosetting resins of the phenol-formaldehyde or urea-formaldehyde type cannot be considered glasses even if these solids are completely amorphous because of the lack of reversibility of the liquid-solid transition on heating and cooling.

As far as commercial glasses are concerned, the last decades have witnessed a great increase in the variety of their compositions. For several thousand years "glass" was essentially an amorphous soda-lime-silicate. The compositions of the antique glasses varied only within narrow limits. Glasses containing more alkali hydrolyzed and were not stable. It was not possible to increase the silica content because that would have raised the melting temperature beyond the accessible range. It was also not possible to increase the CaO because that would have caused the melt to crystallize (devitrification). The narrow composition range was extended for the first time in the 17th Century with the introduction of lead oxide and the development of the flint glasses in England. In the second half of the 19th Century Abbe and Schott, that successful team of physicist and glass technologist, developed a wide range of optical glasses. For the first time, glasses were made commercially which were not based on silica as the

¹⁶ W. Eitel, "Physikalische Chemie der Silikate," 2nd ed., pp. 67-100. Barth, Leipzig, 1941.

¹⁷ G. Tammann, "The States of Aggregation." Van Nostrand, New York, 1925.

"glass former" but contained borates and phosphates. Today the composition has been extended to glasses which are not only free of silica but free of oxygen (fluoride glasses).

In the narrower meaning "glass" always refers to inorganic materials. Morey¹⁸ suggested the following definition: "A glass is an inorganic substance in a condition which is continuous with, and analogous to, the liquid state of that substance, but which, as the result of having been cooled from a fused condition, has attained so high a degree of viscosity, as to be for all practical purposes rigid."

No precise definition of the "vitreous state of matter," as such, has yet been given. A glass can only be defined by the way it has been prepared. The gradual softening and melting of glasses as well as their higher energy content as compared with the crystalline modification of the substance have been emphasized, but none of these features is characteristic. Many crystals (for example, AgI) soften gradually and vitreous phosphorus pentoxide has a lower free energy (lower vapor pressure) than one of its crystalline modifications.

If a liquid can be cooled below its melting point without crystallization, its properties change continuously. The liquid is metastable with respect to the crystal but it remains in internal equilibrium as long as its viscosity permits structural changes to take place during cooling. However, at a certain temperature the viscosity reaches a value which does not permit the structural changes to follow within the experimental times. In this region (transformation region), the supercooled liquid changes into a glass and its physical and chemical properties depend on the equilibrium which has been frozen-in on cooling. For this reason all properties of a glass depend upon the rate of cooling (thermal history). In order to describe the structure of the glass which has been "frozen in" on cooling the term "fictive temperature" has been suggested (see Tool¹⁹). If a rapidly cooled glass is heated to its "fictive temperature" its properties assume their equilibrium values without delay. Heated rapidly to any other temperature but the fictive temperature, the properties of a glass drift.

The temperature at which the substance reaches a viscosity of the order of 10^{14} poises has been called the "transformation point." Here the supercooled liquid changes into a glass and major structural changes cannot take place below this temperature. Actually one should speak of a "transformation region" rather than of a "transformation point" because the exact temperature depends upon the experimental conditions. Experiments of long duration lead to a lower transformation temperature than those in which higher rates of heating or cooling are used. It is amazing,

¹⁸ G. W. Morey, "Properties of Glass," p. 34. Reinhold, New York, 1938.

¹⁹ A. Q. Tool, *J. Am. Ceram. Soc.* **29**, 240 (1946).

however, to see that the chemical composition of the glass has little influence and that it is primarily the viscosity which determines the transformation point. Glycerol reaches this viscosity at -100°C , selenium at room temperature, most commercial silicate glasses around 500°C ., and fused quartz well above 1000°C . In all cases the viscosity of 10^{13} to 10^{14} poises marks the temperature below which major structural changes, such as flow, are frozen in and only minor structural changes can go on. In an alkali-lime-silicate glass, for example, the alkali ions are bonded to the silicate framework by much weaker forces than the calcium ions. As a result, alkali ions can rearrange themselves in the spacious SiO_4 -network at much lower temperature than the more highly charged ions. This gives rise to some characteristic phenomena, e.g., "internal friction" and "ice point depression."

2. THE KINETICS OF GLASS FORMATION

If one looks upon the wide variety of substances which form glasses one realizes that glass formation cannot be related to the nature of the chemical binding forces. Oxygen and selenium can form glasses due to the pairing of electrons. Polar organic compounds—for example, alkaloids, sugar, glycerol—form glasses in which the molecules are bonded together by the sharing of protons (hydrogen bonds). Purely ionic compounds—for example, BeF_2 or Na_2BeF_4 —form glasses, and according to the conventional classification the bonds in most commercial glasses would be called partly ionic and partly covalent.

The fact that a liquid can be supercooled is no indication that it also forms a glass. Small droplets (50μ) of metals, especially of those of the iron and platinum group, have been supercooled more than 200°C below their melting points. Nevertheless, no metal is known in the glassy state. Pure water can be supercooled but on further cooling it does not change into a glass but crystallizes. Tammann²⁰ and his school demonstrated that a large number of organic molecules which are in no way related from a constitutional point of view do form glasses when their melts are cooled in the absence of nuclei. Most significant is his finding that as far as glass formation, nucleation, and crystallization rates are concerned, no difference exists between the low melting elemental selenium or the organic substances on the one side and the high melting ionic silicates, borates, or phosphates on the other.

The importance of the viscosity of glasses and its temperature dependence for glass manufacture has been mentioned in our Introduction. The role which the viscosity plays in the "definition of glass" has been discussed in the preceding section. The kinetics of glass formation involves questions

²⁰ G. Tammann, "Der Glaszustand," Voss, Leipzig, 1933.

such as: Why does potassium chloride form a melt which is fluid down to its freezing point and a potassium silicate one which is so viscous that it fails to crystallize on cooling?

Before we go into the specific case of ionic compounds we shall try to answer this question in a very general way. Liquids consist of particles which exert attractive forces upon one another. The particles are in thermal motion but their positions are not completely random because of the intermolecular or interionic forces. The forces in fused KCl and the geometry of the melt are essentially the same as in the crystal. Obviously the kinetic energy of the ions is greater in the hot melt and the interionic distances are larger in the melt than in the cold crystal because of the thermal expansion. Such a melt consists of K^+ ions, each surrounded by approximately six Cl^- ions, and Cl^- ions, each surrounded by approximately six K^+ ions. However, the coordination number of six is not as rigid a condition for the melt as it is for the crystal. One may predict from crystal chemical considerations that the average coordination number decreases with increasing temperature. However, even if we assume the coordination number of the ions would remain six, we still have to realize that any ionic rearrangement such as nucleation, crystallization, and viscous flow requires that the normal coordination of six changes temporarily to five and seven for some cations.

The rheology of a system is determined by two energy terms, namely, the energy which is required for a temporary change of coordination and the energy (kT) which is available in the system for such a change.

Let us dwell for a moment on this fundamental relation which governs viscosity and glass formation. Liquids which consist of close-packed particles, e.g., metals, organic substances such as benzene, and liquefied rare gases such as argon, are characterized by relatively large coordination numbers which range from 8 to 12. If the coordination number is so high, a temporary change of $+1$ or -1 does not require much energy. For these liquids the activation energy of viscous flow is very small, usually of the order of 0.5 to 1.5 kcal./mole. Argon, mercury, or benzene cannot form glasses because the high coordination number of these atoms and molecules in the liquid state enables them to crystallize easily even at low temperature. The same applies to molten copper and gold. These metals, too, have high coordination numbers but, in addition, the value of kT at their melting points is high. The latter factor alone would make possible considerable changes in the coordination number and would enable these melts to crystallize.

The geometry of the liquid (coordination) and the value of kT which means the absolute temperature of the freezing point of the liquid determine the activation energy of viscous flow and the tendency toward glass forma-

tion. Dipole forces between molecules play only a minor role; they become negligible if the kT of the liquid permits free rotation.

This relation also explains why glass formation becomes a rare event if one goes to compounds which melt at very high temperatures. The high melting nitrides and carbides are "strengthened models" of oxides in the sense of Goldschmidt's model structures²¹ because the change from O^{2-} to N^{3-} or to C^{4-} affects certain properties of crystals in the same fashion as the change from F^- to O^- ions. However, no glass formation has yet been reported among the high melting nitrides and carbides. The high melting point of a substance causes the kT of the liquid phase at the melting point to be so high that the system can overcome even relatively high energy barriers of nucleation. At high temperatures a system has available the energy which is necessary for the temporary unscreening of cations. We picture the activation energy of viscous flow of NaCl and similar ionic compounds as the energy which is required for temporarily partially unscreening Na^+ ions so that two Na^+ ions become neighbors. Such a constellation of ions introduces a repulsive force which depends upon the field strength of the cations, its polarizability and, above all, upon the anion to cation ratio. These parameters have been used by Marboe and Weyl²² for deriving an atomistic picture of the effect of the chemical composition of glasses upon their viscosities.

It is well to keep in mind that glass formation is a rate phenomenon and, for this reason, it is not possible to classify substances into those which do form glasses and others which do not. Many substances, e.g., sodium metasilicate, can be obtained as glasses in small quantities when their melts are chilled rapidly. Large quantities of the same substances, however, crystallize because they cannot be cooled sufficiently fast to avoid the formation of crystal nuclei.

The process of glass formation represents one kind of polymerization process, as will be seen in the following discussion of the atomic structure of inorganic glasses.

3. THE ATOMIC STRUCTURE OF INORGANIC GLASSES

When V. M. Goldschmidt derived the rules which relate the properties and the structures of crystals to their composition he also considered the conditions which cause glass formation. He pointed out that the radius ratio $R_{cation}:R_{anion}$ for glass forming oxides is of the order of 0.3, a value which is favorable for tetrahedral coordination. Indeed, most glasses contain tetrahedral groups SiO_4 , PO_4 , or BO_4 as the characteristic building

²¹ V. M. Goldschmidt, *Geochemische Verteilungsgesetze der Elemente VIII. Skrifter Norske Videnskaps-Akad. Oslo, I. Mat.-naturv. Kl.* **8**, 50, 129-139 (1926).

²² E. C. Marboe and W. A. Weyl, *J. Soc. Glass Technol.* **39**, 16 (1955).

units. These tetrahedral groups are interlinked by having some of their O^- ions in common.

The glass formation of a molten oxide mixture is a function of the "degree of polymerization" and, as such, it depends to a large extent on the number of corners of each polyhedron which are shared. In orthosilicates, for example, there is no need for the SiO_4 tetrahedra to share corners. As a result, the melts of most orthosilicates, for example, Na_4SiO_4 , have a low viscosity and do not form a glass. With increasing acidity of the silicate melt, glass formation develops as the average number of shared corners increases or the system undergoes polymerization of its polyhedra. Pure SiO_2 is the prototype of glass-forming oxides; its melt is extremely viscous because the formula demands that all corners of the SiO_4 tetrahedra be shared.

Goldschmidt's idea of "model structures," i.e., of crystals which have similar structures but either "weakened" or "strengthened" properties, has been extended successfully to glasses. According to Goldschmidt, BeF_2 is the weakened model of SiO_2 . Both compounds have the same radius ratio but different "valence sums." The lower valence sum of BeF_2 ($2 + 2 \times 1 = 4$) as compared with SiO_2 ($4 + 2 \times 2 = 8$) causes the fluoride to have a much lower melting point than the oxide. Fused BeF_2 has a much lower viscosity than fused SiO_2 . The glass forming property of BeF_2 is extended to the complex beryllium fluorides. These weakened models of silicate glasses contain BeF_4 tetrahedra as the structural elements. These model glasses may have the same degree of polymerization as the silicates, but their viscosity is low because of the weaker binding forces between Be^{++} and F^- ions as compared with those between the more highly charged Si^{4+} and O^- ions.

It has been found advantageous to distinguish between (1) cations (network-forming cations) which have a high field strength so that they form the centers of their own polyhedra, thus dominating the polymerization process through their coordination requirements and (2) those cations (network-modifying cations) which play a secondary role and which assume interstitial positions. The environment of the latter is less sharply defined with respect to the number of the surrounding anions and internuclear distances. The oxides of sodium and calcium cannot form a glass by themselves but their presence modifies the extent of polymerization because they increase the anion-to-network-forming cation ratio. The fields of these cations are not strong enough to form polyhedra of their own, but they influence the polarizability of the anions which, in turn, reflects upon the strength of the binding forces within the polyhedron.

Some technically important groups of glasses contain two or more kinds of central cations, for example, $B^{3+} + Si^{4+}$, $Al^{3+} + Si^{4+}$, and $Al^{3+} + P^{5+}$,

so that they could be called copolymers of different polyhedra. Obviously, the distinction between network-forming and modifying cations is sharp only when it refers to extremes, for example, Si^{4+} and Na^{+} ions, but it cannot be applied rigorously to ions of intermediate field strengths.

IV. Factors Determining the Rheological Properties of Glass

1. TEMPERATURE

In spite of the experimental difficulties, a relatively large body of data has been assembled which illustrates the influence of the temperature upon the viscosity of commercial and experimental glasses. The pioneering work of Washburn and associates²³ revealed that glasses have a very high temperature coefficient of viscosity, ranging from approximately 10 to 10^{15} poises.

For the technologically important field of the ternary system $\text{Na}_2\text{O}-\text{CaO}-\text{SiO}_2$ these authors presented their data in the form of lines of equal viscosity (isokoms). Their diagram of the log isokoms for the temperatures between 900°C . and 1500°C . are available in many books.²⁴ Today Washburn's work, which covers seventeen compositions in the most important composition range of industrial glasses, is primarily of historical interest, and more reliable data are now available.

The viscosity of glasses has a very high temperature coefficient. Plotting the logarithm of the viscosity against the reciprocal value of the absolute temperature gives a curve the slope of which is a measure of the activation energy of the flow process. This value increases rapidly with decreasing temperature.

As an example for the influence of the temperature on the viscosity of a simple silicate glass we give some data on a sodium silicate glass of the approximate composition 80 % SiO_2 and 20 % Na_2O (Table I), as measured by S. English.

So far all attempts to derive a meaningful formula which describes the viscosity of a silicate glass as a function of the temperature have failed. Empirical formulas are plentiful and one of the best fitting expressions seems to be that used by Fulcher.²⁵

$$\log \eta = A + \frac{B}{T - T_0}$$

²³ E. W. Washburn, G. R. Shelton, and E. E. Libman, *Univ. Illinois Eng. Expt. Sta. Bull. No. 140* (1924).

²⁴ G. W. Morey, *Am. Chem. Soc. Monograph Ser.* **124**, 143 (1954); W. Eitel, "The Physical Chemistry of Silicates," p. 127 ff. University of Chicago Press, Chicago, Illinois, 1954; W. Eitel, M. Pirani and S. Scheel, eds., "Glastechnische Tabellen," Springer, Berlin, 1932.

²⁵ G. S. Fulcher, *J. Am. Ceram. Soc.* **6**, 339 (1925).

TABLE I
INFLUENCE OF TEMPERATURE ON THE VISCOSITY OF A SODIUM SILICATE GLASS
(20% Na₂O, 80% SiO₂)
(After S. English)

Temperature, °C.	Viscosity, poises
505	6.1×10^{12}
555	9.5×10^{10}
598	7.3×10^9
650	3.2×10^8
992	8.9×10^3
1100	1.9×10^3
1194	5.5×10^2
1315	1.6×10^2
1410	7.0×10

in which T is the temperature and A , B , and T_0 are constants which have to be determined experimentally. Robinson and Peterson²⁶ published precision measurements of 16 analyzed commercial container glasses. The measurements were made over a viscosity range from 10^2 to 10^{14} poises by means of two pieces of equipment, one using the Margules principle; the other, fiber elongation under load. For this group of soda-lime glasses, they found that the above formula fitted the experimental data within 0.5%.

There can be no question about the desirability of an equation which describes the viscosity of a glass as a function of the temperature over a wide temperature region. Such an equation can be helpful in checking experimental data and assist in interpolations. It might also permit extrapolations into those viscosity ranges which are not easily accessible by direct measurements.

Many unsuccessful attempts have been made to derive a formula which has a theoretical basis. This raises an important question concerning the viscosity of glasses, namely: Is it solely the complexity of the system which is responsible for the failure to find a theoretically sound equation for its change with the temperature or is there another more fundamental difficulty involved, namely, the accuracy of existing formulas describing rate phenomena?

Indeed, precision measurements of the activation energies of the sucrose inversion by Moelwyn-Hughes²⁷ reveal a drift of the "constant" E_A from 27.2 to 20.5 kcal/mole when the temperature is raised from 1°C. to 40°C.

²⁶ H. A. Robinson and C. A. Peterson, *J. Am. Ceram. Soc.* **27**, 129 (1944).

²⁷ E. A. Moelwyn-Hughes, "The Kinetics of Reactions in Solution." Oxford Univ. Press, London and New York, 1947.

In dealing with fused silicates we extend the temperature range of observation not 40°C. but 400–1000°C. We are interested in flow of glasses which have a temperature of nearly 1500°C. and we follow their flow properties to temperatures as low as 500°C. This is a rather rare situation in rheology.

The failure to find a theoretically well founded formula describing the change of the viscosity of glasses with temperature may, therefore, be attributed primarily to the tremendous temperature range from 500° to 1500°C. No equation is valid over such a temperature region and an analysis of the reasons reveals that temperature causes several important parameters to change.

In the following discussion of the effect of the composition of a glass upon the viscosity we will see that the strength of the binding forces between Si and O atoms is one of the most important factors. These forces decrease as the temperature is raised because of the thermal expansion of the glass.

Increased internuclear distances increases the polarizability of all ions, a feature which also lowers the viscosity. Hence, increasing temperature not only increases the kT of the glass, that is, the thermal energy which becomes available for viscous flow, but it also decreases the energy barriers in several ways. This feature is not unique for glasses but applies generally to all rate phenomena. However, it is accentuated for silicate glasses by the unusually large temperature range over which the rheological properties are of interest and over which measurements can be made.

2. TIME

In the temperature region where glasses are fluid they are Newtonian liquids. Their viscosity is defined by the temperature and the composition and is independent of the time and the magnitude of the shear.

With decreasing temperature glasses become more viscous and undergo structural changes, the nature of which is not very different from the modification changes of crystals, i.e., changes of the coordination number or the interionic distances and bond angles. The lack of long range order in glasses does not impose a restriction upon these changes with respect to all ions of the same kind. In crystals the coordination number of a cation can change only if all the corresponding ions undergo an identical change by means of a cooperative maneuver. Using colored ions as indicators, Weyl²⁸ showed that in a glass the equilibrium between two coordination complexes, for example, between NiO_4 groups (purple) and NiO_6 groups (yellow), shifts gradually with the temperature. In contrast to the analogous changes in an aqueous solution, these transitions are time consuming so

²⁸ W. A. Weyl, in "High Polymer Physics" (H. A. Robinson, ed.), pp. 3–27. Tudor, New York, 1948.

that they can be frozen in. One has to look upon a glass as being in a non-equilibrium not only with respect to the thermodynamically more stable crystalline phases but with respect to other possible arrangements of its ions having different coordination numbers and different internuclear distances. Before these relations were understood, much confusion arose from the observation that the properties of glasses depend not only upon temperature, pressure, and composition, but, in addition, upon their past thermal history.²⁹

The viscosity of a glass changes strongly with its atomic structure and the temperature. Obviously, the time one can allow for measuring the viscosity of a glass has practical limitations. Hence, only in the high temperature region where the relaxation times are short does one measure the true viscosity as an "equilibrium property." At lower temperature and higher viscosities, the properties of glasses are usually measured under conditions where their atomic structures do not correspond to an internal equilibrium. This phenomenon has been interpreted as a discontinuity of the temperature dependence of the properties of glass or as the transition between a supercooled liquid and a "fourth state of matter." The temperature where this apparent "discontinuity" was observed has been called the "transformation point."

Lillie³⁰ made precise measurements of the viscosity of glasses as a function of the time and of their previous thermal history. In order to reach a constant viscosity, a certain time is necessary for establishing the internal equilibrium (stabilization) and this time increases with increasing viscosity. Lillie's³⁰ experiments demonstrate (Fig. 1) that glasses become non-Newtonian liquids at low temperatures. They do not have a plasticity range because they do not have a yield value but they have "structural viscosity."

The lower the temperature of a certain glass the more pronounced becomes the time effect in viscosity measurements. Systematic work on this subject was done by G. J. Bair³¹ as well as by Taylor and his collaborators.³²⁻³⁴ They used the fiber elongation method for measuring the viscosity of glasses and found delayed elastic aftereffects when the fiber was loaded, the load changed, or when the load was completely released.

Time effects are observed even if the glass is for all practical purposes a

²⁹ W. A. Weyl, in "Phase Transformations in Solids" (R. Smoluchowski, J. E. Mayer, and W. A. Weyl, eds.), pp. 296-334. New York, 1951.

³⁰ H. R. Lillie, *J. Am. Ceram. Soc.* **16**, 619 (1933).

³¹ G. J. Bair, *J. Am. Ceram. Soc.* **19**, 347 (1936).

³² N. W. Taylor, E. P. McNamara, and J. Sherman, *J. Soc. Glass Technol.* **21**, 61 (1937).

³³ N. W. Taylor and P. S. Dear, *J. Am. Ceram. Soc.* **20**, 296 (1937).

³⁴ N. W. Taylor and R. F. Doran, *J. Am. Ceram. Soc.* **24**, 103 (1941).

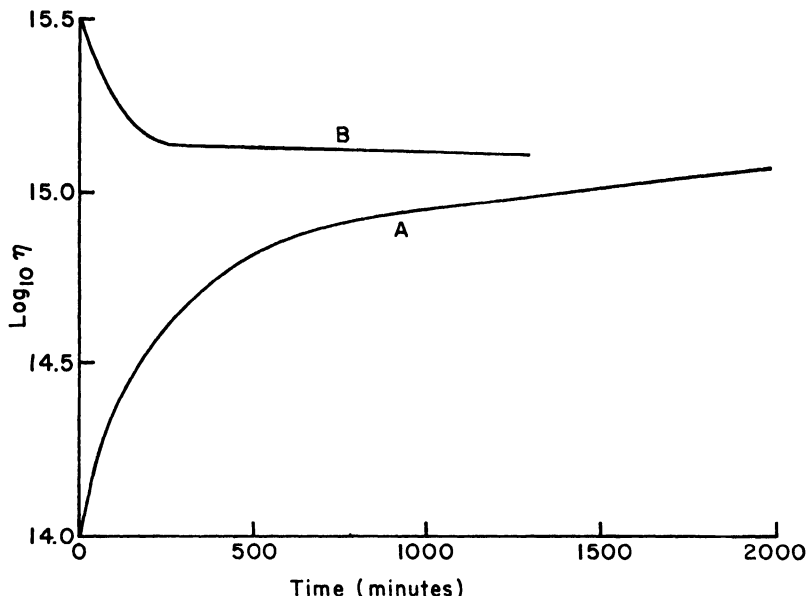


FIG. 1. Viscosity changes as a function of time. (After Lillie.³⁰) Key: curve A viscosity at 486.7°C. of a freshly drawn fiber increases with time; curve B, viscosity at 486.7°C. of a fiber which had been stabilized at 477.8°C. (64 hours) decreases with time.

rigid solid. Taylor considers the elongation of a glass under load as a summation of "elastic adjustment" and constant viscous flow.

In the temperature region just above the transformation point even a "stabilized" glass, i.e., one which has reached thermal equilibrium, still undergoes three distinct changes when a load is applied or when the load is increased: (a) an instantaneous elongation which corresponds to the elastic deformation of the rigid glass; (b) viscous flow corresponding to the Newtonian flow of a liquid which has a viscosity of the order of 10^{10} – 10^{14} poises; (c) a change of length due to a structural rearrangement, which is time-consuming. For this reason the viscous flow reaches a steady rate only some time after the load has been applied or its magnitude changed.

3. COMPOSITION OF THE GLASS

The influence of glass composition on the viscosity is of practical and theoretical interest. The viscosity has always been important for the molding of glass and its control became one of the main problems when automatic glass blowing and pressing machines were introduced. From a theoretical

point of view one may say that understanding viscosity is synonymous with understanding the principles of the glassy state, in particular the forces which are acting between the constituents of the melt and which finally lead to the formation of an amorphous brittle solid.

In the following paragraphs we will discuss the most important structural parameters which determine the viscosity of an inorganic glass as a function of its composition. This analysis, made by Marboe and Weyl³⁵ is based on a large body of viscosity data of glasses, the compositions of which were simple but covered a wide range. The available data on the viscosity of commercial glasses are not suitable for deriving the structural principles which control viscosity. Commercial glasses have to meet many requirements (expansion, light transmission, chemical resistivity), so that by nature their compositions have to be complex. On the other hand, within a certain group, e.g., bottle glass or window glass, only minor variations in the composition can be tolerated. For those reasons even the systematic work of English³⁶ or of Gehlhoff and Thomas³⁷ is of only limited usefulness for our purpose because their glasses did not include cations with sufficient variation of size and electronic configuration.

The Office of Naval Research made it possible for the author to initiate an extensive research program on the viscosity of glasses. Over a period of several years, Enright³⁸ and L. C. Hoffman and co-workers³⁸ produced the data which formed the basis for an atomistic interpretation of viscosity by Marboe and Weyl.³⁵ The atomistic interpretation is based on the screening concept.³⁹

a. The Anion to Cation Ratio

The anion to cation ratio is by far the most important single factor which affects the degree of screening of a cation and, with it, its tendency to share anions, i.e., to polymerize. Pure silica, SiO_2 , which has an anion to cation ratio of only two, can screen its cations only by a three-dimensional polymerization. Additional O^- ions, which are introduced in combination with cations of a weaker field strength than that of the Si^{4+} ion, improve the screening and thus lower the tendency of the system toward polymerization. The data given in Table II illustrate the effect of Na_2O on the viscosity at 1400°C .

The addition of Na_2O to SiO_2 improves the screening of the Si^{4+} ions in two ways. First, the number of O^- ions is increased, which produces

³⁵ E. C. Marboe and W. A. Weyl, *J. Soc. Glass Technol.* **39**, 16 (1955).

³⁶ S. English, *J. Soc. Glass Technol.* **7**, 25 (1923); **8**, 205 (1924); **9**, 83 (1925).

³⁷ G. Gehlhoff and M. Thomas, *Z. tech. Physik* **7**, 260 (1926).

³⁸ D. P. Enright, Office Naval Research Tech. Rept. No. 44, Contract No. N6 onr 269 Task Order 8 NR 032-264, 5. Pennsylvania State Univ., University Park, Pennsylvania, 1952; L. C. Hoffman, T. A. Kupinski, R. L. Thakur, and W. A. Weyl, *J. Soc. Glass Technol.* **36**, 196 (1952).

³⁹ W. A. Weyl, *J. Phys. Chem.* **59**, 147 (1955).

TABLE II
EFFECT OF Na_2O ON THE VISCOSITY OF SiO_2

Composition	O:Si Ratio	Viscosity in poises (1400° C.)
SiO_2	2.0	10^{10}
Na_2O , 2SiO_2	2.5	280
Na_2O , SiO_2	3.0	1.6
$2\text{Na}_2\text{O}$, SiO_2	4.0	<1.0

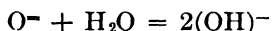
a more favorable anion to network-forming cation ratio and, secondly, O^- ions become more polarizable which means that they become better screeners. The electron clouds of those O^- ions which are exposed to two Si^{4+} ions are strongly tightened and are, therefore, relatively poor screeners. Molten sodium orthosilicate is very fluid because each Si^{4+} ion can have an environment of four polarizable O^- ions without the necessity of sharing them with another silicon. Such a melt contains independent $(\text{SiO}_4)^{4-}$ tetrahedra which are neutralized and linked together by Na^+ ions.

The anion to Si^{4+} ratio of a silicate glass can be increased and the viscosity be lowered in several ways:

(a) Addition of an oxide which contains a cation of low charge. Li_2O , Na_2O , and K_2O are similarly effective in lowering the viscosity of SiO_2 .

(b) Replacing an oxide by a fluoride, for example, CaO by CaF_2 , increases the number of anions. This process accounts for the fluxing action of CaF_2 in glasses and metallurgical slags. The German name of the mineral CaF_2 is *Flussspat*, i.e., fluxing spar.

(c) The presence of water in a silicate melt (volcanic magma) strongly increases its fluidity. Water participates in the structure of fused silicates in the form of OH^- ions, thus increasing the number of anions, according to:



The depolymerizing action of H_2O is utilized in hydrothermal synthesis.

The role which the anion to cation ratio plays in determining the viscosity of glasses is analogous to its influence upon the melting point of simple compounds.³⁹ If the charge of the cation increases, a larger number of anions are needed for neutralization which lowers the melting point of the compound, as can be seen from the following two series.

Fluoride	Mg^{++}	Al^{3+}	Si^{4+}	P^{5+}	S^{6+}
Melting Point	1400°C.	1040°C.	-77°C.	-83°C.	-55°C.
Anion:Cation Ratio	2	3	4	5	6
Oxide	Mg^{++}	Al^{3+}	Si^{4+}	P^{5+}	S^{6+}
Melting Point	2800°C.	2030°C.	1713°C.	570°C.	45°C.
Anion:Cation Ratio	1.0	1.5	2.0	2.5	3.0

b. Binding Forces within the Polyhedra

Next to the anion to cation ratio, the strength of the binding forces within the polyhedra, for example, between Si^{4+} and O^- ions in the SiO_4 groups, is important. At high temperature these two factors are the ones which primarily determine the viscosity. The complex beryllium fluoride glasses, the weakened models of the silicate, provide a good example for the effect of binding forces upon viscosity. These glasses soften in a temperature range approximately 200–300°C. lower than silicate glasses.

Aside from the charge of the cation and anions, there are other factors which can affect the binding forces within an SiO_4 tetrahedron. In order to understand these relations we follow the ideas of Fajans⁴⁰ who treats all chemical binding forces as Coulomb forces between cations and anions which are modified by the electronic interaction, i.e., the mutual polarization. This is brought out quite clearly in the viscosity relations of the alkali silicates.

From the work of Endell and Hellbruegge⁴¹ and Heidtkamp⁴² we learn that the viscosity of alkali ortho- and metasilicates, i.e., of melts with a high O:Si ratio, increases from K to Na and Li. This is to be expected because the SiO_4 tetrahedra are single in the orthosilicate and held together only by the alkali ions. According to the field strength of the alkali ions, the attractive forces between the Li^+ and O^- ions should be greater than those between the larger Na^+ or K^+ ions and O^- ions. However, in glasses with a higher SiO_2 content, i.e., lower anion to cation ration, the viscosities may be reversed and the lithium silicates can form the most fluid melts. In high silica glasses the binding forces between silicon and shared oxygen ions dominate the viscosity because the shared O^- ions are the links between the polyhedra. The stronger field of the Li^+ as compared with Na^+ and K^+ ions tightens the O^- to a greater extent and decreases the Si-O interaction. With Fajans⁴⁰ we describe this effect by stating that the Li^+ ion deforms the electron cloud of the O^- ion and thus weakens the binding forces between the latter and the central Si^{4+} ion.

This effect has to be considered whenever one of the secondary or network modifying cations is replaced by another one which, due to different size, charge, or electronic structure, has a different contrapolarizing effect upon the O^- ions. Even for corresponding compositions, that is, identical Si:O ratio, the Si-O binding forces are subject to change.

c. Polarizability of the Cation

The polarizability of an ion is usually measured as its response to the

⁴⁰ K. Fajans, "Chemical Forces and Optical Properties of Substances." McGraw-Hill, New York, 1931; *Ceram. Age* **54**, 288 (1949).

⁴¹ K. Endell and H. Hellbruegge, *Z. angew. Chem.* **53**, 271 (1940).

⁴² G. Heidtkamp and K. Endell, *Glastech. Ber.* **14**, 99 (1936).

alternating electrical field of light (molar refractivity). With respect to rheology we are interested in the polarizability of an ion as a measure of its ability to adjust its electron cloud to a changing environment and to screen its core under conditions where its coordination is lowered temporarily. According to Fajans⁴⁰ cations of the noble gas-type have lower polarizabilities than ions of similar size but incomplete outer orbitals.

This response of a nonnoble gas-type ion to an asymmetrical environment becomes important for all phenomena which involve temporarily the formation of asymmetrical groups, in particular for flow and diffusion processes. According to Weyl,⁴³ the polarizability of the Ag^+ ion accounts for the plasticity of AgCl and its lower melting point as compared with the harder, more brittle, and higher melting NaCl . Both salts have identical structures and lattice dimensions. Their compressibilities are of the same order of magnitude, because hydrostatic pressure does not change the symmetry of a lattice. Plastic deformation under shear forces and melting are processes which bring some ions into positions where they are incompletely screened. The repulsive force which originates when one Ag^+ ion has to pass another Ag^+ ion is smaller than that between two incompletely screened Na^+ ions passing one another within the same distance.

Comparing the melting points³⁹ of corresponding compounds, one finds that the ones with cations of the nonnoble gas-type have lower melting points than those which contain cations with a complete octet shell. A Pb^{++} compound can increase its entropy at a lower temperature than the corresponding Sr^{++} compound, because the Pb^{++} - Pb^{++} repulsion is decreased by the polarization. The Pb^{++} ion has $18 + 2$ outer electrons, the Sr^{++} ion has 8 outer electrons so that its polarizability is lower.

Figure 2 shows the effect of a substitution of PbO for SrO in a glass of the molar composition, Na_2O , $(1 - x)\text{SrO}$, $x\text{PbO}$, 5SiO_2 , according to D. P. Enright.³⁸

d. Size of the Cation

As far as the viscosity is concerned a change of the size of a cation produces antagonistic effects and the predominant factor will determine the final result. When the size of a cation increases, the geometry requires a larger number of anions for screening it. For a given anion to cation ratio this calls for a stronger polymerization or a higher melting point. Replacing some Si^{4+} ions by Zr^{4+} or Th^{4+} ions causes the low temperature viscosity of the glass to increase because these large ions (having a coordination number of 8), so to speak, withdraw anions from the silicate structure and force the SiO_4 tetrahedra to share more corners. In spite of the fact that the Zr^{4+} and Th^{4+} ions are much more polarizable than Si^{4+} and that the Zr-O and Th-O binding forces should be much smaller than Si-O , their

⁴³ W. A. Weyl, *Glastech. Ber.* **23**, 174 (1950).

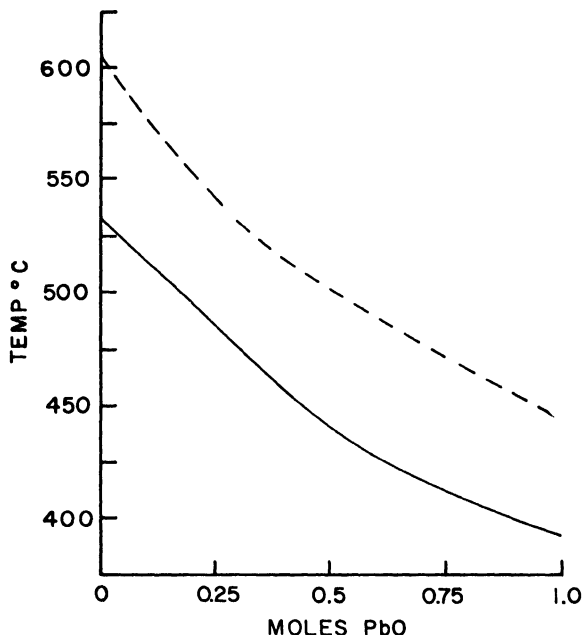


FIG. 2. Substitution of PbO for SrO. Log isokoms for the series of glasses $\text{Na}_2\text{O}, x, \text{PbO}, (1-x)\text{SrO}, 5\text{SiO}_2$. (After Enright.³⁸) Key: solid line, $\log \eta = 13$; broken line- $\log \eta = 10$.

large sizes and their higher coordination requirements raise the viscosity of a sodium silicate glass. This effect is reflected also in the melting points of SiO_2 (cristobalite), ZrO_2 , and ThO_2 , which melt at 1740°C ., 2700°C ., and 3500°C ., respectively.

Unfortunately, it is very difficult to test the influence of size and the polarizability separately. This would be possible by comparing the effects of ZrO_2 and HfO_2 on the viscosity of glass. On account of the lanthanide contraction, these two cations have the same size; but the Hf^{4+} has a larger number of electrons, so that its core should be better screened. On this basis one would expect a hafnium sodium silicate glass to have a lower viscosity than the zirconium analogue.

V. Interpretation of the Viscosity of Some Simple Experimental Glasses of Systematically Varied Compositions

We shall now use the four structural parameters derived in the preceding chapters for interpreting viscosity data of silicate glasses of rather simple but widely different compositions. The parameters which we derived

in the previous chapter consider only the interaction between neighboring ions but they do not consider long range interactions. This treatment is convenient but it is only a first approximation and, consequently, it has definite limitations.

For simplicity's sake we will refer to the four structural parameters by the Roman numbers *I–IV* as follows:

Parameter I: Anion to network-forming cation ratio. This parameter determines the extent to which the SiO_4 tetrahedra or other network-forming polyhedra have to share corners. In alkali silicate glasses, for example, the ratio of O^- to Si^{4+} ions determines the fraction of O^- ions which two neighboring SiO_4 tetrahedra must have in common. The smaller the O:Si ratio, the more corners of SiO_4 tetrahedra have to be shared, the higher is the degree of polymerization and, with it, the viscosity. Vitreous silica has the lowest possible ratio of 2.0.

Parameter II: Binding forces within the polyhedra. The strength of the binding forces between the network-forming cations and the surrounding anions, as well as the fluctuation of these forces with temperature and time, determines the viscosity of the glass. Viscous flow is possible only under conditions which permit the polyhedra to rearrange. The temporary un-screening of network-forming cations during this rearrangement is the major energy barrier of the viscous flow of silicates.

Parameter III: Polarizability of ions. The ability of an ion to adjust its force field to a changing environment increases with its polarizability. Increasing polarizability lowers the viscosity.

Parameter IV: Size of cations with high charges. The number of anions which is required for screening a cation increases with its size. Hence, replacing a fraction of the SiO_2 by ThO_2 causes a silicate glass to increase its degree of polymerization and increases its viscosity.

The measurements of L. C. Hoffman *et al.*⁴⁴ are of particular interest for a structural interpretation of the viscosity because they cover a wide variety of substitutions. The temperatures are chosen to a viscosity range from $\log \eta = 9$ to 13.

FIRST SERIES

In a sodium silicate glass some Si^{4+} ions are gradually replaced by larger ions of the same charge: Si^{4+} , 0.39 Å.; Ge^{4+} , 0.44 Å.; Ti^{4+} , 0.64 Å.; Zr^{4+} , 0.82 Å.; Th^{4+} , 1.10 Å.

The substitution of Ge^{4+} ions for Si^{4+} ions weakens the binding forces between the network-forming cation and its O^- ions (*II*). The polarizability is increased (*III*). At $470^\circ\text{C}.$, however, the substitution does not

⁴⁴ L. C. Hoffman, T. A. Kupinski, R. L. Thakur, and W. A. Weyl, *J. Soc. Glass Technol.* **36**, 196 (1952).

seem to affect the viscosity of the glass $\text{Na}_2\text{O}, 3\text{SiO}_2$ (see Fig. 3). As factor (*I*) is not changed in this series one must assume that the effect of size and of the coordination requirement (*IV*) balances the effect of binding forces (*II*) and polarizability (*III*).

The stable form of GeO_2 has the structure of rutile in which each Ge^{4+} ion is screened by six O^- ions. This tendency of the Ge^{4+} ion to surround itself with more anions than the Si^{4+} ion affects the viscosity of the glass in the same way as a lowering of the anion to cation ratio.

The substitution of GeO_2 for SiO_2 produces two antagonistic effects. The weaker binding forces decrease the viscosity of the glass, but the large size of the Ge^{4+} ion and its higher coordination number increase the viscosity because of the greater degree of polymerization. Such a glass can be called a copolymer of SiO_4 tetrahedra and GeO_6 octahedra. As the substitution did not increase the anion to cation ratio it has to increase the fraction of common corners of the polyhedra.

The substitution of ZrO_2 or ThO_2 for SiO_2 provides additional evidence for the importance of the size of a central cation (*IV*). These ions have a coordination number of at least six to eight with respect to O^- . Germanium dioxide can form a glass by itself, but zirconium and thorium oxide cannot. Their high coordination numbers enable the melt to form nuclei. The oxides should form rather fluid melts because the energy requirements for changing a ThO_3 -group into a ThO_7 or a ThO_9 -group should be relatively small in spite of the strong binding forces between Th^{4+} and O^- ions. In addition, the kT which is available for viscous flow at the melting point, $3500^\circ\text{C}.$, is high. In contrast to SiO_2 and GeO_2 one cannot expect ThO_2 to form a glass.

The Th^{4+} ion is larger (1.10 Å.) than the Zr^{4+} ion (0.87 Å.), but its greater polarizability balances the difference in size. As a result, ThO_2 and ZrO_2 increase the viscosity to a similar extent when replacing SiO_2 on a molar basis.

Replacing SiO_2 by TiO_2 produces an effect which is somewhere in between that of GeO_2 and ZrO_2 , as one would expect. Ti^{4+} ions require six O^- ions for screening, as can be learned from the structure of rutile and from the tendency of the methyl orthotitanate to polymerize. In contrast to GeO_2 , TiO_2 does not form a modification which has the structure of quartz nor can it form a glass by itself.

SECOND SERIES

In a sodium silicate glass some Si^{4+} ions are gradually replaced by cations which have a lower charge: Al^{3+} , Ga^{3+} , and In^{3+} .

The replacement of Si^{4+} ions by Al^{3+} ions increases the low temperature viscosity of a sodium silicate glass (see Fig. 4 on page 322) because it low-

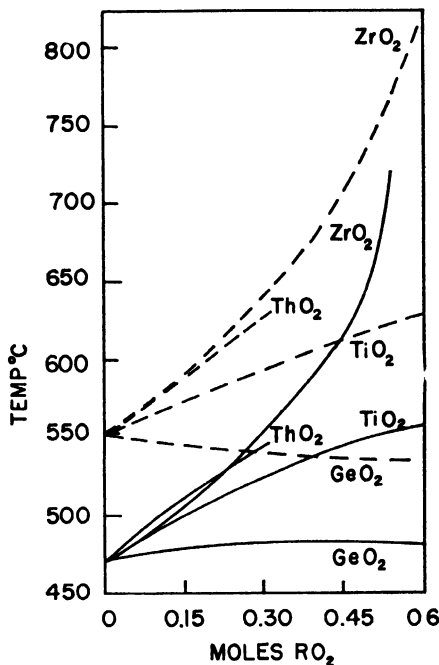


FIG. 3. Substitution of GeO_2 , TiO_2 , ZrO_2 , and ThO_2 for SiO_2 . Log isokoms for the glasses $\text{Na}_2\text{O}, x\text{RO}_2, (3 - x)\text{SiO}_2$. (After Thakur.³⁸) Key: solid lines, $\log \eta = 12$; broken lines, $\log \eta = 9$.

ers the anion to cation ratio (*I*). This ratio can be kept constant only when 2SiO_2 would be replaced by a couple such as $\text{Al}_2\text{O}_3 + \text{CaO}$ or $\text{Al}_2\text{O}_3 + \text{Na}_2\text{O}$.

If one compares the glass $\text{Na}_2\text{O}, 0.3\text{Al}_2\text{O}_3, 2.7\text{SiO}_2$ with the corresponding Ga_2O_3 and In_2O_3 glasses, one can see that for the nonnoble-gaslike Ga^{3+} ion the higher polarizability (*III*) and for In_2O_3 the much larger size (*IV*) dominate the influence of these oxides upon the viscosity. In crystals Al^{3+} ions (0.50 Å.) occur in fourfold, fivefold, and sixfold coordination, but both Ga^{3+} (0.62 Å.) and In^{3+} (0.81 Å.) require sixfold coordination.

THIRD SERIES

In a sodium silicate glass some Si^{4+} ions are gradually replaced by cations which have a higher charge: P^{5+} , Sb^{5+} , V^{5+} and Ta^{5+} .

This group of substitutions leads to a greater anion to cation ratio (*I*) which should lower the viscosity. Indeed, this is the case for Sb^{5+} and V^{5+} ions. With respect to P^{5+} ions, however, the strengthening of the binding forces (*II*) seems to balance the effect of the greater anion to cation ratio (*I*) (see Fig. 5 on page 323). The substitution of large Ta^{5+} ions for Si^{4+}

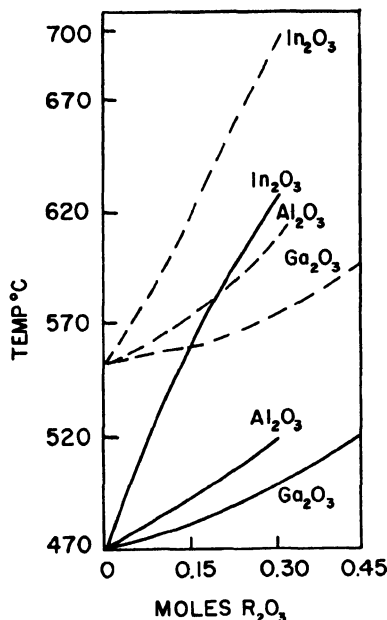


FIG. 4. Substitution of Al_2O_3 , Ga_2O_3 , and In_2O_3 for SiO_2 . Log isokoms for the glasses $\text{Na}_2\text{O}, x\text{R}_2\text{O}_3, (3-x)\text{SiO}_2$. (After Thakur.³⁸) Key: solid lines, $\log \eta = 12$; broken lines, $\log \eta = 9$.

ions increases the viscosity for the same reason as does Zr^{4+} or Th^{4+} . Their fields are sufficiently strong to form their own polyhedra and, because of their size, they surround themselves in the alkali silicate glass with more than four O^- ions, thus increasing the fraction of shared corners: This means a higher degree of polymerization.

FOURTH SERIES

In a sodium silicate glass the Na^+ ions are gradually replaced by the larger K^+ ions. From the work of Gehlhoff and Thomas⁴⁵ it is known that the gradual replacement of one kind of alkali by another causes the low temperature viscosity of a silicate glass to go through a minimum. They also found that this minimum disappears with increasing temperature (see Fig. 6 on page 324).

Poole⁴⁶ confirmed these facts in three series of alkali silicate glasses which contained approximately 18, 25, and 35 % total alkali. The viscosities of the Na_2O glasses are nearly the same as those of the corresponding K_2O

⁴⁵ G. Gehlhoff and M. Thomas, *Z. tech. Physik* **7**, 260 (1926).

⁴⁶ J. P. Poole, *J. Am. Ceram. Soc.* **32**, 230 (1949).

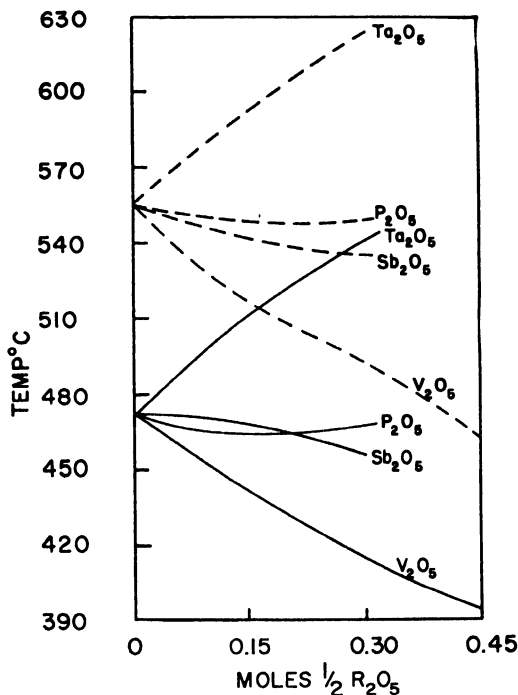


FIG. 5. Substitution of P_2O_5 , Sb_2O_5 , V_2O_5 , and Ta_2O_5 for SiO_2 . Log isokoms for the glasses $Na_2O, 0.5xR_2O_5, (3 - x)SiO_2$. (After Thakur.³⁸) Key: solid lines, $\log \eta = 12$; broken lines, $\log \eta = 9$.

glasses. The glasses in which 40 mole % of the total alkali was K_2O had the lowest viscosity (see Fig. 7 on page 325).

This effect cannot be understood if one considers only the interactions between neighboring ions, because it involves the cooperation of a large number of ions, a feature which Marboe and Weyl⁴⁷ called the key to the understanding of mechanical properties of matter on an atomistic basis.

The simultaneous presence of two cations which have different size and polarization properties makes it easier for the glass to cooperate with the mechanical forces and to group its ions in a fashion which lowers the resistance to shear.

The cooperation of a large number of ions over large distances requires anions of fair polarizability. The dependence of the "mixed alkali effect" upon the polarizability of the O^- ions can be seen from the substitution of alkali oxides in aluminophosphate glasses. The minimum disappears in the aluminophosphate glass and the viscosity is nearly additive if one

⁴⁷ E. C. Marboe and W. A. Weyl, *J. Soc. Glass Technol.* **39**, 16 (1955).

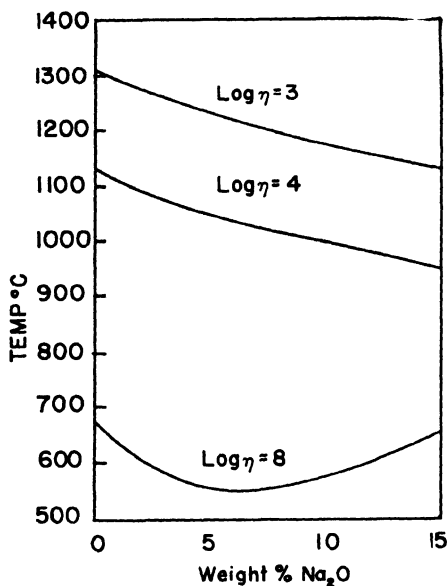


FIG. 6. Substitution of K₂O for Na₂O on a weight per cent basis in the glass: 15% (Na₂O + K₂O), 20% BaO, 65% SiO₂. (After Gehlhoff and Thomas.⁴⁵)

alkali is replaced by another. The phenomenon decreases with decreasing polarizability of the base glass, and PO₄ groups are less polarizable than SiO₄ groups.

FIFTH SERIES

Some Mg⁺⁺ ions of a sodium magnesium silicate glass are gradually replaced by cations of the same charge, similar size, but different electronic configuration: Cu⁺⁺, Mn⁺⁺, Co⁺⁺, Ni⁺⁺, and Zn⁺⁺ (see Fig. 8 on page 326).

The substitution of a nonnoble-gas type cation for a Mg⁺⁺ ion in a compound lowers the melting point. For example, MgF₂ melts at 1396°C. but ZnF₂ at 872°C. A similar effect may be expected for the temperature at which a glass reaches a certain viscosity. The effect of a gradual substitution upon the temperatures at which these glasses (Na₂O, *x*RO, (1 - *x*)MgO, 5SiO₂) reach the viscosities of 10⁹ and 10¹³ poises, respectively, can be seen from Fig. 8.

The substitution of Zn⁺⁺ ions for the smaller Mg⁺⁺ ions has practically no effect upon the viscosity, thus indicating antagonistic influences. The larger size of the Zn⁺⁺ ion (IV) increases the viscosity, and its greater polarizability (18 outer electrons) decreases it.

The concepts of ionic size and ionic radius are based on the assumption that the ions have spherical symmetry and constant size. This approxi-

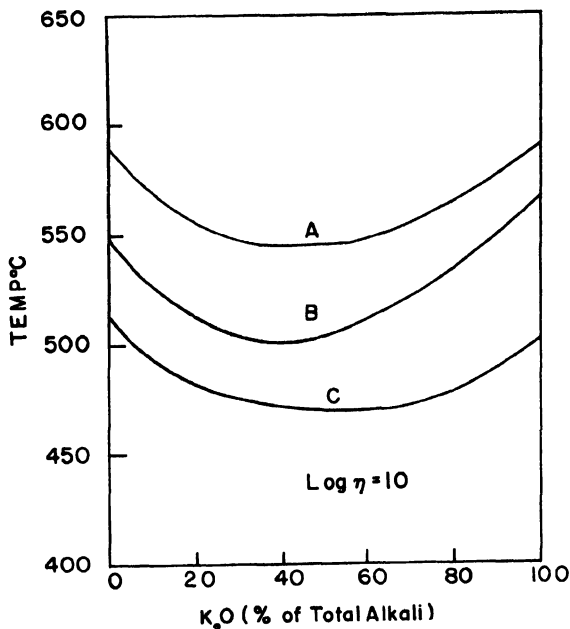


FIG. 7. Substitution of K_2O for Na_2O on a molar basis in alkali silicate glasses containing (A) 18%, (B) 25% and (C) 35% alkali (computed from data of J. P. Poole⁴⁶). $\text{Log } \eta = 10.0$.

mation is justified only for cations of the noble gas type and perhaps for those which have 18 outer electrons. It is not possible, however, to interpret quantitatively the viscosity of glasses containing Cu^{++} , Mn^{++} , and Co^{++} ions with respect to the contributions of their electronic shells (*III*) and their sizes (*IV*).

The group of curves (Fig. 8) reveals the importance of the complexity. In all cases the first additions are by far the most effective. This feature is related to the viscosity minimum of Na-K silicate glasses (Fourth Series).

SIXTH SERIES

The "complexity effect" which can be observed when Na^+ ions are replaced by K^+ ions or Mg^{++} ions are replaced by Cu^{++} ions increases with increasing polarizability of the parent glass.

The response of a complex glass to a shear force can be attributed to the temporary formation of groups ("flow units") which due to mechanical forces, assume asymmetrical force fields. These "flow units" do not represent permanent groups but must be looked upon as chance configurations, the lifetimes of which are prolonged over that expected from statistical considerations as the result of the presence of a force field from stress or an

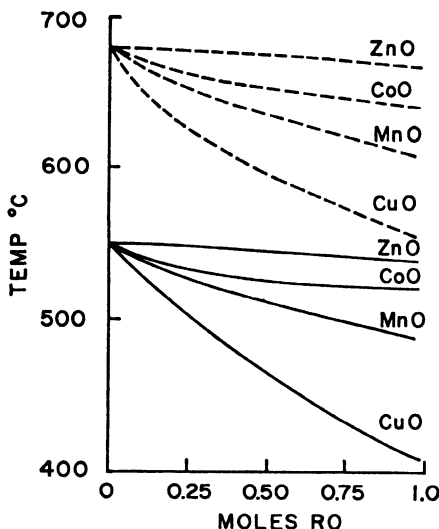
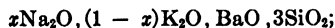
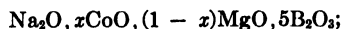
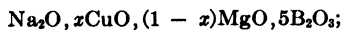


FIG. 8. Substitution of ZnO, CoO, MnO, and CuO for MgO. Log isokoms for the series $\text{Na}_2\text{O}, (1 - x)\text{MgO}, x\text{RO}, 5\text{SiO}_2$. (After T. A. Kupinski.⁴⁸) Key: solid lines, $\log \eta = 13$; broken lines, $\log \eta = 9$.

interface. Formation of these groups requires a change both of the geometry and of the state of polarization of the ions. If all ions were rigid spheres and their interactions were limited to Coulomb forces between neighbors, this effect would not exist; in other words, the physical properties of a random array of ions would be "additive."

For this reason the degree of deviation from additivity becomes a function of the polarizability of the glass, in particular of its O^- ions. It is greater in alkali silicates than in aluminophosphates and it is greater in an alkali barium silicate glass than in a corresponding alkali magnesium silicate. As it was desirable to obtain additional information on the effect which a certain substitution—for example, K^+ for Na^+ or Cu^{++} for Mg^{++} ions—has in different base glasses, Hoffman⁴⁸ examined the viscosity of the following series:



⁴⁸ L. C. Hoffman, Office Naval Research Tech. Rept. No. 34, Contract No. N6 onr 269 Task Order 8 NR 032-264, 5. Pennsylvania State Univ., University Park, Pennsylvania, 1951.

These series show that the "mixed alkali effect" is negligible in the alkali magnesium silicate glass but becomes evident as soon as the small Mg^{++} ion is replaced by the much larger Ba^{++} ion or by one which has an incomplete outer electronic shell (Cu^{++}).

The deviation from additivity caused by the replacement of Mg^{++} ions by Cu^{++} was found to be strong in silicates but weak or practically nonexistent in phosphates and borates.

VI. Viscosities of Some Commercial Glasses

As far as tonnage is concerned, by far the most important glass is based upon the ternary system $\text{Na}_2\text{O}-\text{CaO}-\text{SiO}_2$. However, all commercial glasses contain some alumina, most of them also contain magnesia, and many of them contain K_2O and BaO . These minor constituents are partly unavoidable as they stem from the refractory material (Al_2O_3) or the raw materials (dolomitic limestone). However, some are added on purpose (potash feldspar). These constituents are important as they control the chemical resistivity of the glass and they also affect its viscosity so that their quantities have to be known and controlled. The most reliable systematic work on the viscosity of technical glasses containing these constituents has been published by Poole.⁴⁹

We can present here only the highlights of these very extensive investigations. For details—for example, the melting of the glasses, their chemical analyses, the methods for measuring their viscosities, and the analytical evaluation of the results—the original work should be consulted.

In contrast to the glasses discussed in the preceding Section the commercial compositions are too complex to lend themselves to a theoretical interpretation of their viscosities. Plotting the viscosity data into ternary diagrams, however, allows one to make interpolations and extrapolations to a limited extent. This in itself is very useful because the different glass industries manufacturing plate glass, window glass, container glass, as well as structural glasses (building blocks), are not interested in drastic changes of the composition but have to consider minor changes which are dictated by the economy and the properties.

Table III gives the composition of forty-five glasses in weight per cent and the two constants a and b which describe their viscosity as a function of the temperature by the following equation:

$$\log \eta = a + b(10^3/T)$$

in which η is the viscosity in poises, and T is the absolute temperature. The constants a and b are derived from the experimental data by the method of least squares.

⁴⁹ J. P. Poole, Ph.D. Thesis, Pennsylvania State Univ., University Park, Pennsylvania, 1947; J. P. Poole and M. Gensamer, *J. Am. Ceram. Soc.* **32**, 220 (1949).

No.	Composition in Weight Per Cent								Constants for the equation $\log \eta = a + b(10^3/T)$	
	SiO ₂	Na ₂ O	K ₂ O	CaO	MgO	SrO	BaO	Al ₂ O ₃	a	b
1	74.61	25.39							-17.848	22.759
2	75.73	20.50		3.77					-19.738	25.304
3	77.23	14.22		8.55					-26.462	32.525
4	76.21	9.66		14.13					-24.434	32.665
5	70.43	24.72		4.85					-19.664	24.781
6	66.23	24.17		9.60					-26.269	30.523
7	61.51	24.23		14.26					-30.500	34.115
8	69.06	21.18		8.76					-26.337	31.055
9	65.37	20.61		14.02					-29.384	34.262
10	61.69	19.80		18.51					-31.139	6.080
11	76.02	20.85			3.13				-16.026	21.694
12	79.11	14.98			5.91				-17.736	24.237
13	80.25	10.99			8.76				-17.6394	26.5915
14	70.13	26.55			3.27				-18.7674	23.2986
15	68.90	25.23			5.87				-21.2533	25.2667
16	62.65	27.80			9.55				-21.8421	25.7895
17	71.15	22.89			5.96				-20.4307	25.0437
18	67.14	23.94			8.92				-21.3105	26.2326
19	65.35	22.94			11.71				-23.1862	28.3259
20	72.51	22.42						5.07	-18.4094	23.9588
21	70.42	19.79						9.79	-17.7776	24.4804
22	69.96	24.53						5.51	-18.7333	24.0593
23	64.95	24.87						10.18	-20.1979	25.8912
24	72.38	13.81		9.41				4.40	-21.3265	29.4406
25	70.20	10.59		10.06				9.15	-20.1148	30.1180
26	72.00	15.16		6.99				5.98	-19.9947	27.3730
27	70.16	14.81		4.51				10.52	-18.5155	26.6399
28	69.54	14.93		9.37				6.16	-23.0143	30.2143
29	64.55	15.37		9.43				10.65	-23.3992	30.5806
30	68.97	20.17		4.69				6.17	-21.7770	27.6468
31	64.24	20.12		9.87				5.77	-25.1484	30.9835
32	59.68	25.10		9.45				5.77	-26.9735	31.5619
33	73.84	15.33		5.10				5.73	-18.5813	25.8813
34	64.01	15.52		14.37				6.10	-24.5450	32.0608
35	76.02	16.01		4.92	3.05				-20.6695	26.8568
36	65.60	26.39		4.92	3.09				-21.3784	25.9595
37	70.61	15.90		10.06				3.43	-22.4303	29.3873
38	63.12	22.89				13.99			-24.2300	28.1613
39	58.18	20.44				21.38			-25.6176	29.5204
40	53.67	19.01				27.32			-29.2553	32.6096
41	58.22	19.71					22.07		-24.7299	27.6905
42	51.47	18.58					29.95		-26.6151	29.1132
43	46.19	16.24					37.57		-25.8052	28.3799
44	73.83	12.42	13.75						-16.2244	20.5714
45	73.68		26.32						-16.3025	22.6022

Based on these data Poole⁵⁰ developed a graph which made it possible to read the viscosity of a container glass over a wide temperature range, namely, from the molding to its annealing. The use of the Fulcher equation involves the measuring of the viscosity of the glass at several widely different temperatures, which means the use of at least two types of equipment. He discovered that an approximately logarithmic plot can be used in which the viscosity temperature curve goes through the zero point if the $\log \eta$ is plotted versus the reciprocal value of the absolute temperature on an arc hyperbolic sine graph paper. As $\log \eta$ values are plotted along the \sinh^{-1} ordinate versus $1/T$ he obtained for each glass a nearly straight line which goes through the zero point of the system. One precise viscosity measurement—for example, that of the transformation point (10^{13} poises) or that of the arbitrary softening point ($10^{7.6}$ poises), so to speak—would then be sufficient to characterize the rheological properties of this glass over a temperature range of several hundred degrees centigrade.

This graphical method has been used with very satisfactory results in the container glass industry. Poole points out, however, that this graphical method cannot be used for borosilicate glasses or for lead glasses. As mentioned above, container glasses in different plants vary relatively little in chemical composition, but the glass blowing operation is very sensitive to any minor changes which are made.

VII. Flow Processes within a Rigid Glass

A glass rod fractured under tension shows no sign of flow, the “necking down” which is characteristic for metal rods is absent in glasses. The brittleness of a silicate glass is the result of its inability to dissipate local stresses under impact by flow or plastic deformation. It is this rigidity of glass at room temperature which makes it the best material for supporting the metal films of astronomical telescopes.

In apparent contradiction to this behavior, certain observations seem to indicate flow in a temperature range where the glasses are rigid solids.

1. LOW TEMPERATURE BENDING OF GLASSES

A glass fiber which has been kept wound around a mandrel for some time develops a curvature when it is taken off the mandrel and allowed to move freely, e.g., to float on a pool of mercury.

A glass rod 110 cm. long, clamped at one end in horizontal position over a period of five years, was found to have sagged 9 mm. at the other end under its own weight. Houwink⁵¹ quotes this observation as proof for the

⁵⁰ J. P. Poole, *Glass Ind.* **30**, 19 (1949).

⁵¹ R. Houwink, “Elasticity, Plasticity and Structure of Matter,” p.133. Cambridge Univ. Press, London and New York, 1937.

ability of a silicate glass to flow at an ordinary temperature, analogous to certain organic polymers.

The author prefers to explain these two phenomena on a different basis. Physicists working with high vacua know that the chemisorbed water of their glass vessels is located not only at the surface but that its concentration is highest at the surface and tapers off toward the interior of the glass. Hence, it takes long times to completely remove it and to obtain a good vacuum.

A soda-lime silicate glass is not in chemical equilibrium with the humidity of the atmosphere. Water penetrates into the glass, forming OH^- ions, and causes the glass to swell. The rate of diffusion is determined by the polarizability of the O^- ions of the glass. Protons can diffuse through certain systems by moving within the electron clouds of anions, i.e., they remain screened. By selecting a glass composition which contains highly polarizable O^- ions (cesium disilicate glass), Enright,⁵² in the author's laboratory, performed an experiment in which 15 wt. % H_2O diffused into a glass at room temperature over a period of several months producing a uniform gel.

This diffusion process is accelerated if the glass is brought under tension because the increased internuclear distance in the stretched surface increases the polarizability of the O^- ions. Analogous to the "stress corrosion" of metals, a glass surface under tension is more reactive than one under compression.

If a glass is stressed close to the breaking point, the diffusion of water into its interior causes "delayed fracture." This penetration of water into a glass is one of the reasons why the strength of a glass under load decreases with time and why it depends on the humidity of the atmosphere. On the basis of these facts, the author assumes that a glass rod bent under a load reacts with the water vapor more strongly at that surface which is under tension than with that which is under compression. As a result, the unequal hydration of the two sides produces unequal swelling which, in turn, causes the glass to remain bent. In addition to the migration of water into the glass one must also expect a shift of alkali toward those volume elements which are under tension.

The bending which results from these diffusion processes should not be called viscous flow. The effect, however, is the same as that of a partial release of the mechanical stress through flow.

2. AGING AND COMPACTING OF GLASSES

In addition to the apparent flow of a glass under its own weight at room temperature, other phenomena have been observed which were attributed

⁵² D. P. Enright, Absorption of water by cesium-disilicate glass. Office Naval

to "flow." It was found that precision optical instruments, e.g., prisms, could change their shapes over a period of decades. Precision thermometers revealed that the volume of the glass bulb decreased over decades and caused a "secular rise" of the ice point. When the thermometer was heated and cooled another effect was observed: for some glasses the volume on cooling lagged behind the temperature. A thermometer exposed to boiling water and subsequently immersed in melting ice shows an "ice point depression." When the Jena Glass Works developed their precision thermometer glasses, Weber⁵³ learned to minimize the secular drift by proper heat treatment and the ice point depression by selecting a suitable glass composition. Weber found that for a silicate glass the presence of more than one kind of alkali increased its ice point depression. At this time good thermometers could be manufactured from potash glasses as well as from soda glasses, but mixtures of soda and potash in the same glass had to be avoided.

All these phenomena seem to indicate that in a complex glass there must be particles which flow even at ordinary temperature. When the structure of glasses became better known it was realized that it must be the alkali ions which are "mobile" because they are the most weakly bonded particles in the glass structure.

Today one has learned to control these phenomena. A glass to be used for precision instruments not only has to be properly annealed but also must be "compacted" or "aged." Removal of the stress birefringence alone is not sufficient to guarantee constancy of its properties.

It is very likely that these phenomena are the result of a gradual change of the most mobile particles into energetically more suitable positions. This adjustment of a structure toward an equilibrium should not be called viscous flow. The effect which the redistribution of alkali ions with time exerts upon the volume of a glass is important for precision instruments but its magnitude is very small.

A much stronger effect of a similar nature is observed in the manufacture of the Vycor brand glass. The Vycor brand glass, a 96 % silica glass, has a softening point of 1500°C. which is close to that of pure SiO_2 . The annealing point of the Vycor brand glass is 900°C. and that of fused SiO_2 is 1150°C. Nevertheless, the silica sponge which is obtained by leaching out a partly devitrified sodium borosilicate glass shrinks at a temperature as low as 700°C., according to the observations of Nordberg.⁵⁴

Research Tech. Rept. No. 42, Contract No. N6 onr 269 Task Order 8 NR 032-264, 265. Pennsylvania State Univ., University Park, Pennsylvania, 1952.

⁵³ R. Weber, *Sitzber. deut. Akad. Wiss. Berlin, Math.-naturw. Kl. Abt. II*, 1232 (1883); *Verhandl. deut. chem. Ges.* **21**, 1086 (1888).

⁵⁴ M. E. Nordberg, *J. Am. Ceram. Soc.* **27**, 299 (1944).

It is against all definitions of the fixed viscosity points that a glass with a softening point of $1500^{\circ}\text{C}.$, can show considerable flow at $700^{\circ}\text{C}.$ within a few hours. The shrinking of Vycor is not a reversible flow process, but is analogous to the compacting where the glassware decreases its volume without losing its shape.

3. INTERNAL FRICTION

A perfectly elastic material obeys Hooke's Law. There are several factors such as the thermal conductivity (metal) which may cause a solid to deviate from the ideal behavior and to show "anelasticity." Glasses are poor conductors of heat. Hence, vitreous silica comes close to being perfect in its elastic response; stress and strain are directly proportional. The more complex silicate glasses, however, show deviations from Hooke's Law. Because of structural changes, in particular because of the mobility of the alkali ions, the strain lags behind the stress. This phenomenon, which for glasses involves the diffusion of weakly bonded particles, often called "internal friction," can be measured by several methods.

Guye and Vasileff⁵⁵ studied the damping of torsional oscillations of glass fibers. When the logarithmic decrement of damping was plotted against the temperature, the curves showed maxima around $100^{\circ}\text{C}.$, that is, in a temperature region where the glass is still completely rigid. The maximum could be reproduced on heating or cooling. At this time, when little was known about the constitution of glasses, the phenomenon was attributed to a modification change of the glass, similar to the low-high inversion of quartz.

König⁵⁶ obtained precision data on the elastic aftereffect of a Thüringian glass for different temperatures. A glass rod 2 mm. in diameter and 380 mm. long was clamped in horizontal position at one end. The other end was loaded. The instantaneous deflection and the "elastic aftereffects" were measured for different times and temperatures. Bennewitz and Rötger^{57, 58} made systematic studies of the internal friction of glasses and metals and they were the first ones to offer an acceptable explanation for the origin of the internal friction of glasses where the thermal conductivity is too low to be the cause. They found for vibrating reeds that the damping of the vibration goes through a distinct maximum if the frequency is changed over a wide range. In a particular frequency band the damping constant was found to be as much as ten times larger than the damping constants

⁵⁵ C. E. Guye and S. Vasileff, *Arch. sci. phys. et nat.* **37**, 214, 301 (1914).

⁵⁶ H. König, *Physik*, **Z. 26**, 797 (1925).

⁵⁷ K. Bennewitz and H. Rötger, *Physik. Z.* **37**, 578 (1936); *Z. tech. Physik* **19**, 521 (1938).

⁵⁸ H. Rötger, *Glastech. Ber.* **19**, 192 (1941).

for higher and lower frequencies which were sufficiently far removed. They interpreted the phenomenon by assuming that a glass consists of a rigid elastic network which contains particles of limited mobility. They derived the height of the energy barrier which separates two adjacent possible positions of the moving particle from the effect which the temperature exerted upon the damping. The magnitude of this activation energy (10–20 kcal.) suggests that it is the Na^+ ion which causes the damping. Under stresses these ions can move from one position into another position which, because of the mechanical deformation of the glass structure, has become energetically more suitable.

Fitzgerald and co-workers⁵⁹ made a comprehensive study of the internal friction of a plate glass as a function of frequency and temperature. They recommended this method as a tool for exploring the structure of glass. The internal friction of a glass represents its acoustical absorption spectrum inasmuch as it describes its ability to absorb mechanical energy at different frequencies of vibration. Measuring the internal friction as a function of the frequency at a constant temperature provides the characteristic acoustic absorption spectrum of this glass. The activation energy of the diffusion processes can be derived by applying the Arrhenius' equation to the temperature dependence of absorption maxima.

According to Horton⁶⁰ the damping of the mechanical vibrations of pure silica increases steadily from room temperature to 500°C. without an indication of a maximum. This makes it very probable that it is the introduction of alkali into the glass which is responsible for the appearance of one or more peaks.

In order to understand the internal friction of a silicate glass one has to consider that even the simplest change of the composition, namely, the addition of an alkali oxide to silica, produces three major structural changes: (1) the formation of "single-bonded oxygens," (2) the addition of alkali ions, and (3) a general increase in the polarizability of all anions. The polarizability of all anions is increased or all "bonds" become more "flexible" if the anion to cation ratio is raised.

Even a "pure silica" glass may contain protons or OH^- ions in quantities which will depend upon the way it was manufactured. Anderson and Bömmel⁶¹ observed an absorption maximum for high frequency sound waves (60 kc. to 20 Mc. per second) in vitreous silica at very low temperature (30°–50°K.). This absorption maximum does not appear in quartz but only in vitreous silica. It might be the result of protons moving from

⁵⁹ J. V. Fitzgerald, K. M. Laing, and G. S. Bachman, *J. Soc. Glass Technol.* **36**, 90 (1952).

⁶⁰ F. Horton, *Phil. Trans. Roy. Soc. London, Ser. A.* **204**, 407 (1905).

⁶¹ O. L. Anderson and H. E. Bömmel, *J. Am. Ceram. Soc.* **38**, 125 (1955).

one O^- ion into a neighboring O^- ion. The alternating compression and dilation of the silica under mechanical vibrations cause the internuclear distances and, with them, the polarizabilities of the O^- ions to fluctuate. The protons enter the electron clouds of the most polarizable O^- ion or of that O^- ion which links together two Si^{4+} ions which are stretched apart during the vibrations.

The internal friction as a function of frequency and temperature was measured mostly for commercial glasses. In order to provide a more suitable basis for a theoretical treatment, Hoffman and Weyl⁶² measured the internal friction of glasses which had widely different but very simple compositions.

As anticipated, it was found that the addition of an alkali oxide to a glass affects its internal friction in several ways. Forry⁶³ was able to resolve the effect of sodium oxide into two distinct peaks, which he considered to be related energetically because their activation energies differed by a factor of 2.0.

The latest work on the internal friction of alkali silicate glasses by Rötger⁶⁴ is suited for elucidating its mechanism. We shall interpret his data on the same basis as that used for explaining the viscosity of glasses.

The addition of Na_2O to silica introduces two new structural units, namely, Na^+ ions surrounded by O^- ions and O^- ions which are more polarizable than those in the pure SiO_2 . Each of these units has a characteristic vibration which can be detected by the temperatures at which this frequency has its maximum. One may assume that the vibration of the Na^+ ion with respect to its surrounding O^- ions requires the least energy and that it corresponds to what Rötger⁶⁴ calls the "weak" R^+ group. The value of the activation energies for this group increases from the value 11.9 kcal. for the large K^+ ion to 12.2 kcal. for the Na^+ ion and reaches 14.8 kcal. for the small Li^+ ion. The stronger the electrical field of the ion, the greater will be the energy barrier which has to be overcome in order to move from one position into another. The activation energies refer to glasses of approximately the same molar composition $1R_2O, 2SiO_2$.

As the $O:Si$ ratio increases, the structure as a whole becomes more flexible, i.e., the polarizability of all O^- ions increases. This expresses itself in the lowering of the activation energies of all diffusion mechanisms. With increasing Na_2O content the over-all absorption of the glass increases. Raising the Na_2O content from 15 to 30 mole % lowers the activation energy of the weak group from 13.2 to 12.2 kcal.

The values for the more strongly bonded groups drop from 28.4 kcal.

⁶² L. C. Hoffman and W. A. Weyl, *Glass Ind.* **38**, 81 (1957).

⁶³ K. E. Forry, *J. Am. Ceram. Soc.* **40**, 90 (1957).

⁶⁴ H. Rötger, *Glastech. Ber.* **31**, 54 (1958).

to 26.1 kcal. if the Na_2O content is increased from 15 to 30 mole %. This absorption process is attributed to the motion of R_2O groups by H. Rötger, but it might be better to attribute it to the diffusion of a single-bonded O^- ion. In order to establish electroneutrality in the smallest possible volume the Na^+ ions would have to follow the anion. The two processes amount to the flow of a neutral Na_2O molecule. It is unlikely, however, that the latter migrates as a unit.

The activation energy of a diffusing O^- ion is higher than that of a singly charged Na^+ ion. However, the findings of Forry⁶³ that the two peaks correspond to activation energies having a ratio of 1:2 is very likely a mere coincidence. Treating an O^- ion as a doubly charged rigid particle is an oversimplification. Its electron density distribution and, with it, its binding forces to the Si^{4+} ion are determined by the nature of the neighboring alkali ion. Thus, Rötger⁶⁴ finds that the activation energy of the strongly bonded group is 28.5 kcal in the K_2O silicate but only 23.7 in the Li_2O silicate glass. For the Na_2O silicate the value is intermediate, 26.1 kcal., as one

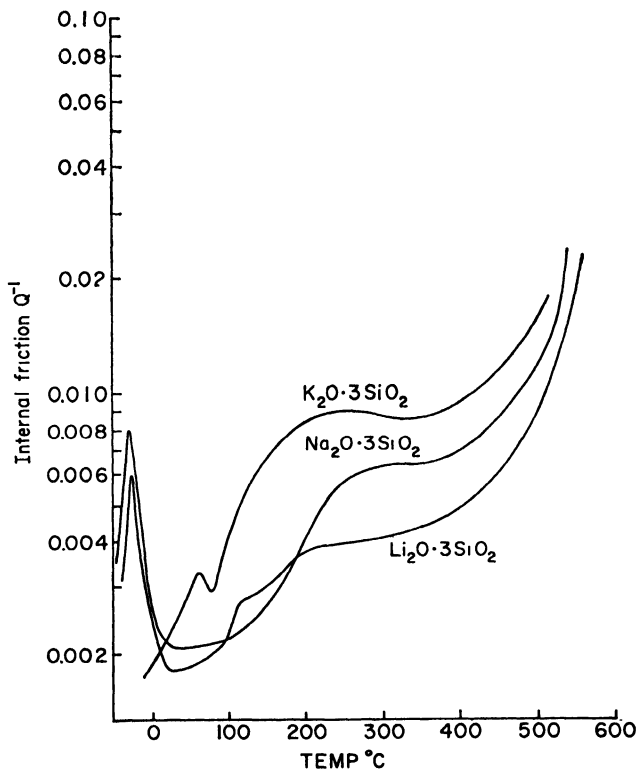


FIG. 9. Internal friction of alkali silicate glasses. (After L. C. Hoffman.⁶²)

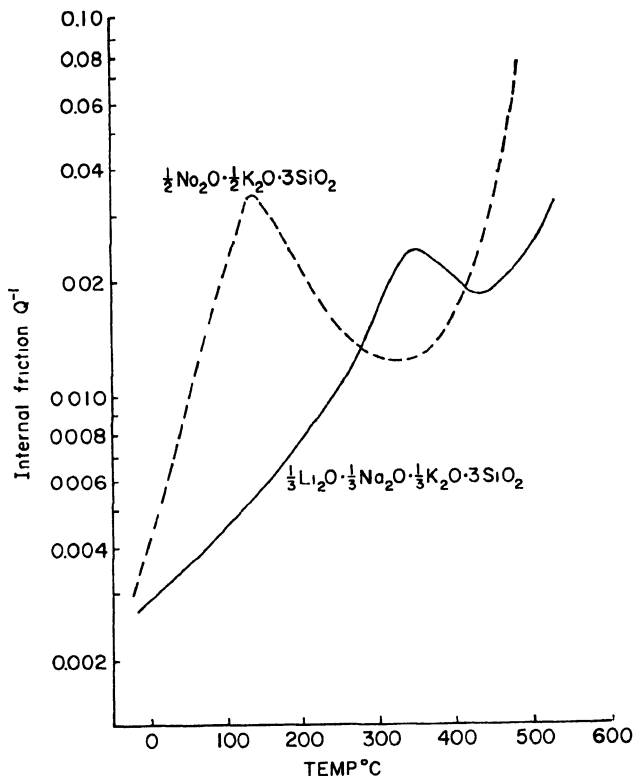


FIG. 10. Internal friction of mixed alkali silicate glasses. (After L. C. Hoffman.⁶²)

would expect. These data indicate that the binding forces of the O^- ion to the Si^{4+} ion are weakest when the anion is polarized by the strong field of Li^+ ions and strongest when it is exposed to the weaker fields of the large K^+ ions. This is precisely what one would expect from the analogy between the internal friction and the viscosities of the alkali silicate glasses.

Figures 9 and 10 are representative curves giving the internal friction of some alkali silicates as functions of the temperature.

4. CUTTING OF GLASS WITH A DIAMOND

During the cutting of glass with a diamond or a steel cutter, phenomena have been observed which seem to indicate flow at room temperature. It is common knowledge among glass cutters that the glass has to be broken shortly after the diamond scratch has been made, otherwise the scratch "heals" and the fracture does not follow the line of the scratch.

This phenomenon is closely related to that associated with internal

friction, where a mechanical force produces a state of polarization in the glass which can be formally described as the formation of a volume element which has a dipole moment. The dipole moment is the result of the flow of alkali ions in one direction. Parts of the glass which are thousands of atoms removed from the scratch have become birefringent and are temporarily weakened. When given sufficient time, however, the induced state of polarization disappears (healing of the glass).

A diamond scratch produces this state of polarization to a considerable depth, but the same phenomenon can be achieved by gently rubbing a glass surface with a piece of cloth. This treatment affects the orientation of the glass to a depth which is far too small to be detected by its birefringence but which is sufficient to induce oriented overgrowth. Zocher and Coper⁶⁶ found that a clean sheet of glass which has been rubbed in one direction induces methylene blue to crystallize on its surface in an oriented fashion. The orientation can be made visible by withdrawing such a glass slowly from a solution of methylene blue in methyl alcohol. Such a glass is then pleochroic and can be used as a Nichol prism.

VIII. Summary and Conclusions

The rheology of glass is unique when one considers the wide range which it covers both with respect to temperature and to mobility. Glasses are Newtonian liquids, they do not have a yield value even in the low temperature range where the viscosity reaches 10^{15} poises. However, in the high viscosity range, additional effects become noticeable which obscure the Newtonian flow unless special precautions are taken to separate them.

In the high temperature range (1400–1500°C.) the silicate glasses are fluid like other fused salts. Frequently fluidity or, generally speaking, mobility has been mistaken for an indication of weak binding forces. There is no relation between these two parameters. Mercury is a fluid metal and the high vapor pressure indicates that the binding forces between the mercury atoms are weak, at least when compared with other metals, e.g., gold and copper. Gallium, too, has a high mobility, it is plastic and melts at 29°C. This metal, however, boils at 2064°C. as compared with 357°C., the boiling point of mercury.

The electronic conductivity of copper or silver is much greater than that of the alkali metals. Nevertheless, the electrons are more tightly bound in copper or silver than in sodium or potassium.

The hydration energy of the proton has been estimated to be of the order of 250 kcal., a value which exceeds that of other cations. Nevertheless, its strong binding forces in an aqueous solution do not prevent it from moving much faster than other cations.

⁶⁶ H. Zocher and K. Coper, *Z. Physik. Chem. (Leipzig)* **132**, 295 (1928).

The low melting point (457°C.) and the softness of AgCl as compared with the higher melting (800°C.) and harder NaCl is not the result of weaker binding of the ions within the AgCl lattice but of the higher polarizability of the Ag^+ ions as compared with the Na^+ ions. AgCl and NaCl crystallize in the same structure and the internuclear distances are the same. The lattice energy of the AgCl, however, is considerably greater (214 kcal.) than that of NaCl (180 kcal.) because of the greater energy of deformation.

In order to clarify the factors which determine the viscosity of ionic systems, the principles of glass formation are discussed. Why do certain fused salts (silicates, borates, and phosphates) polymerize gradually and form a melt whose viscosity increases rapidly, whereas others (NaCl, NaNO_3) do not?

The anion to cation ratio and the coordination requirement of the central cation were found to be the most important factors which determine polymerization and glass formation. Fused oxides which contain large cations of high coordination numbers, for example, ZrO_2 and SnO_2 , cannot form glasses in spite of the very strong forces acting in these fused oxides (low vapor pressure). The binding forces as determined by the charges and the polarization properties of the ions have an important modifying influence on the polymerization.

These factors are discussed on the basis of the viscosity of simple glasses of widely different compositions. The atomistic explanation of Marboe and Weyl⁴⁷ is based on the electrostatic interaction between close neighbors.

The application of crystal chemical concepts to the short range order in glasses and the interpretation of their diffuse X-ray diffraction pattern leads necessarily to a static picture of its structure. One cannot expect that such a picture is suitable for completely understanding viscous flow of glasses. The rheological properties of glass can be explained only when we know how the atomic structure of a glass changes if a mechanical force is applied. This question is answered in a general way by the principle of Le Chatelier, which states that a system under a constraint undergoes, if possible, a change which will minimize the constraint. According to this principle, a shear force which pushes one plane of ions so that it would pass over another plane changes the atomic structure into "flow units" with a minimum cohesive force between the two hypothetical planes. The greater the variety of ions, the greater is the probability of forming groups which exert minimum forces in the direction perpendicular to the hypothetical planes. For this reason the viscosity of glasses is not an additive property. Even the replacement of a weak sodium ion by a potassium ion in a silicate glass causes the viscosity to go through a minimum. The empirical knowledge that low melting glasses of a good chemical resistivity must have a complex composition can be understood on the basis of "flow units"

with strongly asymmetrical force fields. Low melting glazes and enamels contain a large number of constituents, oxides and fluorides, because the presence of ions with a great variety of sizes, charges, and polarizabilities makes it possible for the system to form "flow units" with strongly directional forces which can adjust themselves under shear.

Commercial glasses have a complex composition because they have to meet a large number of requirements with respect to their chemical and physical properties. For this reason no attempt has been made to interpret the viscosity data of technical glasses.

J. P. Poole studied glasses of the soda-lime silica type which contain common constituents such as MgO , Al_2O_3 , etc. These data are presented in tabular form giving the chemical composition in weight per cent and the constants a and b of the equation.

$$\log \eta = a + b(10^3/T)$$

which correlates viscosities as a function of the absolute temperature.

The internal friction of glasses are discussed in order to include one of many phenomena in which particles move in the rigid glass. Mechanical stresses either due to binding or torque produce strains which are conducive to the migration of alkali ions. This is exactly what one would expect from the fact that a flow of alkali ions in one direction causes the volume of the glass to change. This phenomenon has been observed by Quincke (1880) and later by Wüllner and Wien (1902) when they exposed a glass to an electrical field. Especially soda-lime silicate glasses show a volume change with time (electrostriction) which is the result of the alkali ion flowing toward the negative electrode. Migration of alkali ions is also responsible for the volume changes of thermometers (secular drift and ice-point depression). However, it was the internal friction measurements which gave us a better picture of the energy relations of the ions moving within the rigid framework of the silicate structure.

It is not possible to draw a sharp line between those phenomena which constitute the rheology of a glass and others which do not belong in this category. Some readers, for example, may question the author's attitude toward the rigidity of glass at ordinary temperature and point to the flow of glasses under very high pressures which arise during scratching with a diamond or during polishing.

Normally a glass fractures when it is stressed beyond a certain limit. Under certain conditions, however, fracture can be prevented so that the stresses can be increased to such an extent that they can overcome the chemical binding forces and the glass will yield. Bridgman⁶⁶ found that under very high pressures a soda-lime glass can be deformed at ordinary

⁶⁶ P. W. Bridgman, *Proc. Am. Acad. Arts Sci.* **81**, 170 (1952).

temperature. He subjected a flat disc, 0.25 inches in diameter and 0.006 inches thick, placed between two flat carboloy blocks to a pressure of 100,000 kg./cm.². Under the uniaxial pressure the thickness of the disc decreased permanently by 22 %. Prolonged exposure of the glass to this pressure, however, did not change the shape any further. This means that the glass did not behave as a liquid which has a very high but measurable viscosity at ordinary temperature, but it behaved like a crystal which undergoes a structural change.

Pure silica formed by a chemical reaction under very high pressure forms a distinct new crystalline modification, "coesite," named after its discoverer, Coes.⁶⁷ The observation of Bridgman and other similar ones indicate structural changes under pressure rather than viscous flow. In Bridgman's experiment the density of the glass had permanently changed from 2.497 to 2.617.

A glass is an elastic solid up to pressures of 10,000 atm. However, if the pressure is raised to the order of 100,000 atm. the forces reach the magnitude of chemical binding forces and the glass undergoes a structural change during which it can flow temporarily. Pressures of this magnitude are not at all uncommon. A diamond point, when used for writing on glass, exerts a pressure of the magnitude which corresponds to approximately 1 gm./μ². Brüche and Schimmel⁶⁸ made a careful study of the effect of localized pressures on the behavior of glass. With their instrumentation they obtained truly elastic deformation of the glass if the diamond point was loaded with 10 mg. corresponding to a pressure of less than 500 kg./mm.². Loads above 1 gm. produced fracture: the diamond scratches the glass in the same manner as that which occurs when glass is cut. Between these two extremes there is a pressure range in which the diamond point causes the glass to "flow." It produces a groove and two parapets.

These facts were known for quite some time and the development of phase microscopy contributed much to their elucidation. Some observers attribute the flow phenomena to local heating but there is no evidence to substantiate this. The work of Bridgman eliminates temperature as an essential factor.

Very similar situations arise during the polishing of glass. It is well established that polishing is not merely an abrasion. There is evidence that polishing involves "flow." Here, too, the author prefers to speak about a structural change under the directed forces which permit transport of matter temporarily.

⁶⁷ I. Coes, *Science* **118**, 131 (1953).

⁶⁸ E. Brüche and G. Schimmel, *Glastech. Ber.* **27**, 239 (1954).

CHAPTER 9

THE RHEOLOGY OF CONCRETE¹

M. Reiner

I. Introduction	341
II. Fresh Cement paste.	344
1. Structural Considerations.....	344
2. Rheological Properties	345
III. Set Cement	346
1. Structural Considerations ...	346
2. Unstressed Deformations	347
3. Rheological Properties.....	349
IV. Mortar..	351
1. Fresh Mortar ..	351
2. Viscosity of Set Mortar.....	352
3. Elasticity of Set Mortar	354
V. Concrete	356
1. Fresh Concrete ..	356
2. Rheological Behavior of Set Concrete ..	358
3. Viscous Creep.	361
VI. Reinforced Concrete ..	363
Nomenclature..	364

I. Introduction

Concrete is a material consisting of mineral aggregates dispersed in a binder. If the binder is made of cement, one speaks of cement concrete or simply concrete. If it is lime, the term is lime concrete, and so on. The mineral aggregates are usually of two kinds, the fine aggregates called sand and the coarse aggregates which are either broken stone or gravel. In a good concrete both fine and coarse aggregates are well graded so as to give the greatest density. If all grades are present one speaks of "continuous" grading; when a certain class of aggregates is missing in the mix, grading is "discontinuous." The usual designation of a concrete as, e.g., 1:2:4 means one part binder, two parts sand, and four parts stones,

¹ For a more detailed treatment compare the chapters by E. Forslind, E. Torroja, and A. Paez, P. Mason, and A. M. Freudenthal, in "Elasticity and Inelasticity of Building Materials" (M. Reiner, ed.), pp. 64, 222, 253, 290. North-Holland, Amsterdam, 1954.

all measured separately by bulk volume, but cement is actually added in equivalent weight. The water-cement ratio (WC) is the ratio of water to cement by weight. Sometimes very fine aggregates are added directly to the binder: these are called fillers. The mixture of binder and sand is called mortar, and concrete can accordingly be regarded as a mixture of mortar and coarse aggregates. The mortar can be considered as a suspension of sand in the binder. Mortar and concrete will naturally possess voids or pores filled with air and, strictly speaking, air should be considered as one of their constituents.

Commercial cement is sold as a powder. There are two kinds of cement: the natural cement and Portland cement. Natural cements were already used by the Romans. They are produced by calcining limestones associated with a considerable proportion of clay at temperatures usually within a range 1100 to 1300°C. These are then ground to obtain a fine powder. By far the most important cement, however, both technically and economically, is the modern Portland cement, invented in 1824. This differs from most of the natural cements in being an equilibrium product at the kiln temperatures. In the present chapter the term "cement" will always refer to Portland cement.

By the addition of water, cement is made into a concentrated suspension: the *cement paste*. Through the chemical setting process this is converted into "set² cement," which is an artificial stone. The term "cement" is used indiscriminately for the powder, the paste and the stone but their rheological properties are naturally quite different.

The mixture of paste and sand is called fresh mortar: this is converted into "set" mortar. Similarly we have to distinguish between fresh and set concrete.

In order to understand the rheological behavior of concrete it is therefore necessary to consider (a) the fresh cement paste, its setting, and the rheological behavior of the resulting set cement; similarly (b) the fresh cement mortar, its setting, and the rheological behavior of the resulting set mortar; and finally (c) the concrete itself under the same three aspects.

In a different arrangement four kinds of rheological problems can be distinguished: First there are those connected with the rheology of the constituent materials, mainly cement, but also water. Secondly there are the problems connected with the manufacture of the concrete, constituting the rheology of the plastic mix and dealing with such properties as "workability" and "segregation." Thirdly there are those connected with the finished product dealing with elasticity, permanent set, and creep. As concrete has great strength in compression but little in tension, it is re-

² The term "set" is also in use in rheology with an entirely different meaning, compare Section V, 2.

inforced by the insertion of steel rods. The problems specific to the anisotropic material *reinforced concrete* form the fourth group: they are dealt with in Section VI below.

The rheology of concrete started with investigations of its strength. Strength, though the most complicated rheological property, was, as can easily be understood, the first to receive attention and it has remained the one with which the material-testing laboratories are most concerned. From 1845 on, the crushing strength and later tensile strength of cement, mortar and finally of concrete was determined. To date the principal rheological concrete tests which have been standardized in the United States and Britain are determinations of crushing (or compressive) strength, transverse (or bending) strength, and the loading test of concrete floors. Thus the traditional attitude of the average structural engineer to concrete is as if it belonged to the structural materials such as steel and wood not subject to a time factor. When it is felt that this approach is not consistent with facts, sometimes experiments are undertaken which imitate as much as possible the conditions under which the structural elements are required to act in the building structure and the investigator is satisfied with empirical results for these different conditions which can very seldom be correlated among themselves. This method of investigation has on occasion reached a very large scale, e.g., the model tests of the Committee on Arch Dam Investigations, Denver, Colorado, 1931. Since then small-scale rheological experiments have answered the questions raised more fully and certainly more economically.

It appears that the first systematic investigations which may be called rheological were made by Bach in the eighteen-nineties. Bach drew the conclusion that concrete does not obey Hooke's law of the proportionality of stress and strain and that this rule should be replaced by another law in which the strain is proportional to the n th power of the stress. This "power law" is still in use, despite the serious theoretical objections to it.³ Bach was also the first to distinguish between the elastic, recoverable, and the permanent, nonrecoverable part of the deformation, but probably included delayed unrecovered strains in the latter. However, most experimental material collected before the property of creep in concrete was discovered is of little, if any, value. A new era started in the twenties, when McMillan⁴ in the United States reported upon observations of a column in compression which, at the end of a period of 600 days, showed a continuous deformation still proceeding at the average rate.

³ Compare M. Reiner, *Naturwissenschaften* **21**, 294 (1933), but there is no objection to the use of the Nutting-Scott Blair equation as an interpolation formula. Cf. also G. W. Scott Blair and M. Reiner, *Appl. Sci. Research* **A2**, 225-234 (1950).

⁴ F. R. McMillan, *Proc. Am. Concrete Inst.* **17**, 150 (1921).

II. Fresh Cement Paste

1. STRUCTURAL CONSIDERATIONS

The cement paste is formed by mechanically admixing water to the cement powder. The water wets the cement granules, which then form more or less compact agglomerations as is evident under the microscope. As the tendency of a physical system to reduce its interfacial surface is a spontaneous thermodynamic process, it is possible, for example, that certain points of two solid particles can produce a direct bond between them, to the extent of forming part of the same crystalline pattern. This has been revealed by the electron microscope, at least during the early stages of the growing crystalline nuclei. Such a process may be brought about by substances from the solution or by the movement of the intervening liquid or adsorbed film, considering the greater energy of the particles situated along the edges or sharp convexities of the lattice already formed.

Forslind¹ has expounded different views. Regarding the water itself, he points to the fact that the association of the water molecules, which is governed by the hydrogen bond, produces a definite structural arrangement. There results a three-dimensional lattice in ice which is retained above the melting point. At the melting point there takes place a transition from the ice lattice to the water lattice. Thermal vibrations may cause a water molecule to leave its regular lattice point, thus causing a "Frenkel defect." The molecule enters into the interstices of the structure, a process which decreases the over-all thermal expansion of the molecular system and causes the increase of the density of ice to that of water when a thermal equilibrium is attained. The equilibrium is disturbed under the influence of a deformation applied to the system until a new steady state is reached at constant rate of deformation. Intermolecular potential barriers in the crystalline phase prevent all but the largest thermal amplitude fluctuations from contributing to defect formation and thus to flow. The potential barriers are depressed with increase of strain until a yield point is reached. According to this view, aqueous systems therefore possess both a yield point and structural viscosity, and water may thus be regarded as essentially crystalline. When the cement powder is mixed with water a hydrogel is produced. The water molecules are adsorbed on a solid substrate and it may be supposed that the spatial arrangement of the first adsorbed layer corresponds to a crystalline face of the ice lattice. From the interface a crystallization of water molecules proceeds. If adsorption of this type takes place between two layers of substrate the mechanical strength of the water may approach that of ice. A model for the ideal hydrogel is

obtained by imagining layers of solid phase separated by water layers of various thicknesses. The resistance to deformation decreases with the thickness of the water layers. The yield point increases with increased rate of deformation while the instantaneous stress in the crystalline water sheet relaxes in Maxwell fashion. In the close neighborhood of the yield point there occurs a rapid shortening of the relaxation time corresponding to an increase of fluidity, therefore representing non-Newtonian behavior or structural viscosity.

The cement paste itself is formed by gel precipitates obtained on solution of the cement powder in water intermingled with nondissolved clinker residues and crystalline hydration products of low solubility. The ideal hydrogel is thus modified by the introduction of a heterogeneous solid phase of dimensions ranging from molecular size to tenths of millimetres. Hydrophobic materials cause disturbances of the lattice order in the adsorbed water layers and thus lead to augmentation of deformability, to coacervation, and eventually to a visible phase separation known as "bleeding." When the particle size of the solid introduced exceeds the maximum intercrystalline space in the gel, the latter may be considered as a medium of suspension. The system remains plastic as long as the added material, including the filler, is completely dispersed.

2. RHEOLOGICAL PROPERTIES

The rheological properties of fresh cement paste are influenced by the following factors: (a) water-cement ratio; (b) degree of hydration; (c) particle size and size distribution of the cement; (d) amount of filler ($d \leq 0.15$ mm.), its particle shape and size distribution; (e) presence of admixtures affecting the properties of adsorbed water layers; (f) temperature.

In accordance with the structure of fresh cement paste as described in Section II, 1 above, this can be regarded as a first approximation to a Bingham body,⁵ the fundamental rheological properties of which are the yield stress (ϑ) and the plastic viscosity (η_{pl}). The appropriate instruments are the tube and the rotating cylinder plastometer. With the second kind of instrument, as developed by Volarovitch, Lobanov⁶ found, for instance, by applying the Reiner-Riwlin equation,⁵ for a cement paste of 24 % by weight water content, $\vartheta = 480$ dynes/cm.² and $\eta_{pl} = 24$ poises. Applying the Buckingham-Reiner equation⁵ he then estimated that a pressure of 74 atm. would be required to pump the material through 100 m. of a 65-mm.-diameter pipe at a rate of 6 m.³/hr.

⁵ Compare Vol. I, Chapter 2, Section VI, 2.

⁶ V. P. Lobanov, *Kolloid. Zhur.* **12**, No. 5, 352-358 (1950).

III. Set Cement

1. STRUCTURAL CONSIDERATIONS

When the cement paste sets, the paste appears to dry out and water disappears from the surface. If the water-cement ratio is kept within certain limits, the system as a whole will have a gellike structure possessing a certain rigidity and strength. Alternatively this rigidity is viewed as resulting from an interlacing of crystals formed by hydration. As Torroja¹ remarks, the discrepancy between these theories is more apparent than real. The degree of dispersion of the crystals may correspond in size to the colloidal state while the small particles of the solid phase that form the gel will have, in general, a crystalline lattice. In these gels the rigidity can be attributed to the interacting forces between the dispersed particles, and the intermicellar liquid may or may not be an essential factor. The drying-out would correspond to that stage when the interfacial specific surface has become very large and the ratio of solid to liquid phase has increased considerably as a result of the increase of hydrated phases and the reduction of water. Measurements made by Powers and Brownyard⁷ indicate that the solid particles in the hardened cement have an average diameter of the order of 140 Å. and that the distances separating these particles in the gel are of the order of 20 to 40 Å. This implies that the solid phase has a specific surface of the order of 10^6 cm.²/gm. and the free surface energy will, therefore, be high. The water may assume the following states: water chemically combined, water of crystallization, zeolitic water, gel water, adsorbed water, free or capillary water, and water vapor. There is no technique available to determine how water is distributed between these states after setting, and Powers and Brownyard⁷ have resorted to an empirical arbitrary division. They regard as nonevaporable that water which is retained in the paste in equilibrium with a system giving a vapor pressure of 6×10^{-4} mm. Hg. This is substantially equal to the amount of water retained in the paste if dried at 105° C.

The total amount of water present in a sample of hardened saturated paste may be thus divided into two classes, namely, nonevaporable and evaporable water.

Nonevaporable water may be considered to be the water forming part of the solid hydration products, i.e., water chemically combined or water of crystallization, while evaporable water is essentially capillary water, gel water, water adsorbed over the surface of microcrystals, and zeolitic or intercrystalline water that may be present.

The rigidity of the final material and its rheological behavior can be accounted for by the interacting forces between solid and water in the gel,

⁷ T. C. Powers and T. L. Brownyard, *J. Am. Concrete Inst.* **18**, 101, 249, 469 (1946).

when the paste has set. To this must be added the effect of solid to solid linkages, the number of which increases with the age of the material and causes age-hardening. Powers and Brownyard distinguish between two classes of pores: (1) gel pores—small pores between the gel particles, and (2) capillary pores—pores larger than the gel pores, between aggregates of gel.

Hydration proceeds on the expense of capillary volume which thus decreases. It disappears completely if the original WC was 0.4. Capillaries vary in size from 5×10^{-4} to 5×10^{-5} in. in diameter.⁸ Gel pores are about 10^{-7} in. in diameter. The pore volume of cement gel is the lowest possible, the porosity being 26 % which corresponds to the highest packing possible for spheres. The average number of layers of water molecules on the surface of the saturated gel is 2.38.⁹

2. UNSTRESSED DEFORMATIONS

Torroja¹ distinguished two groups of deformations, namely unstressed and stressed deformations. The former are deformations which arise without any externally applied forces, while the latter are the result of externally applied mechanical forces, so that an internal stress system is established in equilibrium with the external forces. He enumerates the following causes of deformation, namely shrinkage, humidity, heat, elasticity, set, and creep. The first three causes are not due to applied forces.

The term *shrinkage* is applied to the apparent reduction in volume of the cement paste (or the mortar and concrete made with it), expressed as change of volume per unit volume. This term is also applied to the reduction in length, expressed as change in length per unit length. The phenomenon is caused by the reduction in volume during the chemical hydration process of anhydrous cement plus water. The decrease in absolute volume of paste will, in general, be greater than the observed shrinkage, because the solid skeletal structure will restrain the movement of the solid particles that make up the paste. L'Hermite¹⁰ attributes shrinkage directly to the loss of "zeolitic" water.

The reduction in absolute volume of a suspension of cement in an excessive quantity of water attains according to him a maximum after 500 days, and is of the order of 16 % of dry cement volume. This volume is substantially larger than the shrinkage observed in practice. If the cement or concrete cannot shrink freely because part of its boundary is fixed, tension stresses develop which will lead to shrinkage cracks. Such shrinkage cracks can also be observed in other materials, for instance, in cheese.¹¹

⁸ G. J. Verbeck, *Am. Soc. Testing Materials, Spec. Tech. Publ.* No. 169 (1956).

⁹ L. E. Copeland and J. C. Hayes, *J. Am. Concrete Inst.* **27**, 633-640 (1956).

¹⁰ R. L'Hermite, *Bulletin Rilem*, Paris, 1953, 1954.

¹¹ M. Reiner, G. W. Scott Blair, and G. Mocquot, *Lait* **29**, 351-357 (1949).

Intrinsic shrinkage occurs within a sealed medium, without possibility of giving off, or absorbing, moisture. *Ecological shrinkage* is operative when gel or evaporable water is adsorbed or eliminated in order to re-establish thermodynamic equilibrium with the surroundings of the paste.

Intrinsic shrinkage is the only one likely to occur in large masses of concrete, such as dams. In these the interchange of water with the surroundings is practically nil because of the very slight permeability of good concrete and the difficulty of water diffusing through the large mass.

In practice the cement hydration process will take a long time to complete. The reaction may be slow or even stop altogether after a certain period of curing, though the ratio of water and cement may be greater than that theoretically necessary for the hydration of the clinker components, as defined by the reaction diagram and the mineralogical composition of the cement. In the set cement the gel water is subjected to interaction forces with hydrated solid particles. This slows up the diffusion of the water toward the anhydrous cement and might even suspend the hydration process. As a result of this, the intrinsic shrinkage, which progressively decelerates, may continue over very long periods.

Usually the setting of cement occurs in air, so that from the start part of the water begins to evaporate. In such conditions it will be less easy for the cement to reach full hydration.

If hardening occurs under water, and the volume of the specimen in relation to its porosity is not sufficiently large to impede the entry of water, the hydration may be completed by absorbing further quantities of water. In such a case the material will experience a noticeable increase in volume which, expressed as a percentage of the total volume, is called *swelling*.

With regard to ecological shrinkage, it is an observed fact that the apparent reduction in volume is accompanied by a loss of water. When the amount of moisture decreases gradually, the test specimen, saturated in water—having been cured in it—will first lose part of the capillary water and will also lose, simultaneously, part of the gel water (making up the less firmly united layers). This will continue until moisture is reduced to 45%. For this value of the moisture Powers supposes that capillary water has disappeared. From this stage on, further shrinkage must be connected entirely with the reduction in the gel water content.

Contradicting this view, Lea and Desch¹² immersed concrete specimens in benzene and showed that this did not cause swelling. Since the benzene penetrated the capillaries only, this proved that moisture transfer to or from the capillaries does not cause change of volume and the latter is, therefore caused by movement of gel water only.

¹² F. M. Lea and C. H. Desch, "The Chemistry of Cement and Concrete." Arnold, London, 1935.

When humidity increases, the cement paste absorbs water so that equilibrium with the surroundings is established. This causes swelling of the cement. In this way the specimen only recovers part of the volume lost in shrinkage, but there always remains *irreversible shrinkage*.

The reversible part of the shrinkage follows variations in environment humidity and can be regarded as a strictly ecological deformation. However, in the course of successive cycles, there is a slight damping in the amplitude of the changes.

To establish thermodynamic equilibrium between the interior of the material and the environment takes time. This period varies much with the size of the specimen. It has been observed that 50 % of the evaporable water at 1 in. from the surface is lost within a month, but that it takes 10 years for the same proportion of evaporable water to be lost at a depth of 3 in. below the surface. Hence a humidity gradient is established inside the cement mass. This alters all ideal uniform states of stresses, produced by elastic and creep stresses, as a result of unevenly distributed internal stresses.

3. RHEOLOGICAL PROPERTIES

Rheological properties refer to stressed deformations. To investigate these Bingham and Reiner¹³ laid beams of hardened cement and cement-mortar stone across two horizontal supports 76.1 cm. apart and allowed them to sag under their own weight, which produced a maximum bending stress of about 5×10^6 dynes/cm². The sections of the beams were 2.27 cm. square. The experiments were extended over a period of 7 months. The curve of the deflection versus time generally starts as a parabola but becomes "linear" beyond a certain point (compare Fig. 1). The slope of the curve is a measure of the "creep fluidity" of the material. As can be seen, the straight-line portions start for all beams approximately at the same age of 45 days. The parabolic curve was interpreted as due largely to chemical hardening which causes a gradual decrease in creep fluidity, with possibly a small elastic fore effect. The experiments were repeated with extended scope by Arnstein and Reiner.¹⁴ The beams were observed not only when acted upon by their own weight but also when supporting concentrated loads at the center producing double and triple bending stresses. The deflections versus time under double and triple stresses, if reduced in proportion to the stress, roughly coincided. Moreover they were "straight lines". The conclusion was accordingly drawn that the set cement flows in the same manner as a very viscous liquid, and that there

¹³ E. C. Bingham and M. Reiner, *Physics* **4**, 88-96 (1933).

¹⁴ A. Arnstein and M. Reiner, *Civil Eng.* **40**, 198-202 (1945).

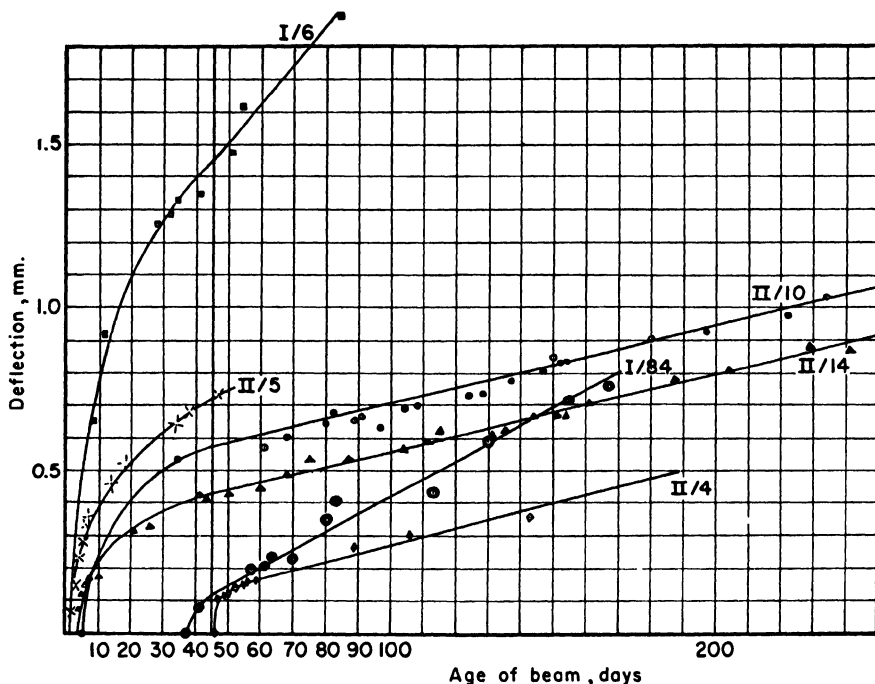


FIG. 1. Creep curves of set cement and cement mortar. I indicates cement; II indicates cement mortar. The denominator indicates the number of curing days. Age of beam = number of days after completion of curing.

is no yield stress which must be exceeded. In contradistinction to the fresh paste, the set cement turned out to be not a plastic solid but paradoxically, could be regarded as a very viscous elastic liquid. Neglecting the possibly very small elastic fore-effect, its behavior could be represented by a Maxwell body.¹⁵ Using equations (69*i*) and (69*ii*) of Volume 1, Chapter 2, Section IV,3, and the viscosity-elasticity analogy mentioned in Section IV,4 of that same chapter, Arnstein and Reiner¹⁴ calculated creep viscosities of 1 to 5×10^{17} poises of set cement at an age of about 60 days. In this view, the cement continues to flow in accordance with this viscosity at a constant rate for about 1 year, after which the rate gradually decreases as a result of internal structural changes described above in Section III,1, without, however, coming to a complete stop during any observed time.

With regard to the elastic response of the set cement, Bingham and Reiner¹³ found proportionality of stress and strain in accordance with

¹⁵ Cf. Vol. I, Chapter 1, Section VI,4.

Hooke's law and calculated a Young's modulus of about 25×10^{10} dynes/cm.² $\sim 35 \times 10^6$ p.s.i.

Recent experiments by J. Glucklich (to be published) on the same lines as those by Bingham and Reiner,¹³ and Arnstein and Reiner,¹⁴ have shed new light on them. He carried out several cycles of loading and unloading of similar beams and found that for equal loading time the beam always reached the same deflections as on the preceding cycle, despite the fact that the beam had not fully recovered on it.

These observations contradict the view expounded previously, that the hardened cement paste can be regarded as a viscous liquid, for such liquid would show progressively increasing deformations with each cycle.

According to the later view, the proportionality found by Arnstein and Reiner to exist between the bending stresses and the deflections would have to be interpreted differently. A rough proportionality may also exist between stresses and deformations when the latter are the result of seepage of water expelled in external loading. It may well be that at least part of the creep is caused by such seepage, which is a nonreversible process due to surface tension effects, while the recoverable creep would be due to delayed elasticity such as is associated with the Kelvin body. Set cement would then have to be pictured as a vesicular solid with the pores partially filled with water, whose spontaneous movement produces shrinkage and whose forced movement produces creep. These contradictory views have not yet been entirely resolved. Some workers in this field, with whom Glucklich's observations were discussed, maintain that the difference between the results obtained by Bingham and Reiner¹³ and those obtained by Glucklich are due to the fact that Glucklich coated the beams with a plastic which prevents moisture transfers from the cement to the atmosphere and *vice versa*.

IV. Mortar

1. FRESH MORTAR

Fresh mortar is a suspension of sand in aqueous cement paste. Its principal property is plasticity. Roller¹⁶ has related the plasticity of a mortar in the compression test to the actual volume of displacement dv^{17} caused by a change of form, and defines a "coefficient of renitence" K by

$$d\sigma/\sigma = K(dv/v_0) \quad (1)$$

where v_0 is the total volume of the material, assumed to be incompressible,

¹⁶ Cf. P. Mason, in "Elasticity and Inelasticity of Building Materials" (M. Reiner, ed.), p. 222. North-Holland, Amsterdam, 1954.

¹⁷ dv should not be mistaken for a *change* of volume.

and σ is the applied uniaxial pressure. He considers the viscous element in the flow of the mortar paste as negligible. The difference in the behavior of the fresh set cement and the fresh mortar paste arises from his experiments by means of a parallel-plate compression apparatus, in which a cylinder of the material was compressed between two flat horizontal plates, both larger than the final cross section of the specimen. The total load P was increased at a constant rate, and Fig. 2 shows the dependence of the height of the cylinder upon P . While the set cement paste can take high loads by mobilizing viscous resistance, the mortar paste fails in flow when the power input is excessive.

Lobanov⁶ extended his experiments mentioned in Section II,2 above to mortars. In contradistinction to Roller he was able to determine the plastic viscosity of a 1:2 fresh cement mortar to be 34 poises. This need not be understood as contradicting Roller's results, considering the very different kinds of flow in their respective experiments. The *yield stress* was 950 dynes/cm.², and the pumping pressure 21 atm.

2. VISCOSITY OF SET MORTAR

Bingham and Reiner¹³ included in their experiments 1:3 mortar beams. Here also chemical hardening stopped at an age of approximately 45 days. However, in contradistinction to the set cement beams, mortar beam

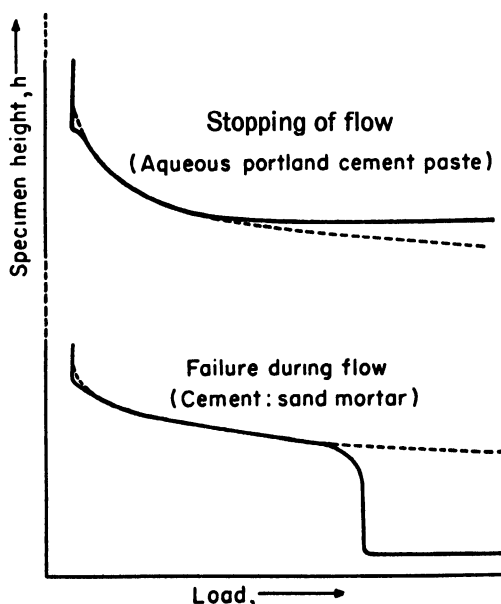


FIG. 2. Behavior of building pastes in the compression apparatus

II/4 (compare Fig. 1) seemed to exhibit a more pronounced foreeffect. It was also found that the creep viscosity increases with increasing curing period and extrapolation to zero creep fluidity seemed to indicate that a beam cured for 80 days or more would not show any viscous creep under a stress of 5×10^6 dynes/cm². This would point to the existence of a yield stress. This feature has not been checked by later investigators, and in any case even if the admixture of sand to the cement would produce in the set mortar a yield value, this seems to be so low as to be negligible for all practical purposes.

Arnstein and Reiner¹⁴ observed mortar beams of 1:1/2, 1:1, 1:2, 1:3, mixes and determined their creep viscosities as 67, 78, 82 and 88 in 10¹⁷ poises (within 10 to 20%) during a period of between 2 months and 1 year.¹⁸ These observations were carried out for the same loading conditions as mentioned for cement, namely own weight, and double and triple load. Within the available accuracy, no yield point could be observed.

It was found that the ratio of creep viscosity of the 1:3 mortar to the one of set cement was approximately the same as in Bingham and Reiner's observations. This was the more remarkable as the rate of creep of set cement in the latter case was about four times the one in the former. The following conclusions were drawn: (a) The creep viscosity of the mortar depends, other factors being equal, upon the creep viscosity of the cement but not upon the nature of the sand. (b) The increase of creep viscosity of the mortar over that of set cement is the result of the interference of the solid sand particles with the flow of the quasi-fluid cement. In other words, it is the cement which creeps, and the sand forms a suspended solid phase. On the other hand, an excess of free water in the mortar over that in the cement will decrease the creep viscosity of the former. Assuming

$$\eta_0 = \eta_0 (1 - c_w) \quad (2)$$

where η_0 is the viscosity of the set cement and c_w the volume concentration of excess water in the cement base of the mortar, Arnstein and Reiner used a generalized Einstein formula.

$$\eta = \eta_0 (1 + \alpha c_s) \quad (3)$$

where c_s is the volume concentration of the sand in the cement base, and found that α turned out to be Einstein's factor = 2.5 which is valid for very dilute suspensions. Reiner¹⁹ explains this surprising result with the following words: "If the viscosity of the dispersion medium, in our case

¹⁸ They remark that the large spreading of observations was probably due to inadequate moisture and temperature control.

¹⁹ M. Reiner, "Deformation and Flow: An Elementary Introduction to Theoretical Rheology." Lewis, London, 1949.

the cement base, is of the order of 10^{17} poises, the flow during one year will be too small to cause either an appreciable change in the orientation of [non spherical] sand particles or an interference [with the flow of the cement base] beyond the [taking-up] of volume proper of the particle. One year of the flow of cement is as much as 10^{-12} seconds in the flow of water. If the observation (of the flow of an ordinary suspension) were to last 10^{-12} seconds only . . . a steady state of flow could not establish itself. To change the picture from a temporal to a spatial one: the distances between particles in a liquid of a viscosity of the order of 10^{17} poises are equivalent to distances in water 10^{19} times as great. We can [regard] the concentration of 60 percent in cement as [very] small in terms of concentration in water." In order to prove this hypothesis it would be necessary to solve the momentum equations of the Maxwell body¹⁵ for unsteady inhomogeneous flow, a mathematical feat which has not yet been attempted. Until then the equation

$$\eta_c = \eta_0 \frac{1 + WC}{1 + \overline{WC}} (1 + 2.5 c_s). \quad (4)$$

for the creep viscosity η_c of the cement mortar of volume concentration c_s of sand in the mortar, with WC the water-cement ratio of neat cement, and \overline{WC} of the cement base in the mortar, which is derived from equations (2) and (3), must be considered as empirical.

These considerations are based upon the assumption that set cement can be considered as a viscous liquid. This view might have to be revised in consideration of Glucklich's experiments with set cement mentioned in Sec. III,3.

3. ELASTICITY OF SET MORTAR

In order to determine the law of elasticity of set mortar Bingham and Reiner loaded beams at midspan in two different manners. (a) The weights were gradually increased to a maximum and likewise decreased, and deflections observed during the cycle as functions of loads. Each experiment took about 1 hr. (b) The beam was loaded with the full weight so that the loading did not take time, and the deflection was observed. This was repeated with increasing loads until a maximum had been reached.

It was found that procedure (a) resulted in a hysteresis loop, both branches being bent upward. Viscous flow could not produce such hysteresis in 1 hr., and it therefore had to be due to delayed elasticity (compare Fig. 3). In case (b) the curve is sufficiently close to a straight line and its slope is the same as the slope of the tangent at the origin of curve (a).

The conclusion may be drawn that the instantaneous strain of set mortar within such sand concentrations as observed by Bingham and

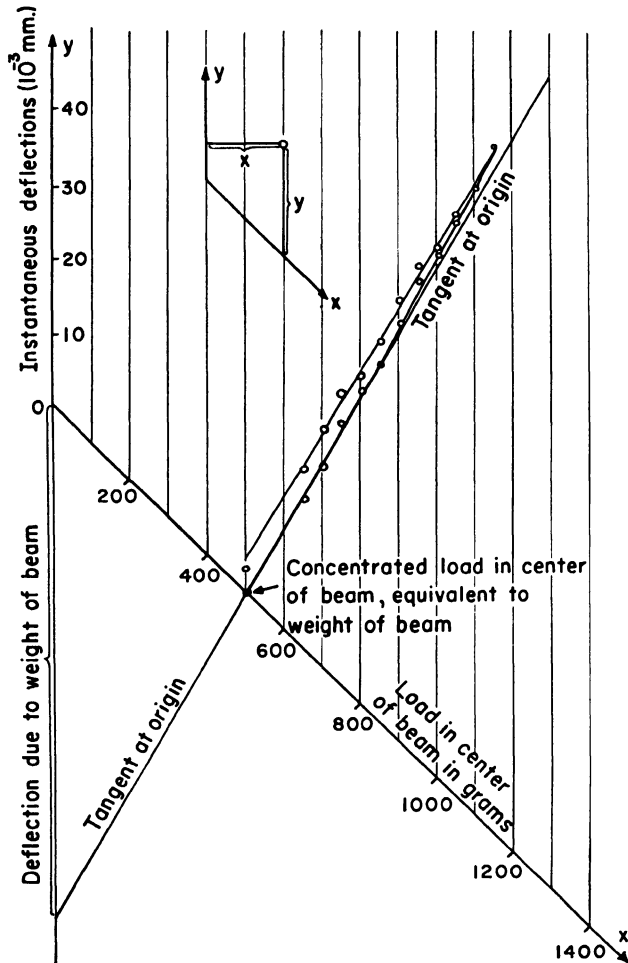


FIG. 3. Stress-strain diagram for beam II/14. An oblique coordinate system, as shown in the upper part of the graph, is used. Instantaneous deflections were under loads superimposed on the weight of the beam.

Reiner obeys Hooke's law. If consecutive strains are measured while the load is gradually increased in time, the strain-stress diagram will be curved and of parabolic shape, with its convex side toward the stress axis. This curvature is due to delayed elasticity. Contrary to general opinions this seems also to apply to the coarse aggregate. Blakey and Beresford²⁰

²⁰ F. A. Blakey and F. D. Beresford, Report C2.2-1, Commonwealth Scientific Industrial Research Organization, Melbourne, Australia, 1953.

state that "there is little evidence of any deviation from a linear tensile stress-strain relationship for concrete below the cracking stress."

A Young modulus of about 28×10^{10} dynes/cm.² was calculated for 1:3 mortars. This implied an increase of about 15 % over the modulus of the set cement as mentioned in Section III,3.

V. Concrete

1. FRESH CONCRETE

In the fresh concrete the fresh mortar forms the medium in which the coarse aggregate is suspended. The most important rheological properties of fresh concrete are (a) *workability* and (b) *stability*.

To evaluate workability, Herschel and Pisapia²¹ designed four tests which determine certain factors, supposed to be at least partially independent of each other. *Harshness*, defined as that relative property which may be illustrated by the smoothness of an oversanded, compared with the roughness of an undersanded mix, is measured by the spread of the concrete on a flow table after a certain number of drops. *Segregation*, the partial or complete separation of one class of materials from a uniform mixture, is measured by the amount of mortar separated from concrete by jolting on the flow table. For *shear resistance* the shear box first evolved by Terzaghi and later developed by Casagrande for soils, is used. Finally *stickiness*, related to the adhesion or bond which keeps the individual particles of the concrete to cling together in a single mass, is measured by the vertical force required to separate a horizontal steel plate from the surface of a freshly made concrete.

L'Hermite²² has investigated shear resistance in greater detail. He uses the apparatus shown in Fig. 4. By placing a piston loaded with a weight P against the free surface of the concrete, a pressure p is obtained on the cutting plane. A horizontal displacement u is then forced upon the upper part of the box, and the corresponding reactive shearing force F measured. Plotting F versus u we find a maximum $F(p) = R(p)$ and a minimum $F'(p)$. Plotting R and F' against p results in a Coulomb straight line, with cohesion C and angle of friction φ .

$$R = C + Kp, \quad F' = C' + K'p \quad (5)$$

The ratio $\rho = K/K'$ is named the *coefficient of interlocking*. The area OAB represents the resilience

$$W \approx R(p)U/2 \quad (6)$$

²¹ W. H. Herschel and E. A. Pisapia, *J. Am. Concrete Inst.* **32**, 64 (1936).

²² R. L'Hermite, *Rev. matériaux construct. et trav. publ.* **405**, (1949), available in English translation, Cement and Concrete Assoc. Transl. No. 9 (1949).

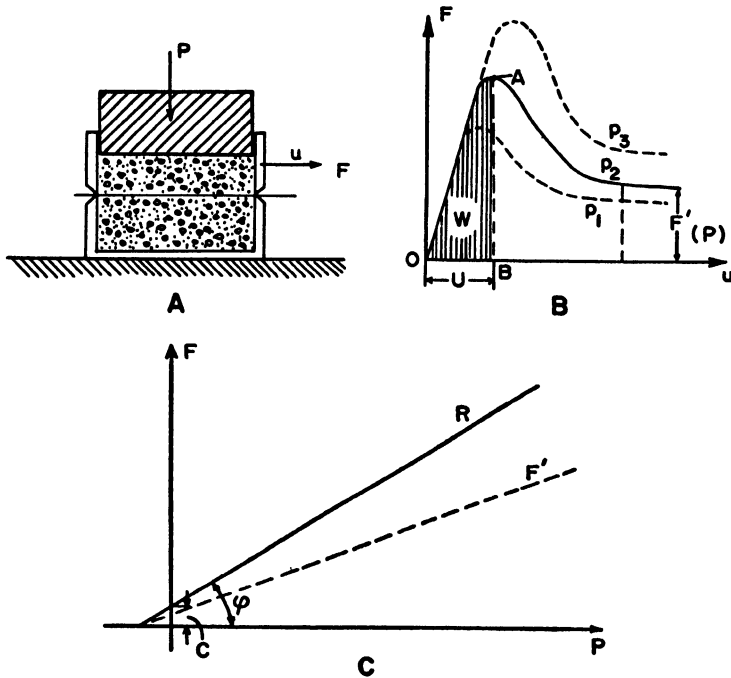


FIG. 4. L'Hermite's observations on shear resistance of fresh concrete. A, apparatus. B, shearing force (F) versus displacement (u). C, Maximum (R) and minimum (F') shearing force versus weight (P).

where U is the maximum shearing displacement. This is approximately $= KpU/2$ and the unit pressure p is $= KU/2$. L'Hermite defines a *coefficient of workability* μ by

$$\mu = 1/KU \quad (7)$$

For a concrete with "continuous" grading, 300 kg. cement/m.³ and $WC = 0.65$, he found $K = 0.7$, $K' = 0.45$, $C = 0.05$ kg./cm.², $\rho = 1.5$, $\mu = 17$.

In a more recent publication, L'Hermite¹⁰ describes another method, more elementary but better suited to field conditions, for measuring shear resistance of fresh concrete. This consists essentially of a rod with a grooved core drill which is being rotated inside the concrete mass at a constant speed. The maximum torque, reached at the moment of rupture, is measured. If the pressure exerted normally by the concrete on the core is known and if an assumption is made with regard to the cohesion, then the angle of internal friction can be calculated.

A "stable" mix is defined by Forslind¹ as one in which the aggregate is completely separated by the paste, and a random sampling shows the

same particle-size distribution, retaining these characteristics during transportation, placing, and compacting. The shearing stresses caused by gravitation must therefore not exceed the yield stress of the paste. The resistance to deformation decreases with increasing layer thickness. The deformability decreases with hindered particle rotation, and therefore with decreasing layer thickness.

The layer thickness depends upon the paste-aggregate ratio and the size distribution of aggregates. Forslind¹ mentions two methods by means of which it is possible to ascertain whether a concrete mix is stable or not. They are the remoulding test of Powers and the plastometers by Erickson and Forslind and Bergstroem.

2. RHEOLOGICAL BEHAVIOR OF SET CONCRETE

When a concrete (or reinforced concrete) slab is loaded, a deflection δ is produced (Arnan *et al.*²³). A certain part of the deflection occurs instantaneously (δ_i). When the load is removed immediately after loading²⁴ part of the deflection ($\delta_{e,i}$) is recovered instantaneously; this is due to the stresses raised by the *instantaneous strain*. The rest which is not recovered is the "permanent set" (δ_s),²⁵ so that

$$\delta_i = \delta_{e,i} + \delta_s \quad (8)$$

As regards δ_s , this may be considered as a kind of plasticity *without a noticeable yield point*. To explain this, we must distinguish between macrostresses and microstresses. The macrostress is the over-all stress as usually calculated in accordance with the theory of elasticity. However, every material body will have notches in its surface and voids or cracks in its interior. These cause local stress concentrations, and these microstresses will much exceed the over-all stress which is recorded in the stress-strain diagram. They will cause local ruptures in a brittle material such as concrete. Therefore, there will be an irrecoverable macrodeformation, called the set, even at very low and practically infinitesimal macrostress, with a corresponding absence of yield point. This set is most pronounced on first loading. It is usually smaller at each further loading which does not exceed the first, and the elasticity of the material is accordingly improved through a series of loadings and unloadings. Arnan *et al.*²³ have shown how this affects the standard loading test for reinforced-concrete structures.

On the other hand, if we leave the slab under load for some time T , δ increases from δ_i to δ_T , and if we now remove the load we shall find, be-

²³ A. Arnan, M. Reiner, and M. Teinowitz, "Research on Loading Tests of Reinforced Concrete Structures." Research Council of Israel, Jerusalem, 1950.

²⁴ Some time must elapse for reading observations, unloading, etc.

²⁵ This is the set to which allusion is made in Section I.

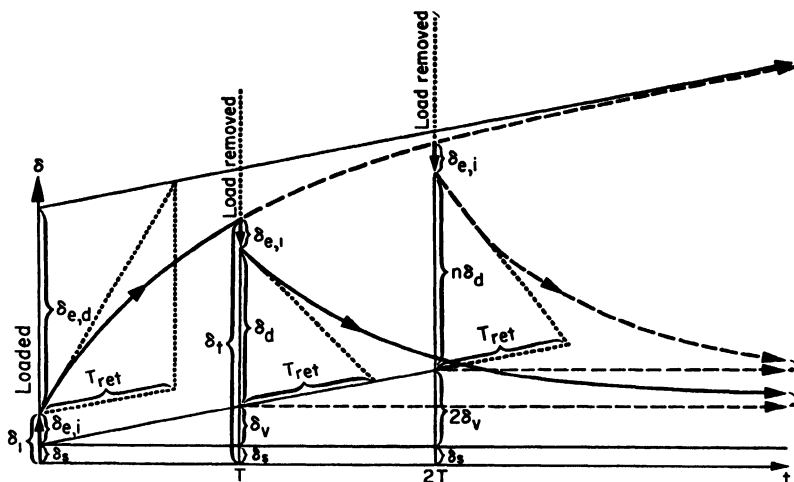


FIG. 5. Deformation-time curve for material with creep; δ = deflection; δ_i = instantaneous deflection; $\delta_{e,d}$ = delayed elastic deflection (primary creep); δ_v = deflection produced by viscous flow (secondary creep).

sides an instantaneous recovery of the same magnitude as before, that after a day or two still more is recovered, and that this process goes on for days and weeks up to a maximum of additional recovery δ_d . This is a measure of the *delayed strain* consisting of elastic fore-effect on loading and elastic aftereffect on recovery, and an indication of the property of delayed elasticity. At the same time the nonrecovered permanent deformation has also increased by, say, δ_v . If we double the time of loading we may find that δ_v has increased to roughly $2\delta_v$ and δ_d to $n\delta_d$ where $1 < n < 2$. If we leave the load on for infinite time, δ_d will not increase beyond a certain maximum $\delta_{e,d}$ which is the *delayed elastic strain*. If δ_v increases both with time and with the load roughly in direct proportion, as in liquids, it could be considered as a case of *viscous deformation*. When first discovered this phenomenon was called plastic deformation, but the rheological behavior described here on the example of concrete is typical for all materials which are not plastic. In rheology, the latter term is connected with plastic behavior in the presence of a yield point, but what is colloquially called a plastic is not a plastic substance in the rheological sense. Fresh concrete, which can be moulded may accordingly be termed a plastic, but it is not a plastic substance after it has set as it does not possess a yield point. When an attempt is made to force upon it a large deformation it breaks in a brittle manner; mild steel, which is a plastic substance, can be deformed by impact but concrete cannot.

As the time-dependent deflections $\delta_{e,d}$ and δ_v proceed with low speed,

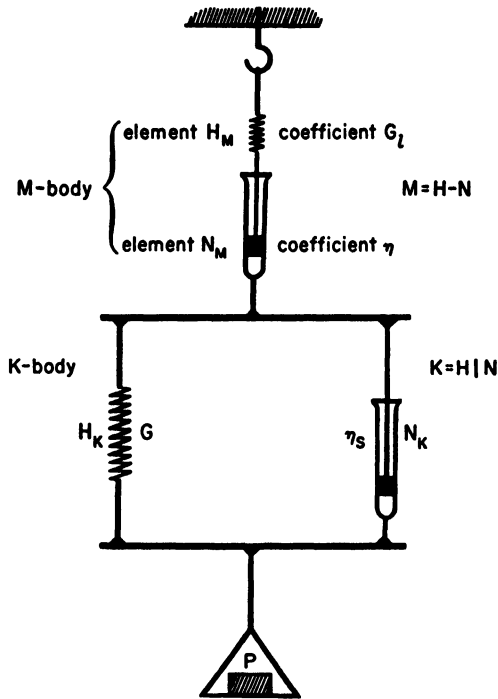


FIG. 6. Model for a Burgers body; H = elastic Hooke element, N = viscous Newtonian element, M = viscoelastic Maxwell body, K = firmo-viscous Kelvin body. The rheological coefficients are: in shear G , η ; in extension E , λ ; in cubical dilatation κ , ζ .

they are called *creep*. They can be separated by unloading only, and are then distinguished as primary or recoverable creep, which is a strain, and secondary or irrecoverable creep which is sometimes considered as a deformation resulting from slow viscous flow. The viscous nature of secondary creep was first stated by Glanville²⁶ with the words, "The movement appears to be . . . in the nature of viscous flow." This points to concrete behaving in one respect as a Maxwell body.²⁴ Primary creep can be represented by a Kelvin body.²⁷ For both acting together the Burgers body,²⁷ a model of which is shown in Fig. 6, is appropriate. In the foregoing we have not taken into account the fact that loading takes time, especially in a loading experiment when the load gradually increases from zero to the test load. An increase of load at constant rate will be accompanied by an increase of instantaneous strain at constant rate together with an increase of set at

²⁶ W. H. Glanville, *Bldg. Research Tech. Papers* **12** (1930).

²⁷ Cf. Vol. I, Chapter 1, Section VI, 5.

roughly constant rate. The Burgers body cannot represent such behavior. Pérez has proposed an appropriate model, and Torroja¹ has developed an analytical theory based upon it.

3. VISCOUS CREEP

From Glanville's observations the following creep viscosities of concrete at an age of two months can be calculated:

mix	1:1:2	1:2:4	1:3:6
η in 10^{17} poises	7.5-10.6	2.8-3.6	1.3-2.0

It is remarkable that in contradistinction to mortars the viscosity decreases with increase of the amount of aggregates in the mix. The reason is to be sought in the presence of voids and the fact that a 1:1:2 concrete, because of better grading, will have less pore space than a 1:2:4 concrete. Equation (4) is therefore not applicable to concretes but may be replaced by

$$\eta_c = \eta_0 \frac{1 + WC}{1 + \overline{WC}} (1 + 40 c_v - 53 c_v^2) \quad (9)$$

The viscosity thus calculated, or observed at the age of two months, gradually increases in the course of time. This has three causes. There is firstly the chemical hardening of the cement base as described in Section III,3 above. Secondly in the course of the deformation aggregates come into contact and develop solid friction between them. Thirdly cement and mortar flow into the voids, decrease the latter, and therefore increase the creep viscosity. The third phenomenon is called *volume flow*.²⁸ While even solid rocks creep through geological periods, it may be assumed that for all practical (i.e., building) purposes the viscosity ultimately becomes infinite and creep stops. Thomas²⁹ has attempted to estimate the limiting value of creep when the creep during the first year is known. Freudenthal³⁰ proposed the equation

$$10^6 D_c = \frac{at}{1 + bt} \sigma \quad (10)$$

for the linear creep deformation as a function of t the period of action of the normal stress σ in kg./cm.², t being measured in years. The parameters a

²⁸ For more information on volume flow of concrete the reader is referred to M. Reiner, *Appl. Sci. Research A1*, 475-488 (1949); M. Reiner, *Bull. Research Council Israel*.

²⁹ F. G. Thomas, *Structural Engineer* **11**, 69 (1933).

³⁰ A. M. Freudenthal, *Intern. Assoc. Bridge & Struct. Eng.* **4**, 249-264 (1936).

TABLE I
Parameters in Freudenthal's equation

Parameters	Age in months		
	1	3	12
<i>a</i>	60	25	5
<i>b</i>	4	2.5	1

and *b* depend upon the age of the concrete at $t = 0$, and have the values shown in Table I. The limiting creep value is accordingly $(a/b) \times 10^{-6}$.

The theory of secondary creep as a case of viscous flow is based on the assumption that creep and shrinkage are independent. However, as Lea and Lee³¹ have pointed out, this view has not been accepted without exception and they quote a view, which they think goes too far, that "the effect of loading is simply to increase the effect of shrinkage." L'Hermite³² also mentions observations according to which a loaded specimen swells under water more than an unloaded one which shrank. He draws the conclusion that creep and shrinkage cannot be separated. Rao³³ has carried out extensive experiments to show that creep is mainly, if not totally, due to shrinkage, the movement being considerably reduced when the specimen is coated with asphalt or kept wet.

Davis and co-workers³⁴ found that creep of concrete made with sandstone aggregates is several times the creep of similar concrete made with limestone. It seems that only the seepage theory can account for this fact.

Others attribute creep to shrinkage. However, since irreversible creep is also present in concretes submerged in water, they are forced to conclude that rheological properties such as sliding and viscosity are also active.

Neville³⁵ explains creep through a reconciliation of the seepage and viscous theories.

He maintains that what is normally measured as creep consists of "true" creep (viscous in nature, with gradual transfer of load to the aggregate) and increased shrinkage (seepage due to evaporation and external force). The magnitude of creep depends on the force applied and the properties of the concrete, but is independent of curing conditions, humidity, temperature, etc. Variations in these parameters affect shrinkage only. This hypothesis would account for the magnitude of creep in water as being the resultant of negative shrinkage (swelling) and positive creep.

³¹ F. M. Lea and R. C. Lee, *Building Research Station Note No. 984*, (May 1946).

³² R. L'Hermite, "Idées actuelles sur la technologie du béton." Paris.

³³ K. L. Rao, *4th Congr. Grands Barrages, (New Delhi) R.64* (1951).

³⁴ R. E. D. Davis, H. E. Davis, and J. S. Hamilton, *Am. Soc. Testing Materials, Proc. 34*, 354-386 (1934).

³⁵ A. M. Neville, *J. Am. Concrete Inst. 27*, 47-60 (1955).

VI. Reinforced Concrete

When designing a reinforced concrete structure there is a tendency to imagine each element to consist of more or less parallel fibres, some in compression (taken by the concrete), others in tension (taken by the steel), separated by a neutral layer. Chaulet³⁶ has drawn attention to the well-known but disregarded fact that this division is entirely unreal. In every point of the body there is compression in one direction and at the same time tension in the direction normal to the first, with shear vanishing in both directions. If the reinforcement follows the tension trajectories, the element can be designed as if it consisted of an isotropic material. Tangential bond stresses do not arise, and hooks at the ends of reinforcing bars can generally be dispensed with. Deviations in the location of the reinforcement from practical considerations cause only secondary stresses.

The two methods of design in use are known as the *elastic* and the *limit* analysis. In the first it is assumed that the concrete is compressed and the steel stressed within their respective elastic ranges, while the concrete "fibres" in tension have fractured. This is the standard method. In the second method the ultimate load corresponding to the fracture pattern is computed and divided by a suitable factor of safety. This method has been developed for steel structures when considering stresses in the plastic (St. Venant) range. Kooharian³⁷ has applied limit design methods to nonreinforced voussoir concrete arches. Cowan³⁸ has described the method in some detail, quoting Freudenthal.³⁹ In a more recent paper Freudenthal⁴⁰ has drawn attention to the fact that the limit design procedure if applied to concrete is essentially different from the "plastic" method used for structural metals. In concrete, which is a viscoelastic material having no yield point, the so-called plastic redistribution of stresses is, in fact, the result of a localized fracture process, the spreading of which along a shear plane is temporarily blocked by the lower stresses in the surrounding material. While in metals the truly plastic redistribution of nonuniform stresses is gradual and continuous, in concrete there is a sharp discontinuity of behavior.

A method in which the viscous creep of the concrete transfers all stress differences to the steel was described by Lohr.⁴¹

In prestressed concrete self-stresses are produced in the reinforced con-

³⁶ M. Chaulet, *Trav. architect., construct. trav. publ. (Paris)* **18**, 295-300, 439-445 (1934); **19**, 172-177, 279-283 (1935).

³⁷ A. Kooharian, *J. Am. Concrete Inst.* **24**, 317-328 (1950).

³⁸ H. J. Cowan, *Engineering* 276-278 (1952).

³⁹ A. M. Freudenthal, "The Inelastic Behavior of Engineering Materials and Structures." Wiley, New York, 1950.

⁴⁰ A. M. Freudenthal, *Proc. 1st U. S. Natl. Congr. Appl. Mech.* pp. 641-646 (1952).

⁴¹ W. S. Lohr, *Eng. News-Record* December (1934).

crete structure by putting the steel into tension, thus reducing both tension and compression in the concrete (compare Abeles⁴²). Olszak⁴³ has treated the problem of prestressing helically bound columns.

Nomenclature

a, b	Parameters	R	Maximum resistance
$A.$	Angstrom unit	s	Set
c_v	Volume concentration	T	Period of time
C	Cohesion	U	Shearing displacement
d	Thickness	v	Viscous
d_v	Volume displacement	WC	Water-cement ratio
D_c	Creep deformation	μ	Coefficient of workability
e	Elastic	η_{pl}	Plastic viscosity
F	Shearing force	σ	Uniaxial pressure
F'	Minimum shearing force	α	Einstein factor
i	Instantaneous	δ	Deflection
K	Coefficient of renitence, coefficient of friction	ρ	Coefficient of interlocking
		ω	Angle of friction

⁴² P. W. Abeles, "Prestressed Concrete." Crosby Lockwood, London, 1952.

⁴³ W. Olszak, *Arch. Mécanique appl.*, Gdansk pp. 80-98 (1949).

CHAPTER 10

THE DEFORMATION OF CRYSTALLINE AND CROSS-LINKED POLYMERS

I. L. Hopkins and W. O. Baker

I. Introduction	365
1. Stress-Strain Behavior	366
2. Cold Drawing	370
3. Planar Movement in Cold Drawing	377
4. Further Consequences of Crystalline Displacements	379
5. Short-range Displacements in Polymers	383
a. Stress Relaxation	384
b. Creep	384
c. Dynamic Modulus	385
d. Dynamic Viscosity-Frequency Product	385
II. Polyethylene	388
1. Dynamic Properties of Polyethylene	388
2. Stress Relaxation in Polyethylene	396
3. Creep of Polyethylene	396
4. Effect of Extrusion Methods on Properties of Solid Polyethylene	398
5. Extrusion of Liquid Polyethylene as Related to Polymer Structure	399
6. Flow Properties of Unmelted Polyethylene in Bulk	401
7. Multiaxial Stressing and Stress-Cracking in Polyethylene	403
III. Hard Rubber: A Highly Polar, Cross-Linked Polymer	408
1. Dynamic Properties of Hard Rubber	408
2. Creep Properties of Hard Rubber	409
3. Stress Relaxation Properties of Hard Rubber	411
IV. Polyamides: Polar Chain Polymers Examined for Both Long and Short Range Behavior	412
1. Dynamic Properties of Polyamides	413
a. Free Oscillations in Polyamides	413
b. Forced Oscillations in Polyamides	414
2. Stress Relaxation in Polyamides	421
3. Creep in Polyamides	423
V. Conclusion	425
Nomenclature	426

I. Introduction

A discussion of the rheology of crystalline and cross-linked polymers should in some ways resemble that of the dentistry of hens' teeth; i.e., what can be said? The reason is that microcrystallinity on one hand and

dense network formation on the other have been developed in polymers largely to prevent flow or, indeed, extensive deformation of any kind. Hence, in contrast to the other topics in this book, the present chapter will involve special kinds of strains. The really reversible, elastic, displacements will be extremely small, generally less than 1 %, and the inelastic ones are likely, in the microcrystalline systems, to be in the range of hundreds of per cent, with a superficial resemblance to true plasticity. Further, they will be of curious interest in polymer technology because, outside of the field of rubbers, only cold drawing, as in fiber formation of microcrystalline polymers, involves important distortions of severalfold.

Unfortunately, neither of these extremes, of minute deformations or enormous ones, is understood theoretically. This is in contrast to rubbery elasticity and its related viscoelastic formalism. Further, this brief survey will not attempt to expose all the phenomenology of these systems. Rather, the simple principles of chain or network segment motion which must govern this rheology will be, where possible, described and related to molecular qualities of particular plastics. Thereby we hope to couple even closer the test tube and the test lab.

1. STRESS-STRAIN BEHAVIOR

Linear microcrystalline polymers subjected to a uniaxial tension characteristically respond with a stress-strain diagram like that shown in Fig. 1. This is for a high molecular weight polyethylene sebacate. Incidentally, this may have been one of the first substances to have been drawn into a synthetic fiber, in the historic experiments of Carothers,¹ although its mechanical properties have not been reported before. The structure of these polymers is essentially paraffinic, with additional cohesion provided by the dipolar layers.² Hence the strain reported in this curve reflects both a sliding of the hydrocarbon groups and the displacement of strong dipoles, and can fairly be said to be characteristic of most chain polymers.

The early part of the curve looks linear, but more detailed examination will show non-Hookean properties. Hence no particular part of the performance of microcrystalline polymers can be identified solely with the perfectly elastic displacements of atoms or distortion of valence bonds, at ordinary temperatures, or, indeed, perhaps short of liquid nitrogen temperatures. This curvature in the stress-strain curve has been studied over a range of temperatures and the moduli it denotes have been represented by an expression $E = E_0 e^{-\alpha \epsilon}$ where E is the slope of a tangent at any point, E_0 = the slope at 0 strain, ϵ = the strain, and α = a constant determined for a particular temperature and polymer. Studies using this expression have

¹ W. H. Carothers and J. W. Hill, *J. Am. Chem. Soc.* **54**, 1579 (1932).

² C. S. Fuller and W. O. Baker, *J. Chem. Educ.* **20**, 3 (1943).

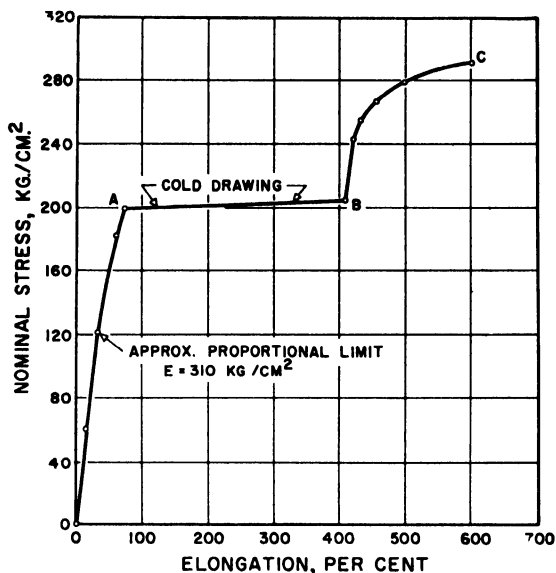


FIG. 1. Relation of elongation to slowly applied stress in the highly crystalline linear polymer polyethylene sebacate.

included polyethylene.³ The effects of molecular weight and of some variations in structure were examined. It was concluded by Carey and co-workers that independently of temperature and molecular weight, the relation was that "The product of the initial modulus and the strain at the elastic limit are proportional to the stress at the elastic limit." Since it is well accepted that the "elastic limit" has to be an arbitrarily defined point, it was desirable to examine the rheology from the very lowest strains upward toward this region in finer detail. Some examples of this have been chosen from recent studies of polyethylene by T. F. Osmer⁴ of Bell Telephone Laboratories. A device giving record of stress-strain behavior at the same time that photoelastic measurements were made has yielded curves shown in the following figures. The complex qualities of this deformation curve (Fig. 2) are well summarized by the creep experiments⁵ of Gohn and associates, wherein even at stresses of 100 p.s.i. with a creep of 0.01"/inch after 10,000 hours of continuous loading, there was still not a steady creep rate. Indeed this had not flattened out at 20,000 hours. These findings appear consistent with a later discussion of the dynamics of solid poly-

³ R. H. Carey, E. F. Schulz, and G. J. Dienes, *Ind. Eng. Chem.* **42**, 842 (1950).

⁴ T. F. Osmer, private communication.

⁵ G. R. Gohn, J. D. Cummings, and W. C. Ellis, *Am. Soc. Testing Materials, Proc.* **49**, 1139 (1949).

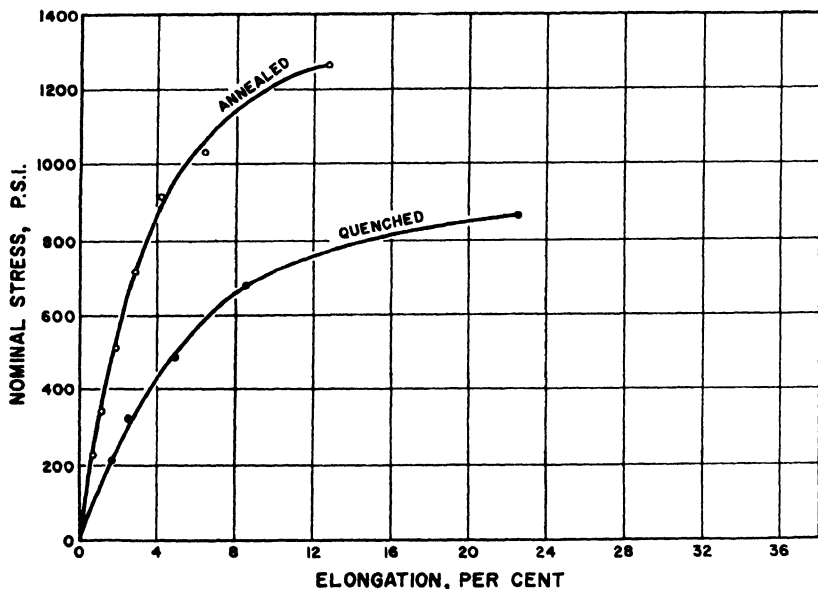


Fig. 2. The effect of different states of crystallinity on the stress-strain curve of low density polyethylene at 25°C. The annealed specimen was 0.035 in. thick; the quenched specimen, 0.037 in. thick. Both were 0.5 in. wide. Average strain rate was 3% per minute.

ethylene, in which evidence for a very broad spectrum of relaxation processes is displayed.

The primary significance of Figs. 2 and 3 is direct evidence of the large influence of crystallites on solid polyethylene rheology. Among the non-polar microcrystalline polymers, a great array of which is now known because of the recent use of Ziegler-type catalysts, polyethylene will be taken as reasonably typical. However, the polyethylene of Figs. 2 and 3, and the rest of this part of the discussion, is a low density, imperfectly linear polymer. The linear polyethylene and isotactic hydrocarbon polymers have even more drastic effects of crystallinity on stress-strain properties.

The quenched specimens on Figs. 2 and 3 cannot be assumed to lack all crystallinity, since polyethylene anneals rapidly at 25° C., where the tests were made. However, both density and X-ray scattering showed a minor ordered component, compared to the annealed samples. The almost double initial modulus testifies strongly to the rigidity conferred by tiny paraffin crystals, even separated as they apparently are by a continuous amorphous or mesomorphous phase.

Indeed, these ordered and disordered regions interact on each other mechanically in many subtle, little-known ways. For instance, when the

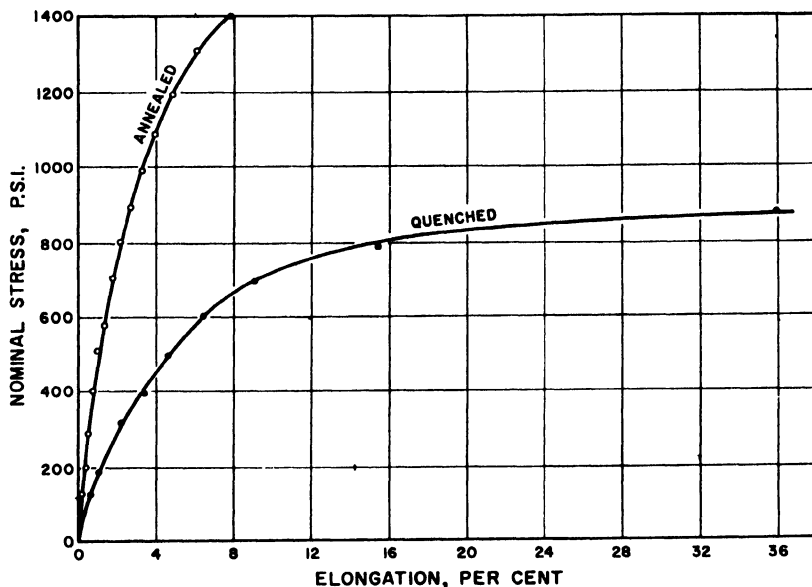


FIG. 3. The effect of different states of crystallinity on low density polyethylene at 25°C at 20X the average strain rate of Fig. 2. The annealed specimen was 0.063 in. thick; the quenched specimen, 0.064 in. thick. Both were 0.5 in. wide. Average strain rate was 60% per minute.

average strain rate of 3% per minute, in Fig. 2, is raised twentyfold to the 60% per minute of Fig. 3, there is little effect on the quenched curves; they almost exactly superpose. This is expected from the short relaxation time of amorphous paraffinic chains, as reflected probably in the very low brittle temperature of polyethylene. However, when a large fraction of crystalline regions obtains, the stress-strain curve of Fig. 3 is markedly steeper than at the lower strain rate. Seemingly, some *organized* rearrangements come in even at a few per cent elongation. They involve large numbers of atoms, both in movement of crystallites in the amorphous solid and probably in plastic slip within the crystallites themselves. Thus, the relaxation times are greatly increased, and the stress builds up rapidly in the strained specimen. Obviously, technical behavior of such systems regarding impact strength, low temperature flexibility, yield point, creep, and tensile strength will greatly depend on crystalline content and distribution.

Stress relaxation is also characteristically exhibited in the curve of Fig. 4, in which, however, the stress-optical effect is precisely linear.^{4, 6} Thus chain orientation over this small strain range seems completely reversible,

⁶ A. Renfrew and P. Morgan, eds., "Polythene." Interscience, New York, 1957.

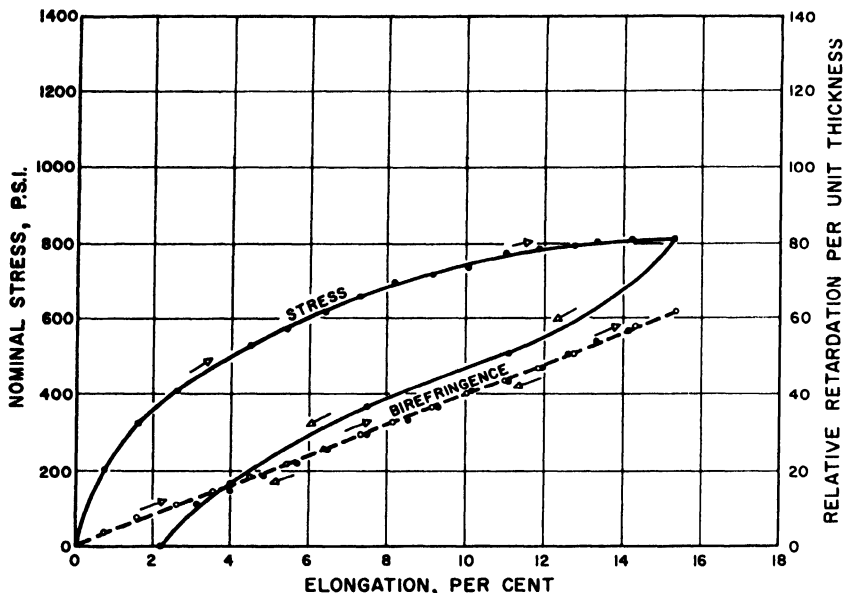


FIG. 4. Stress-strain and birefringence relations of low density polyethylene stressed slowly at 25°C. showing irreversible characteristics of deformation but strict reversibility of birefringence. KEY: ●, ascending stress; ◐, descending stress; ○, ascending birefringence; ●, descending birefringence. Average strain rate was 1.5% per minute.

but unrecovered crystallite deformations give large hysteresis loops for mechanical properties. Indeed, in compression tests, where crystallite properties can be greatly suppressed (by rotational disordering⁷) by elevated temperatures, Fig. 5 illustrates comparative suppression of mechanical hysteresis, compared to Fig. 6. In Fig. 6, low temperature has stiffened both crystals and their "fringes" are so stiffened that recovery progressively disappears. This sort of behavior is usual for chain polymers, and rare except for long times of stressing for chemically cross-linked polymers. If chemical changes in cross linkage accompany the stretching, however, hysteresis is common. The situation with densely cross-bonded structures will be discussed later, particularly for hard rubber.

2. COLD DRAWING

The most spectacular part of the stress-strain curves of microcrystalline polymers for either uni- or multiaxial stressing is where it flattens out into a plateau. This marks the cold drawing phenomenon where a sharp shoulder

⁷ W. O. Baker, in "High Polymers" (S. B. Twiss, ed.), p. 108. Reinhold, New York, 1945.

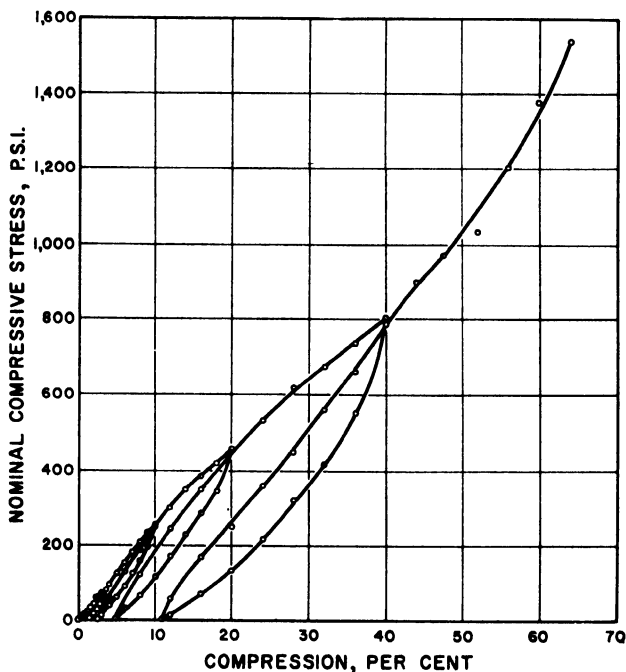


FIG. 5. Compression set curves for low density polyethylene at elevated temperatures where crystalline deformation is minimized. Specimen was a cylinder, $\frac{1}{2}$ " diameter \times $\frac{1}{2}$ " high. Rate of test was approximately 5 min. total for loading and unloading each loop. Test temperature, $+180^{\circ}\text{F}$.

forms and thin material which is molecularly highly oriented is pulled out of a more or less unoriented and frequently opaque bulk. This dramatic reduction in cross section, and the lustrous, clear, strong fibers or sheets which it creates, were once thought especially characteristic of linear microcrystalline polymers. Actually both were also present in many early examples of amorphous polymer studies. Indeed the classic report of Hünemörder⁸ on molecular orientation in polystyrene shows photographs of highly stretched filaments with vestiges of a drawing shoulder visible. In microcrystalline polymers, however, cold drawing which represents roughly elongation at constant stress (referred to the original cross section) is attended by dramatic reorganization of molecular layers and atomic planes. In the linear polyamides, for example, this leads to beautiful filaments giving nylon textiles. In this case, however, the drawing can equally well or actually better be achieved by orientation of the chain axis alone and then subsequent crystallization into oriented crystallites. Similarly,

⁸ M. Hünemörder, *Kautschuk* 3 (3), 106 (1927).

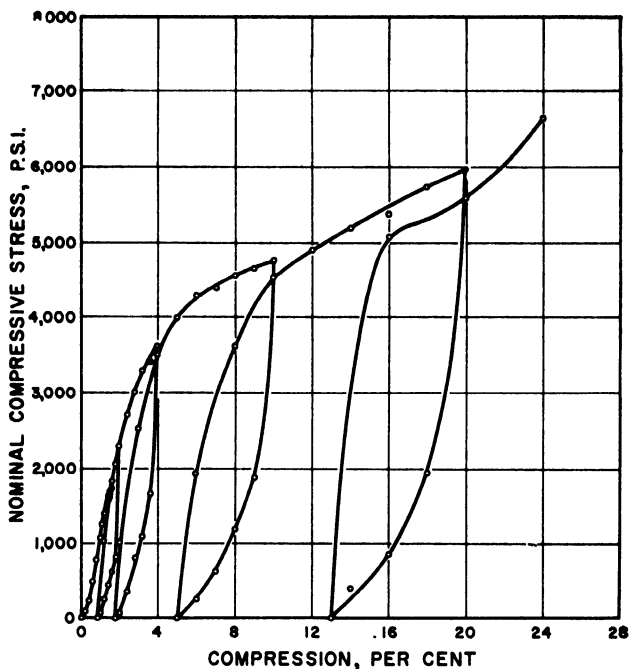


FIG. 6. Compression set curves for low density polyethylene at low temperatures where plastic behavior prevails over elastic responses. Specimen was a cylinder, $\frac{1}{2}$ " diameter \times $\frac{1}{2}$ " high. Rate of test was approximately 5 min. total for loading and unloading each loop. Test temperature, -40°F .

stress-strain curves for polyethylene of crystallinity varied by thermal history are indeed typical of the effects also encountered in proceeding to the stage of full cold drawing in polymers of varying crystallinity. However, the point that cold drawing in a phenomenologically similar way can be achieved for either a noncrystalline polyamide or the same one highly crystallized and organized into spherulites, as was long ago shown,⁹ seems to clarify the question of how this chapter should treat cold drawing. The mesomorphous, but noncrystalline polyamide, which, to repeat, shows typical cold drawing, could not have become heated at the shoulder to within 50°C . or more of the melting point of its crystalline form. If it had, it would have crystallized in the solid according to detailed studies⁹ widely confirmed. Thus, an amount of heating corresponding closely to heat of fusion of linear polymers does not seem to be critical in the drawing of the mass, at least when it is noncrystalline. Hence, it seems proper to focus mostly on the structural and orientation changes in drawing. That is, it

⁹ C. S. Fuller, W. O. Baker, and N. R. Pape, *J. Am. Chem. Soc.* **62**, 3275 (1940).

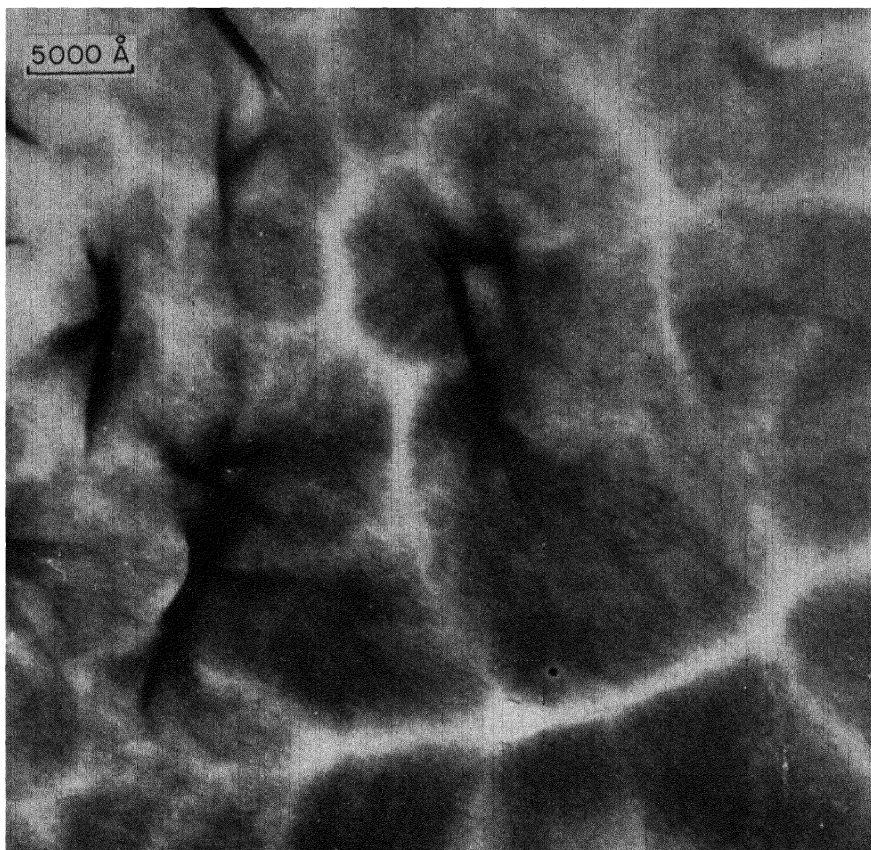


FIG. 7a. Electron micrograph of polyundecanoate polyester showing crystallite sheaves. Original magnification, 3760X.

can be assumed that there is structural continuity between the undrawn and drawn states, although naturally there is a very considerable temperature rise on drawing, as has recently been shown by ingenious observations on thermofluorescent powders.¹⁰ Similarly, the detailed study of Marshall and Thompson¹¹ emphasizes the consequences of the adiabatic working process in polyethyleneterephthalate. Here, there usually is crystallization on drawing of the amorphous polymer, so that the crucial experiment which was noted earlier in the polyamides and might be possible in polyesters at a low temperature, is not normally done.

Microcrystalline polymers characteristically form spherulitic aggregates

¹⁰ P. Brauer and F. H. Müller, *Kolloid-Z.* **135**, 65 (1954).

¹¹ I. Marshall and A. B. Thompson, *Proc. Roy. Soc.* **A221**, 541 (1954).

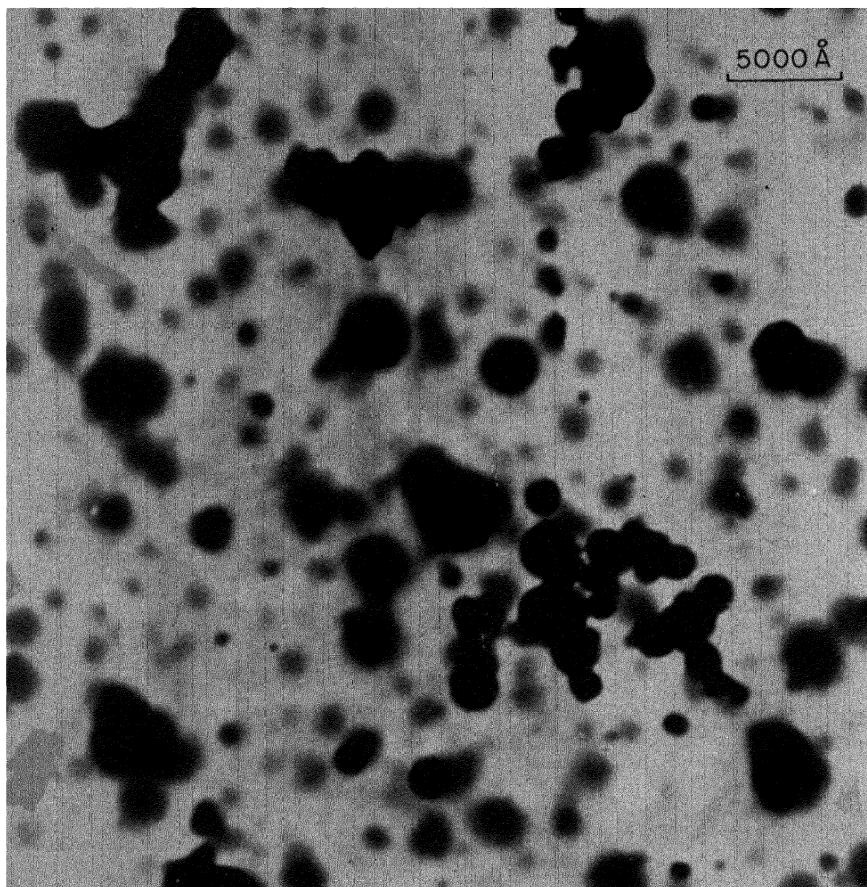


Fig. 7b. Electron micrograph of polydecamethylene sebacamide showing crystal-lite growth from solution. Original magnification, 10,100 \times .

through their bulk.^{12, 13} Generally these are in the form of sections of spherulites containing very fine sheaves of crystallites whose details can be barely discerned in Fig. 7a for a polyundecanoate polyester of weight average molecular weight about 25,000, but which appear beautifully in the diagrams of Brown¹⁴ for polyethylene. Brown's work actually shows a stretched section of one of the thin films which exhibits how the crystallites were made to flow out of the spherulitic sections when the system was

¹² C. W. Bunn and T. C. Alcock, *Trans. Faraday Soc.* **41**, 317 (1945).

¹³ S. W. Hawkins and R. B. Richards, *J. Polymer Sci.* **4**, 515 (1949).

¹⁴ A. Brown, *J. Appl. Phys.* **20**, 552 (1949).

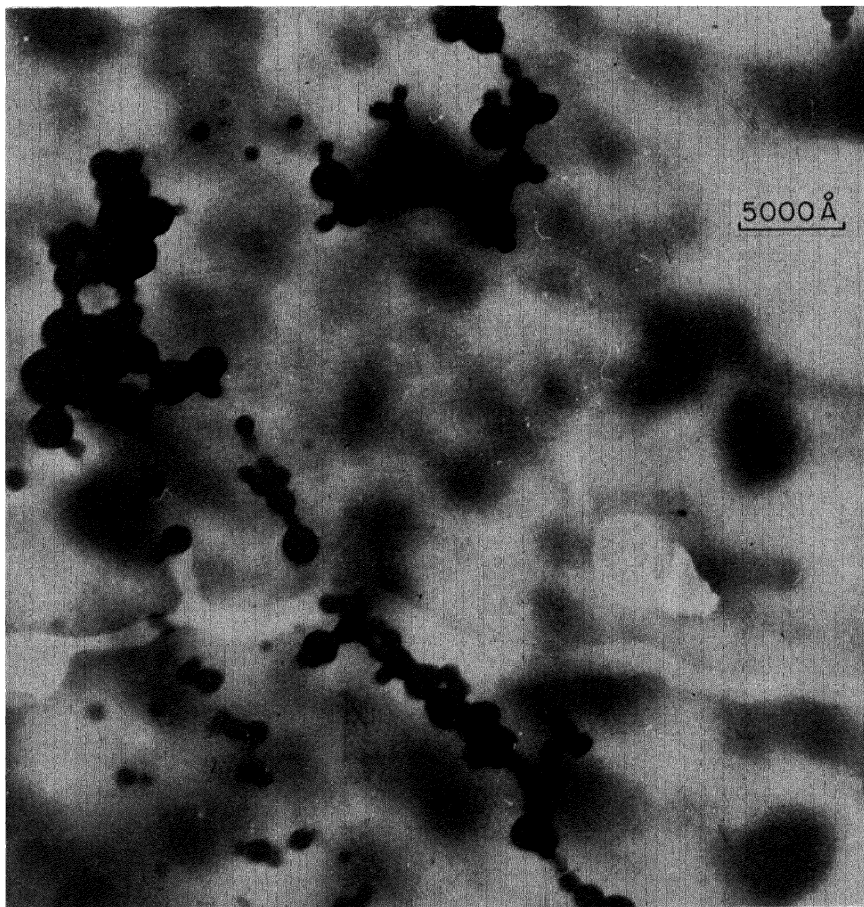


FIG. 7c. Electron micrograph of polyhexamethylene adipamide film showing spherulite clusters of crystalline phase. Original magnification, 10,100X.

oriented. Also, in the linear polyamides, (in a series of electron microscopic studies by C. J. Calbick of the Bell Telephone Laboratories), thin films could be cast on water from cresol or formic acid solution, which then crystallize as the solvent evaporates and grow beautiful spherulites. Fig. 7b shows how these aggregate in polyhexamethylene sebacamide, and Fig. 7c is for the familiar nylon 66. In Fig. 7d appears a section of the film of polyhexamethylene adipamide which was stretched in the beam of the electron microscope. These spherulites can easily be seen to appear to flow continuously into the matter drawn out adjacent to them. Perhaps submicroscopic crystallites are being reoriented as the spherulites are

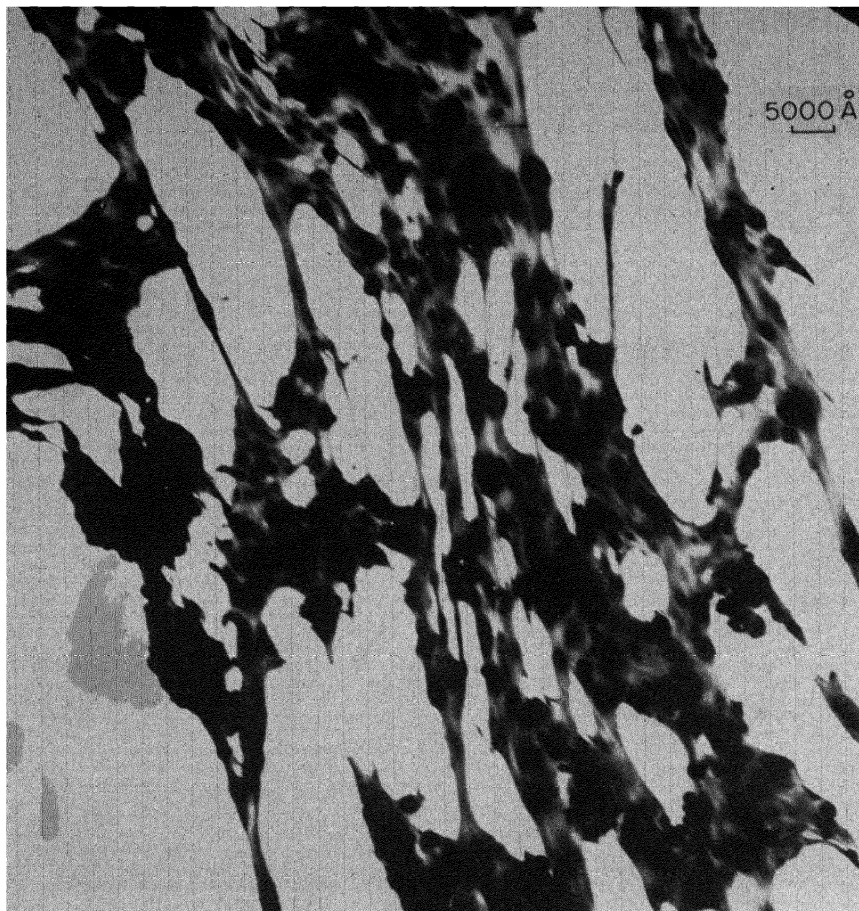


Fig. 7*d*. Electron micrograph of partly drawn film of polyhexamethylene adipamide showing distortion of spherulites by fibering. Original magnification, 3760 \times .

subjected to tension around them, and this is the basic step in the large strain rheology of microcrystalline polymers.

The crystallites and their aggregates, the spherulites already shown to be strongly affected by polymer deformation, are nevertheless largely connected by more or less disordered chains. These disordered chains always tend to pull out so that their long axes eventually line up in the direction of, say, a uniaxial stress. It is therefore important to know how the arrangements of the long chain axis (*c*-axis in the crystallites) take place in the crystallite. In this way, some idea of the transmission of stress from the disordered continuum to the crystallites and spherulites can be gained.

The recently discovered principles of spiral growth of crystals generally seem also to apply to polyethylene, at least,^{15, 16} and probably to polyamides and others.¹⁶ A consequence of this finding was anticipated in an extensive study of the mechanism of crystallization in linear polymers^{17, 18}: it caused a spiral arrangement of long chains into fibrillar crystallites, which seems necessary to account for the observed positions of crystal cells in single spherulites.^{19, 20} Such closely coiled helices of crystallites then are radii of spherulites, or spherulitic sections. Such is the present concept of the chain geometry in the unoriented polymer, on which an external stress (or an internal relaxing force) must work. It leads, in accord with our earlier postulate, to highly organized motions of chain segments along crystal planes and is greatly enriching knowledge of polymer mechanics. Indeed, after the great triumph of the kinetic theory of rubbery elasticity, and even viscoelasticity, based on *independent* segment movements, the new findings about orderly motions are peculiarly complementary. Strikingly, they are appearing as the new isotactic polymers provide overwhelmingly crystalline plastics. For the first time, there may be plastics whose behavior is largely plastic.

3. PLANAR MOVEMENT IN COLD DRAWING

Evidence for this motion of whole planes of atoms occurred in early studies of the disorientation of polyamide filaments caused by heating.⁹ There was selective growth of the X-ray arcs coming from the main equatorial reflections, showing that the crystal planes did not go from the oriented to the disoriented state all together, but rather with a selective ease of gliding. Likewise, examination with a tiny X-ray beam of scattering through and on both sides of the neck of a small nylon filament was done by Fankuchen and Mark.²¹ Here it was established by reference to the earlier structure studies that planes corresponding to sheets of hydrogen-bonded chains were first being drawn around so that the ribbonlike sheets were in the direction of the uniaxial stress. Similar planar motion was observed for various stages in the orientation of cellulose and some of its derivatives, as discussed by Sisson.²² Incidentally, the study of Fankuchen

¹⁵ R. Jaccodine, *Nature* **176**, 305 (1955).

¹⁶ E. W. Fischer, *Z. Naturforsch.* **12a**, 753 (1957).

¹⁷ L. B. Morgan, *J. Appl. Chem.* **4**, 160 (1954).

¹⁸ A. Keller, G. R. Lester, and L. B. Morgan, *Phil. Trans. Roy. Soc. London, Ser. A* **247**, 1 (1954).

¹⁹ A. Keller, *Nature* **169**, 913 (1952); **171**, 170 (1953).

²⁰ A. Keller, *J. Polymer Sci.* **17**, 351 (1955).

²¹ I. Fankuchen and H. Mark, *J. Appl. Phys.* **15**, 364 (1944). 245 *at seq.*

²² W. A. Sisson, in "Cellulose and Its Derivatives" (E. Ott, ed.), p. 245 *et seq.* Inter-science, New York, 1943.

and Mark also revealed large differences in the crystallinity of their monofilament, reflecting variations in the quenching, water annealing and the heating during drawing to which it was exposed. The present interpretation of crystalline rearrangements in the rheology of drawing emphasizes that all these features are important in understanding the force-extension behavior of such systems.

The most striking and intensive probe of the deformations during cold drawing has been done for polyethylene. Here it was found that first stages of the drawing just beyond the yield region caused an extraordinary splitting of X-ray diffraction rings.⁷ The structure these rings represent was pretty well known by the early study of Bunn.²³ The inner strong ring corresponding to (110) planes, and the outer weaker ones to (200) planes, split so that the (200) was readily pulled down to equatorial spots but the (110) arcs split further above and below the equator of the diagram.⁷ This indicates that the (011) axis is tilted at a very large angle to the direction of the stress, and yet this is the axis containing the carbon chains of polyethylene. Hence the very element of structure most capable of supporting the applied stress is, by crystallographic responses to the stress, thrown into a position where it is not pulled on. Weaker, van der Waals', interactions in the solid bear most of the external force. This has turned out to be a predominant feature of microcrystalline polymer mechanics. Recently, detailed studies by Brown,¹⁴ and Horsley and Nancarrow²⁴ have emphasized the quasimetallic features⁷ of polyethylene plastic flow. They have shown that selective planar glide is achieved on relaxing fully stretched fibers from their condition of having the chain axes all parallel to the direction of principal stress. Again, the crystallites, disorienting as in the polyamide cases noted, do not go through random rearrangements, but slip back so that at an intermediate state the long axes are again largely tilted with respect to the principal force axis. However, for polyethylene, this was not found on *stretching* above 95°C., where crystalline anisotropy and probably crystal content are drastically reduced. This is strong support for the earlier thesis that the mechanics of cold drawing of these microcrystalline systems are dominated by crystal planes rather than by the melting of crystallites which reform only in the oriented condition. Thus, in general, a chain polymer whose crystallites respond in an uneven way to plastic flow will have the (1*k*0) lattice points off the equator of an X-ray diagram instead of lying on it, as simple extension of the chain axis in the direction of flow would produce. (110) reflections will not in general be thus split, however.

²³ C. W. Bunn, *Trans. Faraday Soc.* **35**, 482 (1939).

²⁴ R. A. Horsley and H. A. Nancarrow, *Brit. J. Appl. Phys.* **2**, 345 (1951); S. Krimm, *J. Phys. Chem.* **57**, 22 (1953).

For polyethylene, (110) and (100) seem, however, to be planes along which slip could most readily occur during flow, and where indeed it does seem to take place in the latter stages of extension when the chain axes *are* finally in the direction of the force. Correspondingly, on relaxing, movement back appears to occur along these very planes. Then, chain axes come back again to an intermediate position nearly normal to the direction of the original stress. However, the intermediate configurations observed for the original pulling before relaxing seem to be caused by something like crystallite shape or other details such as the nature of the fringes between crystalline and amorphous volumes. Also critical for this extraordinary stretching behavior may be the suggestion of Bunn and Alcock,¹² that molecular orientation will be stepwise and involve some chains at large angles to the stretching direction, because in this way a few potential barriers at a time can be surmounted. In the case of relaxing, the retractive force is provided by the reinking of rubbery amorphous segments.⁹ Then, since this process often occurs near the melting point of the crystallites, an additional factor may be orientation in which the axis with the lowest coefficient of thermal expansion and hence the least sensitivity to the effect of external force on melting point, bears the main stress.²⁴ This would at least put the *a* axis, with its large coefficient, away from the stress direction on stretching at high temperatures. On relaxing, the reverse would happen, with this axis parallel to the direction of stretch.

4. FURTHER CONSEQUENCES OF CRYSTALLINE DISPLACEMENTS

These various interpretations, and many new and ingenious studies, have been critically analyzed by Keller.²⁵ Many new aspects are now being revealed of mechanical properties of the microcrystalline polymers which may clothe (cellulose, polyamides, polyesters, polyvinylidenes, polyacryls, polyolefins, etc.), help to shelter (cellulose, polyolefins, etc.) and otherwise comfort (plastic piping for plumbing, plastic wiring for communications and power) mankind. No longer are the classical intuitions valid that high average molecular weight alone, for instance, sets a high yield strength for a fiber-forming system. For small enough filaments, the crystallite arrangement and statistics of stress distribution would be expected to become significant.

Such an effect, doubtless well-known to all synthetic fiber technologists, was observed in our Laboratories by Mr. R. L. Taylor, some years ago, for many linear polyesters. For instance, polyethylene sebacate of varying weight average molecular weight indicated by the intrinsic viscosity in chloroform solution, at 25° C., shown in Fig. 8, showed marked differences

²⁵ A. Keller, *J. Polymer Sci.* **15**, 31 (1955); see also references therein.

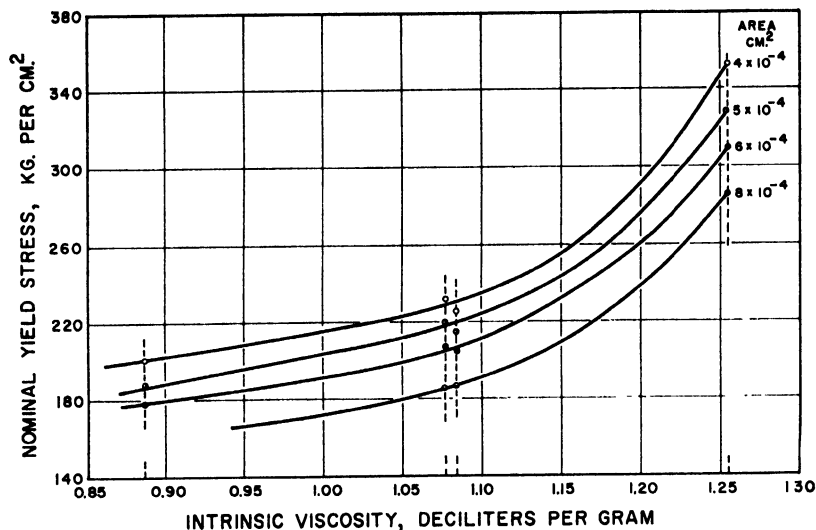


FIG. 8. Relation of nominal yield stress of filaments of polyethylene sebacate to viscosity average molecular weight at different levels of original cross section.

associated with a twofold variation in original cross section. While the yield stress rose regularly with increasing intrinsic viscosity the larger area filaments yielded at consistently lower values than the smaller. Presumably the probability of crystallite and spherulite arrangements favoring easiest planar displacements was greater in the larger diameter specimens.

For tensile strength, or nominal stress at rupture (Fig. 9), the same filaments show little dependence on final cross-sectional area, since now they are all highly drawn with crystallites and chain axes "fully" extended. Even the molecular weight range covered has only the effect of allowing the shorter chain length but more ductile polymer further reduction in area before rupture at the characteristic value. Of course, the lowest molecular weight samples drew so highly that their rupture is at high nominal stress values.

However, when various *very fine* filament sizes of a high molecular weight polyethylene sebacate were tested to rupture, similar strikingly large effects were found, as in Fig. 10. The areas are again down a factor of 10 from those of Fig. 9, and perhaps further reflect the more perfect orientation of large draw ratios (easily six- or sevenfold).

In all cases, the powerful influence of crystallites and cooperative chain orientation on flow and plasticity shows up. Each effect concerns some super-chain displacements, always contained in a disordered matrix. Indeed, under powerful stress, even the noncrystalline chains orient

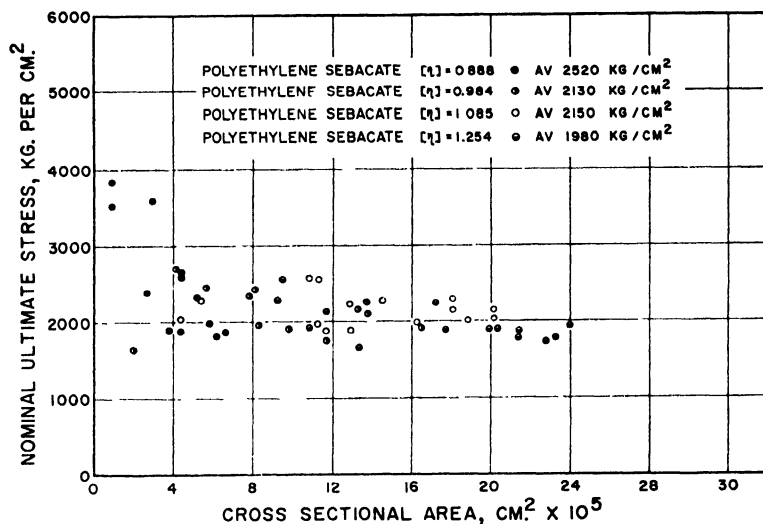


FIG. 9. Breaking strength of polyethylene sebacate polyester fibers of various viscosity average molecular weights as a function of cross sectional area.

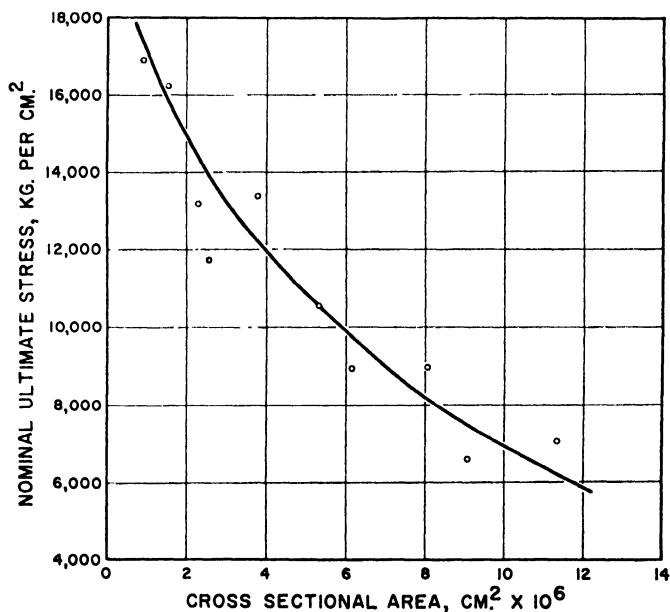


FIG. 10. Breaking strength of polyethylene sebacate polyester fibers of very small cross section as influenced by cross sectional area of fiber.

strongly.²⁶⁻²⁸ Thus, the very transmission of stress to the crystallite regions itself varies.

These subtle structure changes seem to have drastic effects on the mechanics of polymers. This arises because crystallite rotation and planar orientation go through such large angles during a simple uniaxial stretch. Then, it might be expected, during multiaxial stressing with a two-way pull, that occasionally a large stress would meet an arrangement of polymer chains where they could be readily pulled apart sideways, i.e. in directions normal to their long axes. Now the basic element of the physical properties of chain polymers and presumably the source of their amazing utility is that the long chain axes contribute great strength. This is either by sustaining a stress directly or entangling with many others, so that the stress is spread around among primary valence bonds. However, the very element of microcrystallinity is that chain segments are not entangled, but rather neatly laid out laterally and lengthwise. Hence if forces are brought in to meet these chains chiefly normal to their long axes in the crystallites, the structure may show fatal weakness. Examples of this will be discussed in detail in later sections on stress cracking and brittleness of polyethylene and other plastics.

The import of the present discussion, however, is that the purely crystalline rearrangements in the deformation of linear polymers are inadequate to account for all of their properties. Indeed, the rather surprising inter-crystallite (and sometimes intra-) changes sustained by deformed polymers emphasize the importance of the disordered phases. Obviously rheology of these systems involves more intimate and delicate interaction of crystal and liquid mechanics than has been encountered before. While the crystallites are probably also defect structures, and the liquids may have quasi-crystalline packing, certain characteristic properties of each state persist in the presence of the other. Indeed, where such coexistence is practically lost, as in some special stereoisomeric polymers recently synthesized, the domination of microcrystalline properties seems disastrous. Brittle environmental and impact sensitive qualities appear even in certain polyethylenes.

Accordingly, the discussion should turn now to examination of the liquidlike or viscoelastic properties of microcrystalline and cross-linked polymers. Here, the orderly deformation and movement of relatively large arrangements of molecular segments is not expected. Rather, the rapid diffusionlike thermal agitation of single chain segments is thought to be biased by external stresses. The following paragraphs will attempt

²⁶ I. L. Hopkins, W. O. Baker, and J. B. Howard, *J. Appl. Phys.* **21**, 206 (1950).

²⁷ D. R. Holmes, R. G. Miller, R. P. Palmer, and C. W. Bunn, *Nature* **171**, 1104 (1953).

²⁸ W. P. Slichter, *J. Polymer Sci.* **21**, 141 (1956).

to describe the position of these kinetic effects, which are in contrast to the foregoing static structures, in understanding crystalline and cross-linked polymers.

5. SHORT-RANGE DISPLACEMENTS IN POLYMERS

Linear polymers in which long-range molecular movements are either prevented or strongly inhibited by cross-linking, entanglement, partial involvement in crystallites, or other bonding arrangements as in glass, have certain viscoelastic properties in common. In stress relaxation, they are often characterized by a nearly linear relation between stress and the logarithm of time over several units of the latter. The early part of a creep curve represented by deflection against the logarithm of the time may often similarly appear nearly linear. In dynamic tests, in which the mechanical impedance is represented by a spring and dashpot in parallel (Kelvin-Voigt element) the stiffness of the spring (the dynamic modulus) may change only very slowly with frequency over a considerable frequency range, as will the product of the frequency and the viscous resistance of the dashpot. Since the mechanical loss factor $\tan \delta$ is the quotient of these two slowly changing quantities, it will be fairly constant over some decades of frequency change. Specific cases of these phenomena will be adduced in the pages to follow. The discussion throughout will be in terms of the theory of linear viscoelasticity and deviations from it.²⁹

Complete characterization of a material within the range of strains and stresses for which the behavior is linear (within which the superposition principle is valid) requires that measurements be made in some manner over the entire time scale represented by the characteristic relaxation times of the material. For long times stress relaxation or creep measurements are ordinarily used, while for short times measurements at audio

²⁹ The background of the theory of linear viscoelasticity is available in several books. An excellent summary of the theory up to 1943 may be found in H. Leaderman, "Creep of Filamentous Materials and other High Polymers" (The Textile Foundation, Washington, D. C., 1943). A most inclusive discussion of the theory, deviations from it, its application to materials, and approximate methods is provided by Turner Alfrey, Jr., "Mechanical Behavior of High Polymers" (Interscience, New York, 1948). A most complete presentation of the linear theory is given in B. Gross, "Mathematical Structure of the Theories of Viscoelasticity" (Hermann, Paris, 1953). The form of distribution function described here has been treated by W. Kuhn, O. Kunzle, and A. Preissmann [*Helv. Chem. Acta*, **30**, 307, 464 (1947)]. A. V. Tobolsky, B. A. Dunell, and R. D. Andrews [*Textile Research J.* **21**, 404 (1951)] have also discussed this function in detail.

Recent summaries of certain aspects of this field are given by Turner Alfrey, Jr. and E. F. Gurnee, "Rheology: Theory and Applications," Vol. I, Chapter 11, Academic Press, New York, 1956; H. Leaderman, *ibid.*, Vol. II, Chapter 1, 1957; Arthur Tobolsky, *ibid.*, Vol. II, Chapter 2; and John D. Ferry, *ibid.*, Vol. II, Chapter 11.

and supersonic frequencies are required. But generally at ordinary temperatures, the time required for complete relaxation on the one hand, and the extreme frequency of mechanical vibration on the other, are not available, with the result that only by the artifice of introducing temperature as a parameter may a complete analysis be made. The effect of raising the temperature is to reduce the relaxation times to such a range that the long times become short enough for practicable relaxation tests; or lowering the temperature so lengthens them that the shortest of them correspond to an attainable vibration period. This procedure is valid for materials in which a change of temperature is not associated with a change of structure, such as melting of crystallites or dispersion of spherulites. This kind of characterization is complete for but few materials, although many of them show, over part of the time range, some of the characteristics mentioned above.

It has been shown²⁹ that these modes of behavior may be accounted for by the assumption of a distribution of relaxation times

$$\begin{aligned} E(\tau) &= K/\tau, & \tau_1 &\leq \tau \leq \tau_2 \\ E(\tau) &= 0, & \tau &< \tau_1, \tau > \tau_2 \end{aligned}$$

The characteristics of such a distribution have been discussed at length²⁹ and are well known. We shall not repeat the mathematics, but merely state the salient features of the behavior of such a hypothetical material. It is assumed that τ_2 is at least several orders of magnitude greater than τ_1 .

a. Stress Relaxation

Stress is *extremely nearly* although not precisely linear with log time within most of the region between $t = \tau_1$ and $t = \tau_2$. The linear portion of the curve (Fig. 11), if extended, intersects the maximum and the zero stress lines at $\log t = (\log \tau_1 - 0.251)$ and $(\log \tau_2 - 0.251)$, respectively. If $E_r(t)$, the relaxation modulus, is defined as (stress at time t)/strain, then $dE_r(t)/dt = -2.303 K$ is the slope of the linear part of the curve.

b. Creep

If we define a relaxation function as

$$\psi(t) = (\text{stress at time } t)/(\text{stress at time } 0)$$

and a creep function as

$$\varphi(t) = (\text{deflection at time } t)/(\text{deflection at time } 0),$$

then these two functions are related by the integral equation³⁰

$$\int_0^t \varphi(\tau) \psi(t - \tau) d\tau = t \tag{1}$$

³⁰ I. L. Hopkins and R. W. Hamming, *J. Appl. Phys.*, **28**, 906 (1957).

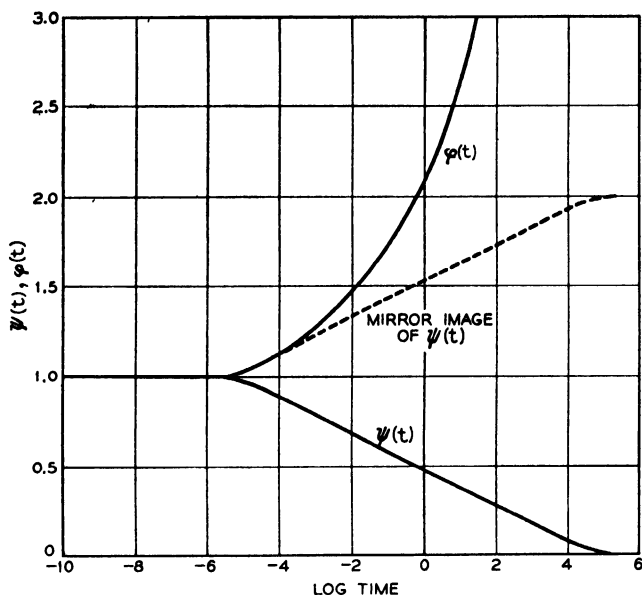


FIG. 11. Relaxation and creep functions for "box" distribution of relaxation times, $\tau_1 = 10^{-5}$ and $\tau_2 = 10^5$.

It is characteristic of this equation that the only functions $\psi(t)$ and $\varphi(t)$ of the forms $\psi(t) = 1 - f(t)$ and $\varphi(t) = 1 + cf(t)$ which will satisfy it are those with $f(t) = 0$; that is, if there were no creep or relaxation at all. If the constant $c = 1$, then $\psi(t) + \varphi(t) = 2$, which is approximately true when $\psi(t)$ and $\varphi(t)$ are near 1, but the deviation is quite appreciable when $\psi(t) = 0.9$ or $\varphi(t) = 1.1$. In fact, it appears from a few calculated cases that if either $\psi(t)$ or $\varphi(t)$ is linear in $\log t$, the approximate identity $\varphi(t) = 1/\psi(t)$ is a satisfactory representation for a considerably greater range.

c. Dynamic Modulus

The dynamic modulus is extremely nearly linear with $\log \omega$ within most of the region between $\omega_1 = 1/\tau_2$ and $\omega_2 = 1/\tau_1$. The linear portion of the curve, if extended, intersects the zero and the maximum modulus lines at $\log \omega = -\log \tau_2$ and $-\log \tau_1$, respectively. The slope is positive and is numerically equal to that of the relaxation curve, $2.303 K$.

d. Dynamic Viscosity-Frequency Product

If $\tau_2/\tau_1 \geq 10^6$, it may be shown that within the limits $\omega_1 \simeq 64/\tau_2$ and $\omega_2 \simeq 1/64\tau_1$, the viscosity-frequency product $\omega\eta$ does not vary more than 1% from its maximum value, which occurs at $\omega = \sqrt{1/\tau_1\tau_2}$. The viscosity itself therefore varies very nearly with $1/\omega$ in this range. While a tentative value of K and limits τ_1 and τ_2 may easily be found for any material which

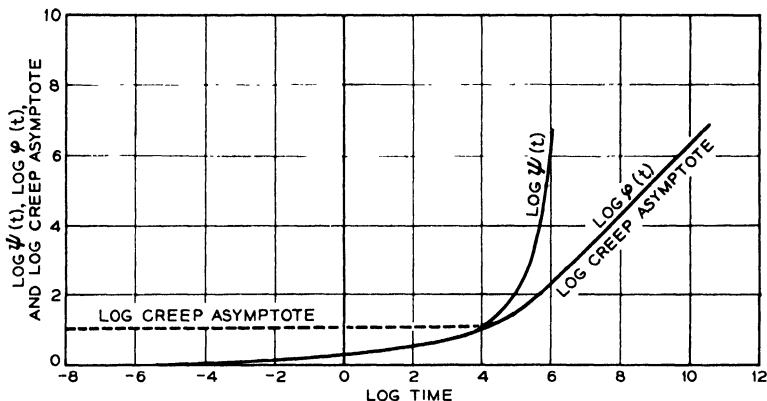


FIG. 12. Log relaxation and creep functions and creep asymptote for "box" distribution of relaxation times, $\tau_1 = 10^{-5}$ and $\tau_2 = 10^5$.

displays any of the behavior mentioned, such a description is usually only partial. For example, a stress relaxation experiment may be compatible with such a characterization, but this test does not even "see" the shorter relaxation times, their effect having vanished even while the initial strain was being applied. On the other hand, dynamic data are usually taken with relatively short periods and characterize a part of the relaxation spectrum which may have quite a different form. It is not surprising, therefore, that complete characterizations are not available for many of these materials. It is in fact not known whether or not certain of them would ever relax completely. Nevertheless, the fact that all the properties mentioned above are so often approximated in reality gives this method of analysis and simplification a certain qualitative value.

For purposes of illustration, Figs. 11 to 14 show the curves derived from a hypothetical material characterized by the relaxation distribution

$$E(\tau) = 0.4342/\tau, \quad \tau_1 \leq \tau \leq \tau_2$$

$$= 0 \text{ elsewhere}$$

where $\tau_1 = 10^{-5}$, $\tau_2 = 10^5$. In Fig. 11 are shown the relaxation and creep functions $\psi(t)$ and $\varphi(t)$, the latter having been calculated by numerical solution of the integral equation (1).³⁰ The asymptote approached by the creep function for times greater than τ_2 is $11.502 + 2.303 \times 10^{-4}t$; this together with the relaxation and creep functions are plotted on a log-log scale in Fig. 12. The dynamic functions are plotted against $\log \omega$ in Fig. 13, and on log-log coordinates in Fig. 14.

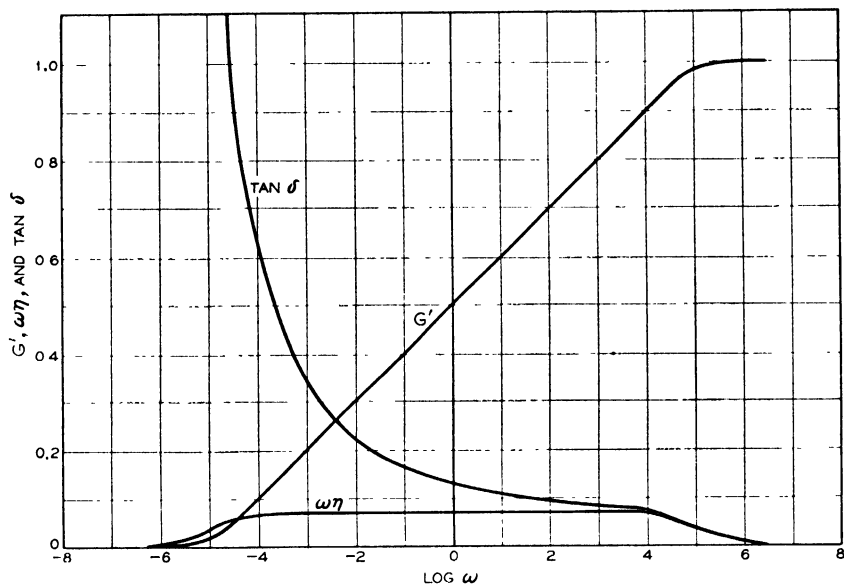


FIG. 13. Dynamic properties for "box" distribution of relaxation times, $\tau_1 = 10^{-5}$ and $\tau_2 = 10^5$.

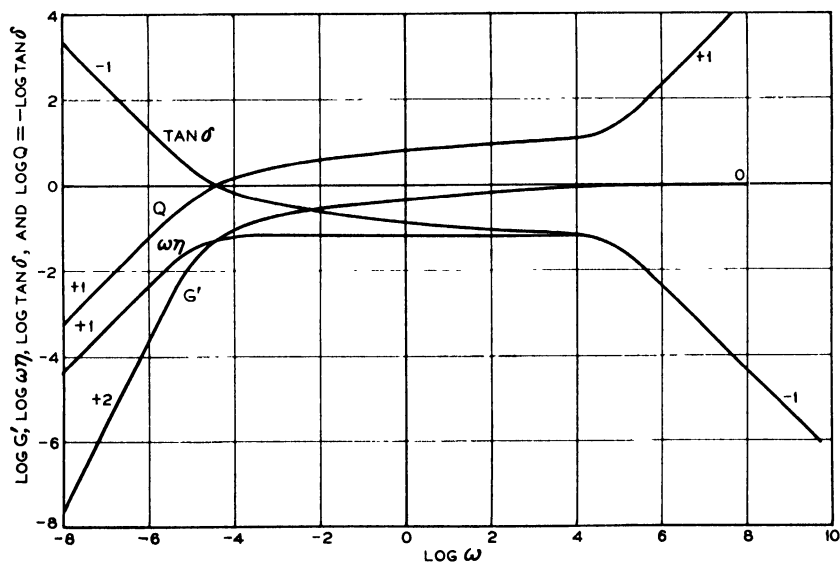


FIG. 14. Log dynamic properties for "box" distribution of relaxation times, $\tau_1 = 10^{-5}$ and $\tau_2 = 10^5$. Numbers at ends of curves are slopes as $\omega \rightarrow 0$ and $\omega \rightarrow \infty$.

II. Polyethylene

1. DYNAMIC PROPERTIES OF POLYETHYLENE

The literature on dynamic testing of polyethylene may be separated into two major groups; tests in which temperature is the main variable, with frequency either being held constant or changing as the change of modulus with temperature causes the resonant frequency of the test system to vary, and tests in which the temperature is held constant while the frequency is varied. The discussion will be in that order; and to bring the data to a common basis, Young's modulus is converted approximately to shear by dividing by 3, a procedure which will be justified later.

In the earlier papers, the identified materials were all standard low-density polyethylenes, and while there were differences between them, the picture that emerges is consistent. The later papers will be discussed separately. The data presented in the literature are in various forms; wherever possible, tabulated data or plots were recalculated to give the shear modulus and mechanical loss factors, $\tan \delta$. While the accuracy of this calculation is not always high, it serves the present purpose.

Nielsen and Buchdahl,³¹ Schmieder and Wolf,³² Oakes and Robinson,³³ and Sauer and Kline³⁴ have used free vibration methods, and Thurn³⁵ and Wada and Yamamoto³⁶ have used forced oscillations over various temperature ranges. Figures 15 and 16 show the shear moduli and loss factors, respectively. Figure 15 shows consistency among the data, with reasonable agreement where the test frequencies are nearly the same, and also demonstrates qualitatively the "reduced variable"³⁷ effect in the maintenance of a high modulus at high frequencies even at the highest temperatures. Fig. 16, in which the mechanical loss factor is plotted against log time, shows the same consistency, except that the data of Thurn at 2 Mc. and the corroborating data of Wada and Yamamoto at 1.46 Mc. show not only a displacement to the right on the log time scale (appropriate to the reduced variable scheme) but also a different form. Schmieder and Wolf attribute the loss peak at circa -100°C . to amorphous unbranched chain parts, that at 5°C . to the "constrained" amorphous at the branch points of the main chain, and that at $+54^{\circ}\text{C}$. to the crystalline. Oakes and Robinson believe the low temperature peak to be possibly associated with flexibility in a limited number of main chain- CH_2 links. The -30° to

³¹ L. E. Nielsen and R. Buchdahl, *SPE Journal* **9**, 16 (1953).

³² K. Schmieder and K. Wolf, *Kolloid-Z.* **134**, 149 (1953).

³³ W. G. Oakes and D. W. Robinson, *J. Polymer Sci.* **14**, 505 (1954).

³⁴ J. A. Sauer and D. E. Kline, *J. Polymer Sci.* **18**, 491 (1955).

³⁵ H. Thurn, *Z. angew. Phys.* **7**, 44 (1955).

³⁶ Y. Wada and K. Yamamoto, *J. Phys. Soc. Japan* **11**, 887 (1956).

³⁷ A. V. Tobolsky and R. D. Andrews, *J. Chem. Phys.* **13**, 3 (1945).

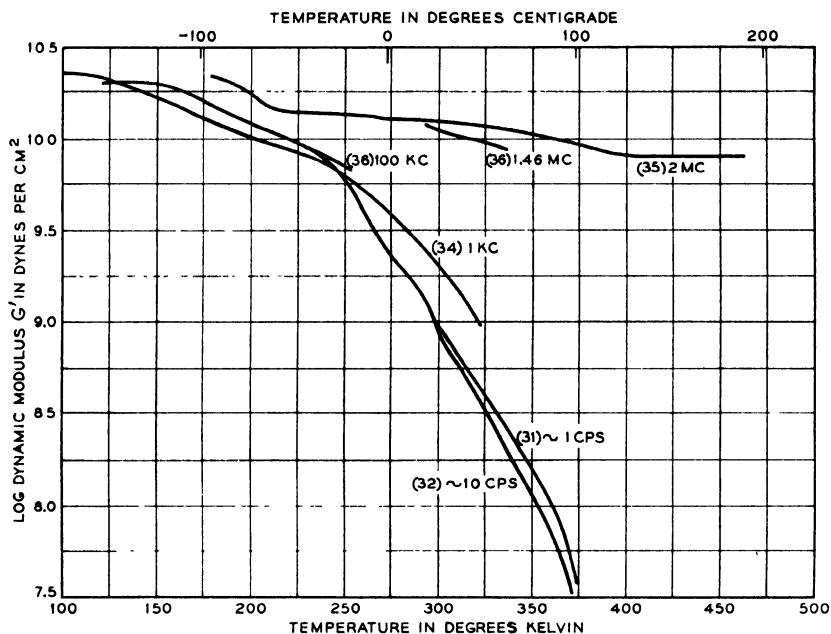


FIG. 15. Dynamic shear modulus as function of temperature for polyethylene with test frequency as parameter. The numbers in parentheses are literature references.

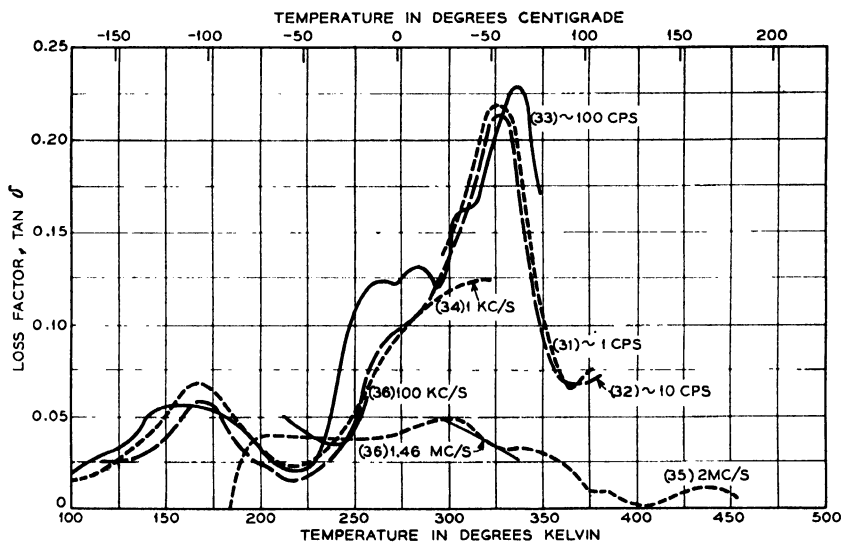


FIG. 16. Dynamic loss factor as function of temperature for polyethylene, with frequency as a parameter. The numbers in parentheses are literature references.

+50° C. range contains signs of multiple loss peak structure, which they believe to be frequency dependent and influenced by molecular weight; the dispersion region from -60 to +40 is absent from loss curves for straight unbranched polyethylenes, as will be discussed later. The high peak at 60-80° C. is attributed by Oakes and Robinson to relatively large scale mobility of the polymer chains, enhanced by the onset of melting in the crystalline regions. The high modulus throughout the temperature range in Thurn's data suggests that at his test frequency, 2 Mc., bond-angle bending is the predominant mode of compliance, with only slightly longer range effects coming into play at the higher temperatures. The constancy of the loss factor from -70° to +70° C. (within $\pm 25\%$) suggests that no new major compliance mechanism has come into play. In other words no movements large enough to distinguish between branch points, crystallites, and amorphous material, have developed in that range.

Dynamic tests over a range of frequencies, with temperature constant, have been made by forced vibration methods by Hillier,^{38, 39} Lethersich,⁴⁰ McSkimin,⁴¹ Dunell and Dillon,⁴² Mason and McSkimin,⁴³ and Philippoff.⁴⁴ The values of shear modulus and the loss factor $\tan \delta$ are plotted against log frequency in Fig. 17. Here again the picture is consistent; and this plot, covering a range of 10^{12} c.p.s., shows that polyethylene requires a tremendous range of logarithmic time or frequency to describe its properties. The maximum value of shear modulus in Fig. 15 is in excess of 2×10^{10} dynes/cm.² at 25° C., while the maximum in Fig. 17 is somewhat less than 10^{10} . The minimum value is about 10^8 , obtained by Philippoff at 75° C. at about 10^{-5} c.p.s. As will be discussed later, the minimum in stress relaxation obtained by Catsiff *et al.*⁴⁵ is about 2×10^7 , obtained after 1 hr. at 105° C. The range of 10^{12} in frequency in Fig. 17 therefore does not encompass the total realizable range of moduli for polyethylene. Philippoff,⁴⁴ utilizing the principle of reduced variables, has synthesized a plot in which a frequency range of 10^{24} is required to include the measurements he has made on the dynamic properties, and even this is not really enough, since in his diagram of modulus versus frequency the curve has not leveled off at either end. Further, the technique of reduced variables itself, in this case, tends to minimize the length of the spectrum of relaxation times. That this is so can be shown by the following considerations.

³⁸ K. W. Hillier, *Proc. Roy. Soc. B***62**, 701 (1949).

³⁹ K. W. Hillier, *Proc. Roy. Soc. B***64**, 998 (1951).

⁴⁰ W. Lethersich, *J. Sci. Instr.* **27**, 303 (1950).

⁴¹ H. J. McSkimin, *J. Acoust. Soc. Am.* **23**, 429 (1951).

⁴² B. A. Dunell and J. H. Dillon, *Textile Research J.* **21**, 393 (1951).

⁴³ W. P. Mason and H. J. McSkimin, *Bell System Tech. J.* **31**, 122 (1952).

⁴⁴ W. Philippoff, *J. Appl. Phys.* **25**, 1102 (1954).

⁴⁵ E. Catsiff, J. Offenbach, and A. V. Tobolsky, *J. Colloid Sci.* **11**, 48 (1956).

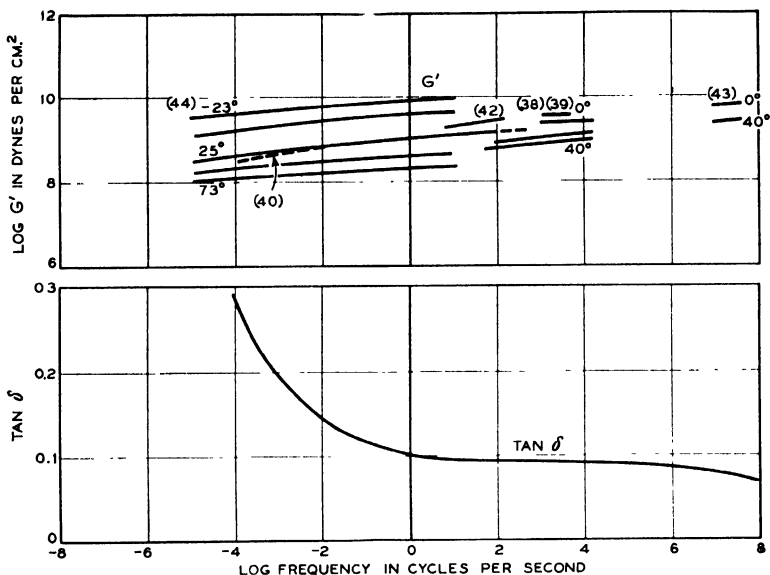


FIG. 17. Dynamic modulus and loss factor for polyethylene as function of frequency with temperature as a parameter. The numbers in parentheses are literature references.

The concept of reduced variables is predicated on the idea that the effect of a change of temperature is to change *all* relaxation times by the same factor;⁴⁶ and this implies that there shall be no structural change associated with the temperature change. However, there is a change in the crystalline content of polyethylene associated with a temperature change from 25° C. to 73° C.^{7, 47} In the dynamic tests at 73° C., the minimum shear modulus will be obtained at the lowest frequency of test, and, by the continued joining of curves from 25° C. (the usual base temperature), the modulus obtained will be ascribed to some lower frequency at 25° C. But the modulus is lower than it would have been had the degree of crystallinity not decreased at the higher temperature; this low modulus in a material at 25° C. would actually have been obtained only at a still lower frequency than that deduced by this method. Thus the low end of the frequency scale has been telescoped, and Philippoff's estimate of 10^{24} is an underestimate. Considering that this accounts only for the decrease of the Young's modulus from something under the ultrahigh-frequency high to something over 10^8 dynes/cm.², or 3×10^7 in shear—a figure corresponding to the stiffness of a fairly stiff soft rubber for a period of seconds or minutes—the long-time,

⁴⁶ R. S. Marvin, E. R. Fitzgerald, and J. D. Ferry, *J. Appl. Phys.* **21**, 197 (1950).

⁴⁷ R. B. Richards, *Trans. Faraday Soc.* **41**, 127 (1945).

or low frequency, end of the relaxation spectrum is undefined, and may be indefinitely long with the crystallites acting as permanent cross links.

The gentle positive slope of the log modulus-log frequency curve, and the moderate change in the mechanical loss factor over the 12 decades covered in Fig. 17 seem characteristic of materials in which long-range movements are prevented either by cross-linking, crystallinity, or other bonding arrangements, as in glass, which prevent unlimited relative movement of chains. Ebonite behaves similarly over the range from 0.0001 to 10,000 c.p.s.,^{40, 48} and fused quartz at 15° C. has a shear modulus of 3.00×10^{11} dynes/cm.² in a static test according to Horton,⁴⁹ and 3.12×10^{11} at 12 Mc./sec. according to McSkimin.⁵⁰

McSkimin and Mason, and McSkimin have measured both the shear and longitudinal wave propagation constants for polyethylene in the megacycle region, and have calculated the Lamé constants λ and μ as well as their associated viscosities χ and η respectively. They found that at 25° C., λ has a value of about 3.0×10^{10} dynes/cm.², and is nearly independent of frequency over the 8- to 30-Mc. range. χ is found to be nearly equal to $\eta/3$, whence the shear and bulk viscosities are about equal.^{53a}

Parks and Richards,⁵¹ Weir,⁵² and Bridgman⁵³ have measured the "static" compressibility of polyethylene. Recalculation of their results to a common basis gives the following bulk moduli at low pressures, in 10^{10} dynes/cm.²: Parks and Richards, 1.8; Weir, 3.9; Bridgman, 3.5.

Weir remarks on the discrepancy between his results and those of Parks and Richards, and on his agreement with Bridgman.

From the formulas in footnote 53a.

$$B = \lambda + 2\mu/3$$

Since for these "static" tests μ , the shear modulus, is only about 4×10^8 , B is very nearly equal to λ . Then, using the mean of the results of Weir

⁴⁸ R. L. Wegel and W. Walther, *Physics* **6**, 141 (1935).

⁴⁹ F. Horton, *Phil. Trans. Roy. Soc. London, Ser. A* **204**, 407 (1905).

⁵⁰ H. J. McSkimin, *J. Appl. Phys.* **24**, 988 (1953).

⁵¹ W. Parks and R. B. Richards, *Trans. Faraday Soc.* **45**, 203 (1949).

⁵² C. E. Weir, *J. Research Natl. Bur. Standards* **46**, 207 (1955).

⁵³ P. W. Bridgman, *Proc. Am. Acad. Arts Sci.* **76**, 71 (1948).

^{53a} The relation between the elastic constants is

$$B = \frac{1}{3}(3\lambda + 2\mu)$$

where B is the bulk modulus. If η_B is the bulk viscosity, then

$$\eta_B = \frac{1}{3}(3\chi + 2\eta)$$

Substituting $3\chi = \eta$,

$$\eta_B = \eta$$

and Bridgman, $\lambda = 3.7 \times 10^{10}$ dynes/cm.². This is nearly the same as the 3.0×10^{10} obtained by Mason and McSkimin⁴³ in the 8- to 30-Mc. range, and seems to confirm their observation of the constancy of λ , although information at intermediate frequencies would certainly be required before the generalization could be fully accepted.

We are now in a position to assess the error in the original assumption that $E = 3G$. From classical elastic theory,

$$E/\mu = (3\lambda + 2\mu)/(\lambda + \mu) = 3 - \mu/(\lambda + \mu)$$

If $\lambda = 3 \times 10^{10}$, the E/μ ratio corresponding to various values of μ becomes

μ	E/μ
10^7	3.000
10^8	2.997
10^9	2.967
10^{10}	2.75

The assumption of a ratio of 3 for E/μ is then justified, with an error of 1% at $\mu = 10^9$, and 8% at 10^{10} .

The only study of dynamic compressibility of polyethylene is that of Philippoff and Brodnyan,⁵⁴ who worked in the range of 0.0003 to 5 cycles per second, and from -24° to $+95^\circ$ C. Their tentative conclusion is that the bulk modulus has no imaginary component.

Taylor⁵⁵ measured the stress-strain behavior of polyethylene in a single compression pulse of about 17 msec. by means of a Hopkinson bar. He found that the effects observed in his experiments could be accounted for by the assumption of a single Maxwell element with a modulus of 2×10^9 dynes/cm.² and a relaxation time of 1.7 msec.

Kolsky⁵⁶ has performed similar measurements with pulse durations of about 20 μ sec. At the maximum rate of stress and strain (in the thinnest specimen) the Young's modulus was about 10^{10} dynes/cm.² at 21° C. The 20- μ sec. half-wave corresponds to a frequency of 25 kc.; from Fig. 17 the shear modulus at this frequency as ascertained from steady-state dynamic tests is about 2×10^9 dynes/cm.², corresponding to a Young's modulus of 6×10^9 dynes/cm.². More recently, Kolsky⁵⁷ found that if the response of the material to sinusoidal stresses over a wide frequency range is known, the pulse shapes can be predicted accurately by means of a numerical Fourier synthesis; and that where the damping loss is not too

⁵⁴ W. Philippoff and J. Brodnyan, *J. Appl. Phys.* **26**, 846 (1955).

⁵⁵ G. I. Taylor, *J. Inst. Civil Engrs. (London)* **8**, 486 (1945-1946).

⁵⁶ H. Kolsky, *Proc. Phys. Soc. (London)* **B62**, 676 (1949).

⁵⁷ H. Kolsky, *Phil. Mag.* [8] **1**, 693 (1956).

large and is "constant" over a wide frequency range, as it is for many polymers, a general solution of the problem can be obtained which gives the pulse shape for all such polymers and for all distances of travel.

Hillier and Kolsky⁵⁸ measured the dynamic Young's modulus of polyethylene filaments at 20° C. and 3 kc., the dynamic strains being superimposed on static strains up to 1.37 in./in. After a slight initial decrease in the dynamic modulus, it was found to be nearly linear with strain. It was 5.65×10^9 at zero strain, and 1.72×10^{10} at a strain of 1.37. Experiments were also made in which the specimen was allowed to relax at a strain of 1.0; it was found that the change in dynamic modulus during this relaxation was extremely small. It would seem, then, that the modulus is a function of strain (i.e., of configuration) rather than of stress—being, in this, reminiscent of birefringence.⁵⁹

The foregoing references have dealt with low density (approximately 0.92 gm./cc.) polyethylenes. Nielsen⁶⁰ measured the shear modulus and logarithmic decrement of six polyethylenes of different densities (0.92–0.96 gm./cc.) at frequencies of 0.2 to 1 c.p.s. and at temperatures from 25° C. to the melting point. He found that for all the materials, and over the temperature range studied, the logarithm of the shear modulus is linearly related to the specific volume. The loss peak at approximately 60° C., shown in Fig. 16, is found to shift along the temperature scale, from a minimum of 50° C. for density 0.92 to 70° C. for density 0.95, and a plateau rather than a peak is found for density 0.96. The variation in the height of the maximum is not great, the limits of the logarithmic decrement being 0.8 to 1.0, corresponding to $\tan \delta$ values from about 0.25 to 0.32.

Kline and co-workers⁶¹ have performed similar experiments at frequencies from about 100 to 2000 c.p.s., and at temperatures from 80° to 380° K. (–193° to 107° C.). The three polyethylenes are characterized in Table I. They confirm the finding of Oakes and Robinson³³ that for the unbranched material the dispersion region from –50° to 60° C. is almost entirely suppressed. The three absorption peaks described by Kline *et al.* are given in Table II. They attribute the α peak to movements of large sections of the main chains themselves, which become possible as the crystallites begin to melt. The peak tends to shift to higher temperatures as the branching is decreased, corresponding to the higher and sharper melting points of the more highly crystalline materials.⁶⁰ The β peak may arise from the onset of diffusional motion of amorphous chain segments containing branch points which cooperate with main and side chain groups in this movement.

⁵⁸ K. W. Hillier and H. Kolsky, *Proc. Royal Soc.* **B62**, 111 (1949).

⁵⁹ R. S. Stein, S. Krimm, and A. V. Tobolsky, *Textile Research J.* **19**, 8 (1949).

⁶⁰ L. E. Nielsen, *J. Appl. Phys.* **25**, 1209 (1954).

⁶¹ D. E. Kline, J. A. Sauer, and A. E. Woodward, *J. Polymer Sci.* **22**, 455 (1956).

TABLE I
CHARACTERISTICS OF THREE POLYETHYLENES INVESTIGATED
BY KLINE AND CO-WORKERS⁶¹

Characteristic	Type designation		
	A	B	C
Methyl groups per 100 carbon atoms	3.2	1.6	<0.1
Density, gm./cc.	0.915	0.922	0.957
Crystallinity, %	55	60	~77
M_n	25,000	32,000	20,000
M_w	900,000	370,000	150,000

TABLE II
ABSORPTION PEAKS OF THREE POLYETHYLENES INVESTIGATED
BY KLINE AND CO-WORKERS⁶¹

Description	Type designation		
	A	B	C
α peak			
Temperature, °K	355	360	>375
1/Q, Maximum	0.14	0.17	>0.14
β peak			
Temperature, °K	265	280	300
1/Q, Maximum	0.145	0.10	<0.01
γ peak			
Temperature, °K	165	165	170
1/Q, Maximum	0.065	0.067	0.08

The α peak is attributed to the development of segmental motion in amorphous areas involving alternate configurations, with cooperative movement of amorphous areas in the main chains.

Baccareda and Butta⁶² have reported the Young's modulus and $Q = 1/\tan \delta$ at 20° C. at 9–14 kc. for three polyethylenes varying from 96 % to 56 % crystallinity, as well as the effect of irradiation on the velocity of wave propagation as a function of temperature from –70° to +45° C. in a polyethylene originally of 60 % crystallinity. Decreasing crystallinity is associated with decreasing modulus and increasing $\tan \delta$ in the unirradiated samples. As irradiation increases, the Young's modulus at 20° C. goes through a minimum (the smallest reported value of 5×10^8 dynes/cm.² not being necessarily the minimum) and $\tan \delta$ passes through a maximum (here 0.6, corresponding to the given value 1.6 for Q). The partly amorphous polymers show a transition, independent of amount of crystallinity, at

⁶² M. Baccareda and E. Butta, *J. Polymer Sci.* **22**, 217 (1956).

about -24°C. ; the sharpness of the transition increases with increasing crystallinity. Below the transition point, the modulus appears to decrease somewhat with increasing crystallinity.

2. STRESS RELAXATION IN POLYETHYLENE

Little has been published on the relaxation of stress in polyethylene, and none of that little covers extended periods of time. Tests extending over a few decades of time show an approximately linear decrease of stress with log time, the rate varying from about 7 to 12% of the original stress per unit of log time.^{58, 63} Measurements⁶⁴ in compression of a cylinder compressed to 50% of its original height over a period of ten days showed similar behavior, with a loss of 5.5% of the initial stress per unit of log time. In all these tests except those of Watson, Kennedy, and Armstrong, the initial reading was generally made within a second to a minute after application of strain; they, however, by means of a spring-loaded weighbar make their initial reading in times of the order of 10 msec. At 23°C. , their 10-msec. value of stress at 3.2% strain is about 1100 lbs./in.² corresponding to a Young's modulus of 34,400 lb./in.², or 2.4×10^9 dynes/cm.², while Catsiff *et al.*⁴⁵ at 25°C. , obtained a first reading of about 1.2×10^9 in a time of about 50 sec. If the materials under test are fairly comparable—and in view of the generally similar behavior of the low density polyethylenes of ordinary properties, as revealed by the foregoing dynamic tests, this is to some extent justified—the modulus difference may be taken to confirm the dynamic data, indicating that there is no major relaxation mechanism between 10 msec. and a minute at 25°C.

3. CREEP OF POLYETHYLENE

Creep—the increasing strain at a constant stress—has been variously defined,^{65, 66} but here we shall regard it as the total strain, including the instantaneous elastic, the viscous (irrecoverable), and the recoverable elastic components. In this form, it is most simply expressed, in a linear viscoelastic material, as another aspect of the relaxation function.

It has been shown³⁰ that the creep function approaches an asymptote which is simply determinable from the relaxation function. The foregoing discussion of relaxation leaves little doubt that the longest relaxation times are extremely long. The longest creep measurements available⁵

⁵⁸ M. T. Watson, W. D. Kennedy, and G. M. Armstrong, *J. Appl. Phys.* **26**, 701 (1955).

⁶⁴ I. L. Hopkins, unpublished data.

⁶⁵ H. Leaderman "Elastic and Creep Properties of Filamentous Materials and Other High Polymers." The Textile Foundation, Washington, D. C., 1943.

⁶⁶ H. Leaderman, Society of Rheology Proposed Nomenclature for Linear Viscoelastic Behavior, Rept. No. 4, August, 1956.

extended over 21,000 hours (875 days) and the rate at the end of that time, while slow, was not yet constant, and it appears that in any test of practicable length the steady state would not be attained. If the crystallites act as permanent cross links, thus blocking large-scale relative movements of molecules, there can indeed be no final steady-state flow, but instead an asymptotic value will be approached. It is of interest that neither Catsiff *et al.*⁴⁵ in stress relaxation nor Philippoff⁴⁴ in dynamic measurements found a modulus lower than 10^7 dynes/cm.², their curves in fact showing a tendency to level off at a value of this order or higher. The creep asymptote, then, would be at a value of strain corresponding to stress/ $(E \approx 10^7)$. Another approach to the slope of the creep asymptote may be made by estimating the total viscosity of the sample. In dynamic tests, the viscosity increases as the frequency decreases, approaching the steady-state viscosity as the frequency approaches zero. The highest value at $\sim 25^\circ \text{C.}$ ¹⁰ is about 10^{11} poises, but the form of the curve is such that it must reach or exceed 10^{12} in the limit. Still another approach is through stress relaxation curves. It is shown³⁰ that the integral

$$G \int_0^\infty \psi(t) dt = \eta,$$

the steady-state viscosity, where $\psi(t)$ is the normalized relaxation function and G is the total relaxable shear modulus. The data of Catsiff *et al.*⁴⁵ furnish in this way another lower bound for the total viscosity. While the same objections to the use of reduced variables as were adduced in the discussion of dynamic testing are applicable here, their use will result in a relaxation curve nowhere higher than the true curve at 25°C. ; the integral under this curve will therefore be less than the true one. Further, the effect of a possible unrelaxable modulus of 10^7 , which would result in the above integral becoming infinite, can be eliminated by decreasing the value of the reduced relaxation modulus by this amount. If this is done, the resulting viscosity is found to have a lower limit of 5×10^{15} poises. At a shear stress of 10^7 dynes/cm.² (150 lb./in.²), for example, the ultimate rate of strain would then be less than $10^7/(5 \times 10^{15}) = 2 \times 10^{-9}$ per second, or 2×10^{-4} per day. This figure is very probably several orders of magnitude too high. The ultimate form of the creep curve is thus undetermined, although upper bounds of terminal deflection or deflection rate, whichever is applicable, have been given.

Lethersich⁶⁷ shows that with shear stresses up to 10^7 dynes/cm.² (150 lb./in.²) the initial elastic strain and the primary creep (that is, the total deflection less the steady-state creep, if it exists) are linear with stress.

⁶⁷ W. Lethersich, *Proc. Intern. Congr. Pure and Applied Chem., 11th Congr., London, 1947* Vol. V, p. 591 (1953).

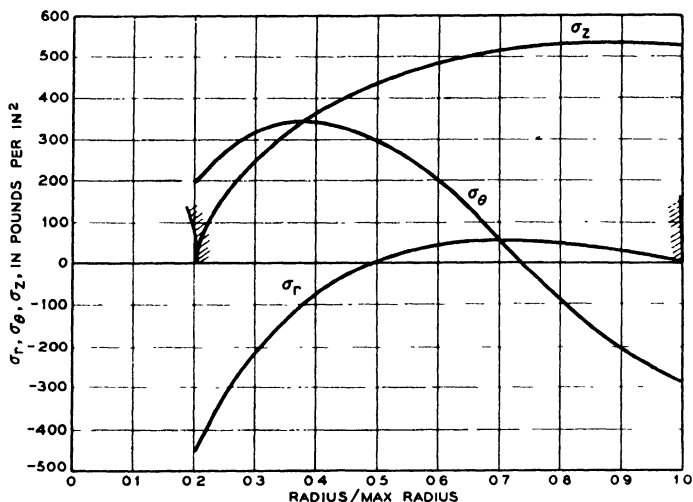


FIG. 18. Stress distribution in polyethylene cable core. Outside diameter of polyethylene, $\frac{5}{8}$ in.; diameter of solid conductor, $\frac{1}{8}$ in.

4. EFFECT OF EXTRUSION METHODS ON PROPERTIES OF SOLID POLYETHYLENE

The effect of fabricating methods upon the state of polyethylene may be illustrated by studies by Kortsch⁶⁸ and Geyling⁶⁹ on polyethylene-sheathed copper conductors. Kortsch measured the magnitude and direction of the maximum refractive index in cross and longitudinal sections of polyethylene cable sheaths and stated that this index is in the direction of orientation of the polymer. He found that in the cross section, the maximum index is radial at the periphery, passing through a neutral zone and then becoming tangential as the copper core is approached. He found also that the maximum index in the longitudinal section is longitudinal in direction. The magnitude of the maximum index in the cross section was strongly influenced by the heating and cooling cycle employed during and after extrusion, while that in the longitudinal section was influenced particularly by the speed of extrusion. Kortsch used the refractive index difference as a measure of stress; Geyling, on the other hand, performed a more rigorous analysis and, using the independently determined stress-birefringence relation for the material in question, determined the stress distribution throughout for three cable cores of the same size and of two different polyethylenes. The radial, tangential, and longitudinal stresses are the principal ones; they are shown in Fig. 18 for one of the cores,

⁶⁸ W. Kortsch, *Kolloid-Z.* **133**, 91 (1953); **137**, 74 (1954).

⁶⁹ F. T. Geyling, unpublished work.

which is fairly representative of the three. The most significant fact here from the point of view of stress-cracking (as will be shown later) is the combination of tensile longitudinal and compressive circumferential stress at the surface of the core, since that is the site of both the greatest tensile and the greatest shear stress, and is furthermore exposed to the action of possible active agents.

Howard and associates⁷⁰ have shown that the longitudinal internal tension in a polyethylene-covered cable core can be minimized by the choice of extrusion parameters. The decrease in length of a three-inch length of polyethylene covering as the result of heating in talc at 130° C. is taken as a measure of the internal stress. It was found that increased speed of extrusion (increased conductor speed) reduces the tension, provided the diameter of the polyethylene is maintained at the size of the die, that is, the conductor speed should not be achieved by slow extrusion followed by draw-down in core diameter. Most important of all, it was found that if material is held in the heated crosshead of the press, either through circulation within the head or artificially by stopping the screw, internal tension is increased. These effects all point to some such phenomenon as cross-linking or gelation in the polyethylene as a function of heating time, even though the effect on the intrinsic viscosity or k' is slight. It is possible that so far as these parameters are concerned the effect of gelation is counterbalanced by oxidative scission.

5. EXTRUSION OF LIQUID POLYETHYLENE AS RELATED TO POLYMER STRUCTURE

The stress and the strain rate of molten polyethylene are not linearly connected except at low strain rates.⁷¹ Further, the material itself undergoes structural changes as a result of heating. These two effects will be considered in relation to the extrusion of molten polyethylene. Tordella⁷² has studied the extrusion of polyethylene and other melts from a capillary rheometer, and given special attention to the conditions at which the extrudate begins to show deviations from the cylindrical. He concludes that there is a critical shear stress at and beyond which the emerging stream becomes irregular in shape. Spencer and Dillon^{72a} observed this phenomenon in polystyrene melts, and concluded that the onset of the deviations corresponds with the excess of a minimum shear stress at the capillary wall. Thus they agree with Tordella that *stress* is the determining factor. Bagley,^{72b} who succeeded in eliminating the length-to-radius ratio

⁷⁰ J. B. Howard, J. D. Cummings, and V. L. Lanza, unpublished work.

⁷¹ W. Philippoff and F. H. Gaskins, *J. Polymer Sci.* **21**, 205 (1956).

⁷² J. P. Tordella, *J. Appl. Phys.* **27**, 454 (1956).

^{72a} R. S. Spencer and R. E. Dillon, *J. Colloid Sci.* **4**, 241 (1949).

^{72b} E. B. Bagley, *J. Appl. Phys.* **28**, 624 (1957).

TABLE III
INTRINSIC VISCOSITY OF POLYETHYLENE DETERMINED IN XYLENE AT 85°C.
(After Wentz⁷⁵)

Sample treatment	Intrinsic viscosity $[\eta]$	Interaction coefficient k'
As received	0.963	0.403
<i>Under pressure at 265°F.</i>		
$\frac{1}{4}$ hr.	0.965	0.418
4 hr.	0.963	0.427
<i>Under pressure at 400°F.</i>		
$\frac{1}{4}$ hr.	0.967	0.422
4 hr.	0.970	0.453
8 hr.	0.975	0.465

as a factor in the shear stress versus shear rate curves by the use of an end correction which is a function of the shear rate, supports Tordella to the extent that both believe the critical event at the inception of roughness of extrudate occurs just before the polymer enters the capillary. Westover and Maxwell,⁷³ on the other hand, find that their data agree with the concept that the appearance of irregularity is associated with a critical Q/D ratio, where Q is the volume rate of flow and D the diameter of the capillary. Since for a Newtonian fluid of given viscosity the Reynolds number is proportional to Q/D , and the inception of turbulence in such a case is coincident with the attainment of a certain Reynolds number, it is concluded that the irregularity is a phenomenon of turbulence. In this view they concur with Nason,^{73a} who associated the roughness and waviness of his melts of cellulose acetate, polystyrene, and polyvinyl resin plastics with Reynolds numbers above 800 to 1000.

The same data cannot support both points of view;⁷⁴ and even though the theoretical idealizations of the viscoelastic behavior of the material in the test apparatus are probably far from the fact in both cases, it should be possible to establish experimentally the domain within which each theory is operative.

A complicating factor in measurements of this kind is the change in the structure of the polyethylene if it is held too long in the rheometer at high temperatures. In one series of tests⁷⁵ intrinsic viscosities were determined in xylene at 85°C., after the material was held in a mold under

⁷³ R. F. Westover and Bryce Maxwell, *SPE Journal* **13**, 27, August (1957).

^{73a} H. K. Nason, *J. Appl. Phys.* **16**, 338 (1945).

⁷⁴ M. Reiner, "Deformation and Flow," p. 304. *Interscience*, New York, 1949.

⁷⁵ R. P. Wentz, unpublished work.

TABLE IV

MELT INDEX OF POLYETHYLENE AS A FUNCTION OF EXCESS TIME IN MELT INDEXER
(After Cummings and Lanza⁷⁶)

Time, min., in excess of prescribed 5 min.	Melt index, gm., in 10 min.	Time, min., in excess of prescribed 5 min.	Melt index gm., in 10 min.
3	0.314	30	0.207
6	0.296	36	0.195
12	0.268	42	0.185
18	0.238	48	0.180
24	0.220	54	0.173

pressure for $\frac{1}{4}$ hr. and 4 hr. at 265° F. and for $\frac{1}{4}$, 4, and 8 hr. at 400° F. The results are given in Table III.

Another result,⁷⁶ probably of greater pertinence here, was obtained by letting polyethylene stand in a melt indexer⁷⁷ for varying lengths of time in excess of the five minutes specified. The melt index (inversely related to the viscosity) as a function of excess time, at 190° C., is given in Table IV. At the beginning of this table, the apparent viscosity is increasing at the rate of 2% per minute, a rate which can be of considerable concern in studies of extrusion.

6. FLOW PROPERTIES OF UNMELTED POLYETHYLENE IN BULK

While extrusion of polyethylene at ordinary temperatures is extremely difficult and not practical technologically, the limiting pressures at which flow occurs may be important. An illustration of the flow pattern obtained at 108° C., together with the apparatus, is shown in Fig. 19. The pattern was obtained by photographing, between crossed Polaroids, a longitudinal slice of the charge after its removal from the cylinder. Here it is seen that there is a considerable amount of dead material in the lower corners, the movement taking place within the boundaries of a long funnel-shaped path. As any disk of thickness dx descends it may be considered as subject to two retarding forces: the first, the vertical component of the force normal to the tapered sides of the funnel necessary to compress the material to a smaller radius; and the second, the vertical component of the shearing force at the boundary between the stationary and moving polyethylene. It is considered that a compressive and a shear yield stress are the only material parameters which need be considered, and that the compressive

⁷⁶ J. D. Cummings and V. L. Lanza, unpublished work.

⁷⁷ Am. Soc. Testing Materials Specification D 1238-52T.

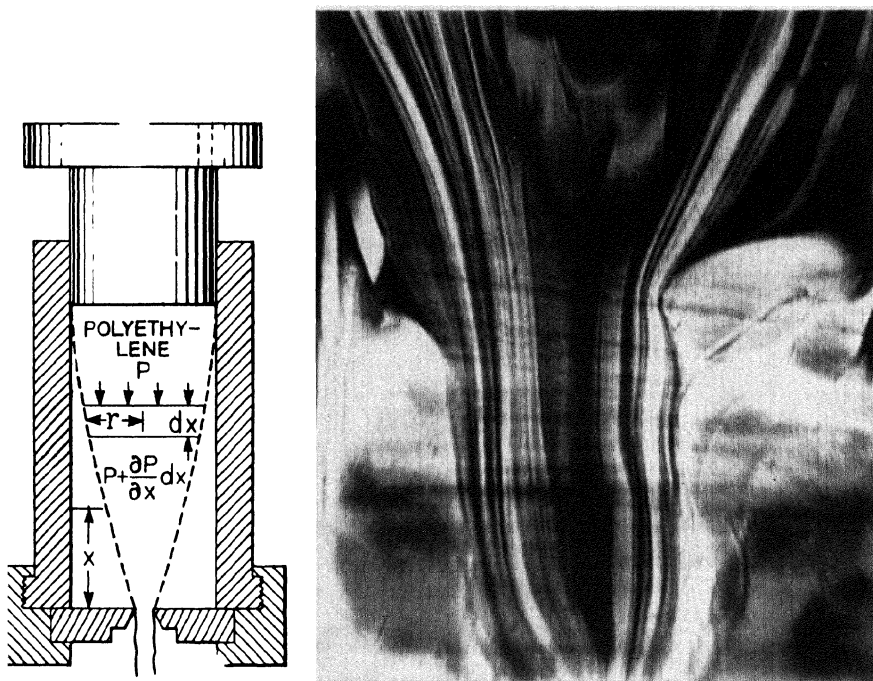


FIG. 19. Left: Diagrammatic cross section of extrusion chamber and die. Right: Flow pattern in polyethylene in extrusion chamber. The bottom edge of the picture coincides with the plane $x = 0$.

is twice the shear.⁷⁸ These considerations lead to the following differential equation:

$$-dp/dx = [1 + (dr/dx)^2]^{1/2} (\text{L.S.S.})/r + 2(\text{L.C.S.})dr/r dx$$

where L.S.S. and L.C.S. are the limiting shear and compressive stresses. If we consider that dr/dx is negligible compared to unity in this example, and with the approximation that

$$r = r_0 - ax^2$$

the equation may be solved to give

$$p = \frac{(\text{L.S.S.})l}{\sqrt{r_0(r_0 - r_1)}} \tanh^{-1} \sqrt{(r_0 - r_1)/r_0} + 2(\text{L.C.S.}) \ln (r_0/r_1)$$

where l is the length of material in the cylinder.

⁷⁸ W. P. Mason, unpublished work.

At room temperature, the material used had a shear yield stress of 940 lb./in.², and a compression yield stress of 1880 lb./in.² For the dimensions of interest, it was calculated that a pressure of 25,400 lb./in.² would be necessary for extrusion. It was demonstrated by test that the pressure necessary was about 30,000 lb./in.²

This development is useful in calculating the maximum permissible pressure which can be withstood without flow; if the pressure is much exceeded and flow results, the extrudate is shattered and fragmentary.

7. MULTIAXIAL STRESSING AND STRESS-CRACKING IN POLYETHYLENE

Richards⁷⁹ first pointed out the brittleness of polyethylenes under the influence of stress in the presence of polar liquids. Hopkins and co-workers²⁶ showed that the brittleness is associated with molecular weight, in particular with the presence of a low molecular weight fraction, and that the effect is correlated with the strain at rupture under biaxial stress. The technique in this early work consisted essentially in the rupture of a diaphragm by nitrogen under pressure, with photographic measurements of the diaphragm configuration and pressure permitting subsequent calculation of stress and strain. The use of gas as the pressure medium had the disadvantage that in specimens with much cold drawing the attainment of the maximum supportable pressure (not coincident with either the maximum stress or strain) was followed by explosive rupture, and data beyond this point were unobtainable. This was followed by the obvious use of water as the pressure medium, and a summary of the findings, published²⁶ and unpublished, follows.

A specimen from a cable sheath which had failed with a brittle fracture was separated into three fractions by extraction with trichloroethylene. The biaxial elongations at rupture were: original, 24 %; low fraction, too weak to test; intermediate fraction, 28 %; high fraction, 73 %. Further, the addition of the low fraction to a satisfactory material (strain at rupture, approximately 100 %) decreased the strain to a fraction of the original. The effect of structure was further demonstrated by comparison of quenched and annealed samples: quenched, the material had a lower biaxial modulus and stress at rupture, but greater strain, than the annealed.

A series of polyethylenes, varying insofar as possible only in molecular weight, was supplied by the Imperial Chemical Industries Ltd. Stress-strain and other data are given in Table V. Here the increase in biaxial strain with molecular weight is evident, as is the uniaxial; but it has been found that generally the former is by far the more reliable indicator of propensity to stress-cracking.

⁷⁹ R. B. Richards, *Brit. Plastics* 17, 146 (1945).

TABLE V
STRESS-STRAIN DATA, MELT INDEX, AND SPECIFIC GRAVITY FOR
A SERIES OF POLYETHYLENES

Sample	Melt index ⁷⁷	Uniaxial tensile rupture		Biaxial tensile rupture		Specific gravity, 25°C.
		Stress	Strain	Stress	Strain	
1	0.08	19,000	700	20,200	385	0.9194
2	0.22	18,830	675	19,600	390	0.9190
3	0.35	18,000	705	18,250	385	0.9190
4	1.25	15,900	670	14,300	360	0.9188
5	8.4	8,050	540	7,600	275	0.9166
6	15.7	8,300	535	6,100	240	0.9162
7	72.	6,400	145	5,400	155	0.9154
8	220.	3,800	95	3,400	90	0.9132

Further information about the relation of structure to physical properties is afforded by the more recent low-pressure, high-density polyethylenes, which are almost completely unbranched. A comparison of one of these materials with a high-pressure, low-density polyethylene is instructive.

Property	High pressure	Low pressure
Density, gm./cc.	0.918	0.960
Melt index ⁷⁷	0.3	0.6
Intrinsic viscosity in xylene (95°C.)	1.067	1.757

Uniaxial stress-strain curves are shown in Fig. 20 with speed of test as a parameter. Here the relative insensitivity of the high pressure material to speed of test is evident, as well as the very considerable sensitivity of the low pressure material. The high value of stress at yield is also noteworthy in the low pressure polyethylene. It is a function of speed, increasing somewhat as speed is increased. The total strain at rupture at low test speeds in the low pressure polyethylene is somewhat greater than in the high pressure polyethylene, and is accompanied by a great deal of fibering; some of the specimens split lengthwise spontaneously at rupture, while all samples of both low- and high-pressure materials may be split with a fibrous fracture if a split is started with a razor blade. The highly drawn part in the (uncolored) low pressure material resembles white satin. This is in contrast again to the high pressure material where the highly drawn part becomes smooth and transparent even though highly ordered. The satiny look is probably due to scattered light from separated fibers; that such separation must occur is shown by the density changes during elon-

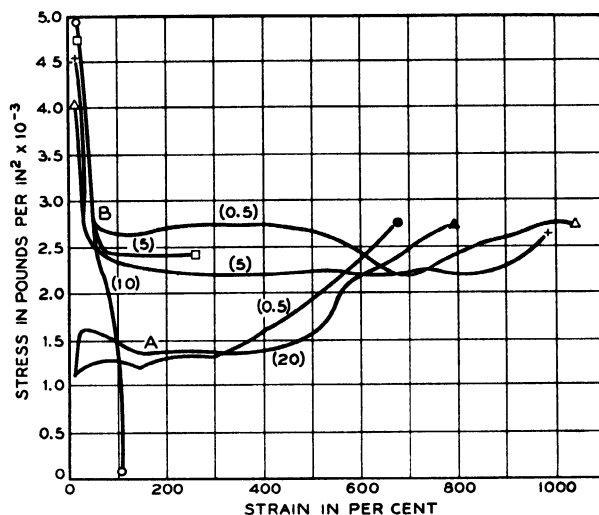


FIG. 20. Uniaxial true stress versus strain curves for high pressure (A) and low pressure (B) polyethylenes, with speed of test as a parameter. The numbers in parentheses are the speed of the testing machine, in inches per minute. The gage length of the specimens was 1 in.

TABLE VI
EFFECT OF TEST SPEED ON DENSITY OF DRAWN HIGH- AND
LOW-PRESSURE POLYETHYLENES
(After Hopkins⁶⁴)

Material	Speed of test, in./min.	Density, gm./cc.	
		Initial	After test
High pressure	20	0.9181	0.9176
High pressure	0.5	0.9181	0.9181
Low pressure	10	0.9604	0.75
Low pressure	0.5	0.9604	0.8476

gation, as illustrated in Table VI by measurements at the most highly drawn sections.

Biaxial stress-strain curves are shown in Fig. 21. Here the greater stiffness of the low pressure material is again evident; the sensitivity to speed has decreased, and the strain at rupture has decreased, as compared with the uniaxial case, from somewhat greater than that of the high pressure polyethylene to less than half as much. This biaxial "shortness" again correlates with susceptibility to stress cracking, for the low pressure material may crack in a few minutes or hours under stress and environmental conditions where a high pressure material would survive indefinitely, and

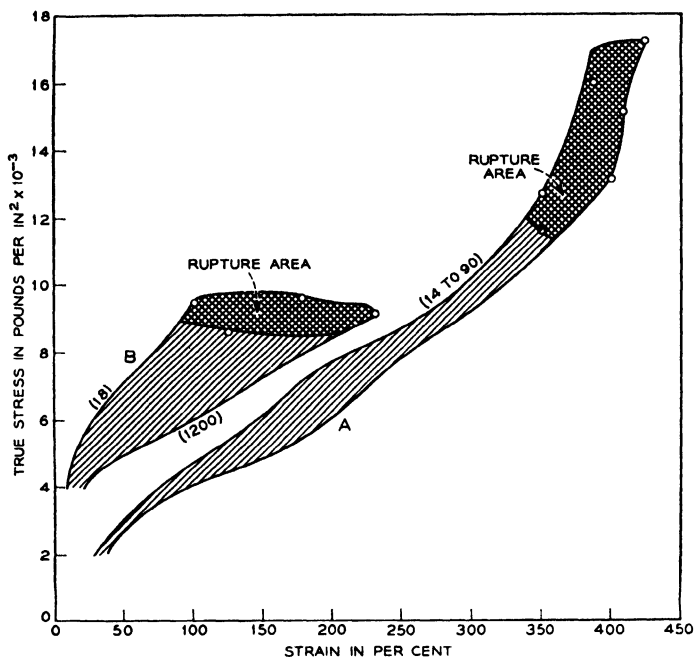


FIG. 21. Biaxial true stress versus strain curves for high pressure (A) and low pressure (B) polyethylenes, with *time of test to rupture* (in parentheses) as a parameter.

indeed the low pressure materials may fail under the stress conditions alone where the other will survive under the effect of a vigorous surface active agent. A number of factors are probably effective here to a yet unknown degree. The higher elastic moduli of the more crystalline material cause it to be under greater *stress* for a given *strain*, and the stress-cracking tests are made with fixed strain. The degree to which molecular weight and its distribution are correlated with stress cracking susceptibility cannot be known until they themselves are reliably known, relatively if not absolutely.

Further examples of biaxial stress-strain properties of crystalline polymers are given in Figs. 22 and 23. Curve A of Fig. 22 is especially interesting, and shows stress and strain at rupture of polytetrafluoroethylene at extraordinarily low levels. There was no sign of cold drawing, even though the same material, tested uniaxially, stretched to several times its original length before it broke. Neither was the rupture brittle; the failure was actually a progressively increasing porosity, a de-sintering in effect, permitting the water under the specimen to pass through and be thrown off as a fine spray. Curves B and C illustrate the effect of the degree of crys-

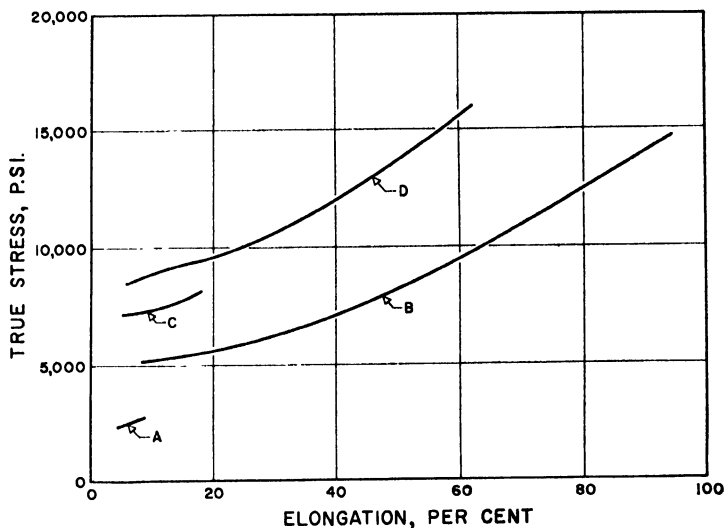


FIG. 22. Biaxial true stress versus strain curves for polytetrafluoroethylene, amorphous and crystalline polytrifluorochloroethylene, and polyvinyl chloride. KEY: A, polytetrafluoroethylene; B, amorphous polytrifluorochloroethylene; C, crystalline polytrifluorochloroethylene; D, polyvinyl chloride.

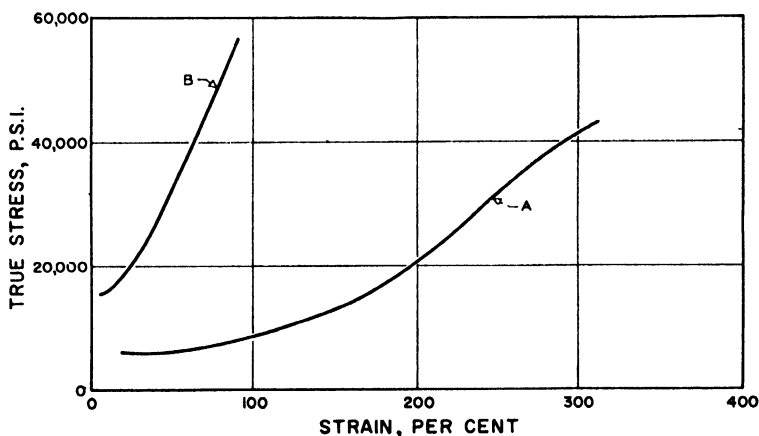


FIG. 23. Biaxial true stress versus strain curves. KEY: A, polyhexamethylene sebacamide (a nylon); B, polyethylene terephthalate.

tallinity on the stress required for cold drawing of polytrifluorochloroethylene. (Specimen C was not stressed to rupture.) Specimen D is an unplasticized polyvinyl chloride. While the crystallites are poorly developed in this specimen, it still showed by X-ray examination evidence of planar

displacements. In Fig. 23, the great strength and stiffness of the originally somewhat oriented polyethylene terephthalate and the ductility of the nylon are both strongly reflected in the biaxial stress-strain curves. Apparently, the crystallite deformations studied in greater detail for polyethylene also have a strong influence here. Naturally a deeper understanding of these effects is important to improvements in bursting strengths, film strengths generally, and other structural uses of these important plastics.

III. Hard Rubber: A Highly Polar, Cross-linked Polymer

Natural rubber, mixed with sulfur and heated, undergoes cross-linking. If the mixture contains about 2% sulfur, a product representative of the "gum rubber" type is obtained. As the quantity of sulfur is increased to a maximum of 30% or thereabouts, the product changes to a polymer which is rigid at room temperature. This is hard rubber, and in this simple form is sometimes called "ebonite." The amount of included sulfur actually participating in cross-linking varies according to the vulcanization time and temperature, and is seldom or never total. Since the total quantity of sulfur may be varied, and the proportion of this which participates in the cross-linking is also variable, hard rubber, even in the absence of other ingredients, is not a specific compound, but merely a relatively highly cross-linked rubber, with considerable variation possible in the amount of cross-linking. In the discussion to follow, therefore, it must be remembered that different experimenters were not working with precisely the same material.

1. DYNAMIC PROPERTIES OF HARD RUBBER

Lethersich⁴⁰ and Wegel and Walther⁴⁸ have made dynamic tests on hard rubber in shear at room temperature. Lethersich used a range of frequencies from 0.0001 to 615 c.p.s. Over this range, the dynamic modulus in-

TABLE VII
DYNAMIC PROPERTIES OF HARD RUBBER AT 10 KC
(After Wegel and Walther⁴⁸)

Property	Value
G (shear modulus)	1.15×10^{10} dynes/cm. ²
η (shear viscosity)	4060 poises
E (Young's modulus)	3.35×10^{10} dynes/cm. ²
η_L (longitudinal viscosity)	10600 dyne sec./cm. ²
B (bulk modulus)	1.27×10^{11} dynes/cm. ²
η_B (bulk viscosity)	8360 dyne sec./cm. ²
λ (Lamé constant)	1.19×10^{11} dynes/cm. ²
χ (Lamé constant-viscosity)	5650 dyne sec./cm. ²
ν (Poisson's ratio)	0.46

creased gradually from 8.1×10^9 to 1.01×10^{10} dynes/cm.²; the viscosity decreased, the log viscosity versus log frequency line having a slope of -0.96 . From Wegel and Walther's data at 10 kc./sec. we find a shear modulus of 1.15×10^{10} dynes/cm.² and a viscosity of 4060 poises, which are quite compatible with Lethersich's findings. In addition to the shear characteristics, Wegel and Walther made longitudinal measurements, permitting the calculation of Young's modulus and its associated viscosity, and also, by combination with the shear properties, the bulk modulus and viscosity. At 10 kc./sec., these values are summarized in Table VII. The bulk modulus in static tests is reported⁸⁰ as $6-7.8 \times 10^{10}$ dynes/cm.².

2. CREEP PROPERTIES OF HARD RUBBER

Lethersich also gives a creep curve for hard rubber over three decades of time, from 0.001 to 1 sec. The creep is linear with log time; the increase is about 5.6 % per decade.

Kobeko *et al.*⁸¹ measured the creep and creep recovery of hard rubber in torsion at temperatures of 60° to 150° C. They found that the creep approaches an upper limit, which appears to correspond to a shear modulus of 5×10^7 dynes/cm.², regardless of temperature. The difference between the highest measured creep value and the deflection after recovery were used to calculate the viscosity of the rubber; but the difference was very small and the method was considered unreliable, yielding only a lower bound (10^{16} poises at 25° C., 10^{11} at 150° C.). They found that a change of 10° C. is associated with a change in rate of creep of about 100; the total viscosity should change in the same ratio.⁸² This would correspond to a change of 10^{25} between 25° and 150° C., rather than the 10^5 ratio shown in their plot of lower limits.

Conceptually, it is in error to suppose that this method of finding the total viscosity can be applied to a material with an unrelaxable component in the modulus. In the simplest case, let us suppose that the material may be characterized by an unrelaxable modulus G_1 and another, G_2 with a relaxation time τ . Then the relaxation modulus is $G_1 + G_2e^{-t/\tau}$. If we define G as the total modulus, $G_1 + G_2$, then

$$(G_1 + G_2e^{-t/\tau})/G = \psi(t),$$

the relaxation function. The creep function corresponding to this can be shown to be⁸⁰

$$\varphi(t) = [G - (G - G_1)e^{-(G_1/G)\tau}]/G_1$$

⁸⁰ L. H. Adams and R. E. Gibson, *J. Wash. Acad. Sci.* **20**, 213 (1930).

⁸¹ P. Kobeko, E. Kuvshinskii, and G. Gurevich, *Tech. Phys. U. S. S. R.* **4**, 622 (1937).

⁸² I. L. Hopkins, *J. Appl. Phys.* **24**, 1300 (1953).

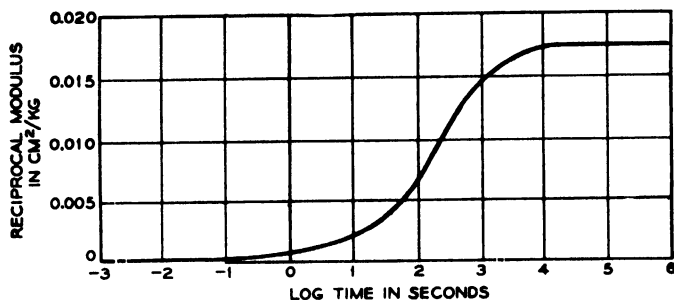


FIG. 24. Master creep curves for hard rubber, constructed from graphs of Kobeko *et al.*⁸¹

If a load is applied for a time t_1 and then released, the deflection for $t \geq t_1$, using the superposition principle and letting $\lambda = G_1/G\tau$, is

$$\begin{aligned} \text{Defl.} &= \varphi(t) - \varphi(t - t_1) = \frac{G - (G - G_1)e^{-\lambda t}}{G_1 - (G - G_1)e^{-\lambda(t-t_1)}/G_1} \\ &= (G - G_1)e^{-\lambda t}(e^{\lambda t_1} - 1)/G_1 \end{aligned}$$

which approaches zero as t approaches infinity. This is in contrast to a completely relaxable material. Suppose such a material with a creep function $\varphi(t)$. Then, if a load is applied at $t = 0$ and released at $t = t_1$, the deflection at $t \geq t_1$ is

$$\text{Defl.} = \varphi(t) - \varphi(t - t_1).$$

For values of $t < (t_1 + T)$, where T is of the order of the greatest relaxation time, the deflection is a function of t . At greater times, $\varphi(t)$ approaches the asymptote³⁰ $(a + bt)$, and the deflection approaches $(a + bt) - [a + b(t - t_1)] = bt_1$. Since b is a function of the total viscosity, the viscosity may be calculated from the residual deflection.

The creep curves of Kobeko *et al.*⁸¹ may be used (by translation along the log time axis) to obtain a reduced creep function.⁸³ The resulting curve is shown in Fig. 24. The important part of the retardation occurs in about 6 units of log time, in contrast to the soft rubber examined by the same authors, which required about 12 units. The modulus at the beginning of these curves is 5×10^9 dynes/cm.²; at the end, the curves approach a modulus of 5.6×10^7 . For the soft rubber, the modulus progresses from 3×10^8 to 8×10^6 dynes/cm.². Much more extreme movement of larger molecular segments is possible and necessary in the soft rubber than in the hard before equilibrium can occur; this may account for the much greater time range in the former.

⁸³ A. V. Tobolsky and H. Eyring, *J. Chem. Phys.* **11**, 125 (1943).

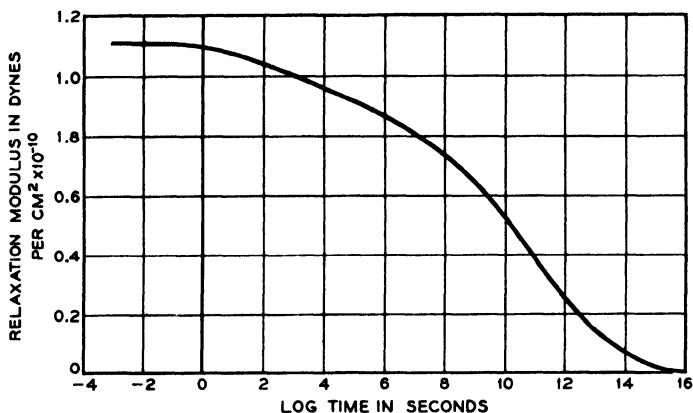


FIG. 25. Stress relaxation in torsion in commercial hard rubber, reduced to 25°C.

3. STRESS RELAXATION PROPERTIES OF HARD RUBBER

The stress relaxation modulus in shear for a commercial hard rubber rod,⁶⁴ reduced to 25° C., is shown in Fig. 25. The viscosity is equal to³⁰

$$\int_0^t [G(t) - G_1] dt$$

where G_1 , the unrelaxed modulus, is actually negligible over the time t over which the integral is taken. By numerical integration the value $\eta = 6.7 \times 10^{18}$ poises was obtained at 25° C.

Creep in compression has also been measured on a lightly cross-linked ebonite⁶⁴ designed particularly for high impact strength and wear resistance. The results are shown in Fig. 26. The viscosity at 50° C., corresponding to the slope at the later part of the curve, is 2×10^{14} poises; if the same conversion factor be applied as before this amounts to 2×10^{19} poises at 25° C. (Even if an unrelaxable modulus of the order of 5×10^7 dynes/cm.² exists, it will have no appreciable influence on the shape of the creep curve at this point. This may be seen by differentiating the previously given

$$\varphi(t) = [G - (G - G_1)e^{-(G_1 t / G\tau)}] / G_1$$

with respect to time

$$\begin{aligned} \varphi'(t) &= (G - G_1)(G_1 / G\tau)e^{-(G_1 t / G\tau)} / G_1 \\ &\simeq e^{-(G_1 t / G\tau)} / \tau, \end{aligned}$$

since

$$G - G_1 \simeq G_1$$

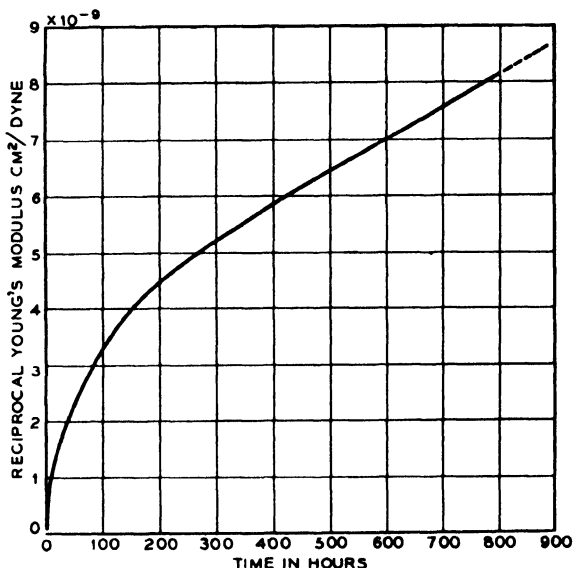


FIG. 26. Creep in compression of commercial hard rubber at 50°C.

When $G_1 t / G \tau < 0.01$, as it is in the early stages of creep, the exponential term is nearly unity, $\varphi'(t) \simeq 1/\tau$, which is the value it would have if the unrelaxable modulus G_1 did not exist.

IV. Polyamides: Polar Chain Polymers Examined for Both Long and Short Range Behavior

A remarkable combination of microcrystalline behavior discussed earlier for simple hydrocarbon chains and highly associated (sheetlike) cross-bonding (not chemical cross links, but strong hydrogen bonding in sheets) of polar groups endows the linear polyamides with a dazzling spectrum of mechanics. With their amide linkages forming analogues to the peptides of proteins, the mechanical tissue of animal life—the nylons are deeply interesting archetypes of polymer versatility. Indeed, the polar groups may be substituted^{7, 84} or distributed⁸⁵ so that properties from the softest rubber to the hardest plastic can be produced at the same temperature. Thus, an understanding of the basic rheology of these microcrystalline solids apparently applies to most other polymer systems. We have accordingly chosen to review particularly the studies of this family.

Writers on nylon have experimented with both single filaments and yarns. Since the characteristics of the yarn structure may be involved in test

⁸⁴ W. O. Baker and C. S. Fuller, *J. Am. Chem. Soc.* **65**, 1120 (1943).

⁸⁵ W. O. Baker and C. S. Fuller, *J. Am. Chem. Soc.* **64**, 2399 (1942).

results, only the work on single filaments or solid material will in general be reviewed here.

1. DYNAMIC PROPERTIES OF POLYAMIDES

a. Free Oscillations in Polyamides

Free oscillations in torsion have been used by several workers, and forced oscillations, either in torsion, bending, or longitudinally, by several more. Early workers generally tested under a single set of conditions; only more recently has the effect of water content or other conditioning been investigated. Nylon presents in a high degree the slow quasi-linear change in dynamic properties with log frequency discussed in the first section of this review, and some measurements over short ranges of frequency were interpreted as confirming the constancy of the dynamic modulus and loss factor; but the assembly of data over as wide a range of frequencies as possible on a single plot, or the data on a single material over a wide frequency range as reported by Fujino *et al.*⁸⁶ show that there is a slow change, accountable for by approximate "box" or "wedge"⁸⁷ distributions of relaxation times extending beyond all times or reciprocal frequencies so far measured.

Schmieder and Wolf³² measured the shear modulus of ten nylons at ~ 1 to 10 c.p.s. by free torsional vibrations, over the temperature range -160° to $\sim 200^\circ$ C. The materials were: polycaprolactam, polycapryllactam, polyaminoundecanoic acid, polyadipic acid hexamethylenediamine, polypimelic acid hexamethylenediamine, polysuberic acid hexamethylenediamine, polysebacic acid hexamethylenediamine, polydecanedicarboxylic acid hexamethylenediamine, polymethyl pimelic acid hexamethylenediamine, polysebacic acid ethylenediamine.

The results are given as plots of modulus and logarithmic decrement against temperature. All curves show two low dispersion regions, at about -120° and -50° C. There is also an especially marked dispersion region at about $+50^\circ$ C., which differs in strength and form with the material. Finally, at the end of the curves at about 200° C., there begins a dispersion region, only the beginning of which could be determined, but which obviously had a different and characteristic form for each material. All had a shear modulus of $2-3 \times 10^{10}$ dynes/cm.² at -160° C., with a gradual decrease to the approximately $+50^\circ$ C. dispersion region, where a steeper decrease occurred. Perhaps the most important generalizations to be made from the curves are that they are very similar in form, and that they are sensitive to the degree of anneal or quenching as evidenced by the measurements on the ninth specimen above. Schmieder and Wolf have discussed

⁸⁶ K. Fujino, H. Kawai, and T. Horino, *Textile Research J.* **25**, 722 (1955).

⁸⁷ A. V. Tobolsky, *J. Am. Chem. Soc.* **74**, 3786 (1952).

very thoroughly the differences in behavior in terms of differences in structures. The original paper should be consulted if detailed treatment is desired.

Speakman and Saville⁸⁸ made free torsional vibration experiments on a 6-6 nylon. The frequency is not given. The shear modulus of dry nylon was found to be 0.89×10^{10} dynes/cm.², which agrees with Schmieder and Wolf's results at 25° C. If the modulus of dry nylon is taken as unity, the rigidity decreases as the moisture content is increased, to about 0.37 at 100% r.h.

Lochner⁸⁹ reported measurements on an unidentified nylon in bending and torsion, the frequency, atmospheric, and drawing conditions not being given. He found the Young's modulus to be 3.5×10^{10} dynes/cm.² with log dec. = 0.491 ($\tan \delta = 0.156$) and the shear modulus to be 2.61×10^{10} dynes/cm.² with log dec. = 0.458 ($\tan \delta = 0.146$).

Hammerle and Montgomery⁹⁰ used free torsional vibrations, of a period between 50 and 400 sec., on drawn nylon 6-6 filaments at 65% r.h., 70° F., and also made stress relaxation measurements in torsion and extension over a coincident time range. The dynamic modulus, as calculated from the stress relaxation on the assumption of a "box" distribution of relaxation times, was within 3% of the measured value; damping was within 13%. The stress relaxation curves in tension and torsion were not of the same form, and this was attributed to the anisotropy of the drawn filaments.

Meredith⁹¹ also used a torsion pendulum, with a period of 4-9 sec. at 65% r.h., 20° C. The modulus found for two unspecified nylon filaments were 5.3×10^9 and 4.9×10^9 dynes/cm.²

b. Forced Oscillations in Polyamides

Ballou and Silverman⁹² found Young's modulus at approximately 10 kc. on unidentified drawn and undrawn nylon at 60% r.h. at 70° F., with the degree of static elongation, upon which the dynamic strain was superimposed, as a parameter. Their findings were:

Drawn nylon		Undrawn nylon	
Elongation, per cent	Young's modulus, dynes/cm. ²	Elongation, per cent	Young's modulus dynes/cm. ²
0	6×10^{10}	0	2×10^{10}
8	1.5×10^{11}	250	1.1×10^{11}

Lyons⁹³ studied Young's modulus and the associated viscosity from

⁸⁸ J. B. Speakman and A. K. Saville, *J. Textile Inst.* **37**, P 271 (1946).

⁸⁹ J. P. A. Lochner, *J. Textile Inst.* **40**, T229 (1949).

⁹⁰ W. G. Hammerle and D. J. Montgomery, *Textile Research J.* **23**, 595 (1953).

⁹¹ R. Meredith, *J. Textile Inst.* **45**, T489 (1954).

⁹² J. W. Ballou and S. Silverman, *J. Acoust. Soc. Am.* **16**, 113 (1944).

⁹³ W. J. Lyons, *Textile Research J.* **19**, 123 (1949).

65–360 c.p.s. and at 21–25° C. on nylon filaments. A dynamic strain of 0.3 % was superposed on a static tension of 8.5×10^8 dynes/cm.². He found that over the frequency range both the modulus and the loss factor were substantially constant; the ratio of the dynamic modulus to the static was 1.86. The dynamic modulus was 8.0×10^{10} dynes/cm.², and the loss factor 0.033. In a later analysis,⁹⁴ Lyons found that the internal friction could be represented equally well, in its frequency dependence, by

$$\mu = [\mu_2/(1 + \omega^2 \tau_2^2)] + \mu_3,$$

with suitable choice of the parameters, and

$$\mu = 2.47 \times 10^9/\omega.$$

Other more recent studies, over a vastly increased frequency range, have shown that the second expression is phenomenologically more acceptable; the first, while satisfactory over a limited range of frequency, must fail at higher or lower frequencies. Much the same may be said of the formulas for cyclic loss by Eyring *et al.*⁹⁶ Longitudinal measurements of energy absorption were made at room temperature and at others between 0 and 65° C., on monofil of 6-6, 6-10 and 2-Me-66 nylon cold drawn 600 %. The frequency of the vibration was from 0.058 to 5.8 c.p.s. at room conditions, and between 0.35 and 5.8 at the others. It was found that the nearly constant cyclic energy absorption in the three materials over this range could be accounted for by two relaxation mechanisms which were invariant in their relaxation times, τ_1 and τ_2 being equal to 0.266 and 0.0274 sec., respectively. These times result in two peaks at frequencies 0.598 and 5.79 c.p.s. Since other parameters were chosen to make the peaks of equal altitude, their sum is relatively constant between 0.598 and 5.79 c.p.s., but approaches zero on each side, contrary to later experimental evidence. Fujino *et al.*,⁹⁶ for example, have shown that a long continuous spectrum, (or alternatively a spectrum of many discrete times), is required for adequate description of nylon; it is manifest that the approximate representation of the data of Eyring *et al.* by only two relaxation mechanisms is possible only because of the restricted frequency range, and that the relaxation times ascribed to the mechanisms are associated with the test frequencies rather than with any special characteristics of the nylons. The conclusion that “the consistent usage of the relaxation times τ_1 and τ_2 implies that the stress response of all three fibers is similar” can now be

⁹⁴ W. J. Lyons, *J. Appl. Phys.* **21**, 520 (1950).

⁹⁵ H. Eyring, M. G. Alder, S. A. Rossmassler, and C. J. Christensen, *Textile Research J.* **22**, 223 (1952).

⁹⁶ K. Fujino, H. Kawai, T. Horino, and K. Miyamoto, *Textile Research J.* **26**, 852 (1956).

TABLE VIII
DYNAMIC PROPERTIES OF UNDRAWN NYLON 6-6
(After Mason and McSkimin⁴³)

Temp., °C.	Frequency, Mc./sec.	Shear		Longitudinal	
		Modulus, $\mu \times 10^{-10}$, dynes/cm. ²	$\tan \delta$	Young's modulus, $E \times 10^{-10}$ dynes/cm. ²	$\tan \delta$
0	10	1.63	0.069	4.54	0.062
	25	1.73	0.080	4.79	0.071
10	10	1.50	0.072	4.18	0.065
	25	1.55	0.083	4.32	0.074
30	10	1.29	0.078	3.61	0.070
	25	1.34	0.103	3.75	0.087
50	10	1.09	0.091	3.06	0.084
	25	1.15	0.108	3.23	0.095

understood to mean only that all the curves were nearly invariant with frequency in the range covered in the tests.

Dunell and Dillon⁴² reported measurements from about 1 to 100 c.p.s. The tests were at 70° F. and 65 % r.h., a tensioning load of 5×10^8 dynes/cm² being used with superposed dynamic stress. It was observed that the dynamic modulus was essentially constant with frequency; the slope of log viscosity with log frequency was -0.9 , which leads to a slope of $+0.1$ for log $\tan \delta$ versus log frequency.

The measurements at the highest frequency are those of Mason and McSkimin.⁴³ The experiments were both in shear and longitudinally on samples of undrawn nylon 6-6. The longitudinal measurements were made on a relatively thin, flat specimen, with the result that the velocity and attenuation were functions of $(\lambda + 2\mu)$, where λ and μ are the Lamé constants, and of the corresponding $(\lambda' + 2\mu')$ —rather than of E (Young's modulus) and E' , its associated loss term. The moduli and loss factors are summarized in Table VIII; E and its associated viscosity were calculated from the values of μ , $(\lambda + 2\mu)$, μ' , and $(\lambda' + 2\mu')$ found experimentally.

Fujino and co-workers⁸⁶ have made longitudinal tests at 20° C. and 65 % r.h. at 0.2 c.p.s. to 200 kc. on filaments of nylon 6, and presented graphically the real and imaginary parts of the complex modulus, the loss factor $\tan \delta$, and the relaxation spectrum as calculated from the imaginary part of the modulus. Over this frequency range, the real part of the modulus increases from $\sim 4.8 \times 10^{10}$ to $\sim 6 \times 10^{10}$ dynes/cm.², the imaginary part decreases from $\sim 5 \times 10^9$ to a very broad minimum of $\sim 4 \times 10^9$ with its center in the vicinity of 100 c.p.s.; it then increases to $\sim 7 \times 10^9$ at 200

kc. The loss factor $\tan \delta$ shows a corresponding minimum. It has a value of ~ 0.1 at 0.2 c.p.s., decreases to ~ 0.07 at ~ 100 c.p.s., and increases again to ~ 0.15 at ~ 200 kc. The relaxation spectrum has a maximum at 3×10^{-6} sec. (corresponding to a frequency of 53 kc./sec.) and a minimum between 0.01 and 0.001 sec. (16 to 160 c.p.s.), after which it increases to the limit of calculated times, about 0.5 sec. (0.3 c.p.s.). The maximum and minimum values shown for the ordinate $E' (\ln \tau)$ of the spectrum are 4.3×10^9 and 2.4×10^9 dynes/cm.², respectively. The box distribution discussed in the Introduction would be of uniform height; the nylon therefore may be said, on the basis of this experiment, to be representable by a box distribution, to a first approximation, within the time of a microsecond to 10 sec.

In a second paper, Fujino *et al.*⁹⁶ performed similar experiments on monofilaments of nylon 6, melt-spun and quenched in ice water under a minimum of tension, followed by various drawing and conditioning treatments. The description of these is given in Table IX.

Samples NY-60-1 and NY-60-2 were drawn as slowly as possible by hand without necking, while the others were drawn at the ordinary commercial rate. NY-60-5B was drawn up to 380% and subsequently boiled in water for 1.5 hr. under constant length for the purpose of extracting the residual lactams, and NY-60-5-BH was prepared by heating the former for 1 hr. at 130° C. under constant length. NY-0-0-H was prepared by heating the quenched filament under constant length for 10 min. at 170° C.

The curves showing the real part of the dynamic modulus are the most regular, increasing almost linearly on the log-log plot, and generally maintaining their relative positions throughout. Except for NY-60-1, the modulus increases with the amount of drawing. At low frequencies, the imaginary parts of the modulus are in the same order of increasing values as the real ones; but those which are slightly drawn and therefore the lowest at low frequencies tend to become the highest at high frequencies, while the most-drawn tend to become the lowest. The $\tan \delta$ curves generally show a tendency to a minimum between 0.2 and 100 c.p.s., and a tendency to a maximum at 10^4 or to level off beyond that point. There is no apparent relation between the degree of drawing and $\tan \delta$ at the low frequencies, but at high frequencies $\tan \delta$ decreases with increasing orientation.

The effect of moisture on NY-60-1, NY-60-5-B, and NY-60-5-B-H was also examined. To supplement the data obtained at 65% r.h., samples were preconditioned for several days at 23° C. at 0% and 90% r.h. The dry specimens were tested at 40% r.h., the moisture content during measurement being about that which would correspond to moisture regain at 5% r.h.; the samples conditioned at 90% r.h. were tested at that condition. With decreasing moisture content the real part of the modulus

TABLE IX
TREATMENT AND X-RAY DIFFRACTION PATTERNS OF NYLON 6
INVESTIGATED BY FUJINO AND CO-WORKERS⁹⁶

Sample No.	Treatment	Density, gm./cc.	Double refractive index ($n_{\gamma} - n_{\alpha}$)	X-ray diffraction pattern*
NY-0-0	Quenched and undrawn (original)	1.127	0.0080	A system of some diffuse rings, almost α type
NY-60-1	Drawn by 30% at 60°C.	1.130	0.0093	Slightly oriented and some diffuse fiber pattern, $\beta \gg \alpha$
NY-60-2	Drawn by 100% at 60°C.	1.134	0.0290	Some oriented and somewhat diffuse fiber pattern, almost β type
NY-60-4	Drawn by 350% at 60°C.	1.140	0.0565	Well oriented and somewhat diffuse fiber pattern of β type
NY-60-5-B	Drawn by 380% at 60°C. and boiled in water for 1.5 hr.	1.143	0.0550	Well oriented and defined pattern of β type, although the crystal orientation is somewhat relaxed
NY-60-5-BH	Heat-treated NY-60-5-B for 1 hr. at 130°C.	1.144	0.0610	Well oriented and defined fiber pattern of β type, although the crystal orientation is somewhat relaxed
NY-0-0-H	Heat-treated NY-0-0 for 10 min. at 170°C.	1.141	0.0133	Slightly oriented and defined fiber pattern, $\beta \gg \alpha$

* The " α " and " β " types in the description of the X-ray diffraction patterns above refer to an orthorhombic and a monoclinic system respectively.⁹⁷

increased considerably for nearly the whole range, while the imaginary part increased at low frequencies and decreased at high. The corresponding relaxation spectrum is noticeably affected by the moisture content. With decreasing moisture content the spectrum generally increases at longer and decreases at shorter times, the effects being especially noticeable when the sample is extremely dry. The effect of decreasing moisture content is very analogous to that of heat treatment. As a result of this work on polycapromide and parallel work on other polymers, the authors were enabled to arrive at generalizations on the effect of drawing, heat treatment, and water content on the structure of the materials and the structural features responsible for the observed viscoelastic behavior. These papers represent the most ambitious attempt to relate structure with viscoelastic behavior so far published; but the conclusions lie outside the scope of this review.

⁹⁷ A. Okada and K. Fuchino, *Kobunshi Kagaku* 7, 122 (1950).

TABLE X
EFFECT OF DRAW RATIO OF NYLON 66 ON THE STATIC AND DYNAMIC YOUNG'S
MODULUS AND ON THE DYNAMIC SHEAR MODULUS
(After Wakelin *et al.*⁹⁹)

Draw ratio	E static, dynes/cm. ² $\times 10^{-9}$	Bending		Torsion		$E/3G$
		Frequency, c.p.s.	E , dynes/ cm. ² $\times 10^{-9}$	Frequency, c.p.s.	G , dynes/ cm. ² $\times 10^{-9}$	
1 (undrawn)	8.6	284-423	16.1	187-224	5.0	1.07
2	17.9	239-1075	20.6	94-182	4.9	1.43
3	23.5	305-709	33.2	91-140	5.5	2.04
4	33.2	285-454	41.7	55-140	5.2	2.75
5	41.9	274-401	49.3	52-106	5.8	2.86
6	50.8	285-464	55.9	54-135	6.0	3.13

The most nearly amorphous material is NY-0-0; if the data of Mason and McSkimin mentioned above at 30° C. are added to the extended plot of Korino *et al.*, they show a further rise in the modulus over two more decades of frequency, and a further decrease in $\tan \delta$. It must be conceded, however, that this procedure is questionable, in view of the differences in materials and test conditions, and the fact that the humidity in the Mason and McSkimin experiments was uncontrolled. It will be shown later that the data of Maxwell⁹⁸ may, with the same qualifications, be used to extend those of Korino *et al.* to lower frequencies.

Wakelin and co-workers⁹⁹ measured the effect of draw ratio of nylon 6-6 on the static and dynamic Young's modulus, and on the dynamic shear modulus. Their results are given in Table X.

These figures show that under the conditions by which the tests were made, the dynamic modulus in bending increased by 3.5 times as the draw ratio increased from 1 to 6; the shear modulus was practically unaffected. If it is assumed that $E/G = 3$ for an isotropic material, the increase of this ratio from ~ 1 to over 3 as the draw ratio increases is taken as evidence of an increasing degree of anisotropy as the draw ratio is increased.

Price and associates¹⁰⁰ measured the dynamic properties of an unidentified nylon filament in a frequency range of 5 to 50 c.p.s. at temperatures of 2° and 25° C. at various relative humidities. Perhaps the most unusual

⁹⁸ Bryce Maxwell, *J. Poly. Sci.* **20**, 551 (1956).

⁹⁹ J. H. Wakelin, E. T. L. Voong, D. J. Montgomery, and J. H. Dusenbury, *J. Appl. Phys.* **26**, 786 (1955).

¹⁰⁰ S. J. W. Price, A. D. McIntyre, J. P. Pattison, and B. A. Dunell, *Textile Research J.* **26**, 276 (1956).

feature of their results is the *decrease* in the dynamic modulus with increasing frequency, which is contrary to the usual results and also to the predictions of viscoelastic theory

$$E(\omega) = \int_0^{\infty} \frac{E(\tau)\omega^2\tau^2 d\tau}{1 + \omega^2\tau^2}$$

in which $E(\omega)$ must increase monotonically with ω , not only for the "step" function as discussed by the authors but also for any other form of $E(\tau)$ which is nowhere negative. The viscosity-frequency product, $\omega\eta$, is nearly independent of frequency over this range, and some success is reported in predicting its magnitude from the slope of the stress relaxation curves.

Maxwell⁹⁸ has provided data at frequencies between 0.001 and 100 c.p.s. and 30° C., obtained from a rotating cantilever beam apparatus. He concluded only that the dynamic modulus changed rather rapidly with frequency, and that two relaxation mechanisms were indicated by the minimum observed in the loss curve. It is interesting, however, that his data, which overlap those of Fujino *et al.*,⁸⁶ agree fairly well in slope of log modulus and $\tan \delta$, showing the minimum in the latter data in the same frequency range.

Chaikin and Chamberlain¹⁰¹ measured the dynamic Young's modulus at 100 kc. by means of the longitudinal pulse velocity as a function of relative humidity on a 15-denier nylon monofil. Their results are given in Table XI.

Tipton¹⁰² measured the dynamic modulus and loss factor of monofilaments at ~40 c.p.s., and determined the effect of static and dynamic strain. The modulus increases and the loss factor decreases with an increase in static strain, the change being small up to strains of 1 %. As the dynamic strain increases, the modulus decreases and $\tan \delta$ increases, the changes being small below strains of 0.2 %. As both strains approach zero, the modulus approaches 3.5×10^{10} dynes/cm.² and $\tan \delta$ approaches 0.1.

Becker and Oberst¹⁰³ measured the effect of water content and temperature on the dynamic properties in bending of nylon 6 at frequencies from 10 to 1000 c.p.s. The nylon was caused to assume two crystalline habits, by choice of cooling rates from the melt. The materials were conditioned roughly to dry, half the saturation value, and saturation at 20° C.; the temperature range of test was -30° to 90° C. Increased water content lowered the modulus, and shifted the dispersion region toward lower temperatures. At the same time the dispersion of the modulus and the absolute

¹⁰¹ M. Chaikin and N. H. Chamberlain, *J. Textile Inst.* **46**, T25, 44 (1955).

¹⁰² H. Tipton, *J. Textile Inst.* **46**, T322 (1955).

¹⁰³ G. W. Becker and H. Oberst, *Kolloid-Z.* **152**, 1 (1957).

TABLE XI
DYNAMIC YOUNG'S MODULUS OF 15-DENIER NYLON MONOFIL AT
100 KC. AS A FUNCTION OF RELATIVE HUMIDITY
(After Chaikin and Chamberlain¹⁰¹)

	Relative humid- ity, %	$E \times 10^{-10}$, dynes/cm. ²
Taut	25	6.5
	40	6.5
	65	6.5
0.5 extension	25	7.5
	40	7.4
	65	7.4

value of the loss factor increased. The difference in behavior of the two crystalline habits was small.

2. STRESS RELAXATION IN POLYAMIDES

The stress relaxation work of Hammerle and Montgomery⁹⁰ on 6-6 nylon has been mentioned in the discussion of the dynamic properties of nylon. Their tests covered periods from 20 to 20,000 sec. in torsion and 10 to 2000 sec. in tension. The experiments were conducted at 65% and 70° F. The torque at 100 sec. after application of the initial strain was taken as the standard. The relative torques at 20 and 20,000 sec. were (from the plot given) 1.07 and 0.80, respectively. The plot of relative torque against log time is nearly linear, but slightly concave upwards; the mean decrease in relative torque is 0.09 per decade, or 8.4% of the 20-sec. torque per decade. The same materials under the same conditions were used for extensional stress-relaxation experiments. Strains of 1, 2, and 5% were used, the load being applied in from 1 to 10 sec. For 1% and 2% extension, the behavior was linear; for 5%, the curve (similar to the one in torsion) is steeper. A formula for the extensional curve is given:

$$F(t)/F(100) = 1 - 0.0570 \ln (t/100)$$

which is equivalent to a loss of 13% per decade.

Attempts to relate the relaxation moduli in shear and tension by means of the usual equation from elasticity theory

$$G(\tau) = E(\tau)/2(1 + \nu)$$

where ν is Poisson's ratio and $G(\tau)$ and $E(\tau)$ are the shear and extension moduli, respectively, of any element comprising the model were not successful, the failure being ascribed to the anisotropy of the filament.

Speakman and Saville⁸⁸ performed relaxation experiments on nylon 6-6,

in buffer solutions of pH from 2.95 to 10.02. The stretch in the filament was 15%. They found the plots to be linear on a semilogarithmic plot up to 100 min.; the rate of decay of tension was independent of pH. In water, however, while the curves at 25° and 45° C. are still linear up to 100 min., those at 35°, 55°, and higher deviate markedly from linearity.

The effect of draw ratio and heat treatment on the relaxation of stress in nylon 6 were studied by Fujita and Kishimoto.¹⁰⁴ The tests were made at 30° C. and 65% r.h., at 10% strain. Cold drawing was performed manually at room conditions up to a draw ratio of 4 at the rate of about 10% per second. The specimens were allowed to rest 24 hr. before test. Curves of stress plotted as functions of log time were not generally linear, but concave upward. At a draw ratio of about 3 the relaxation was somewhat slower, as shown by change in the parameters of an empirical equation which provides a close fit to the curves. The static Young's modulus increases from 0.2×10^{10} dynes/cm.² in the undrawn material to about 1.3×10^{10} at a draw ratio of 3, after which the increase is slower. The elongation of rupture decreases from nearly 400% in the undrawn to about 100% in a draw ratio of 3, after which the decrease is much slower.

The effect of heat treatment was studied by heating undrawn specimens at 1.5° C./min. to the desired temperature, and then cooling in still air for 1 hr. at 30° C. and 65% r.h. At the higher temperatures (up to 130° C.) the initial loads were higher, and the shapes of the curves greatly altered; but they all appear to approach the curve for the untreated material. It was determined that this behavior was due to moisture uptake during the cooling period; if the specimens were cooled for 71 hr. or more, the form of the original curve was reproduced, although the level increased with increasing conditioning times. The initial loads for the untreated specimens and those treated at 130° C. were 2.3 and 2.8×10^8 dynes/cm.² at a strain of 10%.

Continuing this work, Kishimoto and Fujita¹⁰⁶ studied the relaxation of stress in nylon 6 as caused by penetration of water vapor at 40% r.h. and temperatures of 15°, 30°, and 50° C. A theory of chemical relaxation was presented, embodying these assumptions:

The diffusion coefficient is independent of concentration or any other factors.

The rate of breaking hydrogen bonds is proportional to their local concentration and to the local concentration of penetrant.

The remaining (unrelaxed) stress is proportional to the number of unbroken bonds.

The diffusion coefficient of water vapor in nylon could therefore be

¹⁰⁴ H. Fujita and A. Kishimoto, *J. Phys. Soc. Japan* **9**, 867 (1954).

¹⁰⁶ A. Kishimoto and H. Fujita, *Kolloid-Z.* **150**, 24 (1957).

evaluated from chemical relaxation data, as well as from ordinary sorption experiments; it was found that the diffusion is Fickian and that the coefficients agreed quite well when the relaxation-determined values were extrapolated to zero strain.

3. CREEP IN POLYAMIDES

Creep in drawn nylon was systematically investigated by Leaderman.⁶⁵ Emphasis was placed on the behavior of the material in relation to viscoelastic theory, in particular to the Boltzmann superposition principle. The effect of change of temperature in the dry state, and the effect of relative humidity at 75.5° C. were also studied. It is implicit throughout that there is a limiting creep in extension for any set of conditions, although in most cases it was not approximately attained. For small loads (up to 0.2 or 0.35 gm./denier, depending on the particular nylon used, corresponding to stresses of about 2×10^8 and 3.5×10^8 dynes/cm.², respectively), the material was found to conform to the Boltzmann superposition principle provided the principle was modified to permit nonlinearity in the relation between response and load. At higher stresses (up to about 8 gm./denier $\approx 8 \times 10^9$ dynes/cm.²) the behavior is more complex, and the superposition principle no longer holds good, even in modified form. The effect of an increase in temperature or humidity at high loads was similar to that of an increase of load, namely, a shifting of the total deformation curves to higher levels.

In all this work, linearity of deformation (or recovery) with log time occurred occasionally, but by no means generally.

The Young's modulus for these filaments at very low temperatures (or dynamic at very high frequencies) is not given; but if we use Schmieder and Wolf's³² value for shear, approximately 2.5×10^{10} dynes/cm.², and the ratio $E/3G \sim 3$ from Wakelin *et al.*,⁹⁹ the Young's modulus would be $\sim 2 \times 10^{11}$ for reasonably high draw ratios. Stresses of 0.3 gm./denier and 8 gm./denier, corresponding to stresses of 3×10^8 and 8×10^9 dynes/cm.² respectively, would result in instantaneous strains of 0.15 and 2%. The lower figure is at about the upper limit of dynamic strain found by Tipton¹⁰² not to affect the dynamic results; the upper one is above the limit of static strain found not to influence the results. Both these figures were far exceeded in Leaderman's tests, often probably before readings could be made. It may be tentatively concluded that if the strain at no time exceeded the 1% static value mentioned by Tipton, the material would at least obey the modified Boltzmann superposition principle, or even perhaps the linear.

Abbott¹⁰⁶ performed similar work on 16.5-denier nylon 66 monofilaments, but at considerably greater extensions (up to 16%). The work was done

¹⁰⁶ N. J. Abbott, *Textile Research J.* **21**, 227 (1951).

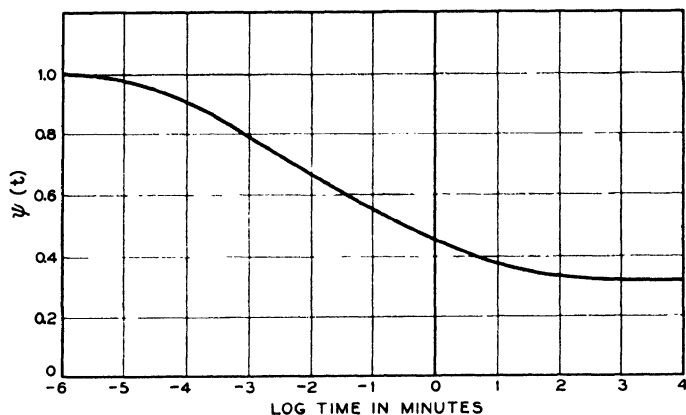


FIG. 27. Stress relaxation curve for nylon 66, at 36°C, 30% r.h., as calculated from the master creep curve.¹⁰⁷

at 65% r.h. and 70° F. He found the creep to be linear with log time, in one case from 10 sec. to 1 year, during which the extension changed from 10.4 to 13.7%. He, like Leaderman, found that an increase in load shifted the curves to higher values of deflection, without altering the slope for loads up to 1.8 gm./denier (1.8×10^9 dynes/cm.²). The deflection at 10 sec. is not proportional to the load. Recovery curves are also parallel but not linear. Abbott also studied the effect of immersion in water during the test. The difference between these results and those made at 65% r.h. is not great.

Catsiff *et al.*¹⁰⁷ attacked the problem of constructing master creep curves for nylon 66 for all loads at several humidity conditions, in such a way that the nonlinear characteristics first reported by Leaderman⁶⁶ and confirmed by their own data would be described. The nylon was in the form of 71-denier 34-filament yarn with $\frac{1}{2}$ twist per inch, cold drawn to 3.6–3.8 times its original length. It is the only yarn discussed in this review, but the paper is of considerable interest as the only attempt to create such a synthesis.

It was found that three operations had to be performed on the experimental curves in order to fit them together into a master curve. Each had to be expanded in ordinate by multiplying by a factor $1/F$, which was a function of the stress; each curve was shifted along the log time axis; and each was shifted vertically. The master curve then includes the time-dependent response, to which must be added the instantaneous elastic response if the total deflection is required. No more than qualitative

¹⁰⁷ E. Catsiff, T. Alfrey, Jr., and M. T. O'Shaughnessy, *Textile Research J.* **23**, 808 (1953).

significance is claimed for these curves outside the range of the experiments on which they were based. But if we take them at face value, three things of interest appear. First, a range of over 10^8 in time is needed to characterize the principal parts of the curve; second, the curve is sigmoidal in shape; and third, there are either relaxation mechanisms of much longer time than is included in the master curves, or else there is a definite upper limit to the creep.

A relaxation curve may be calculated³⁰ from the master creep curve, for what it is worth in view of the perhaps somewhat unreal character of the creep curve itself and the rather dubious use of a transformation based on the assumption of linearity. Such a curve is shown in Fig. 27. The slope of the steepest part is about 10% per decade, and the form of the curve again suggests the box distribution of relaxation times.

V. Conclusion

The foregoing has left unmentioned many materials and many phenomena. It may be said, indeed, that the only satisfactorily clear area in the field of time-dependent phenomena is that of behavior at very small strains and within the time limits attainable by ultrasonic techniques on one hand and the limit of the patience of the observer on the other, with the extensions provided by temperature variation where this is permissible. The ultrashort and ultralong time behavior are generally unknown in crystalline and cross-linked materials. It is perhaps not necessary to know the behavior at the extremes of time; it is not physically possible to deform a material in times shorter than some fraction of a micro-microsecond, for instance, and the creep or stress relaxation in 1000 years is probably not important for most of our uses today, although the archaeologists of the future may feel differently about it. But not to know is tantalizing. Very little has been said about gross distortions; but, for example, the knowledge of the flow of molten polyethylene during extrusion, which was mentioned, is in a sufficiently sad state. The difficulty lies primarily in the nonlinearity of the phenomena, once small strains have been exceeded, and partially in the complexities introduced with anisotropy.

The linear and near-linear behavior of the permanently cross-linked, amorphous polymer, ebonite, differs from an uncross-linked amorphous material principally in that the longer relaxation times may be finite in the latter; stress relaxation can go to completion and creep settles down to a steady rate. The crystalline polymers differ from noncrystalline ones over most of the time and frequency range. The material may be regarded as a crystalline phase in an amorphous matrix and bound to it, the elastic rigidity of the crystalline phase remaining in effect at very low frequencies and very long times, so long as it is not reduced in quantity and character

by partial or total melting. The total stiffness (at very high frequencies or very low temperatures or both) is much the same, however, for all classes of polymers.

Since a very large range of relaxation times is usually required to characterize these crystalline or cross-linked materials, the change in the dynamic modulus and loss factor and the slopes of the creep and stress relaxation curves are small over a small frequency or time range, and in some cases they have been apparently unchanging. This has been shown to be consonant to a high degree with a box distribution of relaxation times. Deviation occurs as the range of times or frequencies in experiments becomes longer; and then the distribution of relaxation times deviates from this simple function.

The theory of linear viscoelasticity has been eminently successful in joining several forms of viscoelastic behavior into a satisfying synthesis. The interest the theory has aroused, and the quantity of work it has stimulated, are an excellent example of the dependence of progress on some unifying concept. No such concepts have been evolved for the large and complex field outside the linear viscoelastic region. Whether such concepts will eventually be based on phenomenological considerations, like the linear theory, or on molecular, structural, and statistical mechanical considerations, remains to be discovered.

Nomenclature

a	Dimensionless parameter in the expression for creep asymptote
b	Parameter in creep asymptote; units, T^{-1}
B	Bulk modulus of elasticity; dynes/cm. ² or lb./in. ²
D	Diameter of capillary; units as convenient
e	Base of natural logarithms
E	Young's modulus; dynes/cm. ² or lb./in. ²
$E(\tau)$	The stiffness associated with relaxation times between τ and $\tau + d\tau$ in a continuous relaxation spectrum; dynes/cm. ² sec., dynes/cm. ² day, etc., as convenient
$E_r(t)$	The stress relaxation modulus, (stress at time t)/strain; units same as E above
G	Shear modulus, dynes/cm. ² or lb./in. ² ; equivalent to the Lamé constant μ
G, G_1, G_2 , etc.	The stiffness of springs in Maxwell elements in shear models, dynes/cm.
$G(t)$	Stress relaxation modulus in shear, (stress at time t)/strain. Units: dynes/cm. ² , lb./in. ² , etc., as convenient
k'	Second virial coefficient in Huggins viscosity equation
K	Absolute temperature; also an arbitrary constant used as required, easily distinguished from the temperature scale
L.C.S.	Limiting compressive stress (yield point in compression of Bingham body representation of polyethylene)

L.S.S.	Limiting shear stress (yield point in shear of Bingham body representation of polyethylene)
M_n	Number average molecular weight
M_w	Weight average molecular weight
p	Pressure; dynes/cm. ² , lb./in. ² , etc., as convenient.
Q	$1/\tan \delta = 1/\text{loss factor in sinusoidal displacement}$
Q	Volume per unit time in capillary flow; units as convenient
r, r_0, r_1	Radii; units as required
t	Time; sec., hr., days, etc., as convenient
$\tan \delta$	Loss factor in sinusoidal displacement
x	General symbol for length, distance, etc.; cm., in., as convenient.
α, β, γ	Designation for absorption peaks, in order of decreasing temperature.
η	Viscosity associated with Lamé constant μ or shear modulus G , in poises
η_B	Viscosity associated with bulk modulus; dyne sec./cm. ²
η_S	Viscosity associated with Young's modulus; dyne sec./cm. ²
λ	Lamé elastic constant; dyne/cm. ²
λ	Relaxation frequency; sec ⁻¹ , days ⁻¹ , etc., as convenient
μ	Lamé elastic constant equivalent to G above; dyne/cm. ²
μ, μ_2, μ_3	In reference 94, internal friction; poises
ν	Poisson's ratio
τ	Relaxation time; sec., min., or days as convenient
τ_1, τ_2	Relaxation times; the minimum and maximum relaxation times, respectively, in a given spectrum. Units: sec., min., or days as convenient
$\varphi(t)$	Creep function, defined as (deformation at time t)/(deformation at time zero)
χ	Viscosity associated with Lamé constant λ ; dyne sec./cm. ²
$\psi(t)$	Relaxation function, defined as (stress at time t)/(stress at time zero)
$\omega, \omega_1, \omega_2$	Circular frequency; radians/sec

CHAPTER 11

THE VISCOSITY AND ELASTICITY OF INTERFACES

Dean W. Criddle

I. Interfacial Viscosity	429
1. Definition of Interfacial Viscosity	429
2. Terminology and Units	431
3. Surface Viscometry Techniques	431
a. Canal Surface Viscometers	432
b. Torsion Pendulum Surface Viscometers	433
c. Rotational Torsion Surface Viscometers	435
4. Review of Data.	436
a. Viscosity Data for Water-Air Interfaces	436
b. Viscosity Data for Water-Hydrocarbon Interfaces	438
c. Viscosity Data for Air-Hydrocarbon Interfaces	439
II. Interfacial Elasticity	439
1. Definition	439
2. Methods of Measurement	440
3. Review of Data	440
III. Significance of Interfacial Viscosity and Elasticity	441
Nomenclature	442

The viscosity and elasticity of interfaces between two fluid phases are a new challenge to surface chemists. Bulk properties, such as viscosity, stress relaxation, and elasticity, have their counterparts in surfaces. The bulk properties have received prior study; increasing attention is being given to the flow and elastic properties of interfaces. This chapter tells what surface viscosity and elasticity are and reviews methods of measuring them. Some typical data are presented and the significance of surface viscosity and elasticity is discussed.

I. Interfacial Viscosity

1. DEFINITION OF INTERFACIAL VISCOSITY

A liquid-liquid or liquid-vapor interface has viscosity if the interface itself contributes to the resistance to shear in the plane of the interface. Pure liquids against their own vapor or against air do not show such viscosity effects. However, many "surfactant" (surface active agent) films adsorbed at interfaces are viscous. Often this surface-induced viscosity is extremely

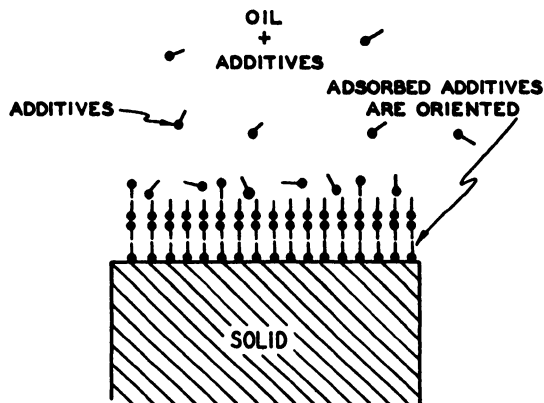


FIG. 1. Surfactant additives adsorb at an interface

high. Brady and Brown showed that the viscosity of lauryl alcohol was a million times larger than the bulk viscosity when this alcohol was spread as a monolayer on a water substrate.¹

The high viscosity of adsorbed films is plausible in view of other known properties of interfaces. For example, surfactants concentrate at interfaces, as shown theoretically by Gibbs and as verified by numerous studies.² These films are also oriented, as evidenced by electron diffraction and surface potential measurements.^{3,4} Viscosity changes in films are expected and found when phase changes occur in surface films. Such phase changes have been studied and the two-dimensional equations of state of the films have been determined.⁵

Surfactants concentrate and orient at an interface, as illustrated in Fig. 1. These chemicals tend to be oriented with the polar portion preferentially in the more polar phase. Monomolecular layers are adsorbed onto solids from low concentrations of surfactants, but multilayers form at high concentrations in some cases.⁶

Surfactants are also oriented at liquid-liquid interfaces. These surface films resist compression by a "film pressure" characteristic of the substrate, surfactant concentration, and temperature. As the film pressure is increased,

¹ A. P. Brady and A. G. Brown, *Mechanical Properties of the Surface Films of an Aqueous Solution of Detergents, "Monomolecular Layers,"* (H. Sobotka, ed.) American Association for the Advancement of Science, Washington, D. C., 1954.

² E. G. Cockbain, *Trans. Faraday Soc.* **50**, 874 (1954).

³ J. T. Davies, *Trans. Faraday Soc.* **49**, 683 (1953).

⁴ B. D. Powell and A. E. Alexander, *J. Colloid Sci.* **7**, 493 (1952).

⁵ W. D. Harkins, "The Physical Chemistry of Surface Films," p. 106. Reinhold, New York, 1952.

⁶ F. P. Bowden and A. C. Moore, *Trans. Faraday Soc.* **47**, 900 (1951).

the surfactant becomes more closely packed and oriented more nearly normal to the surface. Such close-packed films are barriers to diffusion of water vapor through the interface; hence, they are useful in lowering evaporation rates from water surfaces. Some films resist deformation in the plane on the interface.

2. TERMINOLOGY AND UNITS

Surface viscosity is the ratio between shear stress and shear rate for interfacial regions when the stress and shear are in the plane of the interface. The effect of surface viscosity is over and above any viscosity effects which can be attributed to the two bulk phases in contact. Thus, the viscous drag of bulk fluids is a correction on the shear resistance of a surface film.

Surface viscosity has the units of g. sec^{-1} compared to bulk viscosity units $\text{gm. cm.}^{-1} \text{ sec.}^{-1}$. Surface viscosity units are called surface poises.

Some investigators have preferred to report data as apparent surface viscosity because of (1) the uncertainty in the correction to be applied in order to obtain surface poises and (2) the non-Newtonian nature of many surface films.⁷ The latter method of treating data reports the viscous drag of the surface film relative to the viscous drag of the two contacting bulk phases. For example, assume the interface of phases A and B is 100 times as resistant to shear with a film as without a film. The apparent surface viscosity of the film σ is

$$\sigma = 100(\eta_A + \eta_B) \quad (1)$$

where η_A and η_B are the bulk viscosities of phases A and B, respectively. Thus, apparent surface viscosity has the units of bulk viscosity, i.e., poises.

Both of the above methods of reporting data have advantages and utility, but the two methods do not and should not give the same result. Surface poise data is corrected for the drag due to the flow of fluid adjacent to the film. Apparent surface viscosity data include the viscous drag of fluid adhering to the film. Both methods are useful to detect and study viscous surface films.

3. SURFACE VISCOMETRY TECHNIQUES

The three types of apparatus used to measure surface viscosity are canal,⁸ pendulum torsion,⁹ and rotational torsion¹⁰ surface viscometers. Each is described below together with its advantages and limitations.

⁷ D. W. Criddle and A. L. Meader, *J. Appl. Phys.* **26**, 838 (1955).

⁸ W. D. Harkins and J. G. Kirkwood, *J. Chem. Phys.* **6**, 53 (1938).

⁹ R. E. Wilson and E. D. Ries, "Colloid Symposium Monograph," pp. 145-173. University of Wisconsin Press, Madison, Wisconsin, 1953.

¹⁰ M. Joly, *Kolloid-Z.* **162**, 35 (1952).

a. Canal Surface Viscometers

Canal-type surface viscometers are used to measure the rate of flow of a surface film through a "canal" on a surface at a known shear stress. For long, narrow canals, the surface viscosity η_s is given by⁸

$$\eta_s = \frac{Pa^3}{12LA} - \frac{a\eta_0}{\pi} \quad (2)$$

where P is the difference in film pressures at the ends of the canal, L is the canal length, a is the canal width, A is the area flowing per unit time, and η_0 is the viscosity of the substrate. The last term is to correct for the viscous drag of the substrate adhering to the film. This correction term is minimized by using canals of small width. The above equation gives viscosity in units of surface poises, or gm. sec.⁻¹.

An experimental apparatus for canal-type viscosity measurements is illustrated in Fig. 2. A film in "A" at a constant film pressure P_1 flows through the canal to "B" at the lower film pressure P_2 . The film pressures are maintained constant by mechanically adjusting the movable barriers. An alternate method of maintaining constant film pressure is to use "piston

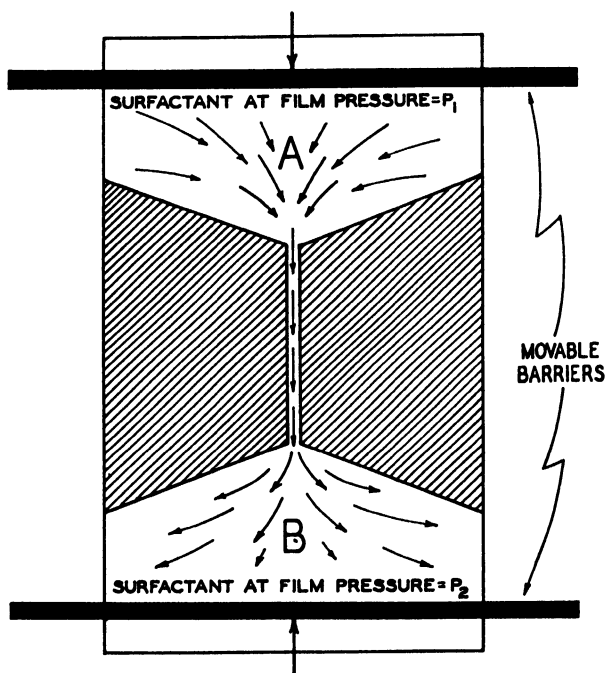


FIG. 2. Canal-type surface viscometer.

oils.”¹¹ Measurements are made of P_1 , P_2 , and the rate of change of area “ A ” as the film flows through the canal.

The canal method has the advantage of giving data in units of surface poises. This method is useful for insoluble films, and it is applicable to soluble surfactants if the modified techniques of Ewers and Sack are used.¹² Liquid-vapor interfaces are easily studied with the canal method, but it is not easily used at liquid-liquid interfaces. This method is limited to surface concentrations which give rise to appreciable film pressures, and, therefore, it cannot be used to study the viscosity of surfactants at low concentrations. Although the data are obtained in units of surface poises, the observed viscosities are the average values of the viscosity over the range of film pressures from P_2 to P_1 . Only for Newtonian films do these measurements have significance in absolute units, and in these cases the surface viscosity must be measured as several shear stresses in order to evaluate the relationship of viscosity to film pressure. Most surface films are non-Newtonian; in these cases a canal-type viscometer uses a complicated range of film pressures and shear rates. The canal method has been little used according to the literature, and, unfortunately, most systems have been studied at only one shear rate. In spite of its limitations, it is useful and sensitive in detecting viscosity effects at interfaces.

b. Torsion Pendulum Surface Viscometers

The second technique of measuring surface viscosity is to observe the damping of a torsion pendulum due to the viscous drag of a surface film. One torsion pendulum viscometer and several variations of the viscometer shearing element⁷ are shown in Figs. 3 and 4. The shearing element is suspended by a torsion wire and positioned at the plane of the interface (Fig. 4). Measurements are made of the period of the pendulum and of the damping as the pendulum oscillates. The apparent surface viscosity σ is¹³

$$\sigma = \eta_0 \left(\frac{\Delta/\Delta_0}{P/P_0} - 1 \right) \quad (3)$$

where η is apparent surface viscosity in centipoises, η_0 is the sum of the bulk viscosities in centipoises of the two phases forming the interface, Δ is the difference in the logarithm of the amplitude of successive swings for the interface with adsorbed surfactant, Δ_0 is the difference in the logarithm of the amplitude of successive swings for the interface without surfactant, P is the period of the pendulum for the film-covered interface, and P_0 is the period of the pendulum for the interface without surfactant.

¹¹ Blodgett, K. B., *J. Am. Chem. Soc.* **56**, 495 (1934).

¹² W. E. Ewers and R. A. Sack, *Australian J. Chem.* **7**, 40 (1954).

¹³ D. W. Criddle, *Lubrication Eng.* **13**, 131 (1957).

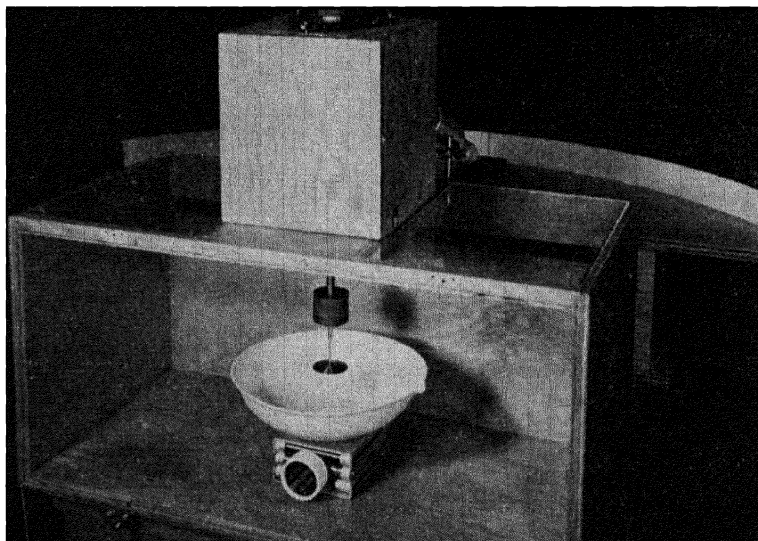


FIG. 3. Torsion pendulum surface viscometer

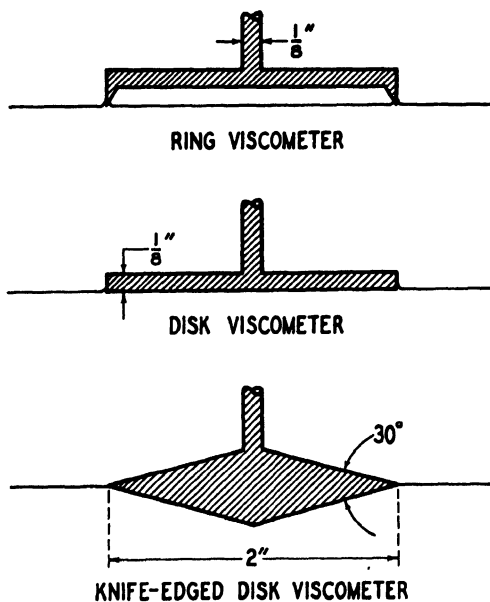


FIG. 4. Surface viscometer designs. Ring, disk, and knife-edged disk viscometers

A relationship used for surface viscosity in surface poises to express data obtained on a torsion pendulum viscometer is¹⁰

$$\eta_s = \frac{C_w I}{2\pi} \frac{R_2^2 - R_1^2}{R_1^2 R_2^2} \left[\frac{\Delta}{7.4 + \Delta^2} - \frac{\Delta_0}{7.4 + \Delta_0} \right] \quad (4)$$

where C_w is the torsion modulus of the wire, I is the polar moment of inertia of the oscillating pendulum, R_1 is the radius of the surface viscometer, R_2 is the radius of the container. Alternate but similar relationships to equation (4) were used by Myers and Harkins¹⁴ and by Langmuir and Schaefer.¹⁵

The torsion pendulum surface viscometer has some advantages and some disadvantages over the canal type. With a single determination of amplitude versus number of swings, one can explore a wide range of shear rates. A further advantage of the torsion pendulum viscometer is the fact that with the same equipment one can detect elasticity of the film and study the viscoelastic range of deformation. Liquid-liquid as well as liquid-vapor interfaces are readily studied by this technique. Film viscosities over a wide range of shear rates can be studied by selecting a pendulum with a suitable polar moment of inertia and torsion constant.

A disadvantage of the torsion pendulum viscometer is that it uses a range of shear rates (amplitudes) in each determination. Hence, data from non-Newtonian films must be considered as an average viscosity over a range of shear rates. However, this type viscometer enables one rapidly to detect and measure the surface viscosity of Newtonian films and to explore the work stability and shear rate dependence of non-Newtonian films.

c. Rotational Torsion Surface Viscometers

The third type of viscometer used is a rotational torsion surface viscometer. In principle, this is a concentric cylinder viscometer adapted to surfaces. A surface film is sheared between rotating concentric rings on a surface. The shear rate can be held constant by rotating one ring at any desired rate and observing the torque on the other ring. The surface viscosity η_s is given by¹⁰

$$\eta_s = \frac{SKt}{8\pi^2} \frac{R_1^2 - R_2^2}{R_1^2 R_2^2} \quad (5)$$

where t is the time of revolution of the ring, K is the torsional moment corresponding to 1° strain, S is the difference in degrees strain for the same velocity gradient in the presence and in the absence of a surface film. A simple derivation of this type equation was given by Ellis *et al.*¹⁶

¹⁴ R. J. Myers and W. D. Harkins, *J. Chem. Phys.* **5**, 601 (1937).

¹⁵ I. Langmuir and F. J. Schaefer, *J. Am. Chem. Soc.* **59**, 2400 (1937).

¹⁶ S. C. Ellis, A. F. Lanham, and K. G. Parkhurst, *J. Sci. Instr.* **32**, 70 (1955).

Data from a rotational torsion viscometer were treated by Brown and co-workers using a Reiner-type equation adapted to surfaces¹⁷

$$\eta_s = \frac{T}{4\pi\Omega} \frac{R_1^2 - R_2^2}{R_1^2 R_2^2} + \frac{f_s}{\Omega} \ln \frac{R_2}{R_1} \quad (6)$$

where T is the torque produced by the film when the angular velocity is Ω and f_s is the surface yield value.

The rotational torsion viscometer also has its advantages and disadvantages. It is the least sensitive method, but at the same time it is convenient to study extremely viscous films. It has the advantage of a constant shear rate, and, hence, it is useful for studying non-Newtonian films. If the clearance between the concentric shearing elements is small, this approaches a canal-type measurement wherein the shear takes place at constant film pressure. This method can be used conveniently to explore work instability and non-Newtonian films. If the clearance between the concentric elements is large, viscosity is measured over a range of shear rates. This type equipment can be used in principle to obtain static surface elasticity by the equation of Langmuir.¹⁵ In practice, the elastic limit of surface films is so small that this method has not been used.

Each of the above three experimental methods for studying surface viscosity is preferred under some circumstances. The one selected for any given problem will depend on the nature of the system and the type of information desired.

4. REVIEW OF DATA

a. Viscosity Data for Water-Air Interfaces

The principal variables affecting the surface viscosity of a film are: the surfactant, interfacial bulk phases, surfactant concentration or film pressure, and temperature. These variables have been studied mainly at water-air interfaces with a wide variety of water-insoluble surfactants. Long chain paraffinic acids on water were studied by Harkins⁶ using a torsion pendulum viscometer. The surface viscosity of the systems are shown in Fig. 5. The data of this figure illustrate that film pressure and molecular size both affect surface viscosity. These acids were studied on a substrate pH of 2.0 and the following four generalizations were made: (a) The logarithm of the surface viscosity was proportional to the film pressures below 19 dynes cm.⁻¹ for all acids with 16 to 20 carbon atoms. (b) The viscosity of fluid films increased rapidly with the length of the hydrocarbon chain. (c) The films were Newtonian at low film pressures and non-Newtonian at

¹⁷ A. G. Brown, W. C. Thuman, and J. W. McBain, *J. Colloid Sci.* **8**, 491 (1953).

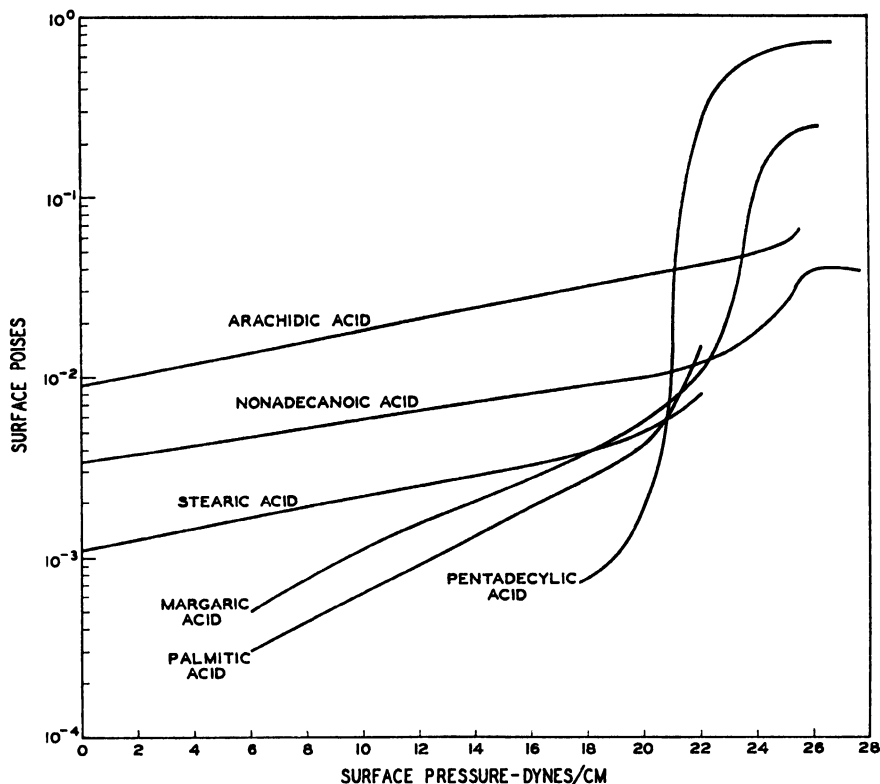


FIG. 5. Viscosity of long chain acids at a water-air interface. The pH is 2.0.

high film pressures. (d) The viscosity of the films decreased with the length of the hydrocarbon chain.

The above four generalizations also apply to long chain alcohols. These alcohols are an order of magnitude more viscous at an air-water interface than the corresponding acids.

Some other surfactants have been studied for surface viscosity at water-air interfaces. Tricaproin, tricaprillin, and oxyethyl stearate are gaslike films (fluid and highly compressible) whose viscosity decreases with pressure. Oleic and myristic acids, tricaprin, trilaurin, triolein, and tricinolein are liquidlike (fluid and with low compressibility). The surface viscosity of these liquidlike films also decreases as the film pressure increases. In contrast, stearic and palmitic acids on $10^{-3}N$ HCl substrate increase in viscosity as the film pressure increases.¹⁰

Aqueous detergents have been studied for water-air interfacial effects.^{17, 18}

¹⁸ B. C. Blakey and A. S. C. Lawrence, *Discussions Faraday Soc.* No. 18, 268 (1955).

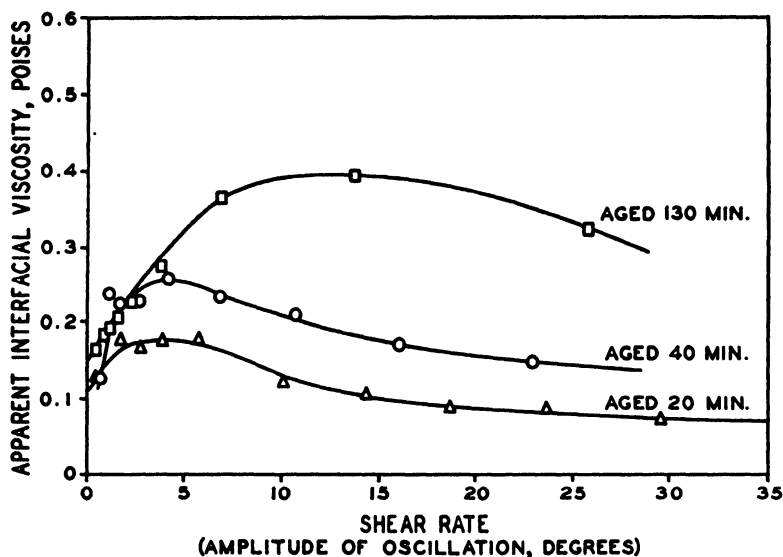


FIG. 6. Effect of shear rate on apparent interfacial viscosity. Four per cent sorbitan sesquileate at oil-water interface. Oil viscosity is 54 centipoises at 24°C.

Stable foams were formed from detergent solutions showing appreciable surface viscosity; unstable foams came from solutions showing low surface viscosity.

The effect of temperature on surface viscosity was shown by Harkins.⁵ In general, an increase in temperature results in a decrease in surface viscosity. However, when phase changes occur in the film as the temperature rises, anomalous results may be observed, as in the case of octadecanol.⁸

b. Viscosity Data for Water-Hydrocarbon Interfaces

A few surfactants are viscous at oil-water interfaces. Alexander and Schulman showed that several emulsifying agents were rigid at oil-water interfaces.¹⁹ Cumber and Alexander found viscosity effects for several proteins at an oil-water interface.²⁰

Several lubricating oil additives are known to be viscous from data obtained on a torsion pendulum viscometer.^{7, 13} These films developed at the interface in a few minutes. All of the aged, highly viscous films were non-Newtonian and work unstable. Figure 6 illustrates, for sorbitan sesquileate, the dependence of apparent interfacial viscosity on shear rate and age of the oil-water interface. These films were non-Newtonian and work un-

¹⁹ A. E. Alexander and J. H. Schulman, *Trans. Faraday Soc.* **36**, 960 (1940).

²⁰ C. W. N. Cumber and A. E. Alexander, *Trans. Faraday Soc.* **46**, 243 (1950).

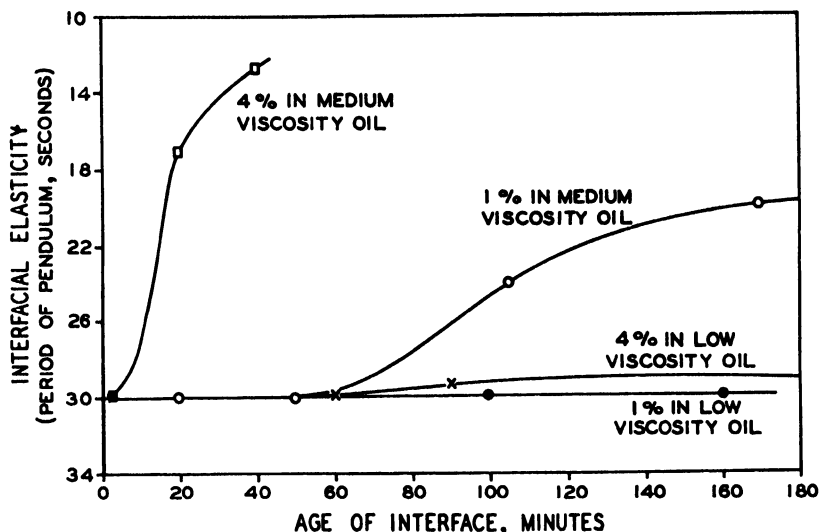


FIG. 7. Development of interfacial elasticity. Sorbitan sesquileate at oil-water interfaces. Data obtained using oscillation amplitudes of less than one degree.

stable after they were aged a few minutes. The concentration of surfactant and the oil viscosity are also important variables, as shown in Fig. 7.

c. Viscosity Data for Air-Hydrocarbon Interfaces

The only known case of viscosity at a hydrocarbon-air interface was reported by Criddle and Meader.⁷ Using a torsion pendulum surface viscometer, they found that sulfurized calcium alkylphenate rapidly formed a viscous non-Newtonian film at an oil-air interface. Several hydrocarbon-air interfaces were tested without evidence of interfacial viscosity.

II. Interfacial Elasticity

1. DEFINITION

Films are elastic if they resist deformation in the plane of the interface and if the surface tends to recover its natural shape when the deforming forces are removed. Analogous to bulk materials, surface films have elasticity which can be measured by both static and dynamic methods. Furthermore, the elastic constant of the surface film depends upon the nature of the deforming stress. If the area of the surface film is held constant and static measurements are made of resistance to deformation in the plane of

the interface, one obtains surface elasticity E_{sm} as defined by Langmuir and Schaefer.¹⁵

$$E_{sm} = \frac{C_w}{4\pi} \left(\frac{\theta_w}{\theta_f} \right) \left(\frac{1}{R_1^2} - \frac{1}{R_2^2} \right) \quad (7)$$

where θ_f and θ_w are the angular displacement in radians of the film and wire, respectively. However, surface films have such a small elastic limit that this relationship has not proven useful.

2. METHODS OF MEASUREMENT

Fourt used a dynamic method to obtain relative surface elasticities. He found that elastic films decreased the period of a lever-type torsion pendulum surface viscometer.²¹ Data from such elasticity measurements, in which the area per molecule of film changes during the measurements, are conveniently expressed in terms of surface shear modulus²²

$$E_s = \pi I \left(\frac{1}{T^2} - \frac{1}{T_0^2} \right) \left(\frac{1}{R_1^2} - \frac{1}{R_2^2} \right) \quad (8)$$

where I is the moment of inertia, and T and T_0 are the periods of the pendulum at the interface in the presence and in the absence of a surface film. The relationships between four different surface elastic moduli were worked out by Tschoegl.²³

Quasi-static methods of measuring the elasticity of films were used by Tachibana and Inokuchi.²⁴ Oka showed that such data could be interpreted in terms of a mechanical model.²⁵

Some investigators have preferred to report their surface elasticity data simply as a decrease in the period of a torsion pendulum viscometer.^{7, 13}

3. REVIEW OF DATA

Interfacial elasticity data are available for only a few systems. Several different proteins spread as films at water-air interfaces are highly elastic in dynamic measurements.^{21, 24} Oil blends of sulfurized calcium alkylphenate form elastic films at oil-air interfaces as detected by the change in period of a torsion pendulum surface viscometer.⁷ The commercial emulsifiers, sorbitan sesquioleate and sorbitan monooleate, are elastic at oil-water interfaces. The rate of development of interfacial elasticity at oil-water interfaces for sorbitan sesquioleate is shown in Fig. 7. Blends of this chemical

²¹ L. Fourt, *J. Phys. Chem.* **43**, 887 (1939).

²² A. A. Trapeznikov, *Doklady Akad. Nauk. S.S.S.R.* **63**, 57 (1958).

²³ N. W. Tschoegl, *J. Colloid Sci.* **13**, 500 (1958).

²⁴ T. Tachibana and K. Inokuchi, *J. Colloid Sci.* **8**, 341 (1953).

²⁵ S. Oka and Y. Sato, *Bull. Kobayashi Inst. Phys. Research* **5**, No. 2 (1955).

FIG. 8

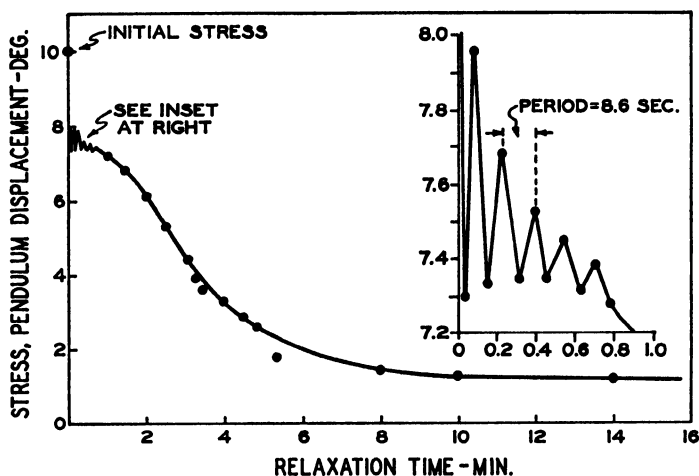


FIG. 8. Stress relaxation curve. Interface of water and SAE 10 mineral oil containing 3% sorbitan monooleate. Interface aged 24 hours.

in low and medium viscosity oils (8.1 and 54 centipoises at 24°C.) differ in the rate of development and in the magnitude of their oil-water interfacial elasticity.

Although no thorough study has been made of the distribution of relaxation times in surface films, there is some information on the subject. Some proteins have relaxation times ranging from a fraction of a second to a few minutes. Films of emulsifying agents have elastic relaxation times known to range from minutes to hours. The stress relaxation curve for an aged film of sorbitan sesquioleate at an oil-water interface shows complex viscoelastic behavior (Fig. 8). A better knowledge of the distribution of relaxation times would help one understand such systems.

III. Significance of Interfacial Viscosity and Elasticity

Interfacial viscosity and elasticity are important in several fields. Studies of proteins at interfaces are motivated by the idea that molecular processes through living membranes are understood better by knowing the rheological properties of protein films.²⁴ The bulk viscosity of some emulsions is explained in terms of the high oil-water interfacial viscosity, and Sherman showed that viscous oil-water films were formed by several emulsifying agents.²⁶ The role of interfacial elasticity in emulsion stability is unknown.

The viscosity of adsorbed films is of interest in the lubrication field. These

²⁶ P. Sherman, *J. Colloid Sci.* **10**, 63 (1955).

films between gears and in bearings protect moving parts from contacting each other. Films which reduce wear and friction may be effective because of their high surface viscosity.¹³

Surface viscosity is believed to be one of the factors contributing to foaming in both aqueous and hydrocarbon solutions. Foam stability has been correlated with the water-air interfacial viscosity of aqueous detergents^{17, 18} and with the oil-air interfacial viscosity of a hydrocarbon detergent. In the latter case, a defoamer, dimethyl silicone, was found to eliminate both the surface viscosity and the foaming tendency of the oil.⁷

Surface viscosity is useful in theoretical studies of intermolecular attraction.²⁷ For example, surface viscosity measurements combined with film pressure-area data give information on the shape and flexibility of macromolecules at interfaces.

The viscous flow of surface films has been treated theoretically and found to be consistent with modern concepts of intermolecular forces. Moore and Eyring²⁸ and Joly²⁹ have discussed surface viscosity in terms of absolute reaction rate theory. Temperature coefficients of surface viscosity enabled Eyring to calculate that the activation energies for viscous flow of fatty acids was about 11 kcal mole⁻¹ compared to about 6 kcal mole⁻¹ for bulk flow. It is likely that a fatty acid surface film has a larger unit of flow than the corresponding acid in bulk. Joly pointed out that Newtonian flow of surface films is expected as long as

$$\eta_s SA \ll kT \quad (9)$$

where S is the shear rate and A is the molecular area. Thus, one expects all high viscosity films to be non-Newtonian. This appears to be true.

Surface rheology is a fertile field for study. Some good experimental techniques are now available, and the next few years will probably see the significance of surface rheological properties appreciated more widely.

Nomenclature

σ	= Apparent surface viscosity in poises	E_{sm}	= Surface elastic modulus for shear
N_s	= Surface viscosity in poises	E_x	= Surface elasticity index.

²⁷ J. T. Davies, *J. Colloid Sci.* **11**, Suppl. 1, 9 (1954).

²⁸ W. J. Moore and H. Eyring, *J. Chem. Phys.* **6**, 391 (1938).

²⁹ M. Joly, *Proc. Intern. Congr. Rheol., 2nd Congr., Oxford, 1963* pp. 365-370 (1954).

RHEOLOGY OF LUBRICATION AND LUBRICANTS

A. Bondi

I. Fluid Lubricants	444
1. Normal Fluids	444
2. Non-Newtonian Flow of Oils	452
3. Flow Properties and Hydrodynamic Lubrication	454
II. Gelled Lubricants	457
1. Lubricating Greases	457
2. Flow Properties of Frozen Oils	463
3. Motion of Gelled Lubricants through Pipes	464
4. Hydrodynamic Lubrication with Gelled Lubricants	467
III. Flow Phenomena in Boundary Lubrication	467
1. Friction of Solid Surfaces	467
2. Lubricated Boundary Friction	474
Nomenclature	478

The primary objective of lubrication is the separation of the rubbing surfaces by a layer which is more easily deformable than the material of the rubbing bodies. This is most successfully accomplished by the hydrodynamic lifting forces of a liquid layer relative to which the rubbing bodies are moving. In some instances it is desirable to impart a small yield strength to the fluid lubricant and gel it, in order to facilitate the sealing of bearings. This conversion has relatively little effect on the mechanics of lubrication and can be handled by the classical methods of continuum physics. In the life of all rubbing machine elements there are time intervals, sometimes of fairly long duration, during which complete separation of the solid surfaces is not possible. The load is then only partly carried by the fluid film and partly by the asperities of the rubbing bodies. Layers of suitable solid or semisolid, usually adsorbed, lubricants reduce, but do not entirely prevent metal-to-metal contact under these conditions. The quantitative treatment of this complex situation is, in spite of considerable efforts, only in its infancy.

The following review will attempt to summarize currently available information on the fundamentals of lubrication and the relevant flow properties of lubricants with only minor attention to historical developments.

I. Fluid Lubricants

1. NORMAL FLUIDS

The only physical property of real importance in journal and slider bearing applications is the viscosity. Exact quantitative treatment of the energy balance and temperature, and therefore viscosity and pressure, distribution throughout the lubricant layer requires in addition also the knowledge of density, heat capacity, and thermal conductivity of the lubricant. The fluids of practical interest differ only very little in the latter three properties, while their viscosity may vary over more than six decades within the temperature and pressure range of interest. Many bearings operate over a sufficiently wide range of temperatures and pressures that the variation of viscosity with temperature and pressure has to be considered when making exact calculations for bearing design.

The requisite viscosity-temperature-pressure data are now available for most groups of commercially important natural and synthetic lubricating fluids. An extensive effort to obtain this information has recently been made as a joint project of the American Society of Mechanical Engineers and of Harvard University.¹ The large number of published data calls now for a concentrated effort to systematize the available information. That such a systematization will be no easy task is at once apparent from an inspection of the data in Figs. 1a-d. The shapes of the viscosity-temperature-pressure diagrams of lubricating fluids differ even in their qualitative aspects so considerably that a generally valid and practically useful formula for the description of these data is very difficult to imagine.

A few viscosity-temperature isobars and viscosity-pressure isotherms of several classes of lubricating fluids are shown in Figs. 2-3. The choice of the ordinates $\log \eta$ vs. $1/T$ and vs. P was dictated by the desire to demonstrate the deviation from the behavior demanded by simple theory.^{2, 3} Many attempts have been made to straighten the $\eta(T)$ function empirically. Best known of these is the plot of $\log^2 (\nu + a)$ versus $\log T$ (where ν is the kinematic viscosity in centistokes and a is 0.8 as proposed by Walther⁴ and adopted in many countries as the standard method of plotting the viscosity-temperature data of petroleum-derived lubricants.⁵ Since its usefulness depends upon the choice of units of viscosity, it can hardly have any theoretical significance. It is, however, surprisingly general and gives straight-line plots over a fairly wide temperature range for many

¹ D. Bradbury, M. Mark and R. V. Kleinschmidt, *Trans. Am. Soc. Mech. Engrs.* **73**, 667 (1951).

² A. Bondi, "Physical Chemistry of Lubricating Oils." Reinhold, New York, 1951.

³ A. Bondi, in "Rheology" (F. R. Eirich, ed.), Vol. I, p. 321. Academic Press, New York, 1956.

⁴ C. Walther, *Erdöl u. Teer* **4**, No. 29/30 (1923); **5**, No. 34 (1929).

⁵ American Society for Testing Materials Method D 341-43.

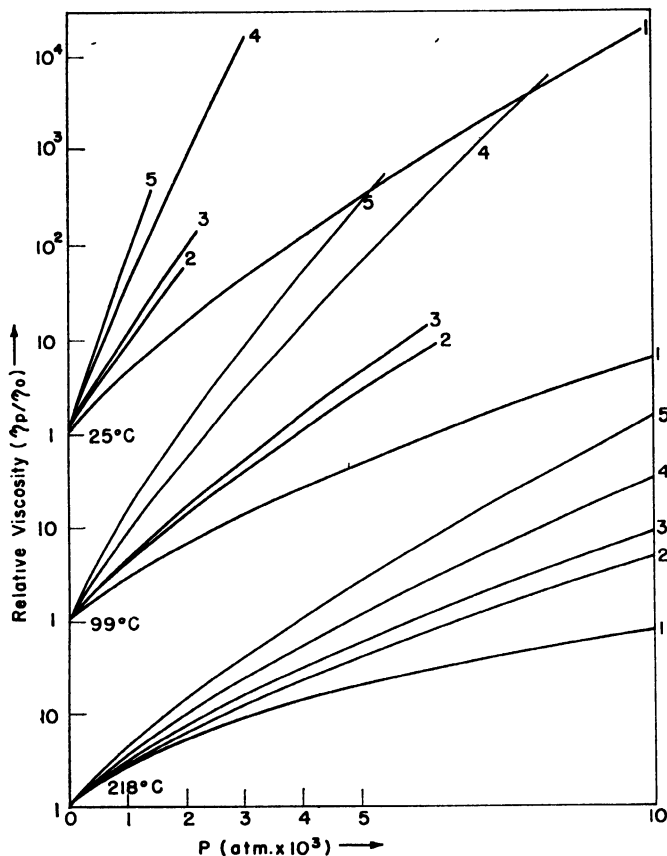


FIG. 1a. Change of viscosity with pressure at three temperatures for a few typical lubricants.^{1, 2} Curve 1: bis(2-ethylhexyl) sebacate. Curve 2: 11- α -decalin heneicosane (temperatures: 20, 99, 204°C.); $\eta_{20} = 1.02$, $\eta_{99} = 0.052$, $\eta_{204} = 0.012$ poise. Curve, 3: 1,1-bis(cyclohexylethyl) *n*-nonane (temperatures: 20, 99, 204°C.); $\eta_{20} = 0.73$, $\eta_{99} = 0.04$, $\eta_{204} = 0.009$ poise. Curve 4: polybutene; $\eta_{25} = 1.00$, $\eta_{99} = 0.05$, $\eta_{218} = 0.010$ poise. Curve, 5: polybutene; $\eta_{25} = 20.0$, $\eta_{99} = 0.16$, $\eta_{218} = 0.016$ poise.

lubricating fluids. Serious deviations from linearity have recently been observed for several types of synthetic lubricants described in Table I.

The Antoine equation, often used for the correlation of vapor pressures, has also been found to represent the viscosity-temperature function of oils tolerably well:^{6, 6a, 6b}

$$\log \eta = A + \frac{B}{T + C} \quad (1)$$

⁶ F. Gutmann and L. M. Simmons, *J. Appl. Phys.* **23**, 977 (1952).

^{6a} H. Vogel, *Physik. Z.* **22**, 645 (1921).

^{6b} U. Rost, *Kolloid- Z.* **142**, 132 (1955); *Erdöl u. Kohle* **8**, 468, 549 (1955).

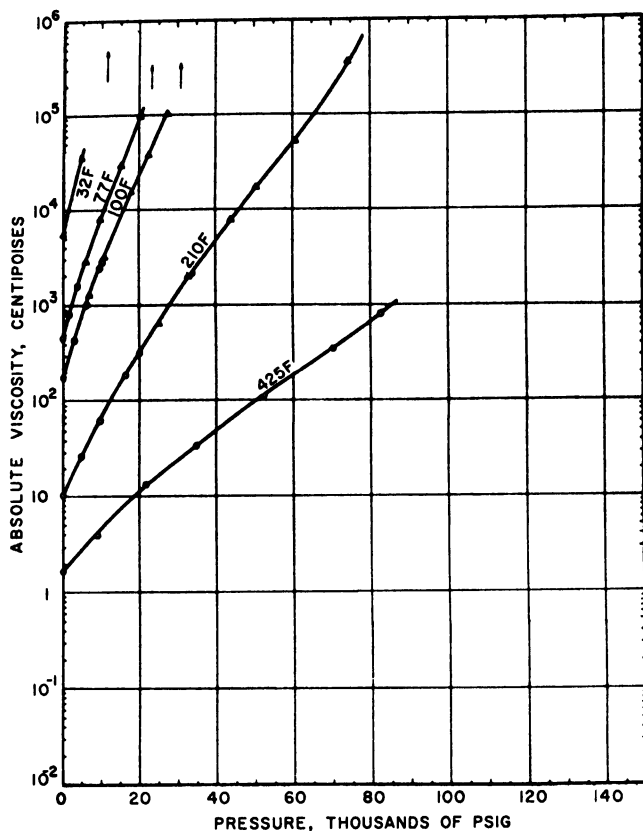


FIG. 1b. Viscosity-temperature-pressure relations for poly(dimethylsiloxane) fluid.¹

Another three-constant expression has been proposed by Cornelissen and Waterman⁷

$$\log \nu = A + (B/T^x)$$

where x has been found to take on values between 2 and 5, for mineral oils being generally near 3. The same equation with $x = 3$ had been obtained earlier for the viscosity of alcohols and polyols.⁸ The awkwardness of dealing with three constants of no particular physical significance will probably preclude widespread use of these expressions, unless general relations between the constants will be found. Not being based on any

⁷ J. Cornelissen and H. I. Waterman, *J. Inst. Petrol.* **42**, 62 (1956).

⁸ T. A. Litovitz, *J. Chem. Phys.* **20**, 1088 (1952).

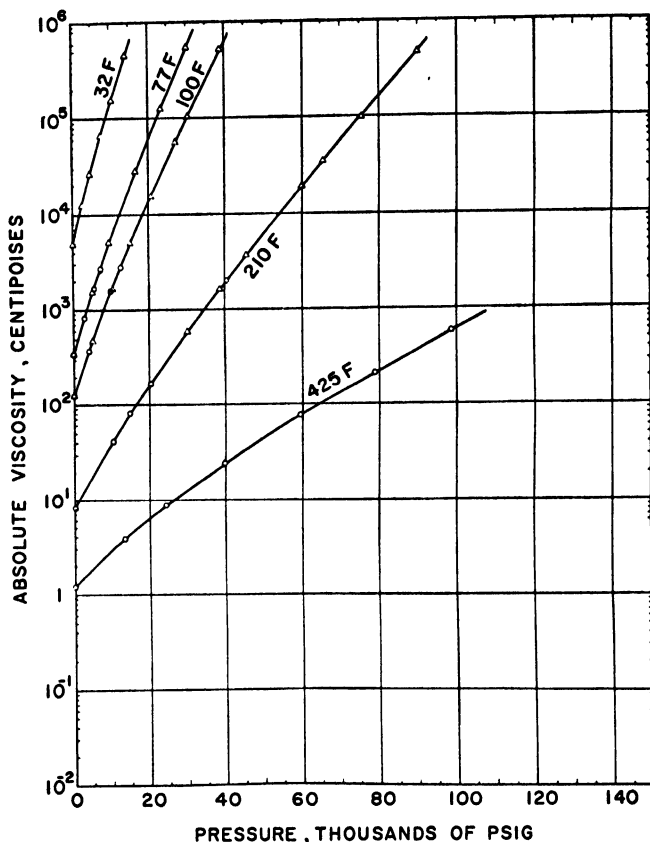


FIG. 1c. Viscosity-temperature-pressure relative for polyisobutylene of the same viscosity at 77°F. and 1 atmosphere as the siloxane sample of Fig. 1b.

theory, all of these relations should be considered as interpolation rules only.

Inspection of the viscosity-pressure curves shows that for a very large number of oils $\log \nu$ versus p is essentially a straight line while $\log \eta$ versus p is slightly curved concave downward in its initial portion. Oils with very flat viscosity-temperature curve tend to exhibit viscosity-pressure curves that are bent concave downward, whereas oils of very steep viscosity-temperature curves exhibit viscosity-pressure curves that are concave upward, and in general it is found that the initial slope of the logarithmic viscosity-pressure curve is related to the slope of the viscosity temperature curve by the simple relation

$$(\partial \log \eta / \partial T^{-1})_p = D(\partial \log \eta / \partial p)_T |_{p \rightarrow 0}$$

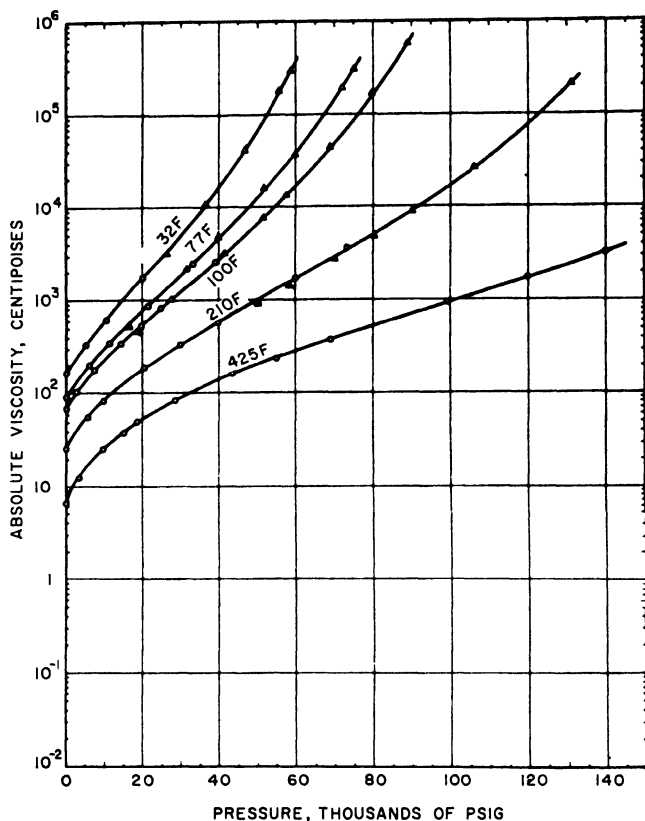


Fig. 1d. Viscosity-temperature-pressure relations for perfluorocarbon fluid.

where

$$D \approx 2.0 \times 10^5 \text{ } ^\circ\text{C. atm. or } 5.3 \times 10^6 \text{ } ^\circ\text{F. p.s.i.}$$

for most hydrocarbon oils.¹ This relation has foundation in theory, since for simple liquids⁹

$$\frac{(\partial \ln \eta / \partial T^{-1})_P}{(\partial \ln \eta / \partial p)_T} \propto (\partial E / \partial V)_T \quad (3)$$

where $(\partial E / \partial V)_T$ = internal pressure or cohesive energy density, a characteristic property of given families of liquids. Hence the relation is valid only for the members of a given family of liquids. The silicones, especially the dimethylsiloxane polymers, occupy a somewhat peculiar position. In keeping with their flat viscosity-temperature curve they exhibit a relatively

⁹ A. Bondi, *Ann. N. Y. Acad. Sci.* **53**, 870 (1951).

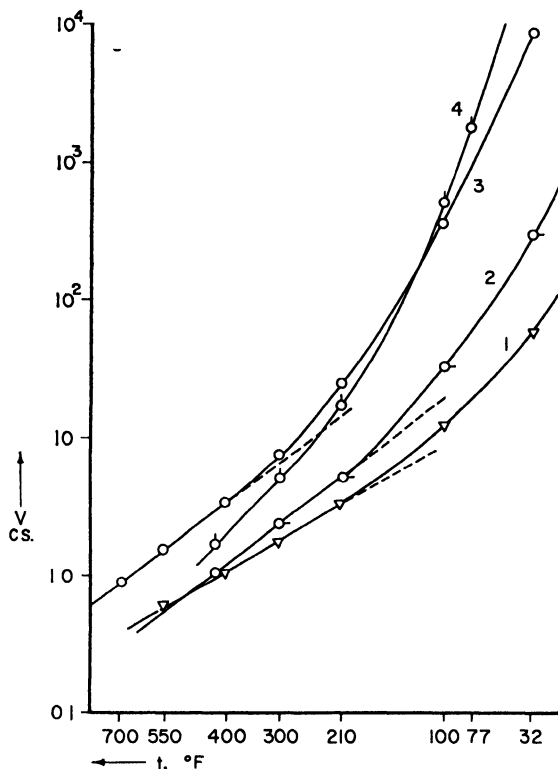


Fig. 2. Viscosity versus temperature curves of typical commercial lubricants. Most of the important range is covered between Curves 1 and 4. The coordinates are log (kinematic viscosity) versus reciprocal absolute temperature. Curve 1, di(2-ethylhexyl) sebacate. Curve 2, light lubricating oil (Sample 24-G of Ref. 1). Curve 3, aviation lubricating oil Navy Symbol 1120. Curve 4, naphthenic oil with 2500 SSU at 100° F. (Sample 38-G of Ref. 1.)

flat initial log ν versus p curve, which is concave downward. At about 3000 to 4000 kg./cm.² pressure the curve inflects and becomes steeply concave upward in character, such that a millionfold increase in viscosity is achieved for most silicone oils^{1, 10} at less than 8000 kg./cm.². This odd behavior has been ascribed to the interlocking of the rather regularly shaped molecules. The very similarly shaped polyisobutylenes also exhibit a sharply concave upward curvature. However, owing to the lesser compressibility of the hydrocarbons than of the siloxanes, the effect is less extreme. The logarithmic viscosity-temperature and pressure coefficients of high polymer solutions in oils (used as so-called viscosity-index

¹⁰ P. W. Bridgman, *Proc. Am. Acad. Arts Sci.* **77**, 115 (1948).

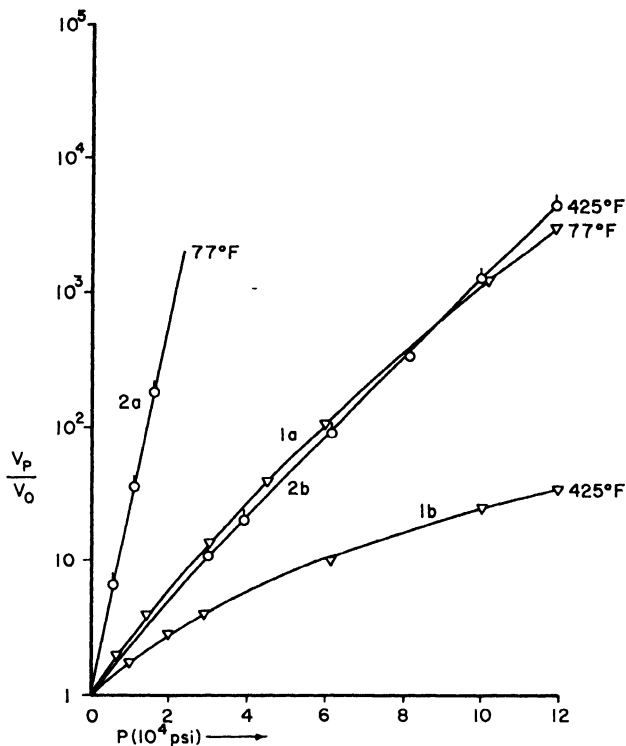


FIG. 3. Relative kinematic viscosity versus pressure curves for the two limiting lubricants of Fig. 2, indicating the large spread of pressure dependence encountered in practice. Curves 1a and 1b, Di(2 ethyl hexyl) sebacate. Curves 2a and 2b, naphthenic oil (2500 SSU at 100° F.). (Sample 38-G of Ref. 1.) All data from Ref. 1.

TABLE I
FIT OF VISCOSITY DATA ON ASTM VISCOSITY TEMPERATURE CHART
(Range Covered: -40 to 350° C.)

<i>Fluids</i>	<i>Viscosity range c.s. at 100°F.</i>	<i>Straight-line range, °C.</i>
Light petroleum oils	10-200	-20 to +150
Heavy petroleum oils	100-2000	0 to +160
Linear diesters	10-50	-40 to +150
Polyethers	20-50	0 to 150
	100	100 to 200
Polysiloxanes (methyl)	5-25	-40 to +50
	higher	-40 to +150
Polysiloxanes (methyl phenyl)	all	+40 to +150
Fluorocarbons		hardly any range

improvers) can to a first approximation be described as those of the oil without the polymer. To the extent that the viscosity increase of such high polymer solutions results from the hydrodynamic interference of the relatively large high polymer particles with the flow, this simple behavior should indeed be expected, viz., the relative viscosity of the polymer solution should be independent of pressure and temperature. Such simple behavior is found for a large number of commercial polymer solutions in oils over wider temperature range and up to a few thousand atmospheres pressure, as is evident from the data of Table II.

The understanding of the specific thickening effect of polymers, expressed as limiting viscosity number

$$[\eta] \equiv \left(\frac{\eta/\eta_0 - 1}{\phi} \right) \bigg|_{\phi \rightarrow 0} = \frac{\ln (\eta/\eta_0)}{\phi} \bigg|_{\phi \rightarrow 0}$$

(where η , η_0 = viscosity of solution and solvent, respectively, and ϕ = volume fraction of solute) has advanced sufficiently that one can predict, at least qualitatively, when the nonideal behavior $d[\eta]/dT' \neq 0$ and $d[\eta]/d_p \neq 0$ should occur. (See Chapter 14 of Vol. I for the theory and the properties of $[\eta]$.) The most general deviation from ideal behavior results from lack of flexibility of the backbone chain (Table III, Case II). The resulting stiffness makes the random coil and hence $[\eta]$ large, but as the flexibility must increase with temperature, the coil diameter and therefore $[\eta]$ decrease to the theoretical limiting value (corresponding to the random arrangement of a flexible molecule) as the temperature is raised. Owing to the preferred alignment with neighboring solvent molecules, a chain is always stiffer in solution than *in vacuo*. This effect becomes the more pro-

TABLE II
EFFECT OF PRESSURE AND TEMPERATURE ON THE THICKENING
EFFECT OF HIGH POLYMERS IN LUBRICATING OILS
(Expressed in Relative Viscosity $\eta_r = \eta_{\text{solution}}/\eta_{\text{oil}}$)
(Derived from Data of Bradbury *et al.*¹)

(Polybutene?)			Polybutene		Polymethacrylate	
Pressure p.s.i.	77°F.	210°F.	77°F.	210°F.	77°F.	210°F.
15	3.76	3.59	2.87	2.44	2.75	3.04
20,000	4.05	3.64	3.25	3.50	2.75	3.8
40,000	3.16*	4.17*	4.74	6.0	3.95	6.5
80,000	3.0	3.74		3.44		3.4
140,000				3.54		2.9

* At 60,000 p.s.i.

TABLE III
SUMMARY OF RELATIONS BETWEEN POLYMER STRUCTURE AND THE
VISCOSITY-TEMPERATURE-PRESSURE FUNCTIONS OF
THEIR SOLUTIONS

	Case I	Case II	Case III	Case IV
Chain flexible	+	-	+	-
Chain stiff	-	+	-	+
Solubility	good	good	bad (increases with temp.)	bad (increases with temp.)
$d[\eta]/dT$	0	negative	positive	S-curve thru 0
$d[\eta]/dp$	0	positive	negative	S-curve thru 0

nounced the closer the molecules approach each other. Hence the coil diameter, and $[\eta]$ for stiff molecules, increase as the pressure is raised.

If the chain is flexible but the solubility is poor (case III), the polymer chain may collapse entirely at some low temperature when the polymer comes out of solution. At all temperatures above the precipitation point, the coil is larger than at the collapse and increases and hence $[\eta]$ increases to the magnitude characteristic of the ideal solution as one raises the temperature. Since such nonideality of a solution usually means that the solution process is accompanied by volume expansion of the system, increasing pressure should decrease the solubility and thereby $[\eta]$, possibly leading to separation of the system at some high pressure.

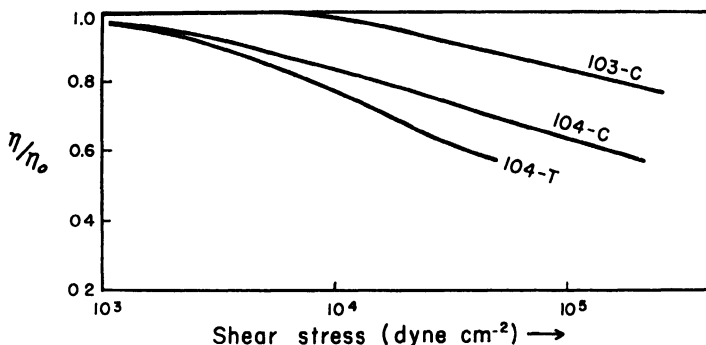
Many actual systems are composed of polymer molecules which are at least somewhat stiff and not in perfect solution in the oil at hand. In those cases (case IV) one observes that the $[\eta]$ versus T and the $[\eta]$ versus p curves go through maxima at those temperatures and pressures where the two opposing effects just balance. The few cases for which experimental data are available exhibit the maximum in the $\eta_r (\equiv \eta/\eta_0)$ versus pressure curve rather well (Table II). All of these general cases have been summarized in the table which also includes the "ideal" case of perfect flexibility and athermal mixture.

2. NON-NEWTONIAN FLOW OF OILS

The viscosity of simple liquids is not affected by the imposition of a shear field. Theoretical speculations indicate that at exceedingly high shear stresses there might be a viscosity reduction even for simple liquids.^{11, 12} Shear-dependent viscosity is of practical significance only for high polymer solutions. Typical data for such systems are shown in Fig. 4

¹¹ A. Bondi, *J. Appl. Phys.* **16**, 539 (1945).

¹² L. Grunberg and A. H. Nissan, *Nature* **156**, 241 (1945)

FIG. 4. Change of the viscosity of polymer solutions with shear stress.²TABLE IV
EFFECT OF SHEAR STRESS ON THE VISCOSITY OF POLYMER* SOLUTIONS

Oil	Temperature °C.	$(\eta/\eta_0)_{\min}\dagger$	$\left(\frac{\Delta\eta}{\Delta\eta_0}\right)_{\min}\S$	$\tau(\eta/\eta_0)_{\min}\parallel$ dynes/cm. ²	Ref.
API-103	38-100	0.80	0.72	10^5	#
API-104	38-100	0.60	0.44	10^5	#
B	38-100	0.77	0.40	2×10^5	**
D	38-100	0.82	0.60	2×10^5	**

* Polymers not identified in published reports.

† Observed relative viscosity at maximum available shear rate of apparatus.

§ Fraction of polymer thickening effect remaining corresponding to $(\eta/\eta_0)_{\min}$.|| Shear stress at which (η/η_0) has the indicated value essentially independent of temperature.# S. J. Needs, *Am. Soc. Testing Materials Spec. Tech. Publ. No. 111* (1951).** E. M. Barber *et al.*, *Anal. Chem.* **27**, 425 (1955).

and Table IV. The general value of this work is rather small since the polymers used have not been characterized. On the basis of a systematic investigation of the relation between viscosity versus shear-rate behavior and the molecular weight and structure of high polymers and their thermodynamic solution parameters one might be placed in a position to predict the behavior of polymer solutions in general.

Existing theory (discussed in Vol. I and Vol. II of this work) predicts in a qualitative way the manner in which molecular structure is related to the reversible shear reduction of the viscosity of high polymer solutions. However, so far the theory has not been put to sufficiently severe experimental tests to consider it as soundly established. In the high shear stress field, especially, under conditions involving cavitation, found in loaded journal bearings and in many oil circulation systems, irreversible reduction

of the viscosity of polymer solutions is experienced owing to the degradation of the polymer. Much of this degradation appears to be oxidative scission facilitated by the mechanical stress to which the system is exposed, and there is evidence that this degradation can be reduced by the addition of suitable oxidation inhibitors.¹³

The non-Newtonian behavior of two-phase lubricant systems, e.g., waxy systems and greases, will be discussed in Section II.

3. FLOW PROPERTIES AND HYDRODYNAMIC LUBRICATION

Elementary hydrodynamic theory of the load-carrying capacity of wedge-shaped fluid films knows only one physical property of fluids, their dynamic viscosity at the operating temperature. In principle nothing has been changed in this in more recent developments. The operating conditions have become so strenuous, however, that the temperature and pressure gradients in the fluid film lead to significant variation of lubricant viscosity throughout the load-carrying area. In order to account quantitatively for the variation of viscosity and thus the load-carrying capacity of the film under such conditions, data regarding the variation of viscosity with temperature and pressure as well as the physical properties have to be incorporated into the bearing equations, which determine the energy balance in the bearing, namely, the heat capacity and the thermal conductivity of the fluid.

The quantitative relationships of the important variables can be summarized in very few expressions. The load carrying capacity W of a wedge-shaped fluid element with constant viscosity η is given (for the journal bearing) by the simple relation

$$\frac{W}{\eta \cdot u} = 1.23 \frac{D^2}{Ch_0}$$

where u = tangential velocity of journal surface, C = diametrical bearing clearance, D = journal diameter, and h_0 = minimum thickness of fluid element. The frictional drag in such a system depends on the same variables in the manner

$$f = K \cdot \sqrt{\eta \cdot u / W}$$

where f = friction coefficient, K = numerical constant of the order of unity. As W acquires very high values it becomes necessary to include the change of viscosity with pressure, $\alpha \equiv (\partial \ln \eta / \partial p)_T$. Then for $\alpha \cdot p < 1$, $W(p)/W(o) = 1 + \alpha p$, where (p) and (o) refer to load-carrying capacity with and without consideration of pressure dependent viscosity, respec-

¹³ W. A. Zisman and H. A. Pohl, Publication Board No. 78601 (May 1943).

tively. It turns out that even for the largest value of $\alpha \cdot p$, $W(p)/W(o)$ can never exceed the value 2.3.^{13a}

The amount of energy dissipated by viscous drag in the film is often sufficiently large to call for explicit consideration of the temperature coefficient of viscosity $\beta \equiv (\partial \ln \eta / \partial T)_p$, and of the amount of heat convected by oil out of the film^{13b} $c\rho \cdot u$ and, at high speeds where radial temperature distribution is also important, the amount of heat conducted out of the film into the bearing, characterized by the thermal conductivity λ .

For the case of dominating circumferential temperature gradient, Vogelpohl^{13c} obtained the load carrying capacity with temperature-dependent viscosity $W(T)$ relative to the temperature independent case $W(O)$:

$$\frac{W(T)}{W(O)} \propto \left(1 + \frac{3\beta\eta_0 u}{\rho c e h_0}\right)^{-1}$$

Hence, for this case, of two oils with the same inlet viscosity η_i the one with the higher value of $\rho c / \beta$ will confer a higher load carrying capacity.^{13d} Where the radial temperature gradient in the oil film is most significant (i.e., at very high speeds) according to Hagg^{13e}

$$\frac{W(T)}{W(O)} \propto \left(1 + \frac{\eta_0 \beta}{2\lambda} u^2\right)^{-1}$$

Here, between two oils with the same viscosity η_0 at the bearing wall temperature the one with a smaller value of β/λ will provide the higher load carrying capacity. In both cases β is the more important property variable since ρc and λ vary only over very narrow ranges for the usual organic lubricating fluids.

It has been demonstrated by Cope^{14,15} that a finite load can be carried by a fluid film with parallel, not wedge-shaped, boundaries in adiabatic flow because of the pressure gradient established through thermal expansion of the fluid. This so-called thermal wedge effect is restricted to (thrust) bearings with very narrow clearances and the oil properties contribute to the load-carrying capacity proportionally with the ratio γ/β , where $\gamma \equiv (\partial \ln V / \partial T)_p$ is the thermal expansion coefficient of the oil.

^{13a} H. Blok, *Ann. N. Y. Acad. Sci.* **53**, No. 4, 779 (1951).

^{13b} ρ = density, c = specific heat, u = linear circumferential velocity of the oil.

^{13c} G. Vogelpohl, *VDI Forschungsheft* **386** (1937).

^{13d} e is a complicated function of the geometry of the film wedge, h_0 is the distance at closest approach.

^{13e} A. C. Hagg, *J. Appl. Mech.* **10**, A-71 (1944).

¹⁴ W. F. Cope, *Proc. Roy. Soc.* **A197**, 201 (1949).

¹⁵ A. Fogg, *Proc. Inst. Mech. Engrs. (London)* **155**, 49 (1946).

The two primary considerations in bearing design or oil selection are the load-carrying ability and the frictional drag. The first is defined as the load at which under the operating conditions the distance of closest approach of the rubbing surfaces is of the order of at least twice, but preferably five times, the average height of the surface irregularities and the frictional drag is a measure of the energy dissipated in the lubricated machine element.

Hydrodynamic separation of the bearing surfaces is sometimes achieved under surprisingly severe conditions. There is increasing evidence that gears with specific loadings as high as 10,000 kg./cm.² can be separated by a continuous film of oil.¹⁶ The conditions governing the formation and maintenance of such films are only now beginning to be understood.¹⁷⁻²⁰ It is rather evident that they are closely related to the mechanical design details of the gear teeth and the infrequency of observation of such types of gear lubrication must be taken as a consequence of the small number of tests which have been carried out with carefully designed and machined gears. The relation of oil properties at such high pressures to hydrodynamic gear lubrication has not yet been studied. The considerable dissipation of energy in the thin layer of lubricant must of necessity lead to the generation of high temperatures as well as high pressures. The evaluation of results is therefore likely to be complex. One may predict on the basis of the published properties (see Fig. 1) that the dimethyl siloxane fluids would develop such high viscosities²¹ that the shear stresses in the "fluid" film in the high pressure zone exceed the shear strength of the gear metals. Consequently shearing may take place in the metal instead of in the lubricant.

Shear stress dependence of viscosity must affect the friction factor of the bearing and its load-carrying capacity. Sharp reduction of viscosity in the region of highest shear rate in the bearing reduces the bearing friction. Such a reduction in bearing friction has indeed been observed with oils containing orientable high polymer molecules.²² The prediction

¹⁶ V. N. Borsoff *et al.*, *Trans. Am. Soc. Mech. Engrs.* **73**, 687 (1951).

¹⁷ A. von Mohrenstein and G. Niemann, private communications.

¹⁸ G. Niemann *et al.* *Z. Ver. deut. Ing.* **95**, 164, 167 (1953); and unpublished reports.

¹⁹ H. Poritsky, 1st Natl. Symposium Fund. Lubr., Am. Soc. Lubrication Engrs. (1952).

²⁰ C. Weber and G. Niemann, unpublished reports.

²¹ The ability of many, especially polymeric, liquids to support shear waves and exhibit shear stiffness may also play a role in gear lubrication.

²² F. W. Ocvirk and G. B. du Bois, *Natl. Advisory Comm. Aeronaut. unpublished report*.

of the load-carrying capacity of such a non-Newtonian oil film requires more subtle reasoning. The theoretical analysis for the general case of a non-Newtonian fluid predicts a flattened radial pressure distribution around the journal bearing compared with that which is obtained with lubricants of uniform velocity.^{23, 24} In that case the over-all load-carrying capacity corresponds to the average viscosity in the pressure zone. Experiments with a lime-soap grease at moderate speeds (and shear rates) are in reasonable agreement with both predictions of the theory.²⁵ Experiments with high polymer solutions in high-speed bearings, on the other hand, showed no reduction in load-carrying capacity although the oil viscosity and consequently the bearing friction had been reduced very appreciably by the flow-orientation effects.²² The explanation of this result is still outstanding.

The same materials which impart non-Newtonian viscosity, especially high polymers, also often impart elastic properties to their solutions. Oils with elastic properties are likely to exhibit the Weissenberg effect, i.e., the tendency to flow from regions of high shear stress to one of low shear stress. As a result such oil blends may be pumped very rapidly out of journal bearings.²⁶

II. Gelled Lubricants

1. LUBRICATING GREASES

Fluid lubricants have numerous advantages over any other form of lubricant. They can be circulated to act as coolant for the bearing, they can carry away the debris of their own decomposition or of extraneous origin and be clarified before their return to the bearing, and so on. But they have one fundamental disadvantage. They have to be retained in the bearing by, sometimes rather elaborate, sealing arrangements. When the cooling of the bearing is not essential, and where a simple bearing design is important, gelled lubricants are often used.

Lubricating greases, as gelled lubricants are generally called, differ therefore from fluid lubricants in the possession of a finite yield stress. The magnitude of the latter is usually just sufficient to prevent loss of lubricant under the operating conditions but not such as to offer significant resistance to the motion of the rubbing surfaces. A Bingham body would be ideally suited for this application. To a first approximation commercial lubricating

²³ K. B. Lawrence, *Trans. Am. Soc. Mech. Engrs.* **72**, 409 (1950).

²⁴ H. Umstatter, *Kolloid- Z.* **116**, 18 (1950); **118**, 37 (1950).

The reader should be warned of the fundamental errors in these papers. See discussion by W. Kochanowsky, *Kolloid- Z.* **142**, 32-45 (1955).

²⁵ G. Cohn and J. W. Oren, *Trans. Am. Soc. Mech. Engrs.* **71**, 555 (1949).

²⁶ G. F. Wood, A. H. Nissan, and F. H. Garner, *J. Inst. Petroleum* **13**, 71 (1947).

greases have indeed been found to act as Bingham bodies.^{27, 28} The gel structure of most greases is far too complicated, however, to fall into the exact pattern of a plastic body. The complex gel structure, made up of soap fibers of widely varying dimensions,^{29, 30} or of bentonite platelets,³⁰ or of sponges of silica gel³⁰ with a wide distribution of particle sizes and bending strengths is hardly likely to exhibit a single well-defined yield stress. One should rather expect successive yielding of structure elements in increasing strength and therefore a pseudoplastic trailing off of the flow curve at low shear stresses.

At very high shear stresses the flow resistance is generally only a small multiple of that offered by the oil itself. It has been argued that at very high shear stresses the cohesion between gel particles makes only a negligible contribution to the flow resistance. One should then be able to consider intrinsic viscosity of the gel agent at high shear stresses as a manifestation of its geometry similar to the case of no interaction, i.e., at infinite dilution.³¹ In the few cases which have been so examined the geometry of the soap fibers deduced from viscosity was in reasonable agreement with electron microscope evidence. The general applicability of such a method appears questionable, however, since the measurements of gel viscosity at high shear stresses is bedevilled by numerous complications, such as temperature gradients in the steaming system, onset of turbulence, induced by the nonhomogeneous nature of the system. Most important, however, is the shear degradation of the gel particles themselves. Their geometry changes often irreversibly under the influence of the applied shear stress,³² further complicating the interpretation of the flow data.

Owing to the relative proximity of the absolute flow resistance value at high shear stresses to that of the oil, their knowledge is of relatively little practical interest. Of far greater practical importance is the behavior of greases under the influence of low shear stresses, i.e., under near static conditions.

At small deformations, e.g., strains of the order of 10^{-2} , many greases exhibit noticeable elastic deformation with deformation versus time curves very similar to those of other elastic-plastic systems, and illustrated in Fig. 5. Numerous curves like these have been discussed in the litera-

²⁷ C. R. Singleterry and E. E. Stone, *J. Colloid Sci.* **6**, 171 (1951).

²⁸ H. E. Mahnke and W. Tabor, *Lubrication Engr.* **11**, 22 (1955).

²⁹ A. Bondi *et al.*, *Proc. 3rd World Petroleum Congr., Hague Sect. 7*, 373 (1951).

³⁰ B. B. Farrington, *Ann. N. Y. Acad. Sci.* **53**, 979 (1951).

³¹ G. B. Moses and I. E. Puddington, *Can. J. Research* **27B**, 616 (1949).

³² R. J. Moore and A. M. Cravath, *Ind. Eng. Chem.* **43**, 2892 (1951).

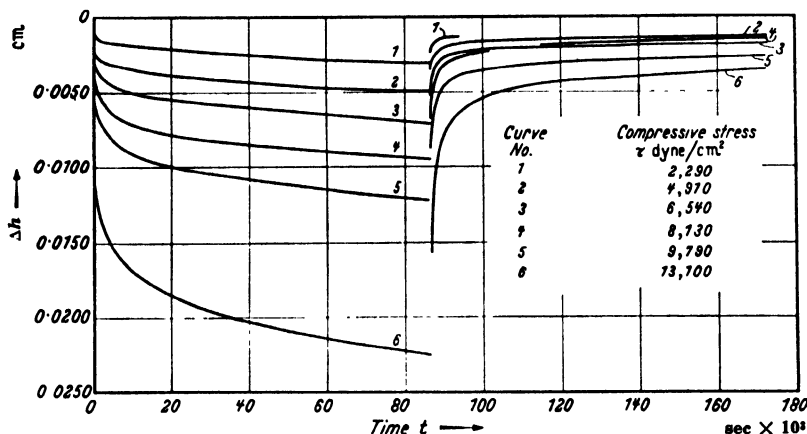


FIG. 5. Elastic recovery of lubricating greases.³³
(Stress released at 90 sec)

ture,³³⁻³⁵ but neither their relation to gel structure (or composition) nor to lubrication problems have as yet been systematically explored.

The yield stress of greases is only rarely measured by theoretically acceptable means. Careful direct measurements have brought to light that many greases have not one but two yield values.³⁶ The "first" yield value, generally of the order of a few hundred to about one thousand dynes per square centimeter, is very difficult to measure and probably represents the yield stress of the mixture of gel fiber ends, gel debris, and oil in the boundary layer between grease and the solid surface of the measuring device. The "second" yield value is more readily determined by a wide variety of instruments, such as the parallel plate plastometer, the cone penetrometer,³⁶ the shear blade²⁷ and the Bingham-type or Goodeve-type evaluation of shear rate versus shear stress curves obtained in viscometers of various types.^{27, 31} Since the yield stress of real bodies is the stress at which measurable permanent deformation takes place during the period of observation, there is great likelihood that the various methods used will differ with respect to what is "measurable" and with respect to the time factor. Considering these inherent differences between instruments the reported agreement²⁷ between different methods on identical samples must

³³ J. F. Hutton and J. B. Matthews, *Proc. 2nd Intern. Rheol. Congr. Oxford*, p. 408 (1953).

³⁴ E. W. J. Mardles "Selected Government Research Reports, Lubricants and Lubrication." H. M. Stationery Office, London, 1952.

³⁵ G. Vinogradov *et al.*, *Neftyanoe Khoz.* **25**, 47 (1947); **26**, 52 (1948).

³⁶ J. F. T. Blott and W. B. Bonner, *Proc. 1st Intern. Rheol. Congr. Scheveningen* Sect. 2, p. 265 (1948).

be considered as about as good as could be expected. For engineering purposes it is sufficient to determine the yield stress of a grease to $\pm 30\%$, and for the more critical identification purposes in the trade one must always adopt standardized methods of measuring procedure.³⁷

The yield stress τ_y determines the equilibrium height H of a self-supporting grease dam according to the relation

$$H = \tau_y / \rho g$$

where ρ = density of the grease and g = gravitational acceleration (acting in compression on the grease). Since the yield stress in shear is of the same order as the yield stress in compression, one can use the same formula to estimate (crudely) the tangentially acting centrifugal acceleration g_c (substituted for g) at which a grease layer of thickness H slides off a rotating surface, if $H \leq 1$ mm. and if the grease sticks well on the surface. If the grease does not wet the surface properly, or if oil is exuded in the grease-solid interface, the formula predicts too high a value for g_c . Acceleration normal to the grease layer acting in tension leads to a more complicated type of rupture, typical of a Taylor instability, while the yield stress plays only a minor role.

Like other plastic materials lubricating greases exhibit creep at (shear) stresses below the yield stress. This creep flow is non-Newtonian in character and has been ascribed to the sliding of the bulk of the grease on a layer of oil and gel ends and debris which tends to form at the interface between solid walls and the grease.³⁹

At stresses slightly in excess of the yield stress one often finds for a limited stress range a pseudo-Newtonian flow, which has been ascribed to the sliding of the bulk grease on the oil layer mentioned above but at shear stresses at which the few gel particles make no contribution to the flow properties. As the shear stress is raised far beyond the yield stress the flow resistance decreases in a regular fashion until it approaches the viscosity of the oil, as mentioned above. When plotted as $\log \eta_{(\text{apparent})}$ vs. $\log \dot{\epsilon}$ nearly straight lines of slopes ~ 0.6 to 0.7 are obtained between $\dot{\epsilon} \sim 5$ and $\dot{\epsilon} \sim 5000$ per second.⁴⁰ Admixture of high polymers, especially to acetylene black gels⁴¹ causes the appearance of steplike discontinuities in the η vs. $\dot{\epsilon}$ curves, the origin of which is as yet obscure, but may be

³⁷ See, for instance, ASTM.³⁸

³⁸ American Society for Testing Materials Method 3 97-47.

³⁹ A. Bondi, *Trans. Soc. Rheol.* **2**, (1958).

⁴⁰ J. P. Patberg, Sproule, L. W. and J. C. Zimmer, *Inst. Spokesman* **6**, (8, 9, 10, 11) (1942/37); **7** (12) (1944); **9** (15) (1945).

⁴¹ Standard Development Co., U. K. Pat No. 607,695 (1948).

caused by the introduction of strongly elastic components of deformation.

All of the aforementioned properties change with temperature in a complicated manner. Initially, i.e., at temperatures far below the first transition temperature of the soap (if that is the gelling agent), all of them decrease in magnitude exponentially as the temperature is raised. A few degrees below the first transition temperature of the soap, the extent depending upon the chemical composition of the oil, the flow resistance, and the yield stress begin to increase with temperature, pass through a maximum, possibly through a minimum and through additional maxima, depending upon the number of phase transitions of the soap. Finally the viscosity decreases steeply to nearly that of the oil, all of the gelling ability of the soap being lost when the soap dissolves in the oil. Only few data have been published on the temperature function of the flow properties of nonsoap gels. Contrary to first thought these need not be simple functions. A flocculate gel structure *in vacuo* would probably not change its strength over a wide range of temperature. However, in a liquid environment the strength of particle interaction is reduced by the adsorption of the molecules of the liquid. Particle cohesion, in liquids of very similar cohesion energy to that of the particles or their surface may even approach zero. Very strongly adsorbed third components of the liquid may so change the particle surface and thus particle cohesion to mask the inherent properties of the solid. The picture is often further complicated by the very different, but often important effect of a thick (duplex or thicker) layer of a second liquid which is insoluble in the bulk liquid and makes the particles stick together by meniscus formation.⁴²

In pure liquids raising the temperature reduces the lifetime of adsorption, and adhesion of collided particles becomes increasingly frequent. Hence the gel strength increases as the temperature is raised. Desorption of a surface active component may accentuate the often steep increase in flocculating tendency with temperature. The concurrent reduction in viscosity of the matrix liquid somewhat counteracts the increasing gel strength of the particle network. The resulting net flow resistance and yield stress may therefore present a far-from-simple temperature curve, the details of which have to be worked out anew for each system. In general one finds the drop in both to be less steep than with many soap greases. In special cases quite the opposite, namely, initially extremely steep curves can also be obtained which tend to flatten out at the higher temperatures.

All of what has been said so far regarding the flow properties of lubricat-

⁴² H. R. Kruyt and F. G. Van Selms, *Rec. trav. chim.* **62**, 415 (1943).

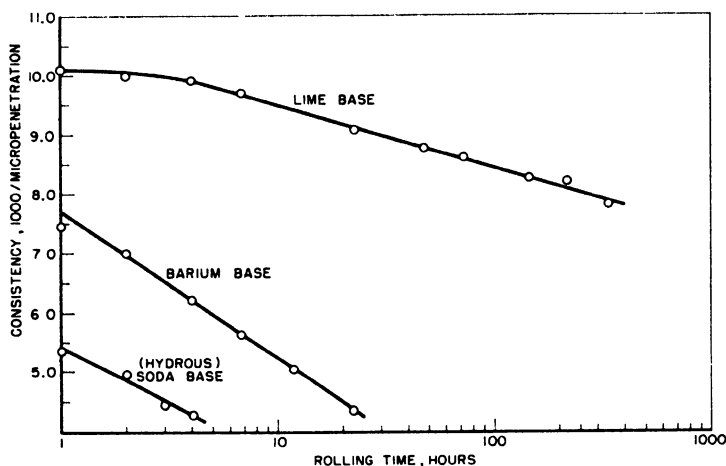


FIG. 6. Shear degradation of lubricating grease.^{29, 32}

ing greases pertains only to the instantaneous values of these properties. Since the bond strength between the gel particles, whatever their nature might be, is of the order of kT , the application of shear energy even in the very act of measurement causes irreversible changes in particle configuration. If the applied shear stress is great enough or the amount of work done on the system large enough, actual particle comminution or in some cases particle agglomeration may be induced. Upon return to rest the changed system will then acquire a new configuration. The result is that all properties of greases are strongly time-dependent and can be thoroughly changed by continued shearing.

In the case of soap grease the shear degradation is primarily associated with the comminution of the particles.³² Typical degradation curves are shown in Fig. 6. The mechanism of consistency recovery upon return to rest of the system is far less understood. It is often called thixotropy⁴³ but is only rarely truly characterized by this designation since the original definition of thixotropy (by Freundlich) implies a reversible process. The fact that very frequently the consistency of the recovered system after severe shearing is far higher than that of the unsheared sample demonstrates the inapplicability of the term thixotropy to these phenomena. Much further work is required to clarify the kinetics of particle bonding responsible for the hardening.

Attempts have been made to describe the flow properties of greases in terms of continuum mechanics or as superposition phenomena of different

⁴³ L. W. MacLennan and G. H. Smith, *Am. Soc. Testing Materials Bull.* No. 152, 71 (1948).

types of bonds which have to be broken.⁴⁴ After what has been described above, such approaches, while courageous, can hardly be expected to provide new insight into the flow processes even if they provide an acceptable formal description of the instantaneous flow curves. Recent simultaneous electrical and mechanical measurements have further shown that the flow of greases is rather likely to proceed in the manner of fruit jams, namely, by relative motion of elastically deforming gel lumps.^{45, 46} On simple consideration of the process of yielding of crystalline solids, which always proceeds through discontinuous flow glide plane production in the crystal lattice, it becomes clear that a body with finite yield stress or yield stress range can only flow if comminuted into smaller macroscopic parts, the size of which depends upon the applied shear stress. A theory describing grease flow on this basis has not yet been developed.

2. FLOW PROPERTIES OF FROZEN OILS

Oils increase in viscosity as the temperature is lowered by two distinctive mechanisms. One type of oil simply turns into a transparent glass, i.e., the viscosity increases smoothly and reaches values which prohibit its use as a lubricant. Other oils, may crystallize partially. The precipitated wax crystals form a coherent network and the oil stiffens before the viscosity of the fluid components has reached very high values. The flow properties of the waxy two-phase mixture do not differ significantly from those of the lubricating grease discussed above. Owing to the weakness of the wax crystals irreversible shear degradation is brought about by relatively small shearing forces.

The flow diagram of frozen waxy oils is therefore rather less well defined than that of grease, its position often depending upon the shear stress at the start of the experiment. In addition, owing to the weakness of the structure the flow resistance becomes effectively Newtonian at relatively low shear stress. The maximum shear stress that can be applied to such systems is limited by the consideration that any appreciable energy dissipation will lead to sufficient temperature rise to melt part of the solid structure. In experiments with continued shearing such partial melting of the structure has been shown to occur.⁴⁷ Continued working at sufficiently low shearing stresses to exclude appreciable temperature rise the shear degradation of the waxy component of many oils has been found to depend only upon the total work input.⁴⁸

⁴⁴ R. E. Powell and H. Eyring, *Nature* **154**, 427 (1944).

⁴⁵ A. Bondi and C. J. Penther, *J. Phys. Chem.* **57**, 72 (1953).

⁴⁶ A. Bondi, *Proc. 2nd Intern. Rheol. Congr. Oxford* p. 274 (1953).

⁴⁷ S. P. Jones, Jr., and T. K. Tyson, *J. Colloid Sci.* **7**, 272, (1952).

⁴⁸ G. Gavlin, E. A. Swire, and S. P. Jones, Jr., *Ind. Eng. Chem.* **45**, 2327 (1953).

The yield stress of frozen oils is of the order of 100 to 1000 dynes/cm.² in the temperature range in which one can handle the oil successfully in pipelines (*v.i.*).^{2, 49} By use of suitable agents, so-called "pour point depressants," the yield stress of frozen oils can be reduced appreciably.^{2, 50} Independent of oil composition, the logarithm of the yield stress of frozen oils has been reported to be generally proportional to the inverse absolute temperature at reasonable distances from the "pour point" of the oil.⁵⁰ The thermal and the mechanical history of the sample must be carefully reproduced to obtain useful information related to the problem that is to be investigated. A common but not very useful measure of the low temperature behaviors of oils is the temperature at which, under carefully specified conditions, an oil column of small height ceases to flow under the influence of gravity. This temperature is called the pour point. Many oils with relatively weak wax structure will easily flow below this temperature under the application of but mild shearing stresses.

The formation of a coherent wax structure can be prevented by a wide variety of compounds, all of which are characterized by the possession of paraffin chains and some noncrystallizing groups in their molecular structure.⁵¹ Since the energy of adsorption on a hydrocarbon surface out of a hydrocarbon solution must be quite small, it is believed that the paraffin chains of these compounds, the pour point depressants, somehow interact, even if only in a two-dimensional way, with the paraffin chains of the wax crystals. The relatively great specificity of interaction between pour-point depressants and certain wax types is in accord with such a view.⁵¹ These agents do not only reduce the yield strength of the wax structure and the temperature at which the oil will stiffen but also reduce the flow resistance at moderate shear stresses by very large factors.²

3. MOTION OF GELLED LUBRICANTS THROUGH PIPES

Gelled lubricants, both frozen oils and greases, have to be moved through pipes. In order to appreciate the problem of doing so one must realize that the available shear stresses in refinery pumping systems, especially the suction lines, range between 100 and 1000 dynes/cm.², while in grease-distributing system they may be of the order of 10,000 to 50,000 dynes/cm.². Obviously in either case the yield stress of the lubricant has to be lower than the available shear stress in order to permit flow to occur. Once flow has set in, the resistance to motion decreases, owing to the shear breakdown of the gel structure.

The prediction of the grease flow rate through pipes can be carried out

⁴⁹ F. Gill and R. J. Russell, *Ind. Eng. Chem.* **46**, 1264 (1954).

⁵⁰ K. S. Ramaya, *Conf. on Viscosity of Liquids and Colloidal Solns. U.S.S.R.* **2**, 179 (1944).

⁵¹ R. A. Ruehrwein, *Proc. 3rd World Petroleum Congr. Hague Sect. 7*, 423 (1951).

in various degrees of sophistication. The simplest approach is to assume that grease is a Bingham body with a well defined yield stress τ_y and a mobility m . The integrated form of the Bingham differential equation for pipe flow, the Buckingham equation then predicts the flow rate as:

$$\dot{q} = \frac{\pi D^4 m \Delta p}{128 L} \left(1 - \frac{4}{3} \Pi + \frac{1}{3} \Pi^4 \right)$$

where $\Pi = \tau_y / \Delta p$ and D = pipe diameter. The agreement between the pipe flow predicted by means of this equation from data obtained with small capillaries or Couette viscometers and actual performance is only moderately good.^{52a}

Very much better results are obtained through use of the empirical Ostwald relation

$$\tau_w \propto \dot{\epsilon}^n \text{ when } \tau_w > \tau_y$$

where τ_w = shear stress at the wall, $\dot{\epsilon}$ = shear rate. For pipe flow, this relation takes the form

$$D \Delta p / 4 L = k (8u/D)^n$$

where u = average velocity of grease in the pipe. The exponent n is a measure of the deviation from Newtonian flow, where $n = 1$. For lubricating greases, n and k are constant only over ranges of about one to two decades in $\dot{\epsilon}$. In the ranges of practical interest in pipe flow ($\dot{\epsilon} = 5$ to 100 sec.^{-1}), n for greases ranges generally between 0.1 and 0.4. Since according to Metzner and Reed^{52b} the velocity profile is essentially that of plug flow for $n = 0.2$, the utility of the Ostwald relation is consistent with Mahnke's (28) visual observation of plug flow for lubricating greases.

From an engineering point of view it is useful to know that pipe flow of greases can be predicted from the usual Fanning friction factor f versus N_{Re} graph if one defines the Reynolds number as

$$N_{Re} = \frac{D^n \cdot u^{2-n} \cdot \rho}{k \cdot 8^{n-1}}$$

where ρ = density of grease. In the laminar flow region, then,

$$\frac{\Delta p}{L} = \frac{32k \cdot 8^{n-1} \cdot u^n}{D^{n+1}} = \frac{32k \cdot 8^{n-1}}{D^{3n+1}} \left(\frac{4\dot{q}}{\pi} \right)^n$$

Hence the pressure drop in grease flow is very much less sensitive to pipe diameter than it is with Newtonian fluids; or conversely one may increase

^{52a} L. C. Brunstrum and R. H. Leet, *Lubrication Eng.* **12**, 316 (1956).

^{52b} A. B. Metzner and J. C. Reed, *A. I. Ch. E. Journal* **1**, 434 (1955).

the grease flow rate \dot{q} through a given pipe many fold without experiencing large increases in pressure drop if n is small.

A large range of τ and $\dot{\epsilon}$ can be covered with a single set of constants when the Powell-Eyring (44) equation

$$\tau = \eta \cdot \dot{\epsilon} + \frac{1}{B} \sinh^{-1} \left(\frac{1}{A} \dot{\epsilon} \right)$$

is employed.^{52a} The experimental determination of the constants η , A , and B is somewhat awkward, and a graphical method^{52a} has been developed to facilitate the process. It has not yet been established whether the constants of this equation really have the physical significance originally attached to them in their theoretical development.

None of the previous equations considered the (thixotropic) breakdown which the grease suffers as it moves through the pipe. An experimental correction for this loss in consistency with time of stress application has been proposed.^{52d} It is based on the empirical observation that

$$\tau = \dot{\epsilon} \cdot C (L/u)^m$$

where C and m are constants, $m < 1$, which can be determined in suitable laboratory experiments. The pressure drop in a pipe is smaller than that calculated in the absence of this effect by a factor of the order of $1/C(u/L)^{1+m}$. A peculiar phenomenon is the delayed and incomplete pressure transmission through lines filled with gelled oils, such that even under static conditions the full pressure is not transmitted to the end of a pipe.⁴⁹ This phenomenon makes the use of pressure taps very ill advised, even on viscometer bodies, and membranes flush with the wall should be used instead.^{52e, 53}

Very viscous oils move through pipes with a distorted velocity profile even in the absence of any structural anomalies if the viscous energy dissipation generates enough heat to create a significant temperature gradient in the oil. The complicated mathematical problem of flow with energy dissipation, heat transfer and the usual steep temperature dependence of viscosity has been solved by von Schlippe.^{52f} The calculations show that an oil flowing at given velocity through a cooled pipe can be cooled only to a certain minimum temperature at which heat generation and heat

^{52a} E. B. Christiansen, N. W. Ryan, and W. E. Stevens, *A. I. Ch. E. Journal* **1**, 544 (1955).

^{52d} J. W. Wilson and G. H. Smith, *Ind. Eng. Chem.* **41**, 770 (1948).

^{52e} P. G. Exline and J. R. Aikens, U.S. Patent 2,503,860.

^{52f} B. von Schlippe, Bericht No. 9, Deutsche Versuchsanstalt für Luftfahrt, Köln, 1956.

⁵³ N. Marusov, U.S. Patent 2,503,676.

flow to the outside just balance. As a consequence of this result, one finds that the pressure drop can be much smaller (by as much as one or two orders of magnitude) than one would have predicted without consideration of the internal heating effect.

4. HYDRODYNAMIC LUBRICATION WITH GELLED LUBRICANTS

Theoretical calculations of the load-carrying capacity and the frictional resistance of macroscopic films of gelled lubricants have been presented recently. The case of journal-bearing lubrication was worked out for a pseudoplastic lubricant utilizing its empirically determined curve of apparent viscosity versus shear rate.²³ The theory predicts, in agreement with experiment, that the pressure distribution around a bearing is rather flatter with a pseudoplastic body than it is with Newtonian fluids. The other published theories start from the assumption that the lubricant can be described adequately as a Bingham body with yield stress τ_y and mobility m . (The inverse of m is often called "plastic viscosity.") The calculations, carried out for a slider bearing,⁵⁴ for the "squeeze-film,"⁵⁵ and for the equivalent of the hydrostatic bearing,⁵⁶ indicate an appreciable gain in load-carrying capacity over that obtainable with a Newtonian fluid of equal mobility, especially at low velocities. In fact, the theory predicts the possession of a finite load-carrying capacity, proportional to τ_y/h (where h = bearing clearance) at zero velocity.

The latter result should not be taken too literally, however, because lubricating greases creep at a sufficiently high rate even at loads of the order of half their short-time yield stress that permanent separation of bearing surfaces at zero velocity should not be expected.

III. Flow Phenomena in Boundary Lubrication

Boundary lubrication always involves the simultaneous deformation of the solid bearing metal and of the lubricant layer. The finite wear rate coupled with a friction coefficient much lower than is obtained for the rubbing of metallic solids in direct contact testify to the importance of the simultaneous incidence of both phenomena.

1. FRICTION OF SOLID SURFACES

The mechanics of the friction of solid surfaces involves deformation and destruction of the rubbing solids on a macroscopic scale. The work

⁵⁴ A. A. Milne, *Proc. 2nd Intern. Rheol. Congr. Oxford* p. 427 (1953).

⁵⁵ F. Osterle and E. A. Saibel, *Lubrication Eng.* **11**, 187 (1955).

⁵⁶ F. Osterle and E. A. Saibel, *Am. Soc. Mech. Engrs.-Am. Soc. Lubrication Engrs. Meeting*, October 1955, Paper 55 LUB-6.

of Holm⁵⁷ and of the Bowden school⁵⁸ has amply demonstrated the deformation in depth which accompanies the rubbing effects on solid surfaces. The surfaces of solids are never smooth on a microscopic scale. Asperities, the size and size distribution of which is determined by the finishing treatment which the surface received, are always contacted first as one solid is lowered on another. The "true" area of contact is thus only a small fraction of the geometrical contact area. By electrical methods it has been shown that over a range of contact pressures the deformation of the asperities follows a law such that the true area of contact is directly proportional to the load, if both solids are metals.^{57, 58}

The specific load at the contact points is always sufficient to cause plastic deformation of the asperities involved. The plastic flow, i.e., the sliding of crystal grains past each other along linear slide paths, is of itself occasionally the source of additional surface irregularity which prevents disengagement of the asperities as they are moved past each other and may lead to their breakage in the cross section just beyond their work-hardened area.⁵⁹ Very often, if not most often, the pressure is sufficient to cause "pressure welding" of the asperity junctions, and subsequent "plucking out" of parts of the weaker asperities.⁵⁷ The friction of metals is probably very often just due to these local adhesions and represents the force necessary to shear the small junctions.

Analysis of the foregoing model led to the conclusion that the friction force $F = As$, where s = shear strength of the weaker of the junctions and A = true area of contact. The latter depends on the load W according to the simple law $A = W/P_m$, where P_m = yield pressure of the softer of the two solids. Hence the friction coefficient μ of unlubricated rubbing solids can be expressed in terms of the flow properties of the softer of the two solids in contact as

$$\mu = F/W = s/P_m$$

More detailed consideration of the life cycle of a single junction in plastic deformation⁶⁰ shows that for the usual surface roughness, where the angle of ascent of the hills is of the order of 10° , the initial shear stress on the junction is $s_1 \sim 1.2 P_m$, the normal stress $P_1 \sim 2P_m$, regardless of the hardness of the metal. For strong junctions which fracture when the normal load is at its maximum, the minimum value of μ is $s_1/P \sim 1/2.6 \sim 0.4$. For a junction which survives to a symmetrical shape, $\mu \sim 1$. For very ductile materials where the junction survives even when W becomes

⁵⁷ R. Holm, "Electrical Contacts." Stockholm, 1946.

⁵⁸ F. P. Bowden and D. Tabor, "Friction and Lubrication of Solids", Oxford Univ. Press, London and New York, 1951.

⁵⁹ I. M. Feng, *J. Appl. Phys.* **23**, 1011 (1952).

⁶⁰ A. P. Green, *Proc. Roy Soc.* **A228**, 191 (1955).

tensile, $\mu > 1$. Superposition of elastic straining of the bulk material behind the junction raises s_1 and reduces P_1 , thus increasing μ . It is apparent from this analysis that brittle substances, fracturing readily in tensile deformation, should exhibit lower friction coefficients than ductile substances, if both sliders form strong junctions.⁶⁰

The macroscopic theory of solid friction by Bowden⁵⁸ and by Holm⁵⁷ leads to useful results only as long as the solid surfaces are covered by a nonmetallic layer—it need only be one atom thick—to prevent gross welding on contact.

If the metal surfaces are absolutely clean, contact leads to instantaneous cementation of the surfaces, the junctions acquiring the bulk shear strength of the solid, and friction coefficients as high as 100+ are observed, if both surfaces are made of the same metal.⁶¹ The usually known friction coefficients of the order of unity or less are generally associated with the presence of oxide layers of low shear strength on the surface. The presence of the oxide layers and their behaviors during sliding, etc., is easily demonstrated by electrical measurements.^{58, 62, 63} If the flow properties of oxide and substrate metal are similar, as for Al, Cd, and Zn, mechanical disruption of the oxide layer has little effect on friction. If the oxide has a greater shear strength than the metal, the friction coefficient drops as the oxide film breaks down, i.e., as the load is raised beyond a certain point, whereas with copper, where the oxide film exhibits the lower friction coefficient, the breakage of the oxide film is accompanied by a sharp rise in the friction coefficient, as is shown by the η versus W curves of Fig. 7. The harder the metal substrate of a given oxide, the lower the depth of penetration into it, hence the lower the coefficient of friction.⁶³ Chromium is so far the only known substance the oxide and metal of which are both so hard that no breakage of the oxide layer occurs over the entire $\sim 10^6$ -fold load range studied, and consequently the friction coefficient likewise does not change over the same load range.

The ultimate-strength properties of macroscopic solids depend on the number of flaws (crystal imperfections, dislocations, and cracks) in the stressed region. Very small samples or very small regions of large samples are therefore much stronger than predicted from measurements on large samples. These strength anomalies have been observed by Smekal⁶⁴ and Hunt⁶⁵ and are likely to become important for surface asperities of the order of one micron or less. Such small roughnesses occur rarely in lubrication.

⁶¹ A. T. Gwathmey, *Ann. N.Y. Acad. Sci.* **53**, 987 (1951); *Proc. Roy. Soc.* **A212**, 464 (1952).

⁶² W. E. Campbell, *Lubrication Eng.* **9**, 195 (1953).

⁶³ R. Wilson, *Proc. Roy. Soc.* **A212**, 450 (1952).

⁶⁴ A. Smekal, *Kolloid-Z.* **131**, 106 (1953).

⁶⁵ F. V. Hunt, *J. Appl. Phys.* **26**, 850 (1955).

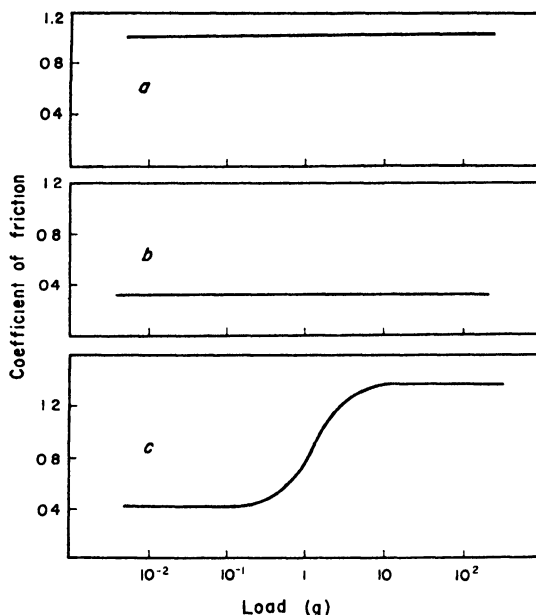


FIG. 7. Coefficient of friction as function of load.⁶⁵ a) Sn sliding on Sn, b) Cr on Cr, c) Cu on Cu.

tion practice, but their peculiar properties should be kept in mind when dealing with wide roughness distributions or with specially treated surfaces.

Combinations of the relatively soft polymeric bearing materials and hard metallic sliders (or shafts) are becoming popular in many applications. This combination differs from the usual metallic systems in several important respects. Since now the deformation of surface asperities is predominantly elastic, we expect, if Hertz's law is followed, that the true area of contact vary not proportionally to the load W as in the plastic case but according to the relation

$$A \propto (W/E)^{2/3}$$

where E = elastic modulus of the substance. Hence the friction force $F \propto W^{2/3}$ and the friction coefficient $\mu \equiv F/W \propto W^{-1/3}$, at least at low loads.^{66, 67} The change of the elastic properties of polymers, especially of rubbers, at large deformations leads to more complicated relations when wide load ranges are considered. A rather good empirical correlation of the data has been obtained with an equation of the form

$$1/\mu = B[1 + (15p/E_0)]$$

⁶⁶ A. Schallamach, *Proc. Phys. Soc. (London)* **B65**, 657 (1952).

⁶⁷ K. V. Shooter, *Proc. Roy. Soc.* **A212**, 488 (1952).

where p = pressure (load per unit surface), E_0 = compression modulus (in the same units as p), and B = a property of the rubber. This relation describes the data for friction of various rubber on smooth hard surfaces over the range $10^{-4} < p/E \leq 10$.⁶⁹

On rough surfaces the true contact area and therefore the friction coefficient against rubbers is also smaller than on polished surfaces. Using a surface of hemispheres as model for the rough hard surface, one obtains $F \propto W^{8/9}$ or $\mu \propto W^{-1/9}$. This peculiar effect of roughness has been verified experimentally.^{68a, 69}

While with ordinary bearing metals the velocity imparted by a given tangential force is constant, and the friction coefficient essentially independent of temperature, the rubbing velocity of a rubber slider increases (at constant F) with path length toward a constant value v . The magnitude of v (at a given F) increases exponentially with temperature and can be described by the relation

$$v = v_0 \exp \{ -(\Delta E_{\neq} - \gamma F)/RT \}$$

where v_0 and γ are constants, and the activation energy ΔE_{\neq} is for Heves rubber about 16 kcal./mole of the magnitude observed for viscous flow. Friction appears to be caused in this case by a viscous, rather than a plastic, flow mechanism.⁶⁹

The behavior at high loads can also be described in terms of Bowden's ploughing model, namely, that for considerable depths of asperity penetration the ploughing contribution P to the friction force

$$F = s + P$$

cannot be neglected. When that happens F depends upon the dimension of the slider. With metals P can be neglected, except at very high loads. With hard plastics, likewise, $P < 0.2F$ as a rule, but with soft plastic and rubbers one may find $P \geq 0.5F$. The steeply increasing high-load portion of the μ versus W curves of soft plastics on Fig. 8 is dominated by the ploughing effect.⁶⁸

While the quotient s/P_m has nearly the same value for most metals, individual components have not, and an interesting application of the insight gained in the course of recent friction research is the coverage of a hard base metal of large P_m value with a very thin layer of soft metal (of low shear strengths) in order to obtain bearing metals of very low solid friction coefficient. The benefit of low penetration (because of the

⁶⁸ K. V. Shooter and D. Tabor, *Proc. Phys. Soc. (London)* **B65**, 661 (1952).

^{68a} B. Lincoln, *Brit. J. Appl. Phys.* **3**, 260 (1952); *Nature* **172**, 169 (1953).

⁶⁹ A. Schallamach, *Kolloid-Z.* **141**, 165 (1955).

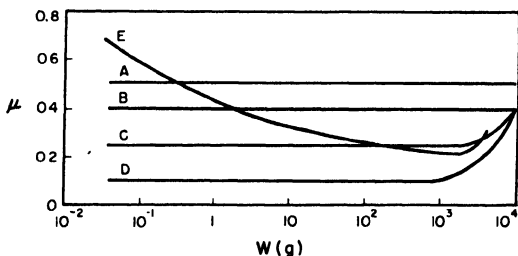


Fig. 8. Coefficient of friction of steel against plastic substances as function of load.⁶⁸ Steel sliding on: A: polymethylmethacrylate, B: polyvinylchloride, C: polyethylene (HMW); D: polytetrafluoroethylene, E: polyethylene (LMW).

hard substrate) is only safeguarded if the layer of soft metal is somewhat, but not much, thinner than the average height of the surface irregularities of the slider, i.e., of the order of microns. Typical applications are indium or copper on steel, or lead on copper.⁵⁸

The change in friction coefficient with sliding velocity u is not very great, if compared with fluid lubrication, where $\mu \propto u^{1/2}$. But it can still be significant, especially in the ranges of extremely low and extremely high speeds. While the total accessible load range is limited at the low end by the accuracy with which significant friction measurements can be carried out ($\sim 10^{-3}$ gm.) and at the high end by the yield strengths of the material ($\sim 10^7$ gm./cm.²) no such limitation applies to velocity. Significant measurements have been carried out between $\sim 10^{-10}$ cm./sec. and $\sim 10^5$ cm./sec. with no principal limitation in either direction. Also from the engineering point of view there is considerable interest in either extreme.

A typical set of curves is shown in Fig. 9 for soft metal bearings. The very slow speed, up to about 10^{-6} to 10^{-4} cm./sec., obviously corresponds to creep in shear with the somewhat unusual condition that a steady state is being observed, just as many junctions being broken as are being formed.^{69a} The drop in friction coefficient with further rise in velocity must be due to the successively greater rate of destruction than of formation of the stronger junctions.

For hard metals, such as iron and copper, the drop in friction coefficient at the low speed side in the creep range has not yet been observed and may not be realizable. The high speed side drop has been studied extensively, however, and has been extended up to 10^4 cm./sec.⁷⁰ A typical friction curve covering the high speed range is shown in Fig. 10, where the specific effect of different surface oxides on the friction coefficient is

^{69a} E. Rabinowicz, *J. Appl. Phys.* **24**, 136 (1953).

⁷⁰ R. L. Johnson and E. E. Bisson, *Natl. Advisory Comm. Aeronaut. Tech. Note* **1442** (1947); **1720** (1948); **2144** (1950).

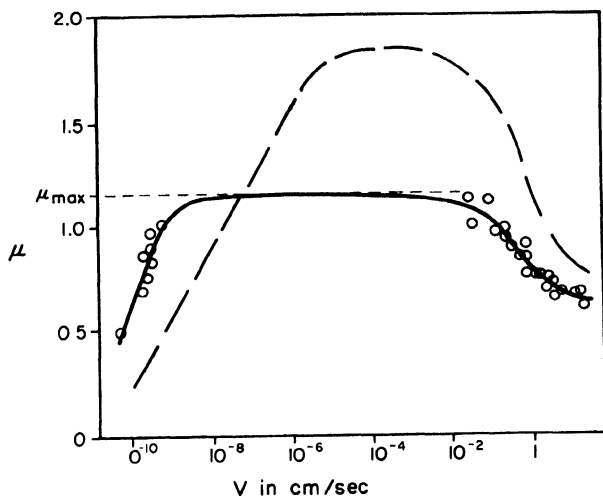
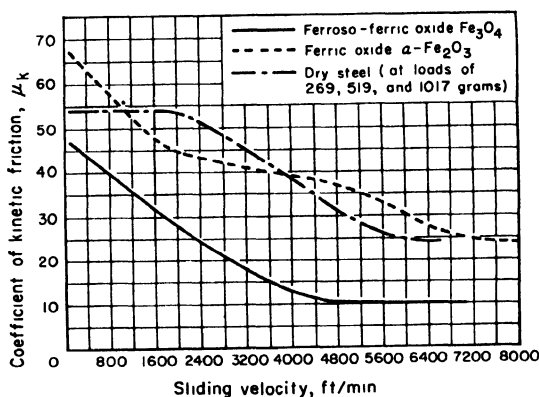


FIG. 9. Coefficient of friction at very low velocity.^{69a}
— Steel on Lead, --- Steel on Indium.



Ferroso-ferric-oxide Fe_3O_4 and ferric-oxide
 $\alpha\text{-Fe}_2\text{O}_3$ films with loads of 269 grams \approx
8,600 kg/cm² nominal surface stress

FIG. 10. Coefficient of friction as function of velocity.^{70a}

well discernible. In the high speed range the friction effects are intimately related to the rate of reformation of oxides, i.e., to chemical reaction rates.

At speeds in excess of about 10^4 cm/sec the friction coefficient drops further and may reach quite low values (at $u \geq 400$ m/sec $\mu = 0.18$ for the

^{70a} R. L. Johnson, M. A. Swikert, and E. E. Bisson, *Lubrication Eng.* **6**, 16 (1950); **11**, 164 (1955).

pair Steel-Cu, and $\mu = 0.1$ for Steel-Duraluminum and $\mu = 0.04$ for Steel-Bi at $u = 200$ m/sec) even with perfectly clean metal surfaces. The reason is, as shown very well by Bowden and Freitag^{70b} that "the contact regions are sheared so rapidly that the heat is generated much faster than it can be conducted away. This causes the surface layer to soften or to melt while the underlying metal is still comparatively hard". This phenomenon is utilized in the practice of ultra-high speed metal cutting that is conducted at surface speeds of several hundred meters per second.

Since the friction process involves the deformation, welding, and breakage of the contacting asperities, dry friction is accompanied by appreciable wear. The wear rate is nearly proportional to the specific pressure until the latter becomes an appreciable portion, about one third, of the yield pressure of the softer metal, whence it rises steeply.⁷¹ This effect is believed to be due to the rather close approach of the actual surface, preventing escape of the primary wear products which thus, in turn, cause secondary wear by their abrasive action.

Rubbing experiments with a radioactive soft steel slider on a (neutral) hardened steel surface demonstrated that the wear process with that pair involves three distinct steps: first, transfer of metal from the slider to the stator; second, oxidation of the transferred, attached metal particles under the effect of local high temperatures; and finally, detachment of the resulting oxide particles from their new host surface as wear products.⁷²

In general it is to be expected that a substance will wear less if it can deform elastically, i.e., without yielding out of the path of the oncoming asperity or abrasive particles. As a quantitative measure of the depth of penetration that a solid can tolerate without exceeding its elastic limit the quotient

$$M_0 = H_B/E = \text{"Modell"}$$

has recently been proposed,⁷³ where H_B = Brinell hardness, a measure of the yield stress or the elastic limit, and E = modulus of elasticity. As shown by the data of Table V M_0 aligns most materials in the order of their known wear resistance. Quantitative comparisons can only be made for series which keep the composition of one of the rubbing surfaces and the operating conditions constant.

2. LUBRICATED BOUNDARY FRICTION

Interposition of a layer of fluid or of an easily deformable solid between two hard solids which have approached each other to within reach of their

^{70b} F. P. Bowden and E. H. Freitag, *Proc. Roy. Soc. A* **248**, 350 (1958).

⁷¹ J. T. Burwell and J. T. Strong, *Proc. Roy. Soc. A* **212**, 470 (1952).

⁷² M. Kerridge, *Proc. Phys. Soc. (London)* **68B**, 400 (1955).

⁷³ T. L. Oberle, *S.A.E. Quart. Trans* **6**, 511 (1952).

TABLE V
MODELL VALUES FOR VARIOUS MATERIALS
(From Oberle⁷³)

<i>Material</i>	<i>Condition</i>	<i>E</i> <i>p.s.i.</i>	<i>Brinell</i> <i>10³ p.s.i.</i>	<i>Modell</i>
Alundum (Al ₂ O ₃)	Bonded	14,000,000	2000	143
Chrome plate	Bright	12,000,000	1000	83
Gray iron	Hard	15,000,000	500	33
Tungsten carbide	9% cobalt	81,000,000	1800	22
Steel	Hard	29,000,000	600	21
Titanium	Hard	17,500,000	300	17
Aluminum alloy	Hard	10,500,000	120	11
Gray iron	As cast	15,000,000	150	10
Structural steel	Soft	30,000,000	150	5
Malleable iron	Soft	25,000,000	125	5
Wrought iron	Soft	29,000,000	100	3.5
Chromium metal	As cast	36,000,000	125	3.5
Copper	Soft	16,000,000	40	2.5
Silver	Pure	11,000,000	25	2.3
Aluminum	Pure	10,000,000	20	2.0
Lead	Pure	2,000,000	4	2.0
Tin	Pure	6,000,000	4	0.7

highest surface asperities reduces the friction coefficient by two mechanisms, by reducing the proneness to local welding and by carrying part of the load. If one assumes linear additivity (per unit area) of the shear strengths of the solid junctions (s_m) and of the interposed lubricants (s_e) one may estimate the total friction force as

$$F' = A[\alpha s_m + (1 - \alpha)s_e]$$

where α = fraction of surface occupied by solid junctions.⁵⁸ In terms of the corresponding friction coefficients μ , μ_m , and μ_e one obtains

$$\mu = \mu_e + \alpha(\mu_m - \mu_e)$$

which is strictly equivalent to a formulation proposed many years ago,⁷⁴ if α is also identified as the fraction of the load carried by the direct metallic contacts. Since generally $\mu_m \gg \mu_e$ one can easily see that even for small values of α , the friction coefficient is entirely determined by the work required to shear the few metallic junctions formed although the bulk of the load may yet be carried by the lubricant film.

In mixed film lubrication where part of the load is carried by the fluid film, one can estimate the fraction of the load to be carried by the film

⁷⁴ G. Vogelpohl, *Oel u. Kohle* **14**, 991 (1937).

from a consideration of the hydrodynamics under the anticipated conditions of close approach^{75, 76} and thus obtain an approximate value of α directly. In view of the rapid increase of α (assuming an entirely "inert liquid") with decreasing distance of approach h ^{76a} the hydrodynamic calculation can give meaningful but probably quite inaccurate answers only for very small values of α .⁵⁴

In the vast majority of cases studied α , and therefore the friction coefficient, depends upon the properties of the wall-nearest layer of but one to perhaps 50 molecules in thickness. Means to calculate or even independently measure the load-carrying capacity, i.e., the yield stress of these layers have not yet been developed. Qualitatively one knows now that plastic solid layers exhibit far greater load-carrying capacity than liquid layers.^{58, 77, 78} Among the latter the more strongly adsorbed and orientable ones appear to exhibit greater load-carrying capacity.

A more sensitive measure of α is the wear rate. If the wear experiments are carried out with radioactive sliders, the autoradiographs of the bearing provide a direct measure of α , the area occupied by the metallic junctions formed.^{77, 79}

Since the shear strength of several metallic soaps, mono- and multi-layers, has been measured both on aqueous and on solid substrates,⁸⁰⁻⁸³ it becomes possible to substitute s_e , s_m , and the radiographically obtained value of α in the above equations and then compare the observed with the calculated friction coefficient. A few such data are assembled in Table VI. While the agreement is reasonably good, it is probably not yet sufficient to reverse the procedure and calculate reliable values of α from the experimental values for μ , s_m , and s_e . The strong temperature and pressure dependence of s_e and the effective viscosity of the layer must be determined more carefully than has been possible to date. Finally the results must be fitted into an energy balance of the sliding surfaces.

Of little interest from the point of view of the rheologist is the fact that the boundary lubricant is often formed by chemical reaction with the surface, e.g., the metal soaps by reactions of fatty acids or their esters, with the metal or metal oxide surface, or the metal halides, sulfides, or

⁷⁵ W. Altrogge, Ph.D. thesis, Munich, 1950.

⁷⁶ A. Bondi, *1st Natl. Symposium Fundamentals of Lubrication*, Am. Soc. Lubrication Engrs. p. 31 (1952).

^{76a} $Y \propto h^{-n}$, one finds n to be of the order 10 to 20.¹⁷

⁷⁷ E. Rabinowicz, and D. Tabor, *Proc. Roy. Soc. A* **208**, 455 (1951).

⁷⁸ D. Tabor, *Proc. Roy. Soc. A* **212**, 498 (1952).

⁷⁹ E. Rabinowicz, *J. Appl. Phys.* **22**, 1473 (1951).

⁸⁰ J. H. Schulman and J. G. Wostenholm, *Trans. Faraday Soc.* **47**, 788 (1951).

⁸¹ A. A. Trapeznikov, *Compt. rend. acad. sci. U.R.S.S.* **18**, 185 (1938).

⁸² A. I. Bailey and J. S. Courtney-Pratt, *Proc. Roy. Soc. A* **227**, 500 (1955).

⁸³ J. R. White, *Lubrication Engr.* **10**, 340 (1954).

TABLE VI
SHEAR STRENGTH OF METAL SOAPS

Substance	Shear Strength (kg/cm² at:				Method	Ref.
	Pressure (kg/cm²):					
	2,200		10,500			
	Temperature (°C):					
	27	100	27	100		
Na-Stearate	31	18	168	100	Bridgman anvil	83
K-Palmitate	57	22	240	—	Bridgman anvil	83
Fe-Stearate	46	—	315	136	Bridgman anvil	83
Ca-Stearate	25 ^a	—	—		Shearing ads. mon- olayer	82
Cu-Palmitate			520 ^b		Measurement of friction coeff. and of true area of contact	77
			315 ^c			77

^a At low (about atmospheric) pressure

^b Pressure = 8,000 kg/cm²

^c Pressure = 6,300 kg/cm²

phosphides by reaction of the metal surface with the respective organo or hydrogen compounds. The last named group involves reactions which take place principally at elevated temperatures and is of importance only when very high loads are applied, and therefore high local temperatures are generated in so called "extreme pressure" applications. The choice of the proper agent is dictated by the relative shear strength of the anticipated metal compound and the metal. Iron sulfide would be a good lubricant on iron or steel surfaces, but copper sulfide would be a poor lubricant on ordinary metallic copper surfaces.

In summarizing one may say that the rheological principles of boundary lubrication are by now fairly well understood. The quantitative details have yet to be worked out, however. From the practical point of view it must be recognized, that wear, the major consequence of boundary lubrication, is in many technologically important cases a problem in corrosion, the mechanical action being just involved in the sloughing off of the corrosion products. In these instances wear is counteracted by strictly chemical means. For this reason most recent efforts in the field of wear prevention deal with chemistry rather than with mechanics.⁸⁴

⁸⁴ R. G. Larsen and G. L. Perry, *Trans. Am. Soc. Mech. Engrs.* **67**, 45 (1945); "Mechanical Wear Symposium," pp. 73-94. American Society for Metals, Cleveland, 1950.

Nomenclature

A	True area of contact; empirical constant	ΔP	Pressure drop
B	Empirical constant	\dot{q}	Flow rate
C	Bearing clearance	R	Gas constant
c	Specific heat of lubricant	S	Shear strength
D	Pipe diameter; empirical constant	T	Temperature (abs.)
E	Internal energy; elastic modulus	u	Velocity
\dot{e}	Shear rate	α	Fraction of area in contact; pressure coefficient of viscosity [p^{-1}]
F	Friction force	β	Temperature coefficient of viscosity [T^{-1}]
g	Acceleration constant	γ	Volumetric expansion coefficient [T^{-1}]
H	Height of grease layer	η	Dynamic viscosity;
h_0	Minimum film thickness of lubricant	$[\eta]$	Intrinsic viscosity
k	Empirical constant	μ	Friction coefficient
L	Length of path for lubricant	ν	Kinematic viscosity
m	Exponent in thixotropy equation	ρ	Density
n	Exponent in Ostwald relation between shear rate and shear stress	τ	Shear stress
n	Exponent in relation between contact frequency and bearing approach	τ_y	Yield stress
P	Pressure	ϕ	Volume fraction

CHAPTER 13

THE RHEOLOGY OF ADHESION

J. J. Bikerman

I. Introduction.	479
II. Application of Adhesives	480
III. Tackiness	481
1. Definition	481
2. The Hydrodynamic Theory.	481
3. Limitations of the Theory	483
IV. Time of Set	485
1. The Mechanism of Setting.	485
2. Physical Changes during Setting	486
3. Chemical Changes during Setting	487
V. Final Strength	488
1. Local Stress and Local Strength	488
2. Stresses in a Strained Bond	491
3. Strength and Thinness of Joints	499
4. The True Adhesion	501
VI. Summary	503
Nomenclature.	503

I. Introduction

As a rule, five layers can be recognized in an adhesive joint. Starting from one of the solids (adherends) they are: first solid, boundary layer, adhesive film, boundary layer, and second solid. If a simple tensile stress is applied to such a joint, normally to the stratification, the weakest of the layers breaks first. In many respects, the knowledge of the layer in which rupture occurs is just as important as that of the value of the breaking load.

Boundary layers are mentioned at the very start of this article because their importance still is often underestimated. Except for very special systems, such as solids condensed in a high vacuum, the composition of a solid surface is always different from that of the bulk of the solid. In addition to ordinary "dirt" there are oxides on metals, silica-rich layers on glass, etc., and adsorbed gases and vapors on everything. For instance, when a glue is applied to what we call metal surface, it has no contact with any metallic phase.

Solid surfaces are also rough or even porous. A simple microscopic observation shows that an adhesive properly applied to paper penetrates into its fibrous structure. Because of the roughness of all solid surfaces, some degree of interpenetration of adhesive and adherends is always present. A striking example of the importance of this interpenetration is afforded by comparison of filter paper and cellophane (that is, regenerated cellulose). The chemical composition of these two materials is almost identical, but paper is porous (great interpenetration) while cellophane films are unusually smooth (little interpenetration). Almost any adhesive can be used for paper but only few compositions are suitable for cellophane.¹ To increase the interpenetration, the solid surfaces often are sandblasted or in another manner roughened before the application of the adhesive.²

Generally, three stages can be recognized in the life history of an adhesive joint. During the first stage the adhesive is applied, during the second it sets, and during the last stage the properties of the system remain, or are supposed to remain, constant.

II. Application of Adhesives

Air occluded by a solid surface or entrapped in its valleys would form a very weak boundary layer. To obtain strong joints this air must be removed. If the adhesive has to displace the air from the surface, it must wet the latter. If the wetting ability is absent (aqueous dextrin solutions and oiled metals are an example), the resulting joints are weak and fail in a boundary layer.

Wetting ability depends on the chemical composition of the two phases (the solid and the liquid) and thus need not be discussed in a book on rheology. However, the *rate* of displacement of air depends on the rheological properties of the liquid glue. Thus, a sheet of filter paper was fully wetted by a sodium silicate solution in 70 sec. when the viscosity η of the solution was 2 gm./cm.sec., in 160 sec. when η was 4 gm./cm.sec., in 240 sec. at $\eta = 6$, and in 320 sec. at $\eta = 8$ (interpolated from the data found in Vail³).

Often the adhesive must displace more than air in the moment of application. Thus in soldering, the flux chemically changes and dissolves the oxide layer on the metal, and then molten solder displaces the flux.

¹ For example, see A. D. McLaren and C. H. Hofrichter, *Paper Trade J.* **125**(19), 96 (1947).

² For example, see N. J. DeLollis, N. Rucker, and J. E. Wier, *Trans. Am. Soc. Mech. Engrs.* **73**, 183 (1951).

³ J. G. Vail, "Soluble Silicates," Vol. 2, p. 370. Reinhold, New York, 1952.

III. Tackiness

1. DEFINITION

There is no accepted definition of tack. Here this term means the resistance of an adhesive joint to separation as long as the adhesive remains liquid. A definition of *liquid* as understood here will be given in Section III,3.

Sometimes a liquid is said to be tacky when it readily forms fibers. The capacity for filamentation depends mainly on the *variation* of viscosity (or consistency) with elongation, while tack, as defined here, is a function of viscosity (or consistency) itself. Thus these two properties are somewhat related but certainly not identical.

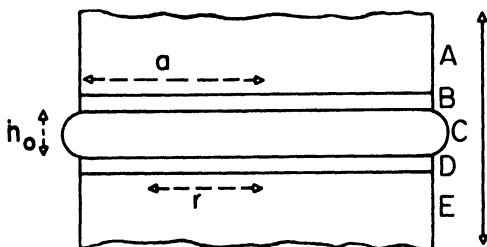


FIG. 1. A and E are adherends, B and D are boundary layers, C is the adhesive film. The pull is applied in the direction of the arrow. (From Bikerman.⁴)

2. THE HYDRODYNAMIC THEORY

The nature of tack is conveniently discussed for the instance of two circular, plane-parallel, solid plates with an adhesive liquid filling the clearance between the plates (see Fig. 1⁴ and disregard the dotted line marked r). When the plates are pulled apart in the direction of the arrow, the liquid flows toward the axis of the system from the bulges shown in the figure. To maintain this movement in a viscous liquid, a stress has to be continually operative. This is the stress f needed to separate the plates. Thus, tack is the viscous resistance of a liquid moving in a slit at a rate determined by the rate of separation of the plates. If the plate radius a is much greater than the initial distance h_0 between the plates, this movement is practically parallel to the plates for almost the whole duration of the experiment; that is, the flow in the direction of the axis (which of course takes place when the plates move apart) may be neglected. For this case and a Newtonian liquid, the relation between stress f and the time t during

⁴ J. J. Bikerman, *J. Colloid Sci.* **2**, 163 (1947).

which the clearance between the plates increased from h_0 to h_1 was derived by Stefan⁵ as

$$ft = \frac{3\eta a^2}{4} \left(\frac{1}{h_0^2} - \frac{1}{h_1^2} \right). \quad (1)$$

A more general equation of the same type was deduced by Reynolds.⁶ A simplified proof of equation (1) was given more recently.⁴

Equation (1) implies that (a) there is no minimum force (such as molecular attraction) which must be overcome to break the bond; only the product ft is important; (b) the forces between the solids and the liquid are not involved at all; the rupture is a purely rheological phenomenon; (c) for complete separation (that is, for $h_1 = \infty$) the product ft is inversely proportional to the square of the initial clearance; and (d) ft is proportional to the viscosity of the liquid.

Experimental confirmation of equation (1) was started by Stefan himself. In later experiments some discrepancies were observed, for instance by Green⁷ and Heidebroek.⁸ An important reason for these discrepancies was disregard of surface roughness.⁹ Figure 2 shows the effect of rugosity on the product ft .

Sometimes separation of the two adherends can be accomplished by peeling or stripping rather than by a tensile pull. Both theoretical and experimental studies of peeling are less advanced than those of tensile separation but it appears¹⁰ that the time of separation by stripping is

$$t = \kappa \frac{\eta E w^2 \delta^3}{F^2 h_0}; \quad (2)$$

κ is a numerical constant, E is the modulus of elasticity of the ribbon which is being stripped off the solid support, η is the (Newtonian) viscosity of the liquid between the ribbon and the support, w and δ are the width and the thickness of the ribbon, F is the applied force, and h_0 the initial clearance.

Comparison between equations (1) and (2) shows that t in peeling tests is much shorter than Stefan's t mainly because the former quantity is proportional to δ/h_0 which usually is of the order of one, while the latter is proportional to a^2/h_0^2 which usually would exceed 10^6 .

⁵ M. J. Stefan, *Sitzber. Akad. Wiss. Wien, Math.-naturw. Kl., Abt. II* **69**, 713 (1874).

⁶ O. Reynolds, *Trans. Roy. Soc.* **177**, 190 (1886).

⁷ H. Green, *Ind. Eng. Chem., Anal. Ed.* **13**, 632 (1941).

⁸ E. Heidebroek, *Ber. Verhandl. sächs. Akad. Wiss. Leipzig Math.-naturw. Kl.* **97**(6), 20 (1952).

⁹ J. J. Bikerman, *Trans. Soc. Rheol.* **1**, 3 (1957).

¹⁰ J. J. Bikerman and W. Yap, *Trans. Soc. Rheol.*, in press.

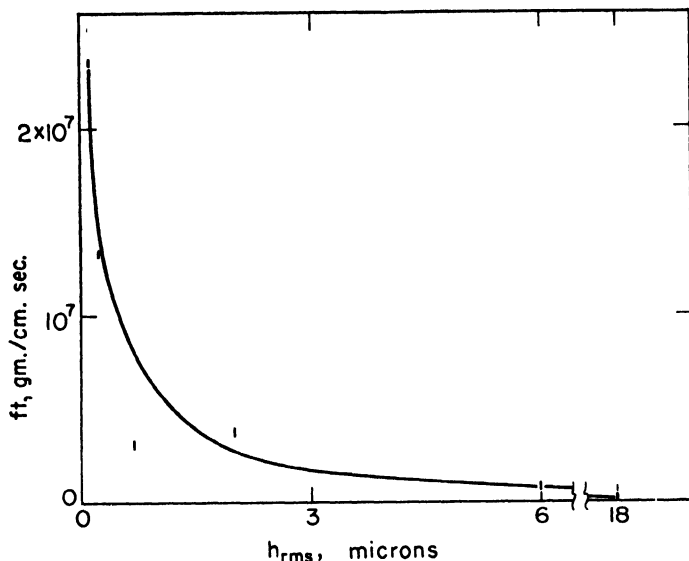


FIG. 2. Effect of surface roughness on tackiness. Abscissa: mean height of hills on the solid surface. Ordinate: product of stress and time. Paraffin oil between two nickel disks. (From the data of Bikerman.⁹)

Earlier experiments¹¹⁻¹⁴ on stripping of adhesive tapes and polymer films have been performed on materials which are neither Newtonian liquids nor Hookean solids (see Section IV,2) and therefore cannot be readily treated mathematically. Qualitatively they agree with the main postulate expounded in this section, namely, that tackiness is a rheological phenomenon not affected by the molecular forces between adherend and adhesive.

3. LIMITATIONS OF THE THEORY

Limitations of equation (1) are many. The theory assumes the viscosity to be a constant. An extension of the treatment to include η variable with velocity gradient could not be found in the literature.

There is only one value of h_0 in equation (1). In reality the distance between the plates varies from point to point because of surface roughness. The effect of rugosity is illustrated in Figure 2.

The centripetal flow of the liquid is directly caused by the pressure differ-

¹¹ R. S. Riwlin, *Paint Technol.* **9**, 215 (1944).

¹² W. F. Busse, J. M. Lambert, and R. B. Verdery, *J. Appl. Phys.* **17**, 376 (1946).

¹³ J. O. Hendricks, G. F. Lindner, and F. J. Wehmer, *Rubber Age (N. Y.)* **63**, 327 (1948).

¹⁴ S. S. Voyutskii, A. I. Shapovalova, and A. P. Pisarenko, *Kolloid. Zhur.* **19**, 274 (1957).

ence between the peripheral and the central portions of the adhesive layer. The theory assumes that this pressure difference cannot be relieved in any other way. However, if, for instance, air channels remain in the valleys of a solid surface, air—more rapidly than the liquid—will move inward and thus facilitate the separation. If air bubbles can form and grow in the underpressure region at a sufficient speed, they will help to eliminate the pressure difference.¹⁵

If the time of separation—that is, t in equation (1)—is very short, the calculated stress f is very large. Indeed it may be greater than the tensile strength of an adherend, in which case breaking of this adherend rather than adhesive flow is the result. Thus gummed kraft paper tape adhering to a glass plate usually can be separated from the plate if slowly pulled away but is torn by a rapid motion.

When the adherends are strong, the adhesive layer gives way also at large stresses (that is, short t). However, the mechanism of the rupture in these instances usually is quite different from that envisaged by Stefan. No noticeable flow of the adhesive occurs; rather a crack advances in it. Thus the adhesive breaks down as a solid even if for slow deformation it behaves as a Newtonian liquid. This effect is readily observed for adhesives whose viscosity is greater than, say, 1000 gm./cm.sec. Equation (1) with $\eta = 1000$, $a^2 = 13.33 \text{ cm.}^2$, $h_1 = \infty$, and $h_0 = 0.001 \text{ cm.}$ affords $ft = 10^{10} \text{ gm./cm.sec.}$ Thus a stress of $10^{10} \text{ gm./cm.sec.}^2$ for 1 sec. would be required to cause the Stefan flow of the adhesive. The "solid fracture" takes place at smaller loads and in much shorter times, and the centripetal flow has no chance to materialize.

An intermediate region also exists, namely when the ratio η/t is not so great as to cause a solid fracture nor so small as to give rise to a uniform liquid flow. In this region the adhesive flows not toward the axis of the whole system but toward many points spread all over the adhesive film; at further separation of the plates, adhesive filaments start from these points. This effect may be crudely accounted for by equation (1), in which a would be the mean half-distance between two nearest filaments; as this distance is small compared with the radius of the plates, the resulting ft is a small fraction of that calculated by Stefan.

At viscosities as high as 1000 gm./cm.sec. the occurrence of a solid fracture can be proved by visual inspection of the broken joint because the forces (gravitation, surface tension, etc.) causing further changes in the surface profile are weak in comparison with viscosity forces. At smaller viscosities, the former forces may alter the surface profile of the adhesive during the time elapsing between the rupture and the inspection. Thus only indirect proofs are available for deciding in any given instance whether

¹⁵ W. H. Banks and C. C. Mill, *J. Colloid Sci.* **8**, 137 (1953).

viscous or elastic forces were more important for the breakdown; that is, whether the adhesive behaved more like a liquid or more like a solid. From experiments on rapidly rolling a cylinder in a shallow layer of a viscous liquid, Voet and Geffken¹⁶ concluded that the observations were better accounted for by elastic effects.

It has been mentioned in Section III,1 that tackiness exists as long as the adhesive is liquid. Now a more detailed definition can be given. According to Stefan's equation the breaking stress f greatly depends on the dimension (that is, a) of the system because the whole adhesive film at all times takes part in the flow. At the other extreme, in brittle fracture, breaking stress little depends on the overall dimensions because rupture is a *topical* phenomenon, i.e., is determined by the properties of one point only (namely the weakest spot in the system) and is not affected by the amount of healthy material around this sick spot. In the intermediate region, the effect of the overall dimensions ranges between these two extremes; presumably, as long as this effect is much greater than for brittle rupture, the adhesive may be called liquid and the resistance to separation may be called tackiness.

The usual definitions of tack refer to two operations: the adhesive is first pressed against a solid and then the joint is ruptured. In this section, only the second operation was considered, but its conclusions seem to be applicable to the first as well; as long as the ratio η/t is small, the adhesive will be able to remove the weak boundary layers and the breaking stress will be determined mainly by the viscous flow. When η/t is very large, the boundary layers will not be displaced, there will be no sticking, and, in a separate rupture test, the adhesive would behave as a solid.

All limitations discussed in connection with equation (1) apply also to equation (2). Moreover, this equation implies also that the ribbon is a Hookean solid, is perfectly flat and smooth, and so on.

IV. Time of Set

1. THE MECHANISM OF SETTING

As soon as an average adhesive is applied, it starts to *set*, that is its consistency starts to increase. The rate of this increase is very small for pressure-sensitive tapes and is greater for joints which are made to be permanent.

The rate of setting often determines whether the adhesive will or will not be suitable for a particular operation. If the final arrangement of the adherends is performed after the application of the adhesive, the setting time must be long enough to allow this arrangement to be completed. Thus,

¹⁶ A. Voet and C. F. Geffken, *Ind. Eng. Chem.* **43**, 1614 (1951).

wall papers are pasted to the wall with slow-setting adhesives. On the other hand, in the rapid automatic manufacture of cardboard boxes, the adhesive may be applied hot and set within a second or two.

The change in the rheological properties of the adhesive during setting depends on the chemical composition of the adhesive, but may crudely be described as solidification. There are three main mechanisms of this process; namely, cooling, drying, and a chemical reaction.

Increase in consistency on cooling is used, for instance, for solders and for the animal glue. In the latter instance it may be classified as sol-gel transformation.

Setting because of the removal of solvent is a very common mechanism. This removal usually is accomplished by evaporation. To allow a rapid evaporation, the adherends must be porous. In some instances the solvent (or a part of it) is imbibed by the adherends. Thus the time of set of an adhesive between two sheets of paper often depends on the degree of dryness of the paper. Also nonporous adherends can imbibe solvents.

Setting of the plaster of Paris is a classical example of solidification caused by a chemical reaction. Many modern adhesives are applied as polymers of a low degree of polymerization and then set because the adhesive further polymerizes *in situ*; this can be achieved, for instance, by adding a polymerization catalyst in the moment of application or by curing the completed joint. In another group (exemplified by the epoxy resins) setting is caused by the cross-linking of a chain polymer with a short bifunctional molecule.

2. PHYSICAL CHANGES DURING SETTING

Increase in the consistency of the adhesive film is accompanied by other physical changes which are of great importance for the fate of the joint.

Setting usually is associated with contraction. If the adherends are in a fixed position—that is, the clearance between them has one definite value—this contraction can break the bond without any external force. Otherwise, the adherends can follow the volume changes of the adhesive. However it is almost impossible, also in this instance, to avoid creating stresses in both adherends and adhesive during the solidification. When solidification is caused by cooling, the remaining stresses will be smaller the more alike the coefficients of thermal expansion of the adherends and the adhesive; thus only those metals can be successfully sealed in glass whose heat expansion is equal to that of the glass used. When solidification results from evaporation of the solvent, the stresses may be strong enough to damage the adherends as sometimes happens in gelatin-glass bonds.

The rheological properties of a solid generally depend on the *rate* of its solidification. This is true also for the adhesive films. Thus, because of the higher heat conductance of copper, a molten adhesive will cool and set

more rapidly between two copper disks than between two lead disks of identical dimensions, and the strength of the adhesive layer should be different in the two instances; no experimental verification of this view could be found in the literature. It has been mentioned in Section IV,1 that the time of set of the glue may depend on the moisture content of the paper to be glued; hence, also the strength of the final bond may be influenced by this content.

Often the periphery of an adhesive film sets when the center is still liquid. On the subsequent solidification and contraction of the central part, the bond will remain under tension (because the unyielding periphery precludes complete contraction of the film). Nuclei of future destruction can form as a result of this tension. If the adhesive film is of sufficient thickness, it can be seen that its periphery (i.e., the adhesive-air boundary) is concave toward the air. This indicates that the three-phase boundary line between air, adherend, and adhesive could not follow the shrinkage of the adhesive. An estimate of the stresses created by this hindred shrinkage was made by Mylonas.¹⁷ In polystyrene-steel bonds rupture is sometimes located in a boundary layer near the periphery and within the polystyrene phase in the center of the joint;¹⁸ this may be a result of stresses set up during solidification on cooling.

3. CHEMICAL CHANGES DURING SETTING

Chemical changes in adhesive joints are important because they affect the strength of one or several of the five layers of usual joints, enumerated in Section I.

The adhesive—or one of its ingredients—may slowly react with the adherends and thus improve or impair their mechanical properties. Thus strongly alkaline adhesives may weaken wood so much that failure occurs in wood at smaller stresses than those needed to break original wood specimens. The inverse phenomenon also occurs; that is, the adhesive may be weakened by substances diffusing into it from the adherends.

Chemical reactions in the boundary layers are not uncommon. Thus tin in the customary solders reacts with many metals to form compounds such as FeSn_2 , Cu_6Sn_5 , etc. Hence, in the majority of soldered joints a boundary between unaltered adherend and unaltered adhesive does not exist; there is a gradual transition from, say, pure copper to copper containing a few crystals of a Cu-Sn compound, to a layer containing less copper and more Cu-Sn compound, etc. Whichever of these layers is the weakest is likely to break first and thus to cause bond failure. When rubber is vulcanized

¹⁷ See N. A. De Bruyne and R. Houwink, "Adhesion and Adhesives," p. 136. Elsevier, Amsterdam, 1951.

¹⁸ H. P. Meissner and G. H. Baldauf, *Trans. Am. Soc. Mech. Engrs.* **73**, 697 (1951).

in contact with brass, CuS forms in the boundary layer; if the rubber contains too much sulfur, the resulting CuS coating is too thick and breaks easily. There is a chemical reaction between enamel and metal during firing.¹⁹

Some chemical reactions in the adhesive, which result in its solidification, are mentioned in Section IV,2. Many reactions continue also afterward and often weaken the joint. Thus rubber adhesives can be oxidized by the air and, consequently, lose their flexibility. If crystals of Cu-Sn compounds invade the solder phase, the tensile strength of the solder usually decreases. Many adhesives become brittle if their moisture loss is too great and require addition of a hygroscopic agent ("humectant") to maintain their resistance to impact. Proteins and some other organic adhesives deteriorate because of attack by microorganisms unless the adhesive composition contains a preservative.

If, after setting, the adhesive film contains many weak spots, its modulus of elasticity is likely to be smaller than that of a flawless film. This modulus can be calculated from the resonance frequency of the joint subjected to ultrasonic vibration.²⁰ By means of such measurements it is possible to separate the chemical from the physical deterioration of bond. If, for instance, a joint between aluminum and aluminum is heated and cooled again, the loss in bond strength is less than when an identical heat treatment is applied to a steel-steel joint with the same adhesive (a phenol-formaldehyde plus vinyl butyral resin); this would be the physical effect since the difference between the thermal expansions of aluminum and resin is smaller than that between steel and resin. On the other hand, temporary deep cooling of joints had a much weaker effect on their strength than a heating of a similar intensity; presumably, heating impaired the strength because of both physical and chemical effects while chemical deterioration was almost absent at low temperatures.

V. Final Strength

1. LOCAL STRESS AND LOCAL STRENGTH

The final strength, f_0 , of a joint usually is even more important than the tackiness of the adhesive at the application stage. The correct calculation of f_0 from the experimental results on bond rupture is not simple, and the simple calculations still common in the literature and the industrial applications are inexact or incorrect.

¹⁹ W. N. Harrison, J. C. Richmond, J. W. Pitts, and S. G. Benner, *J. Am. Ceram. Soc.* **35**, 113 (1952).

²⁰ A. G. H. Dietz, H. N. Bockstruck, and G. Epstein, *Am. Soc. Testing Materials, Special Tech. Publ. No. 138* (1952).

An adhesive joint breaks when and where the local stress exceeds the local strength in the stress direction. The local stress differs from the average stress (arrived at, for instance, by dividing the external force by the area on which it acts) because of three complications.

(a) Often an internal stress acquired during the setting is present in the adhesive film and in the adherends; it has been mentioned in Section IV,2. The local stress then is the sum of this stress and that caused by the external force.

(b) Depending on the geometry of the joint, the stress caused by the external force would vary from point to point even if all the ingredients of the joint were uniform down to molecular dimensions. This macroscopic stress concentration is treated in Section V,2.

(c) There exists also a microscopic or submicroscopic stress concentration at every flaw (such as a crack or a bubble) in a solid. The theory of this effect is extensive,²¹ and only the simplest equation can be reproduced here. If a small ellipse is cut out in a large plate and the plate is subjected to tensile stress of the average value p_0 , then the stress at the two apexes of the ellipse is

$$p = p_0(1 + 2a/b), \quad (3)$$

if a and b are the half-axes of the ellipse, respectively normal and parallel to the stress direction. If the flaw is circular, $a = b$ and $p = 3p_0$; that is, the highest stress is 3 times the average. If the flaw is a crack perpendicular to the stress direction, a is very much greater than b , and p may, for instance, be 1000 times as great as p_0 .

Rupture starts at a point where the local stress (calculated with due regard to the above-mentioned complications) exceeds the local strength. This point, as a rule, is situated in one of the adherends, in one of the boundary layers, or in the adhesive film. Section V,4 discusses the less probable case of the rupture starting *between* an adherend and the adhesive.

If the rupture occurs fully in an adherend, it is clear that the breaking stress is a function of the tensile (or shear) strength of the material of the adherend and has no connection with adhesive forces. When paper, cardboard, or even wood is the adherend, this kind of rupture is quite common.

The rest of the joints may be classified as "proper" and "improper." The "proper" joints break across the adhesive film; in other words, they fail in cohesion. The "improper" joints break in one of the boundary layers.

It would be more truthful to say that "proper" joints do not fail at all. The vast majority of industrial and household adhesive joints are never

²¹ N. I. Muskhelishvili, "Some Basic Problems of the Mathematical Theory of Elasticity," p. 339. Noordhoff, Groningen, Holland, 1953.

ruptured; rather the whole article is discarded or destroyed. The bond between a postal stamp and an envelope is a clear example of this generalization. If such bonds were subjected to abnormally high stresses, they would crack across the adhesive, not in a boundary layer. Thus, we are entitled to state that joints which don't fail would fail in cohesion. On the other hand, joints which break at unexpectedly weak stresses in all probability contain a fragile boundary layer.

When a joint breaks or would break in cohesion, the breaking stress obviously is a function of the tensile (or shear) strength of the adhesive. If the properties of a material were independent of the history and the present state of the sample, the rupture stress of the joint would have been *equal* to that of the material, and one determination of the strength of an adhesive in bulk would be sufficient to predict the strength of all joints made with this adhesive. In reality such a prediction would be grossly inexact, because the mechanical constants of a solid depend on its past and present conditions.

The past. A plastic film has different resistance to rupture according to whether it has been formed from a solution, from a melt, or by extrusion; and the same plastic material used as an adhesive may show a fourth value for its strength because the solidification in a narrow slit between two solids is a process different from the three processes of film formation mentioned above. A possible effect of the adherends on the strength of the adhesive has been mentioned in Section IV,2.

The present. The strength of a material usually is determined on a sample whose dimensions cover the range of 1 to 20 cm. The adhesive film in a joint often is less than 0.01 cm. thick and a few cm. wide. This difference in shape and size may easily cause a difference in the values of the breaking stress (see Section V,3).

In spite of the restrictions pointed out in the two preceding paragraphs it is still true that the rupture stress of a "proper" joint is closely related

TABLE I

Dependence of the strength of a joint on the strength of adhesive in it.

A stands for polyvinyl acetate, B for cellulose nitrate, C for resorcinol resin, D for casein glue, E for gum arabic, F for rubber solution, and G for neoprene solution.

<i>Adherend</i>	<i>Adhesive</i>
Stainless steel	A > B > D > F > G > E > C
Aluminum alloy	A > B > F > G > D > E > C
Paper-phenolic laminate	A > B > C > D > E > G > F
Glass	A > B > E > G > F > C > D
Birch wood	C > B > D > A > E > G > F
Hard rubber	C > B > A > E > G > D > F

to that of the adhesive in bulk. Because the identity of the chemical composition is a more potent factor than the differences in the history and the shape, it is possible for the adhesive manufacturers to specify the strength of the joints made with any adhesive they market. Also laboratory tests show that the nature (that is, the strength) of the adhesive is the most important factor in the bond strength. This can be demonstrated² by Table I, where adhesives are listed in order, from the strongest to the weakest bond. The strong resorcinol resin apparently separated from the hard materials (steel, aluminum, and glass) during setting.

2. STRESSES IN A STRAINED BOND

The stresses operating in a bond when a force is applied to it depend on the geometry of the system. Only a few, the simplest, systems can be considered here.

In a *butt* joint loaded in tension the stresses would be all parallel and normal to the (geometrical) boundaries between the phases, if all the materials involved were perfectly rigid. The situation is different in real solids. As a rule, the macroscopic distribution of stress is more uniform the smaller the ratio F/EA , E being the modulus of elasticity of adherend or adhesive, whichever smaller, F the force, and A the area. When this ratio is small, rupture occurs without a previous significant deformation of the system. At large values of F/EA , marked deformation precedes rupture and alters the stress distribution.

If, for instance, the system is as shown in Fig. 3, i.e., if a relatively thick adhesive film (exaggerated in the figure) is sandwiched between two axially loaded, relatively thin solid plates, then the plates bulge inward, and the stress along the axis of the system is greater than near the periphery of the plates.²² Thus the bond strength may depend on the dimensions of the adherends although the joint fails in the adhesive.

The decrease in the cross section of the adherends and the adhesive film is approximately $\mu F/E$, μ being Poisson's ratio. Since the ratio μ/E as a rule is different for the two materials, the resulting cross sections will tend to be different. Thus a shearing stress is formed along the three-phase boundary of adherend, adhesive, and air (see Fig. 4). In Fig. 4a, μ/E of the adhesive is supposed to be smaller and in Fig. 4b greater than that of the adherends. It has been mentioned in Section IV,2 that shrinkage of the adhesive often results in joints such as illustrated in Fig. 4b even before any application of load. It is clear that combination of stresses caused by shrinkage and by loading may result in failure of the bond at loads smaller than would be required otherwise. Fringe patterns of strained butt joints,

²² J. A. Van den Akker, *Tappi* **35**(4), 155 (1952).

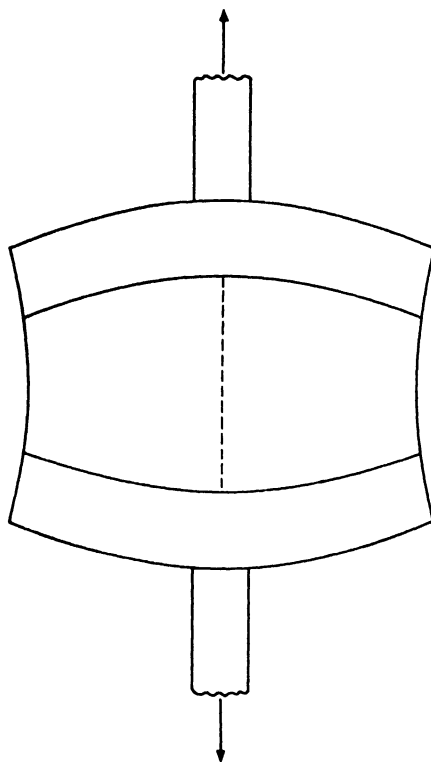


FIG. 3. Deformation of a butt joint between two thin plates

demonstrating the stress concentration near the 3-phase boundaries, have been recently published.²³

The intensity of the stresses shown in Fig. 4 may depend on the radius a of the joint, and this dependence would cause a variation of the breaking stress with a . Not much information on this variation is available. When a was changed in the ratio 1:2 (approximately) the change in F/A was not greater than the difference between repeated measurements at identical a .¹⁸

The breaking load of *scarfed* joints usually is greater than that of butt joints between identical members.

The stress distribution in *lap* joints (Fig. 5) greatly depends on the rigidity of the adherends and the method of application of the load. Suppose that the members cannot bend or are prevented from bending by some external frame. Then shearing stress will be set up between the ad-

²³ C. Mylonas, *Proc. Soc. Exptl. Stress Anal.* **12**(2), 129 (1955).

herends and the adhesive because the stress in each adherend is great at points A and B, respectively (and in the free length of the two bars) and decreases to zero at points C and D. As a result, points C and D do not change their position in space, while point B moves up and point A moves down. Thus, the adhesive film is deformed as illustrated in Fig. 6. A_1 and B_1 are the final positions of A and B just before rupture; the adhesive film is dotted. It is clear from Fig. 6 that stress is concentrated at the ends of the adhesive film, at the levels of points B_1 and A_1 . This stress concentration is noticeable for a distance of about $3h$ from the free edge, if h is the thickness of the film.²³ In this instance again, this stress will be superimposed on any stress originating from solidification.

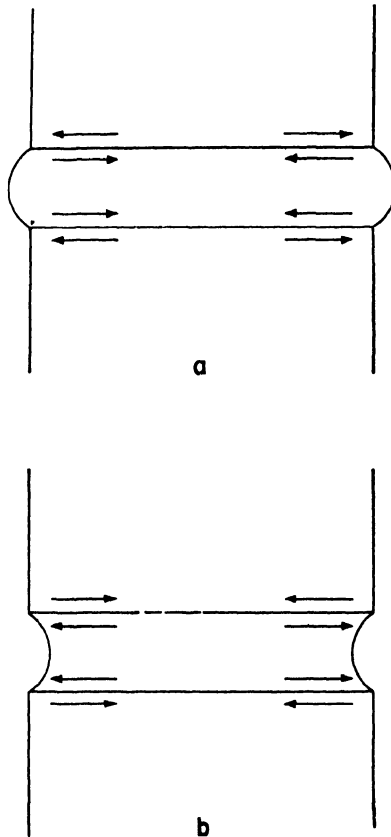


FIG. 4. Shearing stresses set up in butt joints subjected to a tensile stress. 4a. Cross section of the adherends decreases more than that of the adhesive. 4b. Cross section of the adherends decreases less than that of the adhesive.

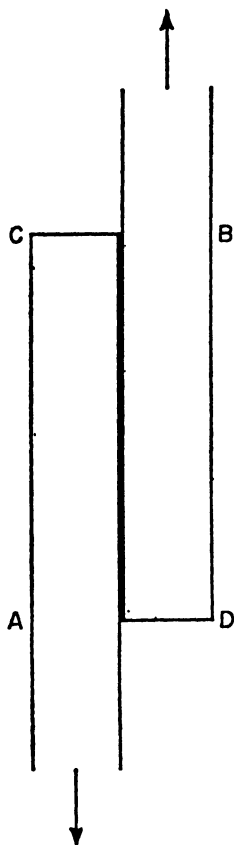


FIG. 5. A lap joint before deformation.

If the members are not restrained, they bend when a pull is applied as pictured in Fig. 5. The tendency is for both forces (represented by the arrows in Fig. 5) to lie on one straight line. Of course, the bond may fail long before this is accomplished. The stresses in a deformed lap joint have been calculated.²⁴ They are small when the thickness of the members is great and the length λ of the overlap is small. In theory, the stress concentration caused by bending increases with the ratio λ/h .

Probably chiefly because of bending, the failing load of a simple lap joint does not increase linearly with λ . An approximate proportionality between F and λ is observed at small values of λ ; the range of validity of the equation $F/\lambda = \text{const.}$ is greater the thinner the members. When 6-mm. thick steel strips were used, this relation was valid for λ smaller

²⁴ M. Goland and E. Reissner, *J. Appl. Mechanics* **11**, 17 (1944).

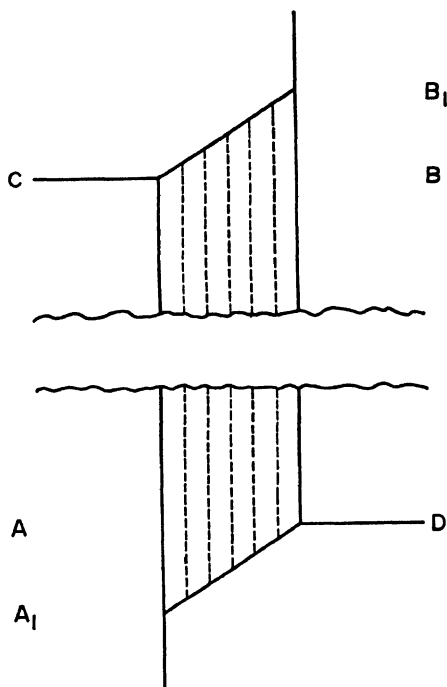


FIG. 6. Deformation of the adhesive layer in a stressed lap joint. The adhesive which was in contact with the solid at the left along AC now extends between A_1 and C; and the length of contact between the adhesive and the solid at the right increased from BD to B_1D .

than 10 mm. only; when λ increased from 1.2 to 2.5 cm., F increased by 16%.²⁵

In a "block shear test" the force is applied as shown in Fig. 7.²⁶ The deformation of the adhesive is as in Fig. 6. The bending of the members should be negligible.

In double lap joints bending is eliminated and these bonds are stronger (for instance, in the ratio 1.65:1) than comparable single lap joints.²⁷

In a cylindrical lap joint (in which the adhesive fills a narrow annular space between two coaxial cylinders) the highest concentration of stress occurs at the loaded end of the inner tube.²⁸ The force carried by this tube

²⁵ N. A. De Bruyne, *J. Sci. Instr.* **24**, 29 (1947).

²⁶ *Am. Soc. Testing Materials, ASTM Standards D 905-49* (1954).

²⁷ Experiments by Nat. Luchtvaart Laboratorium Amsterdam reported in N. A. De Bruyne and R. Houwink, "Adhesion and Adhesives," p. 108. Elsevier, Amsterdam, 1951.

²⁸ J. L. Lubkin and E. Reissner, *Trans. Am. Soc. Mech. Engrs.* **78**, 1213 (1956).

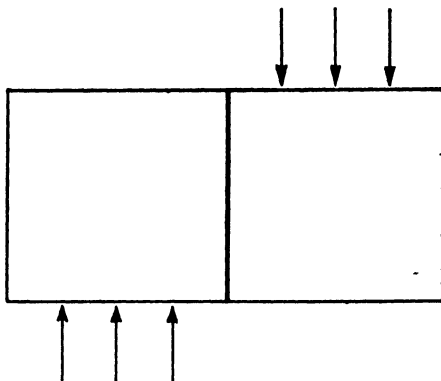
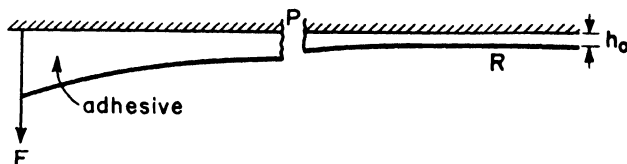


FIG. 7. A specimen for a block shear test

FIG. 8. Peeling test. P is rigid plate, R is flexible ribbon, F is applied force, h_0 is the initial thickness of the adhesive film.

is equal to that carried by the external tube. However the circumference of the former is shorter than that of the latter; hence the stress is greater along the internal than along the external boundary of the cylindrical adhesive film.

In *peeling*, the external force F (see Fig. 8) is balanced by the sum of the stresses produced in the adhesive film by its extension in the directions parallel to F ;²⁹ P is a rigid plate, and R is a flexible ribbon. If the adhesive is a Hookean solid and the force F is applied right at the edge of the adhesive film (as in Fig. 8), then at a first approximation the joint ruptures when³⁰

$$F = 0.3799w\sigma(E/E_1)^{1/4}h_0^{1/4}\delta^{3/4} \quad (4)$$

In this equation, w is the width of the ribbon (that is normal to the plane of paper in Fig. 8), σ is the tensile strength of the adhesive, E and E_1 are the moduli of elasticity of the ribbon and the adhesive, respectively, h_0 is the initial thickness of the adhesive film, and δ is the ribbon thickness. The force required for an idealized tensile rupture (that is, neglecting the

²⁹ G. J. Spies, *Aircraft Eng.* **25**(289), 64 (1953).

³⁰ J. J. Bikerman, *J. Appl. Phys.* **28**, 1484 (1957).

macroscopic stress concentrations) is $\sigma \omega l$, if l is the ribbon length. Hence,

$$\frac{\text{tensile force}}{\text{peeling force}} = \frac{l(E_1/E)^{1/4}}{0.3799 h_0^{1/4} \delta^{3/4}} \quad (5)$$

The quantity $(E_1/E)^{1/4}$ usually would be between 0.1 and 0.5; that is, $(E_1/E)^{1/4}/0.3799$ would not be far from unity. Hence, the ratio of tensile to peeling force is roughly equal to the ratio $l/h_0^{1/4} \delta^{3/4}$. As l in laboratory experiments would be, say, between 1 and 10 cm., while h_0 and δ are between 0.001 and 0.1 cm., the ratio of the two forces is likely to be over one hundred.

When the external force acts not exactly normally to the adhesive film, the breaking load depends also on the angle between that force and the film. Usually, this angle is maintained at either 90° (e.g., Eller³¹) or 180° ³² but that fraction of the external force which really causes peeling depends not only on the angle but also on the stiffness of the ribbon. The experimental material on peeling (e.g., see references 22, 29, 33, 34) is insufficient for a quantitative test of the theory. In many other publications on stripping, its rheology was neglected altogether.³⁵

In some experiments³⁶ a blob of the adhesive was pried loose with a spatula. A similar technique is common in the testing of paints and coatings whose adherence to the support is judged by the ease (or difficulty) of scraping them off. For flexible coatings the rheology of this process is similar to that of metal-cutting, such as in turning or milling.³⁷

The work expended on breaking an adhesive joint is difficult to determine when the rupture is accomplished in a tensile or a shear test. It has been believed (for instance, by Krotova *et al.*³⁵) that the work of peeling, which is readily measured, is identical with the work needed to overcome the molecular or electrostatic forces of adhesion. This belief is not warranted.³⁸ In the instances when equation (4) is satisfactory, the work of stripping for l cm. ribbon length obviously is $0.3799 l w \sigma (E/E_1)^{1/4} h_0^{1/4} \delta^{3/4}$ and depends on the properties of the two materials rather than on their interaction.

The results of all rupture tests depend on the rate of application of the

³¹ S. A. Eller, *ASTM Bull.* **190**, 41 (1953).

³² *Am. Soc. Testing Materials, ASTM Standards D 413-39 and D 1000-48T* (1954).

³³ W. C. Wake, in "Adhesion," p. 94. Society of Chemical Industry, London, 1952.

³⁴ G. W. Koehn, in "Adhesion and Adhesives: Fundamentals and Practice," (F. Clark, J. E. Rutzler, and R. L. Savage, eds.), p. 120. Wiley, New York, 1954.

³⁵ N. A. Krotova, Yu. M. Kirillova, and B. V. Deryagin, *Zhur. Fiz. Khim.* **30**, 192 (1956).

³⁶ H. P. Meissner and E. W. Merrill, *ASTM Bull.* **151**, 80 (1948).

³⁷ W. K. Asbeck, private communication (1957).

³⁸ e.g., K. M. Gorbunova, and P. D. Dankov, *Zhur. Fiz. Khim.* **27**, 1725 (1953).

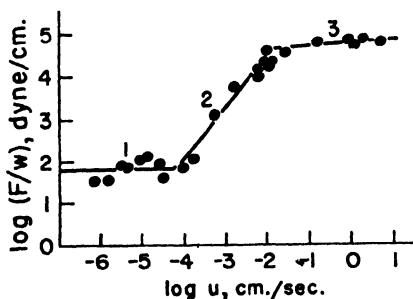


FIG. 9. Relation between force and rate of peeling. Abscissa: log of the rate of peeling in centimeters per second. Ordinate: log of peeling force per centimeter-width. Stripping of a cellulose nitrate film from glass. (From Krotova *et al.*³⁶)

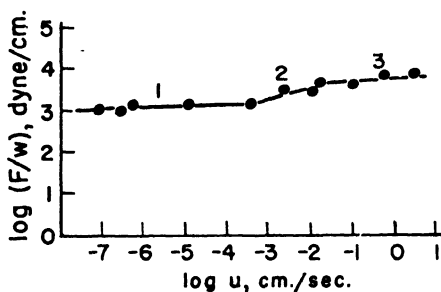


FIG. 10. Relation between force and rate of peeling. Abscissa: log of the rate of peeling in centimeters per second. Ordinate: log of peeling force per cm. width. Stripping of a cellulose acetate film from glass. (From Krotova *et al.*³⁶)

external force. This rate has two main effects. When the load increases slowly, the system has time for rearrangement which tends to relieve the internal stresses. On the other hand, when a load, which is insufficient for rupture in the instant of application, is left acting for a long time, a new and particularly bad flaw may form and cause disruption. Thus, often "constant-rate-of-loading" devices must be used to obtain reproducible results. The rate of separation is particularly easy to change in peeling tests. Fig. 9 and Fig. 10 illustrate³⁶ how different the dependence of the rate u of separation on the force F may be for different adhesives. It can be deduced from some earlier experiments^{39, 40} that u sometimes depends on F according to the equation

$$u = a(e^{bF} - 1), \quad (6)$$

a and b being constant. These experiments were carried out on two-ply

³⁹ S. L. Anderson, *J. Sci. Instr.* **26**, 153 (1949).

⁴⁰ E. M. Borroff, R. Elliott, and W. C. Wake, *J. Rubber Research* **20**, 42 (1951).

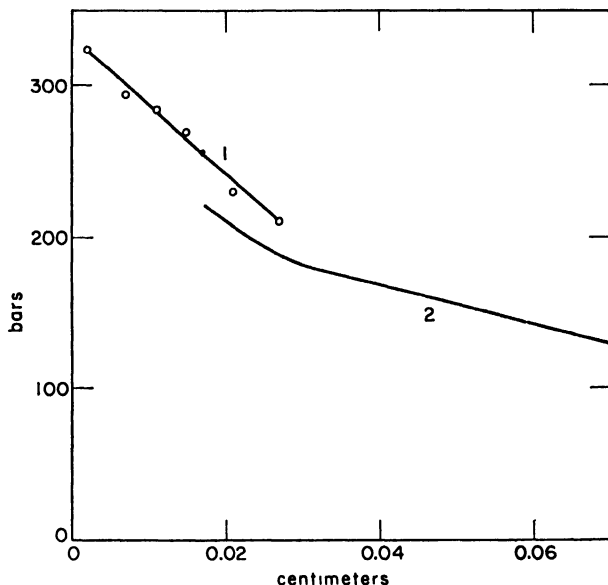


FIG. 11. Increase in breaking stress on reduction of the bond thickness. Abscissa: bond thickness in centimeters. Ordinate: breaking stress in 10^6 dynes/cm². Key: curve 1, steel-polystyrene bonds at -24°C . (from the data of Kraus and Manson⁴¹); curve 2, steel-poly(methyl methacrylate) bonds at 25°C . (from the data of Meissner and Merrill³⁶).

cotton fabric having an interply layer of vulcanized rubber and on conveyor belting plies. In Anderson's tests, u was varied between 0.0008 and 160 cm./sec., and in Wake's work, between 0.04 and 3.1 cm./sec.

3. STRENGTH AND THINNESS OF JOINTS

As long as the continuity of the adhesive is preserved and the adhesive is the seat of the failure, the bonds are stronger the thinner the adhesive film, at least in tensile tests. This rule, known for many years, is illustrated here by two examples taken from Meissner and Merrill³⁶ and Kraus and Manson⁴¹ (see Fig. 11).

A few additional examples:¹⁸ for brass cylinders joined by eutectic solder the breaking stress F/A was about 1600 bars when the thickness (h_0) of the adhesive layer was 0.01 to 0.02 cm. and about 600 bars at $h_0 = 0.5$ cm.; for oxidized steel and paraffin wax F/A was 45 bars at $h_0 = 0.0025$ cm. and 14 bars at $h_0 = 0.25$ cm.

The explanation of the above rule utilizes much of the knowledge pre-

⁴¹ G. Kraus and J. E. Manson, *J. Polymer Sci.* **6**, 625 (1951).

sented in the previous sections of this chapter and illustrates the application of this knowledge to particular problems.

As far as known, there are three main causes of the increase in F/A with diminishing thickness. The first is quite general and, indeed, was pointed out for fibers and wires before being considered in the discussion of bond strength. The second and the third are common but may also be absent in any particular instance. They are:

(a) According to the probability theory of strength (Section V,1) thin layers of an adhesive should be stronger than thick layers because bad flaws are more likely to be present in a larger specimen. In a particularly simple test of this theory⁴² the least breaking stress among n bonds, each of thickness h_0 , is compared with that of a bond nh_0 cm. thick. If the two values are identical, the whole effect of h_0 on F/A is accounted for by the probability. In experiments on paraffin wax joints between metal adherends, about $\frac{2}{3}$ of the effect could be explained in this manner. This cause is more important for adhesives whose total elongation is small than for those having a rubberlike elasticity, as the flaws in the latter class substances are oriented during the rupture test.

(b) The conditions of solidification of a thin layer are different from those of a thick layer. Hence, as mentioned in Section IV,2, the texture of the resulting solid depends on h_0 . For instance, a thin adhesive film which solidified on cooling probably will consist of smaller crystals or smaller oriented domains than a thicker film which has set at identical external conditions. Thus, its tensile strength may be greater than that of thicker films.

(c) The distribution of stresses, both those set up during solidification and those produced by the applied load, depends on the thickness of the adhesive phase. It may be stated in general terms that the breaking load is greater if the specimen tested is free to be plastically deformed, as this deformation tends to equalize the local stresses. But plastic deformation is similar to the flow represented by equation (1) and, consequently, is restrained more the thinner the specimen; thus there is less "work-hardening" or, more generally, adjustment in thin films and they tend to be weaker. On the other hand, "necking" of a specimen reduces its cross section A and thus raises the applied stress F/A ; and this necking occurs more rapidly in a thicker specimen, again in accordance with equation (1) and analogous equations which take care of the non-Newtonian flow. Thus, depending on the properties of the adhesive material, stresses at a constant F may be either greater or smaller the thinner the joint.

The rule "the thinner the joint, the greater the bond strength" explains

⁴² J. J. Bikerman, *J. Soc. Chem. Ind. (London)* **40**, 23 (1941).

cated by the presence of the polymer filament. The appearance of the filament is very much like that of polystyrene filaments extruded at high shearing stresses. Jetting is believed to be responsible for a characteristic type of surface blemish in the molded article. When filling proceeds too slowly after jetting, the filament cools so much that it will not weld perfectly with the incoming hot polymer, thereby blemishing the surface of the molding. This type of blemish may be minimized by keeping the fill time below some arbitrary desirable value.

Another phenomenon which occurs during the filling of some cavities is the formation of weld lines. The presence of a weld line in injection moldings often poses a difficult problem from a standpoint of both strength and appearance. To produce a weld line and observe its formation in the photo mold, small inserts were placed in the center of the cavity between the glass plates. Figures 10 and 11 show two sequences of flow around a circular insert 0.25 in. in diameter and a square insert 0.25 in. on a side. It is evident from these pictures that the flow of polymer adjacent to the insert is greatly retarded. As a result the two polymer streams produced by the insert first join at a distance from the insert. The weld line then forms in toward the insert as well as in the direction of polymer flow. Since a small pocket of air is easily trapped between the insert and the point where the polymer first forms the weld line, it will have little strength adjacent to the insert unless means are provided for allowing this air to escape. If the filling process is rapid enough, this entrapment of air may cause the polymer to burn.

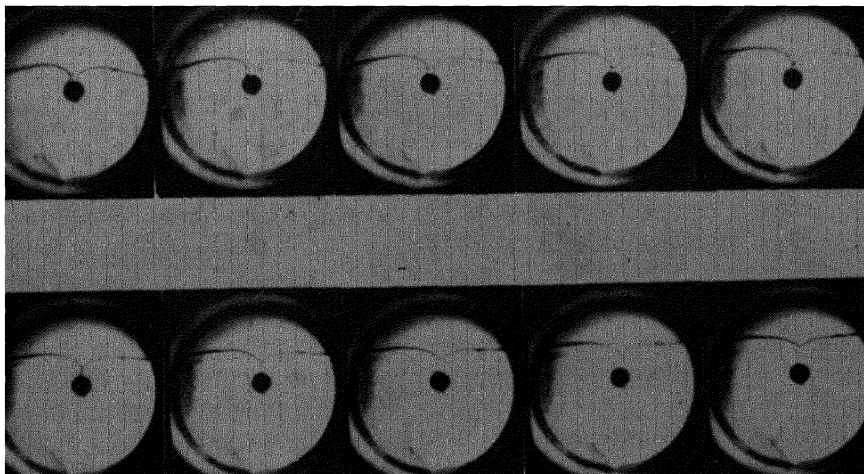


Fig. 10. Sequence of flow around a circular insert

some product of reaction between adhesive and adherend; for a recent example see ref.⁴⁶

This observation can be accounted for by a probability consideration.⁴⁷ In Fig. 12 crosses and circles represent the atoms (or molecules) of the adherend and the adhesive, respectively. Suppose that a crack started, as shown, between the first (from the left) cross and first circle, i.e., as a true failure in adhesion. The crack can continue (toward the right) between the second cross and the second circle but it may also be propagated between two crosses or between two circles. If all these paths are equally probable, the probability of the crack's continuing in adhesion for the length of two atoms is $\frac{1}{3}$. The probability of a crack between adherend and adhesive being three atoms long is $(\frac{1}{3})^2$, and for a crack 100 atoms long (which still is very short) it is $(\frac{1}{3})^{100}$, i.e., practically zero.

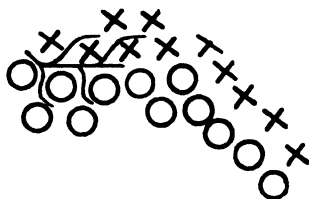


FIG. 12. Explanation, based on probability, of the virtual absence of failures in true adhesion. A predetermined path for the propagation of a crack is improbable.

The probability would be significantly different if there was an enormous bias toward separation between different materials. However, our meager knowledge of molecular forces is sufficient to conclude that a bias of the opposite sign is more likely to exist; that is, the attraction between adherend and adhesive usually exceeds that between two molecules of the adhesive. The constant a in the van der Waals equation is the classical measure of the intermolecular forces. It has been known for many years⁴⁸ that the corresponding constant a_{12} for the equimolecular mixture of two gases (with subscripts 1 and 2) is approximately $a_{12} = (a_1 a_2)^{1/2}$, i.e., greater than the smaller of the two values (a_1 and a_2) for the pure components. It is presumably permitted to extend this reasoning to solids and admit that the attraction between a molecule of adherend and a molecule of adhesive is somewhere between the mutual attractions of two adherend molecules and two adhesive molecules. If, as usual, the latter attraction is weaker

⁴⁶ R. L. Patrick, C. M. Doede, and W. A. Vaughan, *J. Phys. Chem.* **61**, 1036 (1957).

⁴⁷ J. J. Bikerman, in "Surface Activity: Proceedings of the Second International Congress on Surface Activity, London, April, 1957," (J. H. Schulman, ed.), Vol. 3, p. 427 Academic Press, New York, 1957.

⁴⁸ See the review by J. A. Beattie, *Chem. Revs.* **44**, 141 (1949).

than the former, the attraction across the interface is stronger than that in the bulk of the adhesive.

VI. Summary

The problem of bond strength belongs to rheology—except for the removal of surface layers, which is mainly a chemical process. The bond strength is determined by the geometry of the joint and the mechanical properties (viscosity, tensile strength, etc.) of the adherends, the adhesive, or the boundary layers, whichever is weaker, rather than by any interaction between the components of a joint. The mechanical properties of these compounds may be influenced by the composition and the history of the joint.

Nomenclature

a Radius; half-axis of an ellipse; attraction constant in the van der Waals equation; a constant	l Length of adherend ribbon
A Area	n Number of specimens
b Half-axis of an ellipse; a constant	p, p_0 Local and average tensile stress
E, E_1 Modulus of elasticity of ad- herend and adhesive, respec- tively	t Time
f Stress	u Rate of separation
f_0 Breaking stress of a joint	w Width of adherend ribbon
F Force	δ Thickness of adherend ribbon
h, h_0, h_1 Film thickness; initial film thickness; final film thickness	η Viscosity
	κ A numerical constant
	λ Length of overlap
	μ Poisson's ratio
	ρ_1, ρ_2 Density of adhesive and ad- herend, respectively
	σ Tensile strength of adhesive

CHAPTER 14

RHEOLOGY IN MOLDING

C. E. Beyer and R. S. Spencer

I. Introduction	505
II. The Injection Molding Machine	506
1. Description of the Machine	506
2. Description of the Controls	508
3. The Injection Molding Process	509
III. The Injection Molding Cycle	510
1. The Function of the Injection Temperature and Pressure	510
2. The Mold Pressure Cycle	513
IV. Filling the Mold	514
1. Description of Flow into the Mold	514
2. Fill Time Equation	520
V. Packing in the Mold	524
1. Description	524
2. Pressure Losses in the Injection Molding Machine	525
3. Equation of Pressure Loss	529
4. Residual Strains	531
VI. Discharge and Sealing	535
1. Description	535
2. Seal Line	536
VII. Sealed Cooling	537
1. The Equation of State	537
2. Mold Opening Conditions	540
3. Conformity to Mold	541
VIII. Cycle Time	542
1. Limiting Cycle	543
2. Molding Diagram	544
3. Moldability	548
Nomenclature	550
General Bibliography	551

I. Introduction

Injection molding is one of the principal methods by which thermoplastics are fabricated. The conditions that exist in the injection molding machine have presented many new and interesting rheological problems. Most of the problems encountered in the process of injection molding are far too complex to attempt rigorous theoretical solutions. Consider for a

moment the difficulties involved in a mathematical treatment of a hot non-Newtonian compressible liquid flowing through a geometrically complex channel, the walls of which are much colder than the liquid. It is little wonder that in the past, injection molding has been left to develop, for the most part, as an empirical art. Even though obtaining exact theoretical solutions to many injection molding problems is not practical, considerable knowledge of the process can be obtained from various approximations and idealizations which result in only semiquantitative agreement with experience. Such an approach may be used to sketch in the broad forms of relationships, whose finer details can be filled in by suitable experiments.

An attempt will be made in this section to indicate the rheological problems in injection molding and to show how the various flow conditions blend into the more complex situation that we call the Injection Molding Cycle. Most of this work has been done with polystyrene, but the same types of relationships may be expected for other noncrystalline thermoplastics.

II. The Injection Molding Machine

1. DESCRIPTION OF THE MACHINE

In the fabrication of any thermoplastic resin, the basic process consists of (1) heating the polymer to a relatively fluid state, (2) forming the desired shape in the mold, (3) cooling this molding to a solid mass. An injection molding machine is shown in Fig. 1. It can be described in terms of six basic components: (1) a feeding mechanism to meter out a constant

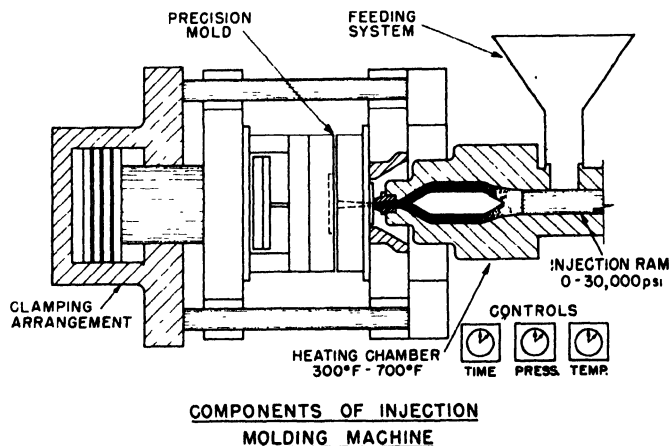


FIG. 1. Schematic drawing of an injection molding machine comprising: (1) feeder, (2) plunger, (3) tunnel, (4) mold, (5) clamping device, and (6) controls.

amount of material for each molding; (2) a plunger or ram to move the polymer through the heating cylinder at an appropriate pressure; (3) a cylinder in which the polymer is heated to a molten condition; (4) a precision-built mold comprising two or more sections which may be opened to remove final product; (5) a clamping mechanism to hold the sections of the mold together; and (6) a system of timers to control the sequence of operation of the injection molding cycle.

The feeding mechanism may be governed either volumetrically or gravimetrically. A volumetric feeder usually consists of a simple sliding chute placed between the hopper of the feeding system and the heating chamber. The polymer is placed into the hopper as pellets and a portion of it falls into a sliding chute. During the injection stroke the chute moves forward, carrying with it a specified volume of polymer which is then released on top of the ram. When the ram returns, the slide travels back into position below the hopper to receive more polymer and the polymer on the ram falls in front of the ram, ready to be pushed into the heating chamber on the next stroke. In weigh feeding the volumetric mechanism is replaced by a sensitive balance device which delivers an exact weight of polymer into the heating cylinder. Since there are some variations in the bulk density of the granular material, weigh feeding gives a more exact control of the amount of material introduced into the mold.

Once the mold is closed the plunger moves forward, pushing cold granules ahead of it into the heating chamber and simultaneously forcing the same amount of molten polymer through a nozzle connecting the front end of the heating chamber with the mold. After holding the pressure on the polymer in the mold for a specified length of time the ram will return to its rear position to await the next cycle.

The heating chamber usually consists of a hollow steel cylinder, jacketed on the outside by electrical heaters. Because of the low thermal conductivity of thermoplastics it is desirable to spread the polymer into a thin layer to obtain more rapid heating. A spreader, or "torpedo," is placed inside the heating chamber for this purpose. However, this torpedo may so restrict the flow of polymer that a large percentage of the pressure exerted by the ram is dissipated in the heating cylinder. To avoid this effect many of the larger molding machines are equipped with preplasticizers, which consist of two consecutive cylinders, each with its own ram. The first cylinder contains a conventional torpedo and is used for heating the polymer. The second cylinder contains no torpedo and leads through a nozzle to the mold. The absence of a torpedo and unmolten polymer permits a greater percentage of the ram pressure to be transmitted into the mold.

The molten polymer moves from the heating chamber through a system of passages into the mold cavity. A conventional mold consists of essentially

three parts: (1) a stationary (cavity) part; (2) a movable (core) part; and (3) an ejector plate with knockout pins in the movable portion of the mold to assist in removing the finished piece from the mold. The mold is clamped between the two platens of the molding press, one of which is stationary and holds the cavity portion of the mold in contact with the nozzle of the heating cylinder. The second platen is movable and allows the mold to be opened upon completion of the molding cycle. It is actuated by a clamping mechanism which also holds the mold halves together while the polymer is being forced into the mold. The clamping mechanism may consist of a hydraulic cylinder or a hydraulically activated toggle.

2. DESCRIPTION OF THE CONTROLS

The three primary variables which govern the operation of the injection molding machine are temperature, pressure, and time. The heating cylinder temperature is maintained at some constant value, usually between 400 and 700° F. At these conditions most polymers have a sufficiently low viscosity to fill the mold with the available ram pressure. The temperature of the heating chamber is maintained by pyrometers connected to the heaters. These are activated by thermocouples imbedded in the cylinder body. The mold is usually held at a relatively constant temperature by means of water flowing through passages surrounding the mold cavity. Mold temperature is regulated either by the amount of water flowing through it, or by controlling the temperature of the water. Ordinarily a range of 90 to 180° F. is used to give a desirable surface luster to the molding.

The injection pressure is set to fill the mold and to develop a hydrostatic pressure in the mold to compensate for the shrinkage of the polymer during cooling. Thus, the right combination of the heater temperature and injection pressure will result in a molding that is an exact reproduction of the mold cavity. The two halves of the mold are clamped together either by a hydraulic cylinder or a hydraulically actuated toggle system. This pressure must be maintained high enough to prevent the mold halves from separating under the injection pressure.

A set of timers on the injection molding machine control the sequence of operation. The first one activated in the cycle controls the length of time that the ram remains in its forward position. When this timer returns the ram to its initial position, another is activated which controls the cooling time and at the end of this time period the mold opens for removal of the molding. This ensures adequate cooling of the article before it is removed from the mold. There are usually two additional, less important timers. One gives the injection ram an extra stroke, thereby obtaining a larger shot. The other regulates the time that the mold remains open for removal of the molding and thus provides a more uniform cycle.

3. THE INJECTION MOLDING PROCESS

There are six major controls available to the operator of the molding machine: (1) temperature of the heating chamber; (2) pressure applied by the ram; (3) the "plunger forward" time; (4) the "mold closed" time; (5) the "mold open" time; and (6) the mold temperature.

The technique of adjustment of these controls and the nature of the polymer are the means by which the acceptability of the finished article is determined. Most of these controls are indirect and are interrelated in some complex manner in their effect on the quality of the finished molding. Before discussing the relations between the controls and the molding let us first consider the flow of polymer through the molding machine.

In the injection molding process a specified volume shot of polymer is fed from the hopper and pushed into the heating chamber by the ram on its forward stroke. Ordinarily, the polymer will take several cycles to move through the heating chamber since the amount of polymer in the heating chamber is at least twice the maximum shot size of the machine. Hence, the amount of time the material will remain in the heating chamber will depend upon both the cycle time and the shot size. The molten polymer leaves the heating chamber through the nozzle and proceeds to the mold cavity via the sprue, runners, and gate. The latter is a restricted passage at the entrance to the mold cavity. After the mold is filled the ram pressure is maintained for a short time. This packs a little more polymer into the mold to compensate for contraction of the polymer during cooling. Some of the polymer is then discharged back out of the mold after the plunger has released its pressure. Following discharge, the polymer in the gate (which is usually the smallest restriction in the mold passages) will be solid enough to withstand the pressure in the mold and will seal the mold cavity from the rest of the system. When a weigh feeder is used the discharge step can be eliminated from the cycle. Here the exact weight of polymer required to make a full molding is forced into the mold. Therefore, the plunger can remain in its forward position until the gate has sealed. It will be shown later that the elimination of discharge greatly reduces the amount of strain in the molded article. The polymer will then cool under conditions of constant mass and constant volume unless the pressure reaches zero during cooling. When the article has cooled to a point where it can be removed from the mold, the rear half of the mold will open and separate from the rest of the mold. As the mold opens, the ejector plate with the ejector pins moves forward, pushing the molding off the core. After the piece is removed from the mold it closes again and the cycle is repeated.

The above discussion indicates that the injection molding cycle may be broken down into the following steps: (1) the dead time, comprising the period from when the plunger starts forward until the polymer begins

flowing into the mold; (2) filling; (3) packing; (4) discharge; (5) sealing; and (6) sealed cooling.

III. The Injection Molding Cycle

1. THE FUNCTION OF THE INJECTION TEMPERATURE AND PRESSURE

As mentioned previously, the six major controls in the molding machine operate interdependently to determine a set of variables which are more directly related to the acceptability of the molded article. The primary variables which determine the quality of the molded article are the pressure and temperature of the polymer, particularly at the time the gate seals and when the mold opens. To determine the relationship between the machine controls and the primary variables it is desirable to know these quantities as a function of time after the mold is filled. Given the geometry of the mold, the temperature of the polymer as it enters the mold, and the mold temperature, the average temperature of the piece may be computed as a function of time from heat conduction theory. This calculation involves idealization of actual conditions, but results can be obtained which are sufficient in most cases to give a relatively accurate picture of what is happening in the mold during the various portions of the cycle. Equations that may be used as approximations for many cases are:

$$\Theta \equiv \frac{T - T_0}{T_i - T_0}$$

Slab

$$\Theta = \frac{8}{\pi^2} \sum_{n=1}^{\infty} \frac{1}{(2n-1)^2} \exp\left(\frac{-(2n-1)^2 \pi^2 h^2 t}{h^2}\right) \quad (1)$$

Sphere

$$\Theta = \frac{6}{\pi^2} \sum_{n=1}^{\infty} \frac{1}{n^2} \exp\left(\frac{-n^2 \pi^2 h^2 t}{R^2}\right) \quad (2)$$

Cylinder

$$\Theta = \frac{6}{\pi^2} \sum_{n=1}^{\infty} \frac{1}{\alpha_n^2} \exp\left(\frac{-\alpha_n^2 h^2 t}{R^2}\right) \quad (3)$$

where T = the average polymer temperature, T_i = the original temperature of the polymer, T_0 = the surface temperature of the mold, t = time, L = the thickness of the slab, R = the radius of the cylinder or sphere, h^2 = the thermal diffusivity of the material = (thermal conductivity)/(specific heat)(density), α_n = the positive roots of the Bessel's equation $J_0(\alpha R) = 0$. The functions defined by these equations are shown in Fig. 2.

Most of the polymers ordinarily used in the injection molding machine are very poor conductors of heat and they normally do not remain in the heating chamber long enough to reach the temperature of the cylinder wall. Therefore the polymer temperature as it leaves the nozzle and enters the mold not only depends upon the heater settings but also upon the rate at which the plastic moves through the heating chamber. By the use of a specially designed thermocouple in the nozzle, the plastic temperature can be measured and related to the heater settings and output rate, so that the average temperature at which the plastic enters the mold is known. Figure 3 shows the observed relationship between the heating efficiency and the output rate of a typical injection molding machine. The heating efficiency is defined as

$$E = \frac{(\text{Average plastic temperature}) - (\text{Room temperature})}{(\text{Cylinder wall temperature}) - (\text{Room temperature})}$$

This relationship permits calculation of the average plastic temperature at any time during the molding cycle from the given machine conditions.

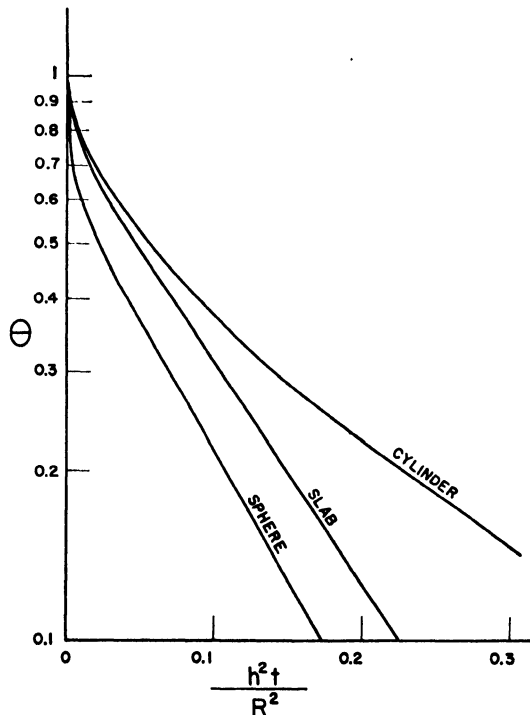


FIG. 2. Reduced average temperature from heat conduction theory

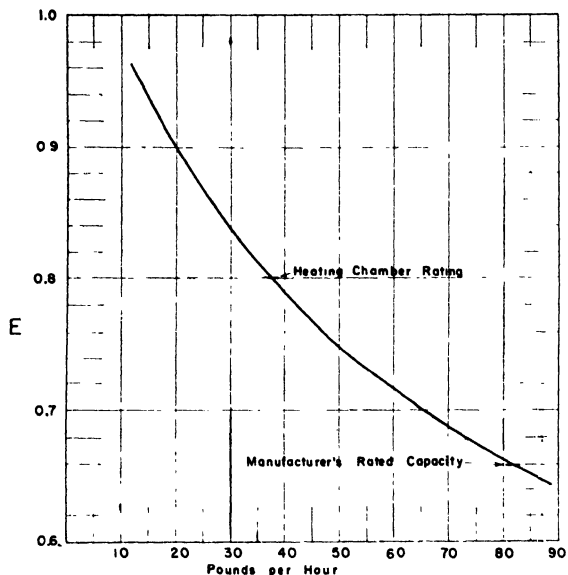


Fig. 3. Heating curve of an injection molding machine

The hydraulic system of the molding machine operates to exert a predetermined pressure on the injection ram. There is a large pressure drop through the granules which will vary with the amount of unmelted polymer ahead of the ram and the temperature of the cylinder wall around these granules. There will also be a pressure drop through all of the restrictions and channels between the ram and the mold, and even through the mold cavity itself. Thus, for any given injection pressure, the pressure in the mold cavity at any point will depend upon: (1) The position of the ram at the end of its stroke. (2) The temperature of the heating chamber wall at the end nearest the ram. (3) The surface lubrication on the granules. (4) The temperature of the polymer, and the relationship between the temperature and viscosity. (5) The size and length of the channels leading to the mold. (6) The geometry of the mold cavity.

As the plastic enters the mold, the outer portion that touches the mold surface will freeze almost instantaneously, and the molded article will consist of a molten core with a solid shell of polymer around it. This frozen layer will become thicker with time until finally the whole molding is frozen. The gate is usually the smallest opening in the system, and hence it is the first location which completely solidifies. The effective size of this orifice keeps decreasing and will depend upon the length of time the material cools. Maximum pressure that the gate can hold in the mold will de-

pend upon the size of the fluid core in the gate, and the fluidity of the polymer in the mold. The longer the material is allowed to cool the smaller will be the orifice size and polymer fluidity. Consequently, the pressure drop that can be maintained across the gate will be higher. When this pressure drop, effective diameter, fluidity and rate of cooling come to an equilibrium condition, so that there is no flow, the mold is then completely separated from the heating cylinder and the gate can be considered sealed. Once the gate has sealed, the pressure will fall off with the temperature according to the equation of state for a system of constant mass and volume. When (1) the pressure in the mold is lowered to a point where the molding will release from the mold as a result of contraction, and (2) the article has hardened enough to maintain its shape after removal from the mold, the mold may be opened.

A primary function of both the injection temperature and pressure is to fill the mold with the required amount of polymer in a fluid state so as to prevent weld lines or surface marks. If the pressure built up in the mold is below that required to offset shrinkage of the polymer during cooling, there will be excessive sink marks or bubbles. To make a good molding, therefore, the pressure in the mold and the plastic temperature when the mold has filled must be greater than the temperature and pressure at which the gate must seal for a given proper amount of material in the mold. In all practical cases, to fill the mold at a reasonable rate with the pressures available, the plastic temperature must be much higher than the temperature at which the gate seals. To maintain the mold pressure while the polymer is cooling down to the sealing temperature, the plunger must hold the pressure on the mold and force a small additional amount of material into the mold. This packing period extends until the plunger forward timer returns the ram. Some of the polymer will then discharge out of the mold, reducing the pressure in the mold to the level that the solidified polymer in the gate will hold in the mold at that temperature.

2. THE MOLD PRESSURE CYCLE

One of the most useful tools in studying the injection molding cycle is the mold pressure gauge. With this gauge the pressure in the mold throughout the molding cycle can be measured as a function of time. A typical mold pressure cycle diagram is shown in Fig. 4. In this diagram are shown the major subdivisions of the cycle, with mold closure denoting zero time. The dead time (1) has little significance other than its contribution to the total cycle time. Filling the mold (2) constitutes the second stage of the process and extends until the pressure starts to rise in the mold. In the packing step (3) the pressure builds up to a maximum very quickly and then remains relatively constant during the remainder of the packing time.

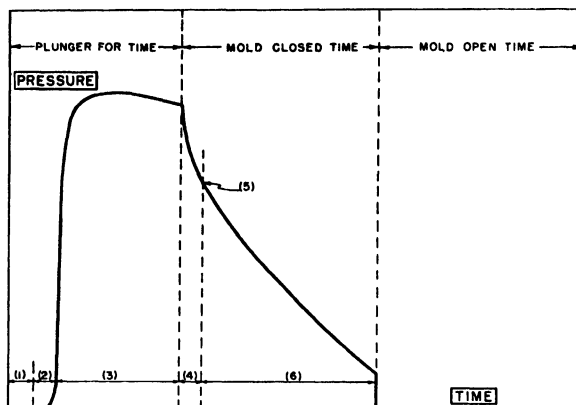


FIG. 4. Pressure in the mold during a typical cycle. Sequence of events is: (1) dead time, (2) filling, (3) packing, (4) discharge, (5) sealing, and (6) sealed cooling.

At the end of the packing period the plunger is released and the excess polymer discharges out of the mold (4). At this point the mold pressure begins to drop rapidly. As the pressure decreases the flow from the mold decreases and eventually ceases at the sealing point (5). A further reduction in pressure results from cooling of the polymer (6). At a given point during cooling the mold is opened and the mold pressure drops to atmospheric pressure. If this residual pressure in the mold when it opens is too high, the product may be scored or broken on ejection.

Since the temperature of the polymer in the mold is related to the time it has cooled in the mold, the time coordinate of the mold pressure diagram can be converted to plastic temperature. Thus, it is possible to draw a diagram representing the pressure-temperature relationships during the injection molding cycle (Fig. 5). The dashed lines on this figure are lines of constant density representing the conditions in the mold during the sealed cooling portion of the cycle where the polymer is cooling under constant density conditions.

IV. Filling the Mold

1. DESCRIPTION OF FLOW INTO THE MOLD

The problems involved in any attempt to treat quantitatively the filling of the mold are very complex. Most thermoplastics have non-Newtonian flow properties; i.e., the flow rate is very sensitive to changes in the pressure gradient which occur under typical filling conditions. The flow rate is also sensitive to temperature gradients arising from contact of the hot polymer with the cold mold walls during filling. Moreover the geometrical complexity

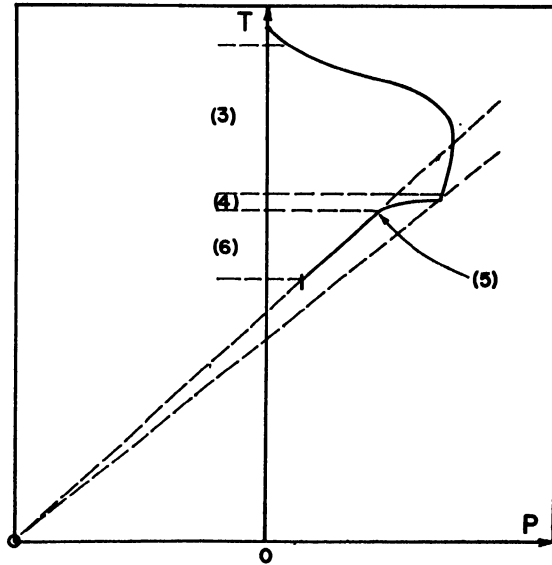


FIG. 5. Pressure-temperature relationships during the injection molding cycle

of the flow channels in the mold, along with the factors noted above enhance the difficulties involved in any theoretical approach.

During filling, the front of the polymer moves across the mold as shown in Fig. 6. In this type of flow between parallel plates the polymer front can be considered as a circular segment of continuously increasing radius, with

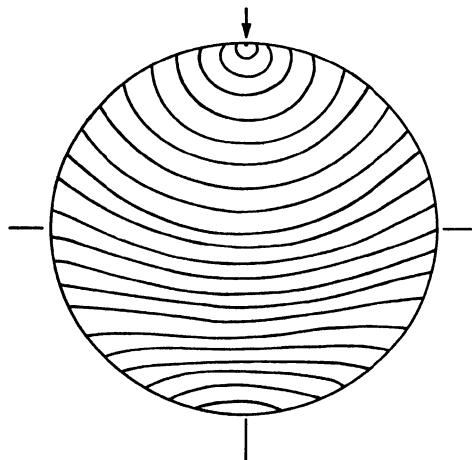


FIG. 6. Successive positions of the polymer front during filling of a disc mold. The time interval between positions is 0.078 sec.

the gate at the center. This is probably an adequate model if one neglects the effect of the circumferential wall. In the early stages of filling, the wall exerts a retarding force, and the polymer front in the vicinity of the wall bends back toward the gate. If the wall were not present, the polymer would flow radially into the cavity from the gate. During the later stages of filling the curved wall deflects the material which would otherwise strike it in radial flow, and this deflected polymer bends the wall ends of the front away from the gate. As a result, the front eventually becomes linear and then curves away from the gate just before completion of the filling operation.

To gain a better insight into the process of filling, a special mold was constructed to fabricate a disc 2 in. in diameter and 0.1 in. thick. Carefully annealed glass plates $1\frac{1}{4}$ in. thick were set into the two sides of the mold and appropriate windows were cut out, making the entire mold cavity visible. Slow-motion movies then were taken of the pattern of flow within the mold during the filling process. During filling, the front of hot polymer advanced across the mold as shown in several of the frames taken from

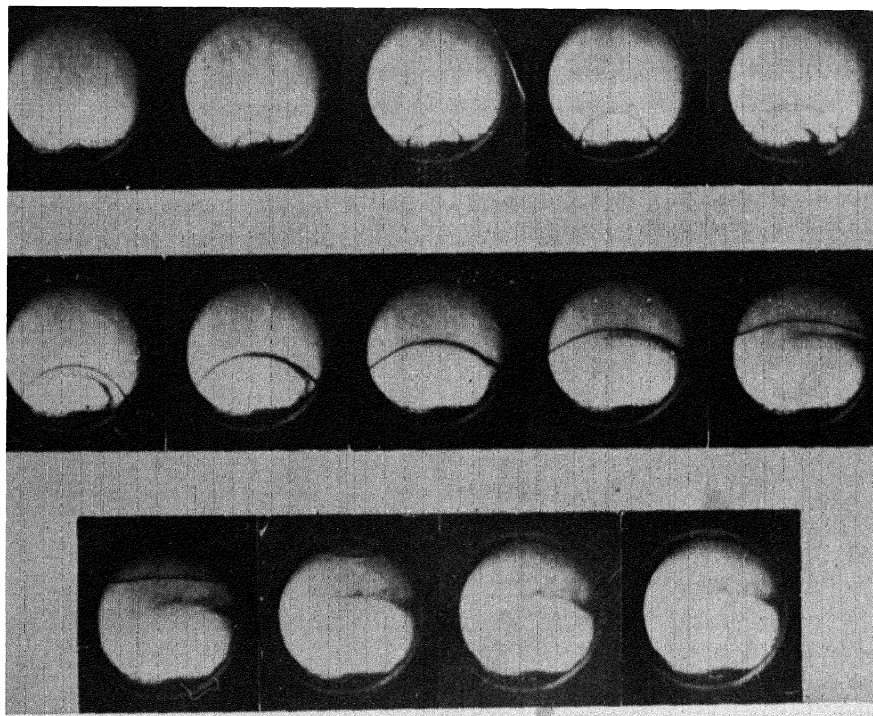


FIG. 7. During filling of the cavity, the polymer front moves across the mold

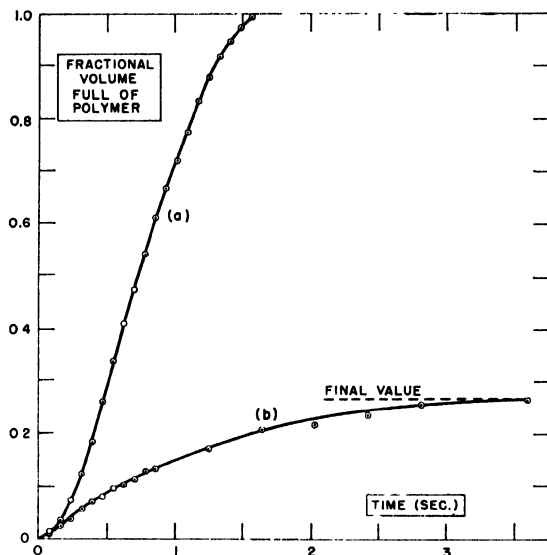


FIG. 8. Volume fraction of polymer in mold during filling; for (a) complete filling, (b) a short shot.

the movie (Fig. 7). The volume of polymer in the mold increases with time as indicated in curve (a) of Fig. 8.

Let us now consider what is going on in the portion of the mold which is already filled. Observation of the flow into the mold was facilitated by mixing a few dark granules with the clear polymer. In the fifth frame of Fig. 7 a streak of black polymer is shown entering the cavity, and in subsequent frames as it travels across the mold in a region centrally located between the parallel glass walls. Its velocity is greater than the velocity of the advancing front. The temperature of this bit of polymer does not drop appreciably in traversing the mold, unless flow is quite slow or the walls very close together. When our bit of polymer catches up with the advancing front it is forced outward against the mold wall. Here it is chilled quite rapidly and remains motionless, while the front traverses the rest of the mold. Thus, in the filled portion of the mold we find two regions; a cool motionless shell, and a relatively hot flow core. At the front the hot flowing polymer is being converted into a stationary shell. The subsequent phenomena of packing and discharge take place within the central core. As soon as the mold is full, the core begins to cool more rapidly and the shell increases in thickness.

Both packing and discharge have been observed in the glass window mold. To get some idea as to the relative polymer flow rates during these processes, measurements of lineal velocities in the neighborhood of the gate

TABLE I
APPROXIMATE POLYMER VELOCITIES AT ABOUT ONE CENTIMETER
FROM THE GATE IN THE GLASS-WINDOW MOLD

<i>Process</i>	<i>Velocity, cm./sec.</i>
Filling (about half full)	15-20
Filling (almost full)	6
Packing	3
Discharge	1
Jetting	70*

* This is the observed lineal velocity of the jet. For comparison with the preceding values this corresponds to 1.7 cm./sec. lineal velocity 1 cm. from the gate if the mold were full of polymer.

were made from the movies taken during filling, packing and discharge. The velocities measured are listed in Table I. Comparison of lineal velocities in the full part of the mold with the velocity of the front permits calculation of the thickness of the hot flowing core. In a typical case this is estimated to be 40 % of the thickness of the disc.

With relatively small gates another phenomenon is sometimes observed, which has been termed "jetting" (Fig. 9). The first polymer entering the mold has sufficient kinetic energy to shoot into the cavity in the form of a jet. The jet continues until the resulting filament of polymer becomes rigid enough, through cooling, to deflect the flow of polymer from the gate. Filling then proceeds in something like the normal pattern, slightly compli-

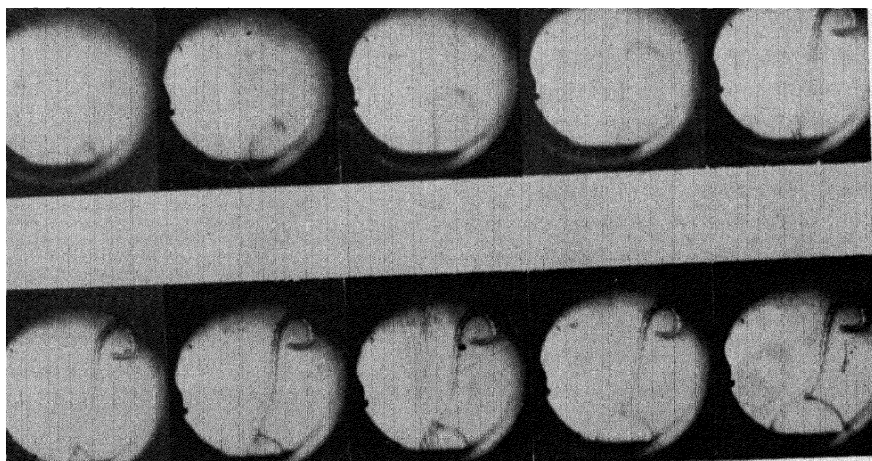


FIG. 9. "Jetting"

cated by the presence of the polymer filament. The appearance of the filament is very much like that of polystyrene filaments extruded at high shearing stresses. Jetting is believed to be responsible for a characteristic type of surface blemish in the molded article. When filling proceeds too slowly after jetting, the filament cools so much that it will not weld perfectly with the incoming hot polymer, thereby blemishing the surface of the molding. This type of blemish may be minimized by keeping the fill time below some arbitrary desirable value.

Another phenomenon which occurs during the filling of some cavities is the formation of weld lines. The presence of a weld line in injection moldings often poses a difficult problem from a standpoint of both strength and appearance. To produce a weld line and observe its formation in the photo mold, small inserts were placed in the center of the cavity between the glass plates. Figures 10 and 11 show two sequences of flow around a circular insert 0.25 in. in diameter and a square insert 0.25 in. on a side. It is evident from these pictures that the flow of polymer adjacent to the insert is greatly retarded. As a result the two polymer streams produced by the insert first join at a distance from the insert. The weld line then forms in toward the insert as well as in the direction of polymer flow. Since a small pocket of air is easily trapped between the insert and the point where the polymer first forms the weld line, it will have little strength adjacent to the insert unless means are provided for allowing this air to escape. If the filling process is rapid enough, this entrapment of air may cause the polymer to burn.

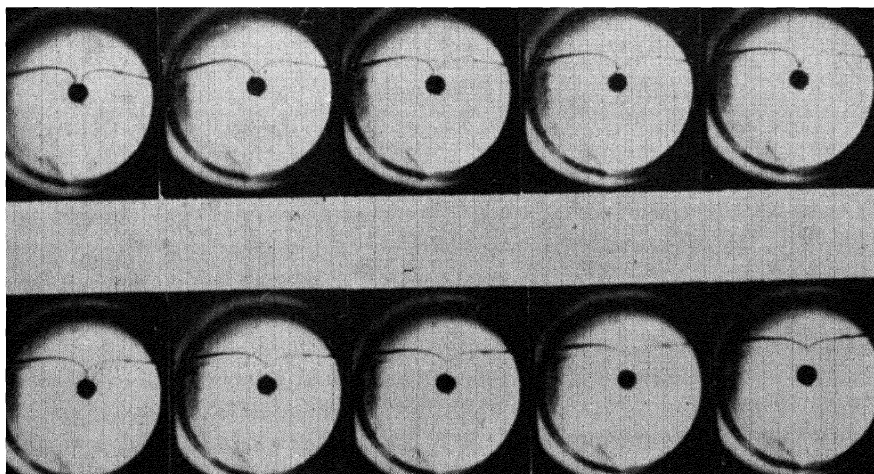


FIG. 10. Sequence of flow around a circular insert

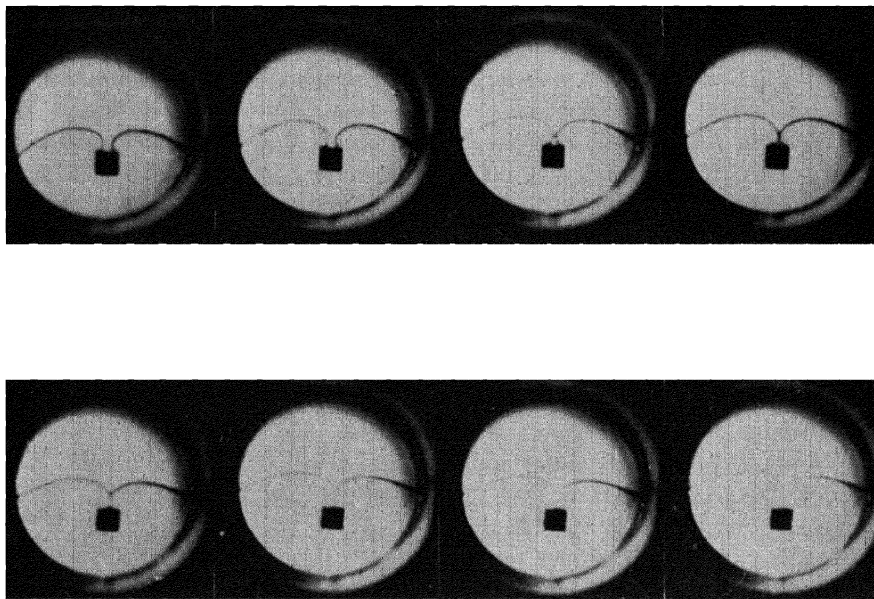


FIG. 11. Sequence of flow around a square insert

2. FILL TIME EQUATION

It is fairly well recognized by now that molten polystyrene is a non-Newtonian fluid because its rate of flow is not proportional to the driving force. The flow of polystyrene through a channel may be described by the following empirical equation:

$$Q = \frac{C_1 D^4 P}{L \eta_0} \left(1 + C_2 K \tau + \frac{C_2^2 K^2 \tau^2}{2!} + \frac{C_2^3 K^3 \tau^3}{3!} + \frac{C_2^4 K^4 \tau^4}{4!} \right) \quad (4)$$

where Q = volume rate of flow, L = length of channel, P = pressure drop, τ = shearing stress at channel wall, D = a characteristic dimension representative of the cross-sectional size, and $C_1 + C_2$ = constants denoting the shape of the channel. Two constants characteristic of the polymer appear in this equation. Of these η_0 is the Newtonian viscosity, and K is a constant proportional to the highly elastic compliance.

Actually, this approach is more detailed than is necessary to satisfactorily discuss the flow characteristics of most commercial polystyrenes, since they fall within a rather limited range of average molecular weight. Since K is directly proportional to molecular weight and independent of temperature, the dependence of flow rate on pressure is relatively invariant over the range of commercial polystyrenes unless they differ appreciably

in content of plasticizer, lubricant, or low molecular weight polymers. However, the Newtonian viscosity is very sensitive to changes in molecular weight or temperature and thus strongly influences the magnitude of flow velocity Q .

A further simplification of equation (4) is possible. The pressure differentials of interest in injection molding are usually in the narrow range. In addition to this the shearing stresses, τ , during flow in molding are relatively high, and a power law equation can be used to approximate the flow:

$$Q = \frac{AP^\alpha}{\eta_0} \quad (5)$$

Here the constant A depends upon the geometry of the channel through which the polymer flows. For a given channel and pressure range one would not expect A and α to vary appreciably with temperature or choice of commercial polystyrene. Further equation (5) will probably be a reasonably good approximation for systems involving channels of noncircular cross sections.

The fill time, f , is defined as the length of time between the instant the polymer begins moving into the mold and the instant the mold becomes full. A detailed consideration of this problem should take into account the geometrical complexity of the channels of flow and the fact that the polymer is being cooled during filling. Needless to say, this makes the problem very difficult, if not completely impossible to solve. The geometrical complexity presents no problem if we are content with an approximate expression, for we can refer to equation (5) and write

$$f = B\eta_0 P_m^{-\alpha} \quad (6)$$

where P_m is the pressure applied to the polymer by the plunger and η_0 is the Newtonian viscosity of the flowing polymer. This last quantity raises a further question. There can be no doubt that the polymer is cooled somewhat while filling the mold, and that the viscosity is highly dependent upon temperature. It has been previously stated that the polymer flowing into the mold passes inside of a layer of frozen polymer. When it reaches the advancing front of flowing polymer it is forced out against the mold surface and cools rapidly. Because of the very low thermal conductivity of most polymers it seems reasonable to assume that in the flowing polymer the temperature will not change rapidly and that the actual cross-sectional area of the channel will be reduced. Hence we may merely compute η_0 at the temperature of the polymer just before it enters the mold, realizing that variations in the surface temperature of the mold may show up in a change in the value of B .

TABLE II
COMPARISON OF EQUATION (6) AND OBSERVED FILL TIMES
[Mold Temperature = 90° F. (32° C.)]

P_m , k.p.s.i.	η_0 , poise	f (calc.), sec.	f (obs.), sec.
19	38,600	1.05	1.2
19	80,500	2.20	1.7
19	115,000	3.14	2.7
19	210,000	5.75	6.7
16	80,500	4.60	4.7
14	9,100	0.94	1.2
14	14,500	1.49	1.2
14	62,500	6.42	6.7
12	12,960	2.63	2.7
12	14,300	2.90	2.7
10	9,100	4.13	4.7
10	12,960	5.88	6.7
10	14,300	6.50	6.7

In the evaluation of B and α the only *a priori* expectation from equation (4) would be that α should be somewhere between 4 and 5 for high shearing stresses. This turned out to be the case for a typical press and mold, where it was found that $\alpha = 4.4$ and $B = 11.4$, with f in seconds, η_0 in poise, and P_m in units of 1000 pounds per square inch (k.p.s.i.). Equation (6), with these values of the constants, was in good agreement with observed fill times when the mold temperature was 90° F. (32° C.), as shown in Table II.

It was found that raising the mold temperature to 120° F. (49° C.) reduced the fill times and this corresponded to a value of $B = 6.15$.

There is a limitation on fill time for many molding presses which must be considered. The plunger forward motion is produced by pumping oil at a constant rate into a cylinder which drives the plunger. A pressure control by-passes the pumps when oil pressure reaches a maximum predetermined value, and subsequently maintains the pressure constant. This corresponds to the pressure P_m . If this maximum pressure is set high enough on the control it is not attained during filling. Instead, the mold fills at a constant rate under some lower pressure. This filling rate is determined by the oil pumping rate and the ratio of polymer displacement to oil displacement. The minimum fill time is determined by this filling rate and the volume of the mold. The filling pressure can be calculated from equation (6) by setting f equal to the minimum fill time. The minimum fill time can be calculated, as just outlined, although it is readily determined experimentally.

Thus far it has been assumed that viscous flow is the mechanism by which polymer moves everywhere within the molding press. This assumption is valid only if that section, through which the incoming cold granules move during filling, is heated so as to soften the surface of the granules contacting it, so that the whole plug-like mass moves ahead by viscous flow of the softened polymer at the wall. In this case the filling time equation would apply as given. If, however, the cylinder wall in the granular zone ahead of the ram is too cool to soften the polymer appreciably, the friction between the polymer and the cylinder wall must be considered. This friction force can be considered to reduce the pressure at the forward moving end of the granular plug to

$$P_d = P_m e^{-(4\mu L_0/D)} \quad (7)$$

where μ is the coefficient of friction of the polymer on the cylinder wall, L_0 is the uncompressed length of the granular zone, and D is the diameter of the cylinder. Substituting this in equation (6) gives

$$f = B e^{4\alpha\mu L_0/D} \eta_0 P_m^{-\alpha} \quad (8)$$

Thus only the apparent value of B is altered; the form of the filling equation is preserved. Consider now the effect of adding a lubricant to the surface of the polymer granules. This would lower the coefficient of friction μ , and hence decrease the time required to fill the mold, according to equation (8). On the other hand if the cylinder section is heated, frictional effects become relatively unimportant and the fill time approaches the value given in equation (6).

Having now considered some of the factors influencing the value of B in the fill time equation let us now turn our attention to the constant α . The rate of flow, Q , through a molding machine during filling may be expressed as

$$Q = \frac{KP}{\bar{\eta}} \sum_{n=0}^4 \frac{A_n}{n!} (\kappa\beta P)^n \quad (9)$$

where K = geometrical constant, P = pressure drop through the machine when frictional losses are neglected, $\bar{\eta}$ = some sort of average polymer viscosity, A_n = geometrical factors, k = polymer constant, proportional to the high elastic compliance, and β = geometrical factor converting pressure drop to average shearing stress at the channel wall. The value α is now defined as

$$\alpha = \frac{d \log Q}{d \log P} = \frac{\sum_{n=0}^4 \frac{A_n(n+1)}{n!} (\kappa\beta P)^n}{\sum_{n=0}^4 \frac{A_n}{n!} (\kappa\beta P)^n} \quad (10)$$

It has been found that $A_r = 1$ for channels of circular or rectangular cross section, so that we are probably justified in writing

$$\alpha = \frac{d \log Q}{d \log P} = \frac{\sum_{n=0}^4 \frac{(n+1)}{n!} (k\beta P)^n}{\sum_{n=0}^4 \frac{1}{n!} (k\beta P)^n} \quad (11)$$

Thus, α will increase as either the shearing stress or the constant k increase. To calculate α , the value of $k\beta$ must be known. This may be found by fitting equation (9) to a set of fill-time or flow-rate data taken at constant temperature conditions but varying pressures. For example, the data of Table II, when reduced to a constant viscosity, give a value of $k\beta = 4.3 \times 10^{-4}$ (p.s.i.)⁻¹. From this $\alpha = 4.25$ at $P = 15,000$ p.s.i., which is more or less the middle of the range covered. This may be compared with a value of $\alpha = 4.4$, found by fitting the fill-time equation to these and many other data for this machine.

If k is known for the polymer used, the method just described also gives the constant β , which is of interest in some cases. Suppose, for example, that one had a series of polymers which one wished to compare as to their relative "fluidity" under injection molding conditions. This could be done by actually molding the materials, but a lot of time and polymer would be needed. In addition, there would be no assurance that the conclusions would apply if some other injection molding machine were to be used. If, however, values of β are known for a few typical molding machines, the properties η and K of each polymer may be measured and then translated into comparable rates of flow at shearing stresses actually encountered in injection molding. For a common 12 oz. press β was found to be 1.7×10^{-3} , and for a 16 oz. press of a different make $\beta = 3.08 \times 10^{-3}$.

V. Packing in the Mold

1. DESCRIPTION

The flow of polymer into the mold does not cease with the filling of the mold. The pressure in the mold is generally quite low at the moment the mold becomes full of polymer. The ram is still exerting pressure, and polymer continues to flow as long as the mold pressure is less than the ram pressure. This flow raises the pressure in the mold very rapidly. Opposed to this, however, is the tendency of the mold pressure to drop because of the cooling of the plastic. As a result, the pressure rises rapidly to some maximum value and then drops off slowly, as shown in Fig. 12. This maximum represents the balancing of the opposing tendencies, and the pressure at this point is substantially less than the ram pressure. Thus, flow con-

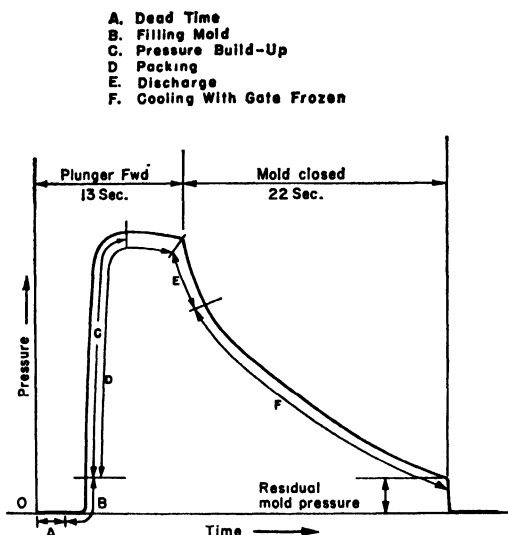


FIG. 12. Mold-pressure cycle

tinues all through the plunger forward time, unless the flow rate drops low enough to permit the plastic to solidify in the gate.

Packing has been observed directly in the photo mold, as illustrated in Fig. 13. Filling is completed after the first frame; packing is evidenced by the subsequent movement of the black streaks near the gate (at the bottom of each picture).

2. PRESSURE LOSSES IN THE INJECTION MOLDING MACHINE

One of the important functions of the molding press is to fill the mold properly, and to transmit enough pressure into it so that the molded piece will be an exact reproduction of the mold cavity. The pressure in the mold after it is frozen off from the heating cylinder must be sufficient to compensate for the shrinkage of the polymer on cooling, or else the piece will shrink away from the surface of the mold, leaving unwanted depressions in the piece. The pressure loss between the injection ram and the mold is considerable. Measurements have been made comparing the maximum pressure in the mold to the ram pressure. These are shown in Fig. 14 for several different injection temperatures. One of the more recent methods of reducing the difference between the injection pressure and the mold pressure is the preplasticizer unit described previously. With this unit hot polymer is fed into a shooting cylinder, without torpedo, so that the pres-

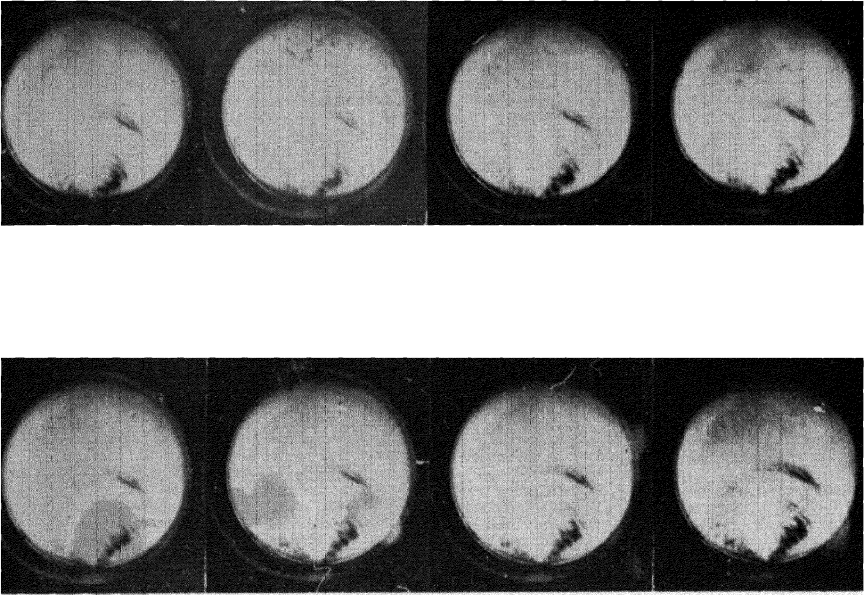


FIG. 13. A series of frames illustrating packing of the mold cavity

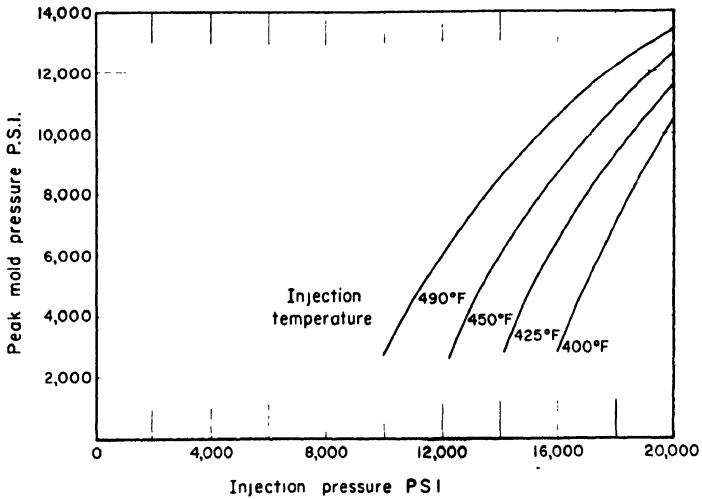


FIG. 14. Machine pressure efficiency determined at varying temperatures of plastic entering the mold, using a 6-oz. shot in a 12-oz. machine on a 60-sec. cycle.

sure loss in the granules and the small channel between the cylinder wall and the torpedo is eliminated.

In going through a conventional molding press the first pressure loss will be the result of the friction through the granular zone. Most thermoplastics are marketed in granular form. In subsequent fabrication operations, such as extrusion or injection molding, it is usually necessary to force the granular polymer through some sort of a channel. Under these circumstances one wishes to know what force has to be applied in order to move the granular plug against a specific resisting force or, conversely, how much of the applied pressure is transmitted through the granular material. This problem has been studied rather thoroughly for the static case where the polymer is just on the verge of moving. The apparatus used for this study is shown schematically in Fig. 15. It consists of a heavy-walled cylinder with two closely fitting pistons. Strain gauges were mounted on the lower piston and the unit calibrated in terms of the force applied to the piston.

As the force is applied the granules first compact down to an almost solid slug. The resisting force, or the force transmitted through the granules, was related to the applied force by

$$F_d = e^{-4\mu L_0/D} F_m \quad (12)$$

in a cylinder, where F_d is the transmitted force, F_m is the applied force, μ is the coefficient of friction, L_0 is the uncompacted length of granules, and D is the diameter of the cylinder.

With the apparatus shown it was convenient to use a number of different loadings and thus check the predicted constancy of F_m/F_d as the loading increased and compaction proceeded. Quite high loads were possible so that compaction down to as little as 60% of the original volume was

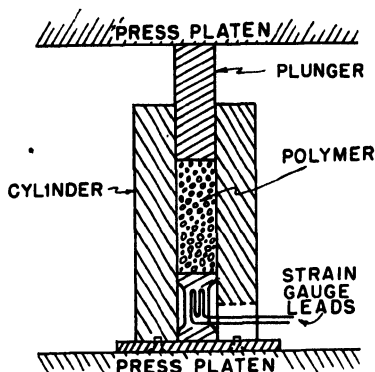


FIG. 15. Experimental arrangement used in the study of pressure transmission through granules.

TABLE III

PRESSURE TRANSMISSION THROUGH GRANULAR POLYSTYRENE. FORCE RATIO F_m/F_d

Poly- mer No.	L_0 , in.	F_m , lb.								Average
		7600	14,700	22,000	29,500	37,000	44,000	51,000	59,000	
1	0.834	1.582	1.530	1.469	1.538	1.457	—	—	—	1.515
	1.594	2.71	2.37	2.44	2.57	2.64	2.51	2.45	2.46	2.52
	2.442	3.80	3.86	3.67	3.69	3.63	3.73	3.64	3.74	3.72
	3.354	6.33	5.65	5.79	6.15	6.17	6.29	6.22	5.57	6.02
2	0.829	1.520	1.362	1.448	1.490	1.516	—	—	—	1.467
	1.611	2.92	2.94	2.75	2.78	2.72	2.68	2.58	2.61	2.75
	2.447	3.80	3.34	3.67	3.69	3.85	3.93	3.98	3.74	3.75
	3.349	9.50	7.35	6.46	6.56	6.38	6.47	6.37	6.55	(6.47)
3	0.794	1.226	1.362	1.266	1.461	1.423	—	—	—	1.348
	2.042	3.17	2.83	2.75	2.74	2.72	2.78	2.96	2.98	2.87
	2.417	4.22	3.68	4.07	3.28	3.43	3.60	3.64	3.83	3.72
	3.314	3.46	3.68	3.66	3.99	4.63	4.89	5.31	5.27	(5.27)

achieved; yet F_m/F_d remained relatively constant as shown in Table III. The effect of the original length is shown in Fig. 16 where the average F_m/F_d from Table III is plotted logarithmically against L_0 . Not only does a fair straight line result, but it may be seen that all three samples of polystyrene tested fall along the same line, which corresponds to a coefficient of friction of $\mu = 0.262$. The effect of external lubrication on the granules is to reduce the force ratio F_m/F_d . Different amounts of lubricant in powder form were mixed thoroughly with polystyrene and the pressure transmission through a fixed size of sample determined. The results are shown in Table IV. The ratio of the pressure at the forward moving end of the granules, P_d , to the pressure exerted by the ram, P_m , will be the same as the force ratio

$$\frac{F_m}{F_d} = \frac{P_m}{P_d} = e^{4\mu L_0/D} \quad (13)$$

In the molding machine the material starts as a cold mass of granules and, as it passes through the heating chamber, it softens and finally becomes a viscous fluid. Once it leaves the nozzle and enters the mold, the polymer starts to cool, with a resultant increase in viscosity. The material solidifying on the surfaces of the mold and the passages leading to the mold cavity reduces the cross-sectional area of molten polymer capable of transmitting pressure. The pressure losses in the mold will depend upon the viscosity and the temperature of the plastic, and the mold temperature. These fac-

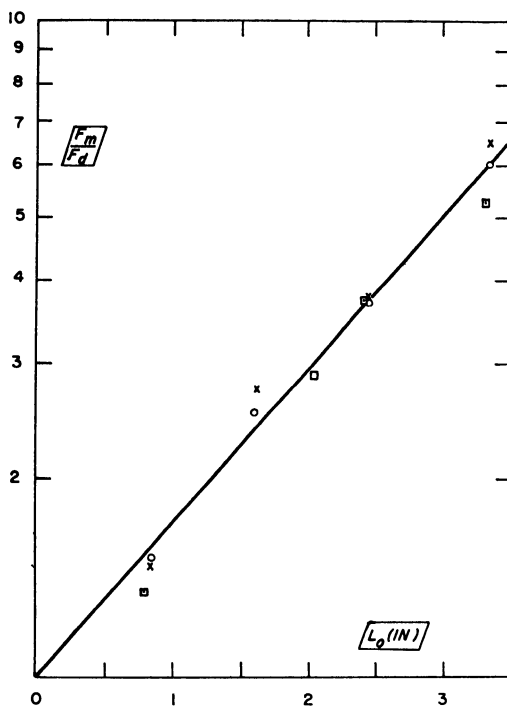


FIG. 16. Dependence of force ratio on length of sample of polystyrene. Circles represent polymer No. 1, crosses No. 2, and squares, No. 3.

TABLE IV
EFFECT OF SURFACE LUBRICATION ON POLYSTYRENE GRANULES

<i>p.p.m. of Lubricant</i>	F_m/F_d
0	4.38
150	3.08
300	2.66
500	2.23
750	1.82

tors, along with the complicated and varied shapes of the channels, make any detailed analysis of the pressure losses in the mold difficult.

3. EQUATION OF PRESSURE LOSS

An approximate equation has been derived to show the relationship between the ram pressure and the peak mold pressure attained during packing. This equation is derived by simultaneously applying the equation

of state to the polymer in the mold cavity and the filling equation to the polymer in the other channels.

$$P_i = P_m \{1 - [f(T_i - T_0)/C]^{1/2}\} \quad (14)$$

where P_i = peak mold pressure, P_m = ram pressure, T_i = temperature of the polymer entering the mold, and T_0 = mold wall temperature.

The magnitude of the constant C depends upon the cooling characteristics of the mold and a little upon the way in which the approximations are carried out. For the particular mold used in the machine, α , which is the same as in the filling equation, equaled 4.4 and $C = 18,300$ when f is expressed in seconds and the temperature in degrees Fahrenheit. In Table V data is presented on two polystyrene samples under a variety of molding conditions. Comparison of calculated and observed values of P_i points out the wide range of application of equation (14).

TABLE V
COMPARISON OF EQUATION (14) AND OBSERVED MOLD
PRESSURES FOR TWO POLYSTYRENES

<i>Polymer</i>	T_0 , °F.	T_i , °F.	f , sec.	P_m , k.p.s.i.	P_i , k.p.s.i.	P_i (calc.), k.p.s.i.
1	90	490	1.2	14.0	9.0	7.9
1	90	490	2.7	12.0	6.1	5.7
1	90	490	2.7	10.0	3.5	3.5
1	90	480	1.7	14.0	8.0	7.4
1	90	460	1.7	16.0	8.9	8.6
1	90	441	1.7	18.0	9.8	9.7
1	90	430	1.7	19.0	10.4	10.3
1	90	450	1.2	19.0	11.3	10.9
1	90	417	4.7	16.0	6.0	6.9
1	90	405	2.7	19.0	8.7	9.5
2	90	400	1.2	20.0	11.8	11.8
2	90	400	1.6	18.0	10.8	10.1
2	90	400	2.7	16.0	8.7	8.1
2	90	400	6.4	14.0	5.5	5.6
2	90	350	4.9	20.0	9.4	9.1
2	120	500	1.6	10.0	5.1	5.3
2	120	450	1.2	14.0	8.7	8.2
2	120	450	2.8	12.0	5.3	5.9
2	120	400	1.6	16.0	9.5	9.1
2	120	400	3.1	14.0	6.4	7.0
2	120	350	7.0	18.0	6.7	7.6

4. RESIDUAL STRAINS

Another phenomenon associated with the flow of polymer into the mold is the formation of frozen orientation in the molded article. It is well known that the flow of hot polymer is accompanied by a partial uncoiling and orienting of the chainlike molecules in the direction of flow. If the polymer is cooled below the softening point while in this state, the orientation is frozen in. Simultaneous flow and cooling occur during three steps of the injection molding cycle: filling, packing, and discharge. Filling is usually a relatively rapid process during which cooling is not very extensive, being ordinarily enough to form a thin skin of cold plastic. Exception must be taken to this, of course, for those cases in which the molding contains very thin sections. For in a thin section this thin shell of molten plastic may be a large portion of the total volume of the molded article and may be responsible for the predominant strains. Packing proceeds during that portion of the plunger forward time that is subsequent to filling. There is a somewhat slower flow of polymer during packing, but the time allowed for this portion of the cycle is usually long enough to permit considerable cooling. Discharge, like filling, occurs during a relatively short time interval. This takes place during later stages of cooling than packing; hence, the cooling process is slower. Both of these factors diminish the contribution of discharge to frozen orientation.

The concentration of frozen orientation in a surface layer, associated with the filling step may be illustrated by cutting tabs from the molded article and relaxing the orientation in an air oven at 230° F. Typical samples are shown in Fig. 17. Shrinkage of the oriented layer is quite evident in the upper tab. Machining off this orientated layer before heating greatly reduced the warpage as shown by the lower tab. The mold temperature also has a large effect on the orientation frozen into the molding. If the mold surface is hot the cooling is less severe, allowing the oriented molecule to relax somewhat before freezing in place. Tests were made where steam was run through the cored passages of the mold during filling; when the mold was full the steam was turned off and cold water run through the mold for cooling. By cycling the mold in this manner the strains in thin section pieces could be almost entirely eliminated. It was even found that on very thick sections where the cooling takes very long, the molding could be removed from the mold while it was still quite warm by cycling the mold in this manner. With this very thick section ($\frac{5}{8}$ in.), even with the extra time taken to heat the mold before filling the over-all cycle could be reduced from 8 to $5\frac{1}{2}$ minutes.

The effect of packing on the residual strain is shown in Fig. 18. Moldings were prepared at different plunger forward times, other conditions being

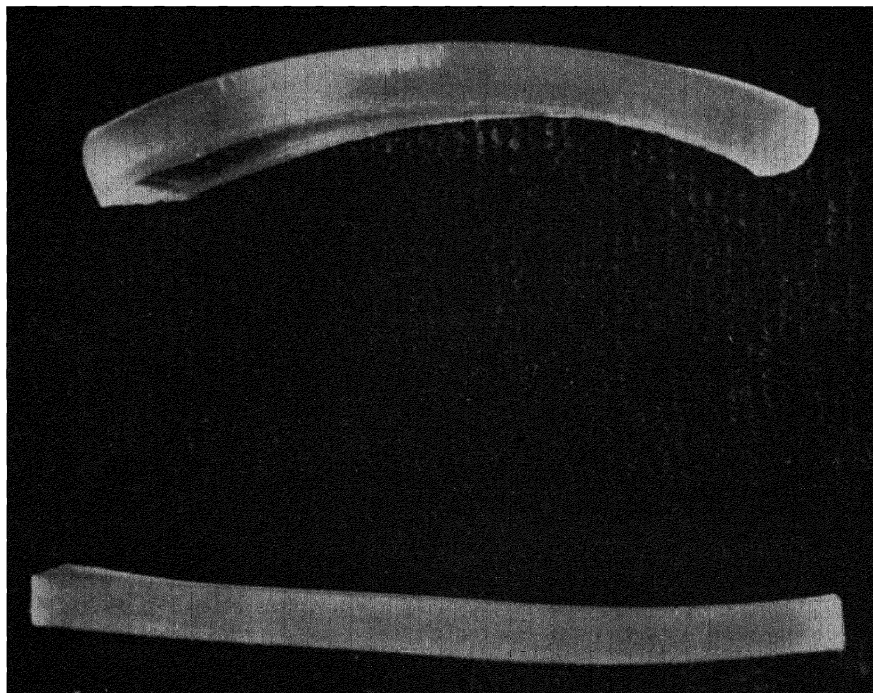


FIG. 17. Pieces cut from box and relaxed at 230° F. Top: Shrinkage of oriented layer is evident in first tab. Bottom: Surface layer machined off before relaxing.

constant. The resultant pieces were examined between crossed polaroids with monochromatic light. It may be seen that the amount of frozen orientation increases markedly with increasing packing. Cross sections of pieces from the same mold were taken near the gate and at the weld line. These were examined between crossed polaroids, as before, with the lines of observation being parallel to the surfaces of the piece and perpendicular to the direction of polymer flow. Typical examples are shown in Fig. 19.

Several distinctive features may be noted. As might be expected, some of the frozen strain is concentrated in a sort of surface skin, which is present in both cross sections and presumably elsewhere throughout the molding. It seems likely that a sizable amount of orientation frozen into this skin may be associated with the filling step. Inside this skin we have a thicker layer in which the orientation was frozen during packing. This packing orientation is present in the gate cross section, but absent in the weld cross section. This is not too surprising when it is realized that the rate of polymer flow during packing is a maximum at the gate and drops off to zero at the weld line. As a further point of interest, the strain pat-

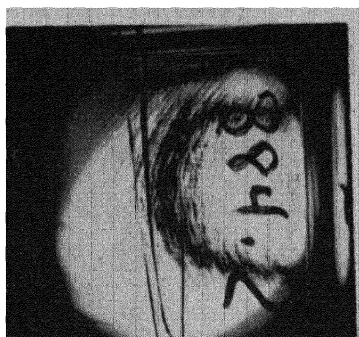
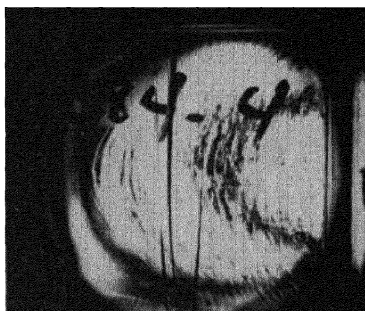
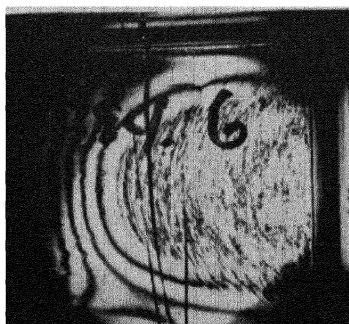
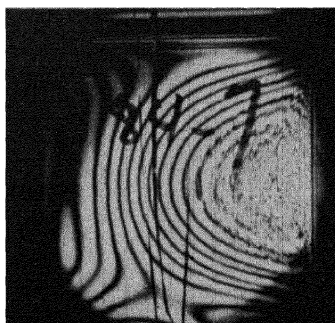
**PF = 14****PF = 16****PF = 18****PF = 20**

FIG. 18. Effect of packing on residual strain. Plunger forward time (P.F.) versus frozen stress pattern. Pieces viewed between crossed polaroids. Large gate 0.375×0.035 in. $P_1 = 13,000$ – $13,500$ p.s.i. $T_1 = 495^\circ$ F., $T_0 = 90^\circ$ F. Cycle = 90 sec. As P.F. rises, the amount of frozen orientation increases.

tern clearly shows the location of the weld and the conditions existing at that point. In Fig. 20 a similar cross section near the gate is shown for a case in which the packing time was appreciably shorter. The reduction in frozen strain in the central portion is apparent.

One very important phenomenon observed in molded articles, which is at least partially associated with frozen orientation, is crazing. By this term is meant the formation of numerous small cracks in the plastic, usually extending only part way into the material. Crazing may be brought about

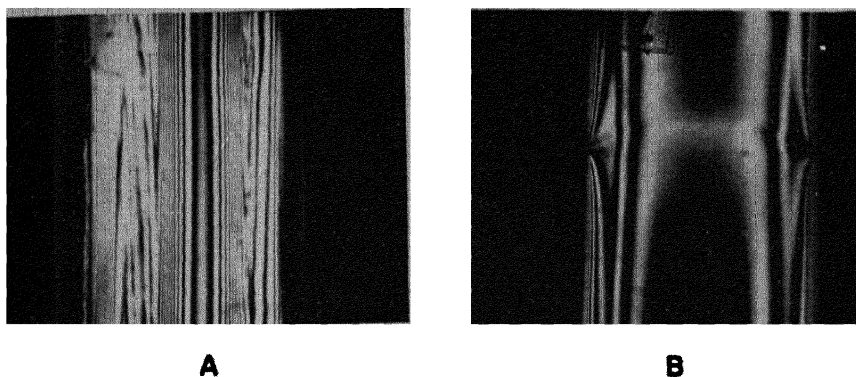


FIG. 19. Cross sections of boxes viewed between crossed polaroids: (a) near weld; (b) at weld with line of sight parallel to box wall planes, perpendicular to polymer flow.



FIG. 20. Box cross sections viewed between crossed polaroids: (a) near gate; (b) at weld. Photo differs from Fig. 19 only in that pieces were made in shorter plunger forward time.

in many ways, but it seems reasonable that in any event it is always produced by tensile stresses. The stresses which produce crazing in use may arise from various causes. Sudden chilling will result in tension in the surface of the article in all directions. This is illustrated in Fig. 21, which is a photograph of a polystyrene box that had seen household use for several months as a refrigerator dish. On all sides of the box the craze cracks follow the flow lines. The tendency of a molded article to craze can be reduced greatly by reducing the frozen orientation.

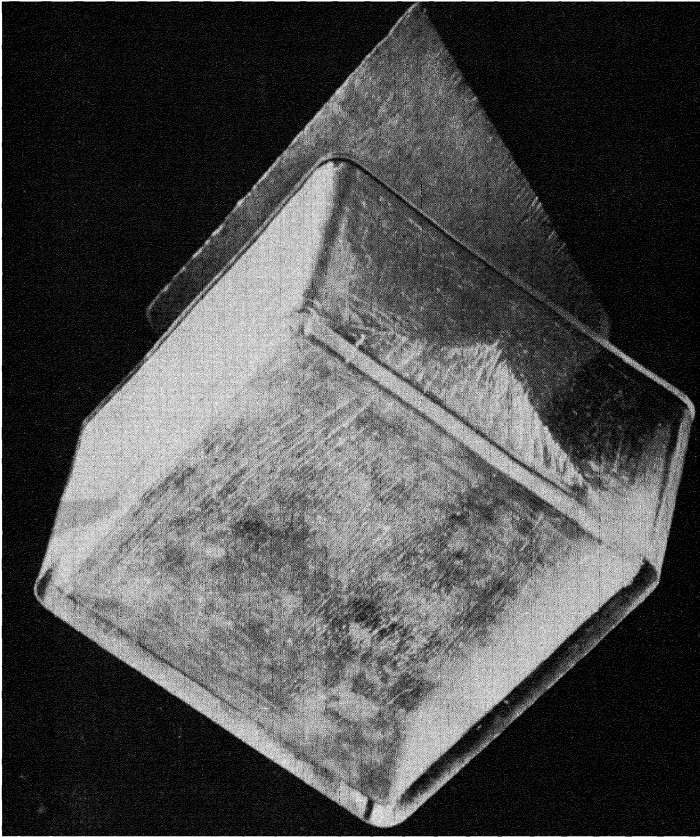


FIG. 21. Crazing of a box which has been used for several months as a refrigerator dish. Cracks follow the lines of flow.

VI. Discharge and Sealing

1. DESCRIPTION

At the end of the packing period the plunger is returned to its starting position. Thus, there is a higher pressure in the cavity than ahead of the gate. If the gate has not frozen shut, the flow in the channel is reversed and the mold discharges. During discharge the pressure in the mold drops quite rapidly, and the rate of discharge decreases as the pressure differential across the gate becomes smaller. When this rate becomes low enough and the polymer temperature becomes cool enough the polymer "freezes" in the gate, sealing the mold. The temperature and pressure in the mold at the instant of sealing are important quantities in considering mold shrink-

age, bubble formation, etc.; to determine the sealing characteristics it is necessary to go back to the polymer cycle, as determined by the pressure measurements, to find the pressure-temperature relations at the time of sealing.

2. SEAL LINE

All that is necessary is to convert time into temperature—from heat-conduction theory—and replot the mold pressure curve by a curve of temperature vs. pressure. The resulting plot is a straight line in the later stages of cooling and the sealing point is the point at which the curve deviates from this straight line. The temperature-pressure plot for a number of plunger forward times is shown in Fig. 22. The relationship between the various sealing points is approximately a linear variation of temperature with pressure. The position of this sealing line will depend largely upon the mold wall temperature, polymer setup temperature, and gate dimensions. For a typical molding situation the experimental sealing points are found to conform to the following equation:

$$P \text{ (k.p.s.i.)} = 22.5 - 0.066 T \text{ (}^{\circ}\text{F.)} \quad (15)$$

Two exceptions must be noted. If the pressure in the mold at the end of the packing period is less than that given by this relationship, only very slight discharge will result, and essentially all of the pressure will be scaled into the mold. The other case may arise if the plunger forward motion is unduly prolonged. After considerable cooling has taken place the rate of

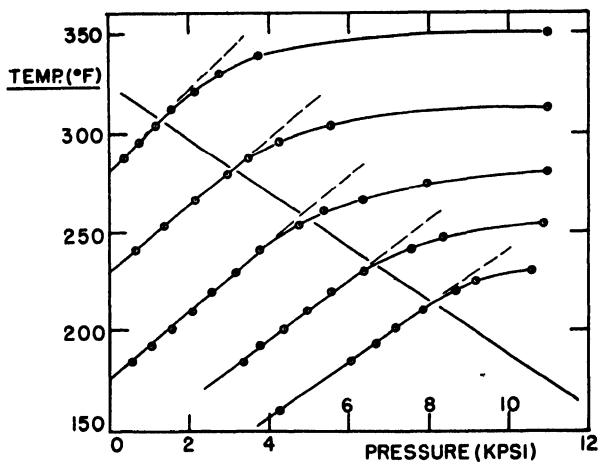


FIG. 22. The relations between the sealing points for various plunger forward times.

flow into the mold during packing is greatly diminished. If this becomes low enough the gate will seal during the plunger forward motion and there will be no discharge at all.

It has been pointed out that frozen orientation may be substantially reduced by minimizing the packing time. With conventional molds and presses this procedure cannot be carried far enough to be of much benefit. As the packing time is reduced, discharge becomes more extensive and less plastic is sealed into the mold. This leads to the formation of sink marks or bubbles. From this it is apparent that extensive reduction of the packing time will become feasible only if a means is provided to reduce or eliminate discharge.

There are several methods used for reducing or eliminating discharge. One method is to use a restricted or pin-point gate. This speeds up sealing of the mold, cuts down on discharge, and hence seals more pressure in the mold. The use of the restricted gate is accompanied by certain disadvantages, in addition to which, it is only a partial solution to the frozen orientation problem.

Another method of reducing strains and also of having the correct amount of plastic in the mold is weigh feeding. In weigh feeding only the correct amount of plastic is placed in the mold during the injection stroke. The injection ram makes a complete stroke and is held in its forward position against a mechanical stop. Thus at the end of the injection stroke essentially all of the plastic is in the mold and there is very little flow through the gate. By holding the plunger in its full forward position the gate is effectively sealed at the end of the injection stroke, and there is very little packing in the mold after this time. The main disadvantage to weigh feeding is that the weight of plastic placed in the mold must be very accurately measured. To do this the accuracy of the weigh feeding apparatus must be very high and also the ram must come to its complete forward position.

Another method of reducing packing is the mechanical shutoff for sealing the mold at the end of the plunger forward time. In this way, discharge can be completely eliminated and the packing time cut back to the point where substantial reduction in frozen orientation is possible. Each of these three methods have their advantages and disadvantages and the particular molding situation will determine which method can be used to the best advantage.

VII. Sealed Cooling

1. THE EQUATION OF STATE

Further cooling subsequent to sealing is usually necessary. The polymer must cool until its average temperature is lower than some effective hard-

ening point, otherwise it will not have sufficient rigidity when removed from the mold, resulting in objectionable distortion.

Among those quantities which are of importance in determining the quality of the piece are the pressure, average temperature, and density of the polymer in the mold just before the mold is opened. These quantities are related through the equation of state.

$$(P + \pi) \left(\frac{V}{M} - \omega \right) = RT \quad (16)$$

where P is the pressure, V/M the specific volume, T the average temperature, and π , ω , and R are constants which have been determined for some of the common polymers. Looking at this equation of state, we see that when the density is held constant the pressure is a linear function of the temperature. This leads to a convenient graphical representation of the sealed cooling portion of the cycle, as illustrated in Fig. 23 where temperature is

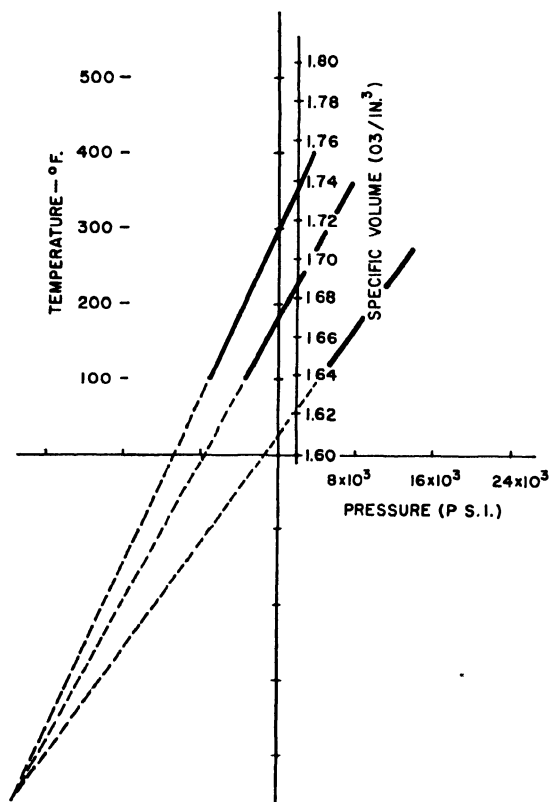


FIG. 23. Sealed cooling curves given by the equation of state

plotted against pressure. When the density is held constant, the temperature and pressure vary along a straight line, the slope of which depends upon the weight of polymer in the mold. All such straight lines pass through a single point, located at $P = -\pi$ and $T = 0^\circ \text{ K}$.

Through the equation of state, the residual pressure in the mold, when opened, will be related to the pressure and temperature in the mold at the sealing point. If we define release as "the ease with which a molding ejects from a mold which has sufficient draft and no reverse draft" the release behavior at the instant of opening the mold is dependent upon the residual mold pressure. This may be shown by a plot of the residual mold pressure and the force required to open the mold as in Fig. 24. The force required to open the mold was measured by the pressure build-up in the clamping cylinder. Since this force is a linear function of the residual mold pressure over a considerable range, we may regard this force as a frictional force arising from the friction between the plastic and the cavity surface. The residual mold pressure may then be considered as the normal force holding the two surfaces in contact. The higher the residual mold pressure, the more difficult it is to open the mold, and the greater the tendency to score the surface of the molding or even to break it, if the piece is relatively thin.

Thus far we have discussed only the effect of residual pressure as the mold opens, but the release from the core is of equal importance. When the mold pressure reaches zero, optimum release can be obtained from either cavity or core. If, at this instant, the molding still has a relatively high average

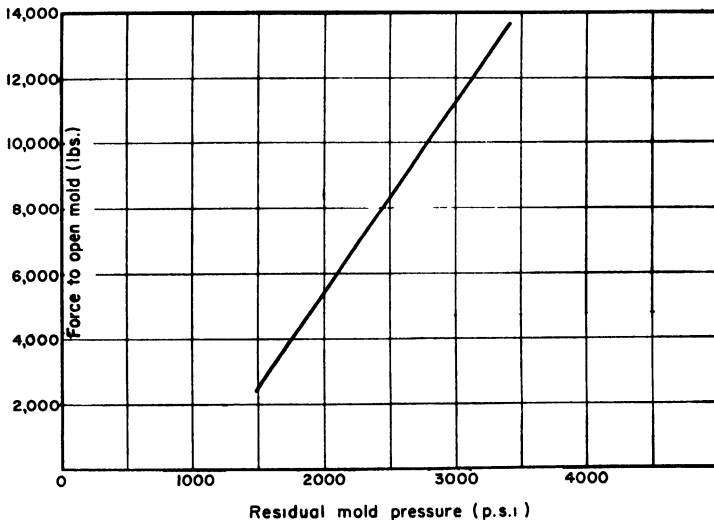


FIG. 24. Residual mold pressure vs force to open mold

temperature, considerable shrinkage can still take place. With this shrinkage and with the mold still closed, pressure builds up between the molding and the core. If this pressure is allowed to build up appreciably, then scoring or cracking is likely to occur, since it will require a correspondingly higher force to strip the molding from the core.

2. MOLD OPENING CONDITIONS

The proper conditions for opening the mold can be established on the pressure-temperature diagram. First of all, the piece must be rigid enough to hold its shape, which means that the polymer temperature must drop to at least some value, T_s . The mold is controlled at some temperature, T_0 , and the molding can not be cooled below this temperature while in the mold. On the pressure scale a maximum allowable residual mold pressure, P_r , is required to avoid sticking or breaking the piece on ejection. The pressure in the mold, then, must be less than P_r when the mold is opened. In a mold containing a core, a negative P_r may be defined also beyond which sticking on the core or insert will occur.

The two pressure and temperature limits define an area within which the mold must be opened. During cooling this region is approached along a constant density line, as illustrated in Fig. 25. Since it would be inefficient to cool the piece below the temperature T_s , it is only necessary to consider the area between the constant density lines which reach the temperature limit, T_s , at $-P_r$ and $+P_r$. To minimize sticking or scoring it would be

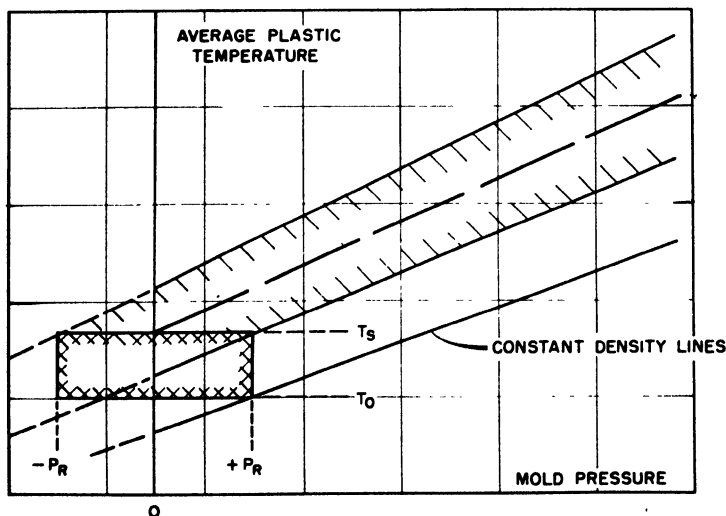


FIG. 25. Pressure-temperature relations in the polystyrene injection cycle determined by mold opening conditions.

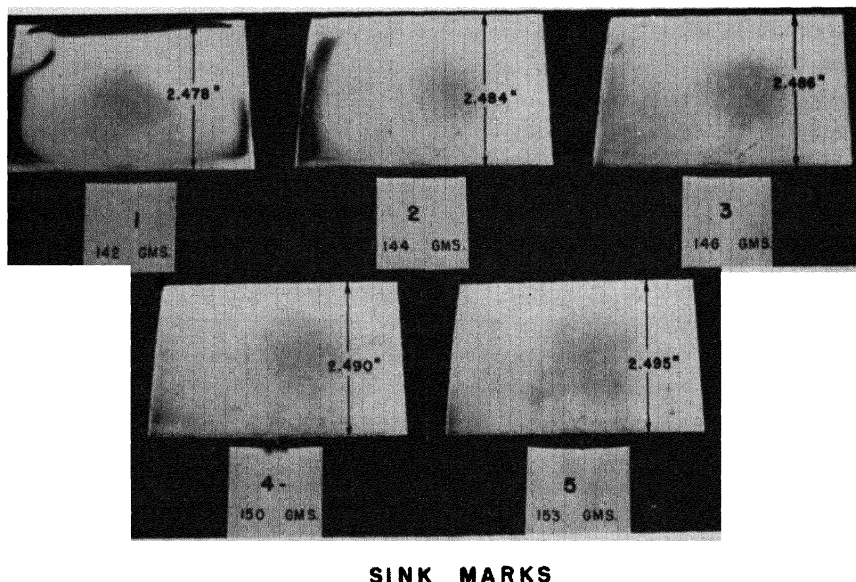
desirable to follow along the constant density line which intersects T , at zero pressure.

3. CONFORMITY TO MOLD

Another phenomenon associated with the sealing point and sealed cooling is the formation of sink marks and bubbles. At the instant the outer surface of the polymer first reaches the freezing point, the stresses acting can only be hydrostatic. A short time later a shell of frozen rigid material has formed, containing within itself a region of hotter, still fluid material. Further cooling of the central region may result in a negative hydrostatic stress and corresponding compressive tangential stresses in the rigid shell. This situation will persist, under certain conditions, even when thermal equilibrium has been attained, leaving residual stresses in the body at room temperature.

In many cases the equilibrium between the negative hydrostatic stress and the compressive tangential stress is unstable, and either the shell collapses in some way or a vacuum bubble is formed in the center of the body. In injection molding the hot plastic is injected into the cold mold cavity, subjected to a hydrostatic pressure, and left to cool under conditions of substantially constant volume. The hydrostatic pressure will drop as cooling proceeds. At some point in the cooling process the pressure inside the frozen shell reaches zero, and further cooling develops negative pressure inside the rigid shell which has been formed. The location of this zero-pressure point is an index to the further behavior of the piece during cooling. If it falls in the earlier stages of cooling, the shell will not be of sufficient thickness to support the ensuing stress and it will collapse in some spot. The resulting defect in the molded article is commonly referred to as a "sink mark." If the zero-pressure point lies in the intermediate stage of cooling, the shell will support stress but the center will still be hot enough to permit the formation of vacuum bubbles. If the zero-pressure point is deferred to the later stages of cooling, neither of these defects form and the resulting molded article contains quenching stresses. If the mold pressure does not reach zero before the mold is opened, then scoring, sticking, or breaking of the piece will occur on ejection, depending upon the magnitude of the residual pressure in the mold.

Thus it is seen that the steps in the progression (sink marks) \rightarrow (bubbles) \rightarrow (satisfactory pieces) \rightarrow (scoring) \rightarrow (sticking) are but different stages in the same process. Experience shows that this is strictly true only for pieces with relatively thick sections; pieces with only thin sections do not customarily show bubble formation. In either case, we can say that the way to reduce or eliminate sink marks or bubbles is to move the zero-pressure point to a later stage of cooling.



SINK MARKS

FIG. 26. One surface of each of moldings produced in pressure cycles shown in Fig. 27. Sink marks are plain in Nos. 1 and 2; almost vanish in 3, 4, and 5.

The equation of state tells us that the average temperature of the polymer in the mold at the zero-pressure point will correlate directly with the weight of the molding. Thus, we might expect the weight of the piece to provide a rough measure of quality with respect to sink marks and bubbles, and this has been our experience. In Fig. 26 we see boxes molded to different weights by varying the plunger forward time. As the weight increases the sink marks gradually disappear. The weight of each molding is shown, ranging from 142 to 153 grams. Measurements have shown that such an increase is not the result of density changes. Mold shrinkage has also decreased, as shown by the dimensions for the height of each box. Figure 27 shows the mold pressure cycle for each of the boxes. It will be noted that as the sealing pressure increases there is a decrease in mold shrinkage as shown in Fig. 28.

VIII. Cycle Time

Up to this point we have been concerned mostly with more or less isolated phenomena in injection molding. The problem of developing a method of synthesis remains; these concepts must be brought together in a unified manner, which will permit us to consider such questions as the optimum molding conditions and a suitable definition of moldability.

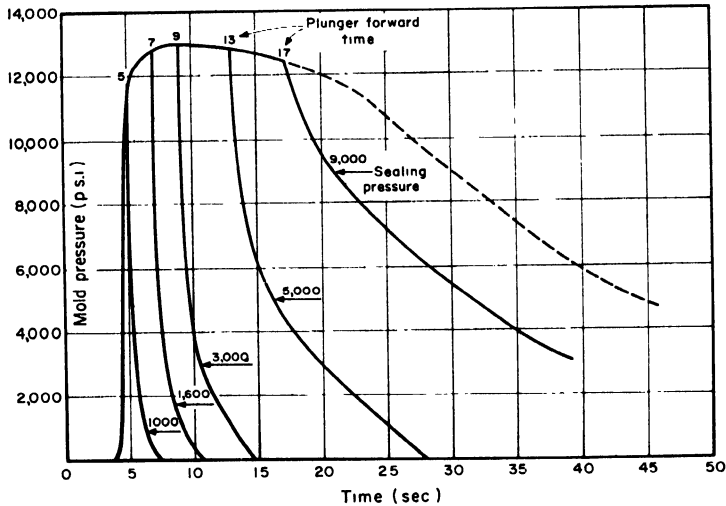


FIG. 27. Mold pressure curves of a 6-oz. shot in a 12-oz. machine on a 60-sec. cycle at injection temperature of 490° F. and a pressure of 16,000 p.s.i.

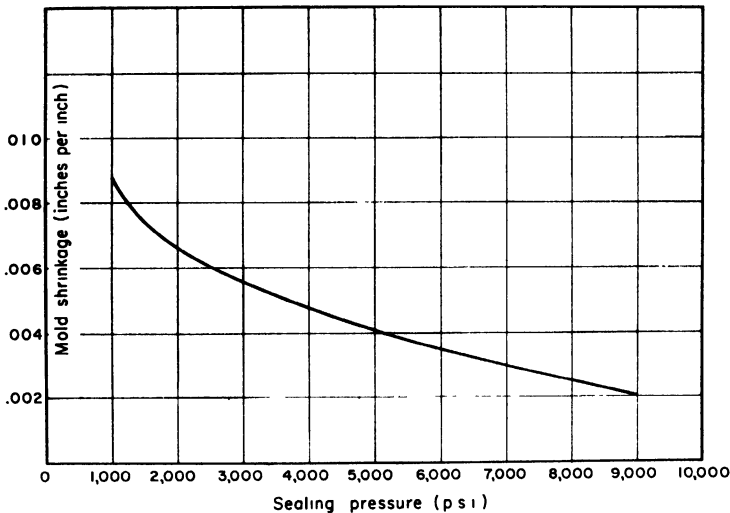


FIG. 28. The dependence of mold shrinkage on sealing pressure and influence of plunger forward time under operating conditions which prevail in Fig. 27.

1. LIMITING CYCLE

One of the paramount interests of the molder is to produce acceptable pieces as rapidly as possible. Bearing this obvious but important fact in mind, emphasis must be placed upon the length of time consumed by a

single molding cycle. This we call the cycle time. In terms of the operation of the press, the molding cycle is customarily broken down into (1) plunger forward time, (2) mold closed time, (3) mold open time.

This breakdown, while convenient for setting the controls of a conventional press, is not suitable for our purposes. Instead we subdivide the cycle as follows: (1) dead time, d ; (2) fill time, f ; (3) cooling time, c ; (4) mold open time.

The first thing in determining the optimum molding conditions is to establish the requirements that must be met by the molded article. The molder seeks to make acceptable pieces as rapidly as possible. Acceptability can best be defined negatively in terms of the defects we require to be absent or at least kept below some level. The acceptability criteria set up will vary from job to job, and may be expanded as our knowledge of molding phenomena increases. Certain of the criteria will be common to most jobs. Given, now, a set of acceptability criteria, we can proceed to introduce cycle time into our considerations. This is done by means of a concept which we term the limiting cycle, which is based on the molder's viewpoint. Under a given set of molding conditions there exists a shortest cycle by which acceptable pieces, under all predetermined criteria, can be produced. This shortest cycle, under the given conditions, we call the limiting cycle.

Let us consider, as an example, the case of molding with normal equipment in which the mold discharges and seals as already described. As our acceptability criteria we take the following: (1) rigidity, (2) release, (3) minimum blemish, (4) conformity to mold.

On the temperature pressure plot of Fig. 25, requirement (1) means that the average temperature of the piece when the mold is opened must be not greater than some effective softening temperature, T_s . Of course, in molding very heavy sections, this condition may be violated successfully by immersing the piece in a cold bath as soon as it is removed. This should be regarded as strictly an emergency procedure, however, as there is very likely to be a tendency to form sink marks or bubbles. Requirement (2) means that the pressure in the mold when it is opened must not be greater than the characteristic release pressure, P_r . If the mold has a core, it also means that the pressure must not become more negative than some other characteristic value. This condition is of no consequence, however, when we are concerned with limiting cycle. Since blemishes are produced by the polymer's cooling as it enters the mold, requirement (3) means that the fill time must be less than or equal to some characteristic value f_B .

2. MOLDING DIAGRAM

Figure 29 shows the relationship between sealing temperature and pressure, and the discharge loci leading to the intersection of the seal line with

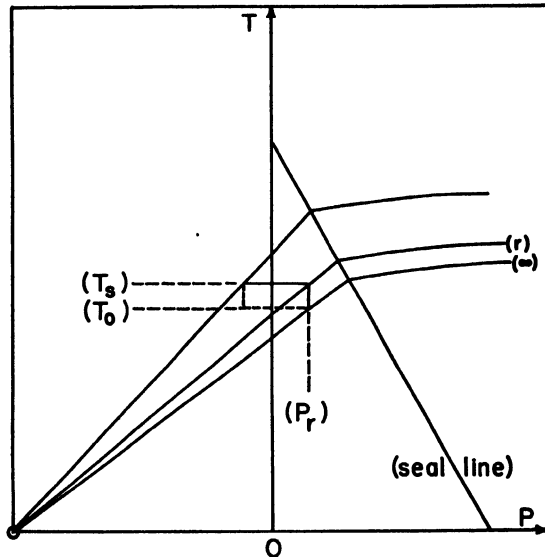


FIG. 29. Pressure-temperature cycle showing discharge loci

the constant-density lines through points (P_r, T_0) , (P_r, T_s) . The line (P_r, T_s) would represent the minimum sealed cooling time and (P_r, T_0) would correspond to an infinite cooling time. If the plot is now converted from polymer temperature and pressure to machine temperature and pressure, the two discharge loci become boundaries specifying the conditions necessary at the time the mold is opened, as in Fig. 30. To these are added two boundaries of constant fill time, one corresponding to the minimum fill time of the machine and the other specified by the acceptability criterion (3) and is the maximum fill time for acceptable blemish characteristics. These boundaries define regions, and equations can be set up to calculate the limiting cycle in each region, the shaded area being excluded.

The two boundaries \bar{f} and r define four regions in this diagram, as shown in Fig. 30. In area I the fill time will be greater than the minimum fill time \bar{f} and will be given by equation (6); the cooling time will then be given by the heat-conduction equation

$$C = \Phi(\Theta)$$

where Φ will be a function of Θ given by either equations (1), (2), or (3). Calling d the dead time, f the filling time, and c the cooling time, the limiting cycle in region I will be

$$L = d + B\eta^{P-\alpha} + \Phi\left(\frac{T_s - T_0}{T_i - T_0}\right) \cdots \text{Region I} \quad (17)$$

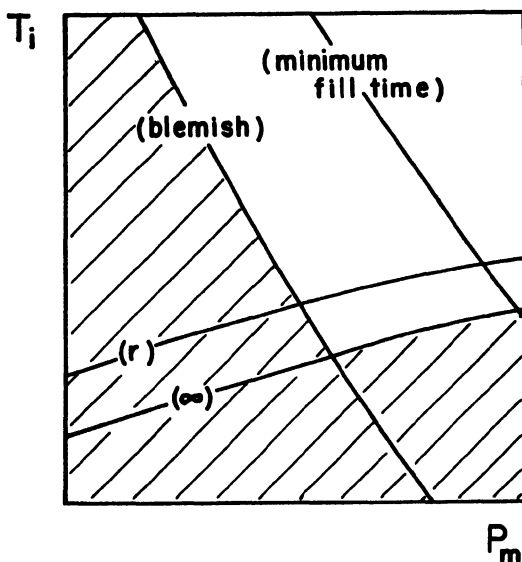


FIG. 30. Molding diagram showing mold-opening conditions

In region II this becomes

$$L = d + \dot{f} + \Phi \left(\frac{T_s - T_0}{T_i - T_0} \right) \cdots \text{Region II} \quad (18)$$

which is a function of temperature alone.

In a typical molding case the (r) -boundary is well below the normal molding range and can be neglected for the moment. Setting L equal to a constant in all four equations and solving for the temperature-pressure function in each region gives an isocycle which turns out to be a closed curve. Varying the value of L gives rise to a family of isocycles, which are arranged in a fashion to which we might refer, rather loosely, as concentric (Fig. 31). As we proceed inward across the isocycles the cycle time decreases. Thus, the isocycles converge on a point where the cycle time is a minimum. This minimum cycle point will be located on the maximum pressure axis, and will either be on or below the minimum fill time boundary.

The case in which the mold is sealed mechanically, so as to prevent discharge, is a little more complicated. Let us assume that the criteria of acceptability are the same as before. We see in Fig. 32 that the seal line is no longer an integral part of our polymer temperature-pressure diagram; rather, the constant-density lines extend across the entire diagram. Present use of the mechanical seal in molding is aimed primarily at reducing frozen orientation. Thus, it is desirable to reduce packing as far as possible, but

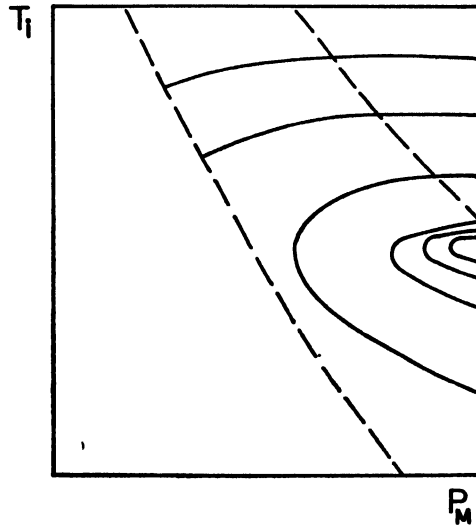


FIG. 31. Molding diagram showing lines of constant limiting cycle

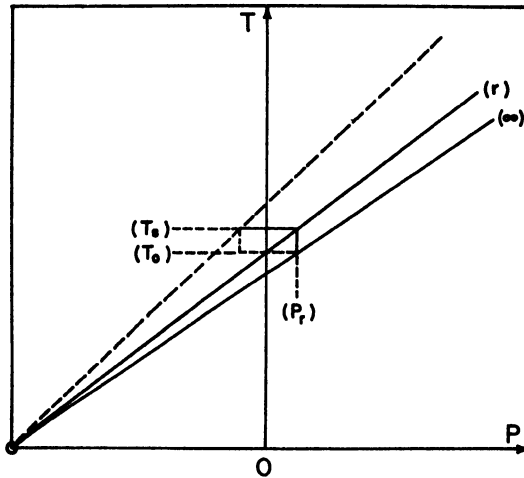


FIG. 32. Polymer pressure-temperature diagram with mechanical seal

this is limited by the fact that a certain amount of packing may be necessary to give the desired conformity to mold geometry, minimize sink marks and bubbles, etc. The balance between these two opposing factors results in a particular constant-density line on the diagram which the molder endeavors to hit every time. A little consideration will show that the biggest influence this can have in our diagram is, in effect, to lower the softening

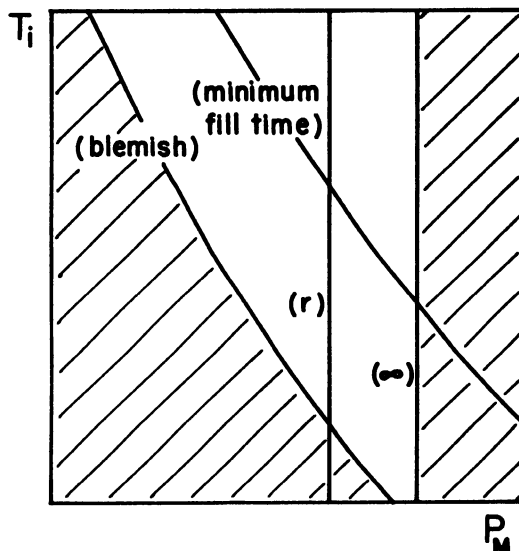


FIG. 33. Molding diagram with mechanical seal

point to some new value. Therefore, this criterion of acceptability need not enter further into the discussion.

To come back to our diagram, the significance of the two constant-density boundaries is the same as that held by the discharge loci in the previous case, except that their orientation in the diagram is different. When the polymer variables are transformed to machine temperature and pressure, as in Fig. 33, these two boundaries become nearly vertical lines, i.e., are approximately defined by characteristic values of machine pressure. The two fill time boundaries are the same as before. The isocycles, or contour lines of constant limiting cycle time, are shown in Fig. 34. The isocycles converge to a minimum cycle point as before. The minimum cycle is usually on the P_r boundary, either at the intersection with the minimum fill time boundary or below it. In some cases the P_r boundary may lie beyond the maximum pressure capacity of the machine; then the minimum cycle point will be on the maximum pressure axis as before.

3. MOLDABILITY

Now let us consider briefly the idea of moldability, a term which has been rather loosely used at times. Obviously the first requirement is to set up some sort of definition as a basis for further discussion. One general definition that has been offered for moldability is as follows:

"Moldability is a measure of the speed and ease with which a polymer can be fabricated to a certain given specification."

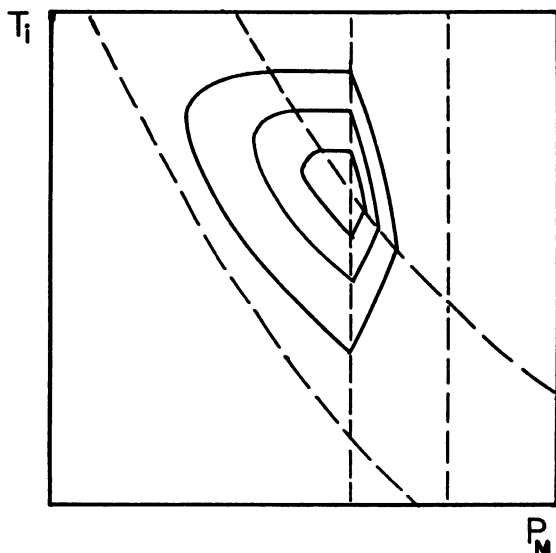


FIG. 34. Lines of constant limiting cycle with mechanical seal

With the given specifications being the acceptability criteria discussed previously, one natural approach is to use the minimum cycle time, or some quantity based upon it, as a measure of moldability. With this thought in mind, let us consider the influence of polymer properties upon moldability. There is one group of polymer properties (melt viscosity, coefficient of friction, etc.) which influences the fill time, and another group of properties (thermal diffusivity, softening point, etc.) which influence the cooling time. The minimum sum of the filling and cooling time will determine the moldability of the respective polymer.

As a simple illustrative example, consider the case of a mold that discharges, with the acceptability criteria listed previously. Table VI shows the location of the minimum cycle point and minimum cycle time for all

TABLE VI
MINIMUM CYCLE
($T_0 = 90^\circ \text{ F.}$) $P_m = 19 \text{ k.p.s.i.}$

<i>Polymer viscosity (437° F.), poises</i>	<i>T_s, °F.</i>	<i>Min. cycle temperature, °F.</i>	<i>Min. cycle time, sec.</i>
50,000	185	433	18.94
100,000	185	464	19.96
50,000	203	433	16.65
100,000	203	464	17.65

four combinations of two different viscosities and two different softening points. Since the actual viscosity of the polymer is not constant but some function of temperature, the viscosity at one temperature is taken only as a relative indication of the flow in the molding machine and is proportional to the viscosity distribution.

The softening point does not influence the location of the minimum cycle point. Raising the viscosity increases the minimum cycle time, and raising the softening temperature lowers the minimum cycle time.

It should be realized by now that moldability, maximum production rate, or whatever you want to call it, is determined by a combination of factors, involving press, mold, polymer, and molding method. None of these can be neglected. Now what is the relative importance of polymer properties in determining moldability? This is a difficult question to answer and depends mainly on the conditions of the mold and press. If the mold is simple in design and requires only a small portion of the capacity of the molding press large polymer variations might be tolerated. But the more difficult the mold and the closer it operates to the capacity of the press, the more influence the polymer properties will have on the molding behavior. If the mold is operated at its minimum cycle very small variations in polymer properties may mean the difference between a good molding and a bad one. In this connection it should be noted that the system of controls on the usual press is somewhat arbitrarily designed and does not give the operator a firm grasp on the fundamental steps of the molding cycle. This permits polymer properties to exert a certain influence on the molding behavior which would be absent in a closely controlled press. That is to say, constant machine settings do not mean constant molding conditions. In fact, this may explain, in part, some of the apparent differences in moldability.

Nomenclature

$A, \alpha, B, \beta,$	empirical constants	P	Pressure
C, π, ω		P_m	Pressure applied by the plunger
D	a characteristic dimension representative of cross-sectional size	P_d	Pressure at forward end of the granules
E	Heating efficiency	P_i	Peak mold pressure
f	Time to fill mold cavity	P_r	Residual mold pressure
F_m	Applied force	Q	Volume rate of flow
F_d	Transmitted force	R	Radius of cylinder or sphere
h^2	Thermal diffusivity	t	Time
k	Constant proportional to elastic compliance	T	Temperature
L	Length	\bar{T}	Average temperature of polymer
L_0	Uncompressed length of granules		

T , Initial temperature of polymer	$\bar{\eta}$ Average polymer viscosity
T_0 The surface temperature of the mold	η_0 Viscosity at zero shear
T_r Temperature at which molding becomes rigid	Θ Reduced average polymer temperature
V/M Specific volume	μ Coefficient of friction
α_n Positive roots of Bessel equation ($J_0(\alpha R) = 0$)	τ Shearing stress at channel wall

GENERAL BIBLIOGRAPHY

The following articles were used as reference material in organizing this chapter.

1. C. E. Beyer and R. B. Dahl, *Modern Plastics* **48** (1952).
2. C. E. Beyer and R. B. Dahl, *Modern Plastics* **54** (1953).
3. C. E. Beyer and F. E. Towsley, *J. Colloid Sci.* **7**, No. 3, 236-243 (1952).
4. R. H. Boundy and R. F. Boyer, "Styrene, Its Polymers, Copolymers and Derivatives," Reinhold, New York, 1952.
5. G. D. Gilmore, *India Rubber World* (1952).
6. G. D. Gilmore and R. S. Spencer, *Modern Plastics* **19** (1950).
7. G. D. Gilmore and R. S. Spencer, *Modern Plastics* **31** (1951).
8. R. S. Spencer, *J. Polymer Sci.* **5**, No. 5, 591-608 (1950).
9. R. S. Spencer and R. E. Dillon, *J. Colloid Sci.* **3**, No. 2, 163-180 (1948).
10. R. S. Spencer and R. E. Dillon, *J. Colloid Sci.* **4**, No. 3, 241-255 (1949).
11. R. S. Spencer and G. D. Gilmore, *J. Appl. Phys.* **20**, No. 6, 502-506 (1949).
12. R. S. Spencer and G. D. Gilmore, *J. Appl. Phys.* **21**, No. 6, 523-526 (1950).
13. R. S. Spencer and G. D. Gilmore, *Modern Plastics* **27** (1950).
14. R. S. Spencer and G. D. Gilmore, *J. Colloid Sci.* **6**, No. 2, 118-132 (1951).
15. R. S. Spencer, G. D. Gilmore, and R. M. Wiley, *J. Appl. Phys.* **21**, No. 6, 527-531 (1950).

CHAPTER 15

RHEOLOGY OF SPINNING

Bruno R. Roberts

I. Introduction	554
II. Description of the Problem	554
III. Discussion of the Physical Characteristics of Spinnable Materials	556
1. Flow Requirements for Fiber-Forming Solutions and Melts	556
2. Structural Properties of Fiber Formers	557
3. Rheological Characteristics of Spin Dopes	558
4. Influence of Solids Content	558
5. Viscosity-Temperature Function of Spin Dopes	559
6. Heat Development during Flow	560
IV. Flow under Fiber-Forming Conditions	561
1. Flow Profile in Spinnerette	561
2. Speed Gradient	561
3. The Role of Shear Stress	562
4. Viscosity Changes Taking Place during Coagulation (Hardening).	562
5. Gel Formation Combined with Mass Transfer (Solution Spinning).	563
a. Dry Spinning (No Chemical Changes Taking Place)	563
b. Wet Spinning.	564
(1) Combined with Chemical Changes	564
(2) Without Chemical Changes	565
6. Gel Formation without Mass Transfer (Melt Spinning)	565
7. The Inversion of the Flow Profile between the Capillary and the Hardening Zone	566
8. The Aligning of the Polymer Chains	567
V. Evaluation Techniques	568
1. Determination of Dope "Viscosity"	568
2. Influence of Shear Stress on Measurements	569
3. Use of the Spinning Machine as Viscometer	570
VI. Interpretation of Phenomena Accompanying the Fiber Formation	571
1. Observation of Dope Cohesion	571
2. Friction between the Coagulating Fiber Structure and Coagulant	572
3. Formation of Crystalline Zones	573
4. The Development of Anisotropy in the Fiber Structure	573
5. Stretch Spinning	574
VII. Summarizing Discussion of Present Knowledge of the Various Rheological Problems Involved in Spinning	575
VIII. Appendix	576
1. Description of the Viscosity Behavior of a Spin Dope	576

2. Anticipated Developments for the Future	583
a. Melt Viscosity of Polymers	584
b. Solution Viscosity.	584
c. Flow Curves of Spinnable Polymers.	585
d. Measuring Techniques.	586
e. New Instruments.	586
Nomenclature	587

I. Introduction

The formation of a fiber structure is the basis of the growth of organisms in the animal and vegetable kingdoms. Nature, in most cases, polymerizes the appropriate compounds in situ and, in a process that is so far only incompletely understood, combines the polymer chains to form physical structures which are adequate for their specific purposes, such as muscle tissue, seed hair, or fur.

The only exception to this rule in the natural formation of organic fibers is the extrusion of prepolymerized protein compounds by such animals as spiders and silk worms. In these cases, fiber formation takes place by a process which served as a model for the preparation of synthetic fibers. The animal produces in its body a spin mass which is extruded through the action of its glands. Contact with air hardens the solution, and by making carefully controlled movements the animal provides the physical fiber structure necessary for building a net, cocoon, etc.

This intricate process of first preparing a polymer mass, then extruding and coagulating it, and bringing it into an appropriate physical pattern serves as a model for the production of man-made fibers. There are two ways of making such fibers: Natural polymers such as cellulose or proteins, are transformed by chemical and physical changes into "semisynthetic" fibers, or man-made polymers are, essentially by physical methods, spun into "fully synthetic" fibers.

The chemical aspects of fiber-forming polymers are outside the scope of this article and, therefore, emphasis will be placed in the following sections on the phenomena which by controlled flow arrangements and modifications of the chain structure form the basis for the physical changes leading to the formation of fiber structures.

II. Description of the Problem

The formation of synthetic fibers is based on the form changes which occur between the statistically random state of a spin mass (solution or melt) and the controlled physical pattern of the preliminary or final fiber structure which appears in the semisolid or the solid state. Simple as this transformation may appear to the outsider, there are a number of com-

plicating factors which control these changes and which are only partly understood.

There is, first of all, the problem of spinnability ("Spinnbarkeit"): As a spin mass is forced through the hole of a spinnerette—a mechanism copied from the procedure the spider and silk worm are using—a continuous "fiber"-shaped structure must be formed which is self-supporting enough to be moved away by mechanical means. (In the case of biological spinning, the fiber structure is stationary and the "spinnerette" of the animal moves away). It also must fulfill certain requirements as to dimensions, uniformity, and physical properties, to name only a few. If the properties of the spin mass or the extrusion conditions are inadequate, one will observe formation of polymer bubbles, of films, of a spray, or other undesirable shapes which cannot be considered as useful for the purpose.

We, therefore, have first to study the relationship between spin mass characteristics and extrusion conditions. They will determine the formation of a continuous and uniform fiber-shaped structure, possibly still in liquid state. Superimposed over these factors is the coagulation or hardening mechanism: The liquid or semiliquid, moving stream must attain a certain minimum "strength" to make it a self-supporting structure. The next step consists in the above-mentioned transformation of the preliminary, self-supporting structure into an arrangement in which the polymer chains contribute to the fulfillment of certain physical and textile requirements. Although the last step is, strictly speaking, not a part of the spinning process, it is obvious that the foundation for the final arrangement is based on the rheological characteristics of the structure and laid in the early stages of fiber formation. Therefore, it is necessary to include in our discussions at least a part of these problems.

The term "spinnability" is very loosely defined. It may be applied to a polymer or to a spin mass. If a polymer is "unspinnable," this implies that no fibers can be obtained from it, regardless of the method used. An unspinnable solution, on the other hand, merely indicates that under given conditions, such as solids content or nature of solvent, no fiber formation takes place. This somewhat colloquial use of the term becomes more obvious if one realizes that even an "unspinnable" polymer might become "spinnable" by modifications in the spinning procedure.

By speaking of "fiber-forming" polymers we gain a little, although the criterion for potential fiber formation is equally uncertain. The qualitative micro- or macroscopic observation of elongated structures drawn by hand from a solution or melt is often taken as proof for the fiber-forming character of the polymer. This is to some extent justified as the quick succession of solvent removal or cooling conditions gives a better chance for the

observation of the development of a fiber structure. Since in some cases structures are formed which have the appearance of fibers but no fiber character, the evidence is not really convincing. Erbring¹ has studied these phenomena and their relationship to the colloidochemical characteristics of spinnable solutions.

The literature applies the term "spinnability" also to the formation of liquid filaments. Methods for the measurement of this property have been developed through determination of the maximum length of a liquid filament prepared under standardized conditions, by Thiele and Lamp.²

Summarizing, we may say that the ability of a polymer to form fiber structures is jointly based on its inherent physical properties and on our knowledge of processes by which it can be brought into a random system (solution or melt) which under proper rheological conditions permits an appropriate arrangement of the polymer chains.

III. Discussion of the Physical Characteristics of Spinnable Materials

1. FLOW REQUIREMENTS FOR FIBER-FORMING SOLUTIONS AND MELTS

The actual rheological factors governing the flow of a spinnable mass are rather complex. It will be attempted to enumerate the more obvious component problems and to combine them into a pattern.

(a) A spin mass flowing through the capillary part of the spinnerette is subjected to friction effects between capillary wall and the outermost liquid layer. In a telescopelike pattern additional friction takes place between concentric cylindrical layers, resulting in a paraboloid-shaped profile of speed distribution.

(b) The rod-shaped polymer chains undergo an orientation in the spinnerette which is strongest near the capillary wall, since the speed gradient has there its highest value. It is, however, probable that the chains are in most cases not sturdy, hard rods but rather of a bent, curled shape which is straightened out to some extent during the flow. Therefore, part of the flow energy is used up to "unroll" the chains before they can be aligned in the direction of the flow.

(c) The dimensions of the spinnerette capillary must have a certain relationship to the physical characteristics of the spin mass, to the dimensions of the primary filament, and to the feeding speed, and will depend on the type of spinning process used.

(d) The influence of temperature is an indirect one. The temperature

¹ H. Erbring, *Kolloid-Z.* **98**, 164-169 (1942).

² H. Thiele and H. Lamp, *Kolloid-Z.* **129**, 25-39 (1952).

affects the mobility of the spin mass and the polymer chains, and can be compensated for to some extent in spinning solutions by concentration changes.

(e) Stationary flow conditions are important since no uniform fiber formation can be expected in their absence. Therefore, turbulence and other sources of irregular flow must be avoided.

(f) The actual fiber formation will be influenced by the surface tension prevailing at the spinnerette exit. Therefore, the viscosity under the conditions of flow must be in a certain relationship to the nature of the coagulating medium (liquid or gas). (The spinning into vacuum is of only theoretical interest and here omitted).

From these factors one may deduce that appropriate flow—preparatory to spin—mass coagulation—depends on a variety of influences. In practical spinning they are determined experimentally by varying the component conditions. Since they mutually depend on each other, it is generally impossible to change only one variable without affecting the others. Luckily, most technically interesting spinnable polymers have a wide range of useful flow conditions. By a trial-and-error method one can narrow the various component conditions to adjust the flow to a combination permitting safe coagulation of a uniform filament of desirable physical characteristics.

2. STRUCTURAL PROPERTIES OF FIBER FORMERS

The investigation of various natural and synthetic fiber-forming polymers has shown that certain dimension and shape standards of the polymer chains have to be met for spinnable compounds.

It is obvious that cross-links which reduce or eliminate solubility and melting characteristics are harmful. (There is no objection against cross-linking imparted into the fibers after they are spun, however.)

Too high a degree of curling of the chains is equally a disadvantage. In certain protein solutions it is necessary to first transform by special chemical denaturing treatments the globular into a fibrous modification.

The absolute length of the polymer chain and the number of repeating units will equally influence the rheological performance of the spin mass and the properties of the obtained fiber. A minimum length—corresponding to a minimum molecular weight—is necessary to make the compound spinnable. While there is no limit to the maximum dimension, it is known that extreme molecular weight values do not improve flow or fiber properties. It is advisable to maintain a reasonable uniformity in chain length (molecular weight).

To obtain desirable flow characteristics in the spin mass, it is most important that the polymer can be brought into a homogeneous solstructure

or into a true melt. Only then a stationary flow can be expected which is the basis of an undisturbed spinning process and of uniform fiber properties.

3. RHEOLOGICAL CHARACTERISTICS OF SPIN DOPES

The flow anomalies of polymer systems, especially spin masses, have been the object of intensive studies by many workers (Philippoff,³ Meskat,⁴ and others).

The basis of these anomalies is the rearrangement of the originally random polymer chains, taking place under the influence of outside forces. A unidirectional movement as it takes place in the passage through conduit tubes, spinnerette capillaries, etc., will affect the relative position of the chains, whether they are curled or straightened out. The unmoved spin mass will oppose strongly any dislocation since there is a large number of contact points between the entangled, randomized chains. As soon as the controlled, unidirectional movement has started, the chains will begin to be straightened out if they are curled, and a disentanglement will take place. Accordingly, the resistance against flow movement will be reduced and with it the apparent viscosity of the spin mass. This viscosity reduction will approach a constant value which may be assumed to be due to a complete straightening out and parallelizing of the chains. In many cases this point will never be reached, however, since turbulence appears before the straightening out and parallelizing process is completed.

For a quantitative description of the force causing these flow effects in capillaries, one may use the intensity of shearing stress as expressed by the term $RP/2L$ (R being the radius of the capillary, L its length, and P the hydrostatic pressure under which the mass is moved.) If the absolute value of this shearing stress is too low, the prearrangement of the chains will prevent fiber formation. If it is too high or turbulence has started, it will be difficult to synchronize the coagulation mechanism with the movement of the spin mass.

4. INFLUENCE OF SOLIDS CONTENT

In spinning solutions the ratio of solute to solvent is an important factor affecting the conditions of fiber-forming flow.

Obviously, the chain length (or the molecular weight) will influence the flow of a solution having a given solids content. A speed gradient sufficient to uncurl and straighten out short chains should leave long chains almost unaffected. Actually, it has been observed that polymers of increasing molecular weight follow this pattern (see, for instance, K. Edelmann.⁵)

³ W. Philippoff, "Viskosität der Kolloide." Dresden-Leipzig, 1942.

⁴ W. Meskat, *Chem. Ing. Tech.* **24**, 333-8 (1952).

⁵ K. Edelmann, *Faserforsch. u. Textiltech.* **3**, 341, 344, 412 (1952).

It is empirically known that under practical conditions fiber-forming flow can be obtained only within a certain range of solids content which depends on the molecular weight (intrinsic viscosity) of the polymer, the nature of the solvent, the temperature, etc. Below that value, the distribution of the chains is insufficient for establishing a network preliminary to fiber formation. Also, the coagulation mechanism cannot be speeded up sufficiently to transform the sol into a gel. (One has to realize that, for example, in a 5% solution, for each weight unit of polymer, 19 units of solvent or at least a large part of them have to be removed to obtain a fiber). If, on the other hand, the solids content is too high, impractical pressures—meaning extreme values of shearing stress—have to be applied to move the solution through the capillary.

Since the capillary dimensions R and L appear in the term describing the shearing stress, it becomes understandable that a certain adjustment can be obtained by modifying radius and length of the spinnerette capillary.

5. VISCOSITY-TEMPERATURE FUNCTION OF SPIN MASSES

Attempts have been made by various investigators to establish a fundamental relationship between temperature and flow curves of spin masses. It appears probable that the shape of the flow curve (shear stress plotted against speed gradient) is not affected by the temperature, but that its location—absolute values in a given system of coordinates—is influenced. One may, therefore, assume that such a family of curves corresponds to parallel dislocation of an imaginary master curve for a given solution type. Such a relationship seems to exist not only between flow curves of a given solution at different temperatures, but also between those of a given polymer in different concentrations at constant⁶ and at varied temperatures.⁵

The influence of increased temperature of a spinning solution is similar to that of dilution. In other words, the flow resistance in movement through a capillary is decreased as if the solvent content had been increased. Actually, of course, the solute-solvent ratio is unchanged, and a quantitative comparison between dilution and temperature increase is not admissible. Also, the above-mentioned relationship between “spinnability” and relative amount of solvent to be removed indicates that the spinning mechanism is different in diluted and in heated spin masses, although they may show similar flow characteristics.

Because a certain speed gradient range is a requirement for fiber formation, it becomes obvious that extreme changes of spinning temperature can cause a normally well-spinnable spin mass to become unspinnable. If the temperature is increased above a certain value at a given pressure, the

⁶ B. Rabinowitsch, *Z. physik. Chem. (Leipzig)* **A166**, 257–69 (1933).

danger of turbulence is an additional adverse factor. Lowering the temperature means the necessity of compensating—generally by pressure increase—for the reduced flow speed; thereby, in addition to other disturbing factors, extreme pressures become necessary. In the case of solution spinning, the reduced diffusion and coagulating speed also must be considered. In melt spinning a natural limit for temperature decrease is given by the melting point of the polymer.

Increased temperature means in solution spinning an increased diffusion speed of dope-solvent and coagulating medium. Their vapor pressures also have to be taken in consideration. Apart from all influences on spin flow, the sudden pressure release taking place at the spinnerette exit may lead to abrupt, explosionlike solvent removal and to simultaneous formation of bubbles or disruption of spinning continuity.

To keep a spinning process within a certain temperature range is therefore necessary for two reasons: to maintain appropriate flow conditions and to avoid disturbances in the coagulation mechanism.

6. HEAT DEVELOPMENT DURING FLOW

While the principle of development of Joule heat in moving liquids is old, little has been done so far to follow up the quantitative temperature changes taking place in moving spin masses. It is obvious that friction of a liquid against a solid, and of polymer chains within a liquid must produce thermal effects. Under certain conditions the developed heat may be dissipated by the disproportionately large system, such as, for instance, the bath in which a spinnerette is immersed.

Experiments by the author⁷ were performed in an adiabatic system (Dewar vessel) in which spin masses were subjected to controlled stirring action by a cylinder rotating at constant speed. Low molecular liquids like glycerin, water, or sugar solutions (bee's honey) and actual spin dopes showed different time-temperature curves. The low molecular weight liquids showed proportionality between stirring time and temperature over a wide range, while the spinning solutions showed an exponential increase of the temperature. In both cases, a flattening-out effect of the time-temperature curve takes place after some time; its meaning is that the temperature reached has lowered the viscosity of the system to a degree where the frictional effects are significantly reduced.

The rheological conditions of flow in spinning, therefore, depend not only on the known viscoelastic properties of the spin mass determined at a given temperature, and the normally controlled extrusion conditions, but also on the thermal behavior of the dope and the heat exchange which

⁷ B. R. Roberts, Paper given at the Gordon Research Conferences, Textiles, New London, New Hampshire, July, 1952.

takes place. Any temperature increase produced by the movement through conduits, metering pump, or spinnerette will have the easily overlooked effect of reducing the "viscosity," thereby affecting the speed gradient and its influence on fiber formation.

IV. Flow Under Fiber-Forming Conditions

1. FLOW PROFILE IN SPINNERETTE

It is well known that a liquid moving through a capillary does not proceed as a cylindrical plug but that the central portions move faster than those in contact with the capillary wall. The layer which touches the inside wall of the spinnerette has theoretically a zero speed, i.e., it stands still. The speed of movement increases toward the center of the capillary gradually, along a parabolic function, in telescopelike concentric cylinders. The speed in the center, therefore, shows a maximum, as mentioned before.

It is the difference in speed between neighboring liquid layers which affects the straightening out of the polymer chains. A chain lying vertical to the capillary axis in the exact center of the capillary should theoretically move parallel to itself without any turning to the capillary axis. A chain near the capillary wall, on the other hand, is exposed to a maximum of tilting action since the speed gradient is highest here. Intermediate cylindrical layers will, therefore, be exposed to an orientation effect gradually decreasing toward the capillary center (see, for instance, Loebering.⁸)

The capillary flow of a spin mass containing polymer chains will, therefore, provide an initial orientation which has a maximum at the outside and a minimum near the center. The absolute value of the amount of orientation will again depend on the shearing stress and all factors governing the shearing stress-speed gradient relation. It does not necessarily determine the final chain arrangements, as will be seen later. However, the chances of strong alignment at the outside are increased by high flow speed, whereas isotropic or nearly isotropic structures may be expected from slow spin-mass movement.

2. SPEED GRADIENT

The speed gradient of a spin mass is proportional to the applied shearing stress at slow speeds but increases along an exponential function with increasing shearing stress values. In some cases proportionality is again observed at still higher shearing stresses. Early experiments by B. Rabinowitsch⁹ showed increases with the second to fourth and higher power, until turbulence set in.

⁸ J. Loebering, *Papier fabr. (Tech.-wiss. Teil)* **37**, 9-15 (1939).

⁹ B. Rabinowitsch, *Z. physik. Chem. (Leipzig)* **A145**, 1-26 (1929).

The speed gradient may be expressed by Q/R^3 in which term Q equals the flow volume per unit time. By plotting values of Q/R^3 against $RP/2L$ (shearing stress) representative flow curves are obtained which show how the four variables (Q , R , P , and L) affect each other.

Since the speed gradient distribution is under otherwise identical conditions indirectly dependent on capillary dimensions, one may, to some extent, adjust its absolute value by changing the spinnerette size and by adapting it to the given system. Depending on the kind of spinning method, one will use other spinnerette types for dry (fast) or wet (slow) spinning, and still others for melt spinning where no mass exchange caused by solvent removal takes place.

3. THE ROLE OF SHEARING STRESS

Since velocity (speed) gradient and shearing stress are mutually dependent on each other, it is obvious that everything said in the previous section is valid for the role of shearing stress. As the latter is easier to control and well defined from capillary dimensions and applied pressure, one can take it as the basis for flow specifications and extrusion under fiber-forming conditions. The only practical disadvantage consists in the fact that in all technical spinning the flow is controlled by a constant feed rate (metering pump) and, therefore, in the above-mentioned shearing stress term $RP/2L$, the pressure P is indirectly depending on the feed rate.

4. VISCOSITY CHANGES TAKING PLACE DURING COAGULATION (HARDENING)

The transition of the flowing spin mass at the spinnerette exit into a self-supporting fiber structure is accompanied by a viscosity increase of several orders of magnitude. The removal of solvent, or cooling, reduces the mobility of the polymer chains and the preliminary fiber structure is affected by the relative position of the chains which prevails during the rather short time interval of coagulation. One also has to consider the mechanical changes taking place near the spinnerette exit: Up to this point the spin mass is moved by a back pressure, "pushed," and surrounded by the capillary walls. Beyond the spinnerette exit the hardening mass is drawn away and is no longer in contact with a solid wall. In technical spinning the drawing force is considerable, but in certain experimental setups it may be reduced to the influence of gravity. (By spinning into a bath having the same density as the coagulated fiber, even the gravity influence may be eliminated.) Obviously, in a very narrow zone near the spinnerette face the hardening mass is exposed to both forces: It is simultaneously pushed and pulled in the same direction. The friction between spin mass and solid capillary wall is, of course, abruptly ended at the

spinnerette exit and replaced by friction against the coagulating fluid (liquid or gas). Therefore, the flow in the transition zone from sol (melt) to gel is changing in quick succession through various stages. Superimposed over the above mentioned effects is the influence of radial restriction caused by solvent removal or cooling. In the case of solution spinning the volume change is compared by various authors with an "implosion" effect meaning a volume reduction comparable in suddenness with the volume increase accompanying an explosion. On account of the small size of the coagulating zone—both in radial and longitudinal direction—and the rather high speed with which an individual section passes through the various stages, it is difficult to determine exactly the sequence of viscosity changes. Observations of flow birefringence are probably the best method of studying the transition from sol (or melt) to gel.

The fact that the extruded mass is able to undergo the changes necessary for formation of an actual fiber, and the size of mechanical forces which are now taken care of without breaking of the structure indicate the enormous viscosity increase which has taken place in the hardening zone.

The coagulation (hardening) profile which is formed near the spinnerette exit is typical for the transition stage in which a hardened or semihardened fiber structure is formed. At the point where the spin mass passes the spinnerette exit it ceases to move as a cylindrical stream. Under the influence of various physical forces the cylindrical stream will in most cases change into a structure moving in the shape of a concave rotation paraboloid. Because of solvent removal, stretching forces, etc., a diameter reduction will take place which after an intermediary stage of a conical shape will lead to a nearly cylindrical fiber structure.

In some cases where the forces restricting the cross-section size are low, a different profile will be formed. Near the spinnerette exit the fiber hardens with formation of an onion-shaped profile. This effect is particularly developed in some cuprammonium rayon spinning processes. It was investigated in detail by H. Pupke¹⁰ who calculated the dimensions of the diameter increase from the spinning conditions.

5. GEL FORMATION COMBINED WITH MASS TRANSFER (SOLUTION SPINNING)

a. Dry Spinning (No Chemical Changes Taking Place)

The industrial dry spinning processes do not combine coagulation with chemical changes. In spite of this simplification, the rheological changes taking place during the gel formation are rather complex. Since the dry spinning process is based on coagulation by solvent evaporation, the mass transfer of solvent toward the surrounding atmosphere must be taken in

¹⁰ H. Pupke, *Faserforsch. u. Textiltech.* **2**, 440-442 (1951).

account. The diffusion of solvent from the central parts of the coagulating stream toward the outside, the evaporation of the solvent, and the resulting volume reduction of the beginning fiber structure are some of the influences affecting the relative position of the polymer chains. The diffusion of air (gas) toward the core of the hardening structure is probably of minor influence. The evaporation of the removed solvent may cause cooling effects which result again in a brief viscosity increase. Since technical dry spinning speeds are high, on the order of 10^3 m./min., the stages through which the hardening structure moves are very short lived. The polymer solution is transformed into a gel within a short fraction of a second with an extremely sudden increase of viscosity. Although in technical dry spinning the hardened fiber still contains a considerable amount of residual solvent it is safe to assume that the overwhelming part of viscosity increase is reached within a very short distance from the spinnerette face.

The relative movement of hardening mass and surrounding gas must be taken in consideration equally. Concurrent and countercurrent direction of fiber and air movement can be applied. The friction between hardening fiber and surrounding air will, of course, be lower in the case of concurrent movement, but other things being equal, the solvent removal will not be as efficient as in the countercurrent arrangement.

b. Wet Spinning

Wet coagulation has, as principal rheological difference compared to dry coagulation, the higher viscosity of the coagulation fluid, a liquid. This causes a considerably higher friction between hardening structure and surrounding bath. Consequently, there are two rheological influences significantly superimposed: First, the flow taking place inside the hardening spin dope. (Telescopic movement in axial, solvent-bath diffusion in radial direction.) Second, the movement of the structure through the spin bath.

The second factor reduces the practical spinning speeds roughly by one to two orders of magnitude, compared with dry spinning.

In the following, the rheological differences of wet spinning with and without simultaneous chemical changes are briefly compared.

(1) *Wet spinning combined with chemical changes.* Since a large part of the synthetic fiber industry (viscose process and others) combines coagulation with chemical changes (regeneration), this type of wet spinning is of considerable technical importance. Complicated as the purely physical rheological changes in the hardening zone are, the superimposition of chemical reactions causes additional effects, such as reaction heat and formation of reaction products.

The chemical precipitation of the spin dope is a nearly instantaneous reaction as far as the outside zones of the dope stream are concerned. When

the precipitant penetrates toward the center, it has to pass through already swollen, regenerated zones, which causes a delay. Obviously, this delay will be shorter for thin diameters than for coarser structures.

(2) *Wet spinning without chemical changes.* The rheological conditions are to some extent here simpler than in "chemical" wet spinning, but still rather complicated. The hardening is caused by the dissolution of the dope solvent in the spin bath and the insolubility of the polymer in the latter. Again, the outlying zones of the dope stream are hardened first, and only by passage of solvent and bath through these semicoagulated zones can the precipitation proceed toward the core.

In addition to the flow of polymer chains in fiber longitudinal direction, and to the moving of the hardening mass within the bath, another type of flow, therefore, must take place: the movement of solvent and bath in opposite directions, roughly perpendicular to the fiber axis. The actual angle will depend on the relative speed of the hardening structure.

The flow directions of dope stream and spin bath may again be concurrent or countercurrent. The relative merits of each arrangement will be analogous to those observed in dry spinning.

6. GEL FORMATION WITHOUT MASS TRANSFER (MELT SPINNING)

The extrusion of a melt into an atmosphere having a temperature lower than the melting point—or melting-point range—of the polymer is the basis of the melt-spinning process. Since no solvent is used in this process, there is no mass transfer taking place except in certain cases where some depolymerization may occur.

The hardening begins again at the outside of the moving spin mass but—in contrast to solution spinning—it can here proceed toward the core without the difficulties caused by the diffusion through swollen shell zones.

The mobility of the polymer chains decreases with progressing cooling. As significant difference from solution spinning, one has to realize that no appreciable volume reduction takes place in melt spinning except that produced by thermal contraction and by tighter packing.

The flow of a cooling melt is again controlled by the viscosity changes of the mass, the positive movement ("push-pull action"), and friction against the surrounding atmosphere. The speeds used in melt spinning are of a similar order as those in dry spinning, namely 10^3 m./min.

The absence of flow in fiber-radial direction promotes a nearly round cross-sectional shape in melt-spun fibers. The symmetry in the micro- and submicrostructure of the hardened fibers is generally much better than in solution-spun fibers.

7. THE INVERSION OF THE FLOW PROFILE BETWEEN THE CAPILLARY AND THE HARDENING ZONE

Schramek and Zehmis¹¹ have pointed out that the relative speed of concentric cylindrical shells of the spin mass passes between spinnerette and hardening through a stage where a complete reversal takes place. This will be understood from the following considerations: Entering the spinnerette, the spin mass moves at uniform speed as long as it is not in contact with the spinnerette walls. In the spinnerette hole, a parabolic flow profile is developed as the result of friction with the capillary walls. The parabola has its apex in the direction of the flow, since the center sections move at higher speed than those at the outside.

The hardened fiber structure, at a certain distance from the spinnerette exit, moves again at uniform speed; i.e., center and outside zones show no relative movement to each other. Obviously, the transition from a centrally accelerated flow into flow uniform over the entire cross section must be accompanied by a retardation along a profile which in each concentric cylindrical layer compensates the original profile: a parabola with the apex in a direction opposite to that of the first parabola.

The cross-section reduction taking place in solution spinning may obscure this effect to some extent. But in melt spinning under a minimum of drawing—where only thermal contraction has to be taken into consideration—its validity seems established.

In the first parabola the center particles, having a higher speed, pass those located at the outside. In the second parabola, the outside particles pass those in the center. (The arrangement is somewhat like a phalanx walking at the start and end of their march at the same uniform speed, while the center members increase their speed at the expense of the outsiders in the first period. In the second period the outsiders speed up, the center members slow down until all march abreast again.)

Depending on their original shape and their flexibility, the polymer chains will pass through various phases as far as shape and relative position are concerned, during these apparently confusing, though actually rather orderly changes of their relative speed. Straight chains may be bent, bent ones straightened out, and alignment in flow direction may be expected. Possibly the interaction of neighboring chains is an important contributing factor in fiber formation. The physical properties of a fiber structure coagulated after passage through a capillary are actually rather different from those found on cast films, and have some analogy to those of films extruded through slits. It is probable that the inversion of the flow profile is in part responsible for these differences.

¹¹ W. Schramek and E. Zehmis, *Kolloid-Beih.* **48**, 93-140 (1939).

The apparent paradox of the inversion of the flow profile has more than merely theoretical interest since it explains some of the structural effects to which the polymer chains are exposed in the spinning process. Their relative position is controlled, as shown above, by the speed distribution during flow and, even more, during hardening. The flow resistance ("viscosity") during the inversion of the profile will, to some extent, determine the differences in crystallinity and orientation prevailing between core and shell of the preliminary fiber structure.

8. THE ALIGNING OF THE POLYMER CHAINS

The technological properties of a fiber structure are based largely on the arrangement of the polymer chains. In spite of the fact that in various processing steps the original position of the chains is modified, the flow taking place in the spinnerette and its changes during hardening are the basis for all later treatments.

One has to realize that a technical fiber is an anisotropic structure. The anisotropy is in part a morphological one (shape of cross section, etc.) and in part based on irregular chain arrangement. The former can be seen in the microscope while special physical methods are necessary to observe the latter.

The morphological anisotropy will depend on the degree of uniformity of flow prevailing in spin mass and coagulating medium. Completely uniform flow of both systems relative to each other should result in fibers of completely round cross sections. In technical processes it is very difficult to realize such conditions. Hardening of neighboring filaments, limited size of the coagulating system, etc., will always cause a certain asymmetry. The latter is strongest in solution spinning where the above-mentioned diffusion flow between solvent and coagulant makes it particularly difficult to obtain symmetric conditions. In melt spinning where the conditions are simplified, it is easier to eliminate asymmetry and melt-spun fibers actually show generally a nearly round cross section, equivalent to a minimum of morphological anisotropy.

The anisotropy based on irregular chain arrangement is a result of the telescopic movement of the spin mass during and after passage through the spinnerette. The variations of the speed gradient from the center to the outside determine the alignment of the chains. In most cases, it will be highest at the outside—at least in the freshly coagulated and not yet processed fiber. There are various methods by which the relative arrangement of the polymer chains over the cross section can be followed up. The absolute intensity of the surface alignment can be controlled by details of the spinning process which indirectly affect the flow properties. Variations in chain length, solids content of spinning solutions, temperature, di-

mension and shape of spinnerette, hardening mechanism, etc., are known to influence the structural anisotropy of a fiber over a wide range. They were the object of numerous investigations.

A fundamental study of these phenomena was made by Sippel^{12, 13} who investigated the relationship between coagulation and orientation. He compared dry- and wet-spun acetate fibers having various amounts of stretch, and concluded from birefringence and tensile measurements that certain speed gradient values have to be obtained for optimum orientation effects.

Elsaesser¹⁴ investigated for the cuprammonium rayon process the structural changes taking place under various spinning and stretching conditions. He determined the optimum coagulation conditions from several series of experiments in which most spinning conditions were varied over a wide range. (For a discussion of his calculations see Pupke.¹⁵)

V. Evaluation Techniques

1. DETERMINATION OF DOPE "VISCOSITY"

From the foregoing it will be understood that a rheological description of a polymeric system as a spinning solution or spin melt cannot be based on any single factor. It is necessary rather to determine the flow curve of such a spin mass over a certain range, which should include shearing stresses to which the mass is subjected in actual spinning.

Determination of values in the region of low shearing stresses often made by the ball-fall method will give a means to compare spinning masses in the initial region of Newtonian flow. It will not yield any information on the deviations to be expected under spinning conditions, however. Even if it were possible to calculate the shearing stress value for a ball-fall experiment one could not predict at which point the flow curve would show beginning non-Newtonian flow, nor could any statement on the shape of the diagram in this region be made.

On certain spinnable polymers these deviations are relatively low. Polymers which are usually melt-spun, as polyamides, polyesters, and vinylidene chloride copolymers were found by Edelmann⁵ to display in solution only minor deviations from Newtonian flow. In these cases, viscosity data determined by the ball-fall method will lead to relatively reliable comparable values although they do not furnish any information on the range where Newtonian flow ceases.

¹² A. Sippel, *Z. Elektrochem.* **50**, 152-163 (1944).

¹³ A. Sippel, *Z. Elektrochem.* **50**, 256-266 (1944).

¹⁴ V. Elsaesser, *Kolloid-Z.* **111**, 174 (1948); **112**, 120 (1949); **113**, 37 (1949).

¹⁵ H. Pupke, *Kolloid-Z.* **118**, 33-37 (1950).

In certain molten systems, as polyethylene terephthalates, there are equally only minor deviations from Newtonian flow found as reported by McKelvey.¹⁶

To determine flow curves, a capillary or rotational instrument may be used which permits variation and control of the shearing stress over a sufficiently wide range. The shearing stress values are plotted against the corresponding speed gradient values, preferably in a double logarithmic system. In this way measurements made over several orders of magnitude can be brought into an easily understandable pattern.

Although apparently no measurements on typical spin masses have been made so far on Weissenberg's Rheogoniometer¹⁷ this instrument in which rotational and vibrational stresses are combined may eventually show interesting possibilities of coordinating rheological characteristics and spinning performance.

On account of the unknown influence of temperature on the flow characteristics of a spinnable polymeric system, it is advisable to perform the flow measurements of a spin mass at the temperature under which the actual spinning takes place. Otherwise extrapolations are made which can easily lead to errors, especially since changes in solvation, of chain shape, etc., may cause unpredictable deviations because of the superimposed influence of the temperature.

Since flow under higher shearing stresses may cause structural disruptions of polymer chains, resulting in changed flow characteristics, a given specimen of a spin mass should be tested only once and not reused for measurements. The influence of thixotropic effects is also reduced by this practice.

2. INFLUENCE OF SHEARING STRESS ON MEASUREMENTS

As mentioned above, a controlled and known amount of shearing stress and its variation over a certain range is a necessity for meaningful viscometric measurements on most types of spin masses. Comparing two given spin masses one may, under certain conditions, obtain two flow curves which intersect each other. The significance of the intersection point lies in the fact that at the corresponding shearing stress values the "viscosity" of the two masses is the same. At lower shearing stress values, one specimen is more "viscous," at higher values the other. In comparing the spinning performance of the two samples one will have to calculate the shearing-stress range prevailing under spinning conditions before a meaningful statement on the relative merits of the samples can be made.

¹⁶ J. M. McKelvey, *Ind. Eng. Chem.* **45**, 982-986 (1953).

¹⁷ K. Weissenberg, *Proc. Intern. Rheol. Congr., 1st Congr., Scheveningen, 1948* Vol. II. p. 114 (1949).

The effect of structural viscosity causes a pseudo-Newtonian behavior at high shear values, namely linear relationship between shearing stress and speed gradient. If measurements are confined to the upper end of the *S*-shaped flow diagram, one may easily be misled into believing that the observed values correspond to the initial, Newtonian part of the curve. Unless flow curves over a wide range of shearing stresses are determined, in which the transition from (initial) Newtonian to non-Newtonian flow is recognizable, one cannot be sure that the comparison of two samples is meaningful.

The turning point of the *S*-shaped flow curve displays according to K. Edelmann⁵ in the case of chemically similar polymers of different molecular weights a peculiar feature: In solutions having a given solids content it is only a function of the shearing stress. In Edelmann's paper 4 % polyacrylonitrile solutions of widely varying molecular weights are shown to have the turning points in their flow curves at approximately 5×10^3 dynes/cm.² shearing stress. On the other hand, solutions of a given polymer, but prepared at different solids contents, were found to have turning points at various shearing stresses, but at constant speed gradient values.

3. USE OF THE SPINNING MACHINE AS VISCOMETER

It has been suggested that the flow characteristics of a spin mass be evaluated under conditions approaching those prevailing in actual spinning by studying the extrusion through a spinnerette in the spinning machine.¹⁸ Such a setup has the advantage of eliminating supplementary equipment and difficulties caused by instrument factors. Since the shearing stress in capillary flow is a function of pressure, capillary diameter, and length, and since the speed gradient is a function of extrusion volume and capillary diameter, one may for a given capillary (spinnerette) dimension either vary the feeding speed and measure the developed pressure, or vary the pressure and measure the obtained speed. In technical spinning machines, the spin mass is fed at constant speed (metering pump) and the developed pressure can be read at a pressure gauge near the spinnerette. Through a slight adaptation the metering pump may be replaced by a constant pressure device, and the extruded volume may thus be measured. If, in the first case, the metering pump is run at technical speeds, or in the second case the mass is extruded under pressures similar to those prevailing in spinning, the obtained data may be used for describing the flow of the spin mass in a range which includes the spinning conditions.

¹⁸ H. L. Bredée and J. de Booy, *Kolloid-Z.* **96**, 24-29 (1941).

VI. Interpretation of Phenomena Accompanying Fiber Formation

1. OBSERVATION OF DOPE COHESION

The various phenomena taking place during the short time elapsing between the instant a spin mass particle leaves the spinnerette exit and its transformation into a link of a self-supporting structure can only partly be understood by studying the influences of flow, surface tension, diffusion, etc.

Weissenberg¹⁹ has observed that polymer solutions brought into proper mechanical conditions will exhibit a phenomenon which seems paradox in view of what is known of the influence of shear, inertia, and other factors on the flow of polymer systems. A polymer solution, e.g., a spin dope, is brought in his experiments into a cylindrical cup or flat dish into which is immersed from above—but not connected with it—a rod or a tube, in such a way that the bottom of the rod (tube) is in contact with the solution. Upon rotation of the cup (dish) the solution is expected to follow the centrifugal force and move away from the center of rotation. Actually it begins to climb up on the rod or tube. By proper adjustment of solution characteristics, cup, rod (tube) dimensions, and rotation speed, one can realize various mechanisms in which the solution rises, overcoming the influence of gravity. For instance, the solution rising at the inside of a wide (e.g., $\frac{1}{2}$ in. i.d.) tube will show a parabolic flow profile comparable to that observed normally in capillary flow.

Instead of a rod or tube a plate may be used which is mounted parallel to the bottom of the cup in such a way that it can slide up and down without rotation. In this case, the polymer solution will, upon rotation of the cup, form a vertical column which lifts the sliding plate under an easily determinable pressure. Schreck and Wille²⁰ have studied this phenomenon in more detail and in a paper "Bemerkungen zum Weissenberg Effect vom Standpunkt der Kontinuumsmechanik" they report on experiments in which gauge-like tubes are mounted in the sliding plate at different distances from the rotation center in such a way that the rise of the solution can be observed during the experiment. They noted, as could be expected, maximum pressure in the center, and compare the phenomenon with the effect of the pressure of a ring surrounding a barrel. In other experiments, these authors have used a Couette apparatus and spread a powder on the surface of the liquid in order to study the speed distribution.

¹⁹ K. Weissenberg, *Nature* **159**, 310-311 (1947); *Proc. Intern. Rheol. Congr.*, 1st Congr., Scheveningen, 1948 Vol. I. p. 29 (1949).

²⁰ C. Schreck and R. Wille, *Kolloid-Z.* **126**, 98-102 (1952).

Frei and Katchalsky²¹ offer "a tentative explanation of the Weissenberg effect", while more recent theoretical and experimental work will be found in Chapters 2 and 10 of Volume I, and Chapter 16 of Volume II of this treatise.

It is safe to assume that dope cohesion has a major, although so far not yet completely understood, influence on the flow of a spin mass, particularly in the zone between spinnerette face and preliminary hardening.

It may be expected that in cases where such effects are observed, a shearing stress applied in one direction causes a stress in a perpendicular direction. If one tries to apply this assumption to the zone of fiber formation, it appears probable that the stress developed in fiber-axial direction will develop another radial stress. This would indicate that the compressive forces resulting from peripheral coagulation are counteracted by the secondary radial stresses.

2. FRICTION BETWEEN THE COAGULATING FIBER STRUCTURE AND COAGULANT

In one of the previous sections it has been mentioned that the coagulation of a spinning solution comprises at least three flow systems: The telescopic movement of the mass in axial directions; the diffusion of solvent and coagulant in opposite and approximately fiber-radial directions; and the relative movement of the hardening mass in the coagulant fluid.

The last of the three flow systems will influence particularly the core-shell development in the fiber structure. The semicoagulated mass is exposed at its surface to a retarding frictional effect which has a tendency to straighten out the still mobile chains. This increases the effect which has taken place during the flow through the spinnerette.

As mentioned before, this friction is minor in gaseous fluids (dry and melt spinning) but considerable in the case of liquid spin baths. Therefore, the wet-spinning speeds are necessarily lower than those obtainable in dry and melt spinning.

The peripheral friction suffered by the fiber while still easily deformable, has an effect similar to that of a ring compressing a barrel. It is known that radial pressure applied to a fiber structure is equivalent to stretch in the longitudinal direction (example: a plastic sphere, as a balloon, will under equatorial pressure be deformed into a longitudinal ellipsoid, as if the poles were pulled apart).

The absolute amount of fiber-bath friction will, of course, depend on shape and size of fiber cross section, relative speed between fiber and bath, their nature, length of contact, and similar factors.

²¹ E. H. Frei and A. Katchalsky, *Bull. Research Council Israel* **1**, 113-6 (1951); *Rubber Chem. and Technol.* **26**, 203-206 (1953); *Chem. Abstr.* **47**, 6167 (1953).

3. FORMATION OF CRYSTALLINE ZONES

The various influences to which a coagulating fiber structure is subjected will cause an arrangement of the chains which is dependent on their mobility and their relative position during the period of hardening. It has been mentioned before that the three types of flow which occur during coagulation will affect the relative position of the chains. Since each of the three flow systems (two in case of melt spinning) take place in a nearly symmetric way, it is understandable that at each instant a large number of polymer chains is subjected to similar conditions. These conditions may and will vary, however, at different distances from the fiber axis, at different intervals of time elapsed from the start of coagulation, etc. The nearly symmetric arrangement of the various forces will cause chain arrangements in concentric layers. As a result of the action of the various physical forces, a parallelizing effect will take place between neighboring chains. A perfect orientation (complete parallelization with respect to fiber axis) can neither be obtained in the coagulation nor would it be desirable. Parallelization in zones of limited dimensions and not necessarily with respect to the fiber axis (crystalline zones) may be expected as consequence of the flow changes during coagulation. The development and stability of crystallinity is, of course, also influenced by various physical factors as moisture, heat, solvent content, etc. Therefore, it must be realized that the crystallinity developed during the spinning process has merely a preliminary character. Depending on the subsequent treatments applied to the fiber, the crystalline zones may be rearranged into zones showing orientation with respect to the fiber axis.

The importance of the development of crystalline zones during the spinning process lies in the fact that the arrangement obtained is the basis for all subsequent changes. Unless the flow in the hardening process has been controlled properly, it will not be possible to obtain technically useful fibers which can be subjected to the stresses encountered in the various processing steps without too great a danger of fiber breaks.

4. THE DEVELOPMENT OF ANISOTROPY IN THE FIBER STRUCTURE

Although the spinning of a synthetic fiber is, strictly speaking, the process of fiber formation, some subsequent steps are intimately related to the spinning process. It is only in a few cases (e.g., acetate) that the physical properties obtained on the fiber in the spinning process are sufficient for certain applications. No major physical changes are necessary in such processes, except removal of residual solvent and similar after-treatments. In most other fibers, however, where the requirements in mechanical performance are higher, the preliminary fiber structure is not

yet sufficient and technical processes have been developed to increase certain physical characteristics above those shown by the original fibers.

Most of these processes are accompanied by a rearrangement of the structural units inside the fiber, and by development of anisotropy. The movements of polymer agglomerations are based on rheological laws. The mobility of these agglomerations (crystallites, micellae) will depend on specific factors such as polymer structure, temperature, presence of swelling agents as water or solvents, and state of (longitudinal) tension. (See, for instance, Happey,²² Krebs,²³ and Mueller.²⁴)

In a perhaps oversimplified way one can make the statement that by proper combination of the above factors an over-all desirable degree of molecular arrangement is obtained which, however, includes desirable and undesirable anisotropy effects. Stretching, relaxing, insertion of permanent crimp or twist, heat setting in fabrics (including ironing) are some of the structural changes obtained by flow arrangements. In addition to mechanical rearrangements chemical modifications also take place indirectly and in subsequent steps. For instance, crystallinity and orientation will affect accessibility to chemical treatments; a rather typical example is the relationship between the physical structure and the dyeability of fibers. Anisotropy in radial or axial fiber direction will cause differences in dye penetration (and actual color intensity) since the flow of a dye bath is slower in tightly packed than in loose zones. Observation of dye penetration in cross-sectional and longitudinal view will demonstrate such effects of anisotropy which are caused by, and are causing, flow anomalies.

There are many other phenomena based on fiber anisotropy because of rheological bases. Their discussion would be outside of the scope of this article, however.

5. STRETCH SPINNING

The flow taking place during fiber formation leads, as mentioned above, in general only to a preliminary fiber structure.

In most cases, it is necessary to subject the hardened fiber to an additional, subsequent treatment in which the relative position of the polymer units or their agglomerations are rearranged. Such treatments require a plastic state which may already be existing as in cold drawing of polyamide and other fibers, or which may be produced by swelling or heat action in nearly hardened fibers.

In some cases, the plastic state prevailing during coagulation can be used for this stretching treatment by combining it with the spinning

²² F. Happey, *Brit. J. Appl. Phys.* **2**, 117-126 (1951).

²³ G. Krebs, *Kolloid-Z.* **98**, 200-212 (1942).

²⁴ F. H. Mueller, *Physik. Z.* **42**, 123-129 (1941).

process ("stretch-spinning"). The oldest example of such a mechanism is the spinning of cuprammonium rayon in which the hardening fiber is led into a conical spin bath container (Thiele funnel).

The bath moves concurrently with the fiber, and as the funnel narrows with increasing distance from the spinnerette, the bath speed is increased. Resulting from bath-fiber friction an accelerated fiber movement will result and a certain orientation effect will take place in the gradually hardening fiber.²⁵ This is enforced by the compressive action of the bath toward the fiber core, an effect equivalent to stretching in longitudinal direction.

It is not possible to stretch-spin by merely increasing the speed (and tension) of a coagulating fiber, since the structure in its transition from sol to gel is not able to absorb the stresses necessary for a desirable deformation. In other words, instead of developing a sufficient amount of flow orientation, the fiber would merely break at its weakest point, near the spinnerette. However, if one takes care to distribute the stresses appropriately by protecting the weak section from extreme deformations, the flow of the micellae inside the fiber can be arranged in a way which leads to satisfactory orientation. Such an arrangement can be made by mounting "fiber-brakes" between spinnerette and stretching zone. These brakes may consist of an arrangement of thread guides around which the fiber is forced to move, thus changing its straight movement into one of an *S*-shaped or similar curve. Schramek and Zehmisch¹¹ have investigated the effect of such a fiber brake by careful control of the directional changes (distance of thread guides and angle to original direction of fiber movement.)

An attempt to establish for such cases a mathematical relationship between spinning conditions and fiber dimensions was made by Sippel.¹² By making diffusion measurements on the coagulating structure, under various conditions, including those of stretch spinning, he was able to analyze mathematically the influence of spinning speed, coagulation length, spinnerette diameter, solids content of spinning solution, and other variables. Experiments on stretch spinning of acetate fibers showed good agreement with the calculated values.

VII. Summarizing Discussion of Present Knowledge of the Various Rheological Problems Involved in Spinning

It has been attempted to show in the foregoing sections how the relative position of the polymer chains affects the various stages of spinning. There are only relatively minor differences between the rheological performance

²⁵ In some cases the fiber will move faster than the bath and thereby suffer a "friction-squeeze."

of a chemically heterogeneous system (spinning solution) and a homogeneous one (melt or fiber). The systematic studies of the last 20 or 30 years have shown that for a given polymer type—even under standard conditions of molecular weight distribution—the flow taking place during spinning will control to a large extent the later developed basic fiber properties. The flow in the formed fiber structure is the basis for many subsequent processing steps and various mechanical and even some chemical properties of the fiber.

Properties such as tenacity, stiffness, toughness, recovery power, energy absorption,—to name only a few—are largely based on the relative position of the polymer chains resulting from flow in spinning and subsequent steps.

There are no universally ideal flow arrangements in spinning as there is no ideal fiber. The various methods of spinning, the requirements for the preliminary and final fiber structure, and finally the use of the fiber in knitted, woven, or other structures, all depend on a combination of flow characteristics. However, a detailed discussion of these factors would lead beyond the limited space of this article.

One may summarize the problem by stating that one of the basic tasks of the synthetic fiber industry consists in finding for a given polymer type appropriate flow conditions which lead to technically satisfactory spinning, and to fibers of desirable characteristics.

VIII. Appendix

In order to illustrate the influence of rheological factors on the spinning process, a few quantitative data and diagrams are given in the following. They should show with the aid of specific examples how laboratory measurements and actual spinning performance are affected by the flow anomalies observed in the case of spinnable compounds.

1. DESCRIPTION OF THE VISCOSITY BEHAVIOR OF A SPIN DOPE

It is obvious that the "viscosity" of a polymer system (as a spinning solution) cannot be described by any single value. Nevertheless, there is an inclination, on the part of some to describe the viscosity of a dope sample in poises, to make statements that a given sample is more viscous than another one, and so forth.

While in certain cases such comparisons may refer to the Newtonian branch of the flow diagram (45 deg. straight line at low shearing stresses) there exists seldom any certainty on this point. The location of the turning points of the curves cannot be predicted unless a flow diagram over a wide range of shearing stresses has been determined. Figures 1 and 2 will illustrate this.

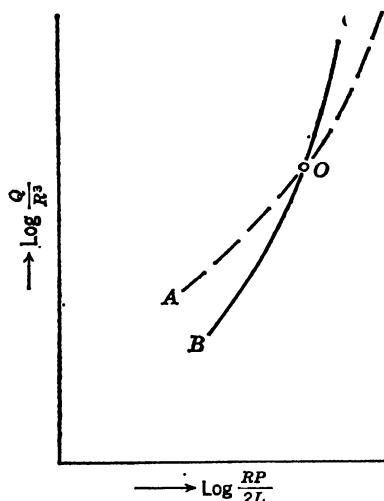


FIG. 1. Flow diagram of two dope samples. From data of Edelmann.

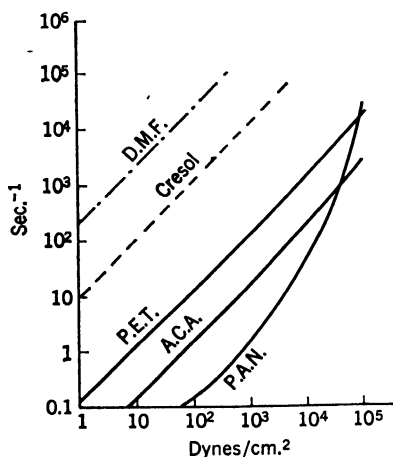


FIG. 2. Flow diagrams of three fiber-forming polymer types. From data of Edelmann.

Figure 1 shows the flow diagram of two dope samples marked A and B, selected in such a way that the two curves intersect each other at a point O. The meaning of the intersection point lies in the fact that at the corresponding shearing stress value ($RP/2L$) the apparent viscosity is the same for both samples. However, at lower shearing stress values, B will appear to be more viscous, while under shearing stresses exceeding those prevailing in O, A will seem to have the higher viscosity.

A quantitative example of such intersection points of flow curves can be seen in Fig. 2. This diagram reproduces the performance of three solutions: (a) "P.E.T." (a 16% solution of polyethylene terephthalate in cresol), (b) "A.C.A." (a 16% solution of an epsilon aminocaproic acid polymer in cresol), and (c) "P.A.N." (a 16% solution of polyacrylonitrile in dimethylformamide "D.M.F.").

The dotted lines in this diagram show the behavior of the two solvents used for the above spinning solutions, namely, cresol and D.M.F. Both solvents are Poiseuille liquids, show Newtonian flow, and appear in the logarithmic scale of the diagram as straight lines inclined under an angle of 45 deg. to the abscissa.

The above curves are condensed from data in Edelmann's paper.

It will be seen that the P.A.N. curve intersects the other two solution curves (A.C.A. and P.E.T.). If the shearing stress range could be extended by a few more orders of magnitude without turbulence effects, the P.A.N. curve would approach its solvent curve.

However, by merely comparing the actual solution curves, one will see that up to a shearing stress value of approximately 3×10^4 dynes/cm.² the P.A.N. solution appears more viscous than that of A.C.A. Above this value, conditions are reversed and the A.C.A. solution seems to have the higher viscosity. At a shearing stress of 3×10^4 dynes/cm.² both solutions display, of course, the same "viscosity."

The P.A.N. and P.E.T. solutions show a similar intersection point at a shearing stress of approximately 10^5 dynes/cm.², and analogous statements can be made for their relative flow performance at shearing stresses below and above the value corresponding to the intersection point.

How these viscosity changes affect the actual performance of a spin mass is illustrated in Fig. 3 (taken from Meskat's paper).⁴ A typical spinning solution (cuprammonium) was investigated by that author over a shearing stress range of approximately 1 to 9×10^4 dynes/cm.² By calculating the actual shearing stresses prevailing at various points of the technical spinning process, Meskat was able to enter the respective ranges in the flow diagram (diagonally shaded areas). Thus, it can be shown in which part of the flow curve the individual steps are performed. For instance, in the conduits at a shearing stress of approximately 1×10^4 dynes/cm.², the "viscosity" of the cuprammonium dope is 3200 poises, while it drops in the spinning pumps at a shearing stress of 4 to 9×10^4 dynes/cm.² to values between 900 and 100 poises. Assuming that two spinning solutions, having an intersecting point in their flow diagrams are investigated at such shearing stresses, one will find for the two samples different relative fluidities at the different stages of the spinning process.

Figure 4 illustrates the inversion of the flow profile, as described by

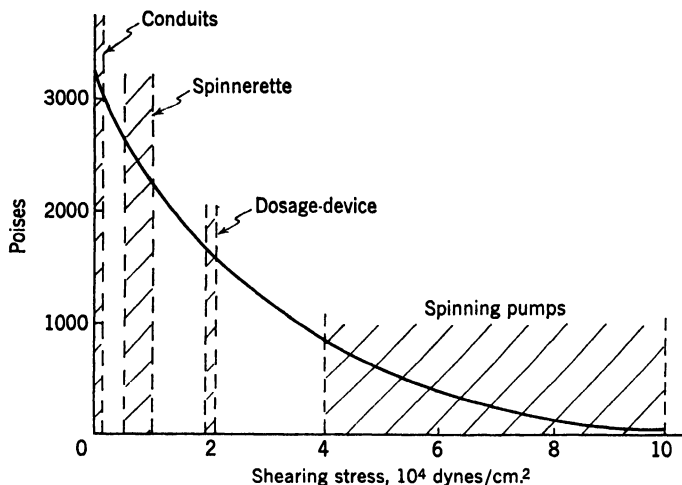


FIG. 3. Shear stresses at typical parts of the spinning machine

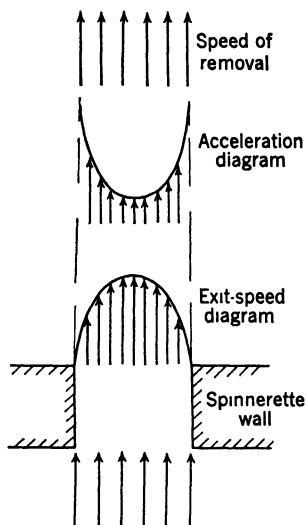


FIG. 4. Inversion of flow profile

Schramek and Zehmisch. The mechanism of this inversion is described in Section IV, 7 and therefore, the diagram should be self-explanatory.

Figure 5 shows the temperature rise obtained by the adiabatic deformation of two liquids. By stirring a sample in a Dewar vessel at constant speed and taking thermometer readings at regular intervals, one obtains rather different curves for Newtonian liquids (in this case a motor oil) and a

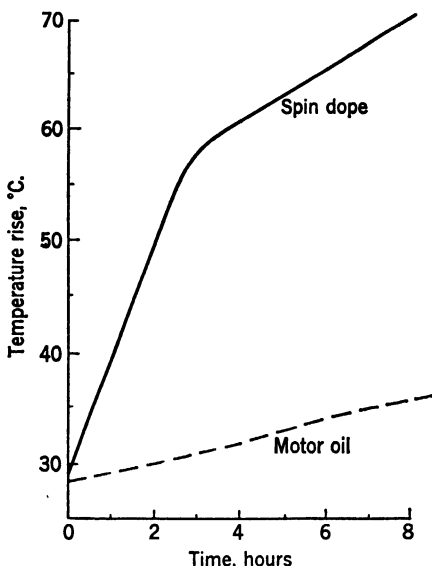


FIG. 5. Adiabatic deformation at constant speed

polymer solution (spin dope). The heat developed in the oil over a period of 8 hr. caused only a temperature rise of 7.5° C. The spin dope (polyacrylonitrile in dimethylformamide) developed within the first 3 hr. a temperature increase of 28.5° C. After that time, the simultaneously decreasing viscosity caused a somewhat reduced rate of temperature rise (in 5 hr. approximately 12.5° C.). Even this reduced rate of heat development exceeds, however, that observed on the Newtonian motor oil of comparable viscosity.

By varying the stirring speed (shearing stress) and calculating from the observed temperature rise the amount of calories developed in the system, a significant difference between Newtonian liquids and polymer solutions becomes apparent. Furthermore, by applying the obtained values to the data shown in Fig. 3, and making certain assumptions with regard to the approximate time a dope unit spends in each of the described phases, one can predict the temperature rise taking place in the spin mass during the various steps between conduits and spinnerette.

Figure 6 shows a diagram of the coagulation profile observed in ordinary solution spinning. It is not drawn to scale and merely reproduces an approximate picture of what is going on in the wet coagulation of a spin dope, without a chemical reaction taking place.

The various superimposed flow systems in the coagulating fiber structure are based on the solvent- spin bath diffusion, the telescopelike sliding of the still movable (not yet completely hardened) concentric cylinder shells

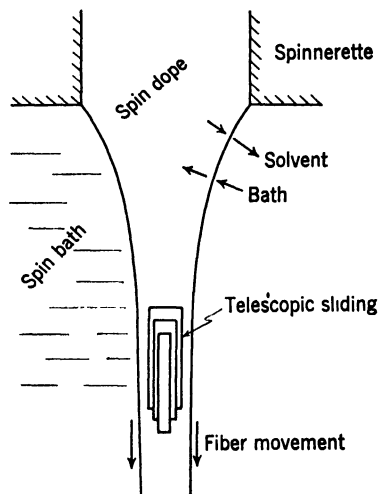


FIG. 6. Coagulation profile in solution spinning

in the structure and the over-all movement of the coagulating fiber in the bath.

The spinnerette diameter is generally below 10^{-2} cm. while the "spinning speeds" (take-up speeds of the coagulated fiber structure from the bath) vary between 10^3 and 10^4 cm./min. The friction between the moving fiber and the surrounding bath causes a considerable drag which is the main factor limiting the wet-spinning speed.

In dry spinning where the spin "bath" is in most cases air, the drag is much lower and, therefore, considerably higher spinning speeds can be realized. Also, in the radial diffusion exchange between outgoing solvent and ingoing bath, the relative amount of air and the vapor nature of the solvent being removed affect the speed of coagulation. These factors explain the fact that dry spinning speeds are 1 to 2 orders of magnitude higher than those obtained in wet spinning, and are on the order of 10^6 cm./min.

The melt-spinning process is in many respects similar to the dry-spinning process, except that there is no solvent removal. Therefore, spinning speeds as high as, or even higher than those obtained in dry spinning, can be applied.

Figure 7 shows a diagram of an onion-shaped coagulation profile as investigated by Pupke on cuprammonium spin dopes. His calculations indicate the following:

The maximum diameter is proportional to the volumetric extrusion speed, inversely proportional to the linear extrusion speed and to the spinnerette hole diameter, and independent from the removal (take-up)

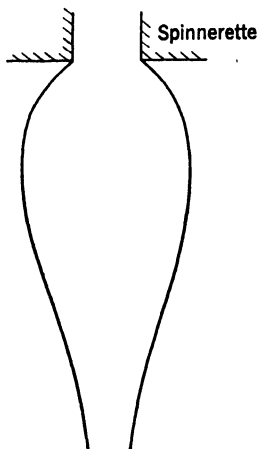


FIG. 7. An onion-shaped extrusion profile

speed. The location of the "equator" of the onion profile depends to some extent on the removal speed, however. At higher take-up speed, the diameter increase will be obtained within a shorter time than at lower speeds.

Finally, as an illustration of the fine structure inside a hardened fiber, birefringence measurements made by G. Bozza (reported in Elsaesser's paper¹⁴) on a cupra fiber of 1.2 denier are reproduced in Fig. 8. Bozza

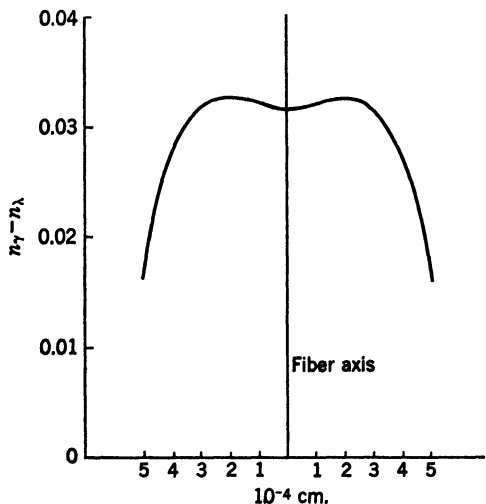


FIG. 8. Birefringence measurements on a cupra fiber of 1.2 denier. Bozza's measurements as reported by Elsaesser.

measured by a special technique the birefringence of that fiber at different distances from the fiber axis. While the shape of the reproduced birefringence distribution curve is restricted to a cupra fiber prepared under special conditions, it is obvious that such curves can be used for the study of the relationship between the flow characteristics of a spin dope—while hardening—and the physical properties of the obtained fiber.

2. ANTICIPATED DEVELOPMENTS FOR THE FUTURE

While the past decades have brought about considerable progress in the understanding of rheological factors in spinning, there are still quite a few unknown influences.

Technological advances^{26a-26e} have confirmed what textile technologists have always realized: that the rheological parameters of a spin mass have a far reaching influence on its actual performance in the spinning process. However, to a large extent, the interpretation of this relationship is mainly a descriptive one. It is possible to explain certain basic phenomena and to give reasons for their occurrence. It is at present, however, not possible to predict beforehand the exact rheological requirements for a desirable fiber-forming mechanism, e.g. by giving ranges of key characteristics.

It is not even possible at present to define the term "spinnability" in a logically unobjectionable manner. Certain restrictions are due to accessible experimental techniques: a polymer, solution, or melt might be considered "unspinnable" under ordinary conditions, as mentioned before. However, it might be found to be fiber-forming by a radical departure from established techniques, by proper adjustment of apparently unimportant or unfeasible mechanical, thermal, or colloidochemical experimental conditions, etc. An example of a development in this direction is the recently achieved technique of "emulsion spinning" as developed by the du Pont Company for the Teflon fiber (polytetrafluoroethylene). An emulsion of the polymer is extruded into a liquid medium and the formed fiberlike structure is subsequently heat sintered. This technique, yielding commercially valuable fibers, is novel in its concept and original in its engineering features.²⁶ The rheological basis of fiber formation from

²⁶ J. F. Lontz, U. S. Patent 2,718,452 (Sept. 1955); British Patents 686,438, (Jan 1953) and 689,801, (April, 1953) all assigned to E. I. Du Pont de Nemours & Co.

^{26a} J. C. Arthur and H. G. Many, *Am. Dyestuff Repr.* **41**, 385-386 (1952).

^{26b} H. Nitschmann and W. Aeschlimann, *Angew. Chem.* **65**, 261-262 (1953).

^{26c} T. Nakagawa, *Bull. Chem. Soc. Japan* **25**, 88-97 (1952); **47**, 10857 (1953).

^{26d} Theory of Extrusion. *Ind. Eng. Chem.* **45**, 969-993 (1953). Symposium comprising the following seven papers: J. F. Carley and R. A. Strub, *ibid.* p. 970; J. F. Carley, R. S. Mallouk, and J. M. McKelvey, *ibid.* p. 974; J. F. Carley and R. A. Strub, *ibid.* p. 978; J. M. McKelvey, *ibid.* 982; R. S. Mallouk and J. M. McKelvey, *ibid.* p. 987; J. F. Carley and M. M. McKelvey, *ibid.* p. 989; C. H. Jepson, *ibid.* p. 992.

^{26e} J. F. Carley, *J. Appl. Phys.* **25**, 1118-1123 (1954).

emulsions and subsequent heat-sintering are, to say the least, rather complicated and probably unexplored at present. However, the process may serve as an example of the changing picture of rheological aspects in spinning. Such and similar problems are being studied by various researchers, but final solutions are in most cases still open.

The research trends in the field, as they are taking shape at present, center on the qualitative observation and quantitative determination of those factors which offer the best chance of understanding the superimposed variables. While the rheology of spinning is primarily concerned with physical effects, it is impossible to eliminate the influence of chemical factors from our studies. Mass transfer (as in the coagulation of a solution or an emulsion) is often accompanied by chemical reactions and they contribute to a further complication of the problem.

Specifically, the interest of fundamental and industrial research is focused on the following problems, as illustrated by a cross section through some recent reports.

a. Melt Viscosity of Polymers

The rheological characteristics of polyamides, polyesters, polyolefins and other fiber-forming melts are of direct and indirect importance. Desirable melt properties will insure a technically safe spinning process. Impurities, often present in only minor amounts, and difficult to determine by analytical methods, may show up in a magnified scale by their effect on flow characteristics of the melt. Obviously, the rather high melting points of the used polymers pose a problem in the experimental performance of satisfactory viscometric methods. Such problems are discussed in the following papers and patents:

Studies on polyamide melts of nylon 6 (before and after extraction of low molecular weight fractions) and on nylon 66 of a wide m.w. range were performed by Kokhomskaya and Pakshver.²⁷

The influence of normal and elevated pressure, also of partial vacuum, on the melt viscosity of polyamides was investigated by Steffens and Sauerwald.²⁸

Imperial Chemical Industries²⁹ has patented an apparatus for the performance of continuous measurements of the melt viscosity of various thermoplastic materials.

b. Solution Viscosity

Parallel to work on the melt viscosity of melt spun polymers go solution viscosity studies. There are numerous investigations of solution viscosity having the object of determining the molecular structure, especially the

²⁷ T. N. Kokhomskaya and A. B. Pakshver, *Kolloid. Zhur.* **18**, 188-192 (1956).

²⁸ H. Steffens and F. Sauerwald, *Kolloid-Z.* **148**, 144-150 (1956).

²⁹ Imperial Chemical Industries, British Patent 755,613. (Aug. 1956)

molecular weight, of the polymer. These are outside the scope of this chapter, and only a few papers having a direct connection with spinning proper shall be mentioned below.

In a paper on the observation of the polycondensation of Perlon by measurement of melt viscosity and solution viscosity, Steffens and Sauerwald³⁰ report on data determining the viscosity changes observed during the first 13 hr. The authors note periodicity effects (including reversals) and influences of movement (stirring conditions).

Solution viscosities of nylon 66 in a number of solvents were studied by Liquori and Mele.³¹ These comparative investigations serve for determining the shape and size of the polymer molecules.

Tordella³² published a paper on fracture in the extrusion of amorphous polymers through capillaries. He observed in various polymers, including nylon 66, that a critical stress causes the stream to become irregular in shape. The effect originates in the approach to the capillary, with tearing or fracture of the molten polymer.

c. Flow Curves of Spinnable Polymers

Various fundamental studies are concerned with a better understanding of the *flow curves of spinnable polymers*. For instance, Edelmann, in a paper on the structural viscosity of solutions of polyacrylonitrile and polymerized amino caproic acid³³ explains the deviations from Newtonian flow by the combined influences of bundle structure, solvent, and shearing stress of the system. The same author³⁴ also studied the influence of shear stress, concentration, and polymerization methods on the flow characteristics of acrylic and polyamide solutions. He thus determines the heterogeneity of polymers from rheological measurements. Based on Edelmann's and other authors' work is a paper by Schurz³⁵ in which the properties of flow curves serve as basis for an understanding of the relationship between molecular weight and the location of the shear stress-velocity gradient turning point.

A paper by F. Schultz-Grunow on viscosity and the role of thermodynamics on rheology of liquids³⁶ discusses the various attempts to interpret the flow principles of non-Newtonian systems.

An increase of the apparent viscosity, due to flow inhomogeneity, is calculated in a paper on the viscosity of polymer solutions in fine capillaries by Lifson.³⁷ The author observes that the increase depends on mo-

³⁰ H. Steffens and F. Sauerwald, *Kolloid-Z.* **149**, 73-83 (1956).

³¹ A. M. Liquori and A. Mele *J. Polymer Sci.* **13**, 589-594 (1954).

³² J. P. Tordella, *J. Appl. Phys.*, **27**, 454-458 (1956).

³³ K. Edelmann, *Kautschuk u. Gummi* **5**, 120-124 (1952).

³⁴ K. Edelmann, *Faserforsch. u. Textiltech.* **6**, 269-277 (1955).

³⁵ J. Schurz, *Kolloid-Z.* **147**, 57-61 (1956).

³⁶ F. Schultz-Grunow, *Kolloid-Z.* **141**, 173-177 (1955).

³⁷ S. Lifson, *J. Polymer Sci.* **20**, 1-6 (1956).

lecular and capillary dimensions, but that it is independent from the flow rate.

An interesting attempt to convert rotational or capillary viscometric data into flow curves corresponding to an "equivalent radius" is made in a paper on the determination of non-Newtonian flow curves from viscometric data by Cram and Whitwell.³⁸ The obtained "absolute flow curves" give instrument-independent data for the shear rate - shear stress relationship.

d. Measuring Techniques

Improvements of rheological measuring techniques are numerous. There is a growing need for increased precision, wider measuring ranges, for apparatus capable of using smaller specimen sizes, etc.

A paper by Frind on limitations of error in the viscometry of high polymer solutions³⁹ discusses the accuracy limitations of visual flow time readings (1-2%). The sources of error (limitations in calibration, stop watch reliability, capillary uniformity, etc.) suggest the use of automatic recording methods.

In a probably independent study Kooy and J. J. Hermans⁴⁰ discuss the use of moving picture techniques for the exact determination of flow times. The authors obtain in this way an accuracy of 0.003 sec., while controlling the temperature within 0.001°C.

"A new consistometer for wide gradient and temperature ranges" is described by Kepes.⁴¹ The described plate-cone viscometer can be used over a temperature range from -70 to +350°C., for small size specimens (1-4 cc.), over a range from 0.01 to 10⁸ poises. The gradient may be varied between 10⁻³ and 10⁺³ sec.⁻¹.

Another attempt to reduce the specimen size was made by Hart.⁴² The author describes a "semimicro dilution viscometer" permitting measurements on 1 cc. of a solution.

e. New Instruments

Of new instruments to determine rheological characteristics should be mentioned the following: "the Caplastometer: a new melt viscometer" by Karam and co-workers,⁴³ an "apparatus capable of use for the study of rheological phenomena," which makes goniometric measurements of flow and pressure distribution of a material,⁴⁴ "automatic and continuously re-

³⁸ K. H. Cram and J. C. Whitwell, *J. Appl. Phys.* **26**, 613-618 (1955).

³⁹ H. Frind, *Faserforsch. u. Textiltech.* **6**, 25-28 (1955).

⁴⁰ J. Kooy and J. J. Hermans, *J. Polymer Sci.* **16**, 417-427 (1955).

⁴¹ M. Kepes, *J. Polymer Sci.* **22**, 409-422 (1956).

⁴² V. E. Hart, *J. Polymer Sci.* **17**, 207-214 (1955).

⁴³ H. J. Karam, K. J. V. *Modern Plastics* **32**, No. 7, 129-134 (1955).

⁴⁴ J. E. Roberts and K. Weissenberg, U. S. Patent 2,752,778.

coding viscosimeters''⁴⁵ which permit indication of the viscosity of a fluid flowing through a line by a variety of thermal and flow variations.

Thus, a variety of theoretical and experimental approaches are being used by physicists, chemists and engineers. The obtained results reflect the common aim: to explain the rheological phenomena involved in spinning and thereby to show the way to technological improvements. The last 30 years have yielded impressive research results but the picture is still obscured in some respects. However, it may be expected that the knowledge of the fundamentals of spinning will keep pace with the development of new fiber types and novel spinning methods.

Nomenclature

$RP/2L$	Shearing stress	L	Capillary length
R	Capillary radius	Q/R^3	Speed gradient
P	Hydrostatic pressure	Q	Flow volume per time unit

⁴⁵ J. M. Jones, Jr., U. S. Patent 2,791,902, assigned to Texas Company.

CHAPTER 16

THEORY OF SCREW EXTRUDERS

W. L. Gore and James M. McKelvey

I. Introduction...	589
1. Pressure Flow	592
2. Drag Flow	592
3. Velocity Distributions	595
4. Power.	596
II. Flow and Power Formulas	599
1. The Flow Formula	600
2. The Power Formula	602
III. Operating Equations for Melt Extrusion	602
1. Isothermal Operation	603
2. Scale-up Rules for Isothermal Operation	606
3. Experimental Results	608
4. Adiabatic Operation	611
5. Scale-up Rules for Adiabatic Operation	616
IV. Extrusion of Non-Newtonian Melts	617
1. Flow Behavior	617
2. Power Consumption	622
V. Plasticating Extrusion	623
1. Metering Zone	627
2. Feed Zone	627
3. Transition Zone	628
4. Torpedo and Screens	629
5. Scale-up of Plasticating Extruders	629
Nomenclature	631

I. Introduction

The use of screw extruders for the fabrication of thermoplastics has increased enormously in the past decade. Today, extruders produce coated wire for electrical uses, plastic pipe for domestic water and for chemical plants, garden hose, packaging film, and many other products. The design and operation of extruders is something of an art and most new developments have evolved by trial-and-error procedures. However, through the application of viscous flow theory, at least part of the process can be described by approximate mathematical relationships and it has been demonstrated that the extrusion theory, when combined with practical experience, is an extremely useful tool.

In the extrusion of thermoplastics the material is usually fed to the extruder in the form of pellets, flakes, or granules. As the screw conveys the material forward, it is heated by a combination of transferred and frictionally generated heat and becomes a highly viscous liquid about halfway down the screw. The action of the screw on the liquid material generates the pressure required to force it through the extruder die, which shapes the molten material into the desired form. As the material leaves the die, it is solidified by quenching with air or water. An extruder which is operated in this manner, that is, fed solid material, is called a *plasticating extruder*.

Extruders also find many applications in which they are used as pumps for the transportation of viscous liquids, such as lubricating oils, polymer melts, or viscous solutions of any kind. In this application the extruder is not required to melt the material and the entire length of the screw acts on a fluid. Such an extruder is called a *melt extruder*.

The present analysis of extruders applies only to fluids. Therefore, the analysis completely describes melt extrusion but only about half of plasticating extrusion. For a complete description of plasticating extrusion, studies must be made of solids transport and the energy relations at the feed end of the extruder.

The most widely used extruders, by far, are the single screw machines. However, multiple screw extruders are also occasionally used in the plastics industry. Multiple screw extruders are of two types: those in which the screw flights intermesh; and those in which the screw flights do not intermesh, but do share a common housing or casing. If the leakage through the clearances is neglected, the intermeshing-flight type is a positive displacement pump and is not treated here. The other type operates on principles similar to the single screw machines.

Figure 1 is a schematic diagram showing the dimensions which establish the geometry of an extruder screw. In order to make the treatment as general as possible, a multiple-flight screw having two parallel channels is

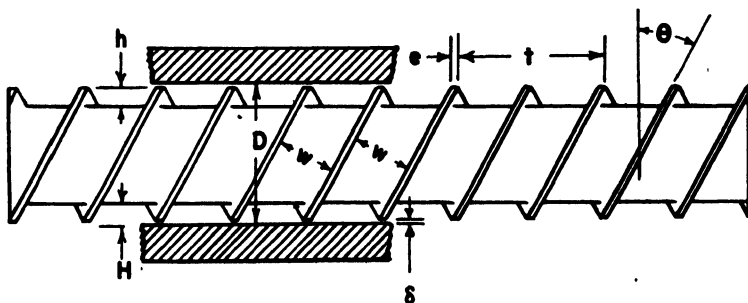


FIG. 1. Geometry of the multiple-flight ($n = 2$) extruder screw

shown. The inside diameter of the barrel is represented by D , while h represents the distance from the root of the screw to the top of the screw flight. The radial clearance between the top of the screw flight and the barrel surface is δ . The pitch of the screw, t , is related to the helix angle by the equation

$$t = \pi(D - 2\delta) \tan \theta \quad (1)$$

where θ is the helix angle measured at the top of the screw flight.

The width of a channel, normal to the helical axis, is w , and for a screw having n flights in parallel the following relation can be deduced:

$$nw = (t - ne) \cos \theta \quad (2)$$

where e is the width of the flight normal to the screw axis.

Extruders can be operated either by rotating the screw and holding the barrel stationary, or by rotating the barrel in the opposite direction and holding the screw stationary. In either case the relative motion is the same and the same operating characteristics are obtained. Since it is easier to build machines in which the screw is driven, this is the usual mode of operation. However, in order to avoid having a moving coordinate system in the derivation of the extruder equations, it is assumed that the barrel is driven and the screw stationary. The equations derived for this case apply equally well to the other mode of operation.

In the derivation of the extruder equations it is assumed that h is small in comparison to D . The root surface of the screw and the barrel surface can then be considered to be parallel plates and the problem is greatly simplified. This parallel plate representation is shown in Fig. 2 along with the three coordinate axes used in the derivations.

The upper plate in Fig. 2 represents the barrel. It moves over the screw channel with velocity W . The magnitude of W is πDN and it is so directed that it makes the angle θ with the screw flight. In the following derivations

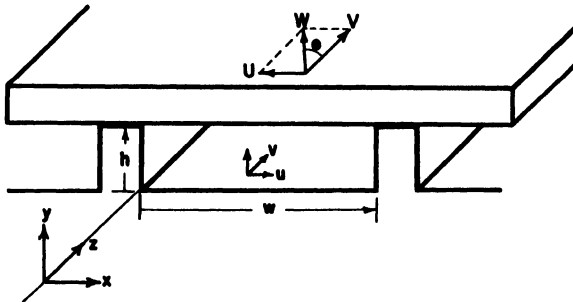


FIG. 2. Parallel plate representation of an extruder screw channel

it is more convenient to work with the U and V components of W . As shown in Fig. 2, V acts parallel to the z axis and U parallel to the x axis. These components can be expressed in terms of the frequency of rotation by the equations

$$V = \pi DN \cos \theta \quad (3)$$

$$U = \pi DN \sin \theta \quad (4)$$

The fluid velocity vector at any point in the screw channel is resolved into components acting in the x , y , and z directions. Although a fluid particle describes a very complex motion in the screw channel, it is only the v component, which acts in the z direction, that is responsible for the advance of the fluid down the screw channel. The other two components, both acting in a plane normal to the z axis, cause a circulatory motion which is important for heat transfer and mixing but contribute nothing to the pumping capacity of the screw. Therefore, in analyzing the pumping capacity of an extruder, it is necessary to consider only the v component of the fluid velocity.

Along the z axis there are two types of flow to be considered. If there is no pressure gradient in the z direction, the v component is due only to the drag effect of the barrel surface. This flow is called the *drag flow*. It always acts in the $+z$ direction, when the convention is adopted that z increases in the direction toward the die of the extruder.

If there is a restriction at the end of the channel (for example, an extrusion die), a positive pressure gradient will be established. This will cause some of the fluid to flow in the $-z$ direction. This flow is called the *pressure flow*. It always occurs in a direction opposite to the pressure gradient.

The analysis of drag flow, pressure flow, and power in this section is based on isothermal, Newtonian flow of an incompressible fluid in a rectangular channel having width w and height h . It is assumed that δ is very small in comparison to h and can be neglected. It is further assumed that the flow is steady and that acceleration can be neglected. Under these conditions the Navier-Stokes equations¹ assume a particularly simple form and solutions are readily obtained. Reference should be made to the papers of Rowell and Finlayson,² Strub,³ and Pigott,⁴ for solutions similar to those presented here.

¹ V. L. Streeter, "Fluid Dynamics." McGraw-Hill, New York, 1948.

² H. S. Rowell and D. Finlayson, *Engineering* **114**, 606 (1922); **126**, 249, 385 (1928).

³ R. A. Strub, Proc. 2nd Midwestern Conf. on Fluid Mechanics, p. 481-494 Ohio State University, Columbus, Ohio, 1952.

⁴ W. T. Pigott, *Trans. Am. Soc. Mech. Engrs.* **73**, 947 (1951).

1. PRESSURE FLOW

Under the conditions mentioned above, the differential equation describing the velocity distribution in the screw channel is written

$$(\partial^2 v / \partial x^2) + (\partial^2 v / \partial y^2) = (1/\mu) (dP/dz) \quad (5)$$

where μ is the viscosity and (dP/dz) the pressure gradient.

The boundary conditions for pressure flow are

$$\begin{aligned} v(x, 0) &= 0 \\ v(x, w) &= 0 \\ v(0, y) &= 0 \\ v(h, y) &= 0 \end{aligned} \quad (6)$$

and a solution of (5) satisfying boundary conditions (6) is

$$\begin{aligned} v = \frac{1}{\mu} \left(\frac{dP}{dz} \right) & \left[\frac{y^2}{2} - \frac{hy}{2} \right. \\ & \left. + \frac{4h^2}{\pi^3} \sum_{g=1,3,\dots}^{\infty} \left(\frac{1}{g^3} \right) \frac{\cosh [g\pi(2x-w)/2h]}{\cosh [g\pi K/2]} \sin \left(\frac{g\pi y}{h} \right) \right] \end{aligned} \quad (7)$$

where $K = (w/h)$. The volumetric pressure flow rate is obtained by integrating (7) over the cross sectional area of the screw channel.

$$Q_P = -(wh^3/12\mu) (dP/dz) F_P \quad (8)$$

where

$$F_P = 1 - (192/\pi^5 K) \sum_{g=1,3,\dots}^{\infty} 1/g^5 \tanh (g\pi K/2)$$

F_P , which depends only on K , is the shape factor for pressure flow. Values of F_P for various values of K are plotted in Fig. 3.

2. DRAG FLOW

The differential equation for drag flow velocity is similar to (5) except that the pressure gradient along the screw channel is zero.

$$(\partial^2 v / \partial x^2) + (\partial^2 v / \partial y^2) = 0 \quad (9)$$

The boundary conditions for drag flow are

$$\begin{aligned} v(x, 0) &= 0 & v(0, y) &= 0 \\ v(x, w) &= V & v(h, y) &= 0 \end{aligned} \quad (10)$$

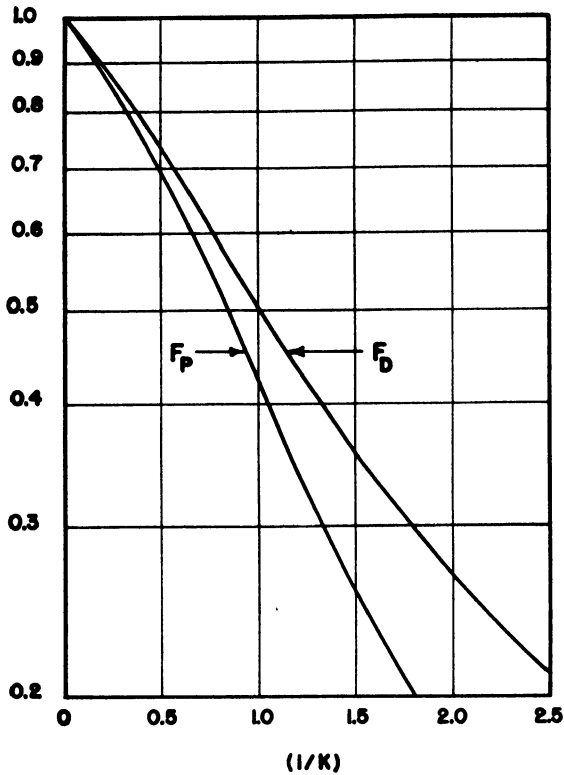


FIG. 3. Shape factors for drag and pressure flow

A solution of (9) satisfying boundary conditions (10) is

$$v = (4V/\pi) \sum_{g=1,3,\dots(1/g)}^{\infty} \frac{\sinh(g\pi y/w)}{\sinh(g\pi/K)} \sin(g\pi x/w) \quad (11)$$

The volumetric drag flow rate is found by integrating (11) over the cross sectional area of the channel.

$$Q_D = (wVh/2) F_D \quad (12)$$

where

$$F_D = (16K/\pi^3) \sum_{g=1,3,\dots}^{\infty} 1/g^3 \tanh(g\pi/2K)$$

F_D depends only on K and is the shape factor for drag flow. Values of F_D for various values of K are also plotted in Fig. 3.

3. VELOCITY DISTRIBUTIONS

It is interesting to examine the flow patterns within the screw channel. The cases of open and closed discharge will be considered. When there is no pressure gradient in the channel open discharge results. The flow is pure drag flow.

Relative velocities (v/V) have been calculated with (11) for three different values of K . Figure 4 shows lines of constant relative velocity for each K .

If the end of the channel is blocked there can be no discharge from the

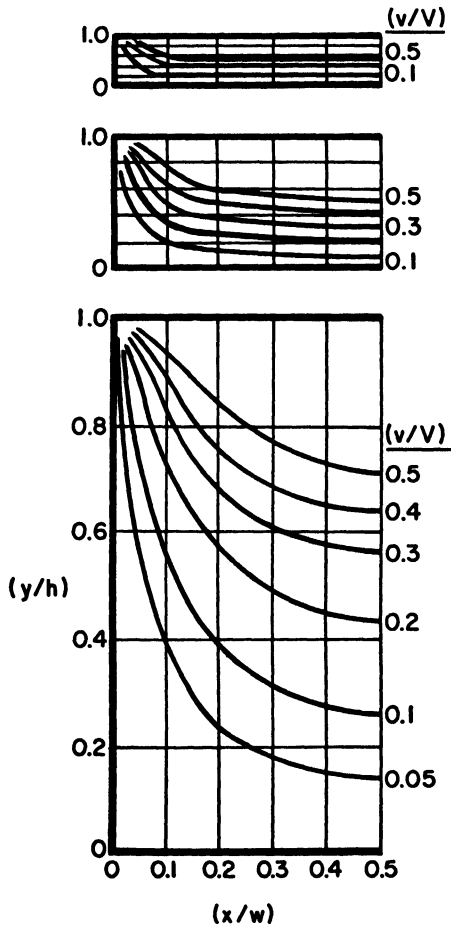


FIG. 4. Lines of constant relative velocity at open discharge. Key: top, $K = 10$; middle, $K = 4$; bottom, $K = 1$.

screw and maximum pressure is developed. Under this condition (neglecting leakage) the forward drag flow is just balanced by the reverse pressure flow and

$$Q_D + Q_P = 0 \quad (13)$$

Substituting (8) and (12) into (13),

$$(dP/dz) = (6V\mu/h^2) (F_D/F_P) \quad (14)$$

By combining (14) and (7) the relative pressure flow velocities for closed discharge are obtained. The resultant closed discharge velocity is obtained by adding the drag and pressure velocities.

$$\begin{aligned} \frac{v}{V} = \frac{4}{\pi} \sum_{g=1,3,\dots}^{\infty} \left(\frac{1}{g} \right) \frac{\sinh(g\pi y/w)}{\sinh(g\pi/K)} \sin(g\pi x/w) + \frac{F_D}{F_P} \left\{ \frac{3y}{h^2} (y-h) \right. \\ \left. + \left(\frac{24}{\pi^3} \right) \sum_{g=1,3,\dots}^{\infty} \left(\frac{1}{g^3} \right) \frac{\cosh[g\pi(2x-w)/2h]}{\cosh[g\pi K/2]} \sin(g\pi y/h) \right\} \end{aligned} \quad (15)$$

Figure 5 shows a typical closed discharge velocity pattern.

4. POWER

Let dZ_s represent the power dissipated in an incremental length dz of the channel. A portion of this power causes the motion of the fluid down the screw channel, while the remainder causes the circulatory motion normal to the channel axis. Let τ_z be the shear stress, *at the barrel surface*, acting in the z direction and let τ_x be the shear stress, *at the barrel surface*, acting in the x direction. The total power dissipated in the screw channel is given by the equation

$$dZ_s = V dz \int_0^w \tau_z dx + U dz \int_0^w \tau_x dx \quad (16)$$

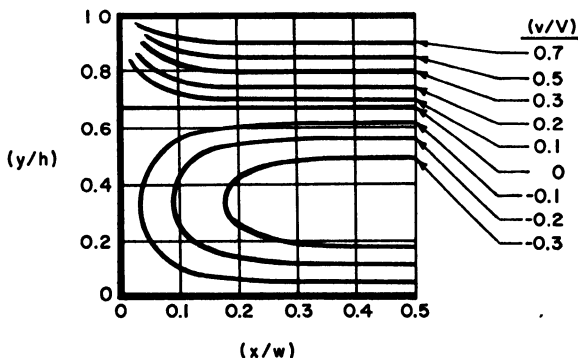


FIG. 5. Lines of constant relative velocity at closed discharge

The shear stresses at the barrel surface are related to the shear rates at the barrel surface by Newton's law.

$$\tau_z = \mu(\partial v/\partial y)_{y=h} \quad (17)$$

$$\tau_z = \mu(\partial u/\partial y)_{y=h} \quad (18)$$

where u is the component of the fluid velocity vector that acts in the x direction.

Combining (16), (17), and (18), the power formula becomes

$$dZ_s = \mu V dz \int_0^w (\partial v/\partial y)_{y=h} dx + \mu U dz \int_0^w (\partial u/\partial y)_{y=h} dx \quad (19)$$

Considering the v component, the shear rate at the barrel surface is obtained by adding the drag velocity (equation 11) to the pressure velocity (equation 7), differentiating with respect to y , and then placing y equal to h .

$$\left(\frac{\partial v}{\partial y}\right)_{y=h} = \left[\left(\frac{4V}{w}\right) \sum_{g=1,3,\dots}^{\infty} \coth\left(\frac{g\pi}{K}\right) \sin\left(\frac{g\pi x}{w}\right)\right] \\ + \frac{1}{\mu} \left(\frac{dP}{dz}\right) \left\{\frac{h}{2} - \frac{4h}{\pi^2} \sum_{g=1,3,\dots}^{\infty} \left(\frac{1}{g^2}\right) \frac{\cosh [g\pi(2x-w)/2h]}{\cosh [g\pi K/2]}\right\} \quad (20)$$

The first term of (19) can now be evaluated.

$$dZ_s = (\mu V^2 w/h) dz F_z + (wVh/2) dPF_D + \mu U dz \int_0^w (\partial u/\partial y)_{y=h} dx \quad (21)$$

where

$$F_z = \left(\frac{10}{\pi K}\right) \sum_{g=1,3,\dots}^{\infty} \frac{(-1)^{g+1}}{(2g-1)} \coth \frac{\pi(2g-1)}{K} \sin \frac{4\pi(2g-1)}{10}$$

F_z is the shape factor for power and is a function of K only. Values of F_z , as calculated by Strub,³ are shown in Fig. 6. For values of K less than unity the shape factor is approximately equal to $(3/K)$.

In the above derivation a divergent series is obtained if the integration indicated by (19) is carried out between the limits of 0 and w . The convergent series represented by (21) is obtained by integrating between the limits of $(0.1w)$ and $(0.9w)$ and then multiplying the result by $(1/0.8)$.

The third term of (21), arising from the circulatory flow, must now be evaluated. This flow has velocity components in both the x and y directions and it would be extremely difficult to obtain a solution of the Navier-Stokes equations. An approximation is obtained by considering only the u component and neglecting acceleration. Under these conditions the differential equation for motion is

$$(d^2u/dy^2) = (1/\mu)(dP/dx) \quad (22)$$

The boundary conditions are

$$u(0) = 0 \quad u(h) = U \quad (23)$$

The solution of (22) for the boundary conditions (23) is

$$u = (Uy/h) + (1/2\mu)(dP/dx)(y^2 - hy) \quad (24)$$

Considering unit length of the channel, the net volumetric flow rate in the x direction is obtained by integrating over the depth of the channel.

$$\int_0^h u \, dy = (Uh/2) - (h^3/12\mu)(dP/dx) \quad (25)$$

Since the flow amounts to a circulatory motion its net value is zero and the pressure gradient in the x direction can be obtained directly from (25).

$$(dP/dx) = (6U\mu/h^2) \quad (26)$$

The shear rate at the barrel surface is obtained by substituting (26) into (24), differentiating with respect to y , and then setting y equal to h .

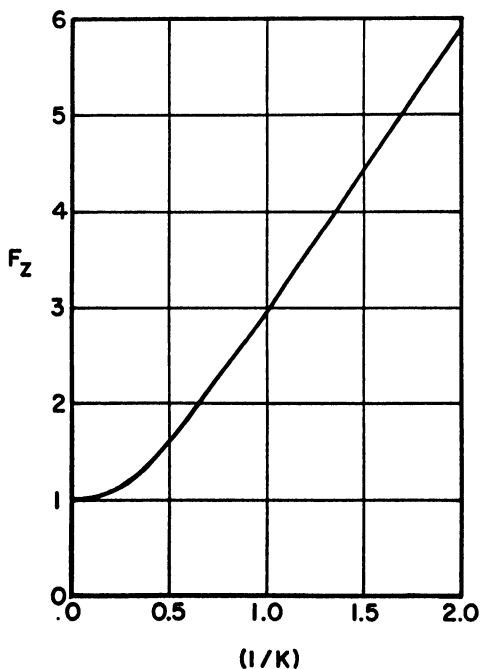


FIG. 6. Shape factor for power

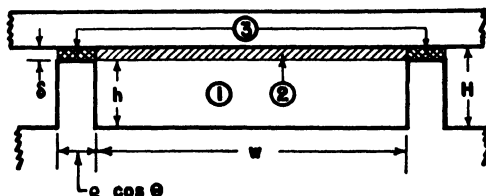


FIG. 7. Cross section of a screw channel

$$(\partial u / \partial y)_{y=h} = (4U/h) \quad (27)$$

After evaluating the third term of (21), the power formula becomes

$$dZ_s = (\mu V^2 w/h) dz F_z + (wVh/2) dPF_D + (4\mu U^2 w/h) dz \quad (28)$$

In view of (3), (4), and (12), the power formula can be written

$$dZ_s = (\mu W^2 w/h)(F_z \cos^2 \theta + 4 \sin^2 \theta) dz + Q_D dP \quad (29)$$

It should be noted that (29) differs from the previously published power formula.⁶ In the previous formula the calculation of the power for the circulatory flow was in error.⁶

II. Flow and Power Formulas

In the preceeding section an analysis of drag flow, pressure flow, and power in a rectangular channel was made. A somewhat similar analysis is made in this section, except that it is based on a one-dimensional velocity distribution. This leads to simple expressions for flow and power which are useful for the design and analysis of many extruder screws. In addition, the restriction of zero radial clearance, which applies to the previous equations, is removed. The derivations are similar to those presented by Carley *et al.*⁷

It should be noted that the simplified flow and power equations are applicable only when the width-to-depth ratio of the screw channel is large, say, $K \geq 10$. Since the most efficient screw designs for thermoplastics usually have a K greater than 10, the formulas are useful for a wide variety of screws.

Figure 7 shows a cross section of the screw channel normal to the z axis. As before, h represents the distance from the root of the screw to the top of the screw flight, w the width of the channel, and δ the radial clearance. The distance from the root of the screw to the barrel surface is H .

⁶ R. S. Mallouk and J. M. McKelvey, *Ind. Eng. Chem.* **45**, 983 (1953).

⁶ It has been brought to the attention of the authors that this error was discovered and the correct formula derived, independently, by R. S. Mallouk and W. D. Mohr of E. I. du Pont de Nemours and Company.

⁷ J. F. Carley, R. S. Mallouk, and J. M. McKelvey, *Ind. Eng. Chem.* **45**, 974 (1953).

1. THE FLOW FORMULA

The differential equation for the one-dimensional velocity distribution in drag flow is obtained directly from (9).

$$(d^2v/dy^2) = 0 \quad (30)$$

The boundary conditions for drag flow velocity are

$$v(0) = 0 \quad v(H) = V \quad (31)$$

The solution of (30) for the boundary conditions (31) is

$$v = (Vy)/(H) \quad (32)$$

In calculating the volumetric drag flow rate it is assumed that drag flow occurs only within the actual boundaries of the screw channel (region 1 in Fig. 7).

$$Q_D = nw \int_0^{H-\delta} (Vy/H) dy = n(wVH/2)(1 - \delta/H)^2 \quad (33)$$

for n channels in parallel.

By combining (2), (3), and (33) the drag flow formula can be written

$$Q_D = \alpha N \quad (34)$$

where

$$\alpha = (\pi DH/2)(t - ne)(1 - \delta/H)^2 \cos^2 \theta \quad (35)$$

α is called the drag flow constant. It depends only on the dimensions of the screw and is independent of the operating conditions.

The differential equation for the one-dimensional velocity distribution in pressure flow is obtained directly from (5).

$$(d^2v/dy^2) = (1/\mu)(dP/dz) \quad (36)$$

The boundary conditions for pressure flow velocity are

$$v(0) = 0 \quad v(H) = 0 \quad (37)$$

The solution of (36) satisfying boundary conditions (37) is

$$v = (1/\mu)(dP/dz)(y^2 - Hy) \quad (38)$$

It is assumed that the pressure flow occurs in the space bounded by the root of the screw, the barrel surface, and the walls of the channel extended to the barrel surface (regions 1 and 2 in Fig. 7).

$$Q_P = nw \int_0^H v dy = -(nwH^3/12\mu)(dP/dz) \quad (39)$$

By combining (2) and (39), the volumetric pressure flow formula can be written

$$Q_P = -(\beta/\mu)(dP/dz) \quad (40)$$

where

$$\beta = (t - ne)(H^3/12) \cos \theta \quad (41)$$

β is called the pressure flow constant. It depends only on the dimensions of the screw and is independent of the operating conditions.

In practice, the pumping capacity of a screw will be less than the sum of the drag and pressure flow rates. This difference is attributed to the "leakage" through the annular space between the top of the screw flight and the barrel surface (region 3 in Fig. 7).

The leakage flow interacts with the drag and pressure flows in a very complicated manner and an exact analysis of it has not been made. However, the leakage flow is usually a small fraction of the pressure flow, so that an approximate expression for leakage can be used with little error.

The leakage flow formula is derived by assuming that the space through which the flow occurs can be approximated by a rectangular slit having width πD and height δ . The length of the slit depends upon the total number of turns that the screw flight makes around the root of the screw and upon the width of the flight. It is given by the formula

$$\text{Equivalent length of slit} = (nel \cos^2 \theta / \pi D) \quad (42)$$

where l is the helical length of the screw channel.

Assuming that the dimensions of the screw are constant over the entire length, that the viscosity is constant, and that the pressure gradient is a constant, the flow rate through the slit is given by the formula

$$Q_L = - \frac{\pi^2 D^2 \delta^3 \Delta P}{12(\mu nel \cos^2 \theta)} \quad (43)$$

where

$$\begin{aligned} \Delta P &= P_d - P_f \\ P_d &= \text{pressure at die} \\ P_f &= \text{pressure at feed port} \end{aligned}$$

To make the form of the leakage flow formula similar to the form of the pressure flow formula, (43) is written

$$Q_L = -(\gamma/\mu) (dP/dz) \quad (44)$$

where

$$\gamma = \frac{\pi^2 D^2 \delta^3}{12ne \cos^2 \theta} \quad (45)$$

To summarize, the extruder flow formula is written

$$Q = Q_D + Q_F + Q_L \quad (46)$$

where Q is the pumping capacity of the screw and Q_D , Q_F , and Q_L are defined by (34), (40), and (44), respectively.

2. THE POWER FORMULA

The simplified power formula is derived using (19) as the basis of the calculation. The shear rate at the barrel surface is found by adding the drag and pressure velocities (equations 32 and 38), differentiating with respect to y , and then setting y equal to H .

$$(dv/dy)_{y=H} = (V/H) + (H/2\mu) (dP/dz) \quad (47)$$

Substituting (47) into (19) and performing the indicated integration

$$dZ_s = (\mu W^2 w/H) (1 + 3 \sin^2 \theta) dz + Q_D dP \quad (48)$$

where the third term of (19) is treated in the same manner as before.

The power dissipated in the radial clearance is calculated under the assumption that the shear rate in the clearance is constant and equal to W/δ . The clearance power is given by the equation

$$dZ_c = [(\mu W^2 ne \cos \theta)/\delta] dz \quad (49)$$

The total power, obtained by adding the channel power to the clearance power, is

$$dZ = \mu W^2 [(w/H) (1 + 3 \sin^2 \theta) + (ne/\delta) \cos \theta] + Q_D dP \quad (50)$$

which can be written

$$dZ = \epsilon \mu N^2 dz + \alpha N dP \quad (51)$$

where

$$\epsilon = \pi^2 D^2 \cos \theta [(t - ne) (1 + 3 \sin^2 \theta)/H + ne/\delta] \quad (52)$$

ϵ is the power constant and is independent of all operating conditions.

III. Operating Equations for Melt Extruders

In the previous section differential equations were derived which describe the flow at a given position along the screw channel. To describe the

over-all performance of an extruder, integrated equations relating output, pressure, temperature, and power to the operating conditions and the machine design are needed. Approximate equations can be obtained for certain special cases, for example, when the channel dimensions vary along the screw, or when the fluid viscosity varies or does not vary along the length of the screw.

In this section some of these special cases are considered. First, the case of isothermal operation, in which the viscosity of the fluid is constant throughout the channel, is discussed. Then, the case of adiabatic operation is discussed. While it is recognized that these are somewhat idealized concepts, the equations have proved extremely useful as a guide in analyzing extrusion operations and in the design of extrusion equipment.

1. ISOTHERMAL OPERATION

Extruder operation is called isothermal if the fluid is maintained at constant temperature throughout the channel of the screw. Since the pumping efficiency of any extruder is always less than 100 %, heat must be continually removed if the temperature is to be maintained constant. In practice, this is not possible or even desirable. However, in some applications the operation may be nearly isothermal, particularly when extruders are operated at low speeds. For these cases of near isothermal operation the isothermal operating equations serve as a very useful guide.

The case where the dimensions of the screw channel are constant is considered first. With a constant screw channel and isothermal operation, the pressure gradient must be constant. Consequently,

$$(dP/dz) = (\Delta P/l) \quad (53)$$

and the flow equation can be written

$$Q = \alpha N - (\beta + \gamma)/(\mu) (\Delta P/l) \quad (54)$$

Equation 54 shows that a plot of Q versus ΔP will be a straight line having a negative slope. This line is called a screw characteristic. For a given fluid and screw, each operating speed gives rise to a different characteristic. The characteristics are parallel and separated by a distance that is directly proportional to the screw speed.

So far only the flow behavior of the fluid in the screw channel has been considered. The performance of the extruder as a whole, however, depends on both the flow through the screw and the flow through the die. The flow rate of Newtonian fluids through a die of any shape is directly proportional to the pressure drop and inversely proportional to the viscosity of the fluid, as shown by the equation

$$Q = (k/\mu) (P_d - P_a) = (k/\mu) \Delta P_d \quad (55)$$

where k depends only on the geometry of the die and can be calculated for certain simple shapes.

The die equation shows that if the pressure drop across the die is plotted against flow rate, the result will be a straight line passing through the origin. This line is called the die characteristic.

In most cases the pressure of the feed, P_f , and the discharge pressure of the die, P_a , are the same, since the feed is usually under atmospheric pressure and the die usually discharges to the atmosphere. In this case ΔP and ΔP_d are identical and the operating point of the extruder can be found by solving the die and screw equations simultaneously.

$$\Delta P = (\alpha\mu N)[(l)/(kl + \beta + \gamma)] \quad (56)$$

$$Q = (\alpha N)[(kl)/(kl + \beta + \gamma)] \quad (57)$$

Equation 57 shows that the output of an isothermal extruder with a uniform screw is directly proportional to the speed of rotation of the screw and is independent of the viscosity of the fluid. Equation 56 shows that the pressure developed by the machine is directly proportional to both the screw speed and the viscosity of the fluid.

The extruder operating point can also be found graphically. Figure 8 shows a plot of the characteristics of a given screw, for different operating speeds. A die characteristic is also shown. The intersection of a screw characteristic with the die characteristic gives the extruder operating point for that particular speed.

The total power required to operate the extruder is calculated from (51).

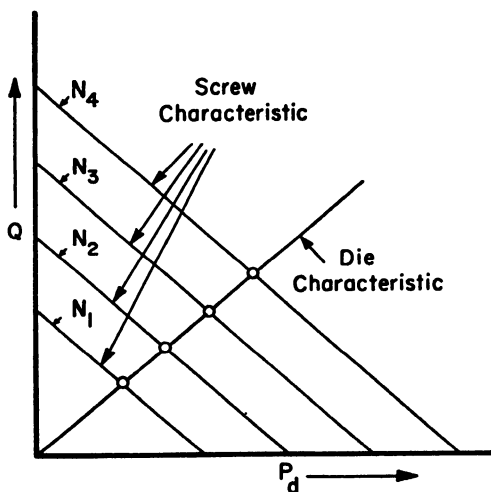


FIG. 8. Isothermal operating characteristics of a given screw for different speeds

Integrating (51) over the length of the screw gives

$$Z = \epsilon \mu N^2 l + \alpha N \Delta P \quad (58)$$

A more general case, that in which the dimensions of the screw channel are a function of position along the screw, will now be considered. It is necessary, in the derivation, to make several simplifying assumptions. It is assumed that e is small in comparison to t and can be neglected and that δ is so small that the leakage term need not be considered. Since the pitch is related to the helix angle by the equation

$$t = \pi D \tan \theta \quad (59)$$

the flow equation can be written

$$Q = \frac{1}{2} \pi^2 D^2 N H \sin \theta \cos \theta - (\pi D H^3 / 12 \mu) (dP/dz) \sin \theta \quad (60)$$

the net flow is constant at all positions along the screw and (60) can be integrated to obtain the total rise in pressure.

$$\Delta P = \int_{P_f}^{P_d} dP = \int_0^l \left[\frac{6\pi D N \cos \theta}{H^2} - \frac{12Q}{DH^3 \sin \theta} \right] dz \quad (61)$$

Assuming that the die discharge pressure and the feed pressure are the same, the flow rate can be determined by combining (61) and (55).

$$Q = \frac{6\pi D N \int_0^l (\cos \theta / H^2) dz}{(1/k) + (12/\pi D) \int_0^l (1/H^3 \sin \theta) dz} \quad (62)$$

Many screws are designed so that the functional relationship between H and z and θ and z is different in different sections. For example, a screw might have a tapered section and then a section of constant root diameter. The generalized form of (62), for a screw of m sections, is

$$Q = \frac{6\pi D N \sum_{i=1}^m \int_0^{l_i} \cos \theta_i / H_i^2 dz}{(1/k) + (12/\pi D) \sum_{i=1}^m \int_0^{l_i} (1/H_i^3 \sin \theta_i) dz} \quad (63)$$

In each section z is taken as a continuous variable and the l_i 's are the helical lengths of the various sections.

It should be noted that with screws of variable channel dimensions, as with constant channel dimensions, the discharge rate is independent of the fluid viscosity.

A common type of screw is one in which the pitch is constant but the channel decreases in depth in a uniform manner in a rear section and then

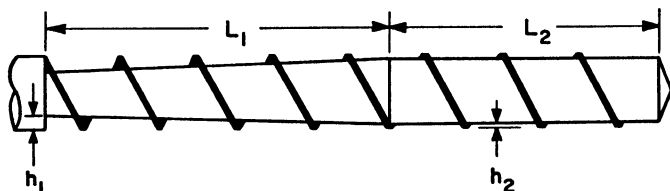


FIG. 9. Extruder screw with compression section

remains constant in a forward section. Figure 9 is a diagram of a screw of this type. In the forward section H and θ are both independent of z , while in the rear section H is a linear function of z . The following formula is obtained by introducing these functions into (63) and then making the necessary integrations and summations.

$$Q = \frac{[(6\pi DN \cos \theta)/H_2][l_2/H_2 + l_1/H_1]}{(1/k) + [12/(DH_2^2 \sin \theta)][l_2/H_2 + (l_1/H_1)(H_1 + H_2)/2H_1]} \quad (64)$$

The effect of using compression ratios in screws is shown by the consideration of an extruder in which the die opening is so large that essentially there is no backward pressure flow. In this case k is quite large and $(1/k)$ drops out. Calculation of the delivery reveals that it is larger than that of a screw with a constant channel depth along the entire length of the screw. For example, if l_1 equals l_2 and H_1 is twice H_2 , then the discharge rate will be 9.1% greater than that of a screw having a constant channel depth. The increased rate is due to pressure being developed in the rear section of the screw and causing a *forward* pressure flow which increases the discharge rate.

2. SCALE-UP RULES FOR ISOTHERMAL OPERATION

The following scale-up rules are derived for any isothermal melt extruder and are not limited to screws of constant cross section. It is assumed that the die discharges at a pressure equal to the feed pressure. The flow equation is written

$$Q = \alpha N - (\beta + \gamma) (1/\mu) (dP/dz) \quad (65)$$

and it follows that

$$\Delta P = \int_0^l (\alpha \mu N) (1/\beta + \gamma) dz - \int_0^l (\mu Q / \beta + \gamma) dz \quad (66)$$

Combining the die flow equation with (66),

$$\Delta P = \frac{\mu N \int_0^l (\alpha / \beta + \gamma) dz}{1 + k \int_0^l (1/\beta + \gamma) dz} \quad (67)$$

Consider now a pair of extruders, one a geometrically similar model of the other. All of the dimensions of the larger are X times those of the smaller, including the die. The two extruders are operated at the same speed and pump the same fluid. Referring back to the definitions of α , β , γ , ϵ , and k , the following relationships can be established.

$$X^2 = (\epsilon_2/\epsilon_1)$$

$$X^3 = (k_2/k_1) = (\alpha_2/\alpha_1)$$

$$X^4 = (\beta_2/\beta_1) = (\gamma_2/\gamma_1)$$

The subscripts 1 and 2 refer to the small and large extruders, respectively.

It will now be shown that the pressure developed by the small extruder is the same as the pressure developed by the large extruder, i.e., the value of equation (67) is the same for both extruders. Consider first the numerator of equation (67). Let $f(z)$ represent $(\alpha_1)/(\beta_1 + \gamma_1)$ and $g(z)$ represent $(\alpha_2)/(\beta_2 + \gamma_2)$. Since any point z on the small extruder corresponds to the point Xz on the large extruder, it follows that

$$f(z) = Xg(Xz) \quad (68)$$

Considering now the numerator of equation (67),

$$X \int_0^{l_1} g(Xz) dz = \int_0^{l_2} g(z) dz \quad (69)$$

since

$$l_1 = (l_2/X)$$

By similar arguments it can also be shown that the value of the denominator of equation (67) is the same for both extruders. Therefore both machines develop the same pressure.

$$\Delta P_1 = \Delta P_2 \quad (70)$$

From equation (54) it follows that

$$Q_2 = X^3 Q_1 \quad (71)$$

and from equation 65 that

$$(dP/dz)_1 = X (dP/dz)_2 \quad (72)$$

The relationship between the power requirements is obtained by writing equation (42) in the form

$$dZ = \epsilon \mu N^2 dz + \alpha N (dP/dz) dz = \nu(z) dz \quad (73)$$

For similar extruders at corresponding points,

$$\nu_2(Xz) = X^2 \nu_1(z) \quad (74)$$

Integrating equation (73), the relation between the total power consumption for the two extruders is found to be,

$$Z_2 = X^3 Z_1 \quad (75)$$

Thus, geometrically similar isothermal melt extruders should develop equal pressures, while the outputs and power consumptions will be in the ratio of the cubes of the diameters.

3. EXPERIMENTAL RESULTS

The literature of experimental extrusion studies is quite limited. The first systematic investigation of screw pumps was reported by Rowell and Finlayson² in 1928. Their apparatus consisted of a 0.5-in. rotor with a right-hand channel starting at one end and a left-hand channel starting at the other end. The rotor fitted inside a cylindrical barrel which was open at both ends and had a discharge port at the center. The feed entered at both ends, was pumped to the center by the two screw flights, and was discharged through a valve. A variety of screws was tested in which the channel depths ranged from 0.003 to 0.062 in. On all of the screws the pitch was 0.375 in. Many experiments were carried out with a wide variety of liquids, such as water, soap solutions, petrol, and oils. The data were correlated on the basis of flow equations which Rowell and Finlayson had previously presented in 1922. These flow equations are similar to those presented in the preceding sections of this chapter, and in all cases the data confirmed the validity of the equations.

Another report of experimental studies on screw pumps was by Pigott⁴ in 1951, who was primarily interested in the extrusion behavior of rubber stocks. In his paper he reviewed the theoretical flow equations and also reported some experimental work on the pumping of Newtonian fluids in a one-inch diameter extruder.

In one series of experiments, the pressures developed at closed discharge by various screws were measured. The experimentally determined pressures were found to agree with the values calculated from the flow equations for the case of closed discharge. In another series of experiments, using a fluid of approximately 1400-poise viscosity, the pressures developed at closed discharge for a given screw design, but for different radial clearances, were measured and agreed closely with calculations made with flow equations which included a leakage flow term.

In still another series of experiments, using oils of 0.5- and 1.1-poise viscosity, Pigott measured the discharge rates and pressures when extruding through dies of various flow resistances. The screw characteristics

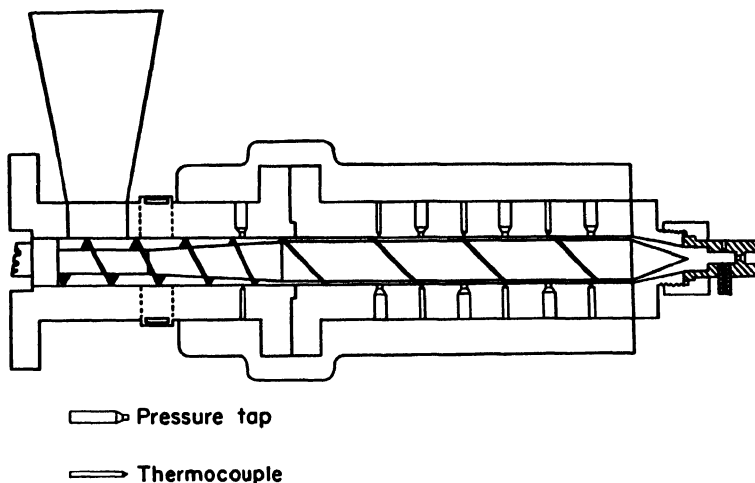


FIG. 10. Experimental extruder

plotted from these data are straight lines, as predicted by the theory. For both oils, the *open* discharge rate is the same. This is to be expected, as the drag flow rate is independent of viscosity. However, the slope of the screw characteristic with the more viscous oil was about twice that with the less viscous oil.

In 1953, further experiments were reported by McKelvey⁸ in which corn syrup was pumped with a 2-in. diameter screw. Corn syrup is essentially a Newtonian liquid. Figure 10 shows a diagram of the apparatus that was used. The barrel was provided with alternating pressure and temperature taps, so that the pressure and temperature gradients along the length of the screw could be measured. The head of the extruder accommodated interchangeable cylindrical dies and also a pressure gage and a thermocouple which measured the pressure and temperature of the fluid just before it entered the die.

Three runs were made using three different size cylindrical dies. During these runs, the pressure at the die, the output, and also the pressures along the barrel were measured.

Figure 11 shows a graph of the pressure points. Lines drawn through these points have a constant slope, which is to be expected for isothermal Newtonian flow in a channel of uniform dimensions.

In all of the runs made during these experiments, the viscosity of the corn syrup was different, owing to differences in temperature and (probably) the water content of the syrup. The viscosity of the corn syrup is

⁸ J. M. McKelvey, *Ind. Eng. Chem.* **45**, 978 (1953).

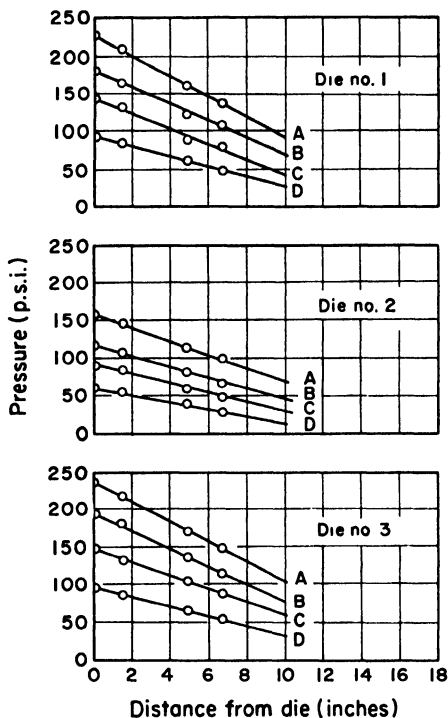


FIG. 11. Pressure profiles. Key: A, 1.24 r.p.s.; B, 0.90 r.p.s.; C, 0.63 r.p.s.; D, 0.32 r.p.s.

very sensitive to moisture content, and since the syrup was reused many times, the moisture content undoubtedly changed with time. However, the theory for this type of operation shows that the discharge rate should be independent of viscosity and depend only on the speed of rotation and the dimensions of the screw and die. Figure 12 shows a plot of the measured discharge rates, plotted as a function of the screw speed. The solid lines show the extruder flow characteristics calculated from flow equations based on the two-dimensional velocity distribution. The dashed lines show the characteristics calculated from the simplified flow equations. The experimental points are evenly distributed close to the solid lines, indicating that the two-dimensional flow equations accurately describe the flow behavior of Newtonian liquids in screw extruders. The slopes of the lines calculated from the simplified flow equations are about 9% higher than those experimentally observed.

The viscosity of the corn syrup can be calculated in two ways. First, the flow rate-pressure drop data for the cylindrical dies can be used with the Poiseuille equation. In this way the Poiseuille viscosity of the corn

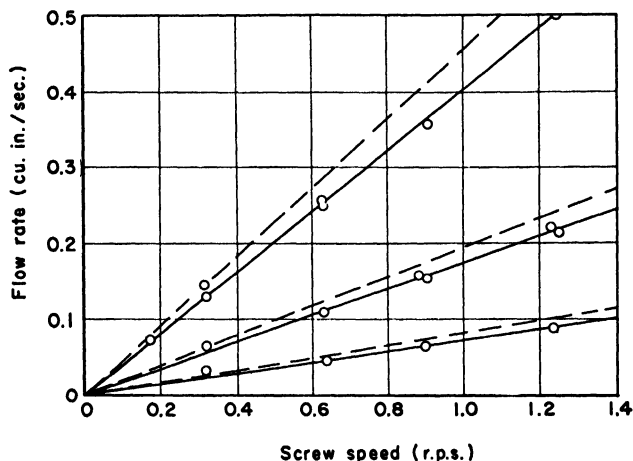


FIG. 12. Extruder flow characteristics. Key: \circ , experimental; —, theoretical; ---, simplified theoretical.

syrup was calculated for each run. The extrusion viscosity of the fluid in the screw channel can be calculated from the pressure profile data with the extruder flow equation.

$$\mu = \frac{(\beta + \gamma)}{(\alpha N - Q)} (dP/dz) = \frac{(\beta + \gamma)}{(\alpha N - Q)} (\Delta P/L) \sin \theta \quad (76)$$

where L is the axial length of the screw. The mean difference between the values is 0.0002 lb. force-sec. per square inch or about 5 %, which is well within the experimental error.

The results reported in these investigations are an experimental verification of the theoretical flow equations. So far, no precise measurements of power consumption of melt extruders have been reported.

4. ADIABATIC OPERATION

The special case in which an extruder is operated adiabatically is considered in this section. The development is similar to that presented by McKelvey.⁹ In adiabatic operation the extruder is assumed to be perfectly insulated and the pressure and thermal energy in the extrudate is obtained only from the action of the screw on the fluid. In adiabatic operation the temperature of the fluid rises continually along the length of the screw, accompanied by a corresponding decrease in viscosity.

For the development of the adiabatic extrusion theory it is necessary to have an analytical expression relating temperature and viscosity. It has

⁹ J. M. McKelvey, *Ind. Eng. Chem.* **46**, 660 (1954).

long been known that viscosity-temperature data for liquids can be correlated, over limited ranges of temperature, by plotting the logarithm of viscosity versus the reciprocal of absolute temperature. Consequently, the viscosity-temperature relationship of liquids is usually given by an equation of the form

$$\mu = Ae^{(E/RT)} \quad (77)$$

where E is the so-called energy of activation for viscous flow. However, when this equation is used in the development of the adiabatic theory, solutions can be obtained only as slowly converging series. This slow convergence would destroy much of the utility of the adiabatic equations. This problem was eliminated by using the following equation to relate viscosity to temperature.

$$\mu = ae^{-bt} \quad (78)$$

In the temperature range which is of interest for the extrusion of polymeric materials (about 100°C. to 300°C.), equation (78) will correlate viscosity-temperature data just about as well as equation (77).

Consider a section of a screw of length dz . Over this length, the pressure rise is dP , the power dissipated is dZ , and the temperature rise of the material is dT . The flow rate through the section is Q . An energy balance is obtained by equating the increase in pressure and heat energy of the material as it passes through the section to the rate at which the mechanical energy is dissipated.

$$CQdT + QdP = \epsilon\mu N^2 dz + \alpha NdP \quad (79)$$

In equation (79), where C is the heat capacity per unit volume, the QdP term represents the increase in pressure energy of the extrudate. In all cases, the pressure energy is much less than the heat energy term, $CQdT$; calculations show that it generally amounts to less than 10%. Therefore,

$$\epsilon N^2 \mu dz \gg (\alpha N - Q)dP \quad (80)$$

and equation (79) becomes,

$$CQdT = \epsilon\mu N^2 dz \quad (81)$$

It is now convenient to write the viscosity-temperature relationship (equation 78) in terms of T_f and μ_f , the temperature and viscosity at the inlet to the extruder.

$$\mu = \mu_f \exp [-b(T - T_f)] \quad (82)$$

By substituting equation (82) into equation (81) and rearranging, a form

convenient for integration is obtained. Integrating between the limits of T_f and T ,

$$T = T_f + (1/b) \ln (1 + MN^2z/Q) \quad (83)$$

where

$$M = (\mu_r b \epsilon)/(C)$$

By differentiating equation (83), the temperature gradient (dT/dz) at any point along the extruder screw is obtained.

$$b(dT/dz) = (MN^2)/(Q + MN^2z) \quad (84)$$

The flow equation can be written in the following form,

$$(dP/dz) = \mu(\alpha N - Q)/(\beta + \gamma) \quad (85)$$

Combining it with (81),

$$(dP/dz) = \left[\frac{CQ(\alpha N - Q)}{(\beta + \gamma)\epsilon N^2} \right] (dT/dz) \quad (86)$$

Substituting (84) into (86) and integrating between the limits of P_f and P ,

$$P = P_f + \left[\frac{CQ(\alpha N - Q)}{b\epsilon N^2(\beta + \gamma)} \right] \ln (1 + MN^2z/Q) \quad (87)$$

In the previous sections the case of isothermal extrusion was considered, and an equation was derived which related the two variables, ΔP and Q , to the screw speed N . This equation was called a screw characteristic and, when it was combined with a die characteristic, the operating point of the extruder was fixed. In a similar manner, an adiabatic screw characteristic which relates the three variables, ΔT , ΔP , and Q to the screw speed N can be obtained. The adiabatic screw characteristic combined with a given die characteristic likewise fixes the adiabatic operating point of the extruder. The pressure developed is obtained from (87) by replacing z with l .

$$\Delta P = \left[\frac{CQ(\alpha N - Q)}{b\epsilon N^2(\beta + \gamma)} \right] \ln (1 + MN^2l/Q) \quad (88)$$

The total temperature rise over the screw is obtained from (83).

$$\Delta T = (1/b) \ln (1 + MN^2l/Q) \quad (89)$$

Combining (88) and (89),

$$\frac{(N^2 \Delta P)}{(Q \Delta T)} = \frac{C}{\epsilon(\beta + \gamma)} (\alpha N - Q) \quad (90)$$

The screw characteristic can also be written in the form

$$(Q/N) = \alpha - [(\beta + \gamma)\epsilon/C](N\Delta P/Q\Delta T) \quad (91)$$

(91) shows that a plot of $(N\Delta P/Q\Delta T)$ versus (Q/N) will be a straight line with a slope equal to $[(\beta + \gamma)\epsilon/C]$. The intercept with the ordinate will be equal to α .

Equation (83) can be written

$$\exp [b(T_d - T_f)] = 1 + MN^2l/Q \quad (92)$$

and from (82)

$$\exp [b(T_d - T_f)] = \mu_f/\mu_d \quad (93)$$

Therefore,

$$R = 1 + MN^2l/Q \quad (94)$$

where

$$R = \mu_f/\mu_d$$

Introducing the die flow equation

$$Q = (k/\mu)\Delta P \quad (95)$$

into (88),

$$\left(\frac{1}{R}\right) = \left[\frac{k}{MN^2(\beta + \gamma)}\right](\alpha N - Q) \ln \left(1 + \frac{MN^2l}{Q}\right) \quad (96)$$

Combining (94) and (96),

$$\left(\frac{\beta + \gamma}{kl}\right) = \left(\frac{R}{MN}\right)\left(\alpha - \frac{MNI}{R - 1}\right) \ln (R) \quad (97)$$

Rearranging (97)

$$\left(\frac{\beta + \gamma}{kl}\right) = \left(\frac{\alpha}{MNI}\right)R \ln (R) - \frac{R \ln (R)}{(R - 1)} \quad (98)$$

Equation (98) is the operating equation for adiabatic operation. It contains one unknown, R , and two dimensionless groups, $(\beta + \gamma)/(kl)$ and $(\alpha)/(MNI)$ which are functions only of the dimensions of the extruder, the frequency of rotation of the screw, and the physical properties of the extrudate. Once the value of R is calculated from (98), the output, pressure, temperature, and power requirement can be determined. The output is obtained by rearranging (94).

$$Q = (MN^2l)/(R - 1) \quad (99)$$

The temperature rise is obtained by combining (93) and (94) and rearranging.

$$\Delta T = (1/b) \ln (1 + MN^2 l/Q) \quad (100)$$

The pressure rise is obtained by combining (94) and (95).

$$\Delta P = \left[\frac{\mu_f MN^2 l}{kR(R-1)} \right] \quad (101)$$

The power requirement is obtained from the extruder energy balance.

$$Z = CQ\Delta T + Q\Delta P \quad (102)$$

The direct calculation of R from (98) is difficult. However, the graph shown in Fig. 13 enables values of R to be obtained quite readily. Various values of R are plotted in Fig. 13 as functions of the two dimensionless groups, $(\beta + \gamma)/(kl)$ and $(\alpha)/(MNI)$. Therefore, to obtain R it is necessary only to calculate $(\beta + \gamma)/(kl)$ and $(\alpha)/(MNI)$ and then read the value of R from Fig. 13.

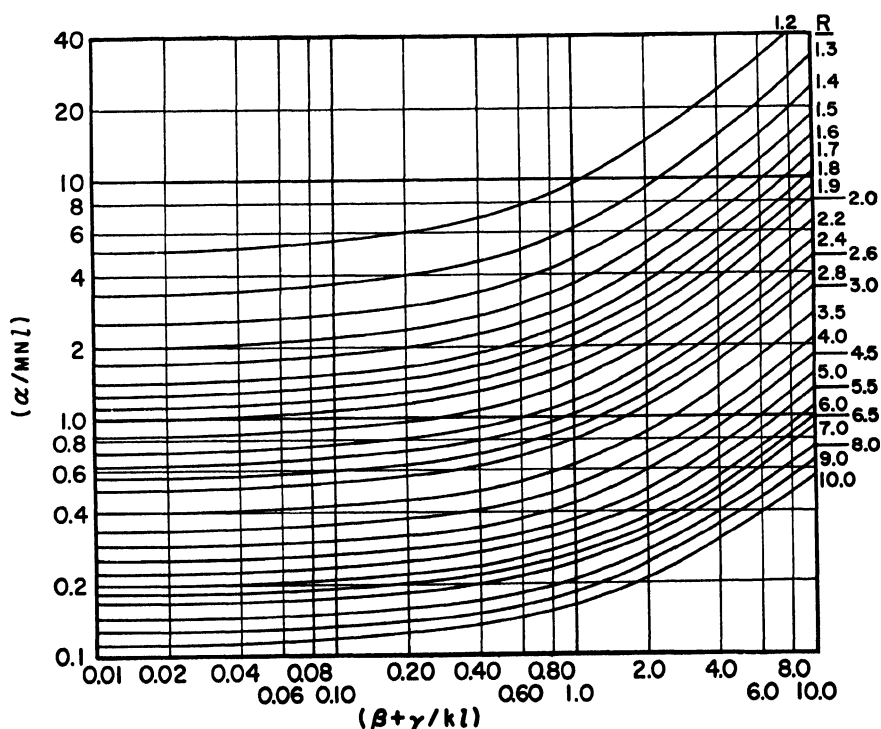


FIG. 13. Values of R

5. SCALE-UP RULES FOR ADIABATIC OPERATION

Consider two adiabatic extruders, a large one and a geometrically similar scale model. The scale model is so constructed that all of the dimensions of the large extruder, including the die, are X time larger than the corresponding dimensions of the model. The subscript 1 refers to the model and the subscript 2 to the large extruder.

$$X = (e_2/e_1) = (D_2/D_1) = (H_2/H_1) = (l_2/l_1) = (\delta_2/\delta_1) \quad (103)$$

and

$$\theta_2 = \theta_1$$

The die constants are related by the equation

$$k_2 = X^3 k_1 \quad (104)$$

where (104) is a general relationship valid for geometrically similar dies of any shape.

Since it is specified that the operating conditions are identical and that the same material is being extruded in both the large extruder and the model,

$$(N_2/N_1) = (b_2/b_1) = (C_2/C_1) = (T_{f_2}/T_{f_1}) = 1$$

The relationships between the screw constants of the two machines are

$$\alpha_2 = X^3 \alpha_1 \quad (105)$$

$$(\beta_2 + \gamma_2) = X^4 (\beta_1 + \gamma_1) \quad (106)$$

$$\epsilon_2 = X^2 \epsilon_1 \quad (107)$$

and from (83),

$$M_2 = X^2 M_1 \quad (108)$$

therefore,

$$\alpha_2/M_2 N_2 l_2 = \alpha_1/M_1 N_1 l_1 \quad (109)$$

$$(\beta_2 + \gamma_2)/k_2 l_2 = (\beta_1 + \gamma_1)/k_1 l_1 \quad (110)$$

Referring to (88),

$$R_2 = R_1 \quad (111)$$

With reference to (99), (100), (101), and (102), the following scale-up rules are deduced.

$$Q_2 = X^3 Q_1 \quad (112)$$

$$\Delta T_2 = \Delta T_1 \quad (113)$$

$$\Delta P_2 = \Delta P_1 \quad (114)$$

$$Z_2 = X^3 Z_1 \quad (115)$$

IV. Extrusion of Non-Newtonian Melts

The theoretical equations which have been presented rest on the assumption of Newtonian flow. Since most applications are concerned with non-Newtonians, the question arises as to how well these equations apply in practice.

Screw extruders are used for a wide variety of materials that differ greatly in their rheological characteristics. For example, screws are used for the extrusion of highly elastic materials such as rubber; for the extrusion of viscoelastic materials such as polyethylene, which deviates considerably from the Newtonian viscosity law; for pumping polymer melts such as nylon, which is mildly non-Newtonian under extrusion conditions; and for metering and pumping simple Newtonian liquids.

For Newtonians the equations rest on a sound theoretical and experimental base. For other materials there is no exact theoretical or empirical method for predicting, quantitatively, the extrusion behavior of the material. The following discussion of non-Newtonians is primarily qualitative in nature. Elastic effects are not considered.

1. FLOW BEHAVIOR

It was previously shown that a linear screw characteristic is obtained for the isothermal extrusion of Newtonian liquids. The dashed lines in Fig. 14

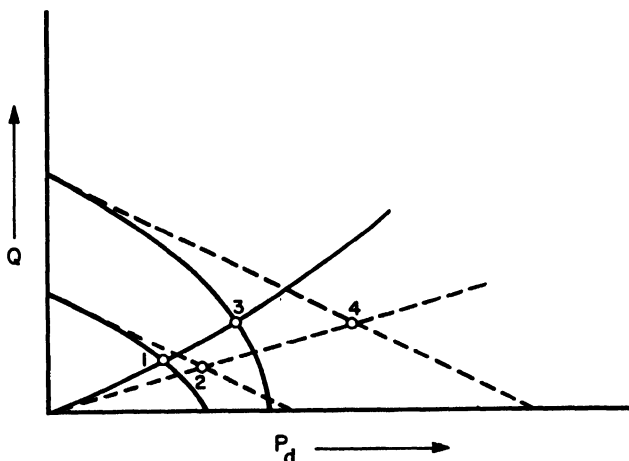


FIG. 14. Screw and die characteristics. Key: —, non-Newtonian; ---, Newtonian

show a set of these linear characteristics. The intercept of a characteristic with the ordinate represents the free discharge flow, or the rate of pure drag flow. For shallow flight screws drag flow is independent of the nature of the liquid, provided that the liquid wets both the screw and barrel surfaces and that there is no slippage at these surfaces. This conclusion is valid only for shallow flight screws. When the difference between the root diameter of the screw and the inside diameter of the barrel becomes appreciable the shear stresses acting on the fluid planes are no longer equal and the apparent viscosity will vary throughout the channel.

An experimental study of non-Newtonian free discharge flow was reported by McKelvey,⁸ in which the free discharge extrusion rate of a molten polymeric material (polyethylene terephthalate) was measured. This material, although non-Newtonian, is characterized by a rather sharp melting point and a mildly non-Newtonian flow behavior which is similar to molten nylon. This material was melt extruded with a 2-in. diameter, double-flight screw of constant pitch. The depth of the screw channel was 0.071 in. A complete description of the screw and of the experimental arrangement is given in reference 8. A series of extrusion runs was made at free discharge during which the polymer melt temperature was kept close to 270°C. Figure 15 is a plot of the free discharge flow rate versus the screw speed. The slope of the straight line drawn through the experimental points agreed exactly with that calculated from the extrusion equation. While this

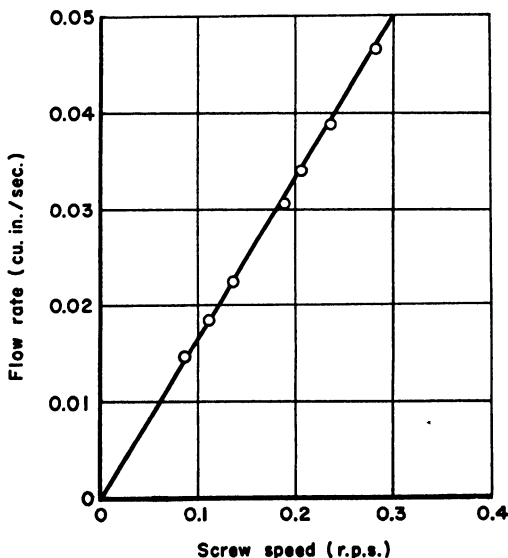


FIG. 15. Free discharge flow. Key: —, theoretical; O, experimental

material is only mildly non-Newtonian, these experiments confirm that the free discharge flow is relatively insensitive to the nature of the liquid.

With a die on the end of the extruder the flow is restricted. Consequently, a pressure is generated which causes back flow along the screw channel. Under these conditions the shear stress varies across the channel and the apparent viscosity of the fluid is different in different parts of the channel. Since for the non-Newtonians the apparent viscosity decreases with increasing shear rate, it is possible to predict, qualitatively, the general shape of the screw characteristic for isothermal operation. First, consider operation at constant speed but against various die resistances. As the die resistance and pressure increase, the driving force for back flow increases. However, since the shear stresses also increase, the apparent viscosity of the fluid decreases. Consequently, the slope of the screw characteristic grows steeper instead of remaining constant as it does with Newtonians. The solid lines in Fig. 14 show how the linear characteristics become distorted.

The screw speed also effects the shape of the characteristic. For Newtonians, characteristics for the same screw turning at different speeds are always parallel. For non-Newtonians this condition does not exist, because the apparent viscosity falls as the speed rises. This causes larger back flows, for the same pressure, at high speeds than at low speeds. Consequently, at high speeds the slope of the screw characteristic steepens more rapidly than at low speeds. Figure 14 shows this difference for the two screw characteristics.

In the design of extrusion equipment for non-Newtonians it is necessary to have an effective extrusion viscosity to use in the flow and power equations. Given a pressure-flow rate point on the screw characteristic it is, of course, possible to solve the flow equation for "viscosity" and to call this the effective extrusion viscosity. However, this method suffers from the liability that if the characteristic has a large curvature, a different effective viscosity will be needed for each die pressure. In theory it would be far better to derive the flow equation anew on the basis of, say, the power law and to use two constants to describe the flow properties of the fluid. However, this has not as yet been done, and in practice the method most commonly used is to calculate an effective extrusion viscosity from measurements made in extruders under similar conditions.

A somewhat different approach was worked out by Pigott⁴ and applied to the extrusion of rubber stocks. He calculated (on the basis of Newtonian velocity distributions) the volume-weighted average shear rate for fluids in extruder screw channels at various back flows. Then from extrusion experiments and also from Mooney plastometer measurements he constructed a graph giving apparent viscosity of rubber stocks as a function

of shear rate. In making extruder calculations the volume-weighted average shear rate is first calculated and then the effective viscosity is obtained from the diagram. Pigott reported some experiments in which there was good agreement between calculated and observed extruder performance.

In many practical cases of plastics extrusion the extruder is not operated with very large back flows and the curvature of the screw characteristics is quite small. This is particularly true for nylonlike materials. For example, the extrusion viscosity of polyethylene terephthalate at 270°C. was determined in a series of experiments reported by McKelvey.⁸ Runs were made using three different multiple orifice dies and the screw characteristics were constructed from the pressure-flow rate data. Figure 16 shows the screw characteristics obtained for three screw speeds. Within the limit of experimental error, the slopes of the three characteristics are identical. The extrusion viscosity calculated from the slope of these lines is 0.0341 lb. force-sec./sq. in. (2350 poises).

On account of the commercial importance of polyethylene, considerably more attention has been devoted to its extrusion behavior than to that of many of the other plastics. However, these studies have had to be carried out with plasticating extruders, as under normal laboratory conditions it is very difficult to supply molten polyethylene to an extruder. When a material is extruded in a plasticating extruder an unknown quantity is

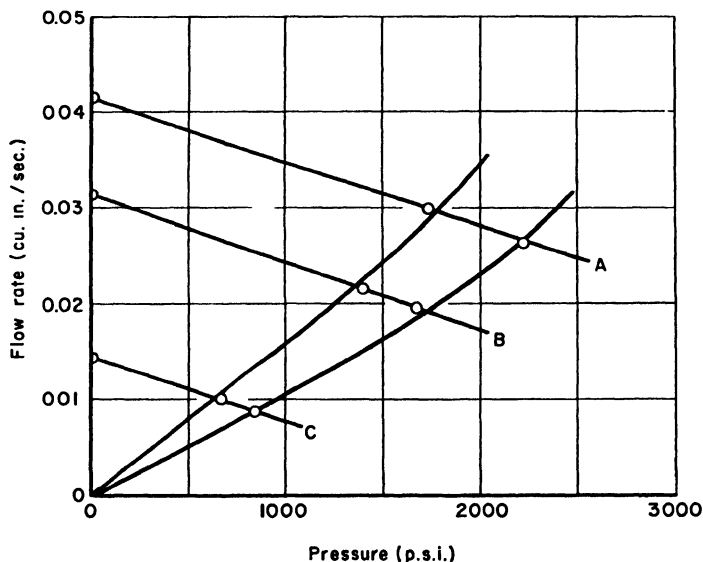


FIG. 16. Screw characteristics for polyethylene terephthalate at three screw speeds. Key: A, 0.256 r.p.s.; B, 0.192 r.p.s.; C, 0.087 r.p.s.

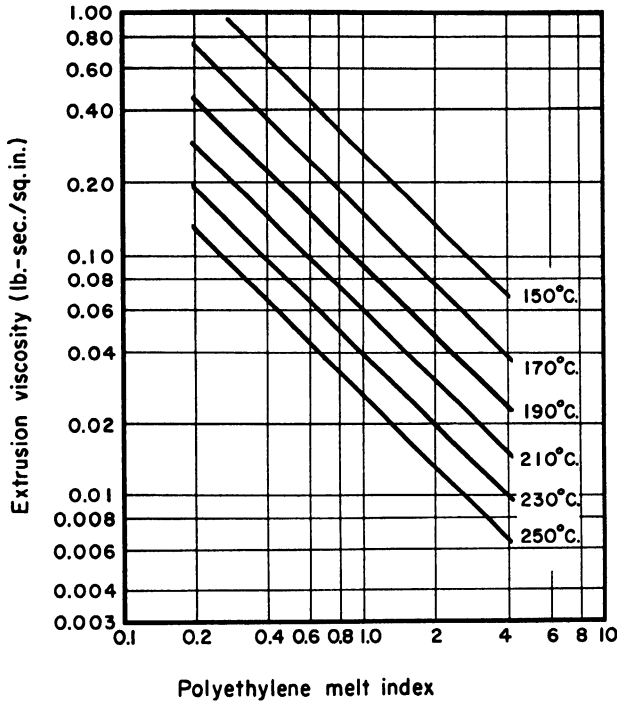


FIG. 17. Polyethylene extrusion viscosities

introduced into the extrusion-viscosity calculations, since the position in the screw where the polyethylene first becomes fluid is unknown. Therefore, with ordinary extrusion equipment this position must be estimated and this introduces a large element of uncertainty into the viscosity calculations. In addition a large amount of heat is generated by viscous shearing in polyethylene, and it is difficult to maintain isothermal conditions. This introduces another uncertainty into the calculations. These problems can be resolved to large degree if pressure measurements are made along the length of the barrel. Then, two pressure points can be selected which are so close together that the temperature error is small.

The apparatus shown in Fig. 10 has been used by the authors to study the extrusion behavior of polyethylene. Experiments have been carried out at different temperatures and with different grades of polyethylene, and effective extrusion viscosities have been calculated. Figure 17 is a diagram¹⁰ which has been constructed on the basis of these measurements. The temperature range has been extended by applying (77) to the flow

¹⁰ J. M. McKelvey, *SPE Journal* 9(3), 12 (1953).

data and using activation energies obtained from experiments with a piston type viscometer. The polyethylene grade is characterized by the melt index,¹¹ which is a measure of the amount of polyethylene which will flow through a standard orifice, at a standard pressure, and at a standard temperature, in a given length of time. High melt indices correspond to low melt viscosities and low molecular weights.

While the viscosities obtained in this manner are approximate, they have proved useful for the design of polyethylene extruders that are intended to operate with small pressure flows and at normal screw speeds (say, 30–60 r.p.m.).

The flow through the die is a pressure flow and it is possible, for dies of simple geometry, to calculate the die characteristic for many non-Newtonians, using a power law. If the power law is written

$$\tau = B(\dot{\gamma})^m \quad (116)$$

where

$$\dot{\gamma} = \text{shear rate}, \quad \tau = \text{shear stress}$$

and B and m are constants, then for cylindrical dies the characteristic is defined by the equation

$$Q = \left(\frac{m}{m+3} \right) (2B)^{-(1/m)} \pi R^{m+3} \left(\frac{\Delta P}{L_d} \right)^{1/m} \quad (117)$$

Equation (117) shows that a logarithmic plot of Q versus P will be a straight line. This has been verified, over limited ranges of shear rate for many high polymeric substances. The die characteristic shown in Fig. 14 has the parabolic shape that is obtained by plotting on arithmetic coordinate paper.

The extruder operating points are located at the intersection of the screw and die characteristics, as shown in Fig. 14. From this, it appears that under the same operating conditions, equal flow rates can be obtained with non-Newtonians as with Newtonians, but that lower pressures will be generated at the die. However, a quantitative theory is needed before any definite conclusions can be drawn.

2. POWER CONSUMPTION

Serious error will result if the power for the extrusion of non-Newtonians is calculated with the usual power formula, because the calculated clearance power will be too large. Since the depth of the screw channel is usually 10 to 20 times that of the radial clearance, the shear rate in the clearance is

¹¹ R. E. Jolly and J. P. Tordella, *Modern Plastics* **31**, 146 (1953).

10 to 20 times that in the channel. Consequently, the apparent viscosity in the clearance is less than it is in the channel, while the power formula assumes that the viscosities are the same.

Assuming that the power law is applicable, a correction to the power formula can be derived. Apparent viscosity is defined by the equation

$$\mu' = \tau/\dot{\gamma} = B(\dot{\gamma})^{m-1} \quad (118)$$

Since the shear rate in the screw channel is inversely proportional to the channel depth, while the shear rate in the clearance is inversely proportional to the clearance,

$$\mu_c' = \mu_s'(H/\delta)^{m-1} \quad (119)$$

where

μ_s' = apparent viscosity in channel

μ_c' = apparent viscosity in clearance

The modified power formula is written

$$dZ = \epsilon' N^2 \mu_s' dz + \alpha N dP \quad (120)$$

where ϵ' , the modified power constant, is defined by the equation

$$\epsilon' = \pi^2 D^2 \cos \theta \left[\frac{(t - ne)(1 + 3 \sin^2 \theta)}{(H)} + \left(\frac{ne}{\delta} \right) \left(\frac{H}{\delta} \right)^{m-1} \right] \quad (121)$$

For Newtonian fluids ϵ' becomes equal to ϵ .

V. Plasticating Extrusion

A distinction has been made between melt and plasticating extrusion and it has been pointed out that the analysis of extrusion via the laws of laminar flow applies only to melt extruders and to the forward zone of plasticating extruders. Plasticating extrusion is inherently a more complicated operation than melt extrusion, since a plasticating extruder, in addition to pumping the melt, must transfer heat to and mechanically work and compact the solid feed. The following discussion of plasticating extrusion is of limited scope and no attempt is made to discuss, in detail, the state of the art.

The book by Simonds *et al.*¹² discussed much of the art of plasticating extrusion up to the time of its publication. A recent article by Gaspar¹³ reviewed problems and trends in European extruder design. The applica-

¹² H. R. Simonds, A. J. Weith, and W. Shack, "Extrusion of Plastics, Rubber, and Metals." Reinhold, New York, 1952.

¹³ E. Gaspar, *Soc. Plastics Engrs. Tech. Papers* **2**, 247 (1956).

tion of extrusion theory to the design of extruder screws has been discussed by Colwell,¹⁴ while Sackett¹⁵ has discussed problems in the selection of extruder screws.

The specification of an apparent or effective viscosity to use with the extrusion formulas is always a problem. Sackett¹⁶ has presented viscosity data for many commercial materials. Techniques involved in the extrusion of nylon resins have been discussed by Toll¹⁷ and Hughes.¹⁸

Another factor involved in the art of extrusion is that of the quality of the extrudate, which is closely related to the homogeneity of the extrudate and the uniformity of delivery. This problem has been discussed, for the case of polyethylene extrusion, by Maddock.¹⁹

Many different extruders developed for special applications and incorporating various special features have appeared on the market and reference should be made to the trade literature for details. One particularly interesting development, reported by Bernhardt,²⁰ is the so-called vacuum extruder screw. In this screw a portion of the screw channel in the middle of the metering section is cut very deep and a vacuum applied through holes in the forward portion of the screw channel. Volatile materials in the plastic are therefore removed, which enables many thermoplastics to be extruded without a previous drying operation.

In discussing plasticating extruders it is convenient to divide the extruder into zones and to consider the function of each zone separately. In general there can be five zones in a plasticating extruder: (1) the feed zone, (2) the melting and transition zone, (3) the pumping or metering zone, (4) the torpedo zone, and (5) the filtering zone. Figure 18 is a diagram of an extruder indicating the location of these various zones. The curve in Figure 18 shows approximately how the pressure increases along the screw and then falls as it forces the melt past the torpedo and through the screens and die. The function and operation of each zone will be discussed separately, but first it is useful to consider briefly the energy requirements of plasticating extruders and two general modes of operation that are sometimes possible with plasticating extruders.

The total amount of energy required by a plasticating extruder depends upon the rate of extrusion and the rise in stock temperature and pressure. Heat losses from the extruder must also be considered. The energy can be

¹⁴ R. E. Colwell, *Soc. Plastics Engrs. Tech. Papers* **3**, 153 (1957).

¹⁵ R. D. Sackett, *Soc. Plastics Engrs. Tech. Papers* **3**, 328 (1957).

¹⁶ R. D. Sackett, *Soc. Plastics Engrs. Tech. Papers* **2**, 265 (1956).

¹⁷ K. G. Toll, *Soc. Plastics Engrs. Tech. Papers* **3**, 295 (1957).

¹⁸ R. L. Hughes, *Soc. Plastics Engrs. Tech. Papers* **3**, 321 (1957).

¹⁹ B. H. Maddock, *Soc. Plastics Engrs. Tech. Papers* **3**, 105 (1957).

²⁰ E. C. Bernhardt, *Soc. Plastics Engrs. Tech. Papers* **2**, 279 (1956).

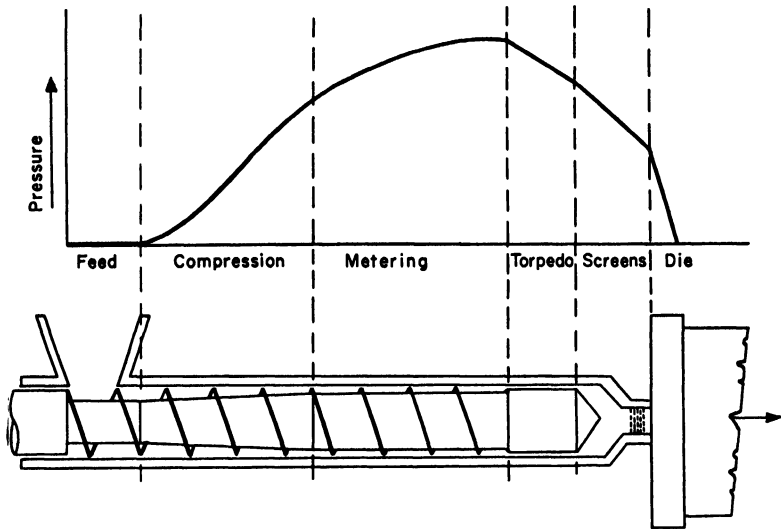


FIG. 18. Zones of a plasticating extruder

supplied either thermally (through heat transfer) or mechanically. The rate of heat transfer to the material is called the thermal power and the rate at which work is supplied by the screw is called the mechanical power.

Under varying extrusion conditions, the percentage of mechanical power used varies over a wide range from about 30 % to greater than 90 %. In other words, depending upon the specific situation, either thermal or mechanical power can predominate. The controlling factor is usually the behavior of the extruder feed. The following two examples illustrate this point.

Nylon is a thermoplastic with a high melting point, a relatively short melting range, and a low melt viscosity. At room temperature nylon flake is a hard, tough, rigid material and it is extremely difficult to shear the individual flakes of nylon until the temperature of the material gets close to the melting point. Therefore, it is not possible to generate much heat through mechanically working nylon flake in an extruder. Nylon extruders must be designed to melt the material with transferred heat and a nylon extruder is, first, a heat exchanger and, second, a melt pump.

As experience with flake nylon in the plastics industry increased, a nearly standard screw design evolved. Figure 19 shows a sketch of this screw. The long section with the constant root diameter is the heat transfer zone, in which the flake is conveyed forward and melted. Usually the heat is transferred from the walls of the barrel, but sometimes the core of the screw is also heated to increase the rate of heat transfer. The transition zone is

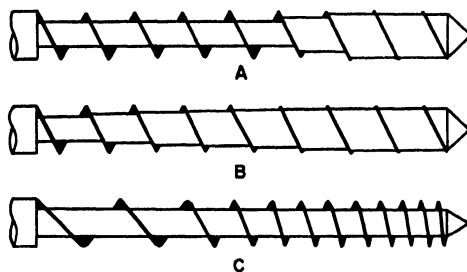


FIG. 19. Typical screw designs. Key: A, nylon type; B, polyethylene type; C, rubber type.

extremely short, as its only function is to squeeze out entrapped air and to compensate for the density change that the material undergoes in changing from a loosely packed solid to a liquid. The metering section is provided with a shallow channel suitable for pumping a low viscosity melt.

In operation, a nylon extruder requires a relatively small amount of mechanical power. However, the thermal power requirements are quite large and heat transfer usually governs the ultimate capacity of the extruder. In other words, the capacity of the metering section can be increased indefinitely by increasing the screw speed, but since the metering zone can pump only as fast as it receives melt, the melting capacity (heat transfer) is the controlling factor.

Turning to the other extreme, consider the plasticating extrusion of a soft material, such as polyethylene. Even at room temperature solid polyethylene can be easily deformed. Therefore, the possibility exists for melting polyethylene by generating heat internally through mechanical working. Of course, acceptable extrusions can be obtained with polyethylene using a nylon type screw and depending upon heat transfer to melt the material. However, screws can also be designed to utilize the easy workability of polyethylene and this method offers certain advantages. For example, higher extrusion rates are possible because the rate is not limited by the amount of heat that can be transferred through the barrel. Also, excessive temperature gradients in the plastic can be avoided since the heat is generated internally. It is also theoretically possible to control the extrusion rate and the extrusion temperature independently merely by varying the screw speed and the die resistance, reserving the barrel heaters to offset heat losses and to provide fine degrees of temperature control. The extrusion of polyethylene using predominantly mechanical power (adiabatic extrusion) has been discussed by Bernhardt and McKelvey.²¹

A sketch of a good screw for the adiabatic extrusion of polyethylene is

²¹ E. C. Bernhardt and J. M. McKelvey, *SPE Journal* **10**, 419 (1954).

also shown in Fig. 19. With a screw of this general design the feed pickup section is just long enough to insure that the material is properly conveyed into the main part of the extruder. Then, compression of the cold material starts immediately, causing the polyethylene to be worked to such an extent that it quickly melts. A screw of this type can be operated with no thermal power whatsoever, as has been demonstrated many times.

In general, therefore, there are two extreme modes of operation for plasticating extruders, and before the designs of the various zones of the extruder can be specified, it is first necessary to decide in what manner the extruder is to operate. This depends primarily on the solid state properties of the plastic. If the solid material is soft and easily worked, consideration should be given to the possibility of operating the extruder under near adiabatic conditions using predominantly mechanical power. On the other hand, if the solid material is hard and difficult to shear, then probably the heat transfer type of operation should be used.

Some of the problems connected with each of the extruder zones will now be considered.

1. METERING ZONE

The purpose of the metering zone is to take the molten plastic from the compression section and to develop the pressure required to pump the melt past the torpedo and through the screens and die at the desired flow rate. The metering section also acts to smooth out irregularities in flow caused by fluctuating pressures at the die or in the transition zone. The design of the metering section depends on the viscous properties of the plastic melt and the characteristic of the die. The methods and formulas described previously can be applied directly to the design of metering zones.

2. FEED ZONE

The purpose of the feed zone is to convey the pellets, flakes, or granules of plastic from the feed hopper into the main part of the extruder. It is, of course, essential that the conveying capacity of this zone be at least equal to the melting capacity and pumping capacity of the rest of the screw.

Darnell and Mol²² have made an analysis of solids-conveying in extruders, but, at the present time, it does not appear feasible to put the design of the feed zone on a quantitative basis. However, some generalizations can be drawn. Certain granular plastics, when conveyed in an extruder screw, pack together to form a plug. This plug advances down the helical channel

²² W. H. Darnell and E. Mol, *SPE Journal* **12**, 20 (1956).

with little deformation. The rate at which the plug moves forward depends upon the back pressure and upon the frictional forces exerted on the plug by the barrel surface, the root of the screw, and the screw flight. These frictional forces, in turn, depend upon the nature of the surfaces and also upon the geometry of the screw, particularly the helix angle. Some limiting cases have been considered. First, if the frictional forces between the plug and the barrel wall were reduced to zero, the plug would merely "ride the screw" and make no forward motion. On the other hand, if the frictional forces on the root of the screw and screw flight could be reduced to zero (while those at the barrel surface remained larger than zero), and there is no back pressure, the plug would move directly down the helix, advancing one pitch for each turn of the screw. A third case might also be considered. If longitudinal grooves were cut into the barrel surface, the helical motion of the plug would be restricted and it would tend to move in a line parallel to the axis of the barrel, much in the same manner that a nut will advance down a screw if its rotation is restricted but its forward motion is free.

Of course, in practice none of these situations are ever met exactly. Frictional forces between the extruder surfaces and the plug are never zero. The back pressure stops the forward motion of the plug down the screw channel if it is large enough to counterbalance the frictional forces driving the plug forward. In general, however, the influence of the helix angle is important. With small helix angles forward motion of the plug is more positive. With large helix angles, a small restricting force or an unfavorable ratio of frictional forces at the top and bottom of the plug (caused perhaps by differences in temperatures at the screw root and the barrel wall or by differences in materials and finishes of root and barrel) may cause forward motion of the plug to cease. In practice it appears that 20° is about as large an angle as can be safely used for the feed zone. Of course, under some conditions larger angles have been successfully used, but usually it is good practice to keep the helix angle in the range of 10° to 20° .

If the resistance to internal shear (either by particle movement or by shearing particles) of the material is less than the shear stress exerted by frictional drag, the movements of the solid become similar to those of fluids and in many cases the same equations apply. In all extruders the mechanism of flow becomes one of internal shear at some point along the screw channel.

More research is needed before a satisfactory understanding can be had of the behavior of solids in extruder screws.

3. TRANSITION ZONE

The transition zone connects the feed zone to the metering zone. In the case of nylon type extruders it is simply a connecting link between the feed

and metering zones. Since it need do no mechanical working it can be quite short. Usually one pitch is satisfactory.

For other materials, such as polyethylene, the transition zone can supply a good part of the mechanical working that is needed to melt the plastic, although there appears to be no agreement among designers as to how long the transition zone should be to accomplish this.

Another question arises in the design of transition zones: Should the reduction in cross sectional area be obtained by reducing the channel depth or by decreasing the pitch, or both? Usually when mechanical working is desired it is better to decrease the depth of the channel. This causes more intense working and also causes the melting process to occur more uniformly. Indeed, the pitch is reduced when it is necessary to minimize mechanical working, as in rubber extrusion. When rubber is extruded, overheating due to excessive shear is always a consideration and the "rubber type" screw shown in Fig. 19 is commonly used for these materials.

4. TORPEDO AND SCREENS

The function of a torpedo is to supply additional mechanical working to the molten plastic. In some cases this is necessary and desirable, particularly where pigments are being added to the feed or where blends or mixtures of plastics are being extruded together. A well designed torpedo will apply an intense shear to the plastic. However, this increased shear can only be obtained at the cost of a loss in extruder capacity. The reason for this is that clearances have to be small and the extruder must generate higher pressures to force the melt through the small annular space. This, in turn, causes increased back flow in the screw and means that larger extruders are required. Therefore, in considering a torpedo the possible beneficial effect must be equated against increased pressures and lower outputs, or conversely, larger machines. Of course, if flights are added to the torpedo the loss of output can be minimized. A flighted torpedo should be considered as an additional metering zone and its performance can be calculated with the screw formulas.

The screen pack serves a different purpose. Its primary function is to filter the melt before it reaches the die. In practice, screen packs are often used to create pressure in the extruder to make the operation smoother or to increase the stock temperature. However, this is a costly way to obtain good extrusions and is unnecessary with properly designed screws. If the screw is properly designed, then the minimum number of screens of the largest possible size that will do a satisfactory filtering job should be used.

5. SCALE-UP OF PLASTICATING EXTRUDERS

From the preceding discussion it is obvious that the design of plasticating extruders is more of an art than an exact science. In some cases the

TABLE I
RESULTS OF SCALE-UP EXPERIMENT

	<i>2-In. model Experimental results</i>	<i>20-In. extruder</i>	
		<i>Calculated</i>	<i>Observed</i>
Capacity (lb./hr.)	2.5	2500	2400
Power (hp.)	0.29	290	245
Stock temperature (°C.)	169	169	156
Pressure (p.s.i.)	1850	1850	1600
Speed (r.p.m.)	15	—	15

design of plasticating extruders can best be carried out by scaling-up small laboratory extruders that are operating in a satisfactory manner. Caution must be observed, however, to use the particular scale-up rules that correspond to the mode of operation of the extruder.

For operation with predominantly thermal power, the capacity of the extruder is proportional to the rate of heat transfer, and the critical factor in the scale-up is the heat transfer area. For a geometric scale-up the heat transfer area is proportional to the square of the screw diameter. Consequently, the capacity is proportional to the square of the screw diameter. Also the thermal and mechanical power requirements, for this case, become proportional to the square of the screw diameter.

When mechanical power is the controlling factor (adiabatic operation) the scale-up rules are different. It has already been shown that the capacity and power requirements of the melt zone of an adiabatic extruder are directly proportional to the third power of the screw diameter. Are the capacity and power requirements of the feed and compression zones also proportional to the cube of the diameter? If they are, then the scale-up rules derived for adiabatic melt extruders can be applied directly to adiabatic plasticating extruders. No conclusive answer can now be given to this question, but in certain cases this appears to be the case. For example, consider the results of a tenfold scale-up experiment on polyethylene reported by Carley and McKelvey.²³ These experiments were carried out with a 2-in. diameter extruder which was a geometrically similar scale model of a 20-in. diameter extruder. Both extruders were operated under nearly adiabatic conditions. Output rates, stock temperatures, pressures, and power consumption were measured on both extruders. Applying the adiabatic scale-up rules, the scale factor for capacity and power consumption is 1,000, while the stock temperatures and pressures should be the same in both the model and the large extruder. Table I gives the results of the experiment.

²³ J. F. Carley and J. M. McKelvey, *Ind. Eng. Chem.* **45**, 985 (1953).

In practice, the operation of many extruders is neither predominantly thermal or mechanical, but falls somewhere in between the two extremes. In this case neither of the sets of scale-up rules apply and the compromise sometimes used by the industry is to assume that the power requirements and capacity are proportional to the 2.5 power of the diameter.

Nomenclature

C	Heat capacity per unit volume	W	Speed of barrel surface
D	Inside diameter of extruder barrel	Z	Total power
F_P	Shape factor for pressure flow	Z_s	Power consumed in screw channel
F_D	Shape factor for drag flow	Z_c	Power consumed in radial clearance
F_Z	Shape factor for power	b	Temperature coefficient of viscosity, defined by equation (78)
H	Distance from root of screw to barrel surface	e	Width of screw flight
K	Dimensionless ratio, (w/h)	h	Depth of channel
L	Axial length of extruder screw	k	Die constant defined by equation (55); helical length of screw channel
L_D	Length of extruder die	m	Exponent in power law
M	Constant defined by equation (83)	n	Number of parallel screw channels
N	Frequency of rotation of extruder screw	t	Pitch of screw flight
P	Pressure at any point in screw	u	Fluid velocity component acting in z direction
P_d	Pressure at entrance to die	v	Fluid velocity component acting in z direction
P_f	Pressure at extruder feed port	w	Width of screw channel
P_a	Pressure at end of die	α	Drag flow constant
Q	Volumetric flow rate	β	Pressure flow constant
Q_D	Volumetric drag flow rate	γ	Leakage flow constant
Q_P	Volumetric pressure flow rate	$\dot{\gamma}$	Shear rate
Q_L	Volumetric leakage flow rate	ϵ	Power constant
R	Radius of extruder die; also dimensionless ratio defined by equation (94)	δ	Radial clearance
T	Temperature at any point in screw	θ	Helix angle
T_f	Temperature at feed port of screw	τ	Shear stress
T_d	Temperature at extruder die	μ	Newtonian viscosity
U	Velocity component normal to z axis	μ'	Apparent viscosity
V	Velocity component acting along z axis		

AUTHOR INDEX

Numbers in parentheses are footnote numbers and are inserted to enable the reader to locate a cross reference when the author's name does not appear at the point of reference in the text.

A

- Abbott, N. J., 423
 Abeles, P. W., 364
 Ackerman, F., 118
 Adams, L. H., 409
 Aeschlimann, W., 583
 Aikens, J. R., 466
 Alcock, T. C., 374, 379
 Alder, M. G., 415
 Aldrich, H. L., 245
 Alexander, A. E., 430, 438
 Alexander, P., 116
 Alfrey, T., Jr., 104, 383, 384(29), 424
 Almy, E. G., 270
 Altrichter, F., 73
 Altrogge, W., 476
 Alves, G. E., 237
 Ammar, I. A., 94
 Anderson, O. L., 333
 Anderson, S. L., 498
 Andrade, E. N. da C., 218, 221
 Andrews, R. D., 383, 384(29), 388
 Anyas-Weiss, L., 115
 Applegate, P. D., 192, 209(23)
 Archivelli, G., 176
 Armstrong, G. M., 396
 Arnold, J. E., 244
 Arnan, A., 358
 Arnold, A. D., 72
 Arnold, R., 104
 Arnstein, A., 349, 350, 351, 353
 Arrhenius, S., 222
 Arthur, J. C., 583
 Asbeck, W. K., 191, 194(6), 235, 244(111), 497
 Atterberg, A., 265
 Auer, P. L., 13
- ### B
- Baccareda, M., 395
 Bachle, O., 123
 Bachman, G. S., 333
 Bacon, L. R., 72
 Bagley, E. B., 399
 Bailey, A. I., 476, 477(82)
 Bailey, F. G., 109
 Bair, G. J., 301, 312
 Baker, W. O., 16, 366, 370, 372, 377(9), 378(7), 379(9), 382, 391(7), 403(26), 412
 Balazs, E. H., 106
 Baldauf, G. H., 487, 492(18), 499(18)
 Ballou, J. W., 414
 Banks, W. H., 171, 174, 182, 484
 Barber, E. M., 192, 453
 Bartell, F. E., 258, 270
 Bary, P., 123
 Basu, S., 106
 Bauman, G. P., 125, 237
 Beattie, J. A., 502
 Bechtel, W. G., 231, 232, 235
 Becker, G. W., 420
 Belcher, H. V., 164
 Belner, R. J., 126, 130, 131, 133(30), 134, 137(30), 138(30)
 Benner, S. G., 488
 Bennewitz, K., 332
 Benson, S. W., 172
 Beresford, F. D., 355
 Bergen, J. T., 178
 Bernal, J. D., 96, 253
 Bernath, L., 173
 Bernhardt, E. C., 624, 626
 Bestul, A. B., 164
 Beyer, C. E., 551
 Bikerman, J. J., 79, 172, 481, 482, 483, 496, 500, 501, 502
 Bilton, N. F., 192
 Bingham, E. C., 124, 158, 191, 198, 254, 255, 349, 350, 351, 352
 Bisson, E. E., 472, 473
 Blakey, B. C., 437, 442(18)
 Blakey, F. A., 355
 Blodgett, K. B., 433

- Blok, H., 214, 455
 Blokhuis, G., 157, 174
 Blott, J. F. T., 459
 Bockris, J. O'M., 94, 96
 Bockstruck, H. N., 488
 Bömmel, H. E., 333
 Bogin, C., 245
 Bondi, A., 214, 444, 445(2), 448, 452, 453(2), 458, 460, 461(7), 462(29), 463, 464(2), 476
 Bonner, W. B., 459
 Booth, F., 90, 91(20), 93(20)
 Borroff, E. M., 498
 Borsoff, V. N., 456
 Boucher, D. F., 237
 Boundy, R. H., 551
 Bowden, F. P., 430, 468, 469, 472(58), 474, 475(58), 476(58)
 Bowles, R. F., 153, 161
 Bowles, R. L., 192
 Boyer, R. F., 551
 Bozza, G., 582
 Braddicks, R., Jr., 159, 192
 Brady, A. P., 430
 Brailey, R. H., 158
 Brass, P., 124
 Brauer, P., 373
 Braun, I., 62
 Bradbury, D., 444, 445(1), 446(1), 448(1), 449(1), 450(1), 451
 Bredée, H. L., 222, 570
 Bridgman, P. W., 339, 392, 449
 Briggs, D. R., 93, 95, 108
 Briggs, L. J., 173
 Brillouin, L., 1
 Brindley, G. W., 250, 264(1), 292
 Bristol, K. E., 258
 Brodnyan, J., 393
 Brookfield, D. R., 165
 Brown, A., 374, 378
 Brown, A. G., 430, 436, 437(17), 442(17)
 Brown, A. R., 104
 Brownyard, T. L., 346
 Brüche, E., 340
 Bruggeman, D., 161
 Brunauer, S., 163
 Brunstrum, L. C., 465, 466(52a)
 Buchdahl, R., 159, 192, 213, 388, 389(31)
 Buckingham, E., 26, 199
 Budgett, R., 173
 Bueche, A. M., 101
 Bueche, F., 1, 16
 Buessen, W. R., 292, 293
 Bull, H. B., 85, 92, 105(8)
 Bungenberg de Jong, H. G., 88, 102
 Bunn, C. W., 374, 378, 379, 382
 Bunzl, M., 84, 158, 222
 Burwell, J. T., 474
 Busse, W. F., 483
 Butler, J. A. V., 110, 111, 112(89b), 114, 115
 Butta, E., 395
- C**
- Campbell, W. E., 469
 Carey, R. H., 367
 Carley, J. F., 583, 599, 630
 Carothers, W. H., 366
 Cathers, G., 106, 107(67)
 Catsiff, E., 390, 396, 397, 424
 Cerf, H., 112, 115(90), 116(90), 118(90), 119(90)
 Chaikin, M., 420, 421
 Chamberlain, N. H., 420, 421
 Chambers, R., 173
 Chapman, A. R., 228
 Chaulet, M., 363, 389(36)
 Christensen, C. J., 415
 Christiansen, E. B., 237, 466
 Clapson, W. J., 229
 Cochran, W. G., 56
 Cockbain, E. G., 430
 Coe, J. R., Jr., 25
 Coes, L., 340
 Cohn, G., 457
 Cohn, R., 265
 Colwell, R. E., 624
 Conway, B. E., 94, 96, 110, 111, 112, 113, 114, 115, 116(95), 119(92)
 Cope, W. F., 455
 Copeland, L. E., 347
 Coper, K., 337
 Cornelissen, J., 446
 Couette, M., 159, 192, 193, 219(28)
 Coughlin, J. H., 244
 Coupe, R. R., 157
 Coutney-Pratt, J. S., 476, 477(82)
 Cowan, H. J., 363
 Cram, K. H., 586
 Cravath, A. M., 458, 462(32)
 Creeth, J., 112, 119(91)
 Crick, F. H. C., 110(104), 116

Criddle, D. W., 431, 433, 438(7, 13), 439,
440(7, 13), 442(7, 13)
Cumber, C. W. N., 438
Cummings, J. D., 367, 396(5), 399, 401
Curado, J. G., 159, 169, 192
Cursin, M. P., 89
Cuthbert, F. L., 252(33), 268, 276
Cutler, M., 102

D

Dahl, R. B., 551
Dahlgren, S. E., 213
Dankov, P. D., 497
Darnell, W. H., 627
Davie, R. P., 192
Davies, J. T., 430, 442
Davis, H. E., 362, 389(34)
Davis, N., 270
Davis, R. E. D., 362, 389(34)
Dean, R. B., 173
Dear, P. S., 301, 312
de Booys, J., 222, 570
De Bruyne, N. A., 487, 495
Debye, P., 101
DeLollis, N. J., 480, 491(2)
Deryagin, B. V., 171, 497, 498(35)
Desch, C. H., 348
Deuel, H., 115
De Vries, N. F., 88, 102(16)
De Vries, O., 123
de Waele, A., 269
DeWitt, T. W., 193
Dickert, C. T., 156, 170
Dienes, G. J., 73, 75, 193, 194(43), 367
Dietz, A. G. H., 488
Dillon, H. J., 390, 391(42), 416
Dillon, R. E., 399, 551
Dixon, H. H., 173
Dobry, A., 95, 96, 98(35), 115, 120
Doede, C. M., 502
Dole, M., 85, 87(10)
Donnet, J. B., 95
Doran, R. F., 301, 312
Doty, P., 106, 108, 109(78), 115(78), 116
Downing, V. F., 171
Drennan, J. W., 115
Droste, W. H., 244
du Bois, G. B., 456, 457(22)
Duclaux, T., 84, 96
Duffie, E., 171
Dundon, M. L., 265

Dunell, B. A., 383, 384(29), 390, 391(42),
416, 419
Dusenbury, J. H., 419, 423(99)

E

Edelmann, K., 558, 559(5), 568, 570, 585
Edelson, D., 109
Ehrlich, G., 108
Eilers, H., 136
Einstein, A., 83, 137, 158, 222
Eirich, F. R., 84, 104, 107, 108(62), 113(62),
118, 158, 165, 222
Eisenberg, H., 106, 112, 116, 119
Eisenschitz, R., 118
Eitel, W., 303, 309
Elder, M. E., 138, 140(38)
Eley, D. D., 176
Eller, S. A., 497
Elliott, R., 498
Ellis, S. C., 435
Ellis, W. C., 367, 396(5)
Elm, A. C., 171
Elrod, H., 32, 35, 126, 130(19)
Elsaesser, V., 568, 582
Elton, G. A. H., 98, 99
Elyash, L. J., 193
Endell, K., 264, 316
English, S., 302, 310, 314
Enright, D. P., 314, 317, 318, 321(38),
322(38), 323(38), 326(38), 330
Epprecht, A. G., 159
Epstein, G., 488
Erbring, H., 556
Ernst, P., 157
Ettisch, E., 274, 275
Evans, M. W., 253, 268
Ewart, R. H., 64, 124, 126, 160, 192, 197
Ewers, W. E., 433
Eyring, H., 133, 410, 415, 442, 463
Exline, P. G., 466

F

Fajans, K., 316, 317
Falkenhagen, H., 85
Fankuchen, I., 377
Farrington, B. B., 458
Farrow, F. D., 28, 202, 203(58)
Faxén, H., 72
Feng, L. M., 468
Ferry, J. D., 16, 29, 79, 80(59), 115, 165,
383, 384(29), 391

- Fetsko, J. M., 153, 155
 Finkelstein, B. N., 89
 Finlayson, D., 592, 608
 Finston, M., 183
 Fischer, E. K., 192, 197, 204, 205, 211, 212,
 219, 220(21), 224(21), 226, 227, 228,
 229, 230, 231, 232, 242, 243, 244(73),
 245(21), 247(73)
 Fischer, E. W., 377
 Fitzgerald, E. R., 391
 Fitzgerald, J. V., 333
 Flory, P. J., 13, 14, 102, 114(52)
 Fogg, A., 455
 Fok, S. M., 128, 130(28), 131(28), 133(28),
 134, 137(28), 138(28), 140
 Fordyze, D. B., 115
 Forry, K. E., 334, 335
 Forslind, E., 341, 358
 Fourt, L., 440
 Fowler, R. H., 96, 253
 Frank, H. S., 253, 268
 Frei, E. H., 116, 119(109), 572
 Freitag, E. H., 474
 Freudenthal, A. M., 341, 361, 363
 Freundlich, H., 191, 202, 206, 216, 252(45),
 263, 272(17), 274, 275, 276, 278
 Frind, H., 586
 Frisch, H. C., 84, 85(4)
 Fröhlich, H., 90
 Fuchino, K., 418
 Fujino, K., 413, 415, 416, 417, 418, 420
 Fujita, H., 106, 422
 Fulcher, G. S., 309
 Fuller, C. S., 366, 372, 377(9), 379(9), 412
 Fuoss, R. M., 85, 89(13), 94, 103, 106, 107,
 108, 109, 119
 Fuwa, H., 69
- G**
- Gamble, D. L., 229
 Gans, D. M., 269
 Gardner, C. S., 13
 Gardner, H. A., 171, 191
 Garner, F. H., 457
 Gaskell, R. E., 155, 177, 179, 182, 183
 Gaskins, F. H., 399
 Gaspar, E., 623
 Gatcombe, E. K., 183
 Gavlin, G., 463
 Geddes, J. A., 192
 Geffken, C. F., 171, 485
 Gehlhoff, G., 314, 322, 324
 Gensamer, M., 327
 Gerjouy, E. J., 172
 Geyling, F. T., 398
 Gibson, R. E., 409
 Gilbert, C. S., 173
 Gilbert, R. H., 171
 Gill, F., 464, 466(49)
 Gillis, J., 101
 Gilmore, G. D., 551
 Glanville, W. H., 360
 Glasstone, S., 172, 173
 Godfrey, T. B., 25
 Goebel, W., 266
 Gohn, G. R., 367, 396(5)
 Goland, M., 494
 Goldberg, H., 49
 Goldschmidt, O., 84
 Goldschmidt, V. M., 307
 Goldstein, S., 71
 Goodeve, C. F., 162, 192, 213(29), 239(29)
 Gorbunova, K. M., 497
 Gourlay, J. S., 158
 Gouy, G., 263, 272(16)
 Grady, L. D., 229
 Graham, T. H., 216
 Gralen, N., 115
 Green, A. P., 468, 469(60)
 Green, G., 27
 Green, H., 158, 159, 169, 192, 193, 194(42),
 197(17, 18), 198, 200, 201, 206, 207(18),
 211(17, 53, 67), 212, 213, 214(18), 215,
 222, 223, 224, 225, 241, 482
 Grieger, P. F., 109
 Grim, R. E., 252(33, 61), 268, 276, 281, 284
 Gross, B., 383, 384(29)
 Grunberg, L., 452
 Gruner, E., 258
 Gulland, J. M., 112, 119(91)
 Gurevich, G., 409, 410(81)
 Gurnee, E. F., 383, 384(29)
 Guth, E., 84, 85(4), 158
 Gutmann, F., 445
 Guye, C. E., 332
 Gwathmey, A. T., 460
- H**
- Haas, E. G., 501
 Hagg, A. C., 455
 Haines, W. B., 287
 Hall, C. E., 110, 114(89a)

- Hamilton, J. S., 362, 389(34)
 Hammarsten, E., 88
 Hammerle, W. G., 414, 421
 Hamming, R. W., 384, 386(30), 396(30),
 397(30), 409(30), 410(30), 411(30),
 425(30)
 Hanig, M., 93, 95(24), 108(24)
 Hankinson, C. R., 93, 95(23), 108(23)
 Happey, F., 574
 Harkins, W. D., 269, 430, 431, 432(8), 435,
 436, 438
 Harmsen, G. J., 95, 96, 97, 98(31), 115(31),
 116(31)
 Harrison, W. N., 488
 Hart, V. E., 586
 Haslam, G. S., 101, 224
 Hatschek, E., 192, 197
 Hauser, E. A., 123, 252(31, 47), 267, 276,
 277(31), 291
 Hauth, W. E., 266
 Hawkins, S. W., 374
 Hayes, J. C., 347
 Hazlehurst, T. H., 162
 Heckler, G. E., 115
 Hedström, B. O. A., 238
 Heidebroek, E., 172, 482
 Heidelberger, M., 106
 Heidtkamp, G., 316
 Heiss, J. H., 16
 Hekker, T., 106
 Hellbruegge, H., 316
 Helmes, E., 192, 209(26)
 Hendricks, J. O., 483
 Henniker, J. C., 278
 Henry, D. C., 90
 Hermans, J. J., 6, 100, 106, 109, 110, 113,
 115(42), 118, 586
 Herschel, W. H., 195, 356
 Hess, K., 222, 224(94)
 Higginbotham, R. S., 193
 Hill, J. W., 366
 Hill, T. L., 102
 Hillier, K. W., 390, 391(38, 39), 394, 396
 (58)
 Hirsch, B., 262, 271(13)
 Hoback, W. H., 148
 Hochwalt, C. A., 247
 Höppler, F., 191
 Hoffman, L. C., 314, 317(38), 318(38), 319,
 321(38), 322(38), 323(38), 326, 334,
 335, 336
 Hoffman, R. D., 179, 181
 Hofmann, U., 252(50), 264, 276, 277
 Hofrichter, C. H., 480
 Holdridge, D. A., 252(62), 286
 Hollis-Hallett, A. C., 56
 Holm, R., 468, 469
 Holmes, D. R., 382
 Homma, T., 106
 Hopkins, I. L., 382, 384, 386(30), 396,
 397(30), 403, 405, 409, 410(30), 411(30,
 64), 425(30)
 Horino, T., 413, 415, 416(86), 417(96),
 418(96), 420(86)
 Horsley, R. A., 378, 379(24)
 Horton, F., 333, 392
 Hosler, C. L., 256, 257
 Hosler, C. R., 256, 257
 Houwink, R., 124, 244, 329, 487, 495
 Howard, J. B., 382, 399, 403(26)
 Howe, J. W., 218
 Huber, G., 115
 Huhnemörder, M., 371
 Hughes, R. L., 624
 Huizenga, J. R., 109
 Hull, H. H., 191, 194(7)
 Hunt, F. V., 469
 Hunt, J. K., 243
 Hutton, J. F., 459

 I
 Ibrahim, A. A. K., 51
 Imai, N., 102
 Inokuchi, K., 440, 441(24)

 J
 Jaccodine, R., 377
 James, D. W. F., 110, 111(89b), 112(89b),
 115
 Jarret, M. E. D., 245
 Jepson, C. H., 583
 Jerome, C. W., 227
 Johnson, A. L., 252(32, 59), 268, 282, 283
 Johnson, R. L., 472, 473
 Joly, M., 431, 435(10), 437(10), 442
 Jolly, R. E., 622
 Jones, G., 85, 87(10)
 Jones, J. M., Jr., 587
 Jones, S. P., Jr., 214, 463
 Jordan, D. O., 112, 119(91)
 Jordan, H., 124
 Juliusberger, F., 202, 216, 278

K

- Kabiell, A. M., 51
 Kagawa, J., 106
 Kalber, T. E., 171
 Kamath, P., 104, 108(62), 113(62)
 Karam, H. J., 586
 Katchalsky, A., 101, 102, 103, 104, 105,
 106, 116, 117, 118(111), 572
 Kato, T., 67, 68(44)
 Kawai, H., 413, 415, 416(86), 417(96),
 418(96), 420(86)
 Keller, A., 377, 379
 Keller, T. A., 236, 237(112), 239, 240(112)
 Kelly, W., 123
 Kendall, F. E., 106
 Kennedy, W. D., 396
 Kenrick, W. B., 173
 Kepes, M., 586
 Kern, W., 94, 102, 103, 106, 108
 Kerridge, M., 474
 Kesler, C. C., 235
 Kilb, R. W., 14
 Kimball, G., 102, 104
 Kimura, I., 69
 Kirillova, Yu. M., 497, 498(35)
 Kirkwood, J. G., 12, 13, 431, 432(8),
 438(8)
 Kishimoto, A., 422
 Klaassens, K. H., 124
 Kleinschmidt, R. V., 444, 445(1), 446(1),
 448(1), 449(1), 450(1), 451(1)
 Klemm, H. F., 73, 193, 194(43)
 Kline, D. E., 388, 389(34), 394, 395
 Knauss, C. J., 162
 Kobeko, P., 409, 410
 Kochanowsky, W., 457
 Kochev, R., 116
 Koehn, G. W., 497
 König, H., 332
 Kokhomskaya, T. N., 584
 Kolsky, H., 393, 394, 396(58)
 Kooharian, A., 363
 Kooy, J., 586
 Kortsch, W., 398
 Kranich, W. L., 125, 237
 Krasny-Ergen, W., 88, 96(15)
 Kraus, G., 499
 Krebs, G., 574
 Krieger, I. M., 29, 32, 35, 36(21), 126, 127,
 128, 129(20), 130(19, 20, 24, 25), 131,
 132(24, 25), 136(25), 138(25)
 Krigbaum, W. R., 13
 Krimm, S., 394
 Krotova, N. A., 497, 498
 Krut, H. R., 88, 102(16), 167, 261, 461
 Kubal, J. V., 115
 Künzle, O., 101, 383, 384(29)
 Kuhn, H., 116, 119
 Kuhn, W., 99, 101, 116, 119, 252(49), 276,
 383, 384(29)
 Kuhns, P. W., 159, 192, 197(32), 203, 209,
 210, 214(62), 219(32)
 Kunst, E. D., 106
 Kupinski, T. A., 314, 317(38), 318(38),
 319, 321(38), 322(38), 323(38), 326
 Kuvshinskii, E., 409, 410(81)
 Kyropoulos, S., 214

L

- Ladenburg, R., 71
 Laiderman, D. D., 235, 244(111)
 Laing, K. M., 333
 Lambert, J. M., 483
 Lamp, H., 556
 Langmuir, I., 435, 436, 440
 Lanham, A. F., 435
 Lanza, V. L., 399, 401
 Larsen, R. G., 477
 Laugier, C., 13
 Laurent, T. C., 106
 Lawley, P., 113
 Lawrence, A. S. C., 437, 442(18)
 Lawrence, K. B., 457, 467(23)
 Lea, F. M., 348, 362, 389(31)
 Leaderman, H., 34, 40(20), 383, 384(29),
 396, 423, 424
 Le Chatelier, H., 290
 Lee, R. C., 362, 389(31)
 Leet, R. H., 465, 466(52a)
 L'Hermite, R., 347, 356, 357, 362, 389(32)
 Lemin, C. E., 72
 Lester, G. R., 377
 Lethersich, W., 390, 391(40), 392(40), 397
 408
 Levy-Pascal, A. E., 128, 130(29), 131(29),
 133(29), 137(29), 138(29), 139
 Libman, E. E., 302, 309
 Lifson, S., 102, 585
 Lillie, H. R., 301, 302, 312, 313
 Lincoln, B., 471
 Lindenthal, J. W., 289

Lindner, G. F., 483
 Lindsley, C. H., 197
 Liquori, A. M., 585
 Litovitz, T. A., 446
 Litt, M., 110, 114(89a)
 Littleton, J. T., 301
 Livingston, H. K., 125
 Lobanov, V. P., 345, 352
 Lochner, J. P. A., 414
 Loeb, J., 88
 Loebering, J., 561
 Loeffel, W. F., 237
 Lohr, W. S., 363
 Lontz, J. F., 583
 Loughborough, D. L., 501
 Lowe, G. M., 28, 202, 203(58)
 Lower, G. W., 158, 159, 160(42), 213
 Lubkin, J. L., 495
 Lustig, A., 73
 Lyons, W. J., 414, 415

M

McAdams, W. H., 236, 238(113)
 McBain, J. W., 252(51), 276, 436, 437(17),
 442(17)
 McDowell, C. M., 277
 Macey, H. H., 252(34, 35), 268, 276, 279,
 291
 McIntyre, A. D., 419
 McKannan, E. C., 63
 McKelvey, J. M., 569, 583, 599, 609, 611,
 618, 620, 621, 626, 630
 McKennel, R., 193, 197(36), 209(36), 215
 (36)
 McLaren, A. D., 480
 Maclay, W. N., 106, 107(68)
 MacLennan, I. W., 462
 MacMichael, R. F., 192
 McMillan, F. R., 343
 McMillen, E. L., 238, 245
 McNamara, E. P., 301, 312
 McSkimin, H. J., 16, 390, 391(43), 392,
 393, 416
 MacWood, G. E., 55
 Maddock, B. H., 624
 Madow, B. P., 128, 130(25, 26, 27), 131,
 132(25, 26, 27), 136(25, 26, 27), 138(25,
 26, 27), 139
 Maegdefrau, E., 264
 Magde, E. W., 124, 140
 Mahnke, H. E., 458
 Mallet, M. W., 266
 Mallouk, R. S., 583, 599
 Malm, C. J., 245
 Manley, R. S., 84, 85
 Manson, J. E., 499
 Many, H. G., 583
 Marboe, E. C., 176, 307, 314, 323, 338
 Mardles, E. W. J., 269, 459
 Margaretha, H., 84, 158, 222
 Margules, M., 302
 Mark, H., 377
 Mark, M., 444, 445(1), 446(1), 448(1),
 449(1), 450(1), 451(1)
 Markovitz, H., 43, 45, 50, 80(25), 104, 193
 Marling, P. E., 247
 Maron, S. H., 29, 32(15), 35, 36(21), 126,
 127, 128, 129(20), 130, 131, 132, 133(28,
 29, 30), 134, 136, 137, 138, 139, 140
 Marquier, P., 95
 Marshall, I., 373
 Martin, C. P., 279
 Marusov, N., 466
 Marvin, R. S., 391
 Mason, P., 341, 351
 Mason, S. G., 84, 85
 Mason, W. P., 16, 390, 391(43), 393, 402,
 416
 Matthews, J. B., 459
 Maus, L., 149
 Maxwell, Bryce, 400, 419, 420
 Maxwell, J. C., 51, 55(31)
 Meader, A. L., 431, 433(7), 438(7), 439,
 442(7)
 Meissner, H. P., 487, 492(18), 497, 499
 Mele, A., 585
 Mellor, J. W., 284
 Meredith, R., 414
 Merrill, E. W., 192, 209(31), 497, 499
 Merrington, A. C., 25
 Meskat, W., 558, 578
 Metzner, A. B., 148, 237, 238(119), 465
 Mill, C. C., 171, 174, 182, 484
 Miller, J. C., 158, 161, 166, 174, 176, 178,
 183, 185
 Miller, R. G., 382
 Milne, A. A., 467, 476(54)
 Miyamoto, K., 415, 417(96), 418(96)
 Mocquot, G., 347
 Moelwyn-Hughes, E. A., 310
 Moffatt, L. R., 224
 Mohiuddin, S. O., 279

Mohr, W. D., 599
 Mol, E., 627
 Montgomery, D. J., 414, 419, 421, 423(99)
 Mooney, M., 64, 124, 126, 160, 192, 197
 Moore, A. C., 430
 Moore, C., 138, 139
 Moore, R. J., 458, 462(32)
 Moore, W. J., 442
 Morawetz, H., 104
 Morey, G. W., 304, 309
 Morgan, F., 214
 Morgan, L. B., 377
 Morgan, P., 369
 Moses, G. B., 162, 200, 458, 459(31), 461
 (31)
 Moses, S., 501
 Mozala, J., 266
 Muller, F. H., 373, 574
 Muenger, J. R., 192
 Muskat, M., 214
 Muskhelishvili, N. I., 489
 Myers, R. J., 435
 Myers, R. R., 153, 156, 159, 165, 166, 170,
 178, 185
 Mylonas, C., 487, 492, 493(23)

N

Nagy, B., 292, 293
 Nakagawa, T., 583
 Nancarrow, H. A., 378, 379(24)
 Nason, H. K., 400
 Neale, S. M., 28, 192, 202, 203(58), 214
 Needs, S. J., 453
 Neukom, H., 115
 Neville, A. M., 362, 389(35)
 Neville, H. A., 162
 Newman, S., 13
 Newton, I., 194
 Nielsen, L. E., 388, 389(31), 394
 Niemann, G., 456, 476(17)
 Nissan, A. H., 452, 457
 Nitschmann, H., 583
 Nordberg, M. E., 331
 Norton, F. H., 252(32, 59), 268, 282, 283,
 287, 301
 Nukiyama, S., 246

O

Oakes, W. G., 388, 389(33), 394
 Oberle, T. L., 474, 475

Oberst, H., 420
 Oevirk, F. W., 456, 457(22)
 Offenbach, J., 390, 396(45), 397(45)
 Ogston, A. G., 116
 Oka, S., 35, 38(22), 39, 40, 44, 45(24, 26),
 46(24), 47(24), 48(23, 24), 53(24), 54
 (24), 55(24), 56(24), 59, 60, 67, 68(44),
 194, 440
 Okada, A., 418
 Oldroyd, J. G., 51
 Olszak, W., 364
 Onsager, L., 85, 89(13)
 Oren, J. W., 457
 Ormsby, W. C., 252(41b), 270, 279(41b),
 293(41b)
 Orowan, J., 176
 Osawa, T., 102
 Oseen, C. W., 71
 O'Shaughnessy, M. T., 424
 Osmer, T. F., 367, 369(4)
 Osterle, F., 467
 Ostwald, W., 165, 191
 Oth, A., 106, 109(78), 115(78)
 Otto, R. E., 148
 Overbeek, J. Th. G., 95, 96(31), 97(31),
 98(31), 100, 104, 106, 115(31, 42), 116
 (31)
 Overholt, J. L., 171

P

Padden, F. J., 193
 Paez, A., 341
 Pakshver, A. B., 584
 Palmer, R. P., 382
 Pals, D. T. F., 106, 109, 110, 113, 118
 Pape, N. R., 372, 377(9), 379(9)
 Parker, K., 191
 Parkhurst, K. G., 435
 Parks, H. C., 191
 Parks, W., 392
 Pasley, P. R., 183
 Patberg, J. P., 460
 Patrick, R. L., 502
 Patterson, G. D., 243
 Patterson, L. A., 109
 Pattison, J. P., 419
 Pawlowski, J., 32

Pearce, C. A. R., 192, 209(27)
 Penther, C. J., 463
 Perry, G. L., 477
 Perry, J. H., 240, 246
 Peterfi, T., 205
 Peterson, C. A., 301, 310
 Philippoff, W., 29, 222, 223(95), 224(94),
 390, 391(44), 393, 397, 399, 558
 Pierce, P. E., 134, 137, 138(32), 140
 Pietsch, E., 172
 Pigford, R. L., 237
 Pigott, W. T., 592, 608, 619
 Piper, G. H., 62
 Pisapia, E. A., 356
 Pisarenko, A. P., 483
 Pitts, J. W., 488
 Plock, R. J., 13
 Podszus, E., 266
 Pohl, H. A., 454
 Poiseuille, J. L. M., 85, 195
 Poole, J. P., 301, 322, 325, 327, 329, 339
 Poretskayeo, A. P., 171
 Poritsky, H., 456
 Pouyet, J., 110, 112
 Powell, A. S., 139
 Powell, B. D., 430
 Powell, R. E., 463
 Powers, T. C., 346
 Preissmann, A., 383, 384(29)
 Price, S. J. W., 419
 Pryce-Jones, J., 192, 209
 Puddington, I. E., 162, 200, 458, 459(31),
 461(31)
 Pupke, H., 563, 568

Q

Quincke, G., 263, 272(14)

R

Rabinowicz, E., 472, 473(69a), 476, 477
 (77)
 Rabinowitsch, B., 23, 118, 203, 559, 561
 Ramaya, K. S., 464
 Rao, K. L., 362
 Rayleigh, J. W. S., 66
 Ree, T., 133
 Reed, C. E., 252(31), 367, 377(31)
 Reed, J. C., 237, 238(119), 465
 Reed, R. F., 169

Reiner, M., 23, 26, 27, 28, 33, 34, 158, 163,
 200, 203, 343, 347, 349, 350, 351, 352,
 353, 358(23), 361, 400
 Reissner, E., 494, 495
 Renfrew, A., 369
 Reynolds, O., 176, 202, 217, 218, 482
 Rhodes, E., 123
 Rice, S. A., 116
 Rich, S. R., 162, 193
 Richards, R. B., 374, 391, 392, 403
 Richmond, J. C., 488
 Ries, E. D., 431
 Riseman, J., 12
 Riwin, R., 22, 200, 483
 Roberts, B. R., 560
 Roberts, J. E., 193, 586
 Robinson, D. W., 388, 389(33), 394
 Robinson, H. A., 301, 310
 Robinson, J. V., 158
 Roe, C., 124
 Röder, H. L., 191
 Rötger, H., 332, 334, 335
 Rogers, W. F., 279
 Romberg, J. W., 192
 Rona, P., 263, 272(17), 274, 275
 Rosen, B., 104, 108(62), 113(62)
 Rosenow, M., 258
 Rossmassler, S. A., 415
 Rost, U., 445
 Roth, W., 162, 193
 Rouse, H., 218
 Rouse, P. E., Jr., 1, 10, 11
 Rowell, H. S., 592, 608
 Rucker, N., 480, 491(2)
 Ruehrwein, R. A., 464
 Ruff, O., 262, 266, 271(13)
 Russell, R. J., 464, 466(49)
 Ryan, N. W., 237, 466

S

Sack, R., 90
 Sack, R. A., 433
 Sackett, R. D., 624
 Sadron, C., 116
 Saibel, E. A., 467
 Saini, G., 104, 106(61)
 Saito, N., 45
 Salmang, H., 258
 Samelson, H., 102

- Sandvik, O., 49
 Sato, Y., 39, 48(23), 440
 Sauer, J. A., 388, 389(34), 394, 395(61)
 Sauerwald, F., 584, 585
 Saunders, B., 245
 Saville, A. K., 414, 421
 Scarr, R. F., 155
 Schaefer, F. J., 435, 436(15), 440
 Schaeffer, W. D., 155
 Schaeffgen, J. R., 14, 106, 108(72)
 Schallamach, A., 470, 471
 Schimmel, G., 340
 Schmieder, K., 388, 389(32), 413, 423
 Schooten, J. V., 95, 96(31), 97(31), 98(31),
 115(31), 116(31)
 Schramek, W., 566, 575
 Schreck, C., 571
 Schremp, F. W., 79, 80(59)
 Schulman, J. H., 438, 476
 Schultz-Grunow, F., 585
 Schultz, W., 109
 Schulz, E. F., 367
 Schurz, J., 585
 Schwander, H., 112, 115(90), 116(90), 118,
 119(90)
 Schweyer, H. E., 192, 224
 Scott, G. W., 178
 Scott Blair, G. W., 191, 343, 347
 Scott, J. R., 62, 76, 172
 Sekar, K., 123
 Shack, W., 623
 Shapovalova, A. I., 483
 Shelton, G. R., 302, 309
 Sherman, J., 301, 312
 Sherman, P., 441
 Shooter, K. V., 470, 471, 472(68)
 Signer, R., 103, 109(56), 112, 115(90), 116
 (90), 118, 119(90)
 Silverman, S., 414
 Simha, R., 84, 85(4), 158
 Simmons, L. M., 445
 Simonds, H. R., 623
 Singleterry, C. R., 458, 459(27)
 Sippel, A., 568, 575
 Sisko, A. W., 127, 134, 137(33), 138(33)
 Sisson, W. A., 377
 Sittel, K., 10, 11
 Sjodahl, L., 168, 174
 Slichter, W. P., 382
 Smekal, A., 469
 Smith, A. H., 157
 Smith, E. H., 104
 Smith, G. H., 462, 466
 Smith, H. F., 123, 124
 Smith, H. L., 245
 Smith, J. W., 192, 209(23)
 Smith, T. L., 79, 80(59)
 Sovokin, S. M., 171
 Spangler, R. D., 63
 Sparta, T. A., 152,
 Speakman, J. B., 414, 421
 Spencer, R. S., 399, 551
 Spies, G. J., 496, 497(29)
 Sproule, L. W., 460
 Stacey, K., 116
 Stanier, J., 116
 Staudinger, H., 102
 Stefan, M. J., 169, 194, 482
 Steffens, H., 584, 585
 Stein, R. S., 394
 Sternberg, N., 116, 117, 118(111)
 Stevens, H. P., 123
 Stevens, W. E., 237, 466
 Stokes, G. G., 22
 Stone, E. E., 458, 459(27)
 Stormer, A. J., 159
 Strasburger, H., 183
 Strauss, U. P., 94, 104, 106(26), 107, 108,
 109, 119
 Streeter, V. L., 592
 Strong, J. T., 474
 Strub, R. A., 583, 592, 597
 Suriani, L. R., 158
 Susuki, K., 102
 Sward, G. G., 171, 191
 Swickert, M. A., 473
 Swindells, J. F., 25
 Swire, E. A., 463
- T
- Tabor, D., 468, 469(58), 471, 472(58, 68),
 475(58), 476, 477(77)
 Tabor, W., 458
 Tachibana, T., 440, 441(24)
 Takami, A., 44, 45(26), 59
 Tammann, G., 303, 305
 Tanasawa, Y., 246
 Taylor, A. M., 228
 Taylor, G. I., 219, 393
 Taylor, N. W., 301, 312
 Teinowitz, M., 358(23)
 Temperley, H. N. V., 173

Tendeloo, H. J. C., 88, 102(16)
 Terzaghi, M., 98
 Thakur, R. L., 314, 317(38), 318(38), 319,
 321, 322, 323, 326(38)
 Thiele, H., 556
 Thimm, J. E., 213
 Thomas, F. G., 361
 Thomas, M., 314, 322, 324
 Thompson, A. B., 373
 Thuman, W. C., 436, 437(17), 442(17)
 Thurn, H., 388, 389(35)
 Tipton, H., 420, 423
 Tobolsky, A. V., 383, 384(29), 388, 390,
 394, 396(45), 397(45), 410, 413
 Todd, W. D., 192, 214, 215
 Toll, K. G., 624
 Tollenaar, D., 157
 Tool, A. Q., 304
 Tordella, J. P., 399, 585, 622
 Torroja, E., 341, 346, 361
 Towsley, F. E., 551
 Trapeznikov, A. A., 440, 476
 Traxler, R. N., 165, 192, 224
 Treves, D., 116, 119(109)
 Tritsch, L., 191
 Tschoegl, N. W., 440
 Tyson, T. K., 214, 463

U

Udy, D. C., 115
 Ulevitch, I. N., 126, 138
 Umstatter, H., 457
 Ungar, G., 58
 Usher, F. L., 252(48), 276, 277

V

Vail, J. G., 480
 Vand, V., 84, 96, 158
 Van den Akker, J. A., 491, 497(22)
 van Gils, G. E., 124
 van Iterson, F. K. Th., 252(30), 267
 Van Loo, M., 235, 244(111)
 van Praagh, G., 271
 Van Selms, E. G., 167, 461
 Vasileff, S., 332
 Vaughan, W. A., 502
 Veis, A., 109
 Verbeck, G. J., 347
 Verdery, R. B., 483
 Verwey, E. J. W., 259, 261

Villforth, F. J., Jr., 192
 Vincent, R. S., 173
 Vinogradov, G., 459
 Voet, A., 151, 153, 158, 161, 171, 485
 Vogel, H., 445
 Vogelpohl, G., 455, 475
 Volkova, Z. V., 278
 von Buzagh, A., 274, 284
 von Engelhardt, W., 252(46), 276
 von Helmholtz, H., 263, 272(15)
 von Mohrenstein, A., 456, 476(17)
 von Schlippe, B., 466
 von Smoluchowsky, M., 87
 Voong, E. T. L., 419, 423(99)
 Voyutskii, S. S., 483

W

Wachholz, F., 191, 194(6)
 Wada, Y., 388, 389(36)
 Wahab, C., 123
 Wake, W. C., 497, 498
 Wakelin, J. H., 419, 423
 Walker, W. C., 149, 151, 153, 155, 156, 159,
 160(42), 170, 213
 Wall, F. T., 109, 115
 Walther, C., 444, 445(2)
 Walther, W., 392, 408
 Ward, A. F. H., 192
 Washburn, E. W., 302, 309
 Waterman, H. I., 446
 Watkins, J. M., 63
 Watson, J. D., 110(104), 116
 Watson, M. T., 396
 Weber, C., 456
 Weber, R., 331
 Wegel, R. L., 392, 408
 Wehmer, F. J., 483
 Weir, C. E., 392
 Weissenberg, K., 118, 569, 571, 586
 Weith, A. J., 623
 Weltmann, R. N., 159, 161, 192, 197(32),
 198, 201, 202, 203, 206, 207, 208, 209,
 210, 211, 212, 213, 214, 219(32), 221,
 222, 223, 224, 225, 236, 237, 238(59),
 114), 239, 240(112)
 Wentz, R. P., 400
 Westover, R. F., 400
 Weyl, W. A., 252(41b), 253, 259, 270, 279
 (41b), 293(41b), 307, 311, 312, 314,
 315(39), 317, 318(38), 319, 321(38),
 322(38), 323, 326(38), 334, 338

- White, J. R., 476, 477(83)
Whitefield, G. W., 162, 192, 213(29), 239
(29)
Whitwell, J. C., 586
Wicker, C. R., 192
Wiederhorn, N. M., 104
Wier, J. E., 480, 491(2)
Wiley, R. M., 551
Wilhelm, R. H., 237
Wille, R., 571
Williams, I., 193, 194(44)
Williams, P. S., 192, 209(25), 213(25)
Williamson, R. V., 202, 243
Williamson, W. O., 268, 288, 293
Wilm, K., 264
Wilson, E. O., 252(23), 265
Wilson, J. M., 106
Wilson, J. W., 466
Wilson, R., 469, 470(63)
Wilson, R. E., 431
Winding, C. C., 125, 237
Winning, M. D., 237
Wint, R. F., 244
Wismer, K. L., 173
Witt, R. K., 501
Witucki, R. M., 252(41b), 270, 279(41b),
293(41b)
Wolf, K., 388, 389(32), 413, 423
Wolff, H., 171
Wood, G. F., 457
Woodward, A. E., 394, 395(61)
Woodward, J. G., 65, 67, 162, 193
Wostenholm, J. G., 476
Wroughton, D. M., 237
Wu, F. C., 115
- Y
- Yamamoto, K., 388, 389(36)
Yap, W., 482
- Z
- Zehmisch, E., 566, 575
Zeidler, G., 171
Zettlemoyer, A. C., 149, 151, 153, 155, 156,
158, 159, 160(42), 166, 170, 185, 213
Zimm, B. H., 11(6), 13, 14
Zimmer, J. C., 460
Zisman, W. A., 454
Zocher, H., 337
Zwanzig, R. W., 13

SUBJECT INDEX

(See also individual Tables of Contents.) Figure in parentheses following page number is equation number; F signifies figure, T signifies table.

A

- Abrasive particles, 474
- Absorption (loss) peaks, polyethylene, 395T
- Acceptability criteria, injection molding, 544, 545, 549
- Acetic acid, 252
- Acetylene tetrabromide, contact angle, 258
- Acrylic solutions, flow characteristics, 585
- Activation energy of flow, 306, 612, *see also* Flow, Relaxation
 - diffusing ions, in glass, 333-335
 - fatty acids, 442
 - rubber friction, 471
- Adherents, 179, 481F
 - tensile strength, 484
- Adhesion
 - boundary layers, 479
 - molecular forces, 497
 - true, 501
- Adhesive film, 479, 481F, 485
 - cylindrical, 496
 - modulus, 488
 - necking, 500
 - work-hardening, 500
- Adhesive joint, 488, 489, 492
 - failing of lap joint, 494
- Adhesives, *see also* Adhesive film, Adhesive joint
 - adherend attraction, 502
 - application, 182
 - boundary layers, 487
 - chemical reactions, 488
 - chemical setting, 486
 - contraction, 486
 - cross-linking, 486
 - displacing ability, 480
 - domains, 500
 - failure, 489
 - filamentation, 484
 - flow, stress concentration, 489
 - hundred shrinkage, 487
 - interpenetration, 480
 - interphase, 501
 - liquid, break as solid, 484
 - local stress, 489
 - physical changes, 486
 - polymerization, 486
 - rate of setting, 485
 - set, 485
 - solidification, 486
 - solvent removal, 486
 - splitting, rolling cylinder, (*see also* Ink, Rolling cylinder), 485
 - strength, 487, 490, 500
 - and dimensions, 491
 - and nature of adhesive, 491
 - stressed lap joint, 495F
 - tapes, stripping, 483
 - tensile strength, 496
 - test by centrifuging, 501
 - test by shaking, 501
 - thickness and rupture, 499F
 - three-phase boundary, 491
 - weak bond, 490
 - wetting ability, 480
- Adiabatic viscous heating, 580
- Adsorption
 - of ions, 91
 - particle enlargement, 164
 - water, clays and quartz, 259T
- Aerosol OT, 226T
- Agar, 229
- Aggregate size and color strength, 231
- Aggregation, fourth state, 267
- Aging dispersions, 219
- Air
 - assisting cavitation, 174
 - channels, effect on tack, 484
 - entrapment, injection molding, 519
 - rate of displacement, 480

- Alcohols, 446
 long chain, surface viscosity, 437
 Alginates, 229
 Alkali barium silicate glass, 326
 Alkali hydroxides, effect on clay, 283
 Alkali ions, in glass, 316
 Alkali redistribution, in glass, 331
 Alkali silicate glasses, 316, 327, 332, 334
 internal friction, 335F
 Alumina, 266
 Aluminophosphate glass, 323
 Aluminum alloy, model value, 475T
 Aluminum, friction, 469
 Aluminum, model value, 475T
 Aluminum sulfate, 273
 Ammonia, liquid, 253, 255
 Ammonium alginate, 141
 Amplitude oscillation, plate viscometer, 65
 Andrade's law, 221
 Anelastic (inelastic, nonelastic) liquid, 29
 Anelasticity (inelastic behavior, non-elasticity), 332, *see also* Creep, Friction, internal, Hysteresis, Viscosity
 Angular displacement, 43, 54, 59
 concentric cylinders, 50
 equation, 43(29)
 spherical, 59(56)
 and torque, 41
 Angular mixer, 149F
 Angular velocity, 30, 31, 53
 concentric cylinders, 129
 double core, 62
 sphere, 57
 Animal glue, 486
 Anion-cation ratio, 317, 319, 321
 Anion deformation, 260
 Anisotropy, 567
 Annealing, nylons, effect on moduli, 413
 Antimony oxide, suspension, 224F
 Antoine equation, 445(1)
 Apidamide polyhexamethylene, 375F, 376F
 Apparent fluidity, viscosity, *see* Fluidity, Viscosity
 Apron nip transfer, 151F
 Argon, 254, 306
 Arrhenius' law, 123(1), 222(20)
 Asperities, elastic, 470
 Asphalts, 233
 mineral powders in, 224
 Attapulgit, base exchange capacity, 281
 Attenuation coefficient, *see* Damping, Friction, internal
 Attraction, interface, 503
 Axial velocity penetrometer, 78
- B**
- Back flow, 619
 Ball mill, 147, 230, 231
 Band viscometer, 191, 194
 Bank, roll flow, 183
 Barium salts, 205, 226T, 265, 274
 Barrel rotating extruder, 591
 Bearing, *see also* Load-carrying design, 456
 equations, 454
 frictional drag, 456
 hydrodynamic separation, 456
 journal, 454, 467
 and slider, 443
 polymeric, 457, 470
 pressure distribution, 467
 sealing, 443
 thrust, 455
 Bending (flexural rigidity)
 nylon 6, effect of conditions, 420
 nylon 66, 419T
 strength, concrete, 343
 Bentonite, 267
 platelets in grease, 458
 suspension, 272
 Benzene, 270, 306
 concrete immersion, 348
 flow through clay, 279
 Beryllia, 266
 Beryllium fluoride, 308
 glasses, 316
 Bessel functions, 45, 46
 Binder, in concrete, 342
 Bingham body, solid, 28(13), 198(5), 199
 capillary flow, 25(10)
 cement, 345
 flow in pipes, plastics, 238
 friction factor, plastics, 238(23)
 in grease, 458
 rotating cylinder viscometer, 33
 yield value, 212

- Birefringence, stress, Optical anisotropy,
 44, 568
 cupra fiber, 582F
 DNA, 112
 streaming, 103
 Blade pressure, 152
 Bleeding, concrete, 345
 Blemishes, injection molding, 544
 Block shear test, 495
 Blom tack tester, 171
 Body force, 36
 Boltzmann's superposition principle,
 nylons, 423
 Bond-angle bending, 390
 Bonds, glasses, 305
 Borosilicate glasses, 329, 331
 Booth's equation, 92(13)
 Borates, 305
 Boundary conditions, 37, 39, 50
 cone and plate, 61
 plate viscometer, 66, 67
 rotating cylinders, 31
 Boundary flow, rolling, 179
 Boundary layers, adhesion, 479, 481F
 Boundary lubrication, 467
 Box distribution, 417, 426
 Brabender viscometer, 192
 Branched molecules, 13, 14
 Breaking, *see also* Rupture, Yield stress
 injection molding, 541
 Brinell hardness, 474
 Brittleness, polyethylene, 403
 Brookfield viscometer, 159, 192
 Brownian motion, 3-5, 7
 clay, 277
 Brush marks, 244
 Brushing, 190, 243, 244
 Bubbles
 injection molding, 537, 541
 roll flow, 186
 tube, 191
 Buckingham equation, 199(9), 465
 Buckingham-Reiner equation, 26, 345
 Bulk modulus, *see* Modulus bulk
 Bulk viscosity, *see* Viscosity, bulk
 Burma shave, 241T
 Burgers body, 360F
 Butanol, flocculation by, 229
 Butt joint, 491, 492F, 493F
- C**
- Cadmium, friction, 469
 Calcium alkylphenate, 439
 Calcium carbonate, 186
 dispersion, 174
 suspension, 226T
 Calcium polymethacrylate, 115
 Calcium stearate, 477
 Calendering of plastics, 177, 182
 Cantilever beam apparatus, 420
 Capillary, *see also* Pipe
 action, paper on ink, 157
 data comparison, 128
 displacement viscometer, 127
 flow, *see* Flow, capillary, Viscometers
 orientation effect, 561
 rheometer, 399
 viscometer, 21, 117, 126, 191, 195, 203,
 see also Viscometers
 water, cement, 348
 Caplastometer, 586
 Carbides, 307
 Carbon black, 232F
 suspension, 95, 198, 201, 224F, 226T
 Carbon tetrachloride, 270
 Carbon, thixotropy of, 276
 Carborundum, colloidal, 99
 Carboxymethyl cellulose, 106, 118
 Caseinate sodium, 93, 94, 104
 Casting slip, 266
 Cataphoretic potential, 89
 Cations
 central in glasses, 308
 hydrated, 273
 maximum screening, 253
 network-forming, 308, 319
 size, effect on glass, and glass poly-
 merization, 317, 319
 Cavitation, 173, 174, 183, 453
 in inks, 175
 in printing, 155
 rate, 186
 Cavities, roll flow, 185
 Cellophane, 480
 printing, 155
 Cellulose, orientation, 377
 Cellulose acetate
 critical extrusion rate, 400
 stripping of a, 498F
 Cellulose cuprammonium, 578, 581

- Cellulose nitrate, stripping of a, 498F
- Cement(s), 233, 342
- age hardening, 347
 - bending, 349
 - bond formation, 344
 - capillary pores, 347
 - chemical hardening, 349, 361
 - coated, deformation of, 351
 - concrete, 341
 - creep fluidity, 349
 - creep viscosities, 353
 - drying-out, 346
 - equilibration rate, 349
 - flow, 354
 - fresh, 342, 344, 345
 - gel pores, 347
 - hardening under water, 348
 - hydration, 348
 - Hooke's law, 351
 - loading cycles, 351
 - as Maxwell body, 350
 - mortar, creep curves, 350F
 - natural, 342
 - particles diameter, 346
 - paste, fresh, 342, 344
 - pore volume, 347
 - Portland, 342
 - pumping pressure, 345
 - sagging, 349
 - seepage, 351
 - set, 342, 350, 350F, 351, 354
 - shrinkage cracks, 347
 - shrinkage irreversible, 349
 - swelling, 348
 - viscosity, 350
 - water, 346, 348
- Center of mass, translation, 7
- Ceramic(s), 250, 266
- bodies, drying process, 286
 - slurries, 233
- Cesium disilicate glass, 330
- Chain molecules, *see also* Configuration, Folding Macromolecules, Segment
- alignment, fiber formation, 567, 573
 - curling, 557
 - end-to-end distance, 13, 100, 101
 - entanglement, 383
 - entropy, *see* Configuration
 - flexibility, mobility, in polyethylene, 388
 - free coiling, 2, 101
 - helical structure, 116
 - length, 557
 - normal modes, 8
 - parallelizing, 558
 - random flexibility and temperature, 451
 - spring representation, 2
 - unrolling in spinnerette, 556
- Change-can mixer, 147F
- Charge
- colloidal particle, 89
 - density, surface, 91
 - distribution, 85
 - net, of polyion, 102
- Charged lattices, 122
- Cheese, shrinkage cracks, 347
- Chemical precipitation, 564
- Chrome plate, model value, 475T
- Chrome yellow, 216, 226T
- Chromium, friction, 469
- Clay, *see also* Clay-water
- adsorption of water, 258, 259T
 - anisotropy, drying shrinkage, 288
 - bodies, microstructure, 293
 - buffering action, 282
 - dimensions, 277T
 - drying shrinkage, 287F
 - filter cake, 279
 - flow curves, 166F
 - green strength, 286
 - heat of wetting, 258, 259T
 - interaction with electrolytes, 281
 - ion sheets, 251
 - leather hard, 286
 - minerals, 250, 251
 - structure, 264
 - mixture, randomly oriented, 292
 - particles, 264
 - primary shrinkage, 287
 - sedimentation, 270
 - slip, 284
 - sticky stage, 284
 - surface energy, 258
 - thixotropy, 277T
 - wet, plasticity, 251
 - white hard, 286
- Clay-water, 291, 292
- deformation, effect of additives, 293
 - mixtures, drying shrinkage, 250

- suspension, 241T
- systems, behavior, 252
- Clearance, shear rate, 623
- Coagulant diffusion, 567
- Coagulation, 555
 - and orientation fiber formation, 568
 - profile, 563
- Coating, 190, 220
- Coaxial, concentric cylinder viscometer,
 - Couette, 29, 77, 116, 125, 159, 192, 193, 196, 200, 204, 210, *see also*
 - Viscometer
 - glass viscosity, 302
- Coaxial cylinders, cemented, 495
- Coefficient of friction, *see* Friction external
- Coefficient of viscosity, *see* Viscosity
- Cohesive strength, liquids, 172
- Cohol, flocculation by, 229
- Coil, coiling, *see* Chain molecules, Configuration, Folding
- Cold drawing, 371
 - polyethylene, 378
 - polyethylene sebacate, 367
 - selective gliding, 377
- Collision frequency, suspended spheres, 84
- Colloids, 291
 - dispersion, 121
 - hydrophobic, electroviscosity, 94
 - mill, 147
 - solutions, electroviscous effect, 88
 - stability, 261
- Color strength, 232F
- Compacting glass, 332
- Compaction, polymer granules, 527
- Complex compliance, *see* Elastic compliance
- Complex modulus, *see* Modulus
- Compressibility, 173, 449
 - bulk moduli, polyethylene, 392
 - dynamic, polyethylene, 393
- Compression, 21, *see also* Plastometers tests, 292, 370
- Concentration
 - dependence, 123
 - polyelectrolytes, 106
 - effect, latex, 142
 - effect on viscosity, *see* Viscosity
 - volume, 223
- Concentric-cylinder apparatus, *see* Coaxial cylinder viscometer
- Concentric-sphere viscometer, 57
- Concrete
 - after effect, elastic, 359
 - aggregates, 361
 - arches, 363
 - bleeding, 345
 - creep secondary, 362
 - creep viscosity, 361
 - dams, 348
 - deflection instantaneous, 358
 - delayed strain, 359
 - elastic analysis, 363
 - fore-effect, elastic, 359
 - fracture localized, 363
 - fresh, 342, 356
 - harshness, 356
 - internal friction, 357
 - limit analysis, 363
 - macrostresses, 358
 - microstresses, 358
 - permanent set, 358
 - plasticity, 358, 359, 363
 - prestressed, 363
 - reinforced, 343, 363
 - remoulding, 358
 - resilience, 356(6)
 - rupture, 357, 358
 - shear resistance, 356, 357F
 - seepage theory, 362
 - segregation, 342, 356
 - set, 342, 358
 - shrinkage, 362
 - stickiness, 356
 - strength, 343
 - swelling, 362
 - under water, 362
 - viscous deformation, 359
 - voids, 361
 - workability, 342
- Conductance, 98
- Conductivity specific, 95
- Cone and disk, rim velocity, 180
- Cone penetrometer, 459
- Cone and plate viscometer, 61, 127, 160, 193, 197, 215
- Configurations 99, *see also* Chain molecules, Macromolecules, Relaxation mechanism, Polymer solvent

- Configurations—*Continued*
 changes in spinning, 566
 and flow anomalies, 558
 polyelectrolytes, 115
Consistency, 221, 233, 241
 ink, 148
Contact angle, 258
 acetylene tetrabromide, 258
Contact area, 468
Contact heating, friction, 474
Contact points, mineral oil, 172F
Container glass, 329
Continuous measurement, melt viscosity, 584
Control, 233
Cooling time, injection molding, 545, 549
Coordination number, 306
Copolymer, *see* Polymer, also individual copolymer
Copper, 306
 friction, 469, 472
 model value, 475T
Copper-palmitate, 477
Copper sulfide, 477
Core release, injection molding, 539
Corn
 industrial viscometer, 231
 starch paste, 204
 syrup, 609, 610
Cornelissen-Waterman equation, 446
Corner-effect, 64
Corrosion, 477
Couette correction, 24
Couette, *see* Coaxial
Counter ions, 108
 sharing, 115
Crack propagation, in adhesive, 502
Crazing, 333–335F
Creep, 360, 384, 396
 asymptote, 386F
 asymptotic value, polyethylene, 397
 concrete, 343
 and crystallinity, 369
 curve, 383
 cement, 350F
 fluidity, cement, 349
 grease, 460
 hard rubber, 409
 limiting value, 361
 lubricating grease, 467
 nylons, 423
 polyethylene, 367
 primary, 359F, 360
 secondary, 359F, 362
 by seepage, cement, 351
 viscosity, cement, 353, 354
Creep function, 384, 386, 409, 411
 hard rubber, 410
 from relaxation function, 396
Crepe, *see* Rubber
Cristobalite, 318
Cross-linked polymer, *see* Polymer, cross-linked, Rubber
Cross-linking, 557
 effect on modulus frequency curve, 392
Crotonic acid, vinyl acetate, copolymer, 96
Crowding effect, non-Newtonian, 141
Crushing strength, concrete, 343
Crystallinity
 effect on modulus frequency curve, 392
 on polymers, 369F, 380
 fiber, 574
 oriented, in fibers, 371
Crystallites, 374
 rotation, polymers, 382
Crystallization
 amorphous polymers, 373
 during fiber formation, 573
 polymers, mechanism, 377
 rates, 305
Cuprammonium rayon, 568, 575
Curtains, 244
Cycle limiting, 544, 549F
Cycle time, 549
 injection molding, 509, 544, 545
Cyclohexylethyl-1,1-Bis, *n*-nonane, 445F
Cylinders, *see* Coaxial cylinders, Viscometer
- D
- Dacron, *see* Polyethylene Terephthalate
Damping, *see also* Absorption, Friction, internal, Hysteresis, Logarithmic decrement
 couple, 54
 oscillating sphere, 60
 glass fibers, 332
 surface torsion pendulum, 433
Dead time, injection molding, 509, 513, 545
Deaggregation, 226, 231

- Debye-Hückel radius, 89, 100, 106
 α -Decalin heneicosane, 445F
Decrement, *see* Logarithmic decrement
Deflocculation, 226
 clay, 283
Defoamer, dimethyl silicone, 442
Deformation, *see also* Displacement,
 Strain
 forms of, cement, 447
Density
 liquid, 24
 molding, 514
 polyethylene, effect of draw speed,
 405F
Deoxyribonucleate (DNA), 110-116
 birefringence, 112
 effect of rate of shear, 118
 stiffness, 110
 urea denaturation, 116
De-sintering, 406
de Waele-Ostwald's law, 28, 34
Dextrin, 229
Diamond
 cutting, 340
 scratch, healing, 336
Die
 characteristic, 613, 622
 Newtonian, 617F
 non-Newtonian, 617F
 equation, extruder, 604
 flow resistance, 608
 geometrically similar, 616
Dielectric constant, 86, 94, 95, 98, 108,
 253
 dispersion, 161
 ink, 161
Dielectric loss, 161
Diesters, 450T
Diffusion, translational and general, (*see*
 also Self-diffusion), 6
 coagulant, 567
 close-packed films barriers, 431
 processes, in glass, 330
 of water, in cement, 348
 in nylon-6, 422
Dilatancy, 163, 165, 242, 293
 concentration limits, 226T
 effect of surface active agent, 226
 rheopexy, comparison, 216
 sand-water, 290
Dilatant flow, 202, 203, 213, 214
 change with treatment, 220
 curve, 195
 thixotropic, 214
Dilatant material, friction factor, 238
 (24)
Dimethylformamide, 578
Dimethyl silicone as defoamer, 442
Dimethyl siloxane fluids, 456
Dip-lacquer, 245
Dipole surface, 260
Dipping, 190, 220, 243
Discharge
 closed, 595
 elimination, 537
 injection molding, 510, 545
 loci, 545, 548
 open, 595
Discone, 178, 182, 183, 186
Disentanglement, 558, *see also* Entangle-
 ment
Disk viscometer, 53-56, 179, 193, 434F
Dispersion, 163, 240
 aging, 219
 form of, 222
 region, nylons, 413
Dissipation energy, *see* Energy dissipa-
 tion
Dissipation extruder power, 596
Dissociation, degree of, 103
Distribution
 charges, 85
 function, 5
 end-to-end length, 7
 Gaussian, 7
 relaxation times, 384
 stress butt joints, 491
Dorn effect, 273
Double-bob method, apparent fluidity,
 35
Double cone viscometer, 63
Double layer, 91, *see also* Electrical,
 double layer
 curvature, 89
 diffuse, electrical, 262, 263
 interaction, 97
 overlapping, 96
 radius, 98
Doublet, suspended spheres, 84

- Draft, injection molding, 539
 Drag flow, 618, *see also* Flow
 boundary conditions, 593(10)
 constant, 600
 differential equation, 593
 screw pump, 592
 shape factor, 594
 velocity distribution, 600
 volume rate, 594(12), 600
 Drage viscometer, 159
 Draw ratios, 380
 and anisotropy, 419
 Drawing, effect on behavior, 418
 Drilling muds, 279
 Droplet size, mean, in gas-atomizing
 nozzle, 246
 Dry spinning, 562, 563, 581
 Drying
 process, ceramic bodies, 286
 shrinkage, clays, 287F, 288
 Dumbbell
 elastic, 2-6
 relaxation time, 7
 Dyeability, 574
 Dynamic,
 complex modulus, *see* Modulus, com-
 plex, dynamic
 loss factor (mechanical loss factor),
 383, 388, 389F
 modulus, 383, 385, 387F, *see also* Modu-
 lus
 polyethylene, 391
 in shear, polyethylene, 389F
 properties, 42
 viscosity-frequency product, 385
- E**
- Ebonite, *see* Hard rubber
 Eddy currents, 217
 Edge effect, 19, 20, 40, 51, 53
 plate viscometer, 68
 Eilers equation, 136(33)
 Einstein's equation, 83(1), 92, 137(38),
 222, 353(3)
 Ejector plate, 508
 Elastic, *see also* Elasticity
 after effect, glass, 332
 analysis, concrete, 363
 chain, 7
 compliance (reciprocal modulus),
 in channel flow, 520
 dumbbell, 2, 3, 6
 length, 4
 mean coordinate, 4
 fluid, 9
 limit, 367
 in wear, 474
 modulus, *see* Elasticity, Modulus
 (moduli)
 recovery (rebound), grease, 459F
 Elasticity
 complex, 19
 delayed, *see* Elasticity, retarded, Fric-
 tion, internal, Voigt body
 dyanmic, *see* Four parameter model,
 Maxwell body, Voigt body
 glass, 301
 interfacial, 439F, 440
 retarded, *see also* Viscoelastic
 glass, 312
 mortar, 354
 static surface, 436
 Elastico-viscous liquids, *see* Elasticity,
 Maxwell body, Non-Newtonian
 liquids
 Elastomer, *see* Rubbers, Chain molecules
 Electrical, *see also* Double layer
 conductivity, suspensions, 272
 currents, local, electrophoretic, 88
 double layer, 88, 262, 263, 272-274, 278
 energy, dissipated, 91
 forces, 88
 long range, 276
 potential, 101
 Electrokinetic potential, 88, 92, 263
 at glass interfaces, 275F
 Electrolytes, in latex, 140, 142
 Electroneutrality, 253
 Electroosmosis, 273, 274
 Electrophoresis, 273, 274
 Electrostatic contribution, 86, 87
 Electrostatic repulsion, 99
 Electroviscous effect, 87
 first, 90
 and ionic strength, 89
 second, 96, 115
 third, 99
 Emulsifier, 138
 polymer ratio, 139
 Emulsions
 effect of concentration, 222
 inversion, 225

- oil-water, 224
- spinning, 583
- Enamels, 242T, 339, 488
 - brushed black, flow properties, 244T
- End effect, 19, 20, 24, 55, 64, 196
 - correction, 37, 53, 197T, 400
 - oscillating cylinder, 46
 - rotational viscometer, 37
- End-to-end length, *see also* Chain molecules
 - distribution function, 7
- End force, penetrometer, 79
- Energy
 - activation, *see* Activation energy
 - barriers, viscous flow, 311, 319
 - free, electrical, 100, 101(23), (24)
 - input, 160, 162
 - storage, 9 *see also* Elastic compliance
- Energy dissipation, 9, 83, 86, 88, 96, 466,
 - see also* Damping, Dynamic loss
- bearing, 455
- Entropy, aqueous solutions, 254
- Epitaxis, Epitaxy, 268, 501
 - on glass, methylene blue, 337
- Equation of motion, 4(5), 45, 55, *see also*
 - Navier-Stokes equation
- Equation of state, 430, 538(16)
- Equilibrium, flow curves, 211, 213
- Ethylhexyl-bis-2, sebacate, 445F
- Ethylhexyl-di-2, sebacate, 449F
- Euler-MacLaurin sum formula, 32
- Euler method, 35
- Evaporation, effect on viscosity, 222
- Exponential flow equation, 128(11), (12),
129(22)
- Extension breaking, *see* Rupture
- Extension, mean square, 6, 7
- Extrudate, 612
- Extruder(s), *see also* Extruder screw,
 - Extrusion
 - adiabatic operation, 611, 613-615(102)
 - apparent viscosity, 619
 - capacity, 630
 - circulation flow, 597
 - closed discharge velocity, 596
 - die characteristic, 604
 - effect of helix angle, 628
 - experimental, 609F
 - feed zone, conveying capacity, 627
 - flow, 602, 610
 - mechanical power, 625
 - melt, 590
 - filtering, 629
 - isothermal, 606
 - nylon, 625
 - operating characteristics, isothermal,
603, 604
 - operating points, non-Newtonian, 622
 - output adiabatic, 614
 - plasticating, 590, 620, 627
 - zones, 624, 625F
 - power, dissipation, 596, 599, 602
 - requirements, 602, 630
 - shape factor, 597
 - scale model, adiabatic, 616
 - isothermal, 607
 - scale-up experiment, 630T
 - shear stress, 597
 - size, power consumption, 608
 - pressure, isothermal, 607
 - solid flow, 628
 - thermal power, 625
- Extruder screw, 590
 - channel, 591F, 599, 605
 - compression, 606F
 - design, 624
 - helical angle, 591
 - pressure profile, 610F
 - selection, 624
 - single, 590
 - temperature gradient, 613(84)
 - types, 626F
 - vacuum, 624
- Extrusion, 266, *see also* Extruder
 - behavior, rubber stocks, 608
 - of blends, 629
 - compressive stresses, 402
 - design, non-Newtonian, 619
 - die, 401
 - fracture, 585
 - Newtonian liquid, 617
 - nylon, 624
 - polyethylene, 399, 401
 - effect of quality, 624
 - profile, 582F
 - rubber stocks, 608, 619
 - speed and fiber profile, 581
 - viscometer, 196, 200, 203
 - viscosity, 611
 - Dacron, 620
 - effective, 619
 - polyethylene, 621F

F

- Falling ball viscometer, 568
- Fanning friction factor, 465
- Fatty acids
 - activation energy, 442
 - surface viscosity, 437
- Feeder, injection molding, 506F, 507
- Ferranti-Shirley viscometer, 127
- Ferric hydroxide, suspension, 96
- Ferry's flow law, 29, 34
- Fibers (filaments)
 - air friction, 564
 - anisotropy, 567, 568, 574
 - birefringence, 583
 - brakes, 575
 - crystallinity, 574
 - formation (filamentation), 481, 555
 - apparatus, 184F
 - chain alignment, 567, 573
 - coagulation and orientation, 568
 - crystallization during, 573
 - ink, 168F
 - rolling, 186
 - solute to solvent ratio, 558
 - and stationary flow, 557
 - synthetic, 554
 - velocity profile, change during, 566
 - volume reduction, 564
 - friction path, 575
 - liquid, 556
 - melt spun, 565
 - microstructure, 565
 - polystyrene, 371
 - semisynthetic, 554
 - single, elongation, 169
 - structure, 563, 567, 582
 - preliminary, 573
- Fick's law, 5
- Fictive temperature, 304
- Fill time, injection molding, 521, 522, 545, 549
- Fillers, in concrete, 342
- Filling, injection molding, 510
 - equation, 523, 530(14)
 - and frozen strains, 532
 - rate, 522
 - process, 516
- Film pressure, 430, 432
 - and molecular size, 436
- Film splitting, 151
 - kinematics, 174
- Filter cake clay, 279
- Flat plate on roll, 176
- Flexibility and crystallinity, 369
- Flexographic printing, 146
- Flint glasses, 303
- Flocculation, 219, 226, 230
 - force, 198
 - in greases, 461
 - pigments, 161
 - by water, 228
- Flow (fluid), 20, *see also* Flow, curve, patterns, Hydrodynamics, Viscosity
 - anomalies, 158, 558
 - birefringence, *see* Birefringence
 - capillary, 24
 - cement, 354
 - centripetal, in tensile separation, 483
 - channel, polystyrene, 520(4)
 - coating, viscosity requirements, 245
 - core, injection molding, 517
 - into crevices, 235
 - through die, 603
 - dilatant, 202, 213
 - distribution measurements, 586
 - energy input, 160
 - exponential equation (low), 128(11), (12), 129(22)
 - field, 8, 15
 - frozen oils, 463
 - grease, by gel lumps, 463
 - inelastic, incompressible, 18
 - intramolecular interaction, 8
 - limit, 265
 - laws, 23
 - Newtonian, *see* Newtonian flow
 - friction diagram, 237F
 - non-Newtonian, *see* non-Newtonian, flow, liquids
 - discharge, 618
 - friction diagram, 237F
 - in pipe, 238
 - orientation, bearing, 457
 - at operational speeds, 235
 - out time, 243, 244
 - in pipes (*see also* Capillary), 236, 238
 - plastic, 198, 201
 - curve, 195
 - effect of concentration, 223

- polymeric systems, 29
- profile, inversion, 578
- properties, and application, 233
 - and color strength, 232F
 - enamel, brushed black, 244T
- pseudoplastic, 213
 - power function, 202
- quasi-viscous, 28
- rate, 127(9)
 - divergence, 6
 - extruder die, 604
 - molding machine, 523(9)
 - rolling, 180
 - screw channel, 593(8)
- rectilinear, 22
- resistance, dies, 608
- rheopectic, 216
- secondary, *see* Creep, Elasticity, Weissenberg effect
- from spatula, 234
- in spinnerette, 556
- split, 183
- stationary and fiber formation, 557
- streamline, 217
- under tension, 172
- thixotropic, 205
- times, determination, 586
- toluene, 278
- turbulent, *see* Turbulence
- viscoelastic liquid, *see* Viscoelasticity
- volume, 21, 22, 27
- water through porous media, 278
- Flow curve(s), 19, 23, 30, 162, 164
 - absolute, 586
 - arbitrary, 22
 - capillary, *see* Capillary
 - clay, 166F
 - dilatant, 195F, 205F
 - effect of water, 207
 - emulsion, 215F
 - entire, need of, 235
 - equilibrium, 211, 213
 - grease, 209F
 - inflection, 585
 - Newtonian, 195F, 234F
 - pastes, 240
 - plastic, 195F
 - power law, 28
 - pseudoplastic, 165F, 195F, 204F
 - rotating cylinders, 32
 - spin masses, 562, 569, 577F
 - inflection point, 570
 - starch, 232F
 - thixotropic, 206F, 210F, 212F, 234F
 - true plastic, 201F, 234F
 - turbulent, 195F
- Flow patterns,
 - discone, 183
 - peeling, 172
 - roll, 176
 - nip, 185F
 - screw channel, 595
- Flow units (rheological flow units) 134, 338
- Fluid films, wedge-shaped, 454
- Fluidity, 29, 34, 127, 129(21), 130, 262
 - apparent, 35, 36, 128(14)
 - and binding forces, 337
 - polymers, 524
 - shear rate and shearing stress, 142
 - true, 129
- Fluoride glasses, 304
- Fluorocarbons, 450T
- Fluorspar, 265
- Flux, 315, 480
- Foams, 438
 - stability and surface viscosity, 442
- Force(s)
 - constant, 4
 - driving capillary, 22
 - between ion, 86
 - plate separation, 482
 - peeling, 496
 - of stripping, 482
 - viscous drag, 3
- Ford cup, 190
- For effect, mortar, 353
- Fountain roller, 152
- Fracture, *see* Rupture, Strength
- Free energy, surface, 261
- Freezing temperature, water, effect of
 - diameter, 257F
- Frenkel, defect, 344
- Fresh cement, *see* Cement, fresh
- Frequency (jump frequency), 10, 19, 43, 383, *see also* Oscillating motion, Sinusoidal, Vibrations
 - natural angular, 55
 - and nylon moduli, 419
 - resonance, plate viscometer, 65

Frequency (jump frequency)—*Continued*

- scale, 391
- shear oscillating, 9
- test, 389F
- effect on viscosity, dynamic, 397
- viscosity product, 385
- Freudenthal equation, 361(10)
- Friction, anelastic, *see* Friction, internal
- Friction diagram
 - generalized for Newtonian and non-Newtonian flow, 237F
 - pipe flow, 239
- Friction external, coefficient
 - brittle substances, 469
 - ductile substances, 469
 - fiber-air, 564
 - metal, 468
 - oxide, 469
 - polymers, 470, 471, 527
 - polystyrene, 528
 - solid surfaces, 467
 - steel against plastic, 472F
 - and velocity, 472, 473F
 - wear, 474
 - work, 475
- Friction factor, 236, 238, 239
 - pipe flow, 218, 236
- Friction force, 468, 475
- Friction, internal, 305, 468, 476, *see also*
 - Damping, Viscoelasticity, Viscosity, Voight model
 - alkali silicate glasses, 335F
 - constant, 101
 - ferric oxide films, 473F
 - frequency dependence, nylon, 415
 - glass, 332, 333, 336F, 339
 - ions, 89
 - junctions, 468, 472
 - liquid, 560
- Frictional drag, bearing, 454, 456
- Frictional effects in spinning masses, 560
- Frictional forces, effect on extruder plug flow, 628
- Fröhlich and Sack method, 90
- Frozen orientation, *see* Frozen strain
- Frozen strain, stress, orientation, 532, 537, 541
- Fruit jams, flow, 463
- Fulcher equation, 309, 329

G

- Gallium, 337
- Gamboge, suspension, 96
- Gardner apparatuses, 171, 191
- Gases, solubility in water, 254
- Gate
 - injection molding, 509, 533
 - pin-point, 537
 - restricted, 537
 - solidification (sealing), 512, 513
- Gaussian distribution function, 7
- Gears, loading and lubrication, 456
- Gegen-ions, 87
- Gel, (Gelation)
 - incipient, 161
 - lacquers, 245
 - rigidity, 276
 - structure, grease, 458
 - set cement, 346
 - transformation, 206
 - water, cement, 348
- Germanium oxide, 320
- Glass(es), 303, 304
 - activation energy, 333, 334
 - acoustical absorption, 333
 - aged, 331
 - alkali, mobility, 331
 - silicate, 325F
 - anion to cation ratio, 312
 - beads, suspension, 198, 201
 - bond flexibility, 333
 - bonds, 305
 - borates, 327
 - cations, central, 308
 - replacement water, 324
 - chemisorbed, 330
 - commercial, 312, 327
 - compacted, 331
 - complexity effect, 325
 - coordination complex, 311
 - cutting of, 336
 - delayed fracture, 330
 - diffusion, 330
 - effect of metal oxide substitution, 326F
 - elastic aftereffect, 332
 - elasticity, 301
 - energy barriers, viscous flow, 331
 - fibers, 301, 332
 - flow, *see* Glass transformation

- formation, *see also* Glass transformation
degree of polymerization, 308
kinetics, 305
rate, 307
temperature, 299, 307
tetrahedral coordination, 307
- fracture, 339
healing of, 337
ice point depression, 331
internal friction, 332, 334, 339
ions, and polymerization, 322
ions polarizability and viscosity, 324
isokoms, effect of substitution, 321F, 322F
leaching, 331
long, 300
mixed alkali effect, 323
non-equilibrium state, 312
phosphates, 327
pleochroic, 337
polarization mechanical, 337
polishing, 339
protons moving, 333
replacement, of alkali, 322
of silicon, 320, 323F
rigidity of, 300
rod fracture, 329
secular drift, 331
setting, 300
short, 300
soda-lime silicate, 301, 303
sodium-magnesium silicate, 324
strain point, 300
substitution, 326F
surface orientation, 337
sweet, 300
swelling, 330
temperature coefficient of viscosity, 300
thermal history, 304, 312
vibration characteristics, 334
viscosity, 338
absolute, 302
characterization, 329
and composition, 307
concentric cylinders, 302
effect of time, 313F
measuring, 301, 303
temperature and, 309, 311, 327
transformation region, 305
Vycor, 331
- Glass transformation (transition), *see also*
Glass, formation, viscosity
flow, as structure changes, 339
flow units, 325
limited mobility, 333
low temperature bending, 329
point, 312
region, 304, 305
softening point, 300, 301
working range, 300
- Glassware, heat-treated, 300
Glossy finish, 242
Glycerin, flocculation by, 229
in quartz powder, 289
Glycol, flocculation by, 229
Gold, 306
Goldschmidt rules, 307
Grading, continuous and discontinuous, 341
Gravel, in concrete, 341
Gravity spinning, 562
Gravure, 146, 153
Grease
as Bingham body, 458, 465
centrifugal acceleration, 460
creep, 460
elastic deformation, 458
elastic recovery, 459F
flow, 209F, 210F, 460, 462, 463, 465
gel structure, 458
line soap, 457
lubricating, 457, 467
shear degradation, 458, 462F
shear hardening, 462
shear stress, 463
time-dependence, 462
yield stress, 459-461
- Green strength, 250
clay, 284
Green viscometer, 159
Grinding
efficiency, 230, 231
effect on flow properties, 230
fineness, 149
- GR-S, latex, 125, 131, 132F, 136, 138, 140
Gums, 93, 94, 229
Guth formula, 123(2)

H

- Hafnium sodium silicate, 318
 Hagen-Poiseuille equation, 24(8), 25(9), 28
 Hagenbach correction, 24
 Hard rubber (Ebonite), 408, 425
 bulk modulus, 408
 creep in compression, 409, 411
 dynamic properties, 408T
 Lamé-constant, 408
 longitudinal viscosity, 408
 master creep curve, 410F
 modulus, 410
 Poisson's ratio, 408
 relaxation modulus, viscosity, 411
 shear modulus, viscosity, 408
 Young's modulus, 408
 Hankel transformations, 39
 Hardening under water, cement, 348
 Healing, glass, 337
 Heat (heating)
 chamber, 506F
 rate of plastic, 511
 conduction equation, 545
 conduction theory, reduced temperature, 511F
 curve, injection molding, 512F
 efficiency, injection molding, 511
 generation, oil flow, 466
 sintering, fibers, 585
 treatment, effect on behavior, 418
 of wetting, clays, 259T
 quartz, 259T
 Helix, chain structure, 116
 Helmholtz double layer, 263, 275
 Hermans-Overbeek theory, 100
 Herschel-Bulkley's law, 28(13)
 Hertz's law, 470
Hevea brasiliensis, 121
Hevea latex, 139
 Hexane, 270
 High polymer, see Macromolecule, Polymer
 High-speed printing, 222
 H  ppler-type viscometer, 123, 191
 Honey, 241T
 Hooke (Hookean)
 element, 360F
 law, 332, 351, 352
 Humectant, in adhesives, 488
 Humic acid, effect on clay, 282
 Humidity
 and cement setting, 349
 effect on uptake of water, 167
 Hydration
 and cement drying out, 346
 clay minerals, 251
 degree, cement, 345
 energy, proton, 337
 Hydrocarbon oils, 448
 Hydrodynamic
 equation, 36
 lubrication, 176
 separation, bearing, 456
 Hydrogel, fresh cement, 344
 Hydrogen-bonding, 116
 Hydrogen cyanide, liquid, 255
 Hygroscopic liquids, addition, 229
 Hydrostatic head, 21
 Hydrothermal analysis, 315
 Hydroxy ions, in water, 253
 Hysteresis loop, 207, 211, 370
 mortar, 354
 polyethylene, 370
 temperature and, 214

I

- Ice, formation, 257
 Iceberg, 256, 273
 structure of water, 253
 Immobilization of adjacent fluid 278, 280,
 see also Rigid film
 Immobilization of water, drying clay, 288
 Impact strength
 on concrete, 359
 and crystallinity, 369
 sensitivity, 382
 Impedance, mechanical, 66
 oscillating penetrometer, 80
 Implosion, 563
 Incompressibility, 36
 Indanthrene dyes, thixotropy of, 276
 Indium oxide, 321
 Inelastic behavior, see Anelasticity
 Inertia, 43, 44, 54, 80
 Inertial reaction, 3
 Injection molding, 505, see also Molding
 air entrapment, 519
 breaking, 541
 blemishes, 544

- bubbles, 537, 541
 - chilled shell, 517
 - cooling with gate frozen, 525F
 - cooling time, 544
 - core release, 539
 - dead time, 544, 525F
 - discharge, 525F, 531
 - draft, 539
 - equation of state, 538(16)
 - filling, 516, 521, 531, 544
 - equation, 523
 - mold, 525F
 - flow core, 517
 - forward time, 544
 - heat chamber, 506F
 - heating curve, 512F
 - jetting, 518
 - mold, closed and open time, 544
 - packing, 525F, 531
 - plunger, 506F, 544
 - polymer velocities, 518T
 - pressure, 508, 512
 - build-up, 525F
 - efficiency, 526F
 - maximum, 524
 - temperature, 515F, 544
 - ram, 506F
 - release, 539
 - scoring, 541
 - seal line, 536
 - sealed cooling, 538F
 - sealing shut off, 537
 - sink marks, 537, 541
 - sticking, 541
 - temperature, 512, 544
 - tunnel, 506F
 - vacuum bubbles, 541
 - weld lines, 519
- Injection stroke, 537
- Ink, 153, 154
 - chalky, 157
 - characterization, 157
 - consistency, 148
 - critical speed, 161
 - dielectric constant, 161
 - elastic limit, 173
 - filamentation, 168F
 - finger test, 169
 - gloss, 157
 - heatset, 146, 170
 - high shear phenomena, 165
 - hysteresis, 161
 - oxidation-polymerization, 166
 - particle-volume interaction, 158
 - pigment, 148
 - premix, 148
 - printing, 233
 - separation patterns, 174
 - set, 157
 - shortness, 165
 - slippage, 161
 - steamset, 146, 170
 - thixotropic break down, 161
 - transfer, 152T
 - vapor set, 222
 - vehicle, 148
 - viscosity anomalies, 150F, 161
 - viscoelasticity, 151
 - wetting down, 148
- Ink film, *see also* Ink
 - split, 154, 156F, 167
 - thickness, 155(2), 170
- Inkometer, 152, 169, 170F, 175F
- Insoluble films, viscosity, 433
- Instrument geometry, 21, *see also* various instruments
- Intaglio plate, 154
- Interaction coefficient, viscosity, 84
- Interface (Interfacial), *see also* Surface
 - elasticity, 439F
 - liquid-liquid, 429, 430
 - liquid-vapor, 429
 - oil-air, 439
 - oil-water, 438
 - solid solution, 90
 - water-air, 436
- Interlocking coefficient, 356
- Intermolecular forces, 442, 502
- Internal
 - coordinates, 7
 - friction, *see* under Friction, internal
 - pressure, 448
 - stresses, cement, 349
 - tension, effect on extrusion parameters, 399
- Intrinsic viscosity, limiting, 9, 12, 101 (22), 451, 452, *see also* Macromolecules, Particles, Polymer, Viscosity
- and branching, 14

Intrinsic viscosity—*Continued*

- molecular weight, 13(11)
- polyethylene, effect of heating, 400T
- ratio, 164
- shear high, 458

Ion(s)

- contribution to viscosity, 85
- coordination number, in glass, 320
- effect on water, 254
- forces between, 86
- frictional coefficient, 86
- glass, 317
- polarizability, effect on glass, 317
- polarizability of, and viscosity, 319

Ionic

- association, 108
- atmosphere, 85, 86, 100
 - diffuse distribution, 89
- elevations, water, 255T
- interaction, shear effect, 119
- mobility, 91, 92
- state, in glass, 316
- strength, 101
 - and electroviscous effect, 88

Ionization

- degree of, 101
- reduced viscosity and, 105
- streaming birefringence and, 105
- uncoiling, 103

Ionogenic sites, 90

Iron-blue, 231

- dispersions, 228T

Iron, friction coefficient, 472

Iron gray, model value, 475T

Iron oxide

- suspension, 205, 219F, 226T
- thixotropy of, 276

Iron salts, 477

Irradiation effect, polyethylene, 395

Isocycles, 548

Isoelectric point, 104

Isokoms, 309

Isotactic hydrocarbon, polymers, 368

J

Jetting, 518, 518F

Joints, *see* Adhesive joints

- butt, *see* Butt, joints

Joule's heat, 560

Journal bearing, 454, 467

Junctions, in friction, 468, 472, 475

K

Kaolin, 258

- suspension, secondary shrinkage, 287
- viscosity minimum, 283T

Kaolinite, 268, 281

- filterabilities, 280F
- stress-deformation, effect of wetting agent, 294F
- suspensions, 271T, 279
- viscosity, 282F
- titration with hydroxides, 283F
- viscosity with alkali, 283F
- water isothermal, 167
- Kelvin body, Kelvin-Voigt element, 260F, 283, *see also* Creep

Ketchup, 241T

Kinematic energy correction, 24, 126

Kinematic viscosity, 217

Kneading, 288

Knife-edged, surface viscometer, 434F

Krieger-Marom formula, apparent fluidity, 35

Kyanite feldspar, 290

L

Lactoglobulin-beta, 93, 94

Lamé constants, 392, 416, *see also* Modulus

Langmuir equation, 436

Lanthanum nitrate, 274

Lap joints, 492, 494, 495

Laplace transforms, 68

Latex (Latices), 123, 233

- concentration effect, 133, 142
- flow, effect of concentration, 123, 135
- through capillaries, 279
- particles, 138
- pseudoplastic flow, 122
- polydispersed, 140

Lead glasses, 329

Lead, model value, 475T

Lead-strontium glass, viscosity, 317

Lead sulfate, 229

Leather hard clay, 286

LeChatelier principle, 338

Lecithin, 229T, 230

Letterpress, 146

- ink, 146T

Leveling, 245, 246

- time, 243T
- versus drying time, 247

- Light scattering, 13
- Lignin sulfonated, 226T
- Lime concrete, 341
- Lime-soap grease, 457
- Limit analysis, concrete, 363
- Linseed oil, 186, 221
 - emulsions, 227F
- Liquid(s), (*see also* Flow, Fluidity, Viscosity), 22
 - associated, 252
 - cohesive strength, 172
 - filaments, 556
 - fracture, 173
 - friction, 560
 - immobilization, 164
 - motion of, 30
 - Newtonian, 18, 43, 61, *see also* Newtonian
 - non-Newtonian, 29, 34, 62, *see also* non-Newtonian
 - pure, lack of surface viscosity, 429
 - supercooled, 304
 - tacky, 481
 - viscoelastic, 49
- Litho varnishes, 160
- Lithographic ink, 146
- Lithographic printing, 146, 217
- Lithol, suspension, 226T
- Load-carrying capacity, 454, 455
 - gelled lubricants, 467
 - non-Newtonian, 457
 - plastic solid, 476
- Load and friction coefficient, 470F
- Loading, constant-rate-of, 498
- Loading cycles, cement, 351
- Logarithmic decrement (*see also* Damping), 44, 48, 55, 59
 - nylons, 413
- Long glass, 300
- Loss, *see also* Damping, Phase angle
 - angle, factor, tangent, 416
 - coefficient, transition, 240
 - mechanical, 383
 - nylon, 416
 - polyethylene, 388, 390, 391
 - peak, 388, 394
- Lubricant(s), *see also* Plasticizer
 - as Bingham body, 467
 - boundary formation, 476
 - commercial, 449F
 - gelled, load-carrying capacity, 467
 - pipe flow, 464
 - grease, 457
 - oil additives, 438
 - viscosity-temperature-pressure data, 443
- Lubrication
 - boundary, 467
 - gear, 456
 - hydrodynamics of, 176
 - mixed film, 475
 - plastic granules, 512, 451T
 - surface, polystyrene granules, 529F
- M**
- Machine pressure, 548
- MacLaurin method, 35
- Macromolecules (macromolecular) *see also* Chain molecules, Polymer
 - branched, 13
 - chain model, 2
 - at interfaces, 442
- Magnesium oxide, 266
 - surface, 262
- Mannide, monooleate, 227F
- Margules equation, 32(21), 36, 58
- Markovits' method, 45, 50
- Master curve (composite, normalized curve) *see also* Scale factor
 - creep, hard rubber, 410F
 - spin masses, 559
- Matte finish, 242
- Maxwell body (element, model, unit), 49, 198, 360F, *see also* Relaxation time
 - cement, 350
 - momentum equations, 354
- Mayonnaise, 241T
- Mechanical loss factor, *see* Dynamic loss factor, Damping
- Mechanical models, *see* Rheological models
- Mechanical power, extruder, 625
- Melt extruder, 590
 - isothermal, 606
- Melt filtering, extruder, 629
- Melt index, 622
 - polyethylene, and heating time, 401T
- Melt spinning, 560, 562
 - speeds, 565
 - volume reduction, 565

- Melting point, *see also* Softening point,
 Setting point
 effect of anion to cation ratio, 315
 and ion type, 317
Melts, non-Newtonian, 617
Meniscus formation, in particle flocculation, 461
Metal(s)
 cutting, 474, 497
 friction of, 468
 lack of glassy state, 305
 to-metal contact, 443
 printing, 155
Metering section, design, 627
Methyl cellulose, 204
Methylene blue, epitaxis on glass, 337
Mercury, 306, 337
Microcrystalline polymers, 366
Mills, types of, 147, 149, 150F, 170, 230
Milling, 182, 497
Mineral oils, 227F, 446
Mineral powders in asphalts, 224
Mineral-water mixtures, 265, 287
Misting, 174
Mixers, 147F, 148, 149F
Mixing
 action, positive displacement, 148
 effect on flow properties, 230
 rate of shear, 231
Model, molecular, 3
Model, rheological, *see* Rheological model
Modell values, of various metals, 475T
Modulus (Moduli), *see also* Elastic compliance, Elasticity
 adhesive film, 488
 bulk, polyethylene, 390
 complex, 42, 44, 46, *see also* Dynamic modulus,
 oscillating sphere, 59
 dynamic, 43, 45(35), 49(41), 385, 420
 oscillating plate, 70(72)
 effect on strain, 394
 frequency curve, 392
 nylon-66, 419T
 operator, 48
 polymers, microcrystalline, 366
 range, polyethylene, 390
 ratio, dynamic to static, nylon, 415
 shear to Young's, 393
 relaxation, 384, 397, 409
 shear and tension ratio, 421
 rigidity (shear, stiffness), 388
 dynamic, 48
 internal, 29, 34
 minimum, 391
 nylon-66, 414
 polyethylene, 390, 393, 394
 and specific volume, polyethylene, 394
 rubbers, comparison, 410
 storage (unrelaxed), 409, 142
 Young's (stiffness in elongation), 388
 mortar, 356
 nylons, 414, 423
 polyethylene, 393-395
 ratio to shear modulus, 393
Mold, 506F
 cavity, 507, 512, 526F
 closed time, 509, 514F
 discharge, 514F, 535
 filling, 514F
 force to open, 539F
 open time, 509, 514F
 opening conditions, 546F
 packing, 514F
 pressure, curves, 543F
 cycle, 525F
 gauge, 513
 residual, 539, 540
 sealing, 514F, 535
 shrinkage, 542, 543F
 sticking, 540
 temperature, 508
 wall temperature, 530
Moldability, 542, 548, *see also* Molding
 effect of polymer, 550
Molding, *see also* Injection molding,
 Mold
 cycle, 507, 513, 544
 dead time, 513
 diagram, 546F, 547F, 548F
 gate, solidification, 512
 isocycles, 546
 machine, flow rate, 523(9)
 setting, 550
 negative pressure, 541
 optimum conditions, 544
 peak pressure and ram pressure, 529
 plunger for time, 514F

press, 508
scoring of, 540
surface luster, 508
weight and flaws, 542
Molecular, *see* Chain molecules, Configuration, Macromolecules, Relaxation mechanism
extension, 9
forces, adhesion, 497
model, 5
orientation, polyethylene, 379
Molecular weight (molecular weight distribution, degree of polymerization (DP)), 11, 12
polymethacrylate, 113
Moment, *see* Torque
Monomer model, 3
Monomer radius, 106
Monomolecular layers, 430
Montmorillonite, 264
base exchange capacity, 281
Mooney and Ewart viscometer, 64, 124, 126
Mortar, 342
chemical hardening, 352
creep viscosities, 353
elasticity, 354, 355
fresh, 342, 351, 352
Hooke's law, 355
hysteresis loop, 354
paste flow, 352
set, 342
stress-strain diagram, 355F
viscosity, 352, 353
water, 353
Young's modulus, 366
Muds drilling, 279
Multiaxial stressing, 382
Multicolor printing, 170
Multicolor trapping, ink, 156
Multilayers, 430
Mustard, 241T
Myosin, 104
Myristic acid, surface viscosity, 437

N

Naphthenic oil, 449F
Natural rubber, *see* Rubber
Navier-Stokes equation, 18, 36, 66, 592

linearized, 18
plastometer, 73
polar coordinates, 61
Necking, adhesive film, 500
Neoprene latex, 125, 131, 139
Network-forming cation, 308
Network segment motion, 366
Newsink, 146
Newtonian flow, liquid, 20, 24(7), 29, 43, 52, 54, 61, 132, 527, 597, *see also* Flow, fluid, Liquids
in bearing, 467
curve, 195, 234F
element, 360F
extrusion, 617
films, 433, 442
laminar, 237F
of spin masses, 568
temperature dependence, 221
turbulent, 237F
viscosity, in oscillation, 45
units, *see* Flow units
Nichol prism, 337
Nip flow
entrance and exit, 182
roll, 183
viscoelastic systems, 183
Nip, material balance, 182
Nitrides, 307
Nitrobenzene, 270
flow through clay, 279
Nitrocellulose lacquers, 244
Nitrocellulose, suspension, 95
Non-Newtonian films, 431-436, 457
Non-Newtonian liquids (*see also* Flow Pseudoplastic, Maxwell body, Weissenberg effect), 20, 29, 34, 62, 64, 198, 221, 235, 622
flow, 19, 21, 41, 98, 128, 133F, 134, 141, 208, 586
ink, 163
temperature dependence, 221
turbulent in pipes, 239
melts, 617
oil film, 457
plate plastometer, 76
Reynolds number, 239
suspension, 224
viscosity, polyelectrolytes, 115, 116

- Normal-coordinates, 4, 10
 relaxation time, 7
 transformation, 6
- Normal-mode
 analysis of rubber, 16
 chain molecule, 8F
 relaxation, 10
- Normal, stress, transversal (*see also* Stress), 19
- Normal vibrations, nodes, 7
- Nucleation, 305, 307
- Nuclei, cavitation, 173
- Nuclei, cement, 344
- Number of velocity head, 240
- Nylon-66, 371, 375, 617, *see also* individual
 Boltzmann superposition principle, 423
 creep, 423-425
 dynamic properties, 416T, 420
 effect of draw ratio, 419T
 effect of moisture, 414
 extruder, 625-628
 Lamé constants, 416
 loss factor, effect of strain, 420
 molten, 584, 618
 screw, 626F
 shear modulus, 413, 414
 solution viscosity, 585
 stress, critical, 585
 relaxation, 422, 424F
 ultrasonic techniques, 425
 yarn, master creep curves, 424
 Young's modulus, 423
- Nylon-6, 6
 bending, effect of conditions, 420
 chemical relaxation, 422
 complex modulus, 416
 effect of conditioning on dynamic properties, 417
 effect of moisture, 417
 loss factor, 416
 melt, 584
 moisture content and relaxation spectrum, 418
 relaxation spectrum, 417
 stress relaxation, 422
 water diffusion, 422
- O
- Octadecanol, 438
- Octyl ester sulfosuccinic acid, 229T
- Oil-air interface, 439
- Oil-based vehicles, 146
- Oil-water emulsion, 224, 227F
- Oil-water interfaces, 438
 of proteins, 438
- Oils
 film, non-Newtonian, 457
 frozen, 463
 gelled, pressure transmission, 466
 thermal expansion, 455
 viscous, velocity profile, 466
- Oleic acid, 227F, 269
 surface viscosity, 437
- Operator, 43
- Orange peel, 246
- Ordered and disordered regions, polymers, 368
- Orientation angle, 104
- Orientation, cellulose, 377
- Orientation, frozen in, polymer, 531
- Orthosilicates, 308
- Oscillating penetrometer, 80
- Oscillating plate, viscometer, 65F
 wall effect, 69
- Oscillating motion (Oscillations, linear and angular), *see also* Frequency
 amplitude of, plate viscometer, 65
 forced, 388
 free, 48
 small, 43
 torsional, 54
 types, 20
- Oseen's equation, 72
- Ostwald equation, 465
- Ostwald flow curve, 166F
- Ovalbumin (eggalbumin), 92, 93
 viscosity-pH dependence, 105F
- Oxidation, in water, 474
- Oxide layers, sliding, 469
- Oxides, fused, 338
 surface friction, 472
- Oxyethyl stearate, surface viscosity, 437
- Oxygen ion, 253
- P
- Packing, 139, 546
 and frozen strains, 532
 injection molding, 510
 time, 537
- Paint(s)
 films, leveling, 243

- flow properties, 242T
- spraying, 222, 245, 246
- thixotropy, 207, 229, 245
- Palmitic acid, surface viscosity, 437
- Paper
 - chromatography, 281
 - coating, 234
 - gummed, 484
 - ink transfer to, 154
 - pores, 154
 - pulps, 233
- Papkous equation, 124(6)
- Paraffin wax joints, 500
- Paraffinic chains, 369
- Parallel plates, *see also* Compression, Plastometer
 - flow in separation, 481
 - separation, 169, 173
 - viscometer, 193, 194
- Particle(s), *see also* Hydrodynamics, Interaction, Macromolecules, Orientation, Rods
 - anisodimensional, 293
 - area, 158
 - charge, 90
 - charged, sedimentation of, 99
 - clusters, 164
 - diameter, 346
 - flocculation, meniscus formation, 461
 - forces between, 269
 - interaction, 96, 163, 164
 - motion, average, 5
 - orientation, 161
 - polymeric, change of shape, 99
 - as rigid rods, 117
 - shape, 99, 162, 207, 223, 252
 - effect of plasticity, 265
 - size, 223, 252
 - latices, 122
 - specific surface, 224
 - suspended, 84
- Pastes, 240
 - flow type, 241T
- Pasting process, 235
- Pectinate sodium, 106, 110, 113
- Pectinates, 115
- Pectons, 216
- Peeling, 172, 482
 - force, 496
 - rate, 498F
- tensile, force, ratio, 497
- tests, 482, 496F
- Penetrometer, 78
- Perfluorocarbon fluid, 448F
- Perlon, *see* Nylon-6
- Petroleum oils, 450T
- Phase difference, *see* Birefringence
- Phenol-formaldehyde resins, 303
- Phosphates, 305
- Phosphorus pentoxide, vitreous, 304
- Picking, ink tack, 154
- Pigment, 146
 - agglomerates, 149
 - concentration, 164
 - dispersions, 229T
 - effect on viscosity, 163
 - ratio, vehicle volume, 158(3)
 - setting, 229
 - suspensions, 212
 - volume content, 224F
- Pipe line
 - pressure, 236(22)
 - roughness, 239
- Pipe, surface roughness, 240
- Pipe (capillary) flow, 236
 - greases, 465
 - rough, 218(18)
 - shear rate, 238
 - smooth, 218(17)
- Piston oils, 433
- Plane-cone viscometer, 586
- Plane-parallel plates, *see* Parallel plates
- Plastic(s), 220
 - calendering, 177
 - deformation asperities, 468
 - friction coefficient, 472
 - granular packing, 627
 - solid, load-carrying capacity, 476
- Plastic flow, *see* Flow, plastic
- Plastic viscosity, *see* Flow, plastic, Viscosity
- Plasticating extruder, 590
- Plasticity (plastic range) *see also* Flow, plastic, Yielding
 - fresh mortar, 351
 - mineral-water mixtures, 265
 - number, 239, 265
 - platelike crystals, 266
 - refractory oxides, 266
 - silver chloride, 317
 - surface chemistry, 266

- Plastisol, vinyl, 215
Plastometer,
 parallel-plate, 74, 352
 Scott's theory, 76
Plate circular, torque, 52
Plates, separation, 481
Pleochroic glass, 337
Ploughing effect, friction, 471
Plug flow, 27, 199, 200, *see also* Flow
 capillary, 26
 extruder channel, 628
 greases, 465
 rotating cylinder, 33
Plunger (Ram), 506F, 507
 forward, 537, 543F
 motion, 522, 536
 time, 509, 533F
 pressure and peak mold pressure, 529
 times, 531
Pochettino viscometer, 77
Poise, 194
Poiseuille's equation, 128(10), 237
Poiseuille flow, 195, *see also* Capillary
Poisson-Boltzmann equation, 89, 99, 100
Poisson's ratio, 421, 491
Polarization
 ionic, effect on glass, 316
 of ions and viscosity, 319
 mechanical, glass, 337
 surface ions, 260, 261
Polyacrylate, reduced viscosity of, 102
Polyacrylic acid, 102
Polyacrylonitrile, 578, 580, 585
 solutions, 570
Polyadipic acid hexamethylenediamine,
 see Nylon-66
Polyamides, 14, 371, 373, 568, *see also*
 Nylons, Polypeptides
 branched, 15
 crystal growth, 377
 filaments, disorientation, 377
 linear, 15, 412
 melt viscosity, 584
Poly- ϵ -aminocaproic acid, 578
Polyaminoundecanoic acid, shear modulus, 413
Polyampholytes, 104
Polybutene, 186, 445F, 451T,
 calcium carbonate dispersion, 174
 oil, 221F
Polycapryllactam, shear modulus, 413
Polydecamethylene sebacamide, 374F
Polydecanedicarboxylic acid hexamethylenediamine, shear modulus, 413
Polydimethylsiloxane, 446F
Polyhedra, in glass, 316
Polyhexamethylene sebacamide, shear-strain curves, 407F
Polyelectrolytes, 106, 115
 concentration dependence, 106, 108
 shape of viscosity curve, 113
Polyester, 379, 568
Polyester fibers, strength, 381F
Polyester, polyundecanoate, 373F
Polyethers, 450T
Polyethylene, Polythene, 368, 617
 absorption (loss) peaks, 395T
 birefringence, 370F
 brittleness, 369, 403
 bulk, moduli and viscosity, 392
 cold drawing, 378
 compression, set, 371F, 372F
 test, 370, 393
 yield, 292, 403
 creep, 367, 396
 asymptotic value, 396
 crystal growth, 377
 crystallinity and stress-strain, 368F, 369F
 crystallites, 374, 395T
 density, effect of draw speed, 405T
 dynamic, loss factor, 389F, 391F
 testing, 388, 393
 effect of branching on loss, 394
 extruder, 622, 629
 extrusion, 401
 effect of quality, 624
 flow pattern, 402F
 shear stress, 399
 viscosities, 621F
 filaments, Young's modulus, 394
 flow, critical rate, 400
 high density, comparison, 404
 hysteresis, 370
 internal mobility, 390, 394
 internal tension and extrusion, 399
 intrinsic viscosity, effect of heating, 400T
 irradiation effect, 395
 low density, 388, 404

- melt index, 404T
 - and heating time, 401T
 - methyl groups, 395T
 - moduli, 367, 390
 - orientation, 378
 - plastic flow, 378
 - quenched, 368, 369
 - relaxation, 379
 - rupture, 403, 404
 - scale up, 630
 - screw, 626F
 - segmental motion, 395
 - shear modulus and specific volume, 394
 - shear viscosity, 392
 - shear yield stress, 403
 - slip planes, 379
 - stress, bearing elements, 379
 - cracking, 399
 - distribution, 398F
 - relaxation, effect of time, 396
 - strain, 367, 370F, 404
 - wave propagation, 392
 - workability, 626
 - Young's modulus, 395
- Polyethylene sebacate, 366, 367F, 379, 380F
- Polyethylene terephthalate, Dacron, Terylene, 569, 578
 - adiabatic process, 373
 - discharge flow, 618F
 - extrusion, 618, 620
 - screw characteristics, 620F
 - stress-strain curves, 407F
- Polyhexamethylene adipamide, *see* Nylon-66
- Polyion, 100
- Polyisobutylene, 447, 449
- Polyisoprene, 121
- Polymer, *see also* Chain molecules, Configuration, Macromolecules, Viscosity
 - amorphous, crystallization, 373
 - bearing, 470
 - in bearing oils, 456
 - chain, alignment, 561
 - cooperative orientation, 380
 - model, 7
 - strain, 366
 - charged, end-to-end distance, 100(19)
 - crazing, 533
 - cross-linked, 370
 - crystallization mechanism, 377
 - crystalline, 376, 425, 426
 - degradation, in shear, 454
 - dilute solutions, relaxation, 16
 - disordered phases, 382
 - effect in lubricating oils, 451T
 - fiber forming, 555
 - flow, 29
 - effect of crystallinity, 380
 - mold filling, 515
 - fluidity, 524
 - friction, 470, 471
 - granular, friction, 527
 - granules, lubrication, 523
 - in grease, 460
 - in heating chamber, 507
 - isotactic hydrocarbon, 368
 - linear, 14
 - melt viscosity, effect of moldability, 550
 - microcrystalline, 366, 368, 378
 - stress-strain, 366
 - model, 3
 - net charge, *see* Polyelectrolytes
 - ordered and disordered regions in, 368
 - orientation frozen in, 531
 - orientation in spinnerette, 556
 - plasticity, effect of crystallinity, 380
 - polyhedra, 309
 - properties, influence on moldability, 549
 - rupture, during drawing, 380
 - shot, 509
 - shrinkage, 508
 - softening point, effect on moldability, 550
 - solutions, oil, 451
 - state in lubricants, 452
 - thickening effect, 451
 - velocities, injection molding, 518T
- Polymethacrylate, 113F, 117, 451T
 - molecular weight, 113
- Polymethacrylic acid, 103, 104
- Polymethyl pimelic acid hexamethylene-diamine, shear modulus, 413
- Polyphosphates, 104
- Polypimelic acid hexamethylenediamine, shear modulus, 413
- Polysalt, 107, 108
- Polysebacic acid ethylenediamine, shear modulus, 413

- Polysebacic acid hexamethylenediamine,
 shear modulus, 413
 Polysiloxanes, 450T
 Polystyrene
 channel flow, 520(4)
 crazing, 535F
 extrusion rate, critical, 400
 filaments, 371
 flow, power law, 521(5)
 friction coefficient, 527
 granules, surface lubrication, 529F
 injection cycle, 540F
 injection molding constants, 522, 524
 latex, 139
 melt viscosity, 522T
 mold opening conditions, 540F
 in toluene, 10, 11
 Polysuberic acid hexamethylenedia-
 mine, shear modulus, 413
 Polytetrafluoroethylene, fibers, 583
 stress-strain curves, 407F
 Polytetrafluoroethylenecarbonate, stress-
 strain curves, 407F
 Polyundecanoate polyester, 373F
 Poly-4-vinyl-N-butylpyridinium bro-
 mide (PVPBr), 103, 106, 107, 109
 112
 Polyvinyl chloride, 407, 407F
 Polyvinyl pyridine, 99
 Polyvinyl resin, critical extrusion rate,
 400
 Pony mixer, 147
 Positive colloids, 276
 Potassium salts, 261, 306, 477
 Potassium soaps, 141
 Potter's flint, 289
 Potter's wheel, 266
 Pour point depressants, 464
 Powder cement, 342
 Powell-Eyring equation, 466
 Power constant,
 extruder, 602
 modified, 623(121)
 Power dissipation, extruder, 596
 Power formula, 623(120)
 Power law, 622(116)
 concrete, 343
 flow curve, 28
 polystyrene flow, 521(5)
 Precipitation chemical, 564
 Premix, ink, 148
 Preplasticizers, 507, 525
 Press
 fountain, 152
 profile, rotating roll, 177F
 speed, 154
 Pressure
 cycle, mold, 513
 difference, capillary, 24
 distribution, bearing, 467
 drop, capillary, 127
 grease flow, 465
 efficiency, injection molding, 526F
 high, on glass, 340
 loss coefficient, 240
 pipe flow, 236
 loss, mold, 528
 maximum, injection molding, 524
 mold cavity, 512
 negative, in cooling molding, 541
 observed, molding, 530T
 pipe line, 236(22)
 plate plastometer, 74
 profile, between rolls, 155F
 discone, 184
 screw extruder, 610F
 pulse, nip, 178
 release, 544
 residual mold, 539
 roll flow, 181
 screw extruder, 604
 sensitive tapes, 48f
 temperature cycle, 515F, 545F
 temperature relations, 405T
 transmission, gelled oils, 405T
 transmission through granu-
 larity, 405T
 viscosity dependence on, 450I
 yielding, 468
 Pressure flow, *see also* Pressure
 boundary conditions, 593(3)
 constant, 601
 forward, 606
 screw pump, 592
 shape factor, 593
 velocity distribution, 600
 volume, 601
 Prestressed, concrete, 363, 364
 Primary shrinkage, clay, 287
 Primers, metal, 242T
 Printing, 182
 inks, *see* Ink

- multicolor, 154
- press, 176
- pressure, 154
- speed, 145
- Production rate, roll mill, 151
- Proteins, *see also* Polyamides, Polypeptides
 - charge effect, 90
 - degree of ionization, 92
 - electroviscous effect, 94
 - films, 440
 - rheological properties, 441
 - on oil-water interfaces, 438
- Proton
 - hydration energy, 337
 - location in water, 253
 - moving in glass, 333
- Pseudoplastic (Pseudoplasticity) 162, 164
 - flow, 131, 213, *see also* Flow, Non-Newtonian, Pseudoplastic
 - change with treatment, 220
 - curve, 195
 - grease, 458
 - latex, 122
 - in pipes, 238
 - thixotropic, 214
- friction factor, 238(24)
- inks, 146, *see also* Ink
- materials, 148
- Pulse shapes, 393
- Pulse velocity, measurements, 420
- Pump, positive displacement, 590
- Pumping capacity, screw, 601
- Pyridine, flow through clay, 278
- Pyrophyllite, 264

Q

- Quartz, 250
 - fused, 305
 - heat of wetting, 259T
 - liquid interaction, 289
 - particle, 273
 - adhesion, 284
 - powder, 262
 - pH, 289
 - suspension, 198, 201, 271
 - solubility, 262
 - water adsorption, 259T
- Quenching, nylons, effect on moduli, 413

R

- Ram, *see* Plunger
- Rayon process, cuprammonium, 568
- RCA viscometer, 162
- Reduced variables, 388, 391
- Reduced viscosity and ionization, 105
- Ree-Eyring theory, 134, 137, 140
- Reed viscometer, 193
- Refractivity, molar, 317
- Refractory oxides, 266
- Reiner equation, surfaces, 436
- Reiner-Riwlin equation, 345
- Relative motion, 18
- Relaxation (Relaxation mechanism), *see also* Creep, Viscosity
 - distribution, 386
 - effects, viscosity, 9
 - modulus, *see* Modulus
 - polyethylene, 379
 - spectrum, nylons, 415
 - viscosity of solutions, 11
- Relaxation function, 384, 385, 409
- Relaxation time, 86, 199, 383
 - "box" distribution, 385F, 387F
 - distribution of, 384
 - nylon-66, 414
 - surface films, 441
 - dumbbell, 7
 - and molecular weight distribution, 12
 - normal coordinates, 7, 10
 - nylons, 415
 - and shear rate, 202
 - spectrum, polyethylene, 390
- Release, injection molding, 539
- Renitence coefficient, mortar, 351(1)
- Residual strain, *see* Strain
- Resilience, *see* Elastic recovery
- Resistance coefficient, 3
- Resonance
 - frequency, adhesive joint, 488
 - plate viscometer, 65
 - oscillating plate, 66, 70
 - rotating cylinders, 46
- Retardation, *see* Elasticity, retarded
- Reversibility, flow curve, 164
- Reynold's number, 71, 148, 217(16), 236, 238, 465
 - non-Newtonian materials, 239
 - polyethylene melt, 400
 - rotational viscometer, 218

- Rheometry, 17
- Rheopeptic (Rheopexy), 163, 165, 216, 220, 278
- Rhombohedral, 139
- Ribbon, 485, 496F
- stiffness, 497
- stripped, 482
- Rigidity, *see also* Bending, Elastic compliance, Macromolecules, Modulus, rigidity, Stiffness
- glass, 300
- set cement, 346
- water, 284
- Ring, surface viscometer, 434F
- Roll (Rolling)
- coating, 182, 235
- cylinder, test, 171
- immersion, 182
- ink, 168
- mill, 147, 150F
- production rate, 151
- nip, 155
- flow pattern, 177
- out limit, 265
- speed, 151
- wetting by liquid, 182
- Rotating cylinder plastometer, 345
- Rotational viscometer, *see also* Coaxial cylinder viscometer
- high shear, 235
- Reynolds number, 219
- turbulent flow, 218
- Rough pipe flow, 218(18)
- Roughness, Rugosity, *see also* Surface roughness
- in friction, 471
- Rubber (Elastomers, rubberlike bodies), 617
- adhesives, oxidation, 488
- cross-linked, 408
- friction, 471
- hard, *see* Hard rubber
- metal sulfide bond, 488
- natural, 408
- latex, 130
- modulus, 410
- normal-mode analysis, 16
- screw, 626F, 629
- stocks, apparent viscosity, 619
- extrusion, 608, 619
- Rubbing bodies, 443
- Runners, injection molding, 509
- Rupture (Fracture), *see also* Strength, Yielding
- adherent, 489
- and adhesive thickness, 499F
- biaxial, polyethylene, effect of structure, 403
- cause, 489
- concrete, 357, 358
- glass, 339
- ink, 173, 174
- joints, low stress, 491
- liquid, 173
- localized, concrete, 363
- rheological, 482
- solid, of liquid adhesive, 484
- strain at, 405
- stress (strength), 490
- tests and rate, 497
- as a topical phenomenon, 485
- Rutile, 320
- S
- Sag marks, 244
- Salts, fused, 338
- Salves, 241
- Sand, 202
- in concrete, 341
- drying, 288
- effect on mortar viscosity, 353
- Sand-water mixtures, 250
- dilatancy, 290
- mechanical strength, 289
- pore volume, 290
- Saybolt viscometer, 190
- Scale-up experiment, extruder, 630T
- Scarred joints, 492
- Schulze-Hardy Rule, 284, 285
- Scoring, injection molding, 540, 541
- Scraping test, 497
- Screen pack, 629
- Screw
- characteristic, adiabatic, 613
- isothermal, 603
- Newtonian, 617F
- non-Newtonian, 617F, 619
- polyethylene terephthalate, 620F
- channel, flow pattern, 595
- flow rate, 592, 593(8)
- shear rate, 623
- velocity distribution, 593

- extruder, compression ratio, 606
 - temperature rise, 613(89)
 - types of, 626F
- leakage, 601
- pitch extruder, 591
- pump, capacity, 601
 - flow, 592
- speed and discharge rates, 610
- Seal line, 546
 - injection molding, 536
- Seal mechanical, 547F
- Sealing
 - injection molding, 510, 538F
 - points, 536(15)
 - pressure, 543F
 - pressure-temperature relations, 536
 - shutoff, injection molding, 537
- Sebacamide polydecamethylene, 374
- Sedimentation
 - of charged particles, 99
 - volume, 158, 269, 270
 - and casting slips, 269
- Sedimentation potential, Dorn effect, 273
- Segment (Segmental), *see also* Chain
 - chain molecules, 382
 - motion, network, 366
 - movement, 377
 - polyethylene, 395
- Segregation, workability, 342
- Selenium, 305
- Semisynthetic fibers, *see* Fibers
- Separation tensile, 482
- Set,
 - cement, 342
 - flow, 349
 - concrete, 358
 - glass, 300
- Severs extrusion meter, 191
- Shaving cream, 241T
- Shear (Shearing), *see also* Deformation, Strain
 - alignment, 202
 - blade, 459
 - breakdown, gelled lubricant, 464
 - degradation, grease, 458, 462F
 - dependence, viscosity, bearing, 456
 - effect ionic interaction, 119
 - and extension moduli, nylon-66, 421
 - flow, two dimensional, 5
 - hardening, clay, 291
 - grease, 462
 - high, during printing, 153
 - intermittent, roller nips, 168
 - melting, structure, 463
 - oscillating, 9
 - resistance, concrete, 357F
 - steady-state, 9
 - strain, *see* Strain
 - strength, *see* Strength, shear
 - test, block, 495
 - viscosity, polyethylene, 392
 - zero, plane, 182
- Shear modulus, *see* Modulus, rigidity
- Shear rate (rate of deformation, strain rate, velocity gradient), 4, 7, 19, 22, 23, 27, 104, 116, 194, 196, *see also* Anelasticity, Creep, Rate process theory, Viscosity
 - average, extruder, 619
 - Bingham body, 200
 - and breakdown, 211, 213
 - brushing, 243
 - capillary, 21(1), 127
 - clearance, 623
 - correlation factor, 202, 204
 - critical, 217
 - dilatant, pipe flow, 238(25)
 - effect on non-Newtonian flow, 220
 - extruder, 597
 - mean, 199, 202, 234
 - nip, 178
 - Pochettino viscometer, 77
 - pseudoplastic, pipe flow, 238(35)
 - rotating cylinders, 31
 - screw channel, 623
 - temperature effect, 214
 - thixotropic, 206
 - viscosity and, 15
- Shear stress, 19, 41, 57, 61, 194
 - butt joints, 493F
 - capillary, 22(1), 127, 196
 - critical, polyethylene, extrusion, 399
 - dilatant, 203
 - effect on polymer viscosity, 453T
 - extruder, 597
 - and fiber formation, 558
 - grease, 463
 - moment of, 44
 - pseudoplastic, 202
 - rotational, 196
 - spinning, 562
 - tensor, 36
 - thixotropic, 208

- Shear stress—*Continued*
 at wall, 27
 capillary, 23
Shock resistant glass, 300
Short, glass, 300
Short, shot, 517F
Shortness, 167, 405
 ink, 155, 165
 size, injection molding, 509
Shrinkage
 cracks, cement, 347
 ecological, 348
 intrinsic, 348
 irreversible, cement, 349
 of oriented layer, 532F
Silica, 266
 fused, 331
 gel in grease, 458
 pure, 333
 sponge, 331
 vibrations, 333
 vitreous, 319
Silicon carbide, suspension, 95
Silicones, 448
 fluid, 210, 221F
Silk screen printing, 235
Silk worms, 554
Silver chloride, 338
Silver iodide, 261
 suspension, 95, 96
Silver, model value, 475T
Single-bob method, apparent fluidity, 36
Sink marks, 513
 injection molding, 537, 541
Size distribution, latex, 139
Slaked lime, 265
Slider bearing, 467
Slip, Slippage
 casting, 266, 288
 molecular, 9
 rotational, 197
 at the wall, 27
Smoluchowsky's equation, 87(7)
Smooth pipe flow, 218(17)
Soap, in grease, 458, 461
Soap, metal shear strength, 477T
Soda-lime silicate, glass, 301
Sodium acrylate, 141
Sodium alginate, 204
Sodium chloride, 338
Sodium magnesium silicate glass, 324
Sodium metasilicate, 307
Sodium silicate glass, 318
 effect of ion substitution, 319
 effect of temperature, 310T
 replacement of silicon, 321
Sodium stearate, 477
Softening point, glass, 301
Solders, 480, 486-488
Sol-gel transformation, 277
Sol-gel-sol transformation, 205
Solid(s), *see also* Glass, Rheological
 models
 fracture of adhesive, 484
 solution interface, 90
 surfaces, 480
Solidifying, polymer in mold, 528
Solution, *see also* under respective sol-
 vent, Birefringence, Colloidal,
 Macromolecular, etc.
 polymers, dilute and concentrated, 16
 spinning, 560
Solvent-chain alignment, 451
Solvent evaporation, effect of, 244T
Sorbitan monooleate, 440
Sorbitan sesquioleate, 438, 440
Sound frequency absorption in glass, 333
Spatula, flow from, 234
Spatula test, 497
Speed gradient, *see* Velocity gradient
Sphere
 angular velocity, 57
 falling, 71
 passing, 97
 suspended, 84
 torsional oscillation, 59
 torque, 59(57)
 viscous resistance, 70
Spheroid rotating, 52
Spherulites, 372-375
 helices, 376
Spiders, 554
Spin dope, *see* Spin mass
Spin mass(es), 554-556, 564, 566
 comparison, 569
 flow anomalies, 558
 flow curves, 562, 569, 577F
 inflection point, 570
 friction effects in, 560
 hardening, 562
 master curve, 559
 non-Newtonian, 570

- pseudo-Newtonian, 570
- temperature flow curves, 559
- temperature rise, 580
- viscosity, 569
- Spinnability, 555, 583
 - chain length and, 557
 - homogeneity and, 557
 - polymers, 557
 - solutions characteristics, 556
- Spinnbarkeit, *see* Spinnability
- Spinnerette, 555, 562, 566, 570, 581
 - capillary flow, 556
 - chain unrolling, 556
 - exit, 562
 - polymer orientation in, 556
 - surface tension at, 557
- Spinning, *see also* Spin, mass, Spinability
 - coagulation, viscosity changes, 563
 - coagulation profile, 581F
 - conditions and fiber dimension, 575
 - dry, 562, 563
 - emulsion, 583
 - melt, 560, 562, 565
 - process, viscosity variation, 578
 - shear stress, 562
 - solution, 560
 - speeds, 564
 - wet, 562
 - coagulation, 564
 - solvent loss, 565
- Spray, Spraying, 190, 243, 245
 - droplet size, 245
 - guns, 245, 246
- Spreading operations, 190
- Spring chain representation, 2
- Sprue, injection molding, 509
- Squeeze-film, 467
- Squibb viscometer, 159, 160F
- Starch
 - cooking two samples, 231
 - flow curves, 232F
 - one-point viscosity control, 235
 - pastes, 202
 - suspension, 205, 226T
- Stearic acid, surface viscosity, 437
- Steel
 - Bismuth, friction, 474
 - in concrete, 363
 - Duraluminum, friction, 474
 - friction coefficient, 472F
 - mild, 359
 - model value, 475T
- Stefan's law, 169(5), 482(1), 485
- Sticking, injection molding, 541
- Stokes' law, 70
 - assumptions, 71
 - charged particles, 95
 - corrections, 71
- Stormer viscometer, 159, 192
- Strain, relative displacement (*see also* Deformation), 360
 - duration, 199
 - frozen, relaxation, 532F
 - gage transducer, 127
 - rate, *see* Shear rate
 - residual, 531
 - at rupture, 405
 - shear, 41
 - sinusoidally varying, 19
- Streaming birefringence, 103
 - and ionization, 105
- Streaming potential, 273, 274
- Streamlines, 22, 30
 - flow, 217
- Strength, shear (*see also* Rupture, Yielding), 311
 - adhesive, 487
 - effect of history, 490
 - in friction, 468
 - joint and strength of adhesive, 490T
 - polyester fibers, effect of diameter, 381F
 - polyethylene sebacate polyester fibers 381F
 - soap, metal, 477T
 - theory, 500
 - ultimate, 469
- Strength, tensile
 - adherent, 484
 - adhesive, 496
 - concrete, 343
 - and crystallinity, 369
 - of fibers, 380
 - liquids, 173(6)
 - separation, 482
- Stress
 - bearing elements, polyethylene, 379
 - concentration, along cuts, 489
 - cooling polymer, 541
 - cracking, environmental, 405

Stress—Continued

- polyethylene, 399
 - tests, 406
 - distribution, adhesive, 500
 - butt joint, 491
 - polyethylene cable, 398
 - electrostatic contribution, 87
 - intercept, 199, 200
 - internal, liquid, 173
 - lap joints, deformed, 494
 - longitudinal, 22
 - normal, 19, 22
 - rolling, 177
 - optical effect, polyethylene, 369
 - pattern frozen, 533F
 - residual, 541
 - shear, *see* Shear, Shear stress
 - sinusoidally varying, 19
 - tangential, rolling, 31, 177
 - transmission to crystallites, 382
- Stress relaxation (*see also* Relaxation),**
199, 283, 284
- interfacial, 441F
 - nylon, 421
 - polyethylene, effect of time, 396
- Stress-strain, *see also* Creep, Deformation, Stress-strain curves**
- biaxial, polyethylene, 405
 - microcrystalline, 366
 - polyethylene, 404T
 - sequence, 192
- Stress-strain curves,**
- mortar, 355F
 - polyethylene terephthalate, 407F
 - polyhexamethylene sebacamide, 407F
 - polytetrafluoroethylene, 407F
 - polytrifluorochloroethylene, 407F
 - polyvinyl chloride, 407F
- Stretch-spinning, 575**
- Strike-through, 234**
- Stripping, 482**
- cellulose acetate, 498F
 - cellulose nitrate, 498F
 - tests, 482
- Structural viscosity, 164**
- fresh cement, 344, 345
- Structure number, 202, 238, 239**
- Sun viscometer, 159**
- Supercooled water, 257**
- Supercooling, 305**

Superposition principle, 383

- Surface, *see also* Interface**
- active agents, 228T
 - effect on polyethylene, 406
 - wetting agent, 226
 - attraction, 503
 - change, 261
 - cylindrical, 22
 - dipole, 260
 - elasticity, 440(7)
 - damping, 440
 - static, 436
 - energy, 259, 262, 269
 - and double layer, 264
 - films, close packed, 431
 - distribution of relaxation times, 441
 - elasticity, 435
 - Newtonian flow, 442
 - water, on solid, 256
- forces, clay, 258**
- fraction, constant friction, 475**
- free energy, 261**
- ions, polarization, 260**
- lubrication, plastic granules, 512**
- luster, molding, 508**
- magnesium oxide, 262**
- poises, 433**
- roughness (rugosity), 468, 482**
- pipes, 218
 - and separating forces, 482
- screening, 281**
- skin, 532**
- solid, 480**
- air occluded, 480
 - friction, 467
 - rubbing, 468
- tension, effect on spray droplet, 246**
- roll flow, 186
 - at spinnerette, 557
- Surface viscometers (*see also* Surface viscosity), 431**
- canal, 432
 - correction, 432F
 - designs, 434F
 - rotational torsion, 435
 - torsion pendulum, 433
- Surface viscosity, 432(2), 435(5), 437**
- alcohols, 437
 - apparent, 431(1), 433(3)
 - fatty acids, 437

- foam stability and, 442
- lack of, in pure liquids, 429
- lubricating films, 442
- reaction rate theory, 442
- shear rate, 438F
- surfactant, 429, 430
- temperature, 438
 - coefficient, 442
- units, 431
- variables, 436
- Surfactant, 429
 - at interface, 430F
 - orientation, 430
- Suspensions (*see also* Particles), 226T, 240
 - dilute, 116
 - effect of concentration, 222
 - of surface active agent, 226
 - flow properties, 227
 - non-Newtonian, 224
 - viscosity, 119(33)
- Sweet glass, 300
- Synthetic fibers, *see* Fibers
- Synthetic lattices, 135
 - shear rate and shear stress, 131
- T
- Tack (tackiness), 175(7), 481, 485
 - effect of air, 484
 - of surface roughness, 483F
 - energy density, 171
 - fingers, 177
 - mechanical, 169
 - force, 183
 - analysis, 168
 - measure, 178
 - ink, 168, 177
 - test, 171
- Tackmeter, 193
 - inclined plane, 171
- Take-off knife, 151
- Take-up speed, 582
- Tangent viscosity, 204
- Tapes, pressure-sensitive, 485
- Taylor's series, 28
- Teflon, *see* Polytetrafluoroethylene
- Temperature
 - average, during the molding cycle, 511
 - coefficient, viscosity, 455
 - of glasses, 309
 - effect on shear rate, 214
 - on spinning, 556
 - on viscosity, 137, 612
 - elastic dumbbell, 6
 - and glass viscosity, 327
 - gradient, bearing, 455
 - oil flow, 466
 - hysteresis loop and, 214
 - loss peak and, 394
 - molded piece, 510
 - molding, 508
 - pressure plot, injection molding, 544
 - reduced, from heat conduction theory, 511F
 - and relaxation times, 384
 - rise, rotational viscometer, 159
 - spin mass, 580
 - viscous, 579
- Tensile strength, *see* Strength tensile
- Tensile stress, *see* Stress
- Tension, internal, polyethylene, 399
- Tensor, shear stress, 36
- Terylene, *see* Polyethylene Terephthalate
- Test, Testing, *see* Creep, Dynamic, Relaxation, Viscometry, etc.
- Thermal
 - agitation, *see* Brownian motion
 - conductivity, 455, 510
 - expansion, 173
 - oil, 455
 - power, extruder, 625
 - wedge effect, 455
- Thermofluorescent powders, 373
- Thermoplastic resin, fabrication steps, 506
- Thickeners, 141
- Thiele funnel, 575
- Thixotropic (Thixotropy), 163, 205, 276, 277
 - breakdown, 206
 - coefficients, 213
 - degree of, 212
 - greases, 466
 - ink, 161
 - dilatant flow curves, 214
 - flow, changes with treatment, 220
 - flow curves, 206F, 210F, 212F
 - grease, 462
 - paints, 207, 244

- Thixotropic—*Continued*
 plastic, flow curve, 234F
 flow evaluation, 213
 pseudoplastic flow, 214
 structure, 207, 211
 aging, 220
 and temperature, 211, 214
 Thorium hydroxide, suspensions, 120
 Thorium nitrate, 273, 275
 Thorium oxide, 318, 320
 suspension, 96
 Thread guides, 575
 Three-roller mill, 230
 Thrust bearing, 455
 Time
 dependence, *see* Creep, Energy dissipation, Frequency, Shear rate, etc.
 effect on practically relaxing metals, 410
 in viscoelasticity, 41
 Tin, model value, 475T
 Titanate, methylortho, 320
 Titanium, model value, 475T
 Titanium dioxide, 229T, 320
 suspensions, 208F, 269
 Torpedo, 507
 flighted, 629
 Torque (Moment, Twist), 30, 31(16), 37,
 39, 47(39) *see also* Stress-strain
 and angular displacement, 41
 concentric cylinder, 129
 cone and plate, 61, 62, 198
 disk, 52
 double cone, 62
 inkometer, 175
 intercept and yield value, 211
 measure, frictionless, 159
 oscillating, 44
 phases, 43
 relaxation, nylon, 421
 splitting ink film, 170
 Torsion, *see also* Coaxial cylinder viscometer
 nylon-66, 419T
 pendulum, surface viscometer, 433,
 435, 440
 Transfer factors, 151
 Transformation region, dependence on
 conditions, 304
 Transition loss coefficient, 240
 Tricaprin, surface viscosity, 437
 Tricaproin, surface viscosity, 437
 Tricapryllin, surface viscosity, 437
 Triethanolamine, 227F
 Trilaurin, surface viscosity, 437
 Triolein, surface viscosity, 437
 Triricinolein, surface viscosity, 437
 True plastic flow curve, 234F
 Tube,
 circular, 21
 critical Reynolds number, 218
 plastometer, 345
 Tungsten carbide, model value, 475T
 Tunnel injection molding, 506
 Turbulence, Turbulent (*see also* Reynolds number), 149, 217, 558, 561
 flow, curve, 195
 rotational viscometer, 218
 mechanism, 218
 Turning, 497
- U
- Ultimate-strength, *see* Strength
 Ultimate-stresses, *see* Strength
 Ultra-Viscoson, 162
 Ultrasonic techniques, nylons, 425
 Ultrasonic vibration, adhesive joint, 488
 Uniaxial stretch, 382
 Universal joints, 3
 Urea-formaldehyde resins, 303
- V
- Vacuum bubbles, injection molding, 541
 Van der Waals' forces, potential, *see also*
 Molecular interaction
 and stress, 378
 Vanadium oxide, suspensions, 216
 Vapor pressure, oils, 445
 Varnishes, 233, 242T
 Vehicle drainage, 156
 ink on paper, 154
 Vehicles oil-based, 146
 Velocity, *see also* Flow, Shear rate
 angular, 30
 average, capillary, 24
 distribution, Bingham body, 26
 capillary, 23
 pressure flow, 600
 gradient, *see also* Shear rate
 roll flow, 185
 and shear stress, 561
 head, number, 240

- profile, between rolls, 155F
 - change during fiber-formation, 566
 - discone, 184
 - nip, 176F
 - rotating roll, 177F
 - viscous oils, 466
- Vibrating reed, 332
- Vibrations, *see also* Frequency, Waves
 - characteristic, glass, 334
 - normal, 2
 - of the crystal lattice, 2
- Vinyl acetate, crotonic acid copolymer, 96
- Vinyl butyral resin, 488
- Vinyl pastes, 202
- Vinyl plastisol, 215
- Vinylidene chloride, 568
- Viscoelasticity (firmo-viscosity) 63, *see also* Anelasticity, Creep, Friction
 - internal, retarded
 - cone and plate, 62
 - deformation, surface films, 435
 - effect of structure, 418
 - ink, 168
 - linear, 19, 41
 - penetrometer, 80
 - plate plastometer, 75
- Viscometers, Viscosimeters
 - capillary, *see* Capillary displacement, 127
 - coaxial cylinder, *see* Coaxial cylinder viscometer
 - concentric-cylinder, *see* Coaxial cylinder viscometer
 - concentric sphere, 57
 - cone and plate, 61, 127, 215
 - conicylindrical, 64, *see also* Coaxial cylinder viscometer
 - corn industries', 231
 - disk, 51-54
 - double cone, 63
 - errors, 586
 - extrusion, 203
 - Ferranti-Shirley, 127
 - hemispherical, 58, 60
 - Höppler, 123
 - melt, 586
 - Mooney-Ewart, 64, 124, 126
 - Oscillating plate, 65F
 - Pochettino, 77
 - rotational, 29, 159
 - semimicro dilution, 586
 - Stormer, 159, 192
 - torsion pendulum, surface, 435
 - torsional, automatic, 209
 - types, 20
- Visco-plastic solid, *see* Bingham body
- Viscose fiber, birefringence, 582
 - process, 564
- Viscosimeters, *see* Viscometers
- Viscosity, 63, 142, *see also* Friction internal, Intrinsic viscosity, Viscometers, Viscosity equations and theories
 - absolute, glass, 302
 - apparent, 198(7), 200, 202, 221, 234, 238, 623
 - capillary viscometer, 29
 - between plates, 98
 - screw channel, 618
 - structure number, 240
 - turbulent flow, 239
 - bulk, polyethylene, 392
 - units, 431
 - cement, 350
 - chain length and, 436
 - in channel flow, 520
 - coefficient, 24, 28, 32, 194(1), *see also* Viscosity, equations and theories, and individual materials
 - complex, *see* dynamic
 - concrete, 361
 - contribution composite, 10
 - cylinder oscillating, 126
 - dynamic, complex, 10, 19, 43, 45(35), 48, 49(48), 51, 454
 - effect of frequency, 397
 - frequency product, 385
 - oscillating plate, 70(72)
 - effect of added salt, 107
 - on grinding, 231
 - on spray droplet, 246
 - of surface active agent, 226
 - of temperature, 612
 - effective, 203
 - extrusion, 619
 - rubber stocks, 620
 - electrostatic contribution, 87
 - extrusion, 611
 - fresh mortar, 352
 - glass, 301, 338

Viscosity—*Continued*

effect of composition, 315T
 effect of time, 312
 index, improvers, 451
 insoluble films, 433
 interaction coefficient, 84
 intrinsic, *see* Intrinsic viscosity
 kinematic, 217, 444
 latex, 135F
 limiting number, *see* Intrinsic viscosity
 melt, 584
 polystyrene, 522T
 minimum, kaolin suspension, 283T
 molecular weight and, 15
 mortar, 353
 Newtonian liquid in oscillation, 45
 one-point, 235
 oscillating, plate, 67
 sphere, 60(60)
 plastic, 25, 28, 165, 211, 467
 effect of concentration, 223
 of surface active agent, 226
 fresh cement, 345
 relative, 158
 plate separation, 482
 polymer solutions, shear dependence, 453F
 pressure, curves, lubricants, 446–449
 dependence, 450F, 454
 function, polymers in oil, 452T
 PVPBr and gradient, 119
 reduced specific, electrolytes, 85(3)
 shear rate, *see* Non-Newtonian liquids,
 Shear rate
 soda-lime-silicate glasses, 302
 sodium glass, 310T
 spin masses, 569
 spinning coagulation, changes, 563, 578
 steady state and relaxation function, 397
 structural effect, 162, 164
 surface, *see* Surface viscosity
 suspensions, 119(33)
 tangent, 202, 204
 temperature, *see also* Temperature
 coefficient, 455
 glass, 300
 function, oils, 445
 polymers in oil, 452T
 water, 254
 zero gradient, 117

Viscosity coefficient, *see* Viscosity
 Viscosity (equation and theories) *see also*
 Flow, Hydrodynamics, Liquids
 electrolytes, 85
 measurements, melt, 584
 glasses, 303
 Viscous, *see also* Viscosity, Flow viscous
 drag, on beads, 3
 plate, 66
 flow, 359F
 oils, velocity profile, 466
 heating, adiabatic, 580
 Vitreous state of matter, *see* Glass
 Voids, concrete, 361
 Voigt body, element, model, Kelvin
 body, *see* Creep, Viscoelasticity
 Volcanic magna, 315
 Volume, *see also* Free volume, Solutions,
 Viscosity
 change, glasses, 339
 flow, 361
 fraction, true, 138(42)
 reduction, fiber formation, 564
 melt spinning, 565
 Vortices, 217
 Vulcanization, 408
 Vycor glass, 331

W

Waele-Ostwald law, 76
 Wall-effects, 19, 20
 falling sphere, 71
 oscillating plate viscometer, 69
 Wall paint, 242T
 Walther equation, 444
 Water, 270
 absorption, clays, 259T
 fresh cement, 344
 quartz, 259T
 adhering film, 256
 air interfaces, 436
 bridges, particles, 167
 cement ratio, 342, 345, 346
 diffusion, in glass, 330
 effect, on flow curve, 207, 225
 on flow properties, 229T
 of pressure, 254
 evaporable, cement, 346
 films, rigidity, 267, 268, 273, 284
 flocculation by, 228

- flow, through clay, 279
 - through porous media, 278
 - freezing temperature, effect of diameter, 257F
 - ionic elevations, 255T
 - isotherm, kaolinite, 167F
 - lattice, cement, 344
 - liquid, network, 253
 - mortar, 353
 - nonevaporable, cement, 346
 - retained, 346
 - rigid film, *see* film
 - solvent power, 255
 - state in set-cement, 346
 - structure, 253
 - effect of ethanol, 96
 - supercooled, 257
 - vapor, 252
 - pressure, on clay, 258
 - viscosity, 254
 - Waves, *see also* Damping, Frequency, Vibrations
 - propagation, polyethylene, 392
 - Wax
 - crystals, 463
 - structure, 464
 - two-phase mixture, 463
 - Wear, 477
 - process, 474
 - product, 474
 - rate, 474, 476
 - resistance, 474
 - Weathering of rocks, 281
 - Wedge effect, thermal, 455
 - Weigh feeding, 507, 537
 - Weissenberg effect, 126, 571, *see also* Normal-stress effect
 - bearing, 457
 - rheogoniometer, 569
 - Weld lines, 513, 532
 - injection molding, 519
 - Welding on contact, 469
 - Wet spinning, 562, 581
 - Wetting, 163
 - ability, adhesive, 480
 - and structure, 480
 - agent, effect on sedimentation, 270, 271T
 - flow through clay, 279
 - heat, on silica gel, 270
 - rate, 480
 - White hard clay, 286
 - White lead, suspension, 224F
 - Wien effect, 109
 - Wildsteiner ion, 258
 - Wire, internal friction, 55
 - Wood, adhesive interaction, 487
 - Work hardening, adhesive film, 500
 - Workability coefficient, 357(7)
 - concrete, 342
- X
- Xanthate, *see* Viscose
 - X-ray, 377, 378
 - Xylene, flocculation by, 230
- Y
- Yarn, nylon, 412, 424
 - Yield (Yielding), *see also* Flow, plastic, Yield value
 - point, and crystallinity, 369
 - fresh cement, 344
 - pressure, in friction, 468
 - strength (*see also* Strength), fluid lubricant, 443
 - stress, 199
 - fresh cement, 345
 - fresh mortar, 352
 - frozen oils, 464
 - grease, 457, 459, 460
 - and temperature, 461
 - polyethylene, 403
 - effect of speed, 404
 - polyethylene sebacate, 380F
 - in wear, 474
 - Yield value, 25, 165, 198, 200, 211, 227, 238, *see also* Yield
 - aging, 220
 - capillary, 28
 - change of, 220
 - effect, of concentration, 223
 - of surface active agent, 226
 - of water, 225
 - and flocculation, 198
 - paint, 243
 - rotating cylinder, 33
 - temperature dependence, 222
 - Young's modulus, *see* Modulus, Young's
- Z
- Zahn cup, 190
 - Zeolite, 251, 264

Zeolitic water, cement, 347

Zeta potential, 92, 95, 98, 274, *see also*

Electrokinetic potential,

Zettlitz kaolin, 258

Zinc, friction, 469

Zinc naphthenate, 229T

Zinc oxide

green seal, suspension, 224F

leaded, suspension, 224F, 225F

suspension, 226T

sedimentation volume, 270T

Zirconium oxide, 266, 318, 320

